



UNIVERSITY OF  

---

LIVERPOOL

**Exploring the Role of Extracellular Vesicles in Equine  
Musculoskeletal Pathologies and Associated  
Regenerative Therapies**

*Thesis submitted in accordance with the requirements of the University of Liverpool for the  
Degree of Doctor in Philosophy*

By

Emily-Jayne Clarke

October 2023

# Table of Contents

Declaration.....	v
Acknowledgements .....	vii
List of Tables.....	ix
List of Figures .....	xi
List of Abbreviations .....	xix
<b>1. Thesis Abstract.....</b>	<b>1</b>
<b>2. Introduction .....</b>	<b>2</b>
2.1. Equine Musculoskeletal Injury .....	2
2.2. Equine Musculoskeletal Limb Anatomy.....	2
2.2.1.Equine Osteoarthritis .....	3
2.2.2.Equine Tendon Injury.....	5
2.3. Experimental Models of Osteoarthritis.....	7
2.3.1.In vitro.....	7
2.3.2.In vivo.....	10
2.4. Experimental Models of Tendon Injury.....	14
2.4.1.In vitro.....	14
2.4.2.In vivo .....	16
2.5. Biological Therapies used in Equine Musculoskeletal Injuries and Disease.....	18
2.5.1. Mesenchymal Stem Cell Therapy.....	18
2.5.2. Platelet-rich Plasma Therapy.....	19
2.6. Extracellular Vesicles.....	19
2.6.1.Overview.....	19
2.6.2. Characterisation.....	20
2.6.3.Biogenesis.....	21
2.6.4.Mesenchymal Stem Cell derived Extracellular Vesicles .....	24
2.6.5.Osteoarthritis associated Extracellular Vesicles.....	27
2.6.6. Extracellular Vesicles derived from Platelets and Platelet-rich Plasma.....	29
2.7. Raman and Optical Photothermal Infrared Spectroscopy.....	31
2.7.1.Applications of Raman and Infrared Spectroscopy to Osteoarthritis.....	33
2.7.2.Applications of Raman and Infrared Spectroscopy to Extracellular Vesicles.....	34
2.8. Mass Spectrometry Proteomics and Lipidomics.....	34
2.8.1. Application of Mass Spectrometry Proteomics and Lipidomics to the Study of Osteoarthritis and Extracellular Vesicles .....	38
2.8.2. Application of Mass Spectrometry Proteomics to the study of Mesenchymal Stem Cell Therapy .....	38
2.8.3. Application of Mass Spectrometry Proteomics to the study of Tendon Injury and Platelet-rich Plasma .....	39
<b>3. Thesis Overview .....</b>	<b>41</b>
3.1. Project starting points.....	41
3.2. Aims and Objectives.....	41
3.3. Outline of Thesis.....	42
<b>4. Materials and Methods.....</b>	<b>43</b>

4.1. <i>Temporal Extracellular Vesicle Protein Changes following Intraarticular Treatment with Integrin <math>\alpha</math>10<math>\beta</math>1-selected Mesenchymal Stem Cells in Equine Osteoarthritis</i> .....	43
4.1.1 Preliminary Studies.....	44
4.1.1.1. Optimisation of Extracellular Vesicle Isolation for Downstream Mass Spectrometry Proteomics Analysis .....	43
4.1.1.2. Optimisation of a Commercially available Extracellular Vesicle Characterisation Platform.....	45
4.1.2. Main Study.....	46
4.2. <i>Optical Photothermal Infrared Spectroscopy can Differentiate Equine Osteoarthritic Plasma Extracellular Vesicles from Healthy Controls</i> .....	53
4.2.1. Preliminary Studies.....	53
4.2.1.1. Optimisation of Extracellular Vesicle Suspension for Spectroscopic Analysis .....	53
4.2.1.2. Using Raman and Optical Photothermal Infrared Spectroscopy to identify Synovial Fluid derived Extracellular Vesicle Biomarkers of Naturally Occurring Equine Osteoarthritis.....	54
4.2.2. Main Study.....	55
4.3. <i>Proteome and Phospholipidome Interrelationship of Synovial Fluid-derived Extracellular Vesicles in Equine Osteoarthritis: An Exploratory ‘Multi-Omics’ Study to Identify Composite Biomarkers</i> .....	58
4.3.1. Main Study.....	58
4.4. <i>Allogenic Platelet-rich Plasma and Platelet-rich Plasma Extracellular Vesicles Change the Proteome of Tenocytes in an In Vitro Equine Model of Tendon Inflammation, Resulting in the Identification of Potential Molecular Modes of Action of platelet-rich Plasma: A Pilot Study</i> .....	66
4.4.1. Preliminary Studies.....	66
4.4.1.1. Optimisation of an In Vitro Inflammatory Model to Study Equine Tendon Injury.....	66
4.4.1.2. Determination of the most appropriate Platelet-rich Plasma Extracellular Vesicle Concentration to use in an In Vitro Equine Tendon Inflammatory Mode.....	68
4.4.2 Main Study.....	70
<b>5. Manuscript 1</b> .....	79
<i>Temporal Extracellular Vesicle Protein Changes following Intraarticular Treatment with Integrin <math>\alpha</math>10<math>\beta</math>1-selected Mesenchymal Stem Cells in Equine Osteoarthritis</i>	
5.1. Abstract .....	80
5.2. Introduction .....	81
5.3. Results.....	83
5.4. Discussion.....	97
5.5. Conclusion .....	102
5.6. Ethics .....	102
5.7. Funding.....	103
<b>6. Manuscript 2</b> .....	104
<i>Optical Photothermal Infrared Spectroscopy can Differentiate Equine Osteoarthritic Plasma Extracellular Vesicles from Healthy Controls</i>	
6.1. Abstract.....	105
6.2. Introduction .....	106
6.3. Results.....	108
6.4. Discussion .....	117
6.5. Conclusion .....	121

6.6. Ethics.....	121
6.7. Funding.....	121
6.8. Acknowledgments.....	122
<b>7. Manuscript 3.....</b>	<b>123</b>
<i>Proteome and Phospholipidome Interrelationship of Synovial Fluid-derived Extracellular Vesicles in Equine Osteoarthritis: An Exploratory ‘Multi-omics’ Study to Identify Composite Biomarkers</i>	
7.1. Abstract.....	124
7.2. Introduction .....	125
7.3. Results .....	127
7.4. Discussion .....	143
7.5. Conclusion.....	146
7.6. Funding.....	146
7.7. Acknowledgments .....	146
<b>8. Manuscript 4.....</b>	<b>147</b>
<i>Allogenic Platelet-rich Plasma and Platelet-rich Plasma Extracellular Vesicles change the Proteome of Tenocytes in an in vitro Equine Model of Tendon Inflammation, Resulting in the Identification of Potential Molecular Modes of Action of Platelet-rich Plasma: A Pilot Study</i>	
8.1. Abstract .....	148
8.2. Introduction .....	149
8.3. Results .....	152
8.4. Discussion.....	170
8.5. Conclusion.....	178
8.6. Ethics.....	178
8.7. Funding.....	178
<b>9. General Discussion.....</b>	<b>180</b>
9.1. Extracellular Vesicle Mediation of Mesenchymal Stem Cell Therapy in an Equine In Vivo Experimental Model of Osteoarthritis .....	182
9.2. Equine Plasma Extracellular Vesicle Biomarkers of Naturally Occurring Osteoarthritis .....	183
9.3. Equine Synovial Fluid derived Extracellular Vesicle Proteomic and Phospholipidomic Biomarkers of Naturally Occurring Osteoarthritis.....	185
9.4. The effect of Platelet-rich Plasma and Platelet-rich Plasma derived Extracellular Vesicles on Cytokine Stimulated Equine Tenocytes.....	186
9.5. Further Work .....	188
9.5.1. Extracellular Vesicle Imaging and Tracking.....	188
9.5.2. Development of Suitable <i>in vitro</i> and <i>in vivo</i> Models.....	189
9.5.3. One Medicine Approach to Research.....	191
9.5.4. Biologic Study Reporting Standards .....	192
9.5.5. Mesenchymal Stem Cell based Therapeutics – Challenges and Future Direction.....	193
9.5.6. Adjuvant Therapeutics.....	194
9.6. Future Challenges.....	195
9.6.1. Extracellular Vesicle Standardisation.....	195
9.6.2. Clinical Translation of Extracellular Vesicles - Therapeutics and Diagnosis.....	196
9.6.3. Commercialisation of Extracellular Vesicle based Therapeutics.....	197
9.7. Conclusion.....	198
<b>10. Supplementary Information.....</b>	<b>199</b>
<b>11. Appendices .....</b>	<b>227</b>
<b>References .....</b>	<b>236</b>

<b>Publications .....</b>	<b>291</b>
<b>Conference Presentations and Posters.....</b>	<b>301</b>

## Declaration

This thesis is the result of work performed whilst registered as a candidate for the degree of Doctor of Philosophy at the University of Liverpool. I declare that no portion of the work referred to in this thesis has been submitted in support of an application for another degree or qualification of this or any other university or institute of learning. I, Emily Clarke confirm that the work included in this thesis is my own. Where information has been derived from other sources, this has been referenced appropriately.

The overall study design was that of myself, Professor Mandy Peffers and Dr Agnieszka Turlo. I conducted the background literature review, and sections of this have been published following peer review by UK-VET Equine, with the title “Extracellular Vesicles in Equine Osteoarthritis: From biomarkers to therapeutic potential” (<https://doi.org/10.12968/ukve.2023.7.6.254>). The below paragraphs outline contributions to each of studies that constitute the thesis results chapters:

**Manuscript 1-** *“Temporal extracellular vesicle protein changes following Intraarticular treatment with integrin  $\alpha$ 10B1-selected mesenchymal stem cells in equine Osteoarthritis”, published in Frontiers in Veterinary Science <https://doi.org/10.3389/fvets.2022.1057667> : Emily J Clarke, Mandy J Peffers, Agnieszka Turlo, Victoria James, and Stine Jacobsen conceived of and designed the study. Stine Jacobsen, Lise Berg, Casper Lindegaard and Camilla Anderson conducted the equine *in vivo* study and collected samples. Kristina Uvebrant and Evy Lundgren-Akerlund provided commercially sourced equine MSCs. Emily J Clarke processed the samples for analysis and acquired the data in conjunction with Rosalind Jenkins; Eva Caamano Gutierrez and Emily Johnson analysed the data using computational approaches. All authors interpreted the data; and all authors reviewed the draft and final manuscript.*

**Manuscript 2-** *“Optical Photothermal Infrared Spectroscopy can Differentiate Equine Osteoarthritic Plasma Extracellular Vesicles from Healthy Controls”, published in RSC Analytical Methods- <https://doi.org/10.1039/D2AY00779G> : Emily J Clarke, Mandy J Peffers, James R Anderson, Alison Beckett Catarina Castanheira, Victoria James, Jacob Hyett, Royston Goodacre and Cassio Lima conceived of the study, produced the manuscript. Emily J Clarke collected samples, and processed samples for spectroscopic analysis and transmission electron microscopy. Transmission electron microscopy was conducted by Alison Beckett. Cassio Lima conducted Raman and Optical Photothermal Infrared spectroscopic analysis. Formal data analysis was conducted by both Emily J Clarke (EV characterisation data) and Cassio Lima (spectroscopic data). Data curation was conducted by Emily J Clarke and Cassio Lima. Emily J Clarke, Mandy J Peffers, James R Anderson, Catarina Castanheira, Royston Goodacre and Cassio Lima conceived of the contributed to the interpretation.*

All authors contributed to the drafted manuscript. All authors read, contributed and approved the final manuscript.

**Manuscript 3** - *“Proteome and phospholipidome interrelationship of synovial fluid-derived extracellular vesicles in equine osteoarthritis: An exploratory ‘multi-omics’ study to identify composite biomarkers”*, available on BioRxiv and will be submitted to *Biochimica et biophysica acta (BBA) Biochemistry & Biophysics Reports*, <https://doi.org/10.1101/2023.08.02.551609> : Emily J Clarke, Laura Varela, P. René van Weeren, Marca H.M Wauben, Chris H.A. van de Lest and Mandy J Peffers conceived of and designed the study. Maciej Przewozny and Anna Cywińska collected samples. Emily J Clarke and Laura Varela, were joint first co-author, and Laura Varela acknowledges the sue of this chapter in this thesis, both processed samples for mass spectrometry analysis of proteins and phospholipids. Rosalind Jenkins assisted with mass spectrometry proteomics data acquisition. Estefanía Lozano–Andrés assisted with flow cytometry data acquisition. Emily J Clarke statistically analysed the proteomics data, and Laura Varela analysed phospholipidomic data, and performed multi-omic integration, with advice from Chris H.A. van de Lest. All authors interpreted the data; Emily J Clarke and Laura Varela wrote the manuscript; and all authors reviewed the draft and final manuscript.

**Manuscript 4** - *“Allogenic platelet-rich plasma and platelet-rich plasma extracellular vesicles change the proteome of tenocytes in an in vitro equine model of tendon inflammation, resulting in the identification of potential molecular modes of action of PRP: A pilot study”*: Emily J Clarke, Mandy J Peffers, Agnieszka Turlo and James R Anderson conceived of and designed the study. David Bardell, Mark Senior and Emily J Clarke acquired samples. Emily J Clarke processed all samples. Alexandra M Gillen assisted with sample characterisation. Emily J Clarke and Mandy J Peffers acquired the data; Emily J Clarke and Anderson Jenson analysed the data ; Mandy J Peffers, Emily J Clarke and Agnieszka Turlo interpreted the data; Emily J Clarke wrote the manuscript; and Mandy J Peffers and Agnieszka Turlo reviewed the draft and final manuscript.

### **Candidate**

Emily Clarke BSc (Hons) MRes AFHEA

### **Supervisors**

Professor Mandy J Peffers BSc (Hons) MPhil PhD BVetMed FRCVS

Dr Agnieszka Turlo PhD MRCVS

## Acknowledgements

Firstly, I would like to thank my primary supervisor, Prof Mandy Peffers. I never would have imagined that a chance interaction at Liverpool horse show would result in meeting an incredible mentor that has provided me with a diverse range of opportunities, opening the doors of veterinary research for me and supporting every endeavour and aspiration I have had wholeheartedly. I am privileged to have met Mandy and words cannot truly express the gratitude I have for her and everything she has done. Her extensive support and world-renowned knowledge in the field of equine musculoskeletal biology have provided me with a priceless platform from which to learn and grow as a researcher, of which I will forever be grateful for.

I would also like to thank my secondary supervisor Dr Agnieszka Turlo for also supporting me throughout my PhD. Her endless encouragement and advice have made this experience profoundly easier, and she has provided me with guidance that has enabled me to prioritise balance with my research endeavours and recognising my worth as a researcher and as an individual, and the value of that truly cannot be underestimated. Thank you.

I would also like to thank Dr James Anderson, without whom I would never have known how to find a pipette or tip box in our lab. James taught me from the start, and every practical lab skill I have I owe to his fantastic teaching, support and confidence in my ability. Encouraging me to grow and trust my own opinion and skill within a lab environment, while also problem solve in a calm manner when required. The data in this thesis would certainly never have been obtained without his teaching in the early stages of my lab career. Thank you.

It goes without saying but I would also like to thank all my colleagues that have become friends: Catarina Castanheira, Kiran Riasat, Hannah Coleman, Lucy Gill, Phaedra Winstanley-Zarach, Sharna Lunn. Sherrin Gotru, Anders Jenson, Anne Stairmand, and Genna Abdullah. You have all had such a profound impact on my life and PhD experience. You have all provided advice, a sounding board and sometimes some well needed emotional support with chocolate and a coffee. I truly cannot thank you enough. I'd also like to thank my academic partner in crime, we've always kept each other on our toes, from our undergrad days to both becoming doctors, and I couldn't be prouder of you and the path you have taken- Laura Davies.

I would also like to extend my sincerest thank to my advisory panel, Prof Pete Clegg and Dr Lesley Iwanjenko. You have both always ensured I was happy and provided the validation I needed to ensure I was confident in my progress and ability to deliver a PhD thesis in a timely manner. Your endless support has always been appreciated.



I would also like to thank collaborators from the University of Liverpool: the computation biology facility for all their support with respect to bioinformatics (Dr Eva Caamano and Dr Emily Johnson), as well as Dr Roz Jenkins, for her infinite mass spectrometry knowledge and support, and all our clinical collaborators from the Phillip Leverhulme Equine Hospital- Dr Alex Gillen, Dr John Stack, Dr David Bardell and Dr Mark Senior.

Next, I would like to thank all the collaborators I have had the honour of working with during my PhD. To connect internationally with world renowned scientists and share ideas is something I will always cherish, and your kindness in teaching me, and entering into new endeavours. The value of team work really cannot be underestimated in science and the opportunities you have provided me with have only highlighted that further. Thank you, Prof Rene Van Weeren, Prof Marca Wauben, Prof Chris Van Hest, Prof Stine Jacobsen and Dr Camilla Anderson.

Through such collaborations I have also had the privilege to meet wonderful people, such as fellow co first author and PhD student Laura Varela. I am so proud of our work together and appreciate the lifelong friendship that has subsequently been forged.

I would also like to thank all those that have been part of my formal education from primary school, high school and sixth form. To the teachers that inspired and challenged me, you know who you are.

I would also like to thank all the funding bodies that have supported me during my journey as a self-funded PhD student, namely: Horserace Betting Levy Board, Liverpool Shared Research Facility, ILCaMS support for research, and the EU COST Association.

Finally, and my most important thank you, to my Mum (Kristian Clarke) and sister (Amy Clarke). Without you both I would not be standing where I am today, you have both supported me in an immeasurable way, moved mountains, and always provided me with everything I could ever need in order to succeed and reach my dreams. You know how much you mean to me, as well as Holly, our family dog that has been their throughout it all.

And of course, I couldn't leave out my favourite border collie Bella, for providing all the cuddles, early morning wake up calls, and hourly reminders to take a break while writing. You might well be my soul dog.

My final thank you goes to Dr Elena Cornara Piscopia, the first female to ever receive a doctorate degree. A fearless pioneer that has paved the way for women to pursue higher education, and subsequently women in STEM. Thank you for being brave enough and bold enough to show we can.

## List of Tables

**Table 2.1. Overview of original research articles on equine *in vitro* studies.** Specifically, between 2018-2023, identified using PubMed and google scholar. Search terms included 'equine', 'osteoarthritis' and '*in vitro*'.

**Table 2.2. Overview of original research articles on equine *in vivo* studies.** Specifically, between 2018-2023, identified using PubMed and google scholar. Search terms included 'equine', 'osteoarthritis', '*in vivo* models', 'surgical', 'carpal osteochondral fragment model', 'lipopolysaccharide', 'synovitis', 'amphotericin', 'il-1'.

**Table 2.3. Overview of original research articles on equine *in vitro* tendon injury studies.** Specifically, between 2018-2023, identified using PubMed and google scholar. Search terms included 'equine', 'tendon injury', 'tendinopathy', 'cytokines', 'mechanical'.

**Table 2.4. Overview of original research articles on equine *in vivo* studies.** Specifically, between 2018-2023, identified using PubMed and google scholar. Search terms included 'equine', 'tendon injury', '*in vivo* models', 'surgical', 'tendinopathy', 'mechanical'.

**Table 2.5. Overview of original research articles on the use of mesenchymal stem cell derived extracellular vesicles and mesenchymal stem cell based secretome therapeutics.** Specifically, between 2018-2023, identified using PubMed and google scholar. Search terms included 'equine', 'MSCs', 'MSC-EVs', '*in vitro*', '*in vivo*', 'human', 'musculoskeletal', 'Extracellular Vesicles'.

**Table 2.6. Overview of original research articles on extracellular vesicles and osteoarthritis.** Specifically, between 2018-2023, identified using PubMed and google scholar. Search terms included 'equine', 'Human', 'Osteoarthritis', '*in vitro*', '*in vivo*', 'pathogenesis', 'musculoskeletal', 'EVs', 'Extracellular Vesicles'.

**Table 2.7. Overview of original research articles on platelet and platelet-rich plasma derived extracellular vesicles.** Specifically, between 2018-2023, identified using PubMed and google scholar. Search terms included 'equine', 'Human', 'Osteoarthritis', 'Tendon injury', '*in vivo*', '*In vitro*', 'musculoskeletal', 'EVs', 'Extracellular Vesicles', 'PRP', Platelet derived EVs'.

**Table 4.1 An overview of experimental groups and the longitudinal time points for synovial fluid collection.**

**Table 4.2 A list of the primers and subsequent primer sequences used for this study.**

**Table 4.3. An overview of the *in vitro* experimental design and donor information.**

**Table 4.4. A list of equine primers and the corresponding base sequences.**

**Table 5.1. The top 10 differentially expressed ( $P < 0.05$ ) proteins following the application of the linear mixed model, accounting for treatment and time point.** Treatment and time were included as main effects, along with a treatment-by-time interaction term. Time point denoting significant pairwise comparisons between control and OA+MSCs is also shown.

**Table 7.1. Top 25 differentially expressed ( $p < 0.05$ ) proteins across synovial fluid derived extracellular vesicle samples derived from healthy joints and joints with mild osteoarthritis**

**and severe osteoarthritis.** Following analysis of variance (ANOVA) and post hoc tukey test analysis, identifying significant experimental group comparisons and heatmap analysis.

**Table 7.2. Top 5 canonical pathways identified using Ingenuity Pathway Analysis.** Following input of proteins correlated to lipids.

**Table 8.1. Top canonical pathways following Functional enrichment analysis using Ingenuity Pathway Analysis for platelet-rich plasma when compared to matched plasma.**

**Table 8.2. Top canonical pathways following Functional enrichment analysis using Ingenuity Pathway Analysis for platelet-rich plasma derived extracellular vesicles compared to matched plasma extracellular vesicles.**

**Supplementary Table 10.1. A table showing all 48 significant proteins.** Including accompanying accession number, FDR corrected P-Value, and direction of expression from MSC injection into the joint, to the end of the 70-day study. All proteins returning to baseline control after 70 days.

**Supplementary Table 10.2. Radiographic criteria used for the classification of the healthy, mild and severe osteoarthritis phenotypes.** Arrows indicate osteophyte formation and subchondral osteolysis, and R and L denote right or left limb.

**Supplementary Table 10.3.** Author Checklist: MIFlowCyt-Compliant Items.

**Supplementary Table 10.4.** MIFlowCyt-EV framework.

**Supplementary Table 10.5. Significantly differentially expressed pathological functions.** As identified by ingenuity pathway analysis for each comparison.

**Supplementary Table 10.6. Candidate proteins for composite osteoarthritis biomarker discovery.**

**Supplementary Table 10.7. A list of all differential ( $p < 0.005$ ) following false discovery rate correction proteins identified as enriched in platelet-rich plasma derived extracellular vesicles compared with plasma derived extracellular vesicles.** The table includes raw p value, FDR corrected p value and  $\log_2(\text{foldchange}/\text{FC})$  to inform direction of protein expression, as compared to plasma- EVs, n=3 samples used for analysis.

**Supplementary Table 10.8. A list of all differential ( $p < 0.005$ ) following false discovery rate correction proteins identified as enriched in platelet-rich plasma compared to plasma.** The table includes raw p value, FDR corrected p value and  $\log_2(\text{foldchange}/\text{FC})$  to inform direction of protein expression, as compared to plasma, n=3 samples used for analysis.

**Supplementary Table 10.9. A list of all 18 differential ( $p < 0.005$ ) proteins identified following two-way analysis of variance analysis and pairwise comparisons.** The included 18 proteins were identified as differential for both status (control or following cytokine stimulation) and grouping (treatment- no treatment, PRP or PRP-EVs). Raw P value and FDR corrected P value are shown.

## List of Figures

**Figure 2.1. A diagram of the equine metacarpal phalangeal joint.** Demonstrating molecular changes and structural changes found within an osteoarthritic joint compared to a healthy joint.

**Figure 2.2. A diagram of the equine distal limb.** Illustrating the major tendon structures in the limb and the microstructure and composition of tendon. Superficial digital flexor tendon (SDFT), deep digital flexor tendon (DDFT), common digital extensor tendon (CDET).

**Figure 2.3. A diagram illustrating the biogenesis of extracellular vesicles.** (1) the process of blebbing in order to form apoptotic bodies, (2) The process of endocytosis and exocytosis in order to secrete exosomes, (3) the budding of the cell membrane in order to form microvesicles.

**Figure 2.4. A diagram illustrating the scientific principles of optical photothermal infrared spectroscopy and Raman spectroscopy.** Highlighting how such spectroscopic techniques can be used simultaneously in order to acquire data on sample metabolic composition.

**Figure 2.5. A diagram illustrating how a mass spectrometer works and the scientific principles that govern how data is acquired from both high-performance liquid chromatography and the use of mass spectrometry.** (A) Illustrates tandem mass spectrometry analysis and the subsequent stages prior to data acquisition. (B) Illustrates how high-performance liquid chromatography works, and how it is used in conjunction with a mass spectrometer in order to generate proteomic data.

**Figure 4.1. A schematic overview of the experimental process.** Specifically, in order to probe the global EV cargo from a carpal osteochondral fragment model of equine OA following  $\alpha$ 101 $\beta$  MSC treatment intraarticularly.

**Figure 4.1 - A schematic overview of the experimental process.** Specifically, followed in order to probe the equine plasma EV membrane between 'healthy' and 'osteoarthritic' diseased states.

**Figure 4.3. Workflow for sample processing.** OA was characterised following clinical and radiographic examinations. SF was collected by sterile arthrocentesis and spun to create cell-free SF. Forty-two donors were used to create 14 samples consisting of a pool of three unique biological samples with a volume of 5mL (Healthy n=7, mild OA n= 4, and severe OA n= 3). EVs were isolated from cell-free SF following differential ultracentrifugation with a sucrose density gradient. EVs were stained using PKH and subsequently characterised following quantitative single EV-based high-resolution flow cytometry. The EV lipidome was probed following a chloroform and methanol lipid extraction, and mass spectrometry lipidomics was performed using a Fusion Orbitrap MS passing through a heated electrospray ionisation. The peaks were detected based on retention time, exact m/z-ratio, and, if present in at least 3 out of 13 samples (Healthy n=6, OA n=4, Advanced OA n=3). The features were annotated using an *in-silico* phospholipid database. The features were also selected to account for isotope distribution and adducts.

**Figure 4.4. An overview of the experimental design of the study.** Venous blood from horses (n=3) was used to produce PRP. PRP was characterised, PRP-EVs isolated using differential ultracentrifugation. The subsequent proteome was quantified. The profiled PRP and PRP-EVs were then used in an *in vitro* equine tendon inflammatory model following cytokine stimulation to ascertain the cellular response to PRP and PRP-EVs. This illustration was created

in biorender.com.

**Figure 5.1. FunRich analysis of the proteins identified from ultracentrifugation derived extracellular vesicles.** This EV isolation technique resulted in the highest number of protein identifications compared to SEC and SEC+UC.

**Figure 5.2. Particle counts identifying for particles positive for CD9, CD81, or CD63.** Equine plasma (5.2.A and 5.2.B), to SF (5.2.C and 5.2.D) derived EVs were compared and their reactivity on both the human (5.2.A and 5.2.C) and murine (5.2.B and 5.2.D) tetraspanin assay chips assessed. 1E demonstrated the colocalisation of surface markers present on plasma and SF EVs, with percentage particle count positive for such surface marker expression.

**Figure 5.3. Size and concentration of synovial fluid-derived nanoparticles.** Nanoparticle tracking analysis was undertaken using a Nanosight NS3000. All error bars are standard error of the mean (SEM). Statistical analysis undertaken in GraphPad Prism 9.0 using Kruskal Wallis Tests with FDR correction and Mann Whitney Tests within time points. ( $p < 0.05$ , \*;  $p < 0.01$  \*\*:  $p < 0.001$ , \*\*\*,  $p < 0.0001$ , \*\*\*\*). (A) EV concentration and (B) EV size.

**Figure 5.4. Sizing and enumeration of synovial fluid-derived extracellular vesicles.** All data was adjusted for dilution of the sample onto the chip. Shown is the average representing mean of three technical replicates that were run for each sample. Particle numbers were quantified by the number of particles in a defined area on the antibody capture spot. All bars are mean and standard error mean. (A) CD9, and (B) CD81-positive particles following probing with fluorescent tetraspanin antibodies. (C) Sizing of CD9 and (D) CD81 labelled EVs, normalised to MlgG control. Limit of detection was 50-200 nm. Statistical analysis undertaken in GraphPad Prism 9.0 using T-tests following parametric evaluation ( $p < 0.05$ , \*;  $p < 0.01$  \*\*:  $p < 0.001$ , \*\*\*,  $p < 0.0001$ , \*\*\*\*).

**Figure 5.5. Visualization of synovial fluid derived extracellular vesicles from control, osteoarthritic and osteoarthritic+ mesenchymal stem cell joints using Exoview at selected time points.** A fluorescent image of a representative spot is shown for each sample comparing (A) control, (B) OA and (C) OA+MSCs with colour denoting surface tetraspanin positive identification (blue-CD9, and green -CD81).

**Figure 5.6. A representative selection of synovial fluid derived extracellular vesicle samples from corresponding experimental groups (control, osteoarthritis, osteoarthritis + mesenchymal stem cells) irrespective of day.** The figure shows corresponding Sodium dodecyl sulphate–polyacrylamide gel electrophoresis (SDS-PAGE) gels used to separate proteins from EV protein extract. A Novex™ sharp protein ladder was used as a band reference, and gels were colloidal coomassie stained in order to visualise protein associated bands.

**Figure 5.7. FunRich analysis output, after mapping 2047 proteins to Gene Ontology Cellular Component terms.** These proteins were identified from a pooled sample of equine synovial fluid (11ml) used to generate the SF-EV spectral library for this study. SF was sourced from healthy, OA and OA+MSC treated joints in order to encapsulate all potential proteins that may be present across all experimental groups.

**Figure 5.8. Multi-level PCA.** The first two principal components are plotted, accounting for ~54% of variance. samples based on SWATH-MS. Each plotted point represents a horse, which are coloured by their treatment and shaped by the day of the study.

**Figure 5.9. PCA per day, highlighting global proteome change across time in association with surgical induction of OA and MSC treatment.** The first two principal components are plotted, samples based on SWATH-MS. Each plotted point represents a horse, which are coloured by their treatment, each panel reflects different day, specifically day 0 (Figure 5.9.A), day 18 (Figure 5.9.B) day 21 (Figure 5.9.C), day 28 (Figure 5.9.D), day 35 (Figure 5.9.E) and day 70 (Figure 5.9.F).

**Figure 5.10. Protein expression changes in osteoarthritic joints treated with mesenchymal stem cells vs control.** (A) Hyaluronan binding protein 2, (B) Complement subcomponent C1r, (C) CD5, (D) Complement factor D, (E) C2, (F) C1. The models were fitted using the lmerTest implementation of lme4. 48 proteins had a significant group, time, or group:time effect after FDR correction. For each protein with a significant effect the model was plotted using the effects and ggplot2 packages. The fitted model is shown as a line for the OA+MSC (blue) and control (red). The 95% confidence intervals for each group are shown as a shaded area. The raw data is included as points. At each time point pairwise comparisons were carried out between the treatment and control using the emmeans package. Significance thresholds were as follows: ( $p < 0.05$ , \*;  $p < 0.01$  \*\*:  $p < 0.001$ , \*\*\*,  $p < 0.0001$ , \*\*\*\*).

**Figure 5.11. Dot plot of Gene Ontology term enrichment analysis of differentially abundant proteins.** The size of the dots indicates the number of proteins that mapped to that term. The x-axis is the protein ratio (number of proteins that map to the term divided by the total number of significant proteins). The dots are shaded by adjusted p-values (BH method).

**Figure 6.1. Dry plasma extracellular vesicle samples imaged using the Raman and Optical Photothermal Infrared Spectroscopy instrument.** O-PTIR measurements were acquired on single-point mode using a mIRage infrared microscope and Raman spectra were acquired simultaneously with infrared data using a Horiba Scientific iHR-320 spectrometer coupled to mIRage. Images obtained compare EV morphology when suspended in (A) water, (B) PBS, and (C) saline. EVs can be identified as white a sphere with red arrows depicting where they colocalized to a given substrate.

**Figure 6.2. Synovial fluid derived extracellular vesicle characterisation.** (A) Nanoparticle tracking analysis (NTA) of synovial fluid- EVs (SF-EVs). Concentrations of EVs in particles/ml and particle size measured in nm. (B) Transmission electron microscopy of SF-EVs to determine morphology. (C) Fluorescent image of EVs highlighting the presence of specific EV surface markers ( CD9 –blue , CD81- green , CD63- red).

**Figure 6.3. Classification model for partial least squares discriminant analysis of infrared and Raman spectra from equine synovial fluid derived extracellular vesicles.** (A) Infrared and (B) Raman spectra showing classification rates for real (blue – from the 10,000 bootstrap analyses) and random (red – from the 10,000 permutation tests).

**Figure 6.4. Characterisation of extracellular vesicles.** (A) Nanoparticle tracking analysis (NTA) of a representative sample of plasma derived EVs (P-EVs). Concentrations of EVs in particles/mL and particle size measured in nm, all measurements recorded using NanoSight NS300, and data analysed by the in-built NanoSight Software NTA 3.1 Build 3.1.46. Hardware: embedded laser: 45 mW at 488 nm; camera: sCMOS. (B) Transmission electron microscopy (TEM) micrograph of negatively stained representative of plasma derived EV samples. Scale bar is equal to 200nm. Samples fixed to grids were visualised using a FEI Tecnai G2 Spirit with Gatan RIO16 digital camera.

**Figure 6.5. ExoView assay results.** (A) Particle counts for plasma EVs from the human tetraspanin chip, (B) a size histogram of plasma EV samples as captured on the CD9 human tetraspanin chip, (C) a scatter diagram demonstrating correlation between the number of CD9 positive EVs (X axis) and CD81 positive EVs (Y axis), (D) colocalization analysis of the presence of surface tetraspanins on equine plasma EVs, and (E) fluorescent microscopy visualizing plasma-derived EVs, with colour denoting surface tetraspanin positive identification (red – CD63, blue – CD9, and green – CD81).

**Figure 6.6. Fingerprint region of averaged spectra.** A) Infrared and B) Raman spectra collected from healthy control (blue line) and OA (red line) samples. Plots are offset for clarity.

**Figure 6.7. Principal component analysis scores and loadings plots.** Plots were obtained by subjecting infrared data to PCA (A and B); (C) PC scores plot of Raman data; Values in parentheses are the percentage total explained variance (TEV).

**Figure 6.8. Classification model for partial least squares discriminant analysis of infrared and Raman spectra.** (A) Infrared and (B) Raman spectra showing classification rates for real (blue – from the 10,000 bootstrap analyses) and random (red – from the 10,000 permutation tests), with a sensitivity, specificity, and positive predictive value of 97.5 %, 97.6 %, 96.7 % for infrared, respectively. (C) and (D) are the average confusion matrices for infrared and Raman, respectively, with rows representing predicted classification and columns representing experimental.

**Figure 7.1. Quantitative flow cytometric analysis of extracellular vesicles isolated from equine joints with a healthy or osteoarthritic phenotype.** A) Single EV-based high-resolution FCM of representative healthy SF-EVs (n=3) and OA SF-EVs (n=2) from the mild OA group and from the severe OA group (n =1). Sucrose density gradient fractions containing EVs labelled with the lipophilic dye PKH67 were measured for 30 seconds. The majority of EVs floated at densities of 1.16-1.10 g/ml. FL – Events: Fluorescent Events. B) EV concentration in SF was calculated as the sum of single fluorescent events measurements (PKH67+ events) in EV-containing sucrose gradient densities (1.16 to 1.10 g/ml). Mean  $\pm$  SD. ns: non-significance by Student's t-test. The uppermost point in the OA group reflects the severe OA phenotype.

**Figure 7.2. Lipidomic profile of equine synovial fluid-derived extracellular vesicles from healthy joints, mild and severe osteoarthritis.** Healthy samples (n=6), mild OA (n=4), severe OA (n=3). Each sample is comprised of a pool of three different biological replicates. Lipids were extracted from EVs isolated by differential centrifugation up to 100,000g, followed by purification with sucrose density gradients. (A) Principal component analysis of lipids isolated from the three different clinical groups. The principal components (PC)-1 and -2 explain 49% and 20% of the variance, respectively. (B) Lipid species correlation of SF-EVs. Combined heatmap (cluster dendrogram) of Lipid-Lipid Spearman correlations between the 50 most abundant lipid species in all EV sample groups. Lipid order was based on Partitioning Around Medoids, also known as K-Medoids, a centroid-based clustering algorithm. On top of the figure is the cluster dendrogram. Below is the group distribution, the relative lipid intensity of each species, and the heatmap. Under the heatmap, the degree of saturation, the lipid class of each lipid, and the respective annotation of each lipid species are indicated. (C) Changes in EV lipid classes during OA development. Vertical slices plot of SF-EVs showing the relative molar abundances for individual lipid classes. Abbreviations: LysoPC, (lysophosphatidylcholine); LysoPG, (lysophosphatidylglycerol); LysoPI, (lysophosphatidylinositol); LysoPS, (lysophosphatidylserine); PC, (ester-linked phosphatidylcholine); PC O-, (ether-linked phosphatidylcholine); PE, (ester-linked

phosphatidylethanolamine); PE O-, (ether-linked phosphatidylethanolamine); PI, (phosphatidylinositol); PS, (phosphatidylserine); SM, (sphingomyelin), PA (phosphatidic acid).

**Figure 7.3. Proteomic profile of equine synovial fluid derived extracellular vesicles derived from healthy joints and from joints with mild and severe osteoarthritis.** A) Unsupervised multivariate analysis using principal component analysis. The first two principal components were plotted, accounting for ~36.4% of the variance. SF-EV samples were plotted based on acquired SWATH-MS data, after PQN normalisation and log transformation. Each plotted point represents a pooled SF-EV sample comprised of three biological replicates. B) Heatmap demonstrating mean average protein intensities between SF-EV healthy (green), mild OA (orange) and severe OA (red) phenotypes. Protein intensities were transformed and are displayed as colours ranging from red to blue. Both rows and columns are clustered using the Ward method, and distance was calculated using Pearson Distance.

**Figure 7.4. Ingenuity Pathway Analysis networks providing an overview of significant related canonical pathways.** Analysis was conducted using the ingenuity knowledge base library and accounting for protein p-value and log<sub>2</sub> fold change following ANOVA and post hoc test analysis. (A) Mild OA compared to healthy (16 significant proteins), (B) Severe OA compared to healthy (20 significant proteins), (C) Severe OA compared with mild OA (9 proteins).

**Figure 7.5. Unsupervised proteomic and lipidomic data integration.** Proteomic and lipidomic datasets from SF-EVs derived from healthy joints, mild OA and severe OA were normalised by the sum. (A) Sparse Partial Least Squares-2 regression (sPLS2) of SF-EV samples projected into the area covered by the averaged components of both datasets. Healthy SF-EVs (green triangle), mild OA SF-EVs (orange cross), and severe OA SF-EVs (Sev. OA; red circle). (B) Unsupervised multivariate sPLS2 arrow plot from the integration of proteomic and lipidomic data. The base of the arrow shows where a specific sample is in relation to the components of the proteomics dataset, and the tip of the arrow shows where the same sample is located concerning the components of the phospholipidomics dataset. Healthy SF-EVs (green circle), mild OA SF-EVs (orange circle), and severe OA SF-EVs (Sev. OA; red circle). The boxes zoom in on certain samples to better show the arrow direction. (C) Clustered Image Map from the sPLS2 data integration performed on the SF-EV omic datasets. The graphic shows the degree of similarity between the proteomic and lipidomic variables clustered over two dimensions and grouped using the Euclidean distance approach.

**Figure 7.6. Network representation derived from the sparsity in partial least squares regression models analysis of the proteomics and lipidomics integrated data.** A relevance network plot with a correlation cutoff of 0.7 was created. Hence, only the variables with a correlation above 0.7 or below -0.7 are shown. The networks are bipartite, and each edge connects a protein (rectangle) to a phospholipid (circle) node based on a similarity matrix. The colour of the connecting lines represents positive (red) or negative (green) correlations.

**Figure 7.7. Discovery of potential composite biomarkers for osteoarthritis.** Phospholipids and proteins were normalised by the sum of the total amount of material (i.e., lipid or protein). Healthy (green), mild OA (orange) and severe OA (red). \*  $p < 0.05$ , Kruskal-Wallis with Dunn's post hoc test A) Phospholipids and proteins that decreased with OA severity, B) phospholipids and proteins that increased with OA severity.

**Figure 8.1. Reverse transcription-quantitative polymerase chain reaction analysis of equine tenocytes (n=3) cytokine stimulation.** Control has no cytokine added; IL-1 had interleukin-1 $\beta$  added), IL-1+TNF- $\alpha$  had interleukin-1 $\beta$  and TNF- $\alpha$ ; and IL-1+TGF had interleukin-1 $\beta$  and TGF-



$\beta$  added (n=3). Error bars are +/- standard deviation of the mean. (A) MMP3 gene expression following treatment with different cytokine combinations. Significant differences were found (Kruskal-Wallis:  $p=0.0118$ ) between control vs IL-1. ( $p=0.0315$ ), control vs IL-1 with TNF- $\alpha$  ( $p=0.0415$ ), IL-1 vs IL-1 with TGF- $\beta$  ( $p=0.0415$ ). (B) MMP13 gene expression following treatment with different cytokine combinations. No significant differences were found. (C) COL1A1 gene expression following treatment with different cytokine combinations. Significant differences were found (ANOVA=  $p=0.0170$ ), between control vs IL-1 ( $q=0.0239$ ) and control vs IL-1 with TNF- $\alpha$  ( $q=0.0262$ ). (D) COL1A2 gene expression following treatment with different cytokine combinations. No significant differences were found following Kruskal Wallis test. Across all box plots standard deviation of the mean error bars are shown and significance was denoted by \* = ( $p<0.05$ ), \*\* = ( $p<0.01$ ), \*\*\* = ( $p<0.001$ ).

**Figure 8.2. Gene expression using analysis of equine tenocytes (n=3) following cytokine stimulation, and varying platelet-rich plasma derived extracellular vesicle concentration treatments.** Control was no cytokine added; IL-1+ TNF $\alpha$  had interleukin-1 and TNF- $\alpha$ ; and both 50 $\mu$ l and 100  $\mu$ l PRP-EV treatments were added to stimulated equine tenocytes. Data was analysed using a one-way ANOVA with multiple comparisons and a post hoc Tukey test, boxplots show standard deviation of the mean error bars. (A) MMP3 gene expression was found to significantly different between control and IL+TNF ( $p=0.0298$ ). (B) MMP13 gene expression was found to significantly change with respect to control compared to 50  $\mu$ l PRP-EV treatment ( $p=0.021$ ), control compared to 100  $\mu$ l PRP-EV treatment  $p=0.0071$ ), and IL1+TNF $\alpha$  compared to 100  $\mu$ l PRP-EV treatment ( $p=0.0375$ ). (C) COL1A1 gene expression was found to significantly vary between control and IL1+TNF ( $p=0.0016$ ), control compared to 50  $\mu$ l PRP-EV treatment ( $p=0.0017$ ) and control compared to 100  $\mu$ l PRP-EV treatment ( $p=0.0013$ ). (D) COL1A2 gene expression was found to change between control and IL1 + TNF $\alpha$  ( $p=0.0017$ ), control and 50  $\mu$ l PRP-EV treatment ( $p=0.014$ ), and control compared with 100  $\mu$ l PRP-EV treatment ( $p=0.0028$ ). Across all box plots significance was denoted by \* = ( $p<0.05$ ), \*\* = ( $p<0.01$ ), \*\*\* = ( $p<0.001$ ).

**Figure 8.3. Platelet-rich plasma characterisation.** (A) The platelet count (K/u) per anonymised equine donor, from whole blood, plasma and platelet-rich plasma (PRP). (B) The mean (n=3) platelet count in plasma and PRP with standard deviation shown.

**Figure 8.4. Exoview of platelet-rich plasma derived extracellular vesicles.** (A) Particle concentration (particles/ml) per EV surface marker for PRP-EVs, with MIgG acting as a negative control, B) Mean average EV size per tetraspanin surface marker for PRP-EVs. Error bars are +/- standard deviation. (C) Visualization of PRP- EVs using Exoview Tetraspanin Assay. A fluorescent image of a representative spots (technical replicates) is shown with colour denoting surface tetraspanin positive identification blue-CD9, and green-CD81). (blue-CD9, and green-CD81). Significance denoted by \* ( $p<0.05$ ), \*\* ( $p<0.01$ ), \*\*\* ( $p<0.001$ ), \*\*\*\* ( $p<0.0001$ ), following Shapiro Wilks normality testing and one-way ANOVA with multiple comparisons, followed by a post hoc Tukey test undertaken in GraphPad Prism.

**Figure 8.5. Proteins identified and quantified between platelet-rich plasma and platelet-rich plasma derived extracellular vesicles with matched plasma samples.** (A) Venn diagram, (B) PCA of the proteome of plasma-EVs and PRP-EVs (n=3) following Pareto scaling, (C) PCA of the proteome of plasma and PRP (n=3), 95% confidence limit regions shown.

**Figure 8.6. A network showing activated upstream regulator nuclear factor erythroid 2-related factor 2, and associated proto-oncogene MyC, nuclear respiratory factor 1 and O-GlcNAc transferase, identified as enriched in platelet-rich plasma compared to plasma made in**

**Ingenuity Pathway Analysis.** This is a graphical representation between molecules identified in our data. Green nodes; reflect decreased measurement and red nodes; highlight increased measurement within the dataset. Intensity of colour is related to higher fold change. Key to the main features in the networks is shown.

**Figure 8.7. A network showing activated upstream regulators, with the highest z score, identified as enriched in platelet-rich plasma derived extracellular vesicles compared to plasma derived extracellular vesicles.** This is a graphical representation between molecules identified in our data. Green nodes; reflect decreased measurement and red nodes; highlight increased measurement within the dataset. Intensity of colour is related to higher fold change. Key to the main features in the networks is shown.

**Figure 8.8. Gene expression analysis of control and cytokine stimulated equine tenocytes following platelet-rich plasma and platelet-rich plasma derived extracellular vesicle treatments.** A) IGFBP6, B) COL1A2, C) MMP13, D)MMP3 using RT-qPCR and relative quantification methods ( $2^{-\Delta\Delta CT}$ ). Significance is denoted by an adjusted p value \* ( $q < 0.05$ ), \*\* ( $q < 0.01$ ), \*\*\* ( $q < 0.001$ ), \*\*\*\* ( $q < 0.0001$ ), following two-way ANOVA analysis and multiple comparison testing. (A)COL1A2, (B) IGFBP6, (C) MMP3 and (D) MMP13.

**Figure 8.9. Unsupervised multivariate analysis using principal component analysis.** Red denotes cytokine treatment and green denotes control, a triangle symbolises no treatment, a cross represents samples treated with PRP and a circle represents PRP-EV treatment. 95% confidence limit are also shown in PCA plots.

**Figure 8.10. Differential abundant proteins following cytokine stimulation of equine tenocytes and the effect of no treatment, platelet-rich plasma and platelet-rich plasma derived extracellular vesicle treatment.** As identified by a two-way ANOVA and post hoc tukey test A) AHNAK nucleoprotein, (B) SAP domain containing ribonucleoprotein, (C) sequestosome 1, (D) translocon associated protein subunit alpha, (E) heme oxygenase and (F) collagen type 1 alpha 1. Significance is denoted by \* ( $p < 0.05$ ), \*\* ( $p < 0.01$ ), \*\*\* ( $p < 0.001$ ), \*\*\*\* ( $p < 0.0001$ ).

**Figure 9.1. An overview of this PhD thesis.** The primary research themes, and subsequent main findings across all results chapters.

**Supplementary Figure 10.1. Clustering of experimental variables and confounding variables as drivers for explained variance for respective principal components before and after appropriate batch correction.** Proteomic data was normalised and log2 transformed, with (A) showing the variables driving separation prior to batch correction, namely horse. (B) Following batch correction using ComBat it can be observed that group\_day, and group are the drivers of variation in the proteomic dataset.

**Supplementary Figure 10.2. Differentially abundant proteins mapped to one of the three most significant functional enrichment pathway.** Graphs demonstrating the results of significant ( $p \leq 0.05$ ) proteins identified after a linear mixed model was applied to the experimental cohort, comparing protein expression between experimental group (treatment OA+MSCs (treatment) and control over time (day 21, 28, 35 and 70), visualizing the expression change longitudinally. Pairwise comparisons were conducted post linear mixed model application to compare control and OA +MSCs protein expression per time point. Significance level, as determined by the generated FDR corrected P Value is shown using ( $p < 0.05$ , \*;  $p < 0.01$  \*\*:  $p < 0.001$ , \*\*\*,  $p < 0.0001$ , \*\*\*\*).

**Supplementary Figure 10.3. Composition of individual lipid species in phosphatidic acid, phosphatidylinositol, ester-linked phosphatidylcholine, ether-linked phosphatidylcholine, ester-linked phosphatidylethanolamine, ether-linked phosphatidylethanolamine, phosphatidylserine, and sphingomyelin classes.** Lipid composition of the most abundant lipid classes of SF-EVs from healthy, mild OA, or severe OA horse patients. The left stacked bars graph in each class shows the lipid species' amount in the overall lipidome. The immediately right stacked bars graph displays the normalised amount of lipid species in each class. Samples were normalised for each class and SF-EV group by expressing the lipid intensity as a fraction of the sum of lipid intensities. Lipids were obtained from 100,000g purified SF-EVs with sucrose density gradients. Healthy samples (n=6), mild OA (n=4), severe OA (n=3).

**Supplementary Figure 10.4. Normalisation of proteomics and lipidomics data for integrated analysis.** Healthy SF-EVs (green triangle, n=6), mild OA SF-EVs (orange cross, n=4), and severe OA SF-EVs (Sev. OA; red circle, n=3). Samples of both datasets were normalised by the sum. A-B) Principal component analysis (PCA) of the proteomics (A) and lipidomics (B) SF-EV datasets. C-D) Unsupervised multivariate Sparse Partial Least Squares regression (sPLS2) of the SF-EV samples in X-variate (for proteomics (C)) and Y-variate (for lipidomics (C)) components projected into the space spanned to the respective dataset.

**Supplementary Figure 10.5. Differential abundant proteins following cytokine stimulation of equine tenocytes and the effect of no treatment, platelet-rich plasma and platelet-rich plasma derived extracellular vesicle treatment.** As identified by a two-way ANOVA and post hoc Tukey test. A) Adenylate kinase 2, mitochondrial, (B) beta galactosidase, (C) centrosomal protein of 162 kDa, (D) D3- phosphoglycerate dehydrogenase, (E) f-actin capping protein subunit alpha (F) heterogenous nuclear ribonucleoprotein U like 1, (G) LRP chaperone MESD, (H) polyadenylate – binding protein, (I) protein disulphide - isomerase, (J) small monomeric GTPase, (K) Sulphide quinone oxidoreductase and (L) THADA armadillo repeat containing .Significance is denoted by \*(p<0.05), \*\* (p<0.01), \*\*\* (p< 0.001), \*\*\*\* (p<0.0001).

**Figure A.11.1. A visual summary of some the prevention modalities used in an attempt to maintain equine distal forelimb functionality.** Created with BioRender.com.

## List of Abbreviations

<b>ACD-A</b>	<i>Acid citrate dextrose- A</i>
<b>ACS</b>	<i>Autologous conditioned serum</i>
<b>ADAM</b>	<i>A disintegrin and metalloproteinase</i>
<b>ALIX</b>	<i>ALG-2-interacting protein X</i>
<b>ANOVA</b>	<i>Analysis of variance</i>
<b>ARF1</b>	<i>ADP-ribosylation factor 1</i>
<b>ARRIVE</b>	<i>Animal Research: Reporting of In Vivo Experiments</i>
<b>BMC</b>	<i>Bone marrow cells</i>
<b>C5</b>	<i>Complement 5</i>
<b>CCL7</b>	<i>C-C Motif Chemokine Ligand 7</i>
<b>CD</b>	<i>Cluster of differentiation</i>
<b>CDET</b>	<i>Common digital extensor tendon</i>
<b>CID</b>	<i>Collision induced disassociation</i>
<b>CILP-1</b>	<i>Cartilage intermediate layer protein 1</i>
<b>CIM</b>	<i>Cluster image map</i>
<b>COL</b>	<i>Collagen</i>
<b>COMP</b>	<i>Cartilage oligomeric matrix protein</i>
<b>COX</b>	<i>Cyclooxygenase</i>
<b>CXCL</b>	<i>Chemokine (C-X-C motif) ligand</i>
<b>DDA</b>	<i>Data dependent acquisition</i>
<b>DE</b>	<i>Differentially expressed</i>
<b>DEPA</b>	<i>Dose of injected platelets, Efficiency of production, Purity of the PRP, Activation of the PRP</i>
<b>DIA</b>	<i>Data independent acquisition</i>
<b>DNA</b>	<i>Deoxyribose nucleic acid</i>
<b>dUC</b>	<i>Differential ultracentrifugation</i>
<b>ECM</b>	<i>Extracellular matrix</i>
<b>EDTA</b>	<i>Ethylenediaminetetraacetic acid</i>
<b>EGF</b>	<i>Epidermal growth factor</i>
<b>ESCRT</b>	<i>Endosomal sorting complexes required for transport</i>
<b>ESI</b>	<i>Electron spray ionisation</i>
<b>EV</b>	<i>Extracellular vesicle</i>
<b>EV-Foundry</b>	<i>The Extracellular Vesicle Foundry</i>
<b>EVOLVE</b>	<i>Extracellular Vesicle Translation to Clinical Perspectives</i>
<b>FDR</b>	<i>False discovery rate</i>
<b>FGF</b>	<i>Fibroblast growth factor</i>
<b>FXR-RXR</b>	<i>Farnesoid X receptor - retinoid X receptor</i>
<b>GAG</b>	<i>Glycosaminoglycans</i>
<b>GAPDH</b>	<i>Glyceraldehyde-3-phosphate dehydrogenase</i>
<b>GC</b>	<i>Gas chromatography</i>
<b>GTPase</b>	<i>Guanosine-5'-triphosphate</i>
<b>HA</b>	<i>Hyaluronan</i>
<b>HCD</b>	<i>High collision dissociation</i>
<b>Hmgn3</b>	<i>High mobility group nucleosomal binding domain 3</i>
<b>HNFA1</b>	<i>Hepatocyte nuclear factor-1 alpha</i>
<b>HPLC</b>	<i>High performance liquid chromatography</i>
<b>IGFBP6</b>	<i>Insulin like growth factor binding protein 6</i>
<b>iKb</b>	<i>Inhibitor of <math>\kappa</math>B</i>
<b>IL-1<math>\beta</math></b>	<i>Interleukin 1<math>\beta</math></i>
<b>IL20</b>	<i>Interleukin 20</i>
<b>ILV</b>	<i>Intraluminal vesicles</i>
<b>iNOS</b>	<i>Inducible nitric oxide synthase</i>
<b>IR</b>	<i>Infrared</i>

<b>ISCT</b>	<i>International society for cell and gene therapy</i>
<b>ISEV</b>	<i>International society of extracellular vesicles</i>
<b>LOXL</b>	<i>Lysyl oxidase homolog 1</i>
<b>LRP</b>	<i>LDL receptor related protein 1</i>
<b>LXR-RXR</b>	<i>Liver X receptor – retinoid X receptor</i>
<b>LysoPC</b>	<i>Lysophosphatidylcholine</i>
<b>MALDI</b>	<i>Matrix Assisted Laser Desorption/Ionization</i>
<b>MARSPILL</b>	<i>Method, activation RBCs, spin, platelet concentration, image guided, leukocyte concentration, light activation</i>
<b>MCP</b>	<i>Metacarpophalangeal</i>
<b>MHC</b>	<i>Major histocompatibility complex</i>
<b>MIFlowCyt-EV</b>	<i>Minimum Information about a FC experiment</i>
<b>MISEV</b>	<i>Minimal information for studies on extracellular vesicles</i>
<b>MMP</b>	<i>Matrix metalloproteinases</i>
<b>MRI</b>	<i>Magnetic resonance imaging</i>
<b>MS</b>	<i>Mass spectrometry</i>
<b>MSC</b>	<i>Mesenchymal stem cell</i>
<b>MyC</b>	<i>MyC proto-oncogene</i>
<b>NFE2L2</b>	<i>Nuclear factor erythroid 2-related factor 2</i>
<b>NF-κB</b>	<i>Nuclear factor-κB</i>
<b>NRF1</b>	<i>Nuclear respiratory factor 1</i>
<b>NTA</b>	<i>Nanoparticle tracking analysis</i>
<b>OA</b>	<i>Osteoarthritis</i>
<b>OC</b>	<i>Osteochondrosis s</i>
<b>OGT</b>	<i>O-linked N-acetylglucosamine transferase</i>
<b>OPTIR</b>	<i>Optical photothermal infrared spectroscopy</i>
<b>PA</b>	<i>Phosphatidic acid</i>
<b>PAW</b>	<i>Platelets, activation, white blood cells</i>
<b>PC</b>	<i>Phosphatidylcholine</i>
<b>PCA</b>	<i>Principal component analysis s</i>
<b>PE</b>	<i>Phosphatidylethanolamine</i>
<b>PEG</b>	<i>Polyethylene glycol</i>
<b>PE-O</b>	<i>Ether-linked phosphatidyl-ethanolamine</i>
<b>PG</b>	<i>Proteoglycans</i>
<b>PGE2</b>	<i>Prostaglandin E2</i>
<b>PGF</b>	<i>Platelet growth factor</i>
<b>PI</b>	<i>Phosphatidylinositol</i>
<b>PkH</b>	<i>Paul Karl Horan</i>
<b>PLS-DA</b>	<i>Partial least squares- discriminant analysis</i>
<b>PMF</b>	<i>Peptide mass fingerprinting</i>
<b>PPD</b>	<i>ε-polylysine-polyethylene-distearyl phosphatidylethanolamine</i>
<b>PRP</b>	<i>Platelet-rich plasma</i>
<b>PS</b>	<i>Phosphatidylserine</i>
<b>PTM</b>	<i>Post translational modifications</i>
<b>QCL</b>	<i>Quantum cascade laser</i>
<b>RA</b>	<i>Rheumatoid Arthritis</i>
<b>RAC1</b>	<i>Ras-related C3 botulinum toxin substrate 1</i>
<b>RhoA</b>	<i>Rhas homolog family member A</i>
<b>RNA</b>	<i>Ribose nucleic acid</i>
<b>ROS</b>	<i>Reactive oxygen species</i>
<b>RS</b>	<i>Raman spectroscopy</i>
<b>SDFT</b>	<i>Superficial digital flexor tendon</i>
<b>SEC</b>	<i>Size exclusion chromatography</i>
<b>SF</b>	<i>Synovial fluid</i>
<b>SM</b>	<i>Sphingomyelin</i>
<b>SNARE</b>	<i>Soluble N-ethylmaleimide-sensitive factor-attachment protein (SNAP) receptor</i>
<b>sPLS2</b>	<i>Sparse multivariate partial least squares</i>

<b>STAT3</b>	<i>Signal transducers and activators of transcription 3</i>
<b>SWATH</b>	<i>Sequential window acquisition of all theoretical fragment ion spectra mass spectrometry</i>
<b>TEM</b>	<i>Transmission electron microscopy</i>
<b>TGF-<math>\beta</math></b>	<i>Transforming growth factor <math>\beta</math></i>
<b>TIMP</b>	<i>Tissue inhibitors of metalloproteinases</i>
<b>TNF-<math>\alpha</math></b>	<i>Tumour necrosis factor <math>\alpha</math></i>
<b>TOF</b>	<i>Time of flight</i>
<b>TSP-1</b>	<i>Thrombospondin 1</i>
<b>VCAM1</b>	<i>Vascular cell adhesion molecule 1</i>
<b>VEGF</b>	<i>Vascular endothelial growth factor</i>
<b>VSP4</b>	<i>Vacuolar protein sorting-associated protein 4A</i>

# 1. Thesis Abstract

Horses are used in a variety of disciplines, including dressage, show jumping, eventing and racing. Thus, the equine athlete is predisposed to the development of musculoskeletal injury. Both equine osteoarthritis and tendon injury are significant causes of pain, lameness and are equine welfare concerns. Osteoarthritis and tendon injuries are usually diagnosed at late stage and treatment includes biological therapies, such as mesenchymal stem cell and platelet-rich plasma therapy. These therapeutics often produce variable clinical outcomes and their mechanistic action is not well characterised. It is hypothesised that extracellular vesicles may be involved in mediating the effect of biological therapies, and could offer a viable cell-free alternative therapeutic. The aims of this thesis were as follows; (1) To investigate extracellular vesicle structure and protein cargo from a longitudinal *in vivo* model of equine osteoarthritis treated with mesenchymal stem cells, in order to determine disease-associated extracellular vesicle cargo, and their potential role in mediating mesenchymal stem cell therapy. (2) Explore the differences in composition of extracellular vesicles from healthy horses and those with clinically diagnosed osteoarthritis using both spectroscopic and spectrometric techniques. (3) Explore the composition of platelet-rich plasma and platelet-rich plasma derived extracellular vesicles using mass spectrometry proteomics. (4) Investigate the effect of platelet-rich plasma and platelet-rich plasma derived extracellular vesicles in an *in vitro* model of equine tendon injury, using mass spectrometry proteomics and gene expression analysis.

Extracellular vesicles were characterised and a range of spectroscopic and spectrometric techniques used including mass spectrometry. This thesis has catalogued extracellular vesicle cargo from synovial fluid in both an *in vivo* models of equine osteoarthritis (carpal osteochondral fragment model) and naturally occurring disease. As some protein content can be attributed to disease progression they could serve as potential biomarkers used in the development of diagnostic tests to aid earlier diagnosis and intervention in osteoarthritis. Further to this, my work has identified altered cargo in association with extracellular vesicles following mesenchymal stem cell treatment, and cellular cargo following platelet-rich plasma derived extracellular vesicle treatment, emphasising their role as mediators of therapy and their capacity to serve as future therapeutics. Therefore, they might be considered as a viable therapeutic alternative that warrants further investigation in the case of mesenchymal stem cell therapy, in order to deliver a safer more reproducible therapeutic. With respect to platelet-rich plasma, extracellular vesicles should be considered when optimising the composition of platelet-rich plasma for more efficacious outcomes, or considered as an alternative to platelet rich plasma.

## 2. Introduction

### 2.1. Equine Musculoskeletal Injury

Equines are used in a variety of disciplines, such as dressage, show jumping, eventing and racing. The equine athlete is predisposed to the development of musculoskeletal injury. Injury can be career limiting and present as a significant equine welfare concern. Poor performance can be the result of pain and the onset of lameness; however, riders and trainers are often unwilling to recognise behavioural changes as a manifestation of impaired welfare. The most common reported injuries in eventing include lacerations, neck trauma and fractures (Murray *et al.*, 2004). In addition, horse size and conformation is also known to affect the likelihood of injury (Dyson, 2017). For example, in racehorses, such as quarter horses, increased length of humerus was associated with osteochondral fractures of the proximal phalanx and synovitis/capsulitis in both carpal joints (McIlwraith, Anderson and Sanschi, 2003). Leg length increased the odds of sustaining osteochondral fracture in the carpus, implying that longer legs could predispose to an increased incidence of fracture. Increased length of toe enhanced the odds of sustaining a carpal chip fragment. As shoulder angle increased, the odds of an osteochondral fracture of the carpus increased (McIlwraith, Anderson and Sanschi, 2003). In addition, a study in 2016 found that in 126 elite show jumpers, 55% and 22% of days lost to training for medical reasons were owing to non- acute and acute orthopaedic injuries respectively (van Weeren and Back, 2016a).

### 2.2. Equine Musculoskeletal Limb Anatomy

The forelimb incorporates the carpus, a compound joint, composed of three articulations; the antebrachio-carpal joint; the middle carpal joint, and the carpometacarpal joint, commonly referred to as the carpal joint (Bertone, 2002). Soft tissue components include intercarpal ligaments, collateral ligaments, a fibrous joint, and the palmar carpal ligament. The metacarpophalangeal joint is comprised of four bones; the third metacarpal bone, the proximal phalanx, and the paired proximal sesamoid bones (Bastiani *et al.*, 2014). As the carpal and metacarpophalangeal regions are imperative for equine locomotion, they can be highly susceptible to injury and disease, most notably tendinopathies and osteoarthritis, specifically traumatic and degenerative. Previously, the metacarpal condyles have been extensively explored as a common site of overload arthropathy in racehorses. A study of note includes that of Olive *et al* (Olive *et al.*, 2017), whereby a retrospective cross sectional study compared magnetic resonance findings in the metacarpophalangeal joint of standardbreds and thoroughbreds. It was found that thoroughbreds developed a much higher rate of stress fractures compared to standardbreds (40.3%).



In addition, standardbreds were found to have more sites of subchondral bone defect and resorption, as well as higher synovitis and joint capsule thickening scores. Moreover, fatigue in horses, particularly those that are extensively active, can affect the kinematics of the metacarpophalangeal joint, with locomotor efficiency often impaired. This resulted in the propensity for injury to be exacerbated, and the equine athlete unable to maintain consistent levels of activity (Pugliese *et al.*, 2020). The current preventative measures used in equine practice to maintain distal forelimb functionality has been discussed previously, and can be found in section A.11.1. The hindlimb of the horse includes the stifle joint and incorporates the patella with parapatellar fibrocartilage, and medial, intermediate and lateral patellar ligaments. The quadriceps femoris muscle inserts into the patella (Schuurman, Kersten and Weijs, 2003; Crook *et al.*, 2008). The hindlimb is also comprised of both the tarsal and metatarsophalangeal joint. The hindlimb can also be susceptible to injury and disease. For example, proximal suspensory desmopathy can be a common cause of lameness in sport horses. It has previously been found that for every degree increase in the tarsal joint angle there was an 11% increase in the likelihood of developing proximal suspensory desmopathy (Routh *et al.*, 2020). In addition, it has been shown that plantar distal phalanx angulation can contribute towards the development of hindlimb lameness in the stifle joint (Clements *et al.*, 2020). The current preventative measures used in equine practice to maintain distal forelimb functionality has been discussed previously, and can be found in section A.11.1.

### 2.2.1. Equine Osteoarthritis

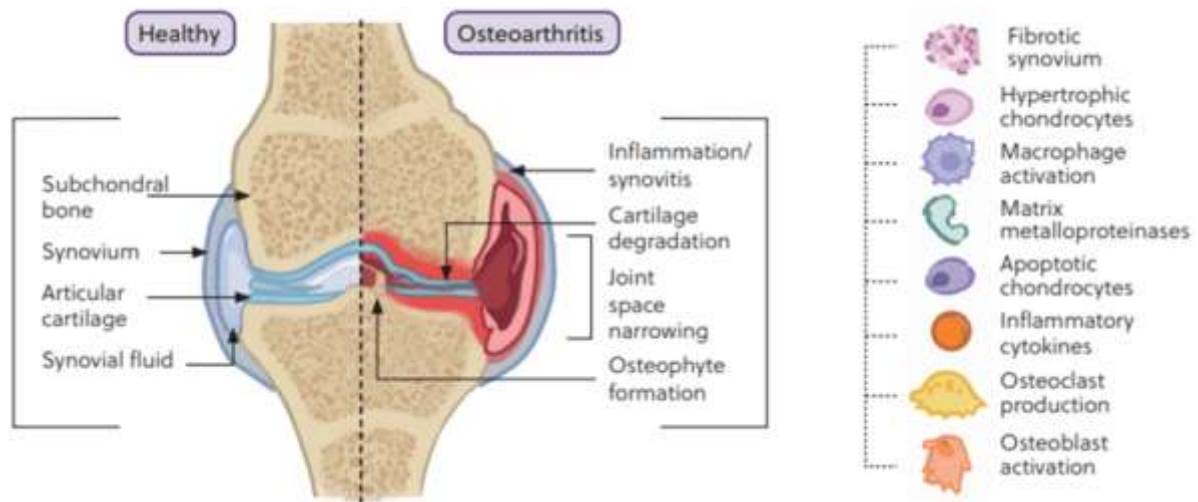
Equine osteoarthritis (OA) is a significant cause of equine pain and lameness, with over 60% of horses reported to develop OA within their lifetime (McIlwraith, Frisbie and Kawcak, 2012a), though its prevalence is thought to be much higher. 80-90% of horses older than 15 years developing such chronic condition (Schlueter and Orth, 2004). It was first reported in 1938 and received clinical interest in 1966 at the American Association of Equine Practitioners, with its relationship with lameness and trauma fundamental to disease understanding. In 1975 it was established that cartilaginous lesions should act as objective criteria for the diagnosis of OA (McIlwraith, Frisbie and Kawcak, 2012b). Today it is understood that OA is a disease of the entire joint, including, subchondral bone, ligaments, synovial membrane and periarticular tissues. OA is recognised as incorporating multiple disorders characterised by a common end stage: the progressive deterioration of articular cartilage accompanied by changes in bone and soft tissue. It is a disease of multifactorial origin, including traumatic injury and idiopathic causes such as ageing. It results in significant pain, reduced mobility and impaired life quality (Jammes *et al.*, 2023). As such it is a leading equine welfare concern.

OA pathophysiology results in synovitis, cartilage degradation, osteophyte formation (Anderson *et al.*, 2023), subchondral bone sclerosis, fibrosis and reduced elastoviscosity of synovial fluid found within the joint capsule, as shown in Figure 2.1 (Clarke, Anderson and Peffers, 2021a). Clinical diagnosis is founded upon radiographic and physical examination as well as reported history, and occurs when cartilage has exceeded its capacity for intrinsic repair (Castanheira *et al.*, 2021). There is a current inability to diagnose the disease at its early stages. In addition, treatment is primarily symptomatic to provide relief, rather than resolve the underlying mechanisms.

Collagen type II composes 90-95% of cartilage, with additional collagens such as type VI, IX, X and XI also present in lower abundance (McIlwraith, 2010). Type II is produced by chondrocytes and forms a collagen framework, producing fibrils that trap proteoglycans (PGs) and hyaluronan (HA). In healthy cartilage PGs are actively turned over. However, in OA PGs, and collagen expression are depleted (Elahi *et al.*, 2023) and HA is reduced resulting in reduced elastoviscosity of synovial fluid, reducing joint lubrication (Costa *et al.*, 2023).

Osteoarthritis is characterised by a range of molecular changes within the joint resulting in the cascade of cartilage destruction and impairment of the microenvironment. These include a reduction of glycosaminoglycans (GAGs) and increased production of catabolic factors within the joint, such as matrix metalloproteinases (MMPs), aggrecanases, prostaglandins, free radicals and cytokines such as Interleukin 1 $\beta$  (IL-1 $\beta$ ) and tumour necrosis factor- $\alpha$  (TNF- $\alpha$ ) (McIlwraith, Frisbie and Kawcak, 2012b). These cytokines have been shown to act on the nuclear factor kappa b (NF $\kappa$ B) pathway; a transcription factor that binds regulatory elements on deoxyribose nucleic acid (DNA) to increase transcriptional activity, and Jun N-terminal Kinase (JNK), a kinase that controls the nuclear and mitochondrial activation of other molecules. Subsequently these intermediates result in the increased expression of other molecules such as MMPs, cyclooxygenase-2 (COX-2) and inducible nitric oxide synthase (iNOS). TNF- $\alpha$  can be found in greater abundance in the synovium, synovial fluid and cartilage of equine OA carpi, and IL-1 $\beta$  expressed in significantly greater amount in cartilage (Kamm, Nixon and Witte, 2010). IL-1 $\beta$  has been referred to as the master cytokine in human OA and this finding is conserved across species (Rivers-Auty *et al.*, 2018; Deng *et al.*, 2021; Watkins *et al.*, 2021). In addition, the increase of such chemokines promotes inflammation resulting in the recruitment of inflammatory cells to bone, connective tissues and cartilage. IL-1 $\beta$  receptors are more concentrated around lesions within OA cartilage, allowing for more binding resulting in the increased production of MMPs and aggrecanases.

These proteins are proteolytic enzymes that target the cartilaginous matrix, resulting in its destruction, and a decrease in cartilage oligomeric matrix protein (COMP) expression and collagen type II; the most abundant collagen found in cartilage.



**Figure 2.1. A diagram of the equine metacarpal phalangeal joint.** Demonstrating molecular changes and structural changes found within an osteoarthritic joint compared to a healthy joint.

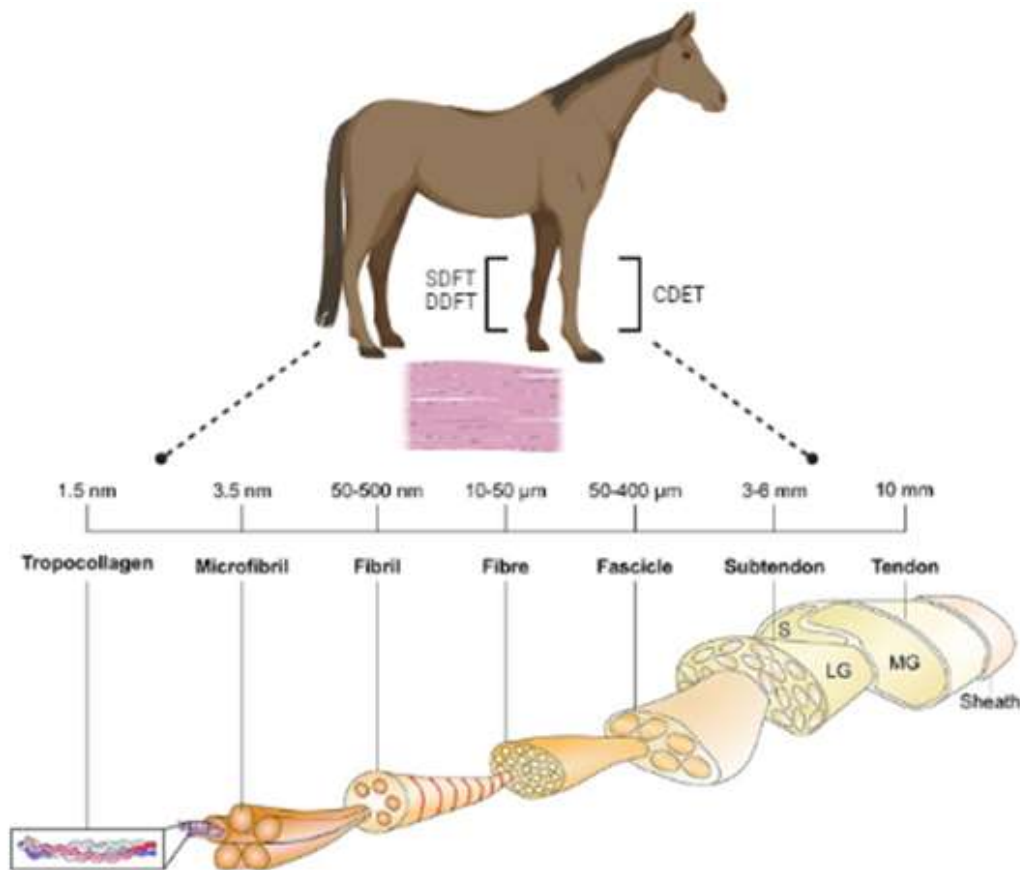
### 2.2.2. Equine Tendon Injury

Tendons are formed of collagenous fascicles (primarily collagen type 1) separated by interfascicular matrix. They enable movement and the retention of energy during equine locomotion. Its structure provides strength and an ability to withstand unidirectional forces. Tendon consists of a dense fibrous extracellular matrix synthesised by tenocytes, tendon specific fibroblasts as shown in Figure 2.2 (Turlo *et al.*, 2018). Tendon also consists of vascular and nerve cells along with Mesenchymal stem cells (MSCs). Proteoglycans (PG) and glycoproteins are the most abundant non-collagenous proteins found in tendon, whereby PGs are thought to regulate fibrillogenesis and organise the extracellular matrix (ECM), contributing to the mechanical properties of tendon.

In addition, cartilage oligomeric matrix protein (COMP) is able to bind to fibrillar collagen and support tendon growth (Thorpe, Clegg and Birch, 2010). Within the tendon, tenocytes synthesise matrix molecules such as collagen as well as proteolytic enzymes that promote degradation and subsequent tendon maintenance, these include MMPs. These MMPs are able to degrade matrix components and are regulated by tissue inhibitors of matrix metalloproteinases (TIMPs) (Thorpe, Clegg and Birch, 2010).

Components of tendon vary based on anatomic location, for example the superficial digital flexor tendon (SDFT) has higher GAG, COMP and water content and increased cellularity compared with the common digital extensor tendon (CDET) (Batson *et al.*, 2003).

As tendons are poorly vascularised the structure is prone to injury and poor healing. The SDFT experiences the most injury compared to the CDET and is analogous to the human Achilles tendon (Smith and McIlwraith, 2021). It has been demonstrated that the SDFT can experience *in vivo* strains of up to 16% during gallop. It has been previously reported that 82% of all injuries to racehorses competing in the national hunt races could be attributed to musculoskeletal injury, with 46% involving tendon or ligament (Thorpe, Clegg and Birch, 2010). Tendon injury can be attributed to both chronic degeneration as a result of micro lesions, or traumatic injury. The healing process for tendons can be divided into three stages: an acute inflammatory phase, proliferative phase, and a remodelling phase. It is hypothesised that in order to maximise healing potential treatment should be administered between inflammatory phases and proliferative phases (Beerts *et al.*, 2017). Tissue that forms typically within these phases are characterised by fibrosis and collagen type III deposition by fibroblasts, producing an inferior structure, and highly regarded as the reason for re-injury (Beerts *et al.*, 2017). During the first phase of healing debridement of damaged materials occurs due to the expression of catabolic and pro-inflammatory genes. During this time platelet derived cytokine signalling results in increased vascular permeability and recruitment of inflammatory cells to the site of injury. Following this, a provisional matrix containing type III collagen is produced by fibroblasts, restoring partial function to the damaged structure and allowing for the migration of cells to the site of injury (O'Brien, Marr and Thorpe, 2021). At this stage there is limited knowledge on the importance of intrinsic and extrinsic cells in the process of healing. However, it is known that chemotactic signalling from a number of important growth factors, including transforming growth factor-  $\beta$  (TGF- $\beta$ ) family, platelet-derived growth factors, insulin-like growth factors and basic fibroblast growth factor stimulate proliferation and migration of fibroblast populations in order to promote healing (Nichols, Best and Loiselle, 2019). During the final stage of healing type III collagen is converted into type I collagen (scar tissue) through granulation, in order for the tendons structure to contract properly as it matures (O'Brien, Marr and Thorpe, 2021). In addition a dramatic decrease in vascularity and cellularity occurs (Nichols, Best and Loiselle, 2019). During this process tendon is prone to the development of peritendinous adhesions and excess scar formation, which further reduce tendon function and lead to chronic complications (Nichols, Best and Loiselle, 2019). However, despite this currently no treatments restore the biomechanical properties of tendon, or enhance the healing process.



**Figure 2.2. A diagram of the equine distal limb.** Illustrating the major tendon structures in the limb and the microstructure and composition of tendon. Superficial digital flexor tendon (SDFT), deep digital flexor tendon (DDFT), common digital extensor tendon (CDET).

## 2.3. Experimental Models of Osteoarthritis

### 2.3.1. *In Vitro*

*In vitro* models are widely used in basic science research to study the pathogenesis of OA in order to identify biomarkers of disease that may serve to improve diagnostics, or to inform the potential of therapeutic interventions. It is most common that 2D monolayer models are used, predominantly involving the use of chondrocytes; the native cell of the articular cartilage, but can also involve the use of synoviocytes, and subchondral bone osteoblasts and osteocytes. However, such models do not consider OA being a disease of the whole joint with multiple tissue involvement. 2D monolayer models often involve the use of primary or immortalised cell lines and have been utilised for the screening of chondroprotective compounds that have been attributed to reducing catabolic factors influencing articular cartilage degeneration. However, the use of such primary lines can be difficult and expensive,

as primary cell sources are limited and have a finite passage time before de-differentiating from their original cellular phenotype due to growing in a planar environment. Subsequently this can result in cellular polarisation altering mechanotransduction and effecting cell to cell signalling (Samvelyan *et al.*, 2020). Alternatively, 3D culture models can be used in the forms of bio fabrication, organotypic, tissue explant, and dynamic culture models (Singh *et al.*, 2021). These provide the opportunity for inter and intra tissue communication compared with 2D monolayer models. However, cellular viability and maintaining tissue volume are disadvantages to their use (Singh *et al.*, 2021). Subsequently, it is necessary to create a robust and reliable *in vitro* model that replicates OA, by involving the various tissues that can become diseased, with the ability to manipulate the microenvironment with respect to mechanical stimulation and cellular interaction. Table 2.1 highlights *in vitro* studies of equine osteoarthritis undertaken between 2018-2023.

**Table 2.1. Overview of original research articles on equine *in vitro* studies.** Specifically, between 2018-2023, identified using PubMed and google scholar. Search terms included 'equine', 'osteoarthritis' and '*in vitro*'.

Author	Journal	Title	Year	Species	Technique	Key Findings
Martins <i>et al</i> (Martins <i>et al.</i> , 2018)	BMC veterinary research	Effects of stanozolol on normal and IL-1 $\beta$ -stimulated equine chondrocytes in vitro	2018	Equine chondrocyte stimulation with IL-1 $\beta$	Gene expression using Real time qPCR	Stanozolol treatment reduced gene expression of MMP-13, MMP-1, IL-6 and COX-2 in both normal and IL-1 $\beta$ treated chondrocytes. Stanozolol
Lofgren <i>et al</i> (Löfgren <i>et al.</i> , 2018)	Research in Veterinary science	Time-dependent changes in gene expression induced in vitro by interleukin-1 $\beta$ in equine articular cartilage	2018	Equine third metacarpal bone cartilage explant stimulated with IL-1 $\beta$	Gene expression using real time qPCR	Cytokines, chemokines, and matrix-degrading enzymes increased in the stimulated explants.
Shakya <i>et al</i> (Shakya <i>et al.</i> , 2020)	Equine Veterinary Journal	Detection of experimental cartilage damage with acoustic emissions technique: An in vitro equine study	2020	Equine metacarpophalangeal joint with mechanical stimulation	Joint acoustic signals	A difference in acoustic emission signal between healthy and damaged joints, and the severity of joint damage.
Haltmayer <i>et al</i> (Haltmayer <i>et al.</i> , 2019)	PLOS ONE	Co-culture of osteochondral explants and synovial membrane as in vitro model for osteoarthritis	2019	Equine osteochondral explant with/without synovial membrane explants, stimulated with IL-1 $\beta$ and TNF $\alpha$	Gene expression using qPCR	Significantly increased expression of MMPs and IL6 compared to their respective control group. In the osteochondral-synovial explant co-culture OA-model the nitric oxide/urea ratio was increased compared to the control group.
Bourdon <i>et al</i> (Bourdon <i>et al.</i> , 2021)	International Journal of Molecular Science	Marine Collagen Hydrolysates Downregulate the Synthesis of Pro-Catabolic and Pro-Inflammatory Markers of Osteoarthritis and Favor Collagen Production and Metabolic Activity in Equine Articular Chondrocyte Organoids	2021	Equine articular chondrocyte organoids with or without BMP-2 and/or IL-1 $\beta$	Gene expression using qPCR	Promerim®40 increased protein synthesis of collagen types I and II, while decreasing transcript levels of proteases such as namely Htra1, and the metalloproteinases Mmp1-3, Adamts5, and Cox2.

*Abbreviations – Matrix metalloproteinase (MMP), cyclooxygenase (COX), Interleukin 1  $\beta$  (IL-1 $\beta$ ), quantitative polymerase chain reaction (qPCR), interleukin 6 (IL6), osteoarthritis (OA), a disintegrin and metalloprotease (ADAM), bone morphogenic protein (BMP), tumour necrosis factor  $\alpha$  (TNF- $\alpha$ ).*

### 2.3.2. *In Vivo*

*In vivo* models are frequently used in translational research in order to quantify long term effects of diseases and subsequent treatments. In addition, with respect to orthopaedic conditions such as osteoarthritis, *in vivo* models are fundamental to understanding the complex disease pathophysiology involving multiple tissues found in the intraarticular joint environment, within a biomechanically functional joint. At least 18 animal models have been developed to study OA, with small animal models including murine, zebrafish, guinea pigs and rabbits (Kuyinu *et al.*, 2016). Large animal models such as canine, porcine, ovine and equine have also been developed and provide an anatomical environment comparable to humans with respect to structure, function, cartilage and subchondral bone morphology, with a shared risk of secondary OA associated with trauma, meniscal tear and osteochondrosis (Teeple *et al.*, 2013; Kuyinu *et al.*, 2016; Hotham and Henson, 2020). Further advantages of large animal models include the prevalence of spontaneous OA, arthroscopic intervention and ability to perform diagnostic imaging such as magnetic resonance imaging (MRI) (Kuyinu *et al.*, 2016). As a result they provide an appropriate model for orthopaedic research with translational capacity (Oláh *et al.*, 2021). The primary disadvantage to large animal models include the cost, time to age, handling, slower OA progression and ethical considerations (Teeple *et al.*, 2013; Kuyinu *et al.*, 2016). Studies involving animals require ethical approval and are tightly regulated by the country in which the study is to be conducted. In the European Union this research is regulated under Directive 2010/63/EU (Macrì *et al.*, 2013). The directive ensures that strategies are implemented to reduce the number of animals used in research while refining techniques to reduce predicted pain, suffering, distress and/or lasting pain whilst also improving animal husbandry.

In large animal models the stifle is most regularly used for research, followed by the metacarpophalangeal (MCP) or middle carpal joints in the horse (Kuyinu *et al.*, 2016). Surgical methods can be used to induce an OA phenotype, and include: joint destabilisation, altered articular contact forces and intra-articular inflammation. Surgical models are often achieved through meniscectomy, anterior cruciate ligament (ACL) transection and osteotomy (Teeple *et al.*, 2013).

Surgical models that have previously been described in the horse include intra-articular injection (Amphotericin, Interleukin-1, and lipopolysaccharide), instability (carpal fracture, cutting collateral & collateral sesamoid and ligaments in metacarpophalangeal joint), osteochondral fragmentation and exercise, trauma (impact on a medial femoral condyle) and disuse (lower limb cast immobilisation) (McIlwraith, Frisbie and Kawcak, 2012a).



Of those surgical models used the carpal osteochondral fragment model is most widely used and validated macroscopically, microscopically and following biochemical profile analysis. It has been found to produce joint effusion, bony lysis, bone proliferation and osteophytosis has also been observed, along with sclerosis, joint capsule thickening and oedema (McIlwraith, Frisbie and Kawcak, 2012a). The model involves creating an 8 mm fragment on the distal dorsal aspect of the radial carpal bone. Subsequently resulting in progressive OA without producing severe lameness. Throughout the time course of studies using this surgical model synovial fluid samples can be collected at regular intervals. In addition, power calculations have indicated that 16 animals are sufficient for a complete *in vivo* study, reducing the number of animals used within research (McIlwraith, Frisbie and Kawcak, 2012a). Table 2.2 demonstrates the recent use of *in vivo* models of equine osteoarthritis.

**Table 2.2. Overview of original research articles on equine *in vivo* studies.** Specifically, between 2018-2023, identified using PubMed and google scholar. Search terms included ‘equine’, ‘osteoarthritis’, ‘*in vivo* models’, ‘surgical’, ‘carpal osteochondral fragment model’, ‘lipopolysaccharide’, ‘synovitis’, ‘amphotericin’, ‘il-1’.

Author	Journal	Title	Year	Species	Technique	Key Findings
Te Moller <i>et al</i> (te Moller <i>et al.</i> , 2021)	Journal of orthopaedic Research	Structural, compositional, and functional effects of blunt and sharp cartilage damage on the joint: A 9-month equine groove model study.	2021	Carpal groove (blunt and sharp) and exercise model	Macroscopic, microscopic, gait analysis and biochemical evaluation	Increase in interleukin-6 expression in synovium from grooved joints and an increased CPII/C2C ratio in synovial fluid extracted from blunt-grooved joints at week. Gait analysis outcome revealed mild, gradually increasing lameness.
Broeckx <i>et al</i> (Broeckx, Pille, <i>et al.</i> , 2019)	American journal of veterinary research	Evaluation of an osteochondral fragment–groove procedure for induction of metacarpophalangeal joint osteoarthritis in horses.	2019	Osteochondral fragment groove model	Radiographic imaging, macroscopic and histologic joint evaluation, biochemical analysis.	synovial fluid interleukin-6, prostaglandin E2, hyaluronic acid, and interleukin-1 receptor antagonist protein concentrations increased surgically induced OA joints. Gross examination of metacarpophalangeal joints revealed synovitis and wear lines.
Thampi <i>et al</i> (Thampi <i>et al.</i> , 2021)	Journal of Orthopaedic Research	Surface Topography as a Tool to Detect Early Changes in a Post-Traumatic Equine Model of Osteoarthritis	2021	Carpal osteochondral fragment model	Surface topography, standard histological grading, and gross evaluation of the joints	Significant differences were observed between OA and non-OA joints for gross evaluation scores. Articular cartilage from the induced OA joint had significantly greater surface topography measurements compared with the sham treatment group.
Peal <i>et al</i> (Peal <i>et al.</i> , 2020)	Journal of Orthopaedic Research	Synovial fluid lubricin and hyaluronan are altered in equine osteochondral fragmentation, cartilage impact injury, and full-thickness cartilage defect models	2020	High-motion joints in horses without clinical signs of joint disease, carpal osteochondral fragmentation, talar cartilage impact injury, and femoral trochlear ridge full-thickness cartilage injury	ELISA and gel electrophoresis	Lubricin concentrations increased post-injury in all osteoarthritis models Sustained loss of Hyaluronic acid was noted post-arthroscopy following carpal osteochondral fragmentation and talar impact injury.
Mohammadi <i>et al</i> (Mohammadi <i>et al.</i> , 2022)	Annals of Biomedical Engineering	Site-and Zone-Dependent Changes in Proteoglycan Content and Biomechanical Properties of Bluntly and Sharply Grooved Equine Articular Cartilage	2022	Carpal groove (blunt and sharp) model	Digital densitometry	Compared to control joints, whole tissue depth PG loss was found in sites adjacent to sharp and, to a larger extent, blunt grooves.

Andersen <i>et al</i> (C. Andersen, Jacobsen, <i>et al.</i> , 2022a)	BMC Research Notes	A detailed macroscopic scoring system for experimental post-traumatic Osteoarthritis in the equine middle carpal joint	2022	Carpal osteochondral fragment model	Macroscopic evaluation	N/A
Reesink <i>et al</i> (Reesink <i>et al.</i> , 2018)	Frontiers in Veterinary Science	Galectins-1 and-3 Increase in Equine Post-traumatic Osteoarthritis	2018	Osteochondral injury	ELISA	Synovial fluid galectin-1 and-3 concentrations increased following experimental carpal osteochondral fragmentation.
Seabaugh <i>et al</i> (Seabaugh <i>et al.</i> , 2022)	Frontiers in Veterinary Science	Examining the Effects of the Oral Supplement Biota orientalis in the Osteochondral Fragment-Exercise Model of Osteoarthritis in the Horse	2022	Carpal osteochondral fragment model	Gait analysis, MRI, serum GAG analysis, macroscopic and histological scoring	BO treated horses with surgical OA significantly decreased synovial fluid prostaglandin E2 concentration and white blood cell counts
McCoy <i>et al</i> (McCoy <i>et al.</i> , 2020)	BMC Genomics	Differential gene expression analysis reveals pathways important in early post-traumatic osteoarthritis in an equine model	2020	Metacarpal joint chip model of PTOA	RNA seq	397 genes were upregulated and 365 downregulated in OA synovium compared to control. There were 17 enriched pathways, involved in ECM turnover, protein metabolism, and growth factor signalling.
Nelson <i>et al</i> (Nelson <i>et al.</i> , 2019)	Osteoarthritis and cartilage	Evaluation of equine articular cartilage degeneration after mechanical impact injury using cationic contrast-enhanced computed tomography	2019	Mechanical impact injury was initiated in equine femoropatellar joints	Cationic agent contrast-enhanced computed tomography,	Cationic CECT attenuation (microCT) of cartilage correlated with GAG, compressive modulus and safranin-O histological score. Cationic CECT (microCT) was found to reflect cartilage properties and enable segregation of subtly degenerated tissue from healthy.
Temple-Wong <i>et al</i> (Temple-Wong <i>et al.</i> , 2020)	American veterinary medical association	Effects of an articular cartilage lubrication with a viscosupplement in vitro and in vivo following osteochondral fractures in horses	2021	Osteochondral fracture model of PTOA	Macroscopic scoring, biochemical analysis, hyaluronic acid molecular weight distribution, and by friction	SF lubrication was altered and hyaluronic acid concentration decreased following surgery.

Abbreviations – Coat protein complex II and collagen 2 degradation protein (CPII/C2C), interleukin 6 (IL6), osteoarthritis (OA), enzyme linked immunosorbent assay (ELISA), proteoglycan (PG), glycosaminoglycans (GAG), magnetic resonance imaging (MRI), ribose nucleic acid sequencing (RNAseq), extracellular matrix (ECM), post-traumatic osteoarthritis (PTOA), synovial fluid (SF).

## 2.4. Experimental Models of Tendon Injury

### 2.4.1. *In Vitro*

Tendon functionally serves to transfer forces from muscle to bone and are fundamental to equine locomotion (Patterson-Kane, Becker and Rich, 2012). However, they are frequently injured and subsequently it is paramount to study the homeostatic mechanisms by which tendon regulate and how this failure results in injury and impaired tissue structure during repair. Various models have been utilised, such as computational models and model *in vitro* systems in order to determine the impact of biochemical factors, inflammatory cytokines and mechanical loading. In addition *in vitro* cell models have been used to assess cyclic strain and growth factors on tenocytes phenotype and function (Theodossiou and Schiele, 2019). It has been identified that a number of growth factors are involved in tenogenic development and regulation, most notably TGF- $\beta$ s. Growth factor upregulation or inhibition can be studied *in vitro* to explore their effect further.

In addition, mechanical factors must be considered when exploring concepts *in vitro*, as mechanical loading has been shown to be a critical factor in tendon development and mechanical factors as fundamental to tenogenesis. As a result, *in vitro* models have been adapted to create bioreactor systems that enable mechanical stimulation with loading enhancing tenogenic markers, collagen production, and mechanical properties of engineered tissues. In addition, alginate gels have been previously used in order to replicate the elastic modulus properties of tendon (Theodossiou and Schiele, 2019). Subsequently, 2-D and 3-D models are appropriate for basic research, but lack many parameters to fully replicate the *in vivo* system and structure. They often fail to incorporate physiological ECM cues and biomechanical cues, effecting the mechanical and metabolic competence of the resulting tissue (Wunderli, Blache and Snedeker, 2020). Tendon explant models can be used instead as they overcome some of these limitations as they retain cell to cell and cell to matrix connections, while providing the ability to control variables such as mechanical loading (Wunderli, Blache and Snedeker, 2020). Table 2.3 outlines *in vitro* tendon studies undertaken between 2018 and 2023 across a range of species and the subsequent findings.

**Table 2.3. Overview of original research articles on equine *in vitro* tendon injury studies.** Specifically, between 2018-2023, identified using PubMed and google scholar. Search terms included ‘equine’, ‘tendon injury’, ‘tendinopathy’, ‘cytokines’, ‘mechanical’.

Author	Journal	Title	Year	Species	Technique	Key Findings
Atkinson <i>et al</i> (Atkinson <i>et al.</i> , 2020)	Journal of Tissue Engineering and regenerative medicine	Cyclical strain improves artificial equine tendon constructs <i>in vitro</i>	2019	Bioreactor- 3D culture of equine tenocytes/ constructs with the application of cyclical strain	Dynamic shear analysis (DSA), dynamic scanning calorimetry (DSC) and Fourier-transform infrared (FTIR) spectroscopy	10% cyclical strain resulted in an increased amount of collagen gel contraction after 7 and 8 days of culture.
Turlo <i>et al</i> (Turlo <i>et al.</i> , 2019)	Cells and biomaterials	Insulin-like growth factor binding protein (IGFBP6) is a cross-species tendon marker	2019	Rat, sheep, human, horse healthy tenocytes	Gene expression	Insulin-like growth factor binding protein 6 (IGFBP6) was identified as a universal tendon marker.
Turlo <i>et al</i> (Turlo <i>et al.</i> , 2018)	BMC technology	Donor age affects proteome composition of tenocyte-derived engineered tendon	2018	Tissue-engineered constructs derived from young and old equine tenocytes	LC-MS/MS	Ageing was associated with altered extracellular matrix composition, and lower cytoskeletal turnover.
Marr <i>et al</i> (Marr <i>et al.</i> , 2023)	Frontiers in Cell and developmental biology	The tendon interfascicular basement membrane provides a vascular niche for CD146+ cell subpopulations	2023	Equine tenocytes	Immunolabelling, flow cytometry	Unique interfascicular cell subpopulation that resides in proximity to a basal lamina which forms extensive, interconnected vascular networks. Isolated CD146+ cells showed limited osteogenesis and adipogenesis.

*Abbreviations – Three dimensional (3D), liquid chromatography tandem mass spectrometry (LC-MS/MS), cluster of differentiation 146 (CD146+).*

#### 2.4.2. *In Vivo*

There are multiple *in vivo* model options for investigating tendon injury for both human and equine purposes as the tendon is prone to injury due to overuse and microdamage (O'Brien, Marr and Thorpe, 2021). The SDFT is analogous to the human Achilles tendon and therefore horses can act as suitable animal models for human Achilles tendon injury (Patterson-Kane, Becker and Rich, 2012). This has served to improve understanding of tendon injury in human and veterinary medicine (Meeremans *et al.*, 2021; Wagner *et al.*, 2021). Previously, in small animal model's treadmill running and artificial muscle stimulation have been employed to induce tendinopathy development. Often these models have been difficult to reproduce, and lesions caused can heal spontaneously when overuse training is discontinued. Further models include the use of collagenase injection in order to cause disruption to tendinous fibres. This model replicates some physiological changes seen in tendinopathy but has been shown to produce inconsistent lesions and stimulate inflammatory responses, involving peritendinous tissues (Cadby *et al.*, 2013), and its applicability to tendinopathy induced by mechanical overload has been questioned (Schramme *et al.*, 2010). Further models have used cytokines, corticosteroids, inflammatory mediators, as well as surgical incision and inclusion of arthroscopic burr (Bosch *et al.*, 2010; Schramme *et al.*, 2010; G. Bosch *et al.*, 2011). Table 2.4 provides an overview of the use of *in vivo* models of equine tendon injury between 2018 and 2023, and the subsequent key findings.

**Table 2.4. Overview of original research articles on equine *in vivo* studies.** Specifically, between 2018-2023, identified using PubMed and google scholar. Search terms included ‘equine’, ‘tendon injury’, ‘*in vivo* models’, ‘surgical’, ‘tendinopathy’, ‘mechanical’.

Author	Journal	Title	Year	Species	Technique	Key Findings
Koch <i>et al</i> (Koch <i>et al.</i> , 2022)	Frontiers in Veterinary Science	Interleukin-1 $\beta$ in tendon injury enhances reparative gene and protein expression in mesenchymal stem cells	2022	Liposome injection	Multiplex assay	Following surgical induction of injury IL-1 $\beta$ and IL-6 had a significantly increased concentration in tendon ultrafiltrate.
Wagner <i>et al</i> (Wagner <i>et al.</i> , 2021)	Veterinary Sciences	Biplanar High-Speed Fluoroscopy of Pony Superficial Digital Flexor Tendon (SDFT)—An In Vivo Pilot Study Franziska	2021	Collagenase injection	Biplanar high-speed fluoroscopic kinematography	Following tendon injury, the mid-metacarpal region contributed less to the overall strain during walk but showed increased contribution during trot.
Gaesser <i>et al</i> (Gaesser <i>et al.</i> , 2021)	Frontiers in Veterinary Science	Evaluation of Autologous Protein Solution Injection for Treatment of Superficial Digital Flexor Tendonitis in an Equine Model	2021	Collagenase injection	Ultrasonography, histology, biomechanical testing and gene expression analysis	Upon APS treatment of tendon injury elastic modulus was higher in APS treated tendon and a reduced expression of COL3A1 in APS treated tendon was observed which may indicate superior healing.

*Abbreviations – Interleukin 1 $\beta$  (IL-1 $\beta$ ), Interleukin 6 (IL6), autologous protein solution (APS), collagen type 3 alpha 1 (COL3 $\alpha$ 1)*

## 2.5. Biological Therapies used in Equine Musculoskeletal Injuries and Disease

### 2.5.1. *Mesenchymal Stem Cell therapy*

Mesenchymal stem cell (MSC) therapy is a popular regenerative therapeutic that can be delivered to an equine patient in both allogenic and autologous form. MSC therapy is often used in the treatment of equine musculoskeletal conditions, with the aim of harnessing the regenerative properties of these cells (Taylor *et al.*, 2007). MSCs are multipotent progenitor cells of mesodermal origin that are often harvested from the sternum for bone marrow derived MSCs (BM-MSCs) or from adipose tissue (Al Naem *et al.*, 2020). Equine MSCs are characterised, as their human counterparts are, based upon the guidance from the International Society for Cell Therapy (Dominici *et al.*, 2006). MSCs are regarded as such if they exhibit plastic adherence, trilineage differentiation (osteogenic, chondrogenic and adipogenic) (Taylor *et al.*, 2007) and expression of surface receptors cluster of differentiation 105 (CD105), cluster of differentiation 90 (CD90), cluster of differentiation (CD73), and inability to express cluster of differentiation 45 (CD45), cluster of differentiation 34 (CD34), cluster of differentiation 14 (CD14) or cluster of differentiation 11b (CD11 b), cluster of differentiation 79a (CD79a) or cluster of differentiation 19 (CD19), and major histocompatibility complex (MHC) II cell surface receptor (HLA-DR) (Dominici *et al.*, 2006; Al Naem *et al.*, 2020; Guest *et al.*, 2022). MSCs exhibit intrinsic properties dependent on tissue source and donor age. This is evidenced by the higher proliferation rate, lower immunogenicity and longer lifespan of perinatal MSCs compared with those sourced from adult donors (Ribitsch, Oreff and Jenner, 2021a). Previously it was hypothesised that MSCs were capable of tissue regeneration through engraftment and differentiation. However, it is now postulated that MSC therapeutic effect can be attributed to the secretion of bioactive factors from such cells (secretome). Consequently, modulating immune response, inflammation, cell death, and induce endogenous repair mechanisms (Ribitsch, Oreff and Jenner, 2021a). However, MSC therapy exhibits variable outcomes in clinical practice, and its use harbours inherent risks- such as uncontrollable proliferation, migration and the induction of patient immune responses. Additionally there are distinct challenges associated with it, such as donor variability, autologous compared to allogenic therapeutic outcomes, the variability observed with MSC tissue source (Voga *et al.*, 2020). Furthermore treatment longevity cannot be guaranteed, with a lack of studies confirming long-term efficacy (Shariatzadeh, Song and Wilson, 2019; Carneiro *et al.*, 2023). As a result, there is a movement towards understanding the secretome and subsequent bioactive factors, such as extracellular vesicles (EVs) in order to develop a safer, reproducible and more efficacious treatment option for both human and veterinary medical fields.



### 2.5.2. Platelet-rich Plasma Therapy

Platelet-rich plasma (PRP) is an autologous orthobiologic used in equine veterinary medicine in order to treat a number of orthopaedic conditions, including OA and tendon injury (Zhou and Wang, 2016). It is a hemoderivative biological therapeutic often administered through intra-articular and intra-tendinous injection (Andia, Atilano and Maffulli, 2021). PRP involves the local administration of bioactive factors, growth factors and platelets, rich in molecules such as vascular endothelial growth factor (VEGF) and platelet growth factor (PGF), known for supporting the three phases of wound healing and repair cascade (Everts *et al.*, 2020). The local release of such growth factors from platelet alpha granules works in tandem with the fibrinolytic system to promote repair and regeneration (dos Santos *et al.*, 2021). There have been multiple *in vitro* and *in vivo* studies demonstrating PRP's anabolic and anti-inflammatory capabilities. However clinical trials often refute this, resulting in variable efficacy (Zhou and Wang, 2016; Everts *et al.*, 2020). This may be attributed to a number of factors, including : donor variability ( sex, age and breed), preparation protocol (commercially available kits or manual centrifugation), PRP activation method used ( thrombin, calcium chloride, and freeze thawing) and recipient tissue variability (Camargo Garbin, Lopez and Carmona, 2021; Wijekoon and de Silva, 2021).

## 2.6. Extracellular Vesicles

### 2.6.1. Overview

EVs are nanoparticles secreted by most mammalian cells enveloped in a phospholipid bilayer membrane without the ability to replicate. First identified as biological entities with enzymatic and functional potential in the 1980s and 1990s (Rowbotham, 1980; Matsuyama, Murakami and Fujita, 1986). Some of the earliest experiments involving EVs were undertaken by Chargaff and West in the 1940s, while studying blood coagulation (Chargaff and West, 1946; Couch *et al.*, 2021). Chargaff and West described coagulant lipoproteins with a high particle weight that were separated from platelets by differential centrifugation, unbeknownst to them this was the first documentation of EVs. Peter Wolf 17 years later identified “material in minute particulate form, sedimentable by high-speed centrifugation and originating from platelets, but distinguishable from intact platelet” and later referred to as ‘platelet dust’ (Wolf, 1967; Couch *et al.*, 2021).

These nanoparticles are involved in intercellular communication, by transporting biological cargo between cells (Cocucci and Meldolesi, 2015; Konoshenko *et al.*, 2018; Battistelli and Falcieri, 2020). This has been defined by the International Society of Extracellular Vesicles (ISEV) within their proposed minimal information for studies involving EVs, in 2014, and updated in 2018 (Théry *et al.*, 2018). EVs can be categorised by size, density and biochemical composition. Broadly, EVs are subdivided into three groups. Exosomes are the smallest of EVs, with a diameter 40 to 120nm. Exosomes are formed as intraluminal vesicles during the assembly of multivesicular bodies. These vesicles are present in most biological fluids and can serve as a source for potential biomarker discovery (Yue *et al.*, 2020). The protein and lipid composition of exosomes reflect cellular origin, with the most common proteins being annexins, tetraspanins (CD63, CD81, CD82, and CD9), as well as heat-shock proteins (Hsp60, Hsp70, and Hsp90) (Battistelli and Falcieri, 2020; Mathieu *et al.*, 2020, 2021). Microvesicles are the second largest form of vesicles, and are formed from the direct budding of the cell membrane, and have a diameter of 100-500nm in size. They carry proteins, nucleic acids, and bioactive lipids of the cell of origin and often express surface markers reflective of the cellular origin. Both EV subtypes have the capacity to induce phenotypical and functional changes, relevant in several physio-pathological conditions (Battistelli and Falcieri, 2020). Lastly, cells undergoing apoptosis are known to secrete apoptotic bodies, that have a diameter of 500nm-2  $\mu$ m. With respect to biomarker discovery, disease pathogenesis, and mediation of biological therapies exosomes and microvesicles are of most relevance.

### 2.6.2. Characterisation

As per MISEV 2018 guidelines EVs must be characterised in order to demonstrate a sample is comprised of EVs, due to their size being comparable to lipoproteins and protein aggregates (Théry *et al.*, 2018; Witwer *et al.*, 2021). It is required that EVs are characterised using global quantification methods, such as protein content particle number, lipid content, or transmembrane /cytosolic proteins. In addition, it is suggested that an assessment of contaminants should be conducted, and the provision of images of EVs using electron microscopy, scanning probe microscopy, super resolution fluorescence microscopy as well as a non-imaged based form of analysing large numbers of EVs. For example: nanoparticle tracking analysis and flow cytometry (Théry *et al.*, 2018).

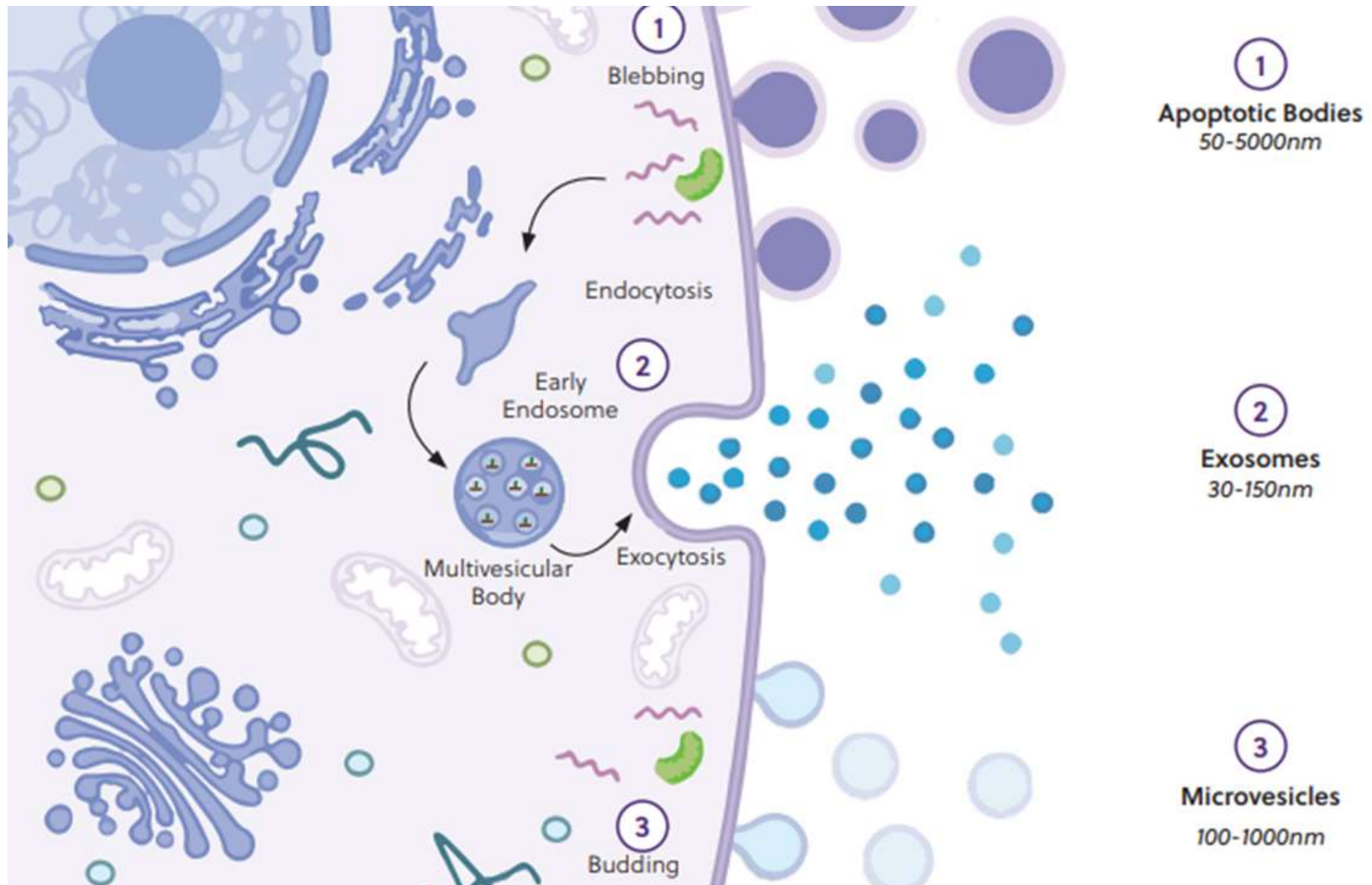
Transmission electron microscopy is a popular form of EV characterisation, and has a resolution of a nanometre. It has the capacity to distinguish EVs from similar sized particles. However, there is a need to improve reproducibility and comparability and eliminate bias in operator image selection (Rikkert *et al.*, 2018). Nanoparticle tracking analysis uses light scattering and the Brownian motion of particles in order to provide rapid sizing and enumeration of vesicles. In addition, the temperature and viscosity of the sample is considered and applied to the Stokes-Einstein equation. Nanoparticle tracking analysis can often be criticised owing to poor reproducibility, due to a number of variables such as: laser wavelength, depth of laser beam, duration of measurements, optical alignment, vibration and operator proficiency (Gardiner *et al.*, 2013).

### 2.6.3. Biogenesis

Exosomes are formed within endosomes and microvesicles from direct budding of the cell membrane. Classically, exosome biogenesis is initiated through the endosomal pathway. This involves the formation of endosomes via the invagination of the plasma membrane. These early endosomes mature, and invagination of the endosomal membrane occurs in order to form lumen and intraluminal vesicles (ILV) (Latifkar *et al.*, 2019; Yue *et al.*, 2020; Gurung *et al.*, 2021). Subsequently resulting in the formation of multivesicular bodies, ultimately fusing with the plasma membrane and releasing the ILVs into the extracellular milieu in the form of exosomes. Alternatively, multivesicular bodies can fuse with lysosomes/autophagosomes to be degraded. These processes are illustrated in Figure 2.3

In order for multivesicular bodies and intraluminal vesicles to form within a cell the formation of endosome sorting complexes required for transport (ESCRT) (Andreu and Yáñez-Mó, 2014; Jackson *et al.*, 2017) are required and comprise of four distinct complexes (ESCRT-0, -I, -II, and -III) and the accessory vacuolar protein sorting 4 (Vps4) complex, with each of them consisting of several subunits (Andreu and Yáñez-Mó, 2014). Within the canonical ESCRT-dependent pathway phosphatidylinositol-3-phosphate (PtdIns3P) recruits the ESCRT-0 complex to early endosomes. Following this HRS (mammalian Master Molecule in Vesicular Transport) recruits clathrin, which induces clustering of HRS to restricted microdomains. Then, ESCRT-0 recruits ESCRT-I to endosomal membranes via direct interaction of HRS with the tumour susceptibility gene 101 (TSG101) subunit of ESCRT-I. ESCRT-I also interacts with the ESCRT-II complex. The function of ESCRT-I and ESCRT-II is thought to be responsible for endosomal membrane invagination. ESCRT-III assembly is initiated by ESCRT-II recruitment. ESCRT-III recruitment is required for intraluminal vesicles (ILV) scission into the multi vesicular body (MVB) lumen. After scission, ESCRT-III is disassociated from the membrane and recycled for additional rounds

of budding. This dissociation process requires interaction with the ATPases associated with diverse cellular activity (AAA-ATPase) and Vps4 (Andreu and Yáñez-Mó, 2014; Teng and Fussenegger, 2021). Alternatively, there are non-canonical ESCRT pathways, and these include the syndecan-syntenin-programmed cell death 6-interacting protein (ALIX) ILV biogenesis pathway. Within this pathway syndecan recruits syntenin and syntenin interacts with ALIX and is modulated by enzymes such as heparinase. Further non-canonical pathways include: ALIX directly binding to protease activated receptor 1, ALIX directly recruiting ESCRT-III and classical non-transmembrane protein tyrosine phosphatase (HD-PTP) recruitment of ESCRT-I through ubiquitin associated protein 1 (Teng and Fussenegger, 2021). Following the formation of the MVB, the MVB is transported to the plasma membrane, involving the cytoskeleton and small GTPases (small (20-kDa to 25-kDa) proteins that bind to guanosine triphosphate). RAB GTPases regulate the intracellular vesicle transport, and involve RAB11, RAB2B, RAB5A, RAB9A, RAB27A, RAB27B and RAB7 (Teng and Fussenegger, 2021). Finally, the MVB fuses with the plasma membrane, and is mediated by soluble NSF attachment protein receptor proteins (SNAREs) (Teng and Fussenegger, 2021). Microvesicle biogenesis is less well characterised. It is suggested that a mechanism of biogenesis involves ESCRT machinery, as previously it has been shown that the knockdown of ESCRT components, such as ALIX reduced hedgehog secretion from EVs (Teng and Fussenegger, 2021). Other potential mechanisms for microvesicle biogenesis that do not include ESCRT machinery include the use of small GTPase proteins such as ADP-ribosylation factor 1 (ARF1), ADP-ribosylation factor 6 (ARF6) and transforming protein RhoA (RhoA) in order to initiate plasma membrane budding (Teng and Fussenegger, 2021).



**Figure 2.3. A diagram illustrating the biogenesis of extracellular vesicles.** (1) the process of blebbing in order to form apoptotic bodies, (2) The process of endocytosis and exocytosis in order to secrete exosomes, (3) the budding of the cell membrane in order to form microvesicles.

#### 2.6.4. *Mesenchymal Stem Cell derived Extracellular Vesicles*

MSCs have been regarded as a poignant source for regenerative therapies, however their use harbours inherent risks, namely: uncontrollable proliferation, migration, and immune response initiation. In addition, the discourse surrounding the mechanistic action of MSCs has altered, in favour of a secretome and extracellular vesicle mediated delivery. MSC-EVs have become a popular area of investigation in the realm of cell free biological therapeutics. MSC-EVs offer a safer alternative to cell based therapeutics, while alleviating the effect of factors such as cell ageing, disadvantageous immune response and inflammation, with the capacity to have bioengineered biological cargo. Hence there is greater control over delivered bioactive materials in order to maximise therapeutic potential (Boulestreau *et al.*, 2020a; Racchetti and Meldolesi, 2021b). MSC-EVs have been shown to modulate immune reactivity, promote angiogenesis, and accelerate cell proliferation and migration through cell signalling pathways (Ni *et al.*, 2020). Specifically in OA they have been shown to promote cartilage repair, inhibit synovitis, and mediate subchondral bone remodelling (Ni *et al.*, 2020). They have many of the same properties as the 'parent' MSC (Zhu *et al.*, 2020), whilst being more stable, adaptable and have a high cellular affinity (Zhu *et al.*, 2020). Their regenerative capacity has been observed in a number of systems including skin, heart, kidney, central and peripheral nerves, as well as musculoskeletal tissues such as cartilage, tendon, ligament and bone (Zhu *et al.*, 2020). Table 2.5 provides an overview of recent original research articles exploring the potential of MSC-EVs across human and veterinary medicine.

**Table 2.5. Overview of original research articles on the use of mesenchymal stem cell derived extracellular vesicles and mesenchymal stem cell based secretome therapeutics.** Specifically, between 2018-2023, identified using PubMed and google scholar. Search terms included ‘equine’, ‘MSCs’, ‘MSC-EVs’, ‘*in vitro*’, ‘*in vivo*’, ‘human’, ‘musculoskeletal’, ‘Extracellular Vesicles’.

Author	Journal	Title	Year	Species	Technique	Key Findings
Cosenza <i>et al</i> (Cosenza <i>et al.</i> , 2017a)	Scientific reports	Mesenchymal stem cells derived exosomes and microparticles protect cartilage and bone from degradation in osteoarthritis	2017	Murine	RT-qPCR and histomorphometric analysis	BM-MSC-derived EVs reinduced expression of chondrocyte markers (type II collagen, aggrecan) and inhibited catabolic (MMP-13, ADAMTS5) and inflammatory (iNOS) markers.
Zhang <i>et al</i> (Zhang <i>et al.</i> , 2018)	Biomaterials	MSC exosomes mediate cartilage repair by enhancing proliferation, attenuating apoptosis and modulating immune reactivity	2018	Rat	RT-qPCR, histology, biochemical assays	exosome-mediated repair of osteo chondral defects was characterised by increased cellular proliferation and infiltration, enhanced matrix synthesis and a regenerative immune phenotype.
Klymiuk <i>et al</i> (Klymiuk <i>et al.</i> , 2019)	BMC Veterinary Research	Exosomes isolation and identification from equine mesenchymal stem cells	2019	Equine	TEM and western blot	Exosomal tetraspanins CD9, CD63 and CD81 were detectable by immunofluorescence staining. EVs detected using TEM. Western blot analysis of CD9 and CD90 presence on surface of exosomes were positive.
Tofino- Vian <i>et al</i> (Tofiño-Vian <i>et al.</i> , 2018)	Cellular Physiology and Biochemistry	Microvesicles from Human Adipose Tissue-Derived Mesenchymal Stem Cells as a New Protective Strategy in Osteoarthritic Chondrocytes	2018	Human	ELISA, RT-qPCR, radioimmunoassay, fluorometry	Microvesicles and exosomes reduced the production of inflammatory mediators such as tumour necrosis factor- $\alpha$ , IL-6, and PGE2. In OA induced chondrocytes. MMP activity was also decreased upon EV treatment of OA chondrocytes
Hotham <i>et al</i> (Hotham <i>et al.</i> , 2021)	Veterinary Record Open	The anti-inflammatory effects of equine bone marrow stem cell-derived extracellular vesicles on autologous chondrocytes	2021	Equine	NTA, TEM, confocal microscopy and RT-qPCR	EVs were incorporated into recipient cells and had an anti-inflammatory effect on stimulated autologous chondrocytes.
Cavallo <i>et al</i> (Cavallo <i>et al.</i> , 2021)	Scientific Reports	Small Extracellular Vesicles from adipose derived stem cells significantly attenuate in vitro the NF- $\kappa$ B dependent inflammatory/catabolic environment of osteoarthritis	2021	Human	RT-qPCR	The inflammatory and catabolic environment was mediated by NF- $\kappa$ B pathway and was found to be significantly attenuated by small EVs derived from adipose stem cells.

Arevalo-Turrubiarte <i>et al</i> (Arévalo-Turrubiarte <i>et al.</i> , 2021)	Equine Veterinary Journal	Extracellular vesicles from equine mesenchymal stem cells decrease inflammation markers in chondrocytes in vitro	2021	Equine	TEM, NTA and RT-qPCR	EVs from bone marrow cells decreased MMP13 expression in stimulated chondrocytes.
Kearney <i>et al</i> (Kearney <i>et al.</i> , 2022)	Frontiers in Veterinary Science	Treatment Effects of Intra-Articular Allogenic Mesenchymal Stem Cell Secretome in an Equine Model of Joint Inflammation.	2022	Equine	Biochemical analysis of SF, clinical parameters such as joint circumference.	MSC secretome significantly reduced joint circumference in phase 1 and increased GAG concentration. In phase 2 no significant difference was observed between MSC secretome treatment and MSC treatment.

*Abbreviations – Reverse transcription quantitative polymerase chain reaction (RT-qPCR), osteoarthritis (OA), nuclear factor kappa b (NF-KB), matrix metalloproteinase (MMP), transmission electron microscopy (TEM), nanoparticle tracking analysis (NTA), inducible nitric oxide synthase (iNOS), a disintegrin and metalloproteinase (ADAM), extracellular vesicles (EVs), synovial fluid (SF), mesenchymal stem cells (MSC).*



### 2.6.5 Osteoarthritis associated Extracellular Vesicles

EVs have been implicated in the pathogenesis of OA and hypothesised to contain biomarkers that may serve as targets for diagnostic tests. All joint tissues and associated structures, including the synovium (synoviocytes), cartilage (chondrocytes) subchondral bone (osteoblasts), and tendon (tenocytes) secrete EVs (Ni *et al.*, 2020). It has been suggested that they regulate joint homeostasis and regeneration in articular tissues (Boere, Malda, Van De Lest, *et al.*, 2018; Herrmann *et al.*, 2021a; Mustonen and Nieminen, 2021a). In OA, it has been postulated and subsequently shown that EVs can propagate disease through the joint by transporting and enhancing the production of inflammatory mediators and cartilage degrading proteinases (Mustonen and Nieminen, 2021a). Table 2.6 provides an overview of original research conducted exploring the role of EVs in OA in recent years in human and horse (2018-2023).

**Table 2.6. Overview of original research articles on extracellular vesicles and osteoarthritis.** Specifically, between 2018-2023, identified using PubMed and google scholar. Search terms included ‘equine’, ‘Human’, ‘Osteoarthritis’, ‘*in vitro*’, ‘*in vivo*’, ‘pathogenesis’, ‘musculoskeletal’, ‘EVs’, ‘Extracellular Vesicles’.

Author	Journal	Title	Year	Species	Technique	Key Findings
Liu <i>et al</i> (Liu, Shortt, <i>et al.</i> , 2020)	Journal of Orthopedic Research	Extracellular Vesicles Released From Articular Chondrocytes Play a Major Role in Cell–Cell Communication	2020	Human	TEM, RT-qPCR, ELISA	EVs isolated from the medium of vehicle-treated chondrocytes inhibited catabolic events and increased expression of aggrecan and type II collagen in IL-1 $\beta$ -treated chondrocytes and stimulated chondrogenesis of C3H10T1/2 cells. EVs from IL-1 $\beta$ -treated chondrocytes inhibited chondrogenesis.
Boere <i>et al</i> (Boere <i>et al.</i> , 2020)	Veterinary Journal	Extracellular vesicles in synovial fluid from juvenile horses: No age-related changes in the quantitative profile	2019	Equine	Flow cytometry, western blotting, biochemical analysis	No difference in EV profile between young and old horses but significant different in biochemical profile.
Ni <i>et al</i> (Ni <i>et al.</i> , 2019)	Nature	The exosome-like vesicles from osteoarthritic chondrocyte enhanced mature IL-1 $\beta$ production of macrophages and aggravated synovitis in osteoarthritis’	2019	Human	NTA, flow imaging, western blot and RT-qPCR	Degraded cartilage produced more EVs than non-degraded. Vesicles from OA chondrocytes increased IL-1 $\beta$ production in macrophages. Resulting in decreased autophagy, promoting the production of mitoROS.
Kolhe <i>et al</i> (Kolhe <i>et al.</i> , 2020)	Life	Sex-Specific Differences in Extracellular Vesicle Protein Cargo in Synovial Fluid of Patients with Osteoarthritis	2020	Human	LC-MS/MS	Haptoglobin, orosomucoid, and ceruloplasmin significantly up-regulated, whereas apolipoprotein down-regulated in female OA EVs. In males, we discovered $\beta$ -2-glycoprotein, and complement component 5 proteins significantly up-regulated and Spt-Ada-Gcn5 acetyltransferase (SAGA)-associated factor 29 down-regulated in male OA EVs.

*Abbreviations – Transmission electron (TEM), reverse transcription quantitative polymerase chain reaction (RT-qPCR), nanoparticle tracking analysis (NTA), extracellular vesicles (EV), osteoarthritis (OA), liquid chromatography tandem mass spectrometry (LC-MS/MS), interleukin 1 $\beta$  ( IL-1 $\beta$ ), enzyme linked immunosorbent assay ( ELISA)*

#### *2.6.6. Extracellular Vesicles derived from Platelets and Platelet-rich Plasma*

Platelets are anucleate cells derived from megakaryocytes that serve as mediators of haemostasis and vascular integrity (Tao, Guo and Zhang, 2017). EVs are readily secreted from the alpha granules upon activation. In addition, EVs derived from platelets have the capacity to cross various tissue barriers, previously inaccessible to platelets (Puhm, Boilard and MacHlus, 2021) and are the most abundant source of EVs in blood. Platelets can synthesise their own molecules, and these can be found in the EVs that are produced. Platelets and subsequent platelet-rich plasma derived EVs have been shown to promote cell proliferation, angiogenesis, enhance osteogenesis and inhibit cell apoptosis (Wu, Piao, *et al.*, 2021). Table 2.7 provides an overview of EVs derived from platelets and PRP, and their potential therapeutically.

**Table 2.7. Overview of original research articles on platelet and platelet-rich plasma derived extracellular vesicles.** Specifically, between 2018-2023, identified using PubMed and google scholar. Search terms included ‘equine’, ‘Human’, ‘Osteoarthritis’, ‘Tendon injury’, ‘*in vivo*’, ‘*In vitro*’, ‘musculoskeletal’, ‘EVs’, ‘Extracellular Vesicles’, ‘PRP’, Platelet derived EVs’ .

Author	Journal	Title	Year	Species	Technique	Key Findings
Ferreira <i>et al</i> (Ferreira <i>et al.</i> , 2020)	Nature	Mode of induction of platelet-derived extracellular vesicles is a critical determinant of their phenotype and function	2021	Human	Flow cytometry and automated thrombography	Agonist stimulation enhanced platelet derived EV release and led to lower negatively-charged phospholipid externalization in platelet derived EVs.
Otahal <i>et al</i> (Otahal <i>et al.</i> , 2021)	International Journal of Molecular Sciences	Effects of Extracellular Vesicles from Blood-Derived Products on Osteoarthritic Chondrocytes within an Inflammation Model	2021	Human	NTA, cryo electron microscopy, western blot, RT-qPCR, ELISA	Gene expression analysis of chondrocytes by RT-qPCR revealed increased type II collagen expression, and cytokine profiling found lower TNF- $\alpha$ and IL-1 $\beta$ levels associated with EV treatment.
Jr <i>et al</i> (Jr <i>et al.</i> , 2021)	Equine veterinary Journal	Effects of endurance racing on horse plasma extracellular particle miRNA	2021	Equine	Electron microscopy, resistive pulse sensing, western blot and RNA seq	MicroRNA differential expression analysis revealed increasing levels of eca-miR-486-5p during and after the race, and decreasing levels of eca-miR-9083 after the end.
Graca <i>et al</i> (Graça <i>et al.</i> , 2022)	International Journal of Molecular Sciences	Therapeutic Effects of Platelet-Derived Extracellular Vesicles in a Bioengineered Tendon Disease Model	2022	Human	RT-qPCR, SEM, NTA, ELISA, LC-MS/MS	Platelet-derived EVs increased the expression of tenogenic markers, promoted ECM remodelling, and the synthesis of anti-inflammatory mediators.
Price <i>et al</i> (Price, Gardiner and Harrison, 2021)	Transfusion	Platelet-enhanced plasma: Characterization of a novel candidate resuscitation fluid's extracellular vesicle content, clotting parameters, and thrombin generation capacity	2021	Human	Capture arrays, thromboelastometry	Platelet enhanced plasma rich in platelet derived EVs may be suitable as a future resuscitation fluid for platelet transfusion.
Liu <i>et al</i> (Liu <i>et al.</i> , 2019)	Journal of Orthopaedic Surgery and Research	Exosomes derived from platelet-rich plasma present a novel potential in alleviating knee osteoarthritis by promoting proliferation and inhibiting apoptosis of chondrocyte via Wnt/ $\beta$ -catenin signaling pathway	2019	Rabbit	ELISA, Assays, western blot	PRP-EVs and PRP both inhibited the release of tumour TNF- $\alpha$ with no statistically significant difference. PRP EVs were significantly better at promoting cellular proliferation, and PRP-EVs in vivo increase chondrocyte count and improved joint phenotype macroscopically according to OARSI scoring system, and performed better than activated PRP.

*Abbreviations – Nanoparticle tracking analysis (NTA), transmission electron microscopy (TEM), reverse transcription quantitative polymerase chain reaction (RT-qPCR), liquid chromatography tandem mass spectrometry (LC-MS/MS), enzyme linked immunosorbent assay (ELISA), ribose nucleic acid sequencing (RNA seq), scanning electron microscopy (SEM), tumour necrosis factor  $\alpha$  (TNF- $\alpha$ ), interleukin 1 $\beta$  (IL-1 $\beta$ ), extracellular matrix (ECM), platelet-rich plasma (PRP).*

## 2.7. Raman and Optical Photothermal Infrared Spectroscopy

Vibrational spectroscopic methods, including Raman and infrared spectroscopies, provide molecular information about the main molecular constituents commonly found in most biological samples such as proteins, lipids, nucleic acids, and carbohydrates based on bond-specific chemical signatures in a non-invasive, non-destructive, and label-free manner (Paraskevasidi *et al.*, 2021). Raman spectroscopy was first developed by the Nobel Laureate Chandrasekhara Venkata Raman and Grigorij Samuilovič Landsberg. In Raman spectroscopy (RS), photons from a monochromatic source interact with the sample and a small fraction of them are inelastically scattered with either higher or lower energies compared with the excitation wavelength. The energy difference between incident and scattered photons corresponds to a Raman shift and it is associated with the chemical structure of molecules in the sample (Lima, Muhamadali and Goodacre, 2021) most photons are scattered elastically and this is known as Rayleigh scatter. Raman spectroscopy can discriminate between different cell and tissue types and detect chemical alterations prior to morphological changes in various pathological states. Raman spectroscopy has previously been used to assess the purity of EV preparations (Gualerzi *et al.*, 2017).

Infrared spectroscopy (IR) is based on the absorption of infrared radiation by molecular vibrations from bonds that possess an electric dipole moment that can change by atomic displacement (Baker *et al.*, 2014). A specific form known as optical photothermal infrared spectroscopy (O-PTIR), often referred to as photothermal IR imaging spectroscopy (PT-IRIS), mid-IR photothermal (MIP), mid-IR photothermal microscopy, and IR photothermal heterodyne imaging (IR-PHI) can be used in order to probe the polar molecular constituents of a sample in a non-destructive manner, with greater spatial resolution than traditional IR while also utilising optical microscopy (Kansiz *et al.*, 2021).

Raman and O-PTIR spectroscopy can be used in tandem. The technique is based on a pump-probe configuration that couples a tuneable infrared quantum cascade laser (QCL) acting as a pump and a visible laser to probe the thermal expansion resulting from the temperature rise induced by the QCL (Gardner *et al.*, 2021). This technique was developed by researchers at the Naval Research Laboratory and other groups (Furstenberg *et al.*, 2012; Kansiz *et al.*, 2021). The principles of Raman spectroscopy and O-PTIR spectroscopy are illustrated in Figure 2.4.

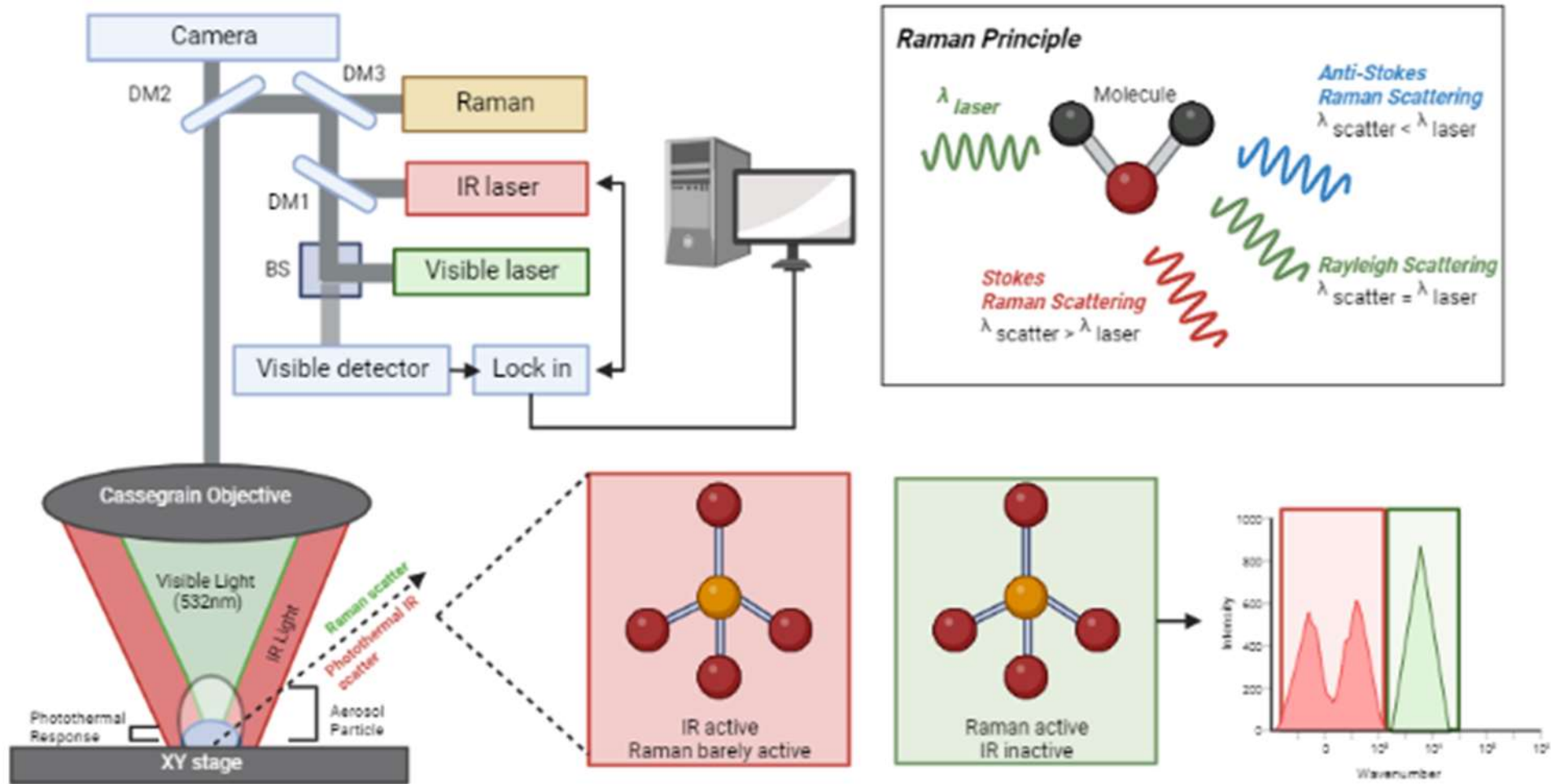


Figure 2.4. A diagram illustrating the scientific principles of optical photothermal infrared spectroscopy and Raman spectroscopy. Highlighting how such spectroscopic techniques can be used simultaneously in order to acquire data on sample metabolic composition.

### 2.7.1 Applications of Raman and Infrared spectroscopy to Osteoarthritis

Spectroscopy based techniques have gained in popularity in the study of OA across species in order to identify disease based biomarkers. In addition, Raman and O-PTIR based spectroscopies have a translation capacity and could be developed in order to be used diagnostically in a 'bed-side' manner, compared with more traditional metabolomics-based methods such as nuclear magnetic resonance (NMR) (de Sousa *et al.*, 2019) and mass spectrometry (MS) (Kim *et al.*, 2022). A previous study conducted by de Souza *et al.* (De Souza *et al.*, 2014) utilised Raman spectroscopy in order to probe molecular changes in collagen deposition and tissue remodelling changes in two surgical models of rat OA (exercise induced and collagenase induced). It identified that the models used were significantly sufficient in inducing OA related changes with respect to tissue remodelling and mineralisation. In addition, significantly lower phenylalanine content and higher crystallinity in the treadmill exercise-induced model of OA than collagenase-induced model of OA was observed (De Souza *et al.*, 2014). Further, studies conducted in human OA patients established that Raman based technologies could be used in order to grade OA patients to improve point of care treatment, with high grade knee OA patients characterised by a decrease in carotenoid associated bands (Bocsa *et al.*, 2019). Moreover, further studies have quantified that specific differences could be resolved from bone composition and inform OA development and progression. Specific differences were quantified using FTIRs and it was identified that mineral and carbonate content varied at different OA stages (Zhai *et al.*, 2019). In addition, the content of acid phosphate, collagen maturity and crystallinity varied with the OA severity. This is suggestive of changes in subchondral bone correlating with cartilage degeneration and subsequently OA (Zhai *et al.*, 2019). Further to this, Afara *et al.* used NIR to spectroscopy to probe the knee of rats with surgically induced OA, identifying that such infrared spectroscopy technique was sensitive to degenerative changes in the joint, distinguishing between mild and advanced OA as determined by gross Mankin score (Afara *et al.*, 2017). AT-FIR has also been used to probe serum samples of clinically diagnosed OA in horses. This enabled 100% discrimination between healthy and OA cohorts and identified changes in peaks associated with proteins and lipids. In OA, it was found that lipid peaks and collagen associated peaks increased, while two peaks decreased and were associated with proteoglycans. Of these a reduction in proteoglycan content was characteristic of OA (Paraskevaidi *et al.*, 2020).

### 2.7.2 Applications of Raman and Infrared Spectroscopy to Extracellular Vesicles

EVs and their associated cargo have also been probed utilising these spectroscopy techniques. Raman spectroscopy has been applied in order to ascertain the purity and function of EV preparations previously, with RS being used in order to assess single vesicles, utilising optical tweezers to conduct single EV fingerprinting (Gualerzi, Kooijmans, *et al.*, 2019). These techniques have been used to explore the cargo of EVs in association with a range of pathologies including Parkinson's disease. This demonstrates its capacity to stratify disease types, highlighting the feasibility and reproducibility of these bio photonic approaches (Gualerzi, Picciolini, *et al.*, 2019). Furthermore, these technologies can be used to visualise biological changes due to their optical component. Recently, MSC-EVs were tracked *in vitro* in 3D models of OA using immunofluorescence and time-lapse coherent anti-Stokes Raman scattering, second harmonic generation and two-photon excited fluorescence. Results showed EV penetration after a few minutes, reaching 30–40  $\mu\text{m}$  depth after 5 hours in both explants and micromasses. This highlighted the techniques ability to monitor EV migration in complex tissues with an ECM, in order to better replicate an *in vivo* environment, compared with standard monolayer culture (Mortati *et al.*, 2020).

### 2.8. Mass Spectrometry Proteomics and Lipidomics

Mass spectrometry (MS) enables the global quantification of a sample proteome or lipidome, sourced from biofluids, media, cells or extracellular vesicles. It is regarded as a high throughput technique that can be utilised in both a targeted and untargeted manner. Techniques have emerged providing the capacity to analyse data on both single proteins and heterogenous complex protein samples, by identifying peptides, protein isoforms and their post translational modifications (PTMs), by using only a microgram ( $\mu\text{g}$ ) of biological material (Rozanova *et al.*, 2021; Neagu *et al.*, 2022). This enables biomarker discovery between conditions, as well as uncovering pathological mechanisms at a phenotypic level.

Proteomic quantification can be divided between label-based quantification methods, whereby a stable isotope label is incorporated into the peptides and proteins, or label-free based quantification methods can be use in which the sample retains native isotope composition (Rozanova *et al.*, 2021). There are two primary forms of MS proteomics – 'top down' or 'bottom up'. In 'top down' proteomics proteins and protein complexes are analysed without prior digestion into peptides. Conversely, in 'bottom up' proteomics ('shotgun') proteolytic peptides (3 to 4 kDa in size) are analysed in a data



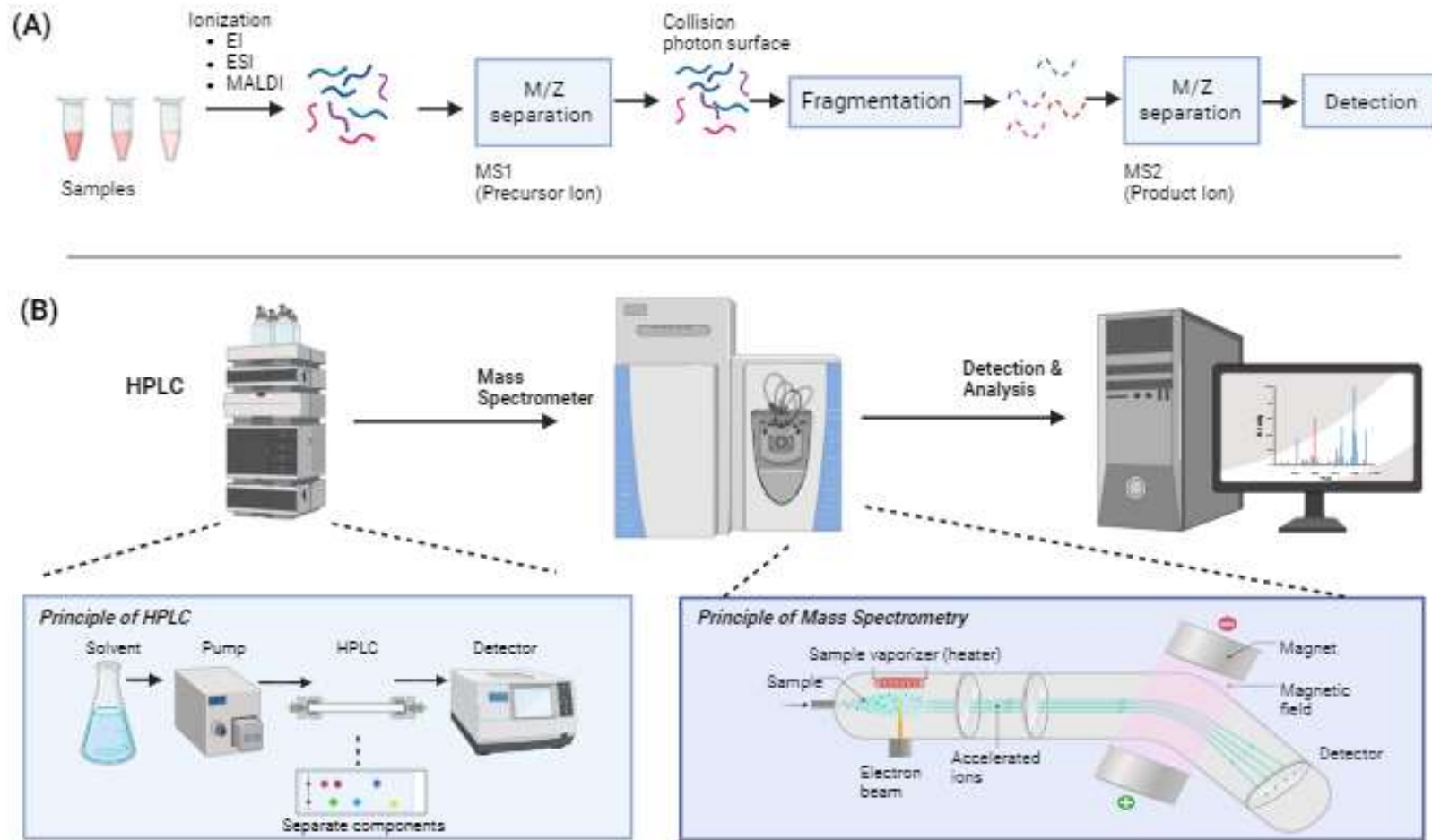
dependant mode (DDA), enabling quantification of a comprehensive proteome (Anjo, Santa and Manadas, 2017; Neagu *et al.*, 2022). Alternatively, data independent acquisition approaches (DIA) can be used in order to improve protein quantification numbers, with higher accuracy and precision (Huang *et al.*, 2015). Sequential window of acquisition of all theoretical mass spectra (SWATH) is a recently developed technique that uses a DIA approach coupled with a peptide spectral library. This DIA based method differs from DDA methods as mass analyser 1 (MS1) and mass analyser 2 (MS2) data is acquired without precursor ion selection within isolation windows in order to generate data across all mass ranges. This overcomes limitations of reproducibility and under sampling often identified when using a DDA approach, that only acquires MS2 data for selected precursor ions (Zhang, Ge, *et al.*, 2020).

MS can also be used in the study of the lipidome. Lipids are heterogenous compounds that contain fatty acyl/alkyl, sphingosine, or isoprene moieties as their hydrophobic components. Such lipids have been classified into eight categories: fatty acyls, glycerolipids, glycerophospholipids, sphingolipids, sterols, prenol lipids, saccharolipids, and polyketides (Züllig, Trötz Müller and Köfeler, 2020). The conventional method use for lipid analysis was gas chromatography MS (GC-MS). This traditional method was time consuming and required large lipid quantities. Now electron spray ionisation (ESI) MS is used, as such 'soft' ionization procedure has simplified lipid analysis by decreasing molecular ion decomposition, allowing for better reproducibility and lower detection limits (Milne *et al.*, 2006).

Fundamentally, MS comprises of the ionization of an analyte (protein or lipid), separation based on their mass to charge ratio ( $m/z$ ) and subsequent detection of these ions. Analytes can be ionized in a number of ways including ESI and matrix assisted laser desorption/ionization (MALDI), atmospheric pressure chemical ionisation source (APCI), atmospheric pressure photo-ionization (APPI) (Pitt, 2009). ESI is often used in tandem with other separation based techniques such as high performance liquid chromatography (HPLC) (Rozanova *et al.*, 2021), as shown in Figure 2.5 . It is known that the sensitivity and resolution of a mass spectrometer is dependent on the form of mass analyser used in order to separate ions. Many are available and include quadrupole, time of flight (ToF) and ion trap analysers such as orbitrap. A quadrupole analyser combines constant and varying radiofrequencies voltages in order to allow for the transmission of a narrow band of  $m/z$  values, by varying the voltage over time a range of  $m/z$  values can be measure resulting in s mass spectrum. Operating at  $<4000$   $m/z$  values, operating at a unit mass resolution with a mass accuracy of  $0.1$   $m/z$  (Pitt, 2009). ToF mass analysers operate by accelerating ions through a high voltage. Subsequently the velocity of ions and the time

taken to travel down a flight tube vary with differing  $m/z$  values. The initial accelerating voltage is often pulsed and detected allowing for the acquisition of mass spectrum (Pitt, 2009). Ion trap analysers use three hyperbolic electrodes to trap ions using static and radio frequency voltages, and ions are sequentially ejected from the trap on the basis of  $m/z$  values in order to produce mass spectrum (Pitt, 2009).

In tandem mass spectrometry (MS/MS) two mass analysers are coupled together, whereby the sample is ionized, and precursor ions are selected by MS1, quantifying the mass to charge ratio ( $m/z$ ). These precursor ions undergo fragmentation that can be conducted by a number of techniques including: collision-induced dissociation (CID), higher-energy collisional dissociation (HCD) and electron transfer dissociation resulting in product ions. These are then sorted by weight and quantified by the second mass analyser (Rozanova *et al.*, 2021), dependent on the type of mass analyser used. The product ions are a pattern of fragments suggestive of the amino acid sequence and subsequent peptide. These peptide fragments are then analysed by a number of methods such as de novo peptide sequencing, peptide mass fingerprinting (PMF) or amino acid sequencing of the peptide, followed by protein database searches. In order to identify the proteins, present within a sample. Identification is conducted by matching the peptide masses quantified with that of theoretical masses from *in silico* digestion on decoy database proteins with the same enzyme used in the experimental digestion (Neagu *et al.*, 2022), the subsequent confidence of correct identification of a protein is then calculated from this. This is illustrated in Figure 2.5.



**Figure 2.5. A diagram illustrating how a mass spectrometer works and the scientific principles that govern how data is acquired from both high-performance liquid chromatography and the use of mass spectrometry. (A) Illustrates tandem mass spectrometry analysis and the subsequent stages prior to data acquisition. (B) Illustrates how high-performance liquid chromatography works, and how it is used in conjunction with a mass spectrometer in order to generate proteomic data.**

### 2.8.1. Application of Proteomics and Lipidomics to the study of Osteoarthritis and Extracellular Vesicles

MS proteomics has been used to explore the underlying molecular mechanisms of OA contributing towards disease pathogenesis, while also characterising the mode of action of a variety of therapeutics. Previously, a study utilising equine MCP joint explants stimulated with IL-1 $\beta$  as a model for OA explored the effect of a non-steroidal anti-inflammatory drug. Upon cytokine stimulation MMP-1, MMP-3 and thrombospondin-1 (TSP-1) expression increased significantly, while cartilage intermediate layer protein (CILP-1) expression decreased (Clutterbuck *et al.*, 2011). In addition, the proteome of septic and non-septic arthropathies in the horse have also be explored, complementing the study by Anderson *et al* (Anderson *et al.*, 2018). Using matched donors, it was found that lactotransferrin was significantly increased in septic joints and insulin like growth factor binding protein 6 (IGFBP6) decreased compared to other diseased groups. Functional enrichment analysis found the downregulation of eukaryotic translation initiation factors and mTOR signalling pathways in both OA and osteochondrosis (OC) (Anderson *et al.*, 2019).

The lipidome of EVs has also been explored using MS lipidomics in order to ascertain the lipid content of vesicles and the physiological function they have. Lipids have been identified in plasma and serum derived EVs. It was identified that following EV isolation using sequential ultracentrifugation. EVs from different fractions following ultracentrifugation were enriched in different lipids. EVs in the highest fraction contained the greatest quantity of lipids, such as phospholipids. The EV pellet contained the lowest concentration of lipid but was enriched in ceramide (Chen, Datta-Chaudhuri, *et al.*, 2019). Synovial fluid derived EVs have also been probed, identifying over 600 lipids and 12 classes, comparing the effect of isolation methods on composition. It was found polyethylene glycol mediated precipitation method (PEG) had the most lipids, but lipoprotein contamination was evident. Whereas lipids from EVs isolated using ultracentrifugation had the highest purity, with the least lipoprotein enriched lipids (Chen *et al.*, 2022).

### 2.8.2. Application of Proteomics to the study of Mesenchymal Stem Cell Therapy

MS proteomics has been used to characterise and quantify the proteome of MSCs in order to further understand how they elicit their therapeutic action. Bundgaard *et al* (Bundgaard *et al.*, 2020) explored the difference between *in vitro* secreted protein profile between naive and chondrogenic differentiating bone marrow-derived (BM)-MSCs and their secretome when exposed to an

inflammatory environment. Key inflammatory proteins such as IL6, chemokine (C-X-C motif) ligand 6 (CXCL6), chemokine (C-C motif) ligand 7 (CCL7) and haptoglobin were identified in the secretome after IL-1 $\beta$  stimulation. Proteins such as TGF $\beta$ 1, vascular cell adhesion molecule (VCAM1), vascular endothelial growth factor A (VEGFA) and TIMP3 were identified in the secretome of MSCs without stimulation (Bundgaard *et al.*, 2020). In addition, Bundgaard *et al* characterised the surface proteome of equine MSCs in order to immunophenotype such cells. A total of 1239 proteins were identified, with 19 attributed to the cluster of differentiation classification system, of which these include CD29, CD44, CD90 and CD105 (Bundgaard *et al.*, 2018). MSC-EVs were analysed due to their potential as a promising alternative, off the shelf, allogenic regenerative and immunomodulatory therapeutic. A recent systematic review identified a number of MSC-EV hallmark proteins from studies across species including rat and pig. These included collagen type 1 alpha 1 (Col1 $\alpha$ 1), collagen type 1 alpha 2 (Col1 $\alpha$ 2), low density lipoprotein receptor related protein 1 (LRP1), actin alpha 1 (ACTN1) (van Balkom *et al.*, 2019).

### 2.8.3. *Application of Mass Spectrometry Proteomics to the study of Tendon Injury and Platelet-rich Plasma*

MS proteomics has been used to quantify proteomic changes in association with ageing and the development of tendinopathies across a range of species. Studies have explored the difference in equine tenocytes derived from core and peripheral SDFT, and identified 4082 proteins from both groups. Of these 27 were more abundant in core tendon and included collagen  $\alpha$ -2(IV). Whereas peripheral tendon had 32 significantly more abundant proteins, such as lysyl Oxidase Like 2 (LOXL2), fibulin 5 and ADAM Metallopeptidase Domain 10 (ADAM 10). However, it was surmised that the proteome were very similar between groups and that other intrinsic or extrinsic factors may contribute towards the tissues response to loading and injury (Yeung, Zhang, *et al.*, 2020). In addition, the protein dynamics of tendinous structures have been explored to further define the maintenance of tissue and their respective turnover rates which can relate to injury and repair. Using isotope labelling and MS proteomics the fascicular and inter fascicular ECM from human Achilles tendon was compared. A 1000 fold difference in protein turnover rate was identified, and an overall faster rate in glycoprotein rich interfascicular matrix compared with collagen rich fascicular matrix (Choi *et al.*, 2020). The response of tenocytes to radial extracorporeal shockwave therapy has also been explored, by stimulating human tenocytes with TNF- $\alpha$ . 40 differentially expressed proteins were identified between healthy and inflammatory tenocytes and inflammatory tenocytes compared to those treated with extracorporeal shockwave therapy. Of those, it was found that integrin alpha, selenoprotein S and

nucleotide-binding oligomerization domain (NOD)-like receptor (NLR) family CARD domain containing protein 4 were important targets for the anti-inflammatory effects observed with the stated therapeutic intervention (Ge *et al.*, 2022).

Tenocyte derived EVs have also been explored in order to determine their role in tissue homeostasis and action within the ECM, and how they may contribute towards dysregulation. A study on human EVs derived from primary tendon cells found that there were higher levels of protein in tendon fibroblast derived EVs than muscle fibroblast EVs. In addition tendon EVs were enriched in proteins contributing to ECM synthesis such as TGF $\beta$ 1 (Yeung, Schoof, *et al.*, 2020). The mode of action of various therapeutic has also previously been explored, such as that of autologous hemoderivative therapeutics such as platelet-rich plasma (PRP).

For example, a study was performed to compare the composition of PRP, platelet poor plasma and blood plasma. Approximately 600 proteins were identified across each plasma formulation. Specifically, 129 proteins were unique to PRP and included TGF $\beta$ 1, collagen 1 alpha 1 (col1 $\alpha$ 1), thrombospondin 1 (THSB1), platelet growth factor (PGF), and heat shock protein 70 (HSP 70). Actin cytoskeleton signalling, integrin signalling, haematopoiesis from pluripotent stem cell signalling, and leukocyte extravasion signalling were upregulated in PRP (Miroshnychenko *et al.*, 2020).

## 3. Thesis Overview

### 3.1. Project Starting Points

The stimulus for this project was the significant welfare and economic burden musculoskeletal diseases have on horses within the UK and worldwide (Anderson, Phelan, Foddy, *et al.*, 2020a). With ineffective diagnostic tests and the inability of current treatment to reverse disease pathology. As such there is a demand to both understand the pathology of disease to identify putative biomarkers, in order to provide better management of disease. While also understanding the mechanisms of action of therapeutics routinely used in clinical practice despite the lack of robust data demonstrating therapeutic efficacy, reproducible outcomes, and inherent risks such as uncontrolled proliferation and migration (Hotham *et al.*, 2021). For many years' cells and biofluids have been probed in order to understand disease. However, a growing research field is gathering momentum with respect to the understanding of biological physiology and cellular communication (Boere, Malda, Van De Lest, *et al.*, 2018; Liu, Cheng, *et al.*, 2020; Tan *et al.*, 2021). The field being extracellular vesicle research. As such it was hypothesised that valuable insight could be provided by exploring the role of EVs in both disease and popular therapeutics such as PRP and MSCs (Taylor *et al.*, 2007; Racchetti and Meldolesi, 2021b; Wu, Zhang, *et al.*, 2021), that would in turn have a translational capacity to human orthopaedic research due to the applicability of equine joint anatomy to humans (McIlwraith, Frisbie and Kawcak, 2012a). As such we wanted to explore EVs in a veterinary medicine capacity primarily, in order to ascertain if they could be a valuable source of biomarkers in orthopaedic disease, and be utilised from appropriate sources to be used therapeutically.

### 3.2. Aims and Objectives

1. To investigate extracellular vesicle structure and protein cargo from a longitudinal in vivo model of equine osteoarthritis treated with mesenchymal stem cells, in order to determine disease-associated extracellular vesicle cargo, and their potential role in mediating mesenchymal stem cell therapy.
2. Explore the differences in composition of extracellular vesicles from healthy horses and those with clinically diagnosed osteoarthritis using both spectroscopic and spectrometric techniques.
3. Explore the composition of platelet-rich plasma and platelet-rich plasma derived extracellular vesicles using mass spectrometry proteomics.

4. Investigate the effect of platelet-rich plasma and platelet-rich plasma derived extracellular vesicles in an in vitro model of equine tendon injury, using mass spectrometry proteomics and gene expression analysis.

### 3.3. Outline of Thesis

The thesis contains a general introduction providing background to fundamental aspects to the project such as equine musculoskeletal conditions, equine osteoarthritis, tendon injury, biological therapies and extracellular vesicles. Along with the 'omics' techniques that have been used throughout, and include: mass spectrometry, Raman spectroscopy and optical photothermal infrared spectroscopy. The following chapters are individual studies written in the format of papers, highlighting the primary findings from this work.

- “Temporal extracellular vesicle protein changes following Intraarticular treatment with integrin  $\alpha 10\text{b1}$ -selected mesenchymal stem cells in equine Osteoarthritis” is published in *Frontiers in Veterinary Science* (2022) - <https://doi.org/10.3389/fvets.2022.1057667>
- “Optical Photothermal Infrared Spectroscopy can Differentiate Equine Osteoarthritic Plasma Extracellular Vesicles from Healthy Controls” is published in *RSC Analytical Methods* (2022) - <https://doi.org/10.1039/D2AY00779G>
- “Proteome and phospholipidome interrelationship of synovial fluid-derived extracellular vesicles in equine osteoarthritis: An exploratory ‘multi-omics’ study to identify composite biomarkers”- preprint on *BioRxiv* and will be submitted to *Biochimica et biophysica acta (BBA) Biochemistry & Biophysics reports*. - <https://doi.org/10.1101/2023.08.02.551609>
- “Allogenic platelet-rich plasma and platelet-rich plasma extracellular vesicles change the proteome of tenocytes in an in vitro equine model of tendon inflammation, resulting in the identification of potential molecular modes of action of PRP: A pilot study”



## 4. Materials and Methods

### 4.1. Temporal Extracellular Vesicle Protein Changes following Intraarticular Treatment with Integrin $\alpha 10\beta 1$ -selected Mesenchymal Stem Cells in Equine Osteoarthritis

#### 4.1.1. Preliminary Studies

##### 4.1.1.1. Optimisation of Extracellular Vesicle Isolation for Downstream Mass Spectrometry Proteomics Analysis

###### 4.1.1.1.1. Sample Selection and Hyaluronidase Treatment

For the purpose of this study one pooled sample (n=3 biological donors, 1.5ml total) of SF was used, and sourced from the University of Liverpool Equine musculoskeletal biobank (VREC561). The pooled sample was HA treated as previously described in section 1.3.3, and then aliquoted into three replicates of 300 $\mu$ l, to be used in order to isolate EVs using one of three isolation techniques, namely: size exclusion chromatography (SEC), differential ultracentrifugation (UC) and SEC + UC.

###### 4.1.1.1.2. Extracellular Vesicle Isolation

EV samples that were isolated using size exclusion chromatography (SEC) or differential ultracentrifugation (dUC). For SEC samples were centrifuged at 2500 $xg$  for 10 minutes, and then 10,000 $xg$  for 10 minutes. Following this qEV single columns (IZON, Lyon, France) were used to isolate EVs, following manufacturer's instructions. In brief, 3.5 ml of PBS (Sigma-Aldrich, Gillingham, UK), previously processed using a 0.22  $\mu$ m polyethersulfone filter (Sartorius, Göttingen, Germany) was passed through the column, followed by 200  $\mu$ l of SF or plasma. The first five 200  $\mu$ l flow through fractions were discarded and the following five 200  $\mu$ l fractions pooled (isolated EVs). For dUC Samples were subjected to a 300  $xg$  spin for 10 min, 2000  $xg$  spin for 10 min, 10,000  $xg$  spin for 30 min in a bench top centrifuge at room temperature. Samples were then transferred to Beckman Coulter thick wall polycarbonate 4 mL ultracentrifugation tubes, and spun at 100,000  $xg$  for 70 min at 4°C (Optima XPN-80 Ultracentrifuge, Beckman Coulter, California, USA) in a 45ti fixed angle rotor, with the use of a 13 mm diameter Delrin adaptor. Sample pellets were suspended in 50  $\mu$ L of filtered phosphate buffered saline (PBS) (Gibco™ PBS, pH 7.4 - Fisher Scientific, Massachusetts, USA), resulting in 50  $\mu$ L EV samples. Vivaspin columns (Sartorius, Göttingen, Germany) were subsequently used to concentrate SEC isolated samples, and were used following manufacturer's instructions.

###### 4.1.1.1.3. Extracellular Vesicle Protein Extraction

EV pellets were suspended in 200  $\mu$ l of urea lysis buffer (6M Urea (Sigma-Aldrich, Dorset, United Kingdom), 1M ammonium bicarbonate (Fluka Chemicals Ltd., Gillingham, UK) and 0.5% sodium deoxycholate (Sigma-Aldrich, Dorset, United Kingdom)). Samples were sonicated at 5  $\mu$ m for 3x 10 seconds per sample, with 1-minute rest on ice between each sonication round.

#### *4.1.1.1.4. Protein Assay*

EV total protein was quantified using the microBCA protein quantification assay (ThermoFisher, Waltham, Massachusetts, United States), and performed as per manufacturers guidelines outlined. In brief, 150  $\mu$ l of each EV protein extract was pipette in triplicate into a 96 well plate, along with known bovine serum albumin (BSA) standards in triplicate (0.5 $\mu$ g/ml-200 $\mu$ g/ml). 150 $\mu$ l of working reagent was added to each sample, and placed on a plate shaker for 30 seconds and then incubated at 37°C for 2 hours. Following this the 96 well plate was placed in a microplate reader and absorbance was measured at 562nm.

#### *4.1.1.1.5. Extracellular Vesicle Protein Digestion*

160 $\mu$ l of AmBic was added to samples, and 10 $\mu$ l of 1% (w/v) RapiGest (Waters, UK) Surfactant (freshly prepared in 25mM AmBic). Samples were then vortexed and incubated at 80°C for 10 minutes. 10 $\mu$ l of dithiothreitol (DTT) (ThermoFisher Scientific, Paisley, UK) (11mg of DTT in 1ml of 25mM AmBic to prepare a 11.1mg/ml solution) was added to each sample. Samples were then incubated at 60°C for 10 minutes. Then 10 $\mu$ l of iodoacetamide (IAA) (ThermoFisher Scientific, Paisley, UK) (46mg IAA in 1ml of AmBic) was added to each sample and samples were incubated at room temperature in the dark for 30 minutes. To prevent overalkylation, 9.4 $\mu$ l of the 11.1mg/ml DTT solution was added in each sample (final DTT concentration 7mM). Trypsin/Lys-C Mix (20 $\mu$ g) (Promega, Southampton, UK) was reconstituted into 100 $\mu$ l of AmBic, and 10 $\mu$ l was added to each sample, and samples were incubated at 37°C in a rotating incubator for 2 hours. After 2 hours an additional 10 $\mu$ l of Trypsin/Lys-C Mix was added to each sample. Samples were then placed in a rotating incubator at 37°C, overnight, to achieve complete protein digestion. Trifluoroacetic acid (TFA- 1 $\mu$ l) (VWR International, Lutterworth, Leicestershire, UK) was added to each sample and acidity was confirmed with pH paper (ThermoFisher Scientific, Paisley, UK). Samples were then incubated at 37°C for 45 minutes. Following incubation, samples were centrifuged at 13,000 $g$  at 4°C for 15 minutes to remove insolubles. Supernatant was transferred to new tubes and samples were centrifuged again at 13,000 $g$  at 4°C for 15 minutes. Supernatant was then removed and placed in new LoBind Eppendorfs ready for LC-MS/MS analysis. Protein LoBind (Eppendorf, Hamburg, Germany) tubes were used throughout. For EV samples both DTT and IAA were diluted 1:5.

#### 4.1.1.1.6. Data Dependent Acquisition Mass Spectrometry Proteomics

Data-dependent LC-MS/MS analyses were conducted on a QExactive HF quadrupole-Orbitrap mass spectrometer (Thermo Scientific, Hemel Hempstead, UK) coupled to a Dionex Ultimate 3000 RSLC nano-liquid chromatograph (Thermo Scientific). Sample digests were loaded onto a trapping column (Acclaim PepMap 100 C18, 75  $\mu\text{m}$   $\times$  2 cm, 3  $\mu\text{m}$  packing material, 100  $\text{\AA}$ ) using a loading buffer of 0.1% (v/v) trifluoroacetic acid, 2% (v/v) acetonitrile in water for 7 minutes at a flow rate of 12  $\mu\text{l min}^{-1}$ . The trapping column was then set in-line with an analytical column (EASY-Spray PepMap RSLC C18, 75  $\mu\text{m}$   $\times$  50 cm, 2  $\mu\text{m}$  packing material, 100  $\text{\AA}$ ) and the peptides eluted using a linear gradient of 96.2% A (0.1% [v/v] formic acid):3.8% B (0.1% [v/v][formic acid in water:acetonitrile [v/v]]) to 50% A:50% B over 30 min at a flow rate of 300  $\text{nl min}^{-1}$ , followed by washing at 1% A:99% B for 5 min and re-equilibration of the column to starting conditions.

For label-free quantification, the raw files of the acquired spectra were analysed by the ProgenesisQI™ software (Waters, Manchester, UK) [9]. The Mascot server (Version 2.8.2), was used in order to identify peptides, searching against the Unihorse database.

#### 4.1.1.1.7. Enrichment Analysis

Functional enrichment analysis was performed on the sample found to have the highest number of proteins, and analysis was performed on all identified proteins in order to determine the cellular components proteins were statistically likely to be attributed to. Horse Uniprot accessions were converted to human Uniprot accession codes in order to use this software. Protein identifications were also compared to validated proteins identified on the Exocarta database.

### **4.1.1.2. Optimisation of a Commercially available Extracellular Vesicle Characterisation Platform**

#### 4.1.1.2.1. Sample Selection

Equine synovial fluid (SF, 200 $\mu\text{l}$ ) (n=1) from the metacarpophalangeal joint and plasma (200 $\mu\text{l}$ ) (n=1) was used. Samples were sourced from the University of Liverpool Equine musculoskeletal biobank (VREC561). SF was HA treated as previously described in section 4.1.1.1.1.

#### 4.1.1.2.2. Extracellular Vesicle Isolation – Size Exclusion Chromatography

SF and plasma were used to isolate EVs following size exclusion chromatography. Firstly, samples were centrifuged at 2500 $\times g$  for 10 minutes, and then 10,000 $\times g$  for 10 minutes. Following this qEV single columns (IZON, Lyon, France) were used to isolate EVs, following manufacturer's instructions. In brief,

3.5 ml of PBS (Sigma-Aldrich, Gillingham, UK), previously processed using a 0.22 µm polyethersulfone filter (Sartorius, Göttingen, Germany) was passed through the column, followed by 200 µl of SF or plasma. The first five 200 µl flow through fractions were discarded and the following five 200 µl fractions pooled (isolated EVs).

#### *4.1.1.2.3. Exoview Analysis*

The ExoView platform (NanoView Biosciences, Malvern Hills Science Park, Malvern) was used to determine EV concentration, surface marker identification and to perform fluorescent microscopy and tetraspanin colocalisation analysis. ExoView analyses EVs using visible light interference for size measurements and fluorescence for protein profiling. Samples were analysed in triplicate using the ExoView Tetraspanin Kit (NanoView Biosciences, USA) and were incubated on the human ExoView Tetraspanin Microarray Chip for 16 h at room temperature. Following this sample chips were incubated with tetraspanin labelling antibodies, namely anti-CD9 CF488, anti-CD81 CF555 and anti-CD63 CF647 and the MIgG negative control. The antibodies were diluted 1:500 in PBS with 2% bovine serum albumin. The chips were incubated with 250 µL of the labelling solution for 1 h. The sample chips were washed and imaged with the ExoView R100 reader ExoView Scanner v3.0. Data were analysed using ExoView Analyzer v3.0. Fluorescent cut offs were set relative to the MIgG control. Total EVs were determined as the number of detected particles bound to tetraspanin antibodies (CD9, CD81, CD63) and normalised to MIgG antibody. Experimental details and methods of characterisation have been uploaded to EV-TRACK, with the EV-TRACK identifier EV230992.

#### **4.1.2. Main Study**

##### *4.1.2.1. Equine Carpal Osteochondral Fragment Model Induction*

The study was approved by the Danish Animal Experiments Inspectorate (#2020-15-0201-00602) as well as the Ethical Committee of the University of Copenhagen (project no 2020-016). OA was induced using a carpal osteochondral fragment-exercise model in a total of 6 Standardbred trotters (mares, 4 to 7 years of age). The model was previously described by McIlwraith *et al.* (McIlwraith, Frisbie and Kawcak, 2012a). OA was induced in the left carpus of all horses and the right carpus was sham operated on to serve as control. Horses were premedicated with a combination of romifidine 6 mg/100 kg (Sedivet®Vet, Boehringer Ingelheim Vetmedica, Missouri, United States), acepromazine 3 mg/100kg (Plegicil Vet, Boehringer Ingelheim Vetmedica, Missouri, United States), atropine sulphate 0.5 mg/100kg (Atropin, Aguetant Ltd, Bristol, United Kingdom), and butorphanol 3 mg/100 kg (Dolorex®, Ag Marin Pharmaceuticals, United States). Anesthesia was induced with ketamine 2.5 mg/kg (Ketador Vet, Richter Pharma AG, Oberosterreich, Austria) and midazolam 4 mg/100 kg

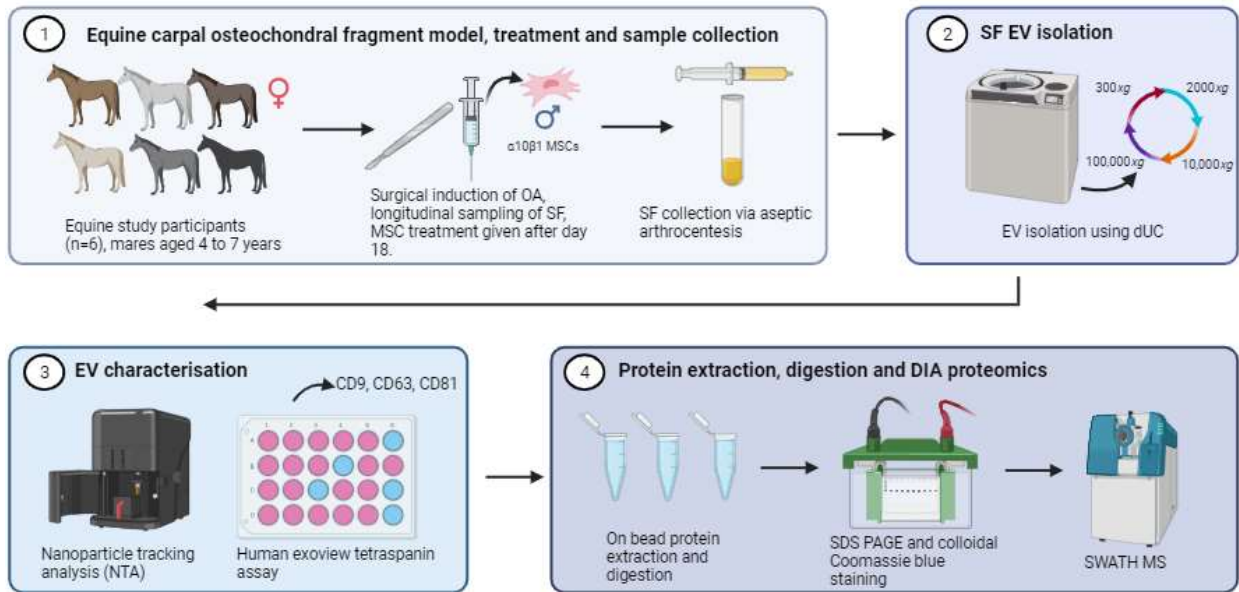
(Midazolam “Accord”, Accord-UK Ltd, Barnstaple, United Kingdom). The horses were placed in dorsal recumbency and anaesthesia maintained with isoflourane (Vetflurane, Virbac, Carros, France). Perioperatively the horses received flunixin meglumine 1.1 mg/kg (Finadyne, MSD Animal Health, New Jersey, United States), penicillin 22.000 IU/kg (Benzylpenicillin PanPharma, Brancaster Pharma, Surrey, United Kingdom), and gentamicin 6.6 mg/kg (Genta-Equine, Dechra Veterinary Products, Shrewsbury, United Kingdom). Arthroscopic portals were made in the right carpus and the carpal joint was inspected for abnormalities. In the left carpus an osteochondral “chip” fragment was made with an 8mm curved osteotome in the dorsal margin of the third facet of the distal surface of the radial carpal bone at the level of the medial plica. The fragment remained attached to the plica. The debris was not flushed from the joint. The horses were stall rested for 14 days after surgery. From day 2 following surgery horses were walked by hand every day. Treadmill exercise was initiated on day 14 after surgery. The horses were exercised 5 days a week for 8 weeks through the following program: 2 min slow trot 16-19 km/h (4.4-5.3m/s), 2 min fast trot 32 km/h (9m/s), 2 min slow trot 16-19 km/h (4.4-5.3m/s). From day 14 the horses were allowed free pasture exercise every day. At day 18 MSCs were injected intraarticularly into the left joint with the osteochondral fragment only. Horses were humanely euthanized at the end of the study and both joints underwent both gross and histological examination. This data is not included.

Aseptic arthrocentesis was conducted on osteochondral chip joints and sham control joints at specific time points: day 0, 18, 21, 28, 35 and 70, as shown in Table 4.1. The synovial fluid (SF) was centrifuged at 2540g at 4°C for 5 minutes and then aliquoted into Eppendorf tubes, and snap frozen. After completion of collection, samples were transported on dry ice to the University of Liverpool, and stored at -80°C. For clarity, experimental groups were control (day 0-day 70), OA (day 0-day 18) and OA +MSCs (day 21- 70) following MSC treatment of the OA group post sampling at day 18, as shown in Table 4.1. An experimental overview is provided in Figure 4.1.

**Table 4.1 An overview of experimental groups and the longitudinal time points for synovial fluid collection.**

		Day						
		0 (prior to surgery)	18		21	28	35	70
Group	Sham Control	→		No treatment	→			
	OA	→		MSC administration	→ OA+MSCs			

Abbreviations: Osteoarthritis and mesenchymal stem cells (OA+MSCs), Osteoarthritis (OA)



**Figure 4.1. A schematic overview of the experimental process.** Specifically, in order to probe the global EV cargo from a carpal osteochondral fragment model of equine OA following  $\alpha 10\beta 1$  MSC treatment intraarticularly.

#### 4.1.2.2. Mesenchymal Stem Cell Therapy

Equine MSCs were isolated from adipose tissue from a 7-year-old healthy gelding. Briefly, the adipose tissue was digested with collagenase, adipose cells were removed, and the stem vascular fraction was isolated and expanded in culture. Cells were cultured to passage 3, and MSCs were then selected for high expression of integrin  $\alpha 10\beta 1$  (integrin  $\alpha 10$ -MSCs) by magnetic-activated cell sorting using a specific biotinylated integrin  $\alpha 10$  monoclonal antibody (Xintela, Sweden) and anti-biotin microbeads (Miltenyi, North Rhine Westphalia, Germany). MSCs were subsequently washed in culture medium, reseeded and expanded for a further passage (passage 4), then frozen in 10% dimethyl sulfoxide (DMSO) cryopreservation medium (Cryosstor, BioLife Solutions, Washington, United States) in liquid nitrogen until use. The frequency of MSCs expressing integrin  $\alpha 10\beta 1$  measured by flow cytometry, was 92.7% before cryopreservation.

On day 18 all six horses were treated with  $20 \times 10^6$  integrin  $\alpha 10$ -MSCs (4ml, in 10% DMSO in cryopreservation medium) immediately after synovial sampling. Cryopreservation medium was not injected into the control joint. Day 18 was selected for MSC treatment to be administered to ensure an OA phenotype had developed within the joint as a response to surgical intervention. This was based on our previous study (Anderson *et al.*, 2022). The integrin  $\alpha 10$ -MSCs were thawed in a sterile water bath at 37°C, aspirated into a syringe through a 14G canula at a slow pace, and injected into the carpal

joint of the OA-induced limb through a 20G canula over a minimum of 10 seconds. The horses were stall rested for 2 days following treatment.

#### 4.1.2.3. *Sample Preparation*

1ml of SF per sample was spun in a benchtop centrifuge (Eppendorf non-refrigerated centrifuge 5420) at 241g for 10 min. The supernatant was removed and treated with hyaluronidase (1 µg/ml) by incubation at 37°C for 1 hour. SF samples were then spun at 1000g for 5 min, and the supernatant was collected.

#### 4.1.2.4. *EV Isolation – Differential Ultracentrifugation*

Equine synovial fluid samples underwent differential ultracentrifugation (dUC) in order to isolate EVs. Samples were subjected to a 300 *xg* spin for 10 min, 2000 *xg* spin for 10 min, 10,000 *xg* spin for 30 min in a bench top centrifuge at room temperature. Samples were then transferred to Beckman Coulter thick wall polycarbonate 4 mL ultracentrifugation tubes, and spun at 100,000 *xg* for 70 min at 4°C (Optima XPN-80 Ultracentrifuge, Beckman Coulter, California, USA) in a 45ti fixed angle rotor, with the use of a 13 mm diameter Delrin adaptor. Sample pellets were suspended in 50 µL of filtered phosphate buffered saline (PBS) (Gibco™ PBS, pH 7.4 - Fisher Scientific, Massachusetts, USA), resulting in 50 µL EV samples.

#### 4.1.2.5. *Nanoparticle Tracking Analysis*

Nanoparticle tracking analysis (NTA) was used to quantify EV concentration and size of all samples, using a NanoSight NS300 (Malvern Panalytical, Malvern, UK). All samples were diluted in filtered PBS 1:50 (10 µL of sample used), to a final volume of 500 µL. For each measurement, three 1-min videos were captured, (at a screen gain of 4 and detection threshold of 12). After capture, the videos were analysed by the in-built NanoSight Software NTA 3.1 Build 3.1.46. Hardware: embedded laser: 45 mW at 488 nm; camera: sCMOS.

#### 4.1.2.6. *Extracellular Vesicle Characterisation*

As described in section 4.1.1.2.3. We had previously tested equine samples on both the human and murine chips and demonstrated the human chips were more compatible (Appendix 1). The ExoView analyses EVs using visible light interference for size measurements and fluorescence for surface protein profiling. Samples were analysed as previously described (Anderson *et al.*, 2022). Experimental details and characterisation information has been uploaded to EV-TRACK, with the EV-TRACK identifier of EV230991.

#### 4.1.2.7. *Extracellular Vesicle Protein Extraction*

As described in section 4.1.1.1.3.

#### 4.1.2.8. *Sodium Dodecyl Sulphate–polyacrylamide Gel Electrophoresis and Protein Staining*

Sodium dodecyl sulphate–polyacrylamide gel electrophoresis (SDS-PAGE) was used to separate proteins from EV protein extract. 7.5  $\mu$ l of 2x Novex™ Tris-Glycine SDS Sample Buffer (ThermoFisher Scientific, Paisley, UK), supplemented with 8% of 2-Mercaptoethanol (Sigma-Aldrich, Dorset, UK), was added to 7.5  $\mu$ l of sample SF-EV protein lysate. Samples were mixed and heated at 100°C for 10 min to denature proteins, then placed on ice. A NuPAGE™ 4 to 12%, Bis-Tris gel (ThermoFisher Scientific, Paisley, UK) was placed in the electrophoretic tank and the tank was filled with 1x NuPAGE® MES Running Buffer (ThermoFisher Scientific, Paisley, UK) (diluted from the 20x stock in ultrapure water). Samples were loaded onto the gel alongside the Novex™ Sharp Pre-stained Protein Standard ladder (ThermoFisher Scientific, Paisley, UK). Gels were run at 100V until completion of electrophoresis and visualised using colloidal coomassie blue (Thermofisher Scientific, Paisley, UK) according to manufacturer's guidelines. The result of this is shown in Supplementary Figure 5.2.

#### 4.1.2.9. *On-bead Protein Digestion*

95  $\mu$ l of lysed and sonicated equine SF-EV were treated with 5mM dithiothreitol (DTT) (Sigma-Aldrich, Dorset, UK) 100 mM Ambic at 60°C and 123xg for 30 minutes. Iodoacetamide (Sigma-Aldrich, Dorset, UK) was then added to a final concentration of 20mM and the samples were incubated at room temperature in the dark for 30 min. Following this 5mM DTT was added to each sample, and incubated at room temperature for 15 min. 12  $\mu$ l hydrophilic and hydrophobic magnetic carboxylate SpeedBeads (SP3 beads, total of 12  $\mu$ l) (Cytiva, Massachusetts, United States) were added to each sample, followed by 120  $\mu$ l ethanol (Sigma- Aldrich, Dorset, UK). Samples were then incubated at 24°C and 123xg for 1 hour. The beads were separated from samples using a magnetic stand and were washed three times with 180  $\mu$ l 80% ethanol. They were resuspended in 100 mM ammonium bicarbonate (Fluka Chemicals Ltd., Gillingham, UK 4  $\mu$ g). Trypsin/LysC (2.4  $\mu$ g) (Promega) was added to each sample. Samples were placed in a sonication bath and sonicated for 30 seconds to disaggregate the beads before being incubated overnight at 37°C and 123g. Beads were removed from the samples using the magnetic stand and the supernatants were acidified by the addition of 1  $\mu$ l trifluoroacetic acid (Sigma- Aldrich, Dorset, UK). Samples were then desalted using an Agilent mRP-C18 column, dried in a SpeedVac and resuspended in 0.1% formic acid. The UV absorbance measured during desalting was used to normalize the loading for mass spectrometry analysis with a final volume of 5  $\mu$ l being loaded on the nano-LC column.



#### 4.1.2.10. *Data-dependent Acquisition for Generation of an Equine Synovial Fluid derived Extracellular Vesicle Spectral Library*

Equine SF was pooled using samples from the metacarpophalangeal joint from equine musculoskeletal biobank at University of Liverpool (VREC561), and samples collected in this study from carpal joint of control group as well as OA, and OA+MSC group, resulting in a total of 11 ml SF. This was hyaluronidase treated (1µg/ml) for 1 hour at 37°C, as outlined in section 2.2. EVs were isolated using dUC, as outlined in section 2.4. The EV pellet was then reconstituted in 200 µl of urea lysis buffer. The samples were digested with trypsin/LysC for 3 hours at 37°C, the concentration of urea was reduced to 1M, and incubation was continued overnight at 37°C. Samples were fractionated on a PolySULFOETHYL, a strong cation exchange column, and 20 fractions were desalted, dried and resuspended in 0.1% formic acid. Aliquots were loaded onto an Eksigent nanoLC 415 (Sciex, Macclesfield, United Kingdom) equipped with a nanoAcquity UPLC Symmetry C18 trap column (Waters, Massachusetts, United States of America) and a bioZEN 2.6µm Peptide XB-C18 (FS) nanocolumn (250mm x 75µm, Phenomenex, Macclesfield, United Kingdom). A gradient from 2–50% acetonitrile /0.1% formic acid (v/v) over 120 min at a flow rate of 300 nL/min was applied. Data-dependent acquisition was performed using nano liquid chromatography-tandem mass spectrometry on a Triple TOF 6600 (Sciex, Macclesfield, United Kingdom) in positive ion mode using 25 MS/MS per cycle (2.8s cycle time), and the data were searched using ProteinPilot 5.0 (Sciex, Macclesfield, United Kingdom) and the Paragon algorithm (SCIEX) against the horse proteome (UniProt *Equus caballus* reference proteome, 9796, May 2021, 20,865 entries). Carbamidomethyl was set as a fixed modification of cysteine residues. The data were also searched against a reversed decoy database and proteins lying within a 1% or 5% global false discovery rate (FDR) were included in the library. Proteins were analysed using GO terms enrichment analysis FunRich.

#### 4.1.2.11. *Data-independent Acquisition Proteomics*

A data-independent proteomic approach was utilised in the form of Sequential Windowed Acquisition of all theoretical fragments (SWATH) (Gillet *et al.*, 2012). Aliquots of 5µl containing equal quantities of peptides were made up to a volume of 5µl with 0.1% formic acid and data were acquired using the same 2h gradient as the library fractions. SWATH acquisitions were performed using 100 windows of variable effective isolation width to cover a precursor m/z range of 400-1500 and a product ion m/z range of 100-1650. Scan times were 50ms for TOF-MS and 36ms for each SWATH window, gave a total cycle time of 3.7 seconds. Retention time alignment and peptide/protein quantification were performed by Data-Independent Acquisition by Neural Networks (DIA-NN) (Demichev *et al.*, 2020),

using the same reference horse proteome as above to reannotate the library. A precursor FDR of 1%, with match between runs and unrelated runs was selected. The mass spectrometry proteomics data were deposited to the ProteomeXchange Consortium via PRIDE (Perez-Riverol and Csordas, 2019) (reference PXD035303).

#### 4.1.2.12. Statistical Analysis

All statistical results were corrected for false discovery rate (FDR) using the Benjamini-Hochberg (BH) method, with the exception of NTA and exoview data analysis, as this did not require FDR correction. Results were considered significant at 5% FDR. Nanoparticle tracking analysis data was analysed using non-parametric tests. A Kruskal-Wallis test was performed for concentration and size, followed by a Mann-Whitney U test per time point. Exoview data was analysed using T-tests following parametric evaluation in GraphPad Prism 9.0. Statistical analysis of proteomics data was carried out using the R statistical programming environment (RStudio, 2015), unless stated otherwise. The data was quality controlled; proteins with complete observations were normalised and log<sub>2</sub> transformed for downstream analysis. Batch effect was detected and corrected via ComBat (Leek *et al.*, 2012) prior to Principal Component Analysis (PCA) and further visualisations, the results of batch correction are shown in Supplementary Figure 10.1. The lmerTest implementation of lme4 was used to fit linear mixed models (LMMs) to the log-transformed data for each protein to determine the effects of treatment, time, and treatment over time on horse joints. For the fitted models pairwise comparisons between the treatment and control were carried out at each time point using the emmeans package with the Kenward-Roger method (Halekoh and Højsgaard, 2014). All graphical representations were undertaken using the package ggplot2 (Villanueva and Chen, 2019). Functional classification and enrichment analyses were performed using the clusterProfiler package (Wu, Hu, *et al.*, 2021). The proteins were annotated with GeneOntology (GO) terms using the UniProtKB ID Mapping tool. Over-representation analysis (ORA) was carried out for GO terms using the enricher function from the clusterProfiler package. The foreground was all the proteins that passed FDR, the background was all the processed proteins after missing values had been removed, i.e., all the proteins that were subjected to statistical analysis. Each term was required to have a minimum of three observed proteins annotated to it and an adjusted p-value <0.05.

## **4.2. Optical Photothermal Infrared Spectroscopy can Differentiate Equine Osteoarthritic Plasma Extracellular Vesicles from Healthy Controls**

### **4.2.1. Preliminary Studies**

#### ***4.2.1.1. Optimisation of Extracellular Vesicle Suspension for Spectroscopic Analysis***

##### *4.2.1.1.1. Sample Collection*

Equine plasma pooled from three donors (n=3) was used for the isolation of EVs in this optimisation study. A total of 800µl of plasma was used, and divided into three technical replicates of 200µl. EVs were isolated and suspended in 50 µl of water, PBS or saline.

##### *4.2.1.1.2. Extracellular Vesicle Isolation*

As described in section 4.1.2.4.

##### *4.2.1.1.3. Nanoparticle Tracking Analysis*

As described in section 4.1.2.5.

##### *4.2.1.1.4. Raman Spectroscopy and Optical Photothermal Infrared Spectroscopy*

For all samples O-PTIR measurements were acquired on single-point mode using a mIRage infrared microscope (Photothermal Spectroscopy Corp., Santa Barbara, USA), with the pump consisting of a tuneable four-stage QCL device, while the probe beam is a continuous wave 532 nm laser. Spectral data were collected in reflection mode using a 40×, 0.78 NA, and 8 mm working distance Schwarzschild objective. A total number of 130 single-point infrared spectra (10 spectra per sample/horse) were acquired over a spectral region of 930–1800 cm<sup>-1</sup>, with 2cm<sup>-1</sup> spectral resolution and 10 scans per spectrum. 130 Raman spectra (10 spectra per sample/horse) were acquired simultaneously with infrared data using a Horiba Scientific iHR-320 spectrometer coupled to mIRage, using a grating of 600 l/mm, 10 s as acquisition time, spectral region of 500–3400 cm<sup>-1</sup>, with 2 cm<sup>-1</sup> spectral resolution and 10 scans per spectrum. It should be highlighted that the volumes used for all samples were the same for both O-PTIR and Raman spectroscopy measurements, samples were not diluted for this analysis.

#### ***4.2.1.2. Using Raman and Optical Photothermal Infrared Spectroscopy to identify Synovial Fluid derived Extracellular Vesicle Biomarkers of Naturally Occurring Equine Osteoarthritis***

##### *4.2.1.2.1. Sample Selection*

Synovial fluid samples (1ml) from the equine metacarpophalangeal joint were utilized from the University of Liverpool Equine Musculoskeletal Biobank (VREC561). Samples were selected on the basis of gross score resulting in a total of 26 samples (control; n= 12 and diseased; n= 14). Synovial fluid was hyaluronidase treated (1ug/ml). In brief, samples were spun at 241g for 10 min. The supernatant was then removed and treated with hyaluronidase (1 µg/ml) by incubation at 37°C for 1 hour. SF samples were then spun at 1000xg for 5 min, and the supernatant was collected. The subsequent sample was then used for EV isolation.

##### *4.2.1.2.2. Extracellular Vesicle Isolation*

As previously described in section 4.1.2.4.

##### *4.2.1.2.3. Nanoparticle Tracking Analysis*

As previously described in section 4.1.2.5.

##### *4.2.1.2.4. Transmission Electron Microscopy*

EV presence and morphology were characterised using transmission electron microscopy (TEM). 10 µL of each sample was placed onto a carbon coated glow discharged grid and incubated at room temperature for 20 min. Samples were then subject to a negative staining protocol. EVs were fixed onto the grid with 1% glutaraldehyde for 5 min. The sample grids were incubated on 1% aqueous uranyl acetate (UA) (ThermoFisher Scientific, Massachusetts, USA), for 60 s, followed by 4% UA/2% Methyl Cellulose (Sigma Aldrich, Gillingham, UK) at a 1:9 ratio on ice for 10 min. Grids were then removed with a 5 mm wire loop and dried. The prepared grids were then viewed at 120KV on a FEI Tecnai G2 Spirit with Gatan RIO16 digital camera.

##### *4.2.1.2.5. ExoView Characterisation*

As previously described in section 4.4.1.1.2.3.

##### *4.2.1.2.6. Raman Spectroscopy and Infrared (O-PTIR) Spectroscopy*

As previously described in section 4.2.1.1.4.

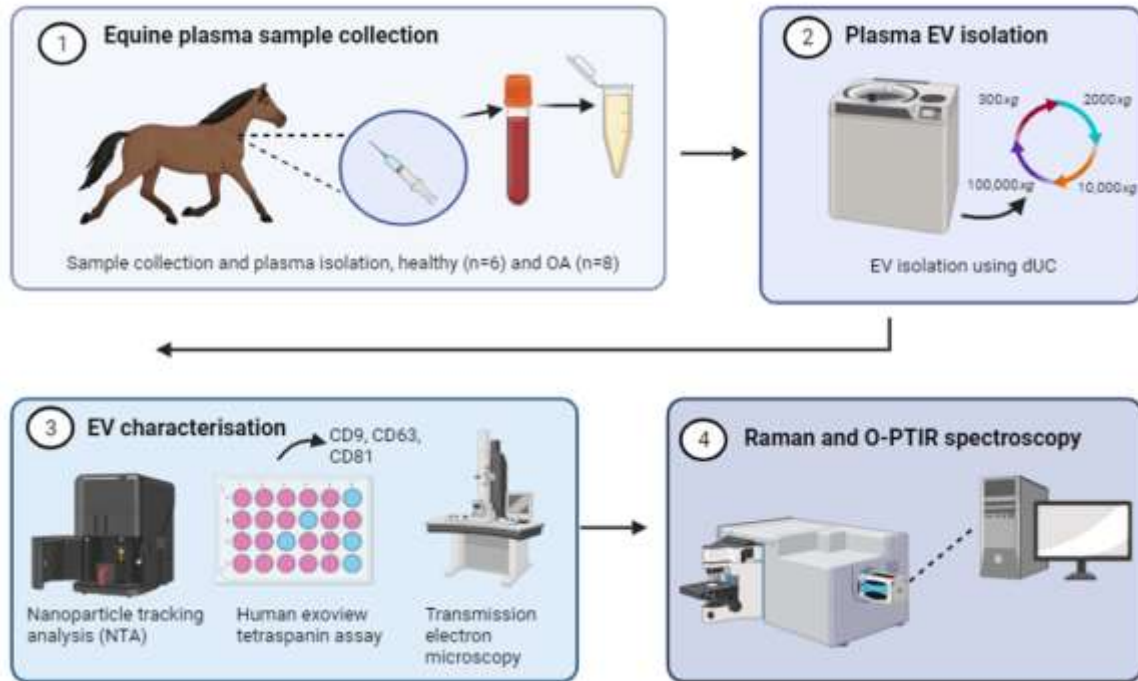
##### *4.2.1.2.7. Statistical Analysis*

Raman and O-PTIR spectroscopic data were analysed using principal component analysis (PCA) to determine each techniques ability to distinguish diseased samples from healthy controls. Before PCA and PLS-DA, spectra were submitted to baseline correction using an asymmetric least squares algorithm, smoothed via a Savitzky– Golay filter, and vector normalized. All spectral data were used as input. Spectral data were also used as input for partial least squares discriminant analysis (PLS-DA) in order to generate a classification model for differentiation of OA from controls. Further analysis with PLS-DA involved using a classification model and confusion matrices, whereby resampling of the data involved both bootstrapping 10,000 times with permutation testing to generate null models to assess whether an EV spectrum was classified as OA or control.

#### **4.2.2. Main Study**

##### **4.2.2.1. Sample Selection**

Plasma samples were collected in accordance with the Hong Kong Jockey Club owner consent regulations (VREC561). Samples were selected due to reflecting a natural model of post-traumatic osteoarthritis. All samples were from thoroughbred racehorses, and were collected between November 2005 and March 2009 from horses actively race training up to the time of death or had previously retired from active race training that were euthanized on welfare grounds. Samples were collected at post-mortem, within 30 minutes of death. The donor cohort had a mean age (+/- standard error of the mean (SEM)) of 6.57 +/- 0.45. The same population has been used in previously published studies by Peffers et al (2015) (Peffers *et al.*, 2015). Horses were selected based on histological scoring of OA severity in the metacarpophalangeal joint using a modified Mankin score (McIlwraith *et al.*, 2010). In addition, osteoarthritis was clinically diagnosed by a qualified veterinary surgeon, to our knowledge these donors had no underlying co-morbidities. Synovitis scores were also obtained for donors, A total of 14 samples were selected: control; n = 6 (mean Mankin score +/- SEM = 1.83 +/- 0.48, and mean synovitis score +/- SEM =3.7 +/-0.33) and diseased; n = 8 (mean Mankin score +/- SEM= 16.25 +/- 1.15, and a mean synovitis score +/- SEM=5 +/- 0.42), reflective of 14 equine donors. An overview of the experimental design is shown in Figure 4.2.



**Figure 4.2 - A schematic overview of the experimental process.** Specifically, followed in order to probe the equine plasma EV membrane between 'healthy' and 'osteoarthritic' diseased states.

#### 4.2.2.2. *Histological Scoring*

Sections were obtained from the left medial distal metacarpal condyle and the left lateral distal metatarsal. Samples were cut with a band saw followed by a saline cooled diamond saw. Cartilage was subsequently dissected and underwent histological staining using Safranin O and Masson's trichrome in order to score cartilage pathologic lesions using a modified Mankin score. This score evaluates cartilage erosion, chondrocyte periphery staining, spatial arrangement of chondrocytes, and background staining intensity. With a higher value denoting a more severe OA phenotype. In addition, the synovial membranes of metacarpophalangeal joints were harvested post-mortem and fixed in cold 4% formaldehyde for at least 30 min before being processed. Processing involved paraffin-embedding, and 10- $\mu$ m section cutting. Synovium sections were Haematoxylin and eosin-stained to assess the level of synovitis, and was determined by three components of synovitis: lining layer hyperplasia, activation of resident cells (stroma) and inflammatory infiltrate. Whereby a higher score denotes a greater severity of synovitis.

*4.2.2.3. Extracellular Vesicle Isolation – Differential Ultracentrifugation*

As previously described in section 4.1.2.4.

*4.2.2.4. Nanoparticle Tracking Analysis*

As previously described in section 4.1.2.5.

*4.2.2.5. Transmission Electron Microscopy*

As previously described in section 4.2.1.2.4.

*4.2.2.6. ExoView Characterisation*

As previously described in section 4.4.1.1.2.3.

*4.2.2.7. Raman Spectroscopy and Optical Photothermal Infrared Spectroscopy*

As previously described in section 4.2.1.1.4.

*4.2.2.8. Statistical Analysis*

As previously described in section 4.2.1.2.7.

### **4.3. Proteome and Phospholipidome Interrelationship of Synovial Fluid-derived Extracellular Vesicles in Equine Osteoarthritis: An Exploratory ‘Multi-Omics’ Study to Identify Composite Biomarkers**

#### **4.3.1. Main Study**

##### *4.3.1.1. Ethical Considerations*

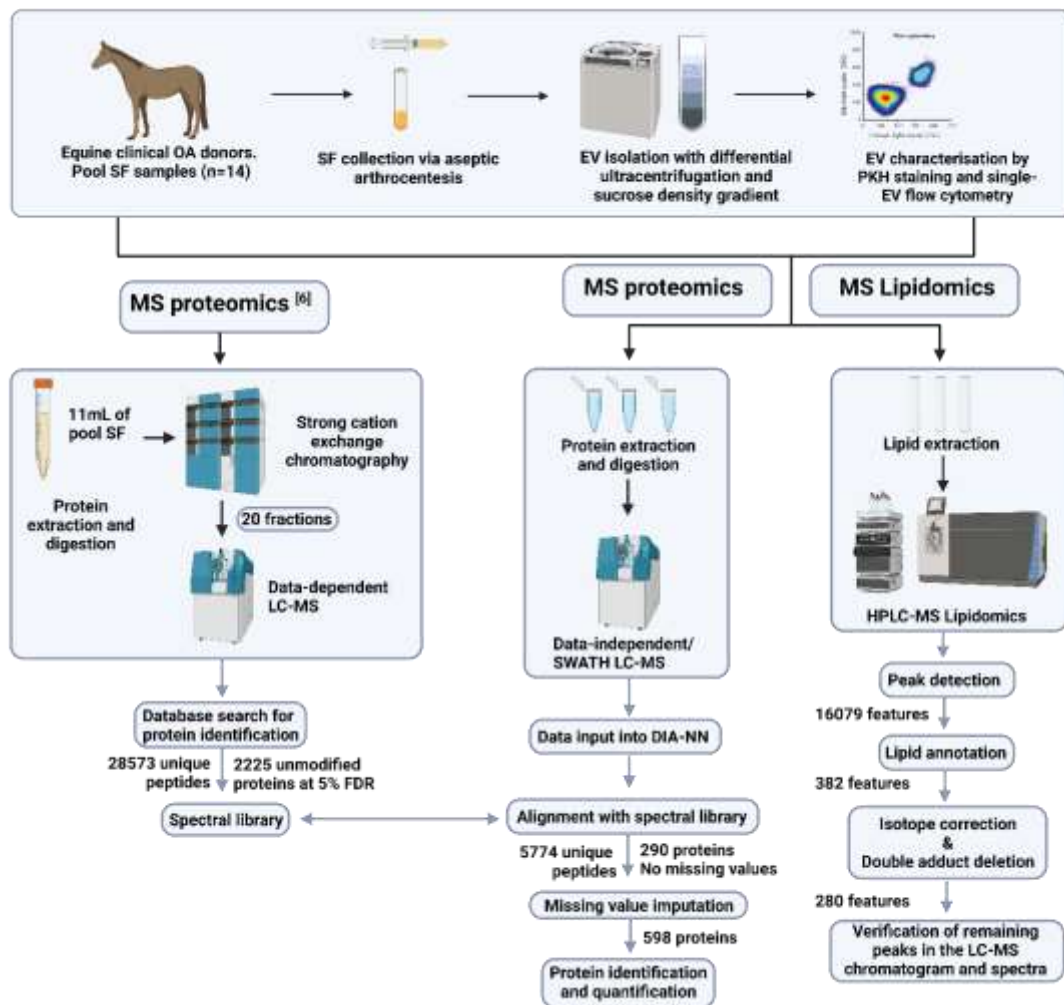
Equine SF was collected from horses at a veterinary clinic (EQUI VET SERWIS) in Buk, Poland, with various disorders of the locomotor system before the intra-articular application of a local analgesic as a standard part of the clinical lameness examination. Sample collection was approved by the University of Liverpool’s Veterinary Research Ethics Committee (VREC1180). Ethical approval was not required in Poland, as the procedures were considered non-experimental clinical veterinary practices, in accordance with the Polish and EU law (Dz. U. 2015 poz. 266 and 2010-63-EU directive).

##### *4.3.1.2. Sample Collection*

SF was collected via aseptic arthrocentesis from the metacarpophalangeal joint into a plain Eppendorf tube. Samples were centrifuged at 2,540  $\times g$  at 4°C for 5 minutes. The supernatant was then transferred to a new Eppendorf tube, snap-frozen in liquid nitrogen and stored at -80°C.

OA was diagnosed based on clinical examination, including subjective lameness scoring according to the American Association of Equine Practitioners (AAEP) lameness scale, radiographic imaging and diagnostic analgesia. Classification as “mild OA” – a mild form of the disease (minor lesions, e.g. small osteophytes and limited subchondral bone sclerosis) and “severe OA” – a severe form of the disease (bone deformation, clear subchondral bone sclerosis, narrowing of joint space and formation of larger osteophytes) was based on radiography; radiographic examples of each OA phenotype are shown in Supplementary Table 9.2. The horses with no lesions in the joints (which featured locomotor abnormalities caused by disorders of other structures) were classified as horses with healthy joints. Three biological replicates were pooled per experimental sample resulting in 5ml of SF. Pooled samples came from horses with healthy joints or joints with the same disease severity. Donors for the pooled samples were randomised with respect to age and sex. A total of 42 donors were used, resulting in 14 pooled samples (Healthy joints n=7, mild OA n= 4, and severe OA n= 3). An experimental overview is shown in Figure 4.3





**Figure 4.3. Workflow for sample processing.** OA was characterised following clinical and radiographic examinations. SF was collected by sterile arthrocentesis and spun to create cell-free SF. Forty-two donors were used to create 14 samples consisting of a pool of three unique biological samples with a volume of 5mL (Healthy n=7, mild OA n= 4, and severe OA n= 3). EVs were isolated from cell-free SF following differential ultracentrifugation with a sucrose density gradient. EVs were stained using PKH and subsequently characterised following quantitative single EV-based high-resolution flow cytometry.

The EV lipidome was probed following a chloroform and methanol lipid extraction, and mass spectrometry lipidomics was performed using a Fusion Orbitrap MS passing through a heated electrospray ionisation. The peaks were detected based on retention time, exact m/z-ratio, and, if present in at least 3 out of 13 samples (Healthy n=6, OA n=4, Advanced OA n=3). The features were annotated using an in-silico phospholipid database. The features were also selected to account for isotope distribution and adducts.

#### 4.3.1.3. Extracellular Vesicle Isolation

4.3.1.3.1. *Differential centrifugation.* EVs from SF were isolated using a published and validated method (Boere, van de Lest, *et al.*, 2016). First, the pooled cell-free SF samples (5 ml) were incubated at 37 °C for 15 minutes with HYase (5 mg/ml; HYase type II from sheep testes, Sigma- Aldrich, St. Louis, USA) while vortexing every 5 minutes. Next, (protein) aggregates and debris were removed by centrifuging at 1,000 $\times$ g for 10 minutes at room temperature (RT) (Avanti J-15R; Beckman Coulter Inc., Brea, USA). Next, the supernatants were transferred into SW40 tubes (Beckman Coulter Inc., Brea, USA) and mixed with phosphate-buffered saline (PBS) to a volume of 12 ml, and centrifuged at 10,000 $\times$ g for 35 minutes (8,900 rpm; RCF average 10,003 $\times$ g; RCF max 14,088 $\times$ g; k-Factor 2,771), followed by 100,000 $\times$ g for 65 minutes (28,000rpm; RCF average 99,004 $\times$ g; RCF max 139,439 $\times$ g; k-Factor 280). The 40 Ti Beckman Coulter rotors were used in an Optima™ L-90K or Optima™ XPN-80 ultracentrifuges. EV pellets were resuspended in 300  $\mu$ l PBS+0.1% Bovine Serum Albumin (BSA) EV-depleted (previously depleted of EVs and protein aggregates).

4.3.1.3.2. *Sucrose density gradient.* EV pellets were thoroughly mixed with 1.2 ml 2.5 M sucrose solution (J.T. Baker; Phillipsburg, USA) in a new SW40 tube and overlaid with fourteen sucrose solutions of decreasing density (from 2 M to 0.4 M), creating a discontinuous sucrose gradient. Gradients were centrifuged at 200,000 $\times$ g for 16 hours at 4 °C in an SW40-Ti rotor (39,000rpm; RCF average 192,072 $\times$ g; RCF max 270,519 $\times$ g;  $\kappa$ -factor 144.5). Twelve fractions of 1 ml were collected from the top (lowest density) to the bottom (highest density). Fraction densities were determined by refractometry. EV-containing fractions were pooled (densities between 1.10-1.16 g/ml) and pipetted into SW32 ultracentrifuge tubes for lipidomics and SW60 for proteomics analysis. EVs were pelleted by centrifugation for 95 minutes at 120,000 $\times$ g at 4°C (SW32 Ti. 32,000rpm ; RCF average 127,755 $\times$ g; RCF max 174,899 $\times$ g; k-Factor 204, or SW60 Ti, 35,000rpm; RCF average 125,812 $\times$ g; RCF max 165,052 $\times$ g; k-Factor 133). Subsequently, EVs for lipidomics were resuspended in 100  $\mu$ l of PBS. For proteomics, dried EV pellets were snap-frozen immediately at - 20°C for later analysis.

Relevant data regarding the experimental details for EV isolation and characterisation have been submitted to the EV-TRACK knowledgebase (EV-TRACK ID: EV230607) (Van Deun *et al.*, 2017b).

#### 4.3.1.4. Single-Extracellular Vesicle-based High-resolution Flow Cytometry

4.3.1.4.1. *Labelling of extracellular vesicle pellets with PKH67.* Generic fluorescent staining of EVs was performed with the PKH67 labelling kit (Sigma-Aldrich, St. Louis, USA). EV pellets were resuspended in 20  $\mu$ l PBS+0.1% BSA EV-depleted with 30  $\mu$ l diluent C. Then, 50  $\mu$ l of diluent C with 1.5  $\mu$ l of PKH67 dye were added. The staining process was halted by adding 50  $\mu$ l of EV-depleted RPMI/10% FBS

(Roswell Park Memorial Institute/fetal bovine serum) after 3 min of incubation at room temperature. Next, the labelled EVs were combined with 2.5 M sucrose to continue the previously described density gradient ultracentrifugation process for EV separation in section 6.3.3. Throughout the whole PKH67 labelling and sucrose gradient ultracentrifugation process, a procedural control sample (20  $\mu$ l PBS+0.1% BSA EV-depleted +30  $\mu$ l diluent C, without sample EVs) was used as a control sample for high-resolution FCM.

*4.3.1.4.2. Single extracellular vesicle-based high-resolution flow cytometry analysis.* An optimised BD Influx jet-in-air- flow cytometer (Becton Dickinson Biosciences, San Jose, CA, USA) fully tailored for single EV analysis was employed (van der Vlist *et al.*, 2012; Arkesteijn *et al.*, 2020). In short, a workspace was loaded that had the optimised PMT parameters and pre-defined gates for the detection of 200 nm yellow-green (505/515) FluoSphere beads (Invitrogen, F8848). After the fluid stream and lasers were aligned, the 200 nm bead population had to fulfil the requirements of pre-defined mean fluorescent intensity and scatter values inside these gates while exhibiting the lowest coefficient of variation for side scatter, forward scatter, and FL-1 fluorescence. All measurements in this study used the same fluorescent threshold level, which was established by running a clean PBS sample and allowing an event rate of <20 events/ second. All samples were run for a fixed period of 30 seconds. The EV concentration was calculated based on the number of fluorescent events detected and normalised for the flow rate of 12.8  $\mu$ l/minute, dilution factor and measurement time. The final EV concentration per ml of SF was determined for the EV-enriched sucrose fractions F7–F10 (densities 1.10 g/ml–1.16 g/ml), adjusted based on the SF starting volume. The procedural control sample revealed no noteworthy background events (<500 events/ 30 secs) in gradient fractions of interest (data not shown).

The BD FACS Software v1.0.1.654 (BD Biosciences, San Jose, CA, USA) was used to collect the data, and the FlowJo v10.07 software (FlowJo, Ashland, OR, USA) was used for analysis. The MIFlowCyt author checklist can be found on Supplementary Table 10.3 and the MIFlowCyt-EV framework on Supplementary Table 10.4 (Welsh *et al.*, 2020).

#### *4.3.1.5. Lipidomic Analysis*

*4.3.1.5.1. Lipid extraction.* Lipids were extracted following the Bligh & Dyer method (Bligh and Dyer, 1959) with slight modifications. First, 0.7 ml of fresh deionised water was mixed with 100  $\mu$ l of samples, 2 ml methanol, and 1 ml chloroform. The samples were incubated for 20 minutes, then 2 ml chloroform and 2 ml of deionised water were added, and the mixture was vortexed. The resultant hydrophilic and hydrophobic phases were separated by centrifugation at RT for 5 minutes at 2,000xg. The hydrophobic bottom phase was transferred to a new conical glass tube. The extraction of the

remaining sample (hydrophilic phase) was repeated with an additional 2 ml of chloroform to ensure that all lipids were collected. The samples were dried under nitrogen gas injection and stored in a nitrogen atmosphere at -20 °C. During the lipid extraction, one sample from healthy joints was lost. Therefore, n=6 SF-EV samples of the group with healthy joints were used for all lipidomics analyses and subsequent omics integration.

*4.3.1.5.2. Mass spectrometry lipidomics.* Dried lipid pellets were resuspended in 30 µL chloroform/methanol (1:1) and analysed as described previously (Jeucken *et al.*, 2019; Varela *et al.*, 2023). A quality control sample composed of all samples in the same ratio together with the SPLASH® Lipidomix® Mass Spec Standard (Avanti Polar Lipids, Inc., Alabaster, USA) was created for subsequent lipid quantification and added in the MS run. A hydrophilic interaction liquid chromatography (HILIC) column (2.6 µm Kinetex HILIC 100, 50 x 4.6 mm, Phenomenex, Torrance, USA) was loaded with 10 µL of lipid extract. Gradient elution on an Agilent 1290 InfinityII UPLC (Agilent, CA) separated the lipid classes. Solvent A consisted of acetonitrile/acetone (9:1) with 0.1% formic acid, and solvent B was composed of acetonitrile/H<sub>2</sub>O (7:3) with 0.1% formic acid and 10 mM ammonium formate. The gradient profile was: minute 0 to 1: 100% A; minute 1 to 3: 50% A + 50% B; minute 3 to 5: 100% B, with a 1 mL/min flow rate. Without further re-equilibration of the column, samples were injected.

The samples were analysed with a Fusion Orbitrap MS (ThermoFisher Scientific, Waltham, USA) via a heated electrospray ionisation (HESI) source with the following parameters: negative ion spray voltage, 3.6 kV; aux sheath gas flow rate, 54Arb; gas flow rate, 7Arb; sweep gas flow rate, 1Arb; ion transfer tube temperature, 350°C; vaporiser temperature, 450°C; scan range, 350–950 m/z at a resolution of 120,000.

*4.3.1.5.3. Lipid annotation.* The msconvert ProteoWizard (Chambers *et al.*, 2012) was used to convert the RAW format to mzML with the “peakPicking filter vendor msLevel = 1-” parameter selected. The package XCMS version 3.10.2 (Benton, Want and Ebbels, 2010) was used to perform LC/MS peak-picking, sample-grouping, and retention time correction on the mzML files running under R version 4.1.2. The identified LC/MS peaks (features) were annotated based on retention time, exact m/z-ratio, and, if present in at least 3 out of 13 pooled samples (Healthy n=6, OA n=4, Advanced OA n=3), MS peaks were annotated using an *in-silico* phospholipid database. The features were also selected to account for isotope distribution and adducts. The RAW and mzML converted mass spectrometry data is deposited in the YODA repository of Utrecht University (Varela, Clarke and van de Lest van Weeren A4 - Marca, Wauben A4 - Mandy, Peffers, 2023).

#### 4.3.1.6. Proteomic Analysis

4.3.1.6.1. *Protein extraction.* As previously described in section 4.1.1.1.3.

4.3.1.6.2. *SDS PAGE & silver stain.* As previously described in section 4.1.2.8.

4.3.1.6.3. *On bead digestion.* Hydrophilic and hydrophobic magnetic beads were used for EV protein digestion in order to remove the urea lysis buffer that was not compatible with downstream analysis. Beads were suspended within the lysed EV samples in order for extracted EV proteins to bind to the surface of the bead, and thus a tryptic digest was performed on bead. Digestion was performed as described in section 4.1.2.9.

4.3.1.6.4. *Data-dependent acquisition for the generation of an equine SF EV spectral library.* As described in section 4.1.2.10.

4.3.1.6.5 *Data-independent acquisition proteomics (SWATH).* As described in section 4.1.2.11. The mass spectrometry proteomics data were deposited to the ProteomeXchange Consortium via PRIDE proteome exchange (Perez-Riverol and Csordas, 2019) (identifier PXD042765). Both proteomics and lipidomics datasets have been submitted to vesiclepedia (Pathan *et al.*, 2019).

#### 4.3.1.7. Statistical Analysis

4.3.1.7.1. *EV characterisation.* EV concentration (particles/mL) was compared between healthy OA groups using a student's t-test to determine statistical significance in the number of EVs identified between groups. Representative healthy SF-EV samples (n=3) and OA samples (i.e. mild OA n=2 and severe OA n=1, each consisting of SF-derived from three different OA-diagnosed horses with the respective severity degree of OA) were used in order to perform statistical analysis. Statistical significance was attributed to  $p < 0.05$ .

4.3.1.7.2. *Proteomics.* Statistical analysis of proteomics data was carried out using the R programming environment version 4.1.2 (RStudio, 2020) or Metaboanalyst (Pang *et al.*, 2021). The data were quality controlled; proteins with complete observations were normalised using probabilistic quotient normalisation (PQN) and log-transformed (base 10) for downstream analysis. Unsupervised multivariate analysis in the form of principal component analysis (PCA) was performed, along with heat map analysis using analysis of variance (ANOVA) and Pearson distance. Statistical significance by ANOVA was attributed to proteins with a p-value  $< 0.05$ . A post-hoc test was also performed in order to identify significant experimental group comparisons. Following ANOVA, a fold change analysis was conducted.

**4.3.1.7.3. Lipidomics and omics data integration.** For lipidomics analysis, the data were normalised based on the sum of total lipids per pool sample – i.e. each lipid value in a pooled sample was divided by the total sum of lipids in the same pool sample and multiplied by 0.01; thus, the relative abundances sum up to 100. A minimum of three biological-pool replicates were used for statistical analyses.

Data analysis was run with R version 4.1.2 (RStudio, 2020). Pareto scaling was performed for the PCA, thus dividing each variable by the square root of its standard deviation. Heatmap and cluster analysis was performed on Spearman correlations with a set speed of two – among the 50 most abundant lipid species in all sample groups – using the R-package ComplexHeatmap v1.12.0 (Gu, Eils and Schlesner, 2016).

Data integration was performed with the R package MixOmics v6.12.2. (Rohart *et al.*, 2017) on lipidomic and proteomics data normalised by the sum (as described for lipidomics analysis) followed by R scaling and centring, which determines the vector's mean and standard deviation, deducts the mean from the vector and divides it by the standard deviation. An unsupervised sparse Partial Least Squares (a linear, multivariate regression method for data reduction to assess the relationship between independent and dependent variables) was used to integrate the datasets. The relevance network plot was set with a correlation cut off of 0.7 to allow readability of the displayed proteins and phospholipids. Differences between the proposed proteins and phospholipid percentages for the composite biomarker were analysed with the rank-based non-parametric Kruskal-Wallis test, followed by the multiple pairwise comparisons with Dunn's test. Significance was defined as p-value < 0.05. Statistical tests were done with GraphPad Prism 9.

#### **4.3.1.8. Functional Enrichment Analysis**

Functional enrichment analysis was performed on all proteomic data using Ingenuity Pathway Analysis (IPA, v2.1; Qiagen, Hilden, The Netherlands) in order to provide functional analyses, networks, canonical pathways, and related molecular and pathological functions by using protein p-values from ANOVA followed by a post hoc test, and associated log<sub>2</sub> fold change. UniProt\_Horse accession codes were used as protein identifiers, and the Qiagen Ingenuity Knowledge Base was used as a reference for exploratory pathway analysis. For network generation, default settings were used to identify molecules whose expression was significantly differentially regulated. These molecules were overlaid onto a global molecular network contained in the Ingenuity Knowledge Base. Networks of 'network-eligible molecules' were then algorithmically generated based on their connectivity. The functional analysis identified the biological functions and diseases that were most significant to the data set. A right-tailed Fisher's exact test was used to calculate p-values. Canonical pathway analysis identified the pathways from the IPA library that were most significant to the data set. Analysis was performed

on significant proteins following ANOVA and post hoc Tukey test analysis, comparing healthy, mild OA and severe OA groups. A second analysis was conducted on proteins correlated to phospholipids.

#### **4.4. Allogenic Platelet-rich Plasma and Platelet-rich Plasma Extracellular Vesicles Change the Proteome of Tenocytes in an In Vitro Equine Model of Tendon Inflammation, Resulting in the Identification of Potential Molecular Modes of Action of platelet-rich Plasma: A Pilot Study**

##### **4.4.1. Preliminary Studies**

###### **4.4.1.1. Optimisation of an In Vitro Inflammatory Model to Study Equine Tendon Injury**

###### *4.4.1.1.1. Tenocyte Collection*

The tenocytes were isolated from the SDFT of a three-year-old and two five-year-old horses (n=3), obtained from University of Liverpool Veterinary Biobank (VREC561). A 2cm mid-section piece of tendon was removed using a scalpel, maintaining sterile conditions.

###### *4.4.1.1.2. Tissue Culture*

The tendon segments were cut into smaller 0.2cm sections and suspended in Dulbecco's Modified Eagle's Medium (DMEM) (Invitrogen, Paisley, UK) complete (low glucose DMEM (Gibco,UK), 10% foetal calf serum, 100 units/mL penicillin (Invitrogen, Paisley, UK), 100mg/mL streptomycin (Invitrogen, Paisley, UK) and 500 ng/mL amphotericin B (BioWhittaker, Lonza, USA) supplemented with 1mg/mL type II collagenase (Worthington Laboratories, USA). The tendon pieces were incubated at 37°C in a shaking incubator overnight. Undigested tendon was removed using a 70µm cell strainer and centrifuged at 2400rpm for 15 minutes. The subsequent cell pellet was then placed in media and the number of cells were counted using a haemocytometer. Tenocytes were then seeded into T75 flasks at  $1.5 \times 10^6$  cells/cm<sup>2</sup> and kept in a 37°C incubator in hypoxic conditions. Cytokines were added once cells reached 75% confluence.

###### *4.4.1.1.3. Cytokine and Transforming Growth Factor-β Treatment*

All experiments were undertaken in serum-free DMEM complete media. Equine SDFT derived tenocytes were treated with cytokines in a 12-well plate at 70,000 cells/cm<sup>2</sup> in four conditions: (1) control (2) IL-1β, (3) IL-1β + TNF-α, (4) IL-1β + TGF-β, all at a concentration of 10ng/mL for 24 hours. Cytokines were provided by R&D systems (Abingdon, Oxfordshire, United Kingdom) was added to determine its ability to counter changes in gene expression. A control condition for each donor was included with no cytokine added. Following treatment tenocyte samples were washed with PBS and suspended in 500 µl Trizol (Invitrogen, Paisley, UK) and scraped. The subsequent cellular suspension in Trizol was stored at -80°C for later RNA extraction.



#### 4.4.1.1.4. Ribose Nucleic Acid Extraction

A phased extraction technique was used as outlined in section 2.8. Samples were cleaned up using RNeasy™ Mini column including a DNase step using manufacturer's instructions (Qiagen, UK). A nanodrop spectrophotometer was used to determine the RNA concentration and purity. Samples were stored at -80°C.

#### 4.5.1.1.5. Complementary Deoxyribose Nucleic Acid Synthesis

cDNA was made from 1ng/μL RNA diluted with RNase-free water added in a 10-fold dilution with one-part random primer (Eurogentec, Belgium). To denature the RNA; this was then thermocycled at 70°C for 5min, then left at 40°C until placed on ice for annealing. 8μL master mix, containing 1μL reverse transcriptase, 5μL 5x buffer and 2μL dNTP mix per sample, was then added to each sample. Samples were subjected to 37°C for 60min then 95°C for 10min for transcription. This mix was diluted using 132μL of RNase-free water to get a final volume of 150μL of cDNA stock per sample.

#### 4.4.1.1.6 Reverse Transcription- quantitative Polymerase Chain Reaction

Primer sequences are listed in Table 4.2. Primer master mixes containing 2μL combined forward and reverse primer (Eurogentec, Belgium), 10μL Takyon™ No ROX SYBR 2X MasterMix blue dTTP (Eurogentec, Belgium) and 3μL RNase-free water per gene: Gapdh (Glyceraldehyde 3-phosphate dehydrogenase) (housekeeper), mmp3, col1a1 (Type I collagen alpha chain 1), IL-6 (Interleukin 6), mmp13, Comp (Cartilage Oligomeric Matrix Protein), Acan (Aggrecan), col1a2 (Type 1 collagen alpha chain 2). Each sample was run in triplicate technical replicates on a 96-well plate. 5μL aliquots were amplified by PCR in 20mL reaction volumes on a Lightcycler 96. Instrument settings were set to manufacturer's instructions: preincubation for 2min at 95°C, denaturation for 10s at 95°C and data collection for 60s at 60°C.

**Table 4.2 A list of the primers and subsequent primer sequences used for this study.**

Gene	Primer sequence
GAPDH	Forward: GCATCGTGGAGGGACTCA
	Reverse: GCCACATCTTCCCAGAGG
MMP3	Forward: TCTTGCCGGTCAGCTTCATATAT
	Reverse: CCTATGGAAGGTGACTCCATGTG
MMP13	Forward: GAGCATCCTCCCAAAGACCTT
	Reverse: CATAACCATTAAGAGCCCAAAT
COL1A1	Forward: TGCCGTGACCTCAAGATGTG
	Reverse: CGTCTCCATGTTGCAGAAGA
COL1A2	Forward: GCACATGCCGTGACTTGAGA
	Reverse: CATCCATAGTCATCCTTGATTAGG

*Abbreviations – Glyceraldehyde-3-phosphate dehydrogenase (GAPDH), matrix metalloproteinase 3(MMP3), matrix metalloproteinase 13 (MMP13), collagen 1 alpha 1(COL1A1), collagen 1 alpha 2 (COL1A2)*

#### *4.4.1.1.7 Statistical Analysis*

Normality was checked using a Shapiro-Wilk test at a threshold of ( $p < 0.05$ ). The data for COL1A1 and MMP13 was normally distributed so an ANOVA and pairwise comparisons test were used. For MMP3 and COL1A2, the data was not normally distributed, so a Kruskal Wallis test followed by Benjamini Hochberg false discovery rate correction was used.

#### **4.4.1.2 Determination of the most appropriate Platelet-rich Plasma Extracellular Vesicle Concentration to use in an In Vitro Equine Tendon Inflammatory Model**

##### *4.4.1.2.1. Tenocyte Collection*

As previously described in section 4.4.1.1.1.

##### *4.4.1.2.2. Tissue Culture*

As previously described in section 4.4.1.1.2

##### *4.4.1.2.3. Whole Blood Collection*

Venous whole blood was collected from an abattoir (VREC561) from equine donors ( $n=3$ ). 55ml of whole blood was collected in acid citrate dextrose tubes (ACD-A). Samples were inverted and kept at room temperature until PRP isolation. Samples were collected from an abattoir as a by-product of the agricultural industry and processed within 12 hours of euthanasia. The Animals (Scientific Procedures) Act 1986, Schedule 2, does not define collection from these sources as a scientific procedure.

##### *4.4.1.2.4. Platelet-rich plasma Isolation & Characterisation*

PRP was isolated using the V-PET Equine Platelet Enhancement Therapy System (Vet Stem Biopharma, Poway, California). The V-Pet system was flushed with the 9ml of capture solution. Following this 55ml of anticoagulated whole venous blood was transferred into the V-PET system and mixed well with the capture solution (clinical sterile water). The V-PET system was then hung in a vertical position and the

samples allowed to filter through to the lower aspect of the system. 8ml of hypertonic saline (2% sodium chloride (NaCl)) harvest solution was then flushed through in order to collect the platelet concentrate. The 8ml platelet concentrate (PRP) was then collected. Whole blood samples and PRP from samples from each of the three donors were analysed using a IDEXX ProCyte Dx haematology analyser (IDEXX, Hoofddorp, the Netherlands) in order to obtain a full blood profile and ensure PRP has >2x platelet count than baseline whole blood values (Fortier, 2010; Parrish *et al.*, 2016).

#### *4.4.1.2.5. Extracellular Vesicle Isolation*

Equine PRP samples (50µl and 100µl) underwent differential ultracentrifugation (dUC) in order to isolate EVs, as described in section 4.1.2.4.

#### *4.4.1.2.6. Cytokine Treatment*

As previously described in section 4.4.1.1.3.

#### *4.4.1.2.7. Platelet-rich Plasma Derived Extracellular Vesicle Treatment*

Following cytokine treatment (IL-1 $\beta$  + TNF $\alpha$ ) for 24 hours, tenocytes were washed with sterile PBS three times and treated with foetal bovine serum depleted Dulbecco's Modified Eagle's Medium (DMEM) (Invitrogen, Paisley, UK) complete (low glucose DMEM (Gibco,UK), 10% foetal calf serum, 100 units/mL penicillin (Invitrogen, Paisley, UK), 100mg/mL streptomycin (Invitrogen, Paisley, UK) and 500 ng/mL amphotericin B (BioWhittaker, Lonza, USA). Cells were then treated accordingly platelet-rich plasma extracellular vesicles (PRP-EVs) derived from 100µl of PRP or 50µl of PRP. Cell were treated with such EV treatments for 24 hours, then harvested for gene expression analysis.

#### *4.4.1.2.8. Ribose Nucleic Acid Extraction*

As previously described in section 4.4.1.1.4.

#### *4.4.1.2.9. Complementary Deoxyribose Nucleic Acid Synthesis*

As previously described in section 4.4.1.1.5.

#### *4.4.1.2.10. Reverse Transcription-quantitative Polymerase Chain Reaction*

As previously described in section 4.4.1.1.6. Primer used can be found in Table 4.2.

#### *4.4.1.2.11. Statistical Analysis*

Gene expression analysis was performed using RT-qPCR on protein coding genes (MMP3, MMP13, COL1A1 and COL1A2). Data was processed using relative quantification and GAPDH served as an internal housekeeping gene. Subsequently data was then analysed in GraphPad prims software. Gene expression data was subject to shapiro-wilks normality testing, and upon confirmation of gaussian distribution experimental groups were compared using a one-way ANOVA with multiple comparisons and a post-hoc Tukey test.

### **4.4.2. Main Study**

#### *4.4.2.1. Sample Collection*

Tenocytes were extracted from SDFT tendons (n=6) collected under ethical approval and owner consent for tissue use in research (VREC561). These were sourced from Thoroughbreds (n=5) and Irish Sports horses (n=1). Within the study four mares and two geldings were included with a mean age of 11.2 (standard error of the mean, SEM = +/-2.2) years old.

#### *4.4.2.2. Whole Blood Collection*

Venous whole blood was collected as described in section 4.4.1.2.3.

#### *4.4.2.3. Platelet-rich plasma Isolation & Characterisation*

PRP was isolated using the V-PET Equine Platelet Enhancement Therapy System (Vet Stem Biopharma, Poway, California), as described in 4.4.1.2.4.

#### *4.4.2.4. Extracellular Vesicle Isolation*

Equine PRP and plasma samples (100 µl) underwent differential ultracentrifugation (dUC) in order to isolate EVs, as described in section 4.1.2.4. All isolation and characterisation procedures followed were uploaded to the EV-TRACK database; EV-TRACK ID EV230986.

#### 4.4.2.5. Extracellular Vesicle Characterisation – Exoview

The ExoView platform (NanoView Biosciences, Malvern Hills Science Park, Malvern) was used to determine EV concentration, surface marker identification (CD9, CD81 and CD63) and to perform fluorescent microscopy and tetraspanin colocalisation analysis on selected samples, as previously described in section 4.1.1.2.3.

#### 4.4.2.6. Cell Isolation

SDFT explants were dissected from the forelimbs of donors. Tendon explants were collected in sterile Dulbecco's modified eagle medium (DMEM) (Sigma-Aldrich, Dorset, UK) supplemented with penicillin and streptomycin (P/S) (100 units/ml penicillin, 100 mg/ml streptomycin) (all from Invitrogen, Paisley, UK). Explants were cut into small pieces and suspended in type II collagenase (1mg/ml) prepared in complete media, (DMEM, phenol red, 10% foetal bovine serum (FBS), P/S (all from Invitrogen, Paisley, UK) and amphotericin B (Bio Whittaker, Lonza, USA), and incubated horizontally at 37°C in a shaking

incubator overnight. The cellular suspension was then passed through a 70µm cell strainer and centrifuged at 2400RPM for 15 minutes to retrieve the cellular pellet. The cellular pellet was resuspended in complete media and a cell count was performed using a haemocytometer. Tenocytes were then seeded in T-75 flasks at approximately  $0.5-1 \times 10^6$  cells per flask (seeding density (SD) of 20,000 cells/ cm<sup>2</sup>) and incubated at 37°C in a hypoxic incubator (a humidified environment at 37°C and 5% carbon dioxide and 5% oxygen) until 80% confluent. The required number of tenocytes were subsequently used in the *in vitro* experiment and remaining tenocytes were then centrifuged at 2400rpm, media was removed and replaced with 10% dimethyl sulfoxide (DMSO) media, frozen at -80°C and then transferred to liquid nitrogen.

#### 4.4.2.7. In Vitro Experimental Design

Equine tenocytes were seeded into 12 well plates at a SD of 10,000 cells/cm<sup>3</sup> at passage 3 (P3). Equine tenocytes (P3) were grown in 12 well plates in phenol red-free, complete media with the addition of L-glutamine until 70% confluent. Nine plates were used in total, six for technical duplicates for qPCR analysis and three for proteomic analysis. Upon confluency cells were washed in PBS and serum starved for 24 hours. From this point on media was not supplemented with FBS. Following this, tenocytes were treated with cytokines; 10 ng/ml of IL-1β and TNF-α (Recombinant Equine IL-1β, R&D Systems, Abingdon, UK) for 24 hours.

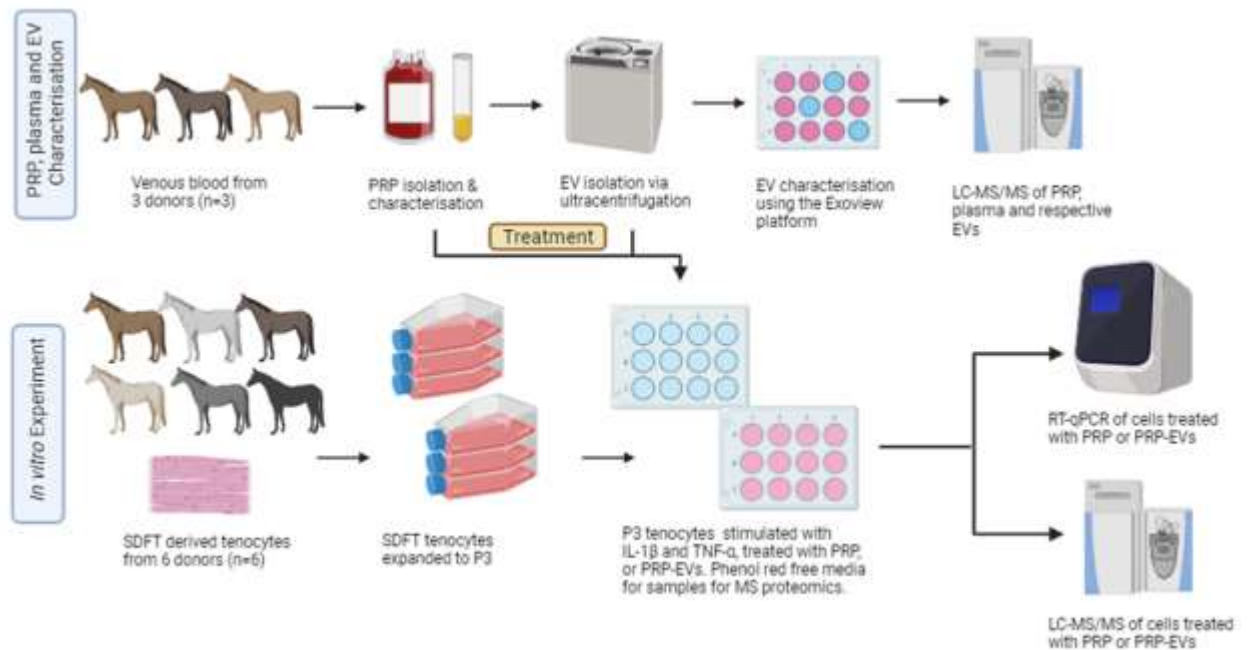
This was chosen following preliminary studies, as shown in section A.7.10.1, Appendix 1. Cells received no treatment (control) or were treated with PRP (100µl) and PRP- EVs (EVs derived from 100µl of PRP, (~500,000 EVs per µl), (3.3%(v/v%)) accordingly and incubated for 24 hours at 37°C in hypoxic conditions. PRP and PRP-EV dose were selected based on previous preliminary studies as shown in A.7.10.2, Appendix 2. It should be noted that PRP was treated with 100 U/ml heparin(U) prior to use in tissue culture to prevent coagulation. The experimental groups for this study are as outlined in Table 4.3.

Tenocyte samples were collected as follows; for RNA, cells were washed with PBS and suspended in Trizol (Invitrogen, Paisley, UK) and scraped and stored at -80°C for later RNA extraction. Cells for proteomics were also washed, trypsinised as previously described, and cells were counted. Cells were then centrifuged at 2400rpm and stored in 25mM ammonium bicarbonate (AmBic) (Sigma-Aldrich, Dorset, UK) at -80°C. An overview is provided in Figure 4.4

**Table 4.3. An overview of the in vitro experimental design and donor information.**

Donor	Age	Breed	M/G	Control			Cytokine stimulation		
				Control	Control + PRP	Control + PRP EVs	Cytokine stimulation	Cytokine stimulation +PRP	Cytokine stimulation + PRP EVs
1	5	TB	G	→	→	→	→	→	→
2	12	TB	M	→	→	→	→	→	→
3	18	TB	M	→	→	→	→	→	→
4	12	TB	M	→	→	→	→	→	→
5	8	ISH	M	→	→	→	→	→	→
6	9	TB	G	→	→	→	→	→	→

*Abbreviations - platelet-rich plasma (PRP), platelet-rich plasma extracellular vesicles (PRP-EVs), mare (M), gelding (G).*



**Figure 4.4. An overview of the experimental design of the study.** Venous blood from horses (n=3) was used to produce PRP. PRP was characterised, PRP-EVs isolated using differential ultracentrifugation. The subsequent proteome was quantified. The profiled PRP and PRP-EVs were then used in an *in vitro* equine tendon inflammatory model following cytokine stimulation to ascertain the cellular response to PRP and PRP-EVs. This illustration was created in biorender.com.

#### 4.4.2.8. Ribose Nucleic Acid Extraction

RNA was extracted following a chloroform phase extraction protocol (Chomczynski and Sacchi, 1987; Peffers, Liu and Clegg, 2013). As described in section 4.4.1.1.4.

#### 4.4.2.9. Complementary Deoxyribose Nucleic Acid Synthesis

Total RNA (500ng), was made up by diluting RNA samples with RNase free water and cDNA was synthesised as described in section 4.4.1.1.5.

#### 4.4.2.10. Reverse Transcription-quantitative Polymerase Chain Reaction

cDNA was diluted to 5ng/μl and 5μl of sample was pipette per well into a 96 well PCR plate in technical duplicates. Reverse transcription- quantitative polymerase chain reaction was then performed as per section 4.4.1.1.6. Table 4.4 has a list of primers used.

**Table 4.4. A list of equine primers and the corresponding base sequences.**

Gene	Species	Sequence	
GAPDH	Equine	F	GCATCGTGGAGGGACTCA
		R	GCCACATCTCCAGAGG
COL1A2	Equine	F	GCACATGCCGTGACTTGAGA
		R	CATCCATAGTGCATCCTTGATTAGG
IGFBP6	Equine	F	GAACCGCAGAGACCAACAGA
		R	ACGGGCCCATCTCCGT
MMP3	Equine	F	TCTTGCCGGTCAGCTTCATATAT
		R	CCTATGGAAGGTGACTCCATGTG
MMP13	Equine	F	GAGCATCCTCCCAAAGACCTT
		R	CATAACCATTAAGAGCCCAAAATT

*Abbreviations- GAPDH (Glyceraldehyde 3-phosphate dehydrogenase), COL1A2 (collagen type I alpha 2 chain), IGFBP6 (insulin like growth factor binding protein 6), MMP3 (matrix metalloproteinase 3), MMP13 (matrix metalloproteinase 13). F (forward primer) and R (reverse primer).*

#### 4.4.2.11. Protein Extraction

For cellular lysates the supernatant was removed from cells and the cellular pellet was dissolved in 100μl of freshly prepared 25mM AmBic (Sigma Aldrick, Dorset, UK). 7.5U of Benzonase nuclease (Merck Millipore) was added to each sample, in order to increase extraction of proteins. Cellular lysates were then sonicated on ice using a probe sonicator for 3 rounds at 40% maximum of amplitude for 10 seconds with 50 seconds rest. PRP and plasma EVs were processed as described in 4.1.1.1.3.

#### 4.4.2.12. Protein Assay – Pierce 660nm

Total protein quantified following a Pierce 660nm assay. A standard curve was prepared using bovine serum albumin (BSA) between a working range of 50-2000μg/ml. 10μl of each standard and unknown sample was added in triplicate to a microplate. Following this 150μL of the Protein Assay Reagent was added to each well, and the plate was incubated at room temperature on a plate shaker for 1 minute. Then a plate reader (SPECTROstar Nano, BMG LabTech, Ortenberg, Germany) quantified absorbance at wavelength 660nm and protein concentration was calculated based on these values and the standard curve. All reagents were sourced from (Invitrogen, Paisley, UK).



#### 4.4.2.13. Protein Enrichment Using Proteominer™

Proteominer™ columns (Bio-Rad, Watford, UK) were used to dilute high-abundance proteins and concentrate low-abundance proteins in PRP and plasma samples. Proteominer™ columns were used as per manufacturer guidelines. In brief, columns were centrifuged at 1000 $\times$ g for 30 seconds in order to remove the column storage solution. Following this 200  $\mu$ l wash buffer was flushed through each column, and columns were inverted over 5 minutes, the wash buffer was then collected after a 1000 $\times$ g centrifugation for 30 seconds. This wash step was repeated three times. 20 $\mu$ l of beads remained and 1000 $\mu$ l of PRP or plasma, equal to 2.5mg of total protein was loaded onto each Proteominer™ column. Columns were then left to rotate for 2 hours at room temperature on a rotational shaker. After this, the supernatant was removed, and 200  $\mu$ l wash buffer was passed through the column, and collected. Thus sample protein was bound to beads within the column, ready for on bead protein digestion (Anderson, Phelan, Rubio-Martinez, *et al.*, 2020).

#### 4.4.2.14. Protein Digestion of Platelet-rich Plasma Derived Extracellular Vesicles, Plasma Extracellular Vesicles and Cell Lysates

PRP-EVs (10 $\mu$ g), plasma-EVs (10 $\mu$ g) and tenocyte cell lysates (100 $\mu$ g) were trypsin digested in-solution. Samples were processed as described in section 4.1.1.1.5.

#### 4.4.2.15. Label Free Liquid Chromatography Tandem Mass Spectrometry

Data-dependent LC-MS/MS analyses were conducted on a QExactive HF Quadrupole-Orbitrap mass spectrometer (Thermo Scientific, Hemel Hempstead, UK) coupled to a Dionex Ultimate 3000 RSLC nano-liquid chromatograph (Thermo Scientific, Oxford, United Kingdom). Sample digests were loaded onto a trapping column (Acclaim PepMap 100 C18, 75  $\mu$ m  $\times$  2 cm, 3  $\mu$ m packing material, 100 Å) using a loading buffer of 0.1% (v/v) trifluoroacetic acid, 2% (v/v) acetonitrile in water for 7 minutes at a flow rate of 12  $\mu$ l min<sup>-1</sup>. The trapping column was then set in-line with an analytical column (EASY-Spray PepMap RSLC C18, 75  $\mu$ m  $\times$  50 cm, 2  $\mu$ m packing material, 100 Å) and the peptides eluted using a linear gradient of 96.2% A (0.1% [v/v] formic acid):3.8% B (0.1% [v/v][formic acid in water:acetonitrile [80,20] [v/v]) to 50% A:50% B over 120 min at a flow rate of 300 nl min<sup>-1</sup>, followed by washing at 1% A:99% B for 5 min and re-equilibration of the column to starting conditions.

The column was maintained at 40 °C, and the effluent introduced directly into the integrated nano-electrospray ionisation source operating in positive ion mode. The mass spectrometer was operated in DDA mode with survey scans between m/z 350–2000 acquired at a mass resolution of 60,000

(FWHM) at  $m/z$  200. The maximum injection time was 100 ms, and the automatic gain control was set to  $3e6$ . The 12 most intense precursor ions with charges states of between  $2+$  and  $5+$  were selected for MS/MS with an isolation window of 2  $m/z$  units. The maximum injection time was 100 ms, and the automatic gain control was set to  $1e5$ . Fragmentation of the peptides was by higher-energy collisional dissociation.

For label-free quantification, the raw files of the acquired spectra were analysed by the ProgenesisQI™ software (Waters, Manchester, UK). A local Mascot server (Version 2.8.2), was used to identify peptides, searching against the Unihorse Reviewed database with carbamidomethyl cysteine as a fixed modification and methionine oxidation as a variable modification, peptide mass tolerance of 10 ppm and a fragment mass tolerance of 0.01 Da. The mass spectrometry proteomics data have been deposited to the ProteomeXchange Consortium via the PRIDE (Perez-Riverol and Csordas, 2019) partner repository with the dataset identifier PXD046066 and 10.6019/PXD046066.

#### *4.4.2.16. Statistical Analysis*

##### *Platelet-rich Plasma Characterisation*

PRP platelet count was analysed in GraphPad Prism 10.0 (California, United States of America). Mean average platelet count ( $n=3$ ) was compared between PRP and whole blood. Subsequent box plots were made to visualise data and include standard deviation error bars. Normality tests were performed following Shapiro-Wilk analysis, and subsequent T-test analysis was used to determine any statistically significant difference in platelet count.

##### *Extracellular Vesicle Characterisation*

EV concentration and size was quantified using the Exoview Human Tetraspanin Assay. Three technical replicates were analysed in order to ascertain concentration and size. Data was analysed using GraphPad Prism 10 (California, United States of America). Following Shapiro-Wilk normality testing data was subject to a one-way analysis of variance (ANOVA) with multiple comparisons, followed by a *post hoc* Tukey test to ascertain significant concentration and size variation with respect to EV surface marker expression.

##### *Reverse Transcription-quantitative Polymerase Chain Reaction Analysis*

Statistical analysis was performed using GraphPad Prism 10 (California, United States of America). Outlier tests were performed on all gene expression datasets. Following this a two-way ANOVA with

multiple comparisons using a *post hoc* Tukey test was performed and significance was determined with a  $p < 0.05$ .

#### *Platelet-rich Plasma and Platelet-rich Plasma Derived Extracellular Vesicle Proteomic Analysis*

Statistical analysis of proteomics data was carried out using Metaboanalyst V5.0 (Pang *et al.*, 2020). The data were quality controlled; proteins with more than 50% missing observations were removed from the dataset. Unsupervised multivariate analysis in the form of principal component analysis (PCA) was performed, along with T-test and fold change analysis, following Pareto scaling of data. P values ( $p < 0.05$ ) were corrected for multiple testing resulting in acquiring q-values. Statistical significance was attributed to proteins with a q-value  $< 0.05$  following a T-test.

#### *Cellular Proteomic Analysis Following Platelet-rich Plasma or Platelet-rich Plasma Derived Extracellular Vesicle Treatment*

Statistical analysis of proteomics data was carried out using the R statistical programming environment or Metaboanalyst V5.0 (Pang *et al.*, 2021). The data were quality controlled; proteins with 25% or more missing observations were removed from the dataset, as were contaminating blood associated proteins, then remaining data was normalised using probabilistic quotient normalisation (PQN) of the control group and log-transformed (base 10) for downstream analysis. Unsupervised multivariate analysis in the form of a multiple factor PCA was performed. In addition, a two-way ANOVA was performed and a multiple comparison test was used in the form of a *post hoc* Tukey test. Statistical significance was attributed to proteins with an unadjusted p-value  $< 0.05$ .

#### *4.4.2.17. Functional Enrichment Analysis*

Functional enrichment analysis was performed on proteomic data using Ingenuity Pathway Analysis (IPA; Qiagen, Hilden, The Netherlands) in order to provide functional analyses, networks, canonical pathways, and related molecular and pathological functions by using protein p-values and associated log<sub>2</sub> fold change. UniProt\_Horse accession codes were used as protein identifiers, and all identified protein were used as a background reference for exploratory pathway analysis. For network generation, default settings were used to identify molecules whose expression was significantly differentially regulated. These molecules were overlaid onto a global molecular network contained in the Ingenuity Knowledge Base. Networks of 'network-eligible molecules' were then algorithmically generated based on their connectivity. The functional analysis identified the canonical pathways, biological functions and diseases that were most significant to the data set. A right-tailed Fisher's exact test was used to calculate p-values, activation z scores were provided. Canonical pathway analysis

identified the pathways from the IPA library that were most significant to the data set. Analysis was performed using significant ( $p < 0.05$ ) proteins identified following t test comparing PRP to plasma, in order to identify enriched pathways in PRP. Similarly, analysis was performed comparing PRP-EVs to plasma EVs.

## 5. Manuscript 1

### **Temporal Extracellular Vesicle Protein Changes following Intraarticular Treatment with Integrin $\alpha$ 10 $\beta$ 1-selected Mesenchymal Stem Cells in Equine Osteoarthritis**

**Emily J Clarke**<sup>1\*</sup>, Emily Johnson<sup>4</sup>, Eva Caamaño Gutierrez<sup>4</sup>, Camilla Andersen<sup>2</sup>, Lise C Berg<sup>2</sup>, Rosalind E Jenkins<sup>3</sup>, Casper Lindegaard<sup>2</sup>, Kristina Uvebrant<sup>5</sup>, Evy Lundgren-Åkerlund<sup>5</sup>, Agnieszka Turlo<sup>1</sup>, Victoria James<sup>6</sup>, Stine Jacobsen<sup>2</sup> and Mandy J Peffers<sup>1</sup>

<sup>1</sup> University of Liverpool, Institute of Life Course and Medical Sciences, William Henry Duncan Building, 6 W Derby St, Liverpool L7 8TX.

<sup>2</sup> University of Copenhagen, Department of Veterinary Clinical Sciences, Agrovej 8, 2630 Taastrup

<sup>3</sup> University of Liverpool, Centre for Drug Safety Science Bioanalytical Facility, Liverpool Shared Research Facilities, Department of Pharmacology and Therapeutics, Institute of Systems, Molecular and Integrative Biology

<sup>4</sup> University of Liverpool, Computational Biology Facility, Liverpool Shared Research Facilities, Faculty of Health and Life Sciences

<sup>5</sup> Xintela AB, Medicon Village, 223 81 Lund, Sweden.

<sup>6</sup> School of Veterinary Medicine and Science, University of Nottingham, Sutton Bonington, Loughborough LE12 5RD

#### **Key words**

**Equine, Osteoarthritis, Extracellular Vesicles, Biologics, Integrin  $\alpha$ 10 $\beta$ 1-selected MSC Therapy, Proteomics**

#### **Declaration of author contributions**

Conceptualization, **MJP, VJ** and **SJ**.; methodology, **EJC, MP, SJ, CA, LCB, EJ, ECG, RJ, AT**; formal analysis, **EJC, EJ, ECG, RJ, AS**; investigation, **EJC, EJ, RJ**.; data curation, **EJC,RJ, EJ,AS**.; writing—original draft preparation, **EJC**.; writing—review and editing, **EJC, MP, SJ, CA, LB, EJ, ECG, RJ, AS, AT,LCB, CL,KU, ELA** ; visualization, **EJC, RJ, AS, EJ, ECG**.; all authors have read and agreed to the published version of the manuscript.

## 5.1 Abstract

Equine osteoarthritis is a heterogeneous, degenerative disease of the joint with multifactorial causation, characterised by a joint metabolic imbalance. Extracellular vesicles are nanoparticles involved in intracellular communication. Mesenchymal stem cell therapy is a form of regenerative medicine that utilises their properties to repair damaged tissues. Despite its wide use in veterinary practice, the exact mechanism of action of mesenchymal stem cells is not fully understood. The aim of this study was to determine the synovial fluid extracellular vesicle protein cargo following integrin  $\alpha 10\beta 1$ -selected mesenchymal stem cell (integrin  $\alpha 10$ -MSC) treatment in an experimental model of equine osteoarthritis with longitudinal sampling. Adipose tissue derived, integrin  $\alpha 10$ -MSCs were injected intraarticularly in six horses 18 days after experimental induction of osteoarthritis. Synovial fluid samples were collected at day 0, 18, 21, 28, 35, and 70. Synovial fluid was processed and extracellular vesicles were isolated and characterised. Extracellular vesicle cargo was then analysed using data independent acquisition mass spectrometry proteomics. A total of 442 proteins were identified across all samples, with 48 proteins differentially expressed ( $FDR \leq 0.05$ ) between sham-operated control joint without mesenchymal stem cell treatment and osteoarthritis joint treated with mesenchymal stem cells. The most significant pathways following functional enrichment analysis of the differentially abundant protein dataset were serine endopeptidase activity ( $p=0.023$ ), complement activation (classical pathway) ( $p=0.023$ ), and collagen containing extracellular matrix ( $p=0.034$ ). Due to the lack of an osteoarthritis group without mesenchymal stem cell treatment, findings cannot be directly correlated to only mesenchymal stem cells. To date this is the first study to quantify the global extracellular vesicle proteome in synovial fluid following mesenchymal stem cell treatment of osteoarthritis. Changes in the proteome of the synovial fluid-derived extracellular vesicles following mesenchymal stem cell injection suggest extracellular vesicles may play a role in mediating the effect of cell therapy through altered joint homeostasis. This is an important step towards understanding the potential therapeutic mechanisms of mesenchymal stem cell therapy, ultimately enabling the improvement of therapeutic efficacy.

## 5.2 Introduction

Osteoarthritis (OA) is a common disease of the joint, and is the cause of up to 60% of all lameness cases in horses (McIlwraith, Frisbie and Kawcak, 2012a). It is a progressive degenerative pathology of synovial joints and results from an imbalance of catabolic and anabolic processes affecting cartilage and bone remodeling (Ratneswaran, Rockel and Kapoor, 2020). This is associated with pain, reduced mobility and impaired welfare. OA is a complex heterogeneous condition with multiple causative factors, including mechanical, genetic, metabolic and inflammatory pathway activation, with a non-functional joint as the shared endpoint (Thysen *et al.*, 2015). In the disease there is a loss of articular cartilage, reduced elastoviscosity of synovial fluid, thickening of subchondral bone, joint space narrowing and osteophyte formation (Smith *et al.*, 2014). Currently, OA is predominantly diagnosed based on clinical signs and radiographic imaging, capturing changes that are typical of the later disease stages. Treatment is symptomatic, with no current cure available to rescue the joint environment.

Biological cell-based therapies include autologous conditioned serum, platelet-rich plasma, and expanded or non-expanded mesenchymal stem cells (MSCs). These regenerative therapies have the potential to enhance repair of damaged tissues or organs (Bogers, 2018). Mesenchymal stem cell (MSC) therapy most commonly uses cells derived from bone marrow or adipose tissue (Al Naem *et al.*, 2020). They are highly proliferative, plastic-adherent, fibroblast-like cells that express CD44, CD90, CD105 and do not express MHC class II or CD45 (Barberini *et al.*, 2014). MSCs are able to modulate and down-regulate immune system activity, reducing inflammatory cytokines associated with acute inflammation (Carrade *et al.*, 2012). However, MSC preparations display substantial heterogeneity of cell types that varies between donors and between tissue sources, which has led to varying results in tissue regeneration studies (McLeod *et al.*, 2017). Selection of MSCs to generate homogenous MSC preparations thus has the potential to improve the therapeutic outcome of MSC therapies (Johal, Lees and Reid, 2016; Nielsen *et al.*, 2016). Integrin  $\alpha 10\beta 1$ , a collagen-binding receptor originally discovered on chondrocytes (Camper, Hellman and Lundgren-Åkerlund, 1998) is also expressed by MSCs (Varas *et al.*, 2007) and can distinguish MSCs from other cell types in MSC preparations. MSCs selected for the expression of integrin  $\alpha 10\beta 1$  (integrin  $\alpha 10$ -MSCs) have shown improved adhesion to chondral and subchondral lesions in explant studies, improved chondrogenic differentiation ability as well as improved secretion of the immunomodulatory factor prostaglandin E2 (PGE2) *in vitro*, compared to unselected cells (Uvebrant *et al.*, 2019). It has been demonstrated that to mitigate the progression of osteoarthritis in an equine talar impact model such MSCs reduce cartilage fibrillation and subchondral bone sclerosis (Delco *et al.*, 2020). In addition, labelled integrin  $\alpha 10$ -MSCs have been shown to home to cartilage defects in rabbit model after intraarticular administration and to directly participate in the regeneration of the cartilage (C. Andersen, Uvebrant, *et al.*, 2022).

MSC secreted factors are believed to have a critical role in the therapeutic efficacy. Thus, there is a drive to investigate and potentially develop cell-free therapeutics including extracellular vesicles (EVs) that reflect the biophysical characteristic of 'parent' cells (Mocchi *et al.*, 2020). EVs are nanoparticles enveloped in a phospholipid bilayer membrane and are secreted by most mammalian cells. EVs facilitate intercellular communication through the paracrine action of protein, lipid and nucleic acid cargo. EV subtypes, namely microvesicles and exosomes, have been demonstrated to act in a protective manner, but also pathologically, dependent on the 'parent' cell phenotype and subsequent *in vivo* environment (Cvjetkovic *et al.*, 2016; Latifkar *et al.*, 2019). Previous evidence has shown that EVs may at least partially drive the therapeutic effect of MSC treatment, by increasing cellular proliferation and infiltration in exosome-mediated cartilage repair by promoting a regenerative immune phenotype, characterised by higher infiltration of CD163+ macrophages and a reduction in proinflammatory cytokines such as interleukin 1 $\beta$  (IL-1 $\beta$ ) (Zhang *et al.*, 2018), tumour necrosis factor- $\alpha$  (TNF- $\alpha$ ) and interleukin 6 (IL-6) (Tofiño-Vian *et al.*, 2018).

In *in vitro* equine models of OA, it has been found that chondrocytes stimulated with inflammatory cytokines had a reduced inflammatory phenotype following treatment with MSC -EVs. MSC-EVs also have an anti-catabolic effect evidenced by decreased expression of matrix metalloproteinase 13 (MMP-13) (Arévalo-Turrubiarde *et al.*, 2021; Hotham *et al.*, 2021). These observations were conserved across different species. In mice it was demonstrated that MSC-EVs reinduced the expression of chondrocyte markers (type II collagen, aggrecan) but inhibited catabolic (MMP-13) and inflammatory (nitric oxide synthase; iNOS) markers. Thus the authors suggested that MSC-EVs act in a chondroprotective manner by inhibiting apoptosis and macrophage activation (Cosenza *et al.*, 2017b).

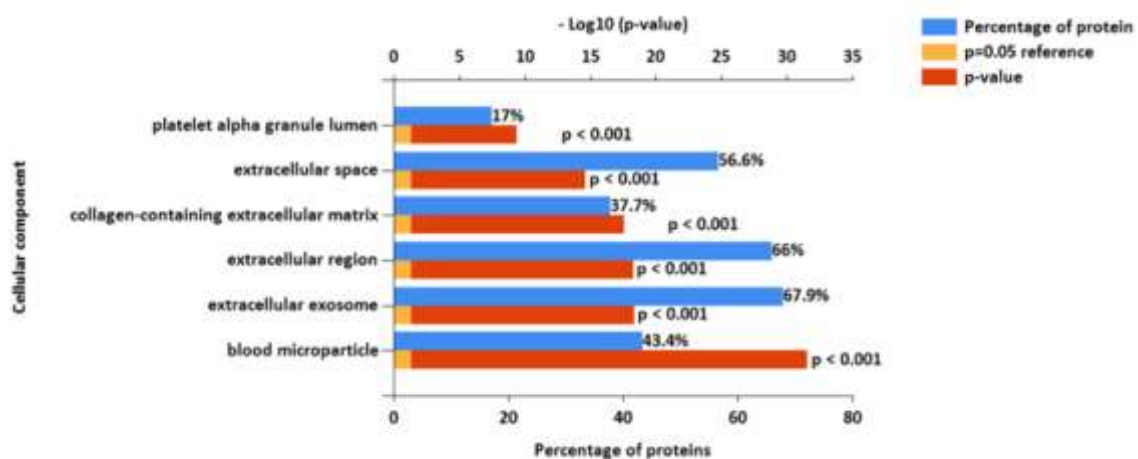
It is paramount to determine the mechanism of therapeutic action of MSCs and determine the contribution of secreted factors such as EVs in rescuing the OA phenotype, with the aim of producing a more targeted treatment. We demonstrate that intraarticular injection of MSCs affects protein cargo of synovial fluid EVs in an equine model of OA, decreasing the expression of proteins associated with pathways related to OA pathogenesis.



### 5.3 Results

#### 5.3.1 Optimisation of Extracellular Vesicle Isolation for Downstream Mass Spectrometry Proteomics Analysis

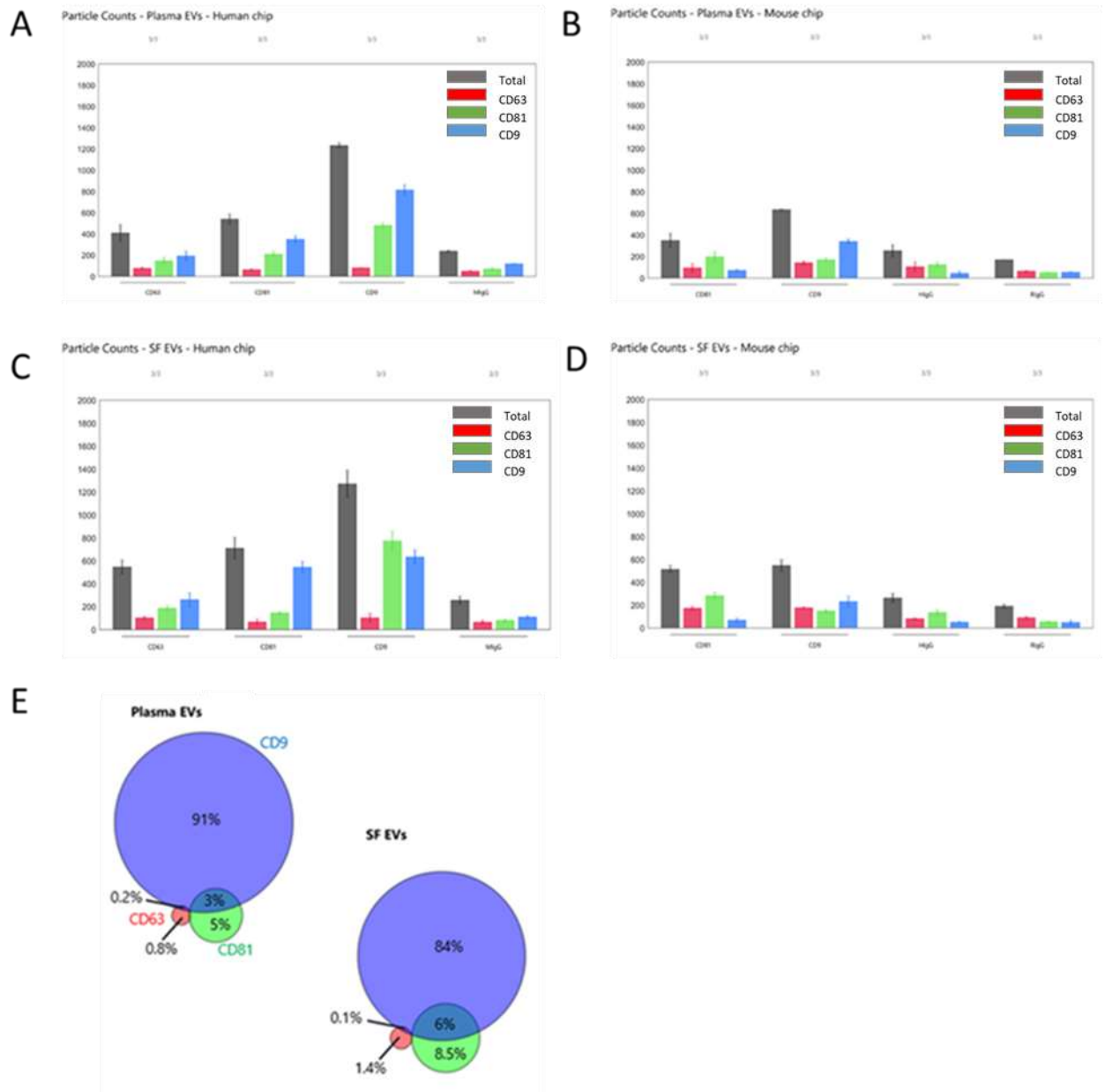
Following mass spectrometry analysis of EV samples isolated using different techniques it was identified that UC yielded the highest number of protein identifications (154 proteins), followed by SEC (89 proteins), then SEC+UC (17 proteins). Subsequently, proteins identified from the EV sample isolated using UC were compared to the Exocarta database (Keerthikumar *et al.*, 2016). It was found that 24 proteins had previously been validated as exosomal proteins. UC derived EV proteins were input into FunRich, and it was identified that the proteome could be attributed to cellular components such as extracellular space ( $p < 0.001$ , 56.6% of proteins), extracellular exosome ( $p < 0.0001$ , 67.9% of proteins) and collagen containing extracellular matrix ( $p < 0.001$ , 37.7% of proteins) (Figure 5.1). In this study it was found that UC isolated EVs yielded the highest number of proteins compared to SEC or SEC and UC. UC presents with a number of advantages, including: isolation of EVs from large volumes, requirement of a small number of consumables, minimal impact on EVs, good reproducibility, and can result in the removal of contaminating lipoproteins (Konoshenko *et al.*, 2018). In addition, further enrichment steps can be included when using UC isolation strategies, such as sucrose density gradients. It should be noted that a limitation of this study was the lack of EV quantification. Future studies could utilise this and correlate this with protein content and identifications. Subsequently, EVs were isolated using UC in the main study and throughout this PhD thesis.



**Figure 5.1. FunRich analysis of the proteins identified from ultracentrifugation derived extracellular vesicles.** This EV isolation technique resulted in the highest number of protein identifications compared to SEC and SEC+UC.

### 5.3.2 Optimisation of a Commercially available Extracellular Vesicle Characterisation Platform

The ExoView system demonstrated human antibody cross-reactivity for CD9 (mean average concentration-  $1.4 \times 10^8$  particles/ml), CD63 (mean average concentration-  $6 \times 10^7$  particles/ml) and CD81 (mean average concentration-  $7 \times 10^7$  particles/ml), for both equine plasma and SF derived EVs, as shown in Figure 5.2 A and C. Minimal cross reactivity was observed with the murine tetraspanin assay, as shown in Figure 5.2. B and D. Most EVs detected were  $<100\text{nm}$ , and plasma EVs were 5-10% larger than SF EVs. Colocalization analysis found the majority of exosomes were CD9+ (SF= 84%, plasma =91%) or CD9+/CD81+ (SF= 6%, plasma = 3%), as shown in Figure 5.2 E. In this study the ExoView human tetraspanin chip was found to be compatible with equine EVs, enabling the identification of equine exosome surface markers. Thus using this technology equine EVs could be characterised according to MISEV2018 guidelines enabling the expansion of EV research (Théry *et al.*, 2018). It should be noted that a constraint of this technology is that it specifically selects for exosomes and uses exosomal markers, therefore characterisation is primarily on a subpopulation of EVs, present within a heterogenous sample. Though, the ability to characterise EVs cannot be underestimated and is fundamental to studying the role of EVs in pathophysiology of OA, and musculoskeletal regenerative therapeutics.



**Figure 5.2. Particle counts identifying for particles positive for CD9, CD81, or CD63.** Equine plasma (5.2.A and 5.2.B), to SF (5.2.C and 5.2.D) derived EVs were compared and their reactivity on both the human (5.2.A and 5.2.C) and murine (5.2.B and 5.2.D) tetraspanin assay chips assessed. 1E demonstrated the colocalisation of surface markers present on plasma and SF EVs, with percentage particle count positive for such surface marker expression.

### 5.3.1. Equine Carpal Osteochondral Fragment Model

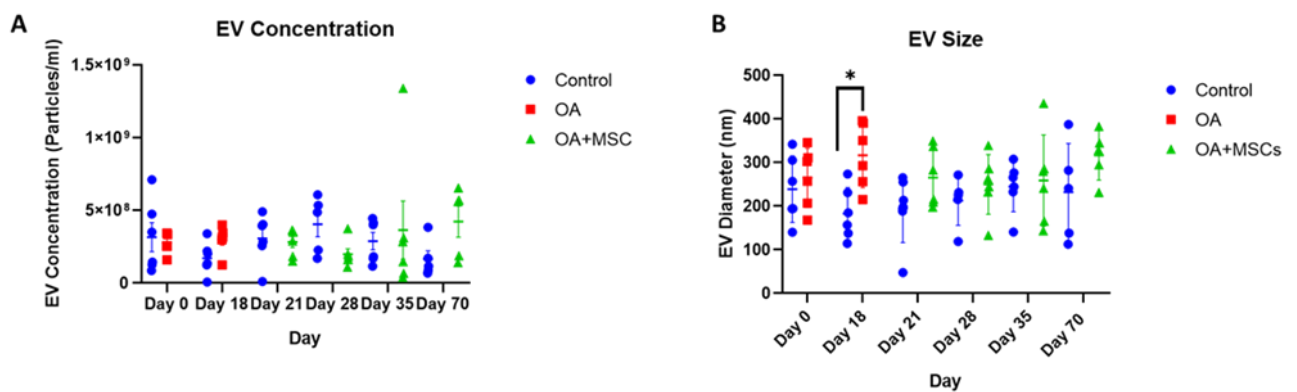
The carpal osteochondral fragment-exercise model used in this experiment has been shown to result in an OA phenotype with respect to clinical parameters, (Frisbie *et al.*, 1997, 2002, 2009; McIlwraith,

Frisbie and Kawcak, 2012a) and responded to integrin  $\alpha 10$ -MSC treatment by reduced lameness and joint degradation, as shown by Andersen *et al* (Andersen *et al.*, 2022).

### 5.3.3. Main Study

#### 5.3.3.1 Nanoparticle Tracking Analysis (NTA) to Quantify EV Size and Concentration

Total particle concentration and size characterisation was performed using NTA. NTA determined the average SF-EV sample concentration between control, OA and OA+MSCs across specific time points, specifically quantifying all nanoparticles within the sample (Figure 5.3.A). No significant difference was observed in EV concentration between experimental groups, however a significant difference in EV size was found irrespective of time when comparing control and OA ( $p=0.02$ ) and control compared to OA+MSCs ( $p=0.02$ ). Specifically, EV size was significantly different between control and OA at day 18 before MSC treatment ( $p=0.02$ ) (Figure 5.3.B). Results were suggestive of a heterogeneous population of nanoparticles.

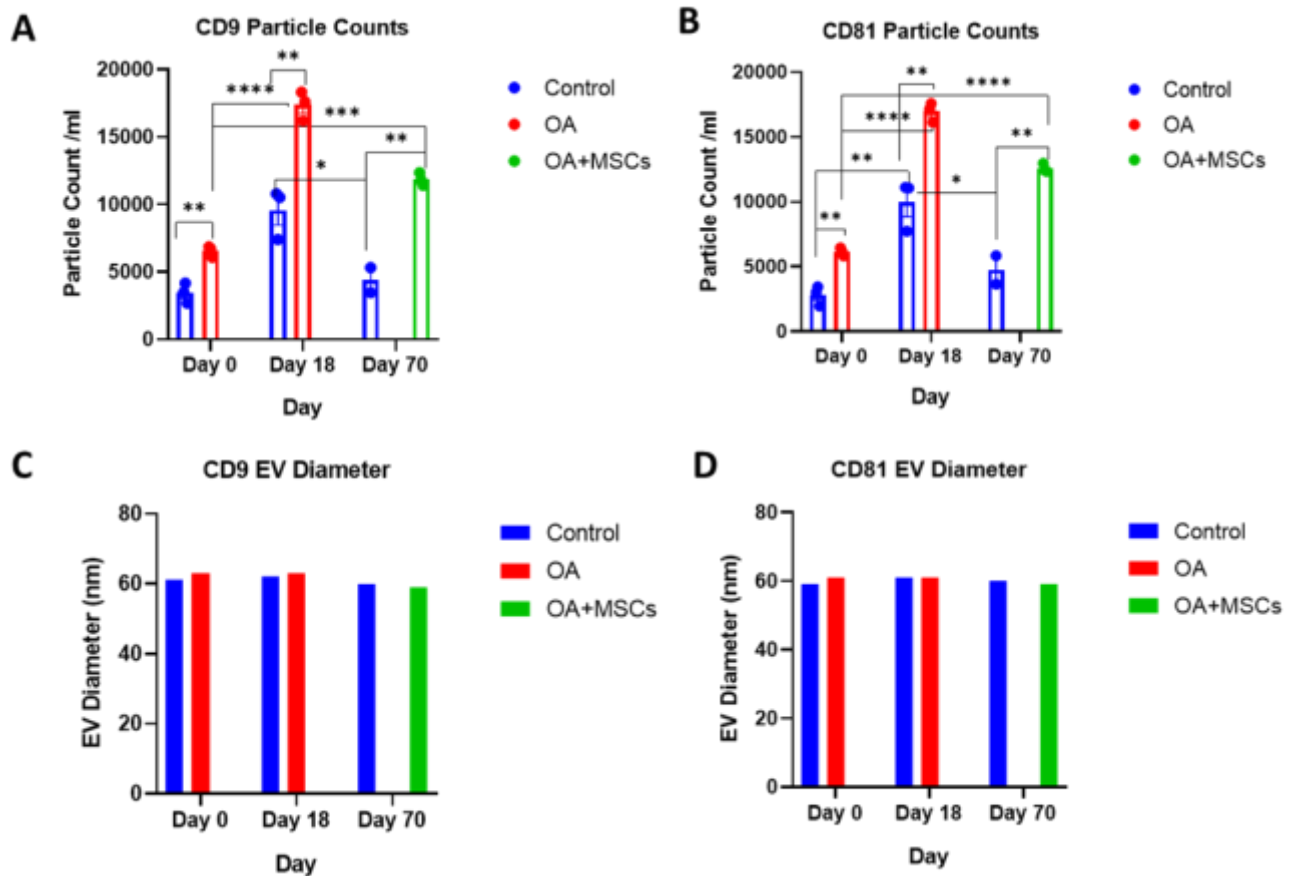


**Figure 5.3. Size and concentration of synovial fluid-derived nanoparticles.** Nanoparticle tracking analysis was undertaken using a Nanosight NS3000. All error bars are standard error of the mean (SEM). Statistical analysis undertaken in GraphPad Prism 9.0 using Kruskal Wallis Tests with FDR correction and Mann Whitney Tests within time points. ( $p < 0.05$ , \*;  $p < 0.01$  \*\*,  $p < 0.001$  \*\*\*,  $p < 0.0001$  \*\*\*\*). (A) EV concentration and (B) EV size.

#### 5.3.3.2. Exoview Assay Characterises Equine Synovial Fluid Extracellular Vesicles, including Morphology and Surface Tetraspanins

In addition to NTA, representative EV samples were characterised using the human exoview tetraspanin chip assay. This assay specializes in characterizing the exosome subpopulations of EVs. Control at day 0, OA and control at day 18 and OA+MSCs and control at day 70 were compared. OA and OA+MSCs groups had a significantly higher concentration of EVs when compared with controls. For CD9 expression, control had  $4.63 \times 10^3$  particles, OA had  $21.91 \times 10^3$  particles, and OA with MSCs

had  $15.97 \times 10^3$  particles. Similarly, for CD81, control had  $3.41 \times 10^3$  particles, OA had  $17.23 \times 10^3$  particles and OA with MSCs had  $12.48 \times 10^3$  particles (Figure 5.4). CD63 was not reported due to low particle counts for this tetraspanin; this has been attributed to poor protein homology between equine and human CD63 tetraspanins. EVs were visualised between groups with fluorescent microscopy, highlighting tetraspanin expression and EV morphology (Figure 5.5).



**Figure 5.4. Sizing and enumeration of synovial fluid-derived extracellular vesicles.** All data was adjusted for dilution of the sample onto the chip. Shown is the average representing mean of three technical replicates that were run for each sample. Particle numbers were quantified by the number of particles in a defined area on the antibody capture spot. All bars are mean and standard error mean. (A) CD9, and (B) CD81-positive particles following probing with fluorescent tetraspanin antibodies. (C) Sizing of CD9 and (D) CD81 labelled EVs, normalised to IgG control. Limit of detection was 50-200 nm. Statistical analysis undertaken in GraphPad Prism 9.0 using T-tests following parametric evaluation ( $p < 0.05$ , \*;  $p < 0.01$  \*\*,  $p < 0.001$ , \*\*\*,  $p < 0.0001$ , \*\*\*\*).

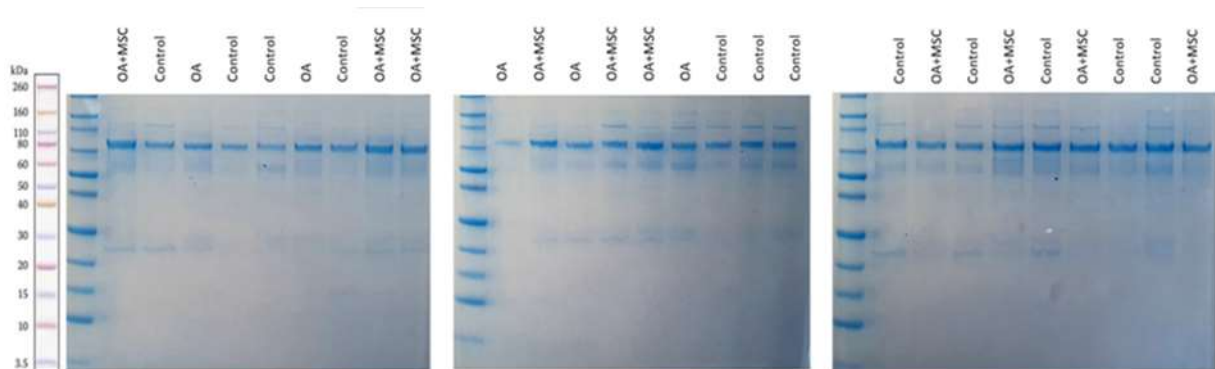
CD81	(A)	CD81 1.001	CD81 1.002	CD81 1.003
CD9		CD9 1.007	CD9 1.008	CD9 1.009
CD81	(B)	CD81 3.001	CD81 3.002	CD81 3.003
CD9		CD9 3.007	CD9 3.008	CD9 3.009
CD81	(C)	CD81 5.001	CD81 5.002	CD81 5.003
CD9		CD9 5.007	CD9 5.008	CD9 5.009
IgG negative control	/	MiGg 3.010	MiGg 3.011	MiGg 3.012

**Figure 5.5. Visualization of synovial fluid derived extracellular vesicles from control, osteoarthritic and osteoarthritic+ mesenchymal stem cell joints using Exoview at selected time points.** A fluorescent image of a representative spot is shown for each sample comparing (A) control, (B) OA and (C) OA+MSCs with colour denoting surface tetraspanin positive identification (blue- CD9, and green -CD81).

#### 5.3.3.3. Sodium Dodecyl Sulphate Polyacrylamide Gel Electrophoresis showing a Representative Selection of Synovial Fluid derived Extracellular Vesicle Samples from Corresponding Experimental Groups

Sodium dodecyl sulphate polyacrylamide gel electrophoresis was used to visualise the global proteome and complexity of EV associated proteins (Figure 5.6). Qualitatively Colloidal Coomassie

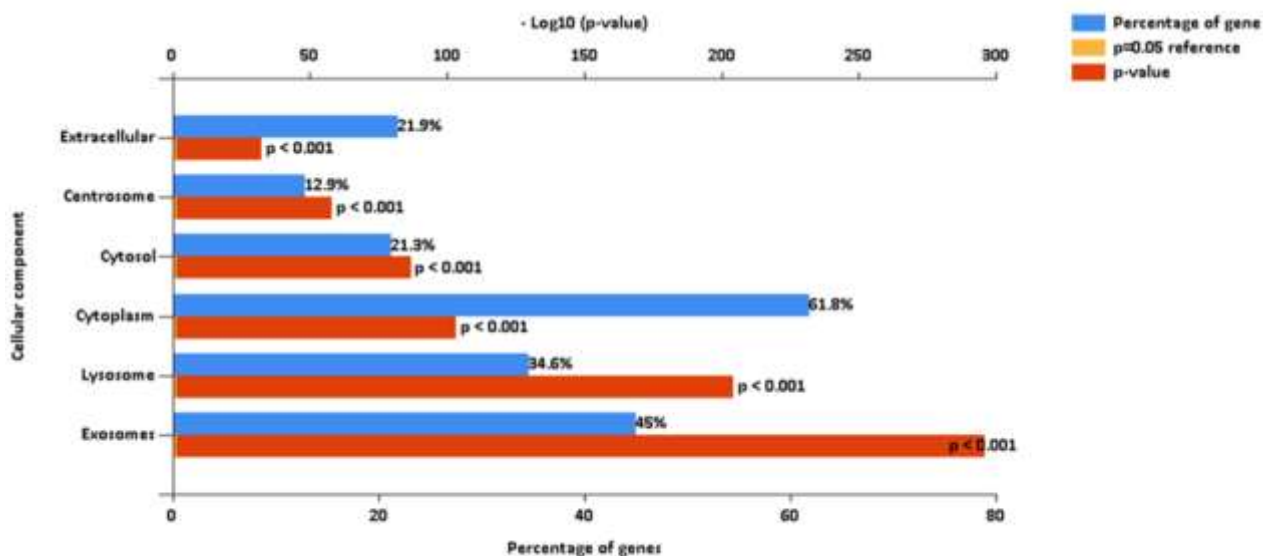
Blue staining did not yield distinct differences in protein associated bands corresponding with experimental group, but demonstrated sufficient protein content per sample for mass spectrometry proteomics analysis.



**Figure 5.6. A representative selection of synovial fluid derived extracellular vesicle samples from corresponding experimental groups (control, osteoarthritis, osteoarthritis + mesenchymal stem cells) irrespective of day.** The figure shows corresponding Sodium dodecyl sulphate–polyacrylamide gel electrophoresis (SDS-PAGE) gels used to separate proteins from EV protein extract. A Novex™ sharp protein ladder was used as a band reference, and gels were colloidal coomassie stained in order to visualise protein associated bands.

#### 5.3.3.4. Spectral Library for Equine Synovial Fluid Extracellular Vesicles

Mass spectrometric analysis of the SF-EV pooled sample identified 2271 proteins, mapping at least one unique peptide. Of these proteins 2047 were identified and mapped to GO Cellular Component terms using FunRich. Proteins were attributed to various cellular components, including extracellular space and exosomes, both  $p \leq 0.001$ , as shown in Figure 5.7. This library was then used to identify the proteins present within the individual samples.

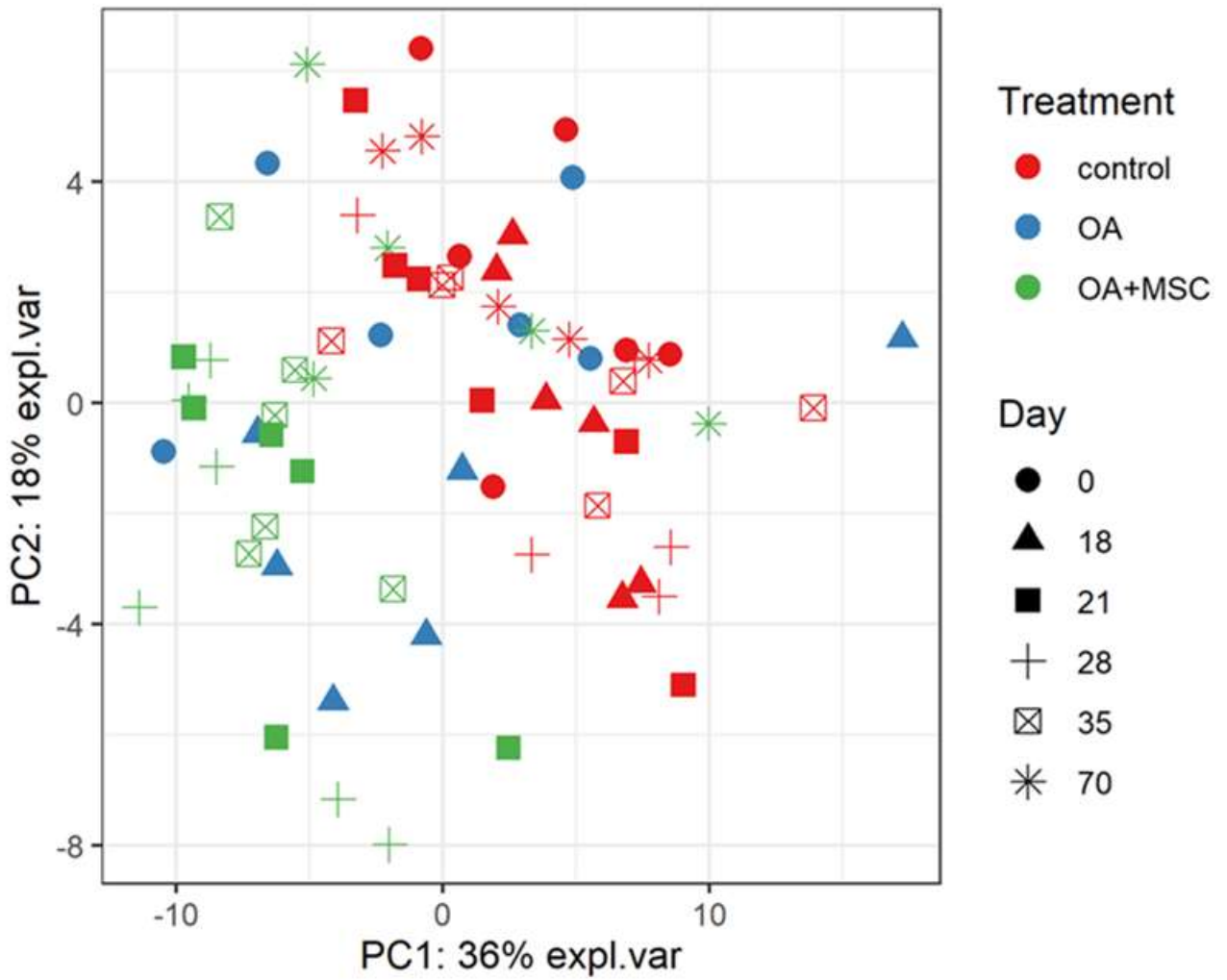


**Figure 5.7. FunRich analysis output, after mapping 2047 proteins to Gene Ontology Cellular Component terms.** These proteins were identified from a pooled sample of equine synovial fluid (11ml) used to generate the SF-EV spectral library for this study. SF was sourced from healthy, OA and OA+MSC treated joints in order to encapsulate all potential proteins that may be present across all experimental groups.

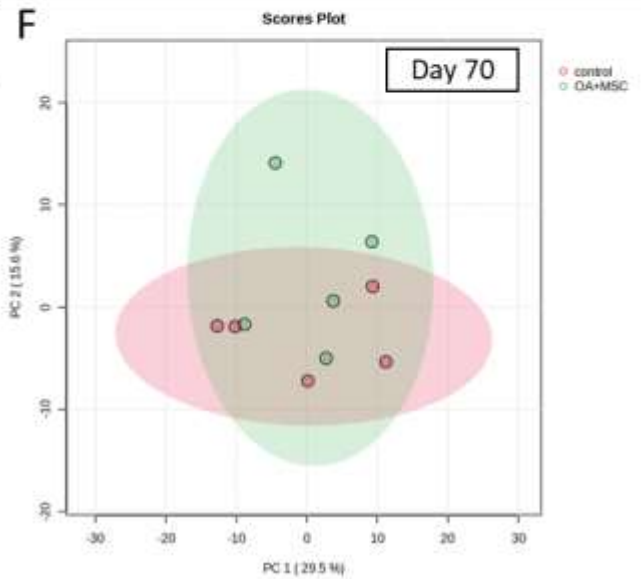
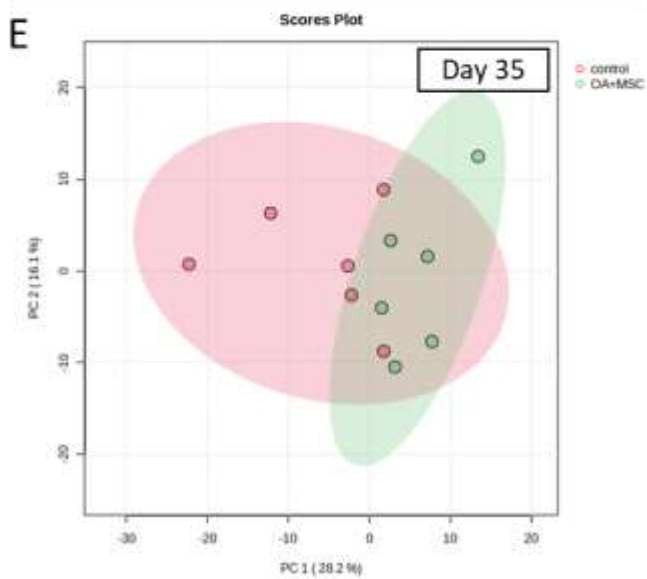
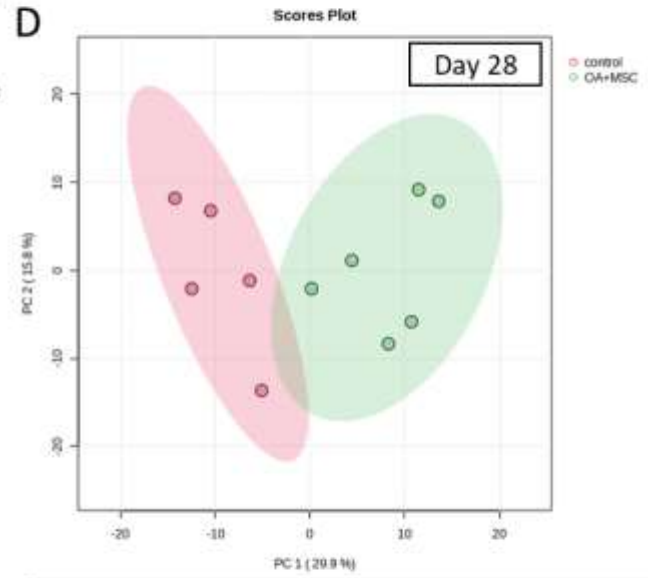
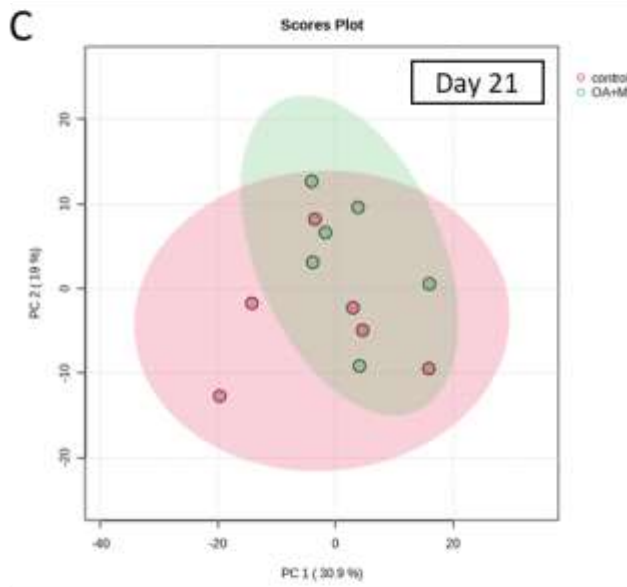
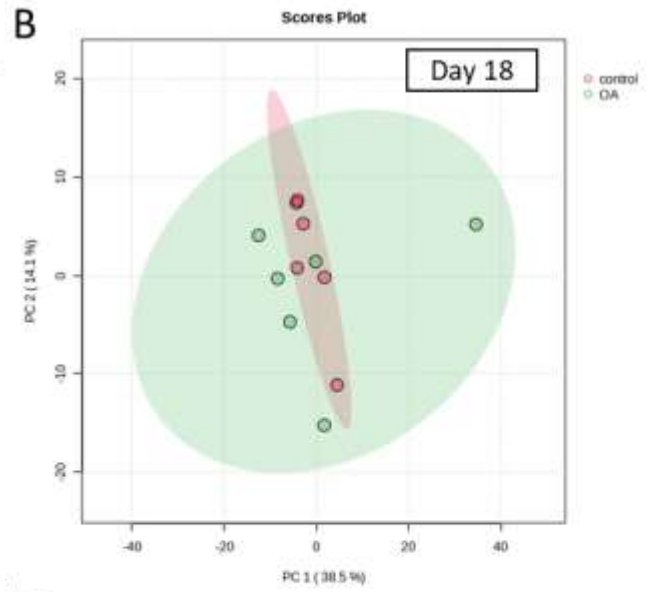
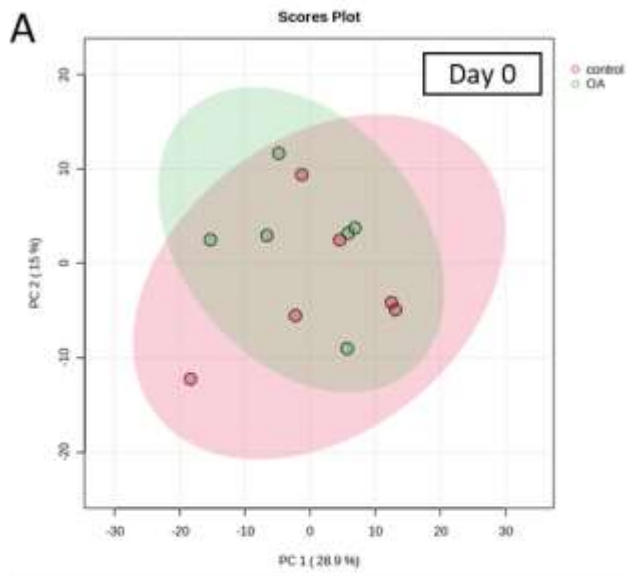
### 5.3.3.5. *A Multivariate Approach identified a Time-dependent difference between Disease Stages Pre- and Post-treatment*

A total of 442 proteins were identified across all samples submitted for SWATH-MS analysis. Multi-level PCA (mPCA) was carried out using the MixOmics R package principal component analysis (mPCA). PCA normally assumes the variables are not correlated. However, this study employed a repeat-measures design on the same horses. To account for the intraclass correlation between horses mPCA was employed. The first two principal components accounting for 54% of the variance were associated with the biological effect and demonstrated that the control and OA+MSC samples clustered by treatment (Figure 5.8). The later OA+MSC time points (day 70) appeared to cluster together with the control samples, reflecting a return to protein expression levels comparable to the healthy controls. Figure 5.9 depicts individual principal component analysis per day, specifically day 0 (Figure 5.9.A), day 18 (Figure 5.9.B) day 21 (Figure 5.9.C), day 28 (Figure 5.9.D), day 35 (Figure 5.9.E) and day 70 (Figure 5.9.F).





**Figure 5.8. Multi-level PCA.** The first two principal components are plotted, accounting for ~54% of variance. samples based on SWATH-MS. Each plotted point represents a horse, which are coloured by their treatment and shaped by the day of the study.



**Figure 5.9. PCA per day, highlighting global proteome change across time in association with surgical induction of OA and MSC treatment.** The first two principal components are plotted, samples based on SWATH-MS. Each plotted point represents a horse, which are coloured by their treatment, each panel reflects different day, specifically day 0 (Figure 5.9.A), day 18 (Figure 5.9.B) day 21 (Figure 5.9.C), day 28 (Figure 5.9.D), day 35 (Figure 5.9.E) and day 70 (Figure 5.9.F).

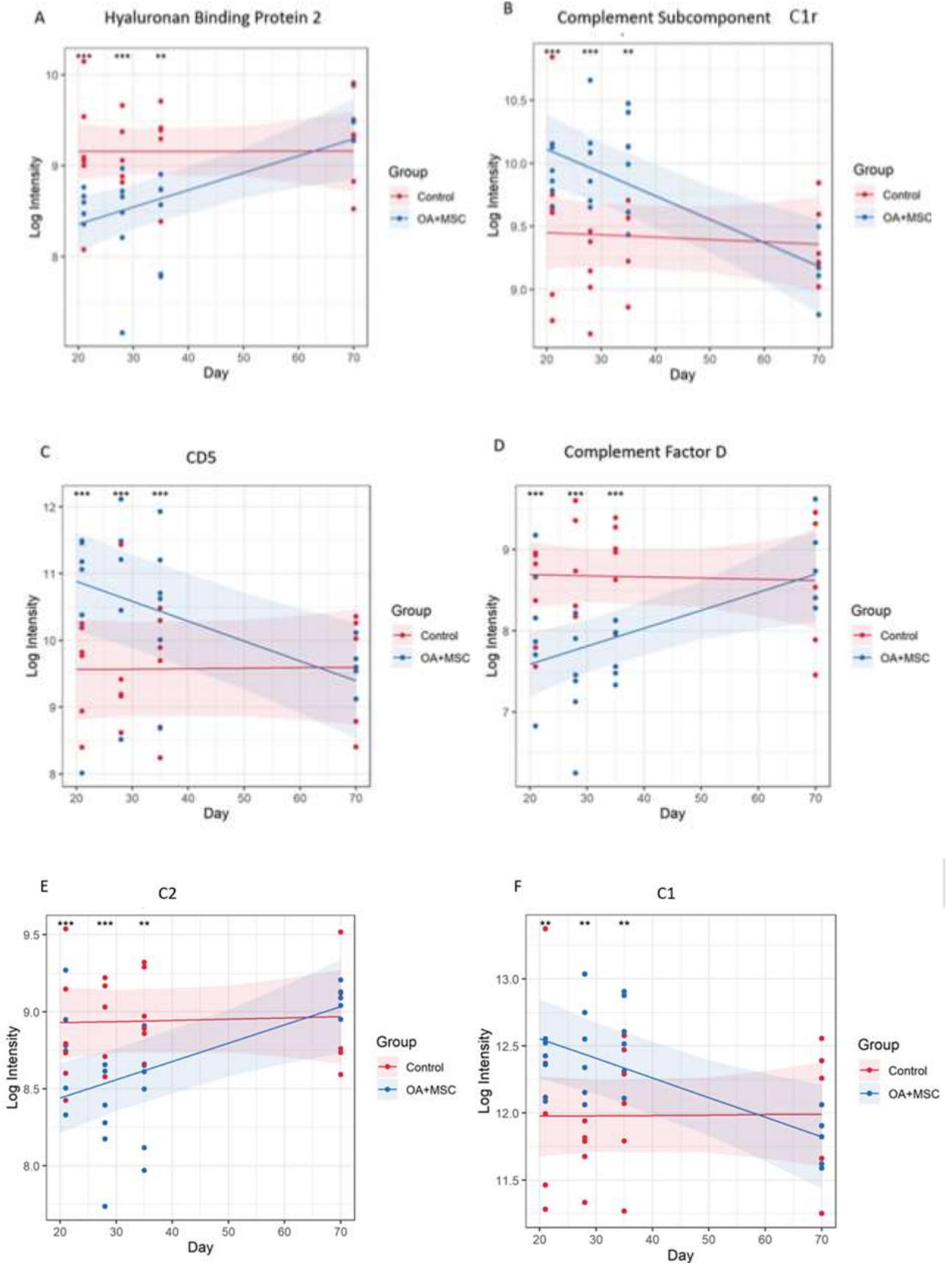
#### 5.3.3.6. *Longitudinal Differential Expression Highlights Key Pathways related to Disease Progression and Treatment*

Differentially expressed (DE) proteins were identified with the application of a linear mixed model with regressed factors comparing protein expression between experimental groups across time. Statistical significance was attributed to any protein with an FDR corrected p-value (BH) of  $p \leq 0.05$  meeting a minimal 95% confidence interval. Of the 442 proteins identified, 48 were present at significantly different levels ( $p \leq 0.05$ ) between control and OA+MSCs regardless of time. Interestingly, there were no proteins DE after FDR correction in SF-EVs between control and OA at baseline and day 18 after OA induction, or between day 18 control and OA. The 10 proteins with the most statistically significant altered levels are shown in Table 5.1, including the time points at which pairwise comparisons show significant differences between control and OA+MSCs, and all 48 can be found in Supplementary Table 10.1. Figure 5.10 shows proteins attributed to the serine endopeptidase ( $p=0.02$ ) and complement pathways ( $p=0.03$ ), including hyaluronan binding protein 2 ( $p=0.04$ ) (Figure 5.10.A), complement subcomponent C1r ( $p=0.03$ ) (Figure 5.10.B), CD5 ( $p=0.01$ ) (Figure 5.10.C), complement factor D ( $p=0.03$ ) (Figure 5.10.D), C2 ( $p=0.04$ ) (Figure 5.10.E), and C1 ( $p=0.04$ ) (Figure 5.10.F). Other proteins attributed to the serine endopeptidase pathway include haptoglobin ( $p=0.03$ ), HtrA1 serine peptidase ( $p=0.03$ ) and complement factor B ( $p=0.04$ ). Proteins mapped to the collagen containing extracellular matrix ( $p=0.02$ ) included cartilage oligomeric matrix protein ( $p=0.001$ ), microfibril associated protein 4 ( $p=0.001$ ), thrombospondin 4 ( $p=0.003$ ), retinoic acid receptor responder protein 2 ( $p=0.03$ ), periostin ( $p=0.03$ ), EGF containing fibulin extracellular matrix protein 1 ( $p=0.03$ ), and cartilage intermediate layer protein ( $p=0.04$ ). (Supplementary Figure 10.2). The third most significant pathway was identified as complement activation classical pathway, with the following proteins attributed to it; two uncharacterized proteins, C9 ( $p=0.01$ ), C8A ( $p=0.02$ ), C1r ( $p=0.03$ ), C7 ( $p=0.03$ ), C2 ( $p=0.04$ ), and C1 ( $p=0.04$ ) (Supplementary Figure 10.2). In all proteins shown in Figure 5.10, protein expression was significantly different at day 21, 28 and 35 when compared to control. Expression of all these proteins returned to control by day 70.

**Table 5.1. The top 10 differentially expressed (P<0.05) proteins following the application of the linear mixed model, accounting for treatment and time point.** Treatment and time were included as main effects, along with a treatment-by-time interaction term. Time point denoting significant pairwise comparisons between control and OA+MSCs is also shown.

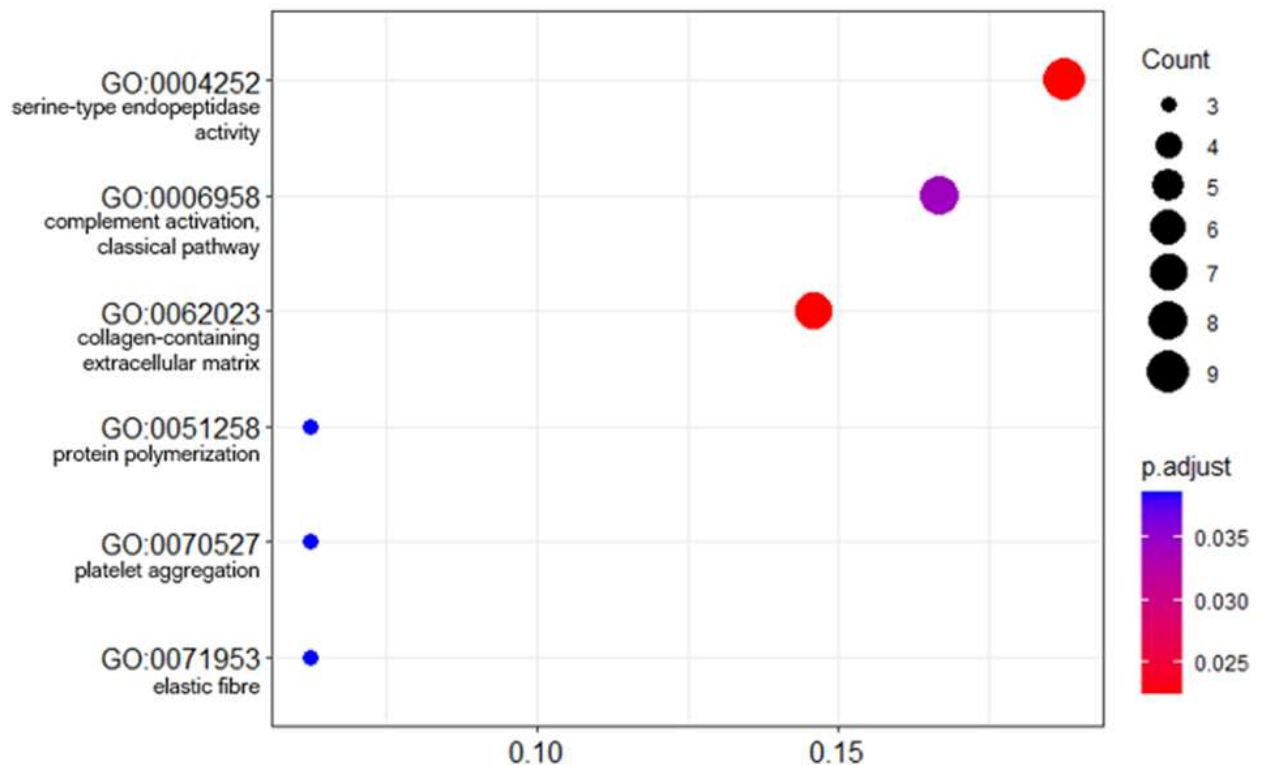
Protein	Accession number	P-Value (FDR adjusted)	Time point (Day)	Expression direction in OA+MSC group compared to control
Fibrinogen beta chain	F6PH38	0.0001	21,28,35	Increase
Fibrinogen gamma chain	A0A5F5PPB8	0.0001	21,28,35	Increase
Joining chain of multimeric IgA and IgM	A0A3Q2HW24	0.0003	21,28,35	Increase
Dynein heavy chain domain 1	A0A3Q2HE28	0.0005	21,28,35	Increase
Fibrinogen alpha chain	A0A3Q2HTG2	0.0005	21,28,35	Increase
Gelsolin (Actin-depolymerizing factor, ADF) (Brevin)	Q28372	0.0006	21,28,35	Decrease
Cartilage oligomeric matrix protein	A0A3Q2HRL2	0.001	21,28,35	Decrease
Microfibril associated protein 4	A0A3Q2HNN0	0.001	21,28,35	Increase
Glutathione peroxidase	A0A5F5PST7	0.003	21,28,35	Decrease
Insulin like growth factor binding protein 6	F7DEB1	0.003	21,28,35	Decrease

*Abbreviations: Osteoarthritis and mesenchymal stem cells (OA+MSCs), Immunoglobulin A (IgA) and Immunoglobulin M (IgM)*



**Figure 5.10. Protein expression changes in osteoarthritic joints treated with mesenchymal stem cells vs control.** (A) Hyaluronan binding protein 2, (B) Complement subcomponent C1r, (C) CD5, (D) Complement factor D, (E) C2, (F) C1. The models were fitted using the lmerTest implementation of lme4. 48 proteins had a significant group, time, or group:time effect after FDR correction. For each protein with a significant effect the model was plotted using the effects and ggplot2 packages. The fitted model is shown as a line for the OA+MSC (blue) and control (red). The 95% confidence intervals for each group are shown as a shaded area. The raw data is included as points. At each time point pairwise comparisons were carried out between the treatment and control using the emmeans package. Significance thresholds were as follows: ( $p < 0.05$ , \*;  $p < 0.01$  \*\*,  $p < 0.001$  \*\*\*,  $p < 0.0001$  \*\*\*\*).

The lists of significant proteins were used for functional enrichment analysis with the aim of identifying biological processes involving these proteins. Using an overrepresentation analysis (ORA) approach on gene ontology (GO) annotations yielded six enriched biological processes: serine endopeptidase activity ( $p = 0.023$ ), complement activation (classical pathway) ( $p = 0.023$ ), collagen containing extracellular matrix ( $p = 0.034$ ), protein polymerization ( $p = 0.039$ ), platelet aggregation ( $p = 0.039$ ), elastic fibre ( $p = 0.039$ ) (Figure 5.11).



**Figure 5.11. Dot plot of Gene Ontology term enrichment analysis of differentially abundant proteins.** The size of the dots indicates the number of proteins that mapped to that term. The x-axis is the protein ratio (number of proteins that map to the term divided by the total number of significant proteins). The dots are shaded by adjusted p-values (BH method).

## 5.4. Discussion

This study aimed to determine the EV protein cargo following integrin  $\alpha 10\beta 1$ -selected mesenchymal stem cell (integrin  $\alpha 10$ -MSC) treatment in an experimental model of equine OA. To our knowledge this is the first study of its kind to quantify the global EV proteome *in vivo* after MSC treatment.

The osteochondral fragment model used in this study has been shown to produce reliable post-traumatic OA in the middle carpal joint of horses (Frisbie *et al.*, 1997, 2002, 2009; McIlwraith, Frisbie and Kawcak, 2012a). The mitigating effect of MSC treatment on the development of post-traumatic OA has been shown in a number of equine studies, although in different models, such as an osteochondral fragment model of the fetlock (Broeckx, Martens, *et al.*, 2019; Bertoni *et al.*, 2021) a blunt impact model of the tarsus (Delco *et al.*, 2020) and injection of the irritant amphotericin B (Barrachina *et al.*, 2018). In all studies, the MSC-treated horses developed significantly less severe OA over time compared to the untreated control horses in terms of decreased synovial effusion and a higher SF viscosity and glycosaminoglycan content, decreasing lameness over time, less severe macroscopic cartilage erosions, less radiographic signs of OA, and less histologic cartilage fibrillation and subchondral sclerosis.

In our study, we identified a global change in the EV proteome, and identified a possible mechanism of MSC therapy. A time-dependent change in the EV protein cargo was also observed, suggestive of a time associated therapeutic effect, which is in line with previous reports of the effects of MSC-treatment.

We used dUC to isolate EVs following hyaluronidase treatment of SF. Hyaluronidase was used in order to break down hyaluronic acid as its presence in SF increases viscosity making the biofluid difficult to handle. This pre-treatment is known to increase EV yield (Boere, Lest, *et al.*, 2016). In addition, it has also been suggested that SF-derived EVs should be sedimented at a speed of at least 100,000xg for optimal EV recovery, hence the decision to use this step within our isolation protocol (Boere, van de Lest, *et al.*, 2016).

EVs were isolated from SF obtained from OA joints that were treated with MSCs and from untreated control joints. The EVs isolated were a heterogenous population that may have been derived from cells found in the intraarticular environment, such as synoviocytes and chondrocytes, and possibly from the MSCs injected into the joint. Nanoparticle tracking analysis conducted on all samples across all time points found no changes in EV concentration with time. It should be noted that NTA quantifies all nanoparticles within a sample and includes lipoproteins, proteins, viruses, nanovectors and drug delivery systems (Pellequer *et al.*, 2021). This accounts for the difference in EV concentration between

our NTA analysis and exoview analysis. We had limited resources to enable Exoview of all samples, and so used the platform for a subset of samples. Exoview analysis specifically focuses on the exosomal population of EVs by using antibodies for surface tetraspanins such as CD9, CD81 and CD63. In this study and our previous study, we were able to show species cross reactivity with the CD9 and CD81 tetraspanins, but not CD63 (Anderson *et al.*, 2022). Exoview analysis demonstrated an increase in the number of exosomes after OA-induction surgery prior to MSC injection. However, this may be due to immune cell infiltration within the first 18 days contributing to the difference. This is in contrast to a human study by Mustonen *et al.* (2022) which identified no change in EV concentration between SF-EVs from healthy and human late stage OA patients (Mustonen *et al.*, 2021a). Those differences could be due to the stage of disease post-traumatic model used in our model (early) versus the end-stage nature of the human study. Our results tentatively suggest that the OA-induction surgery actively increases the number of exosomes as a result of the acute trauma. This could be due to the access of subchondral bone to the SF environment following production of an osteochondral fragment or from tissues within the joint as a response to the formation of the fragment or both. However, our experimental design does not enable us to decipher this. A greater number of CD9+ and CD81+ EVs were identified across all experimental groups using the exoview assay. CD9+ exosomes have been postulated to be a target for inflammatory regulation in specific pathologies. In addition, the increase count observed in OA+MSC groups compared with control could be attributed to its presence on hematopoietic cells, and the role of CD9 in regulating hematopoietic stem cells differentiation (Brosseau *et al.*, 2018). With respect to CD81, there is limited literature available postulating the role of specifically CD81+ EVs. However, the tetraspanin CD81 is involved in providing a scaffold enabling the recruitment of complementary proteins, enabling the function of many cellular processes. CD81 expression has been strongly associated with cancerous pathologies, and has been shown to promote tumour growth and metastasis in human melanoma, while its knockdown in osteosarcoma models has reduced tumour progression (Vences-Catalán *et al.*, 2021). Across all time points the sham control protein expression remained significantly lower than the experimental group at all time points, suggestive of a minimal effect of the arthroscopy. In addition, highlighting that there was a limited systemic effect from the surgical induction of OA.

In this study, SF samples following OA induction and then following the addition of MSCs to the joint were available up to day 70 following OA induction. Unfortunately, SF samples from OA joints without MSC treatment were not available for this study. This makes it difficult to be definitive about the source of the EVs in the SF following addition of MSCs. We believe these will be a combination of tissue-derived and MSC-derived EVs, resulting from MSC-to-cell interactions, cell-to-MSC interactions,



and cell-to-cell interactions. Allogeneic MSCs have been traced in the joint of an ovine OA model up to 14 weeks after injection (Feng *et al.*, 2018) and up to 12 weeks after injection in an OA model in rats (Horie *et al.*, 2009). Therefore, it is possible that MSCs were present in the joint at study termination 52 days (7½ weeks) after MSC-injection.

Following intraarticular injection of MSCs increased EV COMP expression was observed returning to baseline control by day 70. COMP is a key protein present in cartilage extracellular matrix and is a target of degradation in early OA (Maly *et al.*, 2021). In addition, proteins such as gelsolin, which had increased expression in the OA+MSC group, has previously been attributed to chondrocyte migration. It could be postulated that proteins highly associated with the joint tissues may be sourced from EVs secreted by joint cells, raising the question of how EVs interact in their *in vivo* environment in response to stimuli.

The most significant GO term associated with DE EV-proteins following MSC treatment was serine endopeptidase activity. Serine type endopeptidases, or serine proteinases have been attributed to proteolytic cartilage destruction. In addition, serine proteinases perform vital functions such as cytokine regulation and receptor activation (Wilkinson *et al.*, 2019). Degradomic studies have demonstrated that an increase in proteases activity in OA, such as in HtrA1 was responsible for cartilage proteolysis. (Bhutada *et al.*, 2022). HtrA1 decreased across time following MSC injection. In a murine model the genetic removal of HtrA1 delayed the degradation of articular or condylar cartilage in mice (Chen, Tang, *et al.*, 2019). Moreover, a previous study profiling the synovial fluid-derived EV proteome cargo in OA patients of both sexes identified sex-specific differences in cargo, with enriched pathways including proteins involved in endopeptidase activity, specifically in women (Kolhe *et al.*, 2020). This is of note as all horses included in this study were female. With respect to serine endopeptidase activity in MSCs, it has previously been reported that interactions between BM-MSCs and natural killer cells are fundamental to improving MSC therapeutic efficacy. It has been stated that serpin B9 has a cytoprotective function in MSCs (Najar *et al.*, 2018). In other diseases such as colorectal cancer, the use of MSCs identified serpins as having immunomodulatory effects, acting on immune cells in order to induce a wound healing phenotype, as well as angiogenesis and epithelial to mesenchymal transition (Leonard *et al.*, 2021). Therefore, we hypothesize that the change in SF-EV proteome post MSC injection has the capacity to affect the serine endopeptidase pathway that is known for its detrimental effect on cartilage degradation.

A further altered GO term included collagen containing extracellular matrix, often linked with joint homeostasis. Exosomes from embryonic MSCs were found to balance synthesis and degradation of the cartilage extracellular matrix in an *in vitro* murine model (Wang *et al.*, 2017). In our study, we

observe a significant change in the expression of proteins associated with cartilage structure, such as COMP, hyaluronan binding protein 2, cartilage intermediate layer protein, chondroadherin and gelsolin. These proteins return to baseline control level by the end of our study. This suggests a restorative effect and return towards a healthy cartilage phenotype. It may be that such increased expression is more likely to be attributed to EVs secreted by native tissues than MSCs, which contribute to collagen extracellular matrix homeostatic function which could be beneficial in OA treatment. In addition, MSCs could be upstream regulators of these effects in native tissues.

In this study, the level of complement proteins in SF EVs decreased with time and returned to baseline in horses treated with MSCs, potentially affecting disease progression. The complement cascade was also a significantly enriched pathway. This pathway is activated in the early stages of OA, with C3a and C5a attributed to OA progression (Schäfer and Grässel, 2022). In addition, it has been linked to extracellular cartilage matrix degradation, chondrocyte and synoviocyte inflammatory responses, cell lysis, synovitis, disbalanced bone remodelling, and osteophyte formation (Silawal *et al.*, 2018). Several complement components have previously been identified as upregulated in OA SF. It was reported that C3a and C5a promoted chemotaxis of neutrophils and monocytes, and increased leukotriene synthesis (Woodell-May and Sommerfeld, 2020). In our study multiple complement factors were identified as differentially expressed, including C7, C8, C9 and C2 (C3/C5 convertase) when comparing control to OA+MSCs across time.

There are a number of limitations to our study. The duration of the study only enabled the quantification of the effect of MSCs *in vivo* on the global EV proteome in the short term. MSC viability following treatment could not be quantified. Thus, there is an inability to determine the number of EVs contributing to the SF-EV proteome derived from injected MSCs and those from joint tissues themselves.

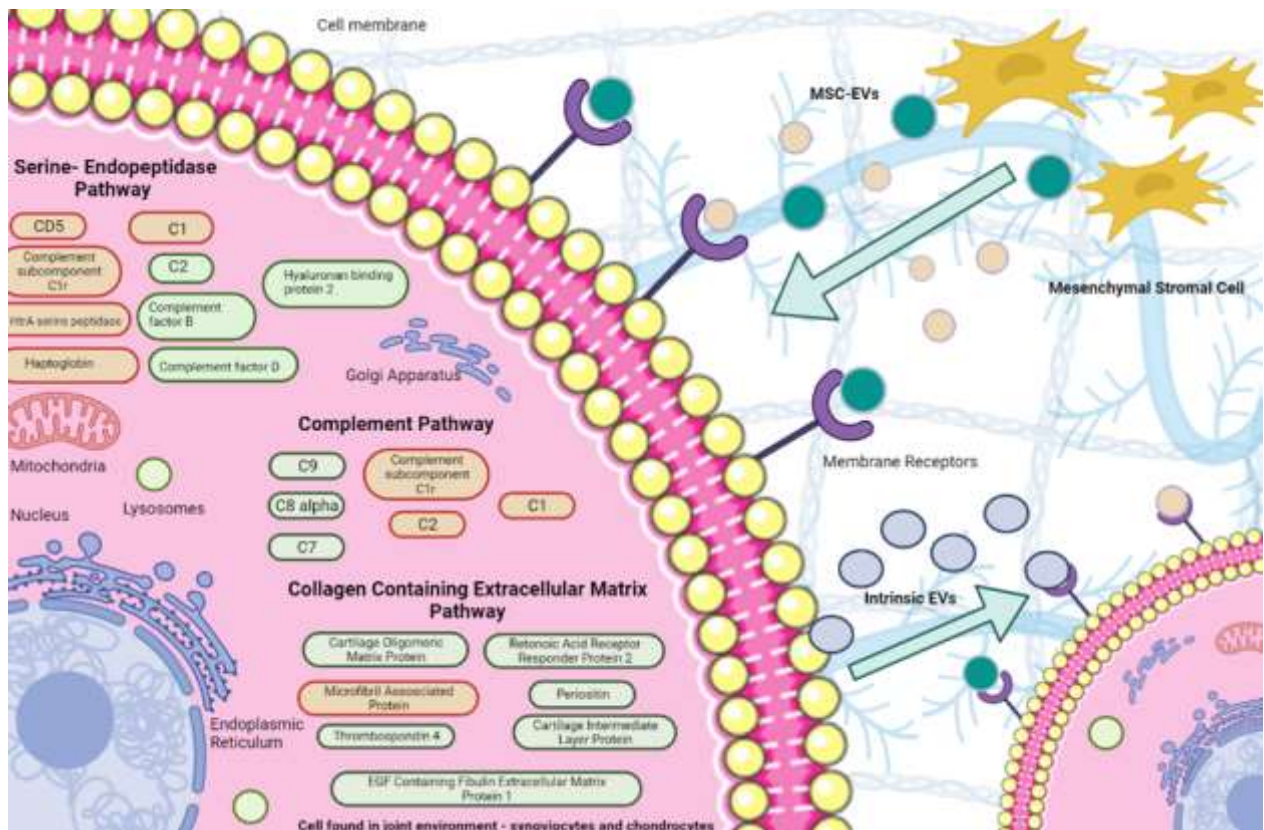
The purpose of this study was to characterize EVs in the SF after MSC administration in equine joints with OA. The specific role of EVs secreted by the MSCs only still need to be elucidated through comparisons to untreated OA joints. One way to study MSC-derived EVs specifically could be to identify MSC-derived EVs based on surface markers.

The severity of OA phenotype is also a limitation, as the model has been shown to produce a post-traumatic OA phenotype with respect to clinical parameters, but there were no significant differences in protein abundance between control and OA joints. Previous studies using the same OA model have shown an increase in the SF concentration of PGE2 and glycosaminoglycans in the OA joints shortly after OA induction (within the first two weeks) and an increase in the matrix degradation products CPII, CS846 and C1,2C only towards the end of the 70-day study period (Frisbie *et al.*, 2008). Prior to

FDR correction ANOVA identified 39 DE proteins with respect to group (control and OA), including: Spondin-1 ( $p=0.005$ ), HtrA1 serine endopeptidase ( $p=0.02$ ), and serotransferrin ( $p=0.01$ ), all of which have been previously implicated in OA pathogenesis (Aspden and Saunders, 2019; Sulaiman *et al.*, 2020; Tossetta *et al.*, 2022). Thus, whilst the confidence in these findings is lower, there appears to be an effect on the EV proteome following OA induction that would require further validation.

It needs to be determined if the MSC-EVs were acting in a causative or reactionary manner to the *in vivo* environment. There is a significant degree of variability with respect to MSC properties dependent on the donor or tissue source. Our study used integrin  $\alpha 10\beta 1$ -selected adipose-derived MSCs and different results may have been achieved with an alternative source of MSCs or different MSC preparation methods. A study by Roelefs *et al.* found that synovium-derived adult GDF5-lineage MSCs had a significant role in response to joint injury (Roelofs *et al.*, 2017). Thus, it is likely that the EV cargo will be MSC source dependent, potentially for the MSC-derived EVs as well as the joint tissue-EV response to MSCs. Another study by Broeckx *et al.* have shown reduced signs of OA following injection of chondrogenically induced peripheral blood-derived MSCs (Beerts *et al.*, 2017) in horses with induced OA. Barrachina *et al.* showed that proinflammatory primed MSCs have improved immunomodulatory abilities in the equine joint compared to naïve MSCs (Barrachina *et al.*, 2018). A recent study showed that integrin  $\alpha 10$ -MSCs were able to home to a cartilage defect in rabbits and to directly participate in cartilage regeneration through chondrogenic differentiation *in vivo* (C. Andersen, Uvebrant, *et al.*, 2022), which has not previously been demonstrated with other MSC preparations. Therefore, we acknowledge that results of this study could have been different if another cell type was used.

With the caveat that we did not have a group of horses with OA but no MSC treatment and that we were unable to confirm the MSC survival time, we have postulated a potential mechanism of action of MSCs in our model. We hypothesize that after the introduction of MSCs into the joint, MSC-EVs deliver proteinous cargo into recipient cells found within the intra-articular environment, while also promoting intrinsic cellular changes altering the cargo of EVs secreted from native cells. We suggest they act partially through effects on the serine endopeptidase pathway, subsequently reducing its activity and OA pathogenic effect. In addition, altered EV proteins are implicated in the complement system and collagen containing extracellular matrix pathway, as shown in Figure 5.12. These altered pathways may provide potential targets for therapeutic intervention and require further exploration in the context of MSC therapy and the use of MSC-EVs in OA.



**Figure 5.12. Potential mechanisms of action of synovial fluid derived extracellular vesicles following mesenchymal stem cell treatment.** EVs were sourced from both MSCs and the intraarticular environment. We hypothesized that MSC-EVs affect the intraarticular cells through their differential protein cargo, resulting in altered EV secretion from intrinsic cells. DE proteins attributed to given pathways are red (decreased expression to meet baseline or surpass it by day 70) or green (increased expression to reach baseline at day 70).

## 5.5. Conclusion

We characterized for the first time using an unbiased approach the SF-EV protein cargo in a model of OA after MSC administration. Changes in the proteome of the synovial fluid-derived EVs following allogeneic integrin  $\alpha 10$ -MSC administration are suggestive of EVs playing a role in mediating the effect of cell therapy. A time-dependent change in potential therapeutic efficacy of the injected MSCs was also observed. Potential targets were identified that warrant further investigation in order to determine their significance in pathophysiology and management of equine OA.

## 5.6. Ethics

The animal study was reviewed and approved by Danish Animal Experiments Inspectorate (#2020-15-0201-00602) and the Ethical Committee of the University of Copenhagen (Project No: 2020-016).

## **5.7. Funding**

Emily Clarke is a self-funded PhD student. Mandy Peffers is funded through a Wellcome Trust Intermediate Clinical Fellowship (107471/Z/15/Z). This work was supported by the Horserace Betting Levy Board in conjunction with the racing foundation (SPrj048). Our work is also supported by the Medical Research Council (MRC), Xintela AB, and Versus Arthritis as part of the MRC Versus Arthritis Centre for Integrated research into Musculoskeletal Ageing (CIMA). This work was funded by the Horserace Betting Levy Board (HBLB), project code SPrj048. The Authors acknowledge use of the CDSS Bioanalytical Facility and the Computational Biology Facility, services funded partially by the Liverpool Shared Research Facility Voucher Scheme (Liverpool Shared Research Facilities, Faculty of Health and Life Sciences, University of Liverpool).

## 6. Manuscript 2

### **Optical Photothermal Infrared Spectroscopy can Differentiate Equine Osteoarthritic Plasma Extracellular Vesicles from Healthy Controls**

**Emily J Clarke<sup>†\*1</sup>**, Cassio Lima<sup>12</sup>, James R Anderson<sup>1</sup>, Catarina Castanheira<sup>1</sup>, Alison Beckett<sup>3</sup>, Victoria James<sup>4</sup>, Jacob Hyett<sup>1</sup>, Royston Goodacre<sup>2</sup> and Mandy J Peffers<sup>1</sup>

<sup>1</sup>*Department of Musculoskeletal Biology and Ageing Science, Institute of Life Course and Medical Sciences, University of Liverpool, William Henry Duncan Building, 6 W Derby St, Liverpool L7 8TX.*

<sup>2</sup>*Centre for Metabolomics Research, Biochemistry and Systems Biology, Institute of Systems, Molecular and Integrative Biology, University of Liverpool, Biosciences Building, Crown Street, Liverpool, L69 7BE*

<sup>3</sup>*Biomedical Electron Microscopy Unit, University of Liverpool, UK.*

<sup>4</sup>*School of Veterinary Medicine and Science, University of Nottingham, Sutton Bonington, Loughborough LE12 5RD*

#### **Key words**

**Osteoarthritis, Equine, Plasma, Extracellular Vesicles, Spectroscopy**

#### **Declaration of author contributions**

Conceptualization, **MJP, RG, CL, and EJC.**; methodology, **EJC, MP, RG, CL, CC, JA, JH, VJ, AB**; formal analysis, **CL and EJC**; investigation, **CL and EJC.**; data curation, **CL and EJC.**; writing—original draft preparation, **EJC** ; writing—review and editing, **EJC, CL, MP, RG, CC, JA, VJ, JH, AB**; visualization, **CL and EJC.**; all authors have read and agreed to the published version of the manuscript.

## 6.1 Abstract

Equine osteoarthritis is a chronic degenerative disease of the articular joint, characterised by cartilage degradation resulting in pain and reduced mobility and thus is a prominent equine welfare concern. Diagnosis is usually at a late stage through clinical examination and radiographic imaging, whilst treatment is symptomatic not curative. Extracellular vesicles are nanoparticles that are involved in intercellular communication. The objective of this study was to investigate the feasibility of Raman and Optical Photothermal Infrared Spectroscopies to detect osteoarthritis using plasma-derived extracellular vesicles, specifically differentiating extracellular vesicles in diseased and healthy controls within the parameters of the techniques used. Plasma samples were derived from thoroughbred racehorses. A total of 14 samples were selected (control; n = 6 and diseased; n = 8). Extracellular vesicles were isolated using differential ultracentrifugation and characterised using nanoparticle tracking analysis, transmission electron microscopy, and human tetraspanin chips. Samples were then analysed using combined Raman and Optical Photothermal Infrared Spectroscopies. Infrared spectra were collected between 950-1800  $\text{cm}^{-1}$ . Raman spectra had bands between the wavelengths of 900-1800  $\text{cm}^{-1}$  analysed. Spectral data for both Raman and Optical Photothermal Infrared Spectroscopy were used to generate clustering via principal components analysis and classification models were generated using partial least squared discriminant analysis in order to characterize the techniques' ability to distinguish diseased samples. Optical Photothermal Infrared Spectroscopy could differentiate osteoarthritic extracellular vesicles from healthy with good classification (correct classification rate= 93.4%) whereas Raman displayed poor classification (correct classification rate = 64.3%). Inspection of the infrared spectra indicated that plasma-derived extracellular vesicles from osteoarthritic horses contained increased signal for proteins, lipids and nucleic acids. For the first time we demonstrated the ability to use optical photothermal infrared spectroscopy combined with Raman spectroscopy to interrogate extracellular vesicles and osteoarthritis-related samples. Optical Photothermal Infrared Spectroscopy was superior to Raman in this study, and could distinguish osteoarthritis samples, suggestive of its potential use diagnostically to identify osteoarthritis in equine patients. This study demonstrates the potential of Optical Photothermal Infrared Spectroscopy to be used as a future diagnostic tool in clinical practice, with the capacity to detect changes in extracellular vesicles from clinically derived samples.

## 6.2 Introduction

Osteoarthritis (OA) is a common degenerative disease of the synovial joint, characterised by catabolic processes observed in articular cartilage, and a notable imbalance in bone remodelling. It results in pain, inflammation and reduced mobility (Mustonen and Nieminen, 2021b). OA is the most prevalent cause of equine lameness, with over 60% of horses developing OA within their lifetime; a significant welfare concern (McIlwraith, Frisbie and Kawcak, 2012a). It is a complex heterogeneous condition of multiple causative factors, including mechanical, genetic, metabolic and inflammatory pathway involvement (Clarke, Anderson and Peffers, 2021b). OA pathophysiology is conserved across species, resulting in synovitis, cartilage degradation, osteophyte formation, subchondral bone sclerosis, fibrosis and reduced elastoviscosity of synovial fluid found within the joint capsule (Kuyinu *et al.*, 2016). The horse is of interest not only as a target species for veterinary equine medicine, but also as a model organism to study osteoarthritis due to these established similarities, as well as comparable anatomic structures of the human carpal joint within equine carpal and metacarpophalangeal joints (McIlwraith, Frisbie and Kawcak, 2012a).

Extracellular vesicles (EVs) are nanoparticles enveloped in a phospholipid bilayer membrane, secreted by most mammalian cells, that transport biologically active cargo, such as proteins, RNAs, DNAs, lipids, and metabolites (Boere, Malda, van de Lest, *et al.*, 2018). EVs are divided into subgroups determined by their size and biogenesis. EVs elicit their effects through paracrine signalling, proving fundamental in intercellular communication (Herrmann *et al.*, 2021b). EVs have been implicated in OA progression, and have been shown to be released and enter chondrocytes, synoviocytes and inflammatory cells (Withrow *et al.*, 2016; Esa *et al.*, 2019; Lin *et al.*, 2021). Interestingly EVs can serve as disease propagators; promoting an increased expression of cytokines, chemokines and matrix degrading proteinases, or disease preventing; increasing cellular differentiation and reducing apoptosis (Lin *et al.*, 2021).

As EVs are microscopic they require physicochemical characterisation and we consider that vibrational spectroscopic methods, including Raman and infrared spectroscopies, could provide valuable information about the main molecular constituents commonly found in biological samples such as proteins, lipids, nucleic acids, and carbohydrates. This is based on functional group bond-specific chemical signatures being generated by these techniques in a non-invasive, non-destructive, and label-free manner (Paraskevaidi *et al.*, 2021). In Raman spectroscopy, photons from a monochromatic source interact with the sample and a small fraction of them are inelastically scattered with either higher or lower energies compared with the excitation wavelength. The energy difference between incident and scattered photons corresponds to a Raman shift and it is associated with the chemical



structure of molecules in the sample (Lima, Muhamadali and Goodacre, 2021). Raman spectroscopy can discriminate between cell and tissue types, and detect chemical alterations prior to morphological changes in various pathological states. It has previously been used to assess the purity of EV preparations (Gualerzi, Kooijmans, *et al.*, 2019), as well as identify cellular origin of mesenchymal stem cell (MSC)-derived EVs (Gualerzi, Picciolini, *et al.*, 2019). Infrared spectroscopy is based on the absorption of infrared radiation by molecular vibrations from bonds that possess an electric dipole moment that can change by atomic displacement (Baker *et al.*, 2014).

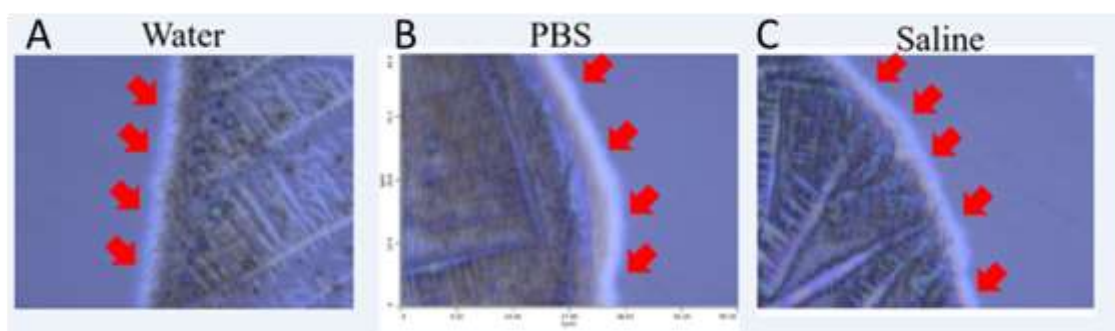
Although Raman and infrared spectroscopies provide molecular information about the overall biochemistry of samples by monitoring the internal motion of atoms in molecules, each method has advantages and disadvantages for different types of samples due to their different working principles. Thus, having both techniques combined in a single platform is a powerful tool with promising applications. More recently, a novel far-field optical technique has been developed in order to acquire Raman and infrared signatures simultaneously from the same location on the sample. In this method, the infrared signatures are collected via Optical Photothermal Infrared Spectroscopy (O-PTIR), which is based on a pump-probe configuration that couples a tuneable infrared quantum cascade laser (QCL) acting as pump and a visible laser to probe the thermal expansion resulting from the temperature rise induced by the QCL. The probe laser also acts as excitation source for acquiring Raman spectrum simultaneously with infrared data at the same spatial resolution (ca. 500 nm spot diameter). This scheme has been used to interrogate tissue samples, mammalian cells (Banas *et al.*, 2021; Gardner *et al.*, 2021) and bacteria (Goodacre *et al.*, 2021) but this is the first study, to our knowledge, to use it in EV or OA samples.

We hypothesised that Raman and O-PTIR can be used to identify potential biomarkers of OA using equine plasma-derived EVs and aimed to test this using a combined vibrational spectroscopic platform.

## 6.3 Results

### 6.3.1 Optimisation of Extracellular Vesicle Suspension for Spectroscopic Analysis

EVs were present in all samples irrespective of the suspension buffer (water, PBS or saline), as shown in Figure 6.1. Qualitatively, EV samples suspended in PBS or saline had the greatest signal. Visually there were a reduced number of EVs present in samples suspended in water. This preliminary study elucidated minimal differences between the EV morphology and integrity of samples suspended in PBS, water or saline. Subsequently plasma EV samples in the main study were suspended in PBS. Such suspension buffer choice has previously been used with EV samples from bovine placenta, bovine peripheral blood mononuclear cells (Zhang, Silva, *et al.*, 2020), and serum and plasma from patients with multiple myeloma (Russo *et al.*, 2020) and sporadic amyotrophic lateral sclerosis (Morasso *et al.*, 2020), that were probed by spectroscopic techniques such as Raman spectroscopy.



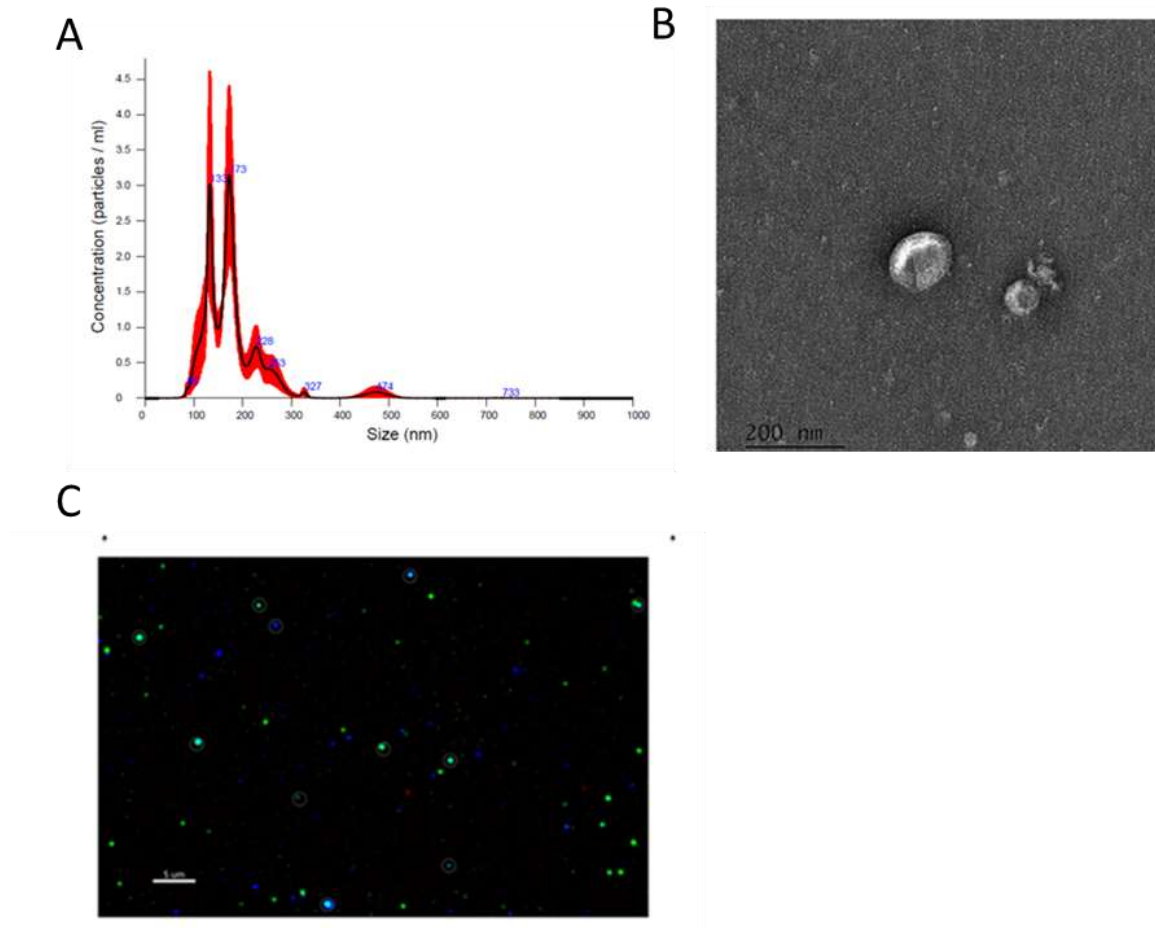
**Figure 6.1. Dry plasma extracellular vesicle samples imaged using the Raman and Optical Photothermal Infrared Spectroscopy instrument.** O-PTIR measurements were acquired on single-point mode using a mIRage infrared microscope and Raman spectra were acquired simultaneously with infrared data using a Horiba Scientific iHR-320 spectrometer coupled to mIRage. Images obtained compare EV morphology when suspended in (A) water, (B) PBS, and (C) saline. EVs can be identified as white a sphere with red arrows depicting where they colocalized to a given substrate.

### 6.3.2. Using Raman and Optical Photothermal Infrared Spectroscopy to identify Synovial Fluid derived Extracellular Vesicle Biomarkers of Naturally Occurring Equine Osteoarthritis

#### 6.3.2.1 Extracellular Vesicle Characterisation

Nanoparticle tracking analysis found that SF-EVs had a mean average concentration of  $1.16 \times 10^8$  particles/ml (Figure 6.2.A). To confirm the particles isolated from SF were EVs, samples were negatively stained and visualised using transmission electron microscopy, in order to identify characteristic EV morphology (Figure 6.2.B). Spherical structures within EV size ranges were identified with a clearly defined peripheral membrane in Figure 6.2.B. Finally, EVs from SF were visualised using

fluorescent microscopy, highlighting positive surface marker expression of CD81, CD9 and CD63 (Figure 6.2.C). No significant difference was observed in EV characteristics between control and disease groups.



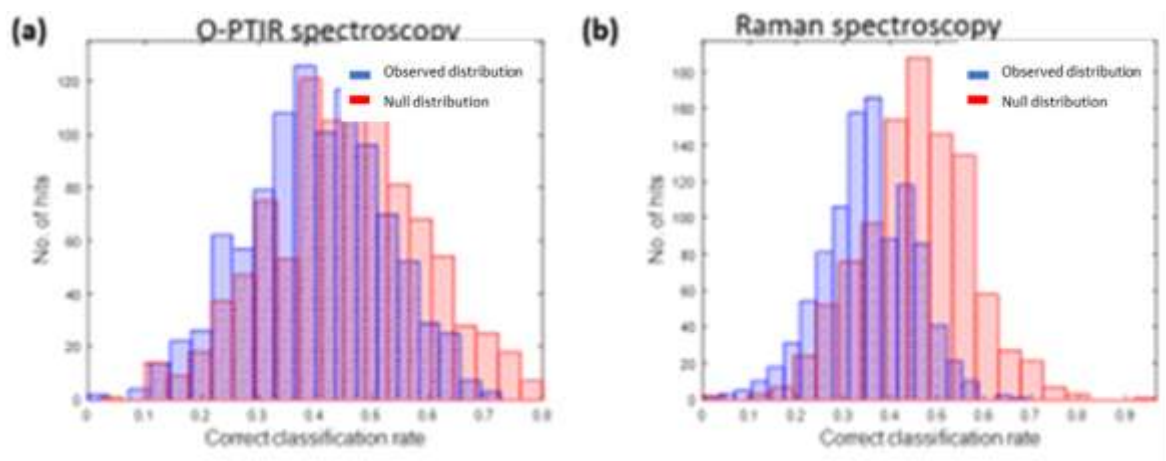
**Figure 6.2. Synovial fluid derived extracellular vesicle characterisation.** (A) Nanoparticle tracking analysis (NTA) of synovial fluid- EVs (SF-EVs). Concentrations of EVs in particles/ml and particle size measured in nm. (B) Transmission electron microscopy of SF-EVs to determine morphology. (C) Fluorescent image of EVs highlighting the presence of specific EV surface markers ( CD9 –blue , CD81- green , CD63- red).

### 6.3.2. Raman and Optical Photothermal Infrared Spectroscopic Analysis

The classification model obtained for the PLS-DA using O-PTIR and Raman data is shown in Figure 6.3. A and B, respectively. Bootstrapping was performed 10000 times to permute whether the EV spectrum was disease or control. The output shows two distributions; a ‘real’ (in blue) and ‘null/random’ (in red) model. These models displayed poor correct classification rates for both O-PTIR and Raman data, indicating no biochemical differences in signal between EVs from diseased and control samples. This study utilised Raman and O-PTIR spectroscopy to probe SF-EVs in order to identify biomarkers for

equine OA. SF-EVs were characterised accordingly, and no significant differences in Raman and OPTIR signals were identified between control and diseased samples. This has been seen previously in orthopaedic conditions in horses (Mustonen *et al.*, 2021b, 2023). Following the use of computational models, it was identified that SF-EV signal reflective of biological cargo did not significantly change in response to disease pathology. This is converse to previous Raman spectroscopy studies in human OA, such studies have identified a significant decrease in glycosaminoglycans, proteoglycans and a significant increase in collagen disorganization, with OA severity (Casal-Beiroa *et al.*, 2021), and protein variance enabled the classification of low-grade and high-grade OA groups with an accuracy of 91% (Bocsa *et al.*, 2019). In addition, comparatively there was a lower concentration of EVs found in SF ( $1.16 \times 10^8$  particles/ml) compared to EVs derived from plasma in the main study ( $2.02 \times 10^9$  particles/ml). As a result, we hypothesised that there may not have been a sufficient number of EVs present in SF compared to that of plasma, and the signal to noise ratio was subsequently too low when SF was suspended in PBS.

Future work should look to use an increased SF volume for EV isolation, type of EV isolation method and explore the effect of sample suspension buffer on this specific biofluid to determine its potential interaction with downstream analysis techniques. Alternatively, it may be regarded that plasma may be a more appropriate source of EVs in a diagnostic context, due to being a less invasive and subsequently more ethical biofluid to source.



**Figure 6.3. Classification model for partial least squares discriminant analysis of infrared and Raman spectra from equine synovial fluid derived extracellular vesicles.** (A) Infrared and (B) Raman spectra showing classification rates for real (blue – from the 10,000 bootstrap analyses) and random (red – from the 10,000 permutation tests).

### 6.3.3 Main Study

#### 6.3.3.1. Statistical Evaluation of Histological and Synovitis Scores

##### *Osteoarthritic Phenotype determined based on Histological and Synovitis Scores*

For statistical evaluation of histological scoring parametric T-test was used. For evaluation of synovitis score non-parametric Mann-Whitney-U test was used. Statistical evaluation was performed between control and diseased using GraphPad Prism 8 (San Diego). Histological score was significantly different between groups ( $p < 0.0001$ ). Synovitis score between groups was not significant ( $p = 0.12$ ).

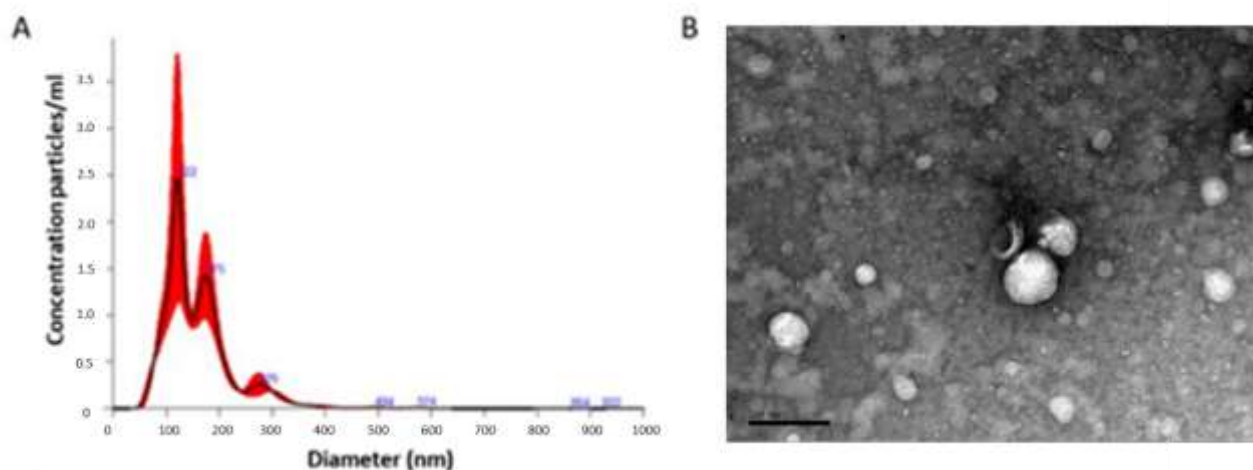
#### 6.3.3.2. Extracellular Vesicle Characterisation

##### *Nanoparticle Tracking Analysis quantifies Extracellular Vesicles from Equine Plasma*

Particle size and concentration characterisation was performed using NTA. NTA determined the average plasma sample concentration to be  $2.02 \times 10^9$  particles/mL. Analysis was suggestive of a heterogeneous population of EVs, ranging from exosomes to microvesicles (Figure 6.4.A).

##### *Transmission Electron Microscopy provides Visualisation of Extracellular Vesicle Morphology*

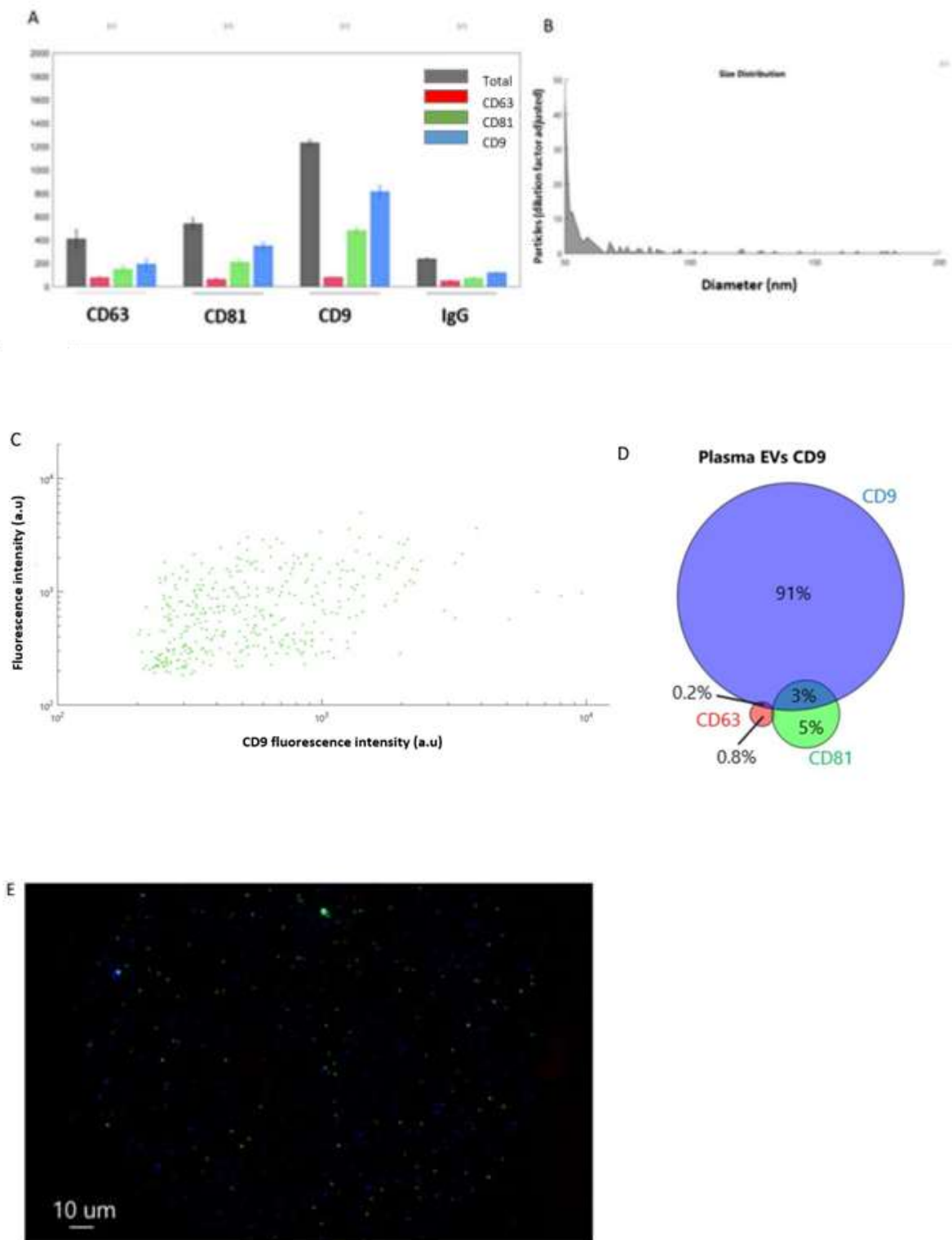
To confirm the particles isolated from plasma samples were indeed EVs we negatively stained and visualised them using TEM. Spherical structures within EV size ranges (30 nm – 100 nm (exosomes) and 100 nm – 1000 nm (microvesicles) were identified with a clearly defined peripheral membrane as shown in Figure 6.4.B.



**Figure 6.4. Characterisation of extracellular vesicles.** (A) Nanoparticle tracking analysis (NTA) of a representative sample of plasma derived EVs (P-EVs). Concentrations of EVs in particles/mL and particle size measured in nm, all measurements recorded using NanoSight NS300, and data analysed by the in-built NanoSight Software NTA 3.1 Build 3.1.46. Hardware: embedded laser: 45 mW at 488 nm; camera: sCMOS. (B) Transmission electron microscopy (TEM) micrograph of negatively stained representative of plasma derived EV samples. Scale bar is equal to 200nm. Samples fixed to grids were visualised using a FEI Tecnai G2 Spirit with Gatan RIO16 digital camera.

#### *Exoview Analysis identifies Exosomal Surface Markers present on Plasma derived Extracellular Vesicles*

ExoView was used on a representative pool of plasma samples. The EVs isolated from plasma had the highest particle counts on the CD9 capture spots, equating to a concentration of approximately  $1.4 \times 10^8$  CD9 positive particles/mL. CD81 ( $7 \times 10^7$  particles/mL) and CD63 ( $6 \times 10^7$  particles/mL positive particles) were also detectable (Figure 6.5.A). It was observed that most EVs detected were less than 100 nm (Figure 6.5.B). It was also found that with plasma derived EV samples, the greater the expression of CD9 the greater the corresponding expression of CD81, whereby a distinct positive correlation was observed (Figure 6.5.C). Co-localisation analysis was also performed and identifying that 91% of plasma-derived EVs were positive for the CD9 surface tetraspanin, followed by 5% expressing CD81, and 3% expressing both CD81 and CD9. CD63 expression was lowest at 0.8% (Figure 6.5.D). Finally, EVs were visualised using fluorescent microscopy, as shown in Figure 6.5.E.



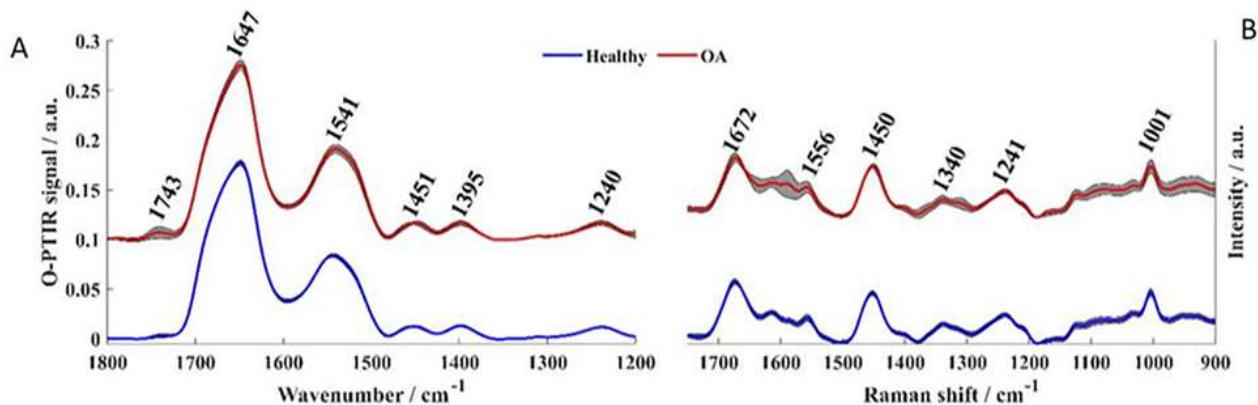
**Figure 6.5. ExoView assay results.** (A) Particle counts for plasma EVs from the human tetraspanin chip, (B) a size histogram of plasma EV samples as captured on the CD9 human tetraspanin chip, (C) a scatter diagram demonstrating correlation between the number of CD9 positive EVs (X axis) and CD81 positive EVs (Y axis), (D) colocalization analysis of the presence of surface tetraspanins on equine plasma EVs, and (E) fluorescent microscopy visualizing plasma-derived EVs, with colour denoting surface tetraspanin positive identification (red – CD63, blue – CD9, and green – CD81).

### 6.3.3.3. *Raman Spectroscopy and Optical Photothermal Infrared Spectroscopy*

#### *Optical Photothermal Infrared Spectroscopy superior to Raman Spectroscopy in identifying Disease associated changes in Equine Plasma Extracellular Vesicles*

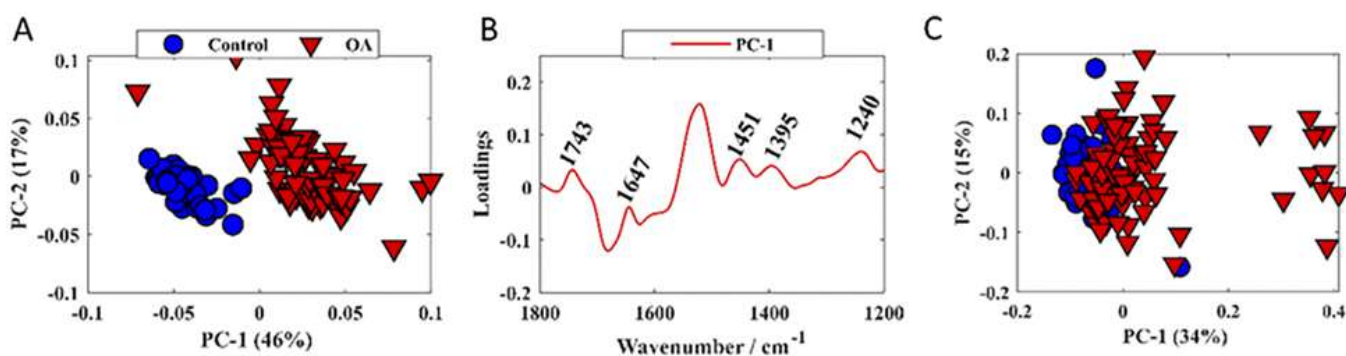
Infrared and Raman spectral data collected from healthy control and diseased plasma derived EV samples displayed similar biochemical features with subtle changes in signal intensity, while appearance or disappearance of peaks were not observed (Figure 6.6 A and B). Infrared signatures acquired by O-PTIR spectroscopy were recorded from 950-1800  $\text{cm}^{-1}$  as this is the spectral range covered by the tunable QCL used as excitation source, however, bands peaking below 1200  $\text{cm}^{-1}$  were removed from the analysis due to interference from bands attributed to minerals from PBS. The band peaking at 1743  $\text{cm}^{-1}$  arose from C=O ester groups from lipids including phospholipids, triglycerides and cholesterol. Amide I vibration, peaking at 1647  $\text{cm}^{-1}$  was associated mainly to C=O stretching vibration from peptide bonds in proteins (Barth, 2007; Mihály *et al.*, 2017; Paolini *et al.*, 2020). Amide II band absorption was found in 1544  $\text{cm}^{-1}$  and is attributed to the out-of-phase combination of the N-H in-plane bend and C-N stretching vibration with smaller contributions from the C-O in-plane bend and the C-C and N-C stretching vibrations of peptide groups (Barth, 2007; Mihály *et al.*, 2017; Paolini *et al.*, 2020). The band observed at 1240  $\text{cm}^{-1}$  results from the coupling between C-N and N-H stretching from proteins (amide III) (Barth, 2007), but it was also influenced by PO<sub>2</sub><sup>-</sup> asymmetric stretching from phosphodiester bonds in nucleic acids (Paraskevaidi *et al.*, 2021). The peak at 1451  $\text{cm}^{-1}$  corresponded to bending vibration (scissoring) of acyl CH<sub>2</sub> groups in lipids (Barth, 2007; Mihály *et al.*, 2017; Paolini *et al.*, 2020), whereas the band peaking at 1395  $\text{cm}^{-1}$  arises from COO<sup>-</sup> symmetric stretching from amino acid side chains and fatty acids (Barth, 2007; Mihály *et al.*, 2017; Paolini *et al.*, 2020). Although Raman signatures were collected between 500-3400  $\text{cm}^{-1}$ , only the fingerprint region (500-1800  $\text{cm}^{-1}$ ) was evaluated as the vast majority of molecular vibrations are found peaking in this region. Spectral signatures from minerals were also observed in Raman spectrum acquired from healthy and diseased samples in the low wavenumber region (below 900  $\text{cm}^{-1}$ ), therefore, only bands peaking between 900-1800  $\text{cm}^{-1}$  were analysed. In Raman spectra, peaks associated with amide I, II, and III from peptide bonds were observed peaking at 1672, 1556, and 1241  $\text{cm}^{-1}$  respectively (Gualerzi, Kooijmans, *et al.*, 2019; Zhang, Silva, *et al.*, 2020). The band at 1450  $\text{cm}^{-1}$  originated from CH<sub>2</sub>/CH<sub>3</sub> bending vibrations from lipids and proteins, while the peak at 1004  $\text{cm}^{-1}$  was attributed to the phenylalanine ring breathing, and the peak at 1340  $\text{cm}^{-1}$  was associated to nucleic acids (Gualerzi, Kooijmans, *et al.*, 2019; Zhang, Silva, *et al.*, 2020).





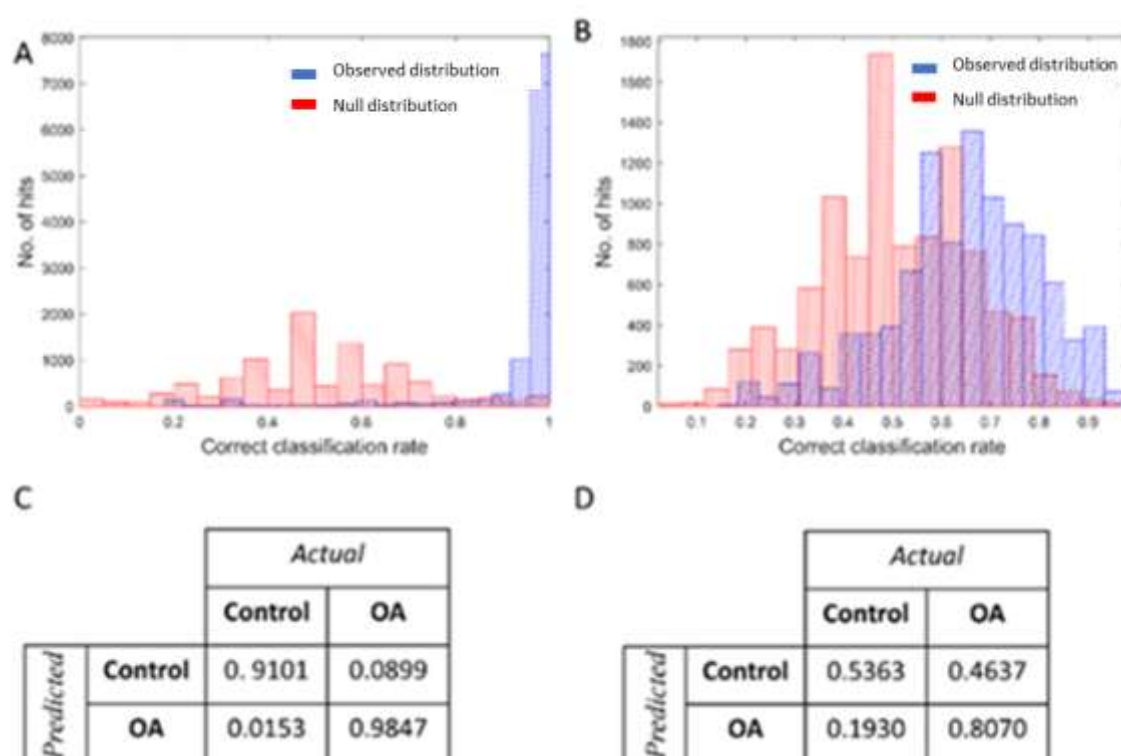
**Figure 6.6. Fingerprint region of averaged spectra.** A) Infrared and B) Raman spectra collected from healthy control (blue line) and OA (red line) samples. Plots are offset for clarity.

Infrared and Raman were first subjected to principal component analysis (PCA) in order to examine the ability of both techniques to discriminate healthy control and diseased plasma-derived EV samples (Figure 6.7). PC scores plot obtained from O-PTIR (infrared signatures) as input data showed satisfactory discrimination between healthy control and diseased samples (Figure 6.7.A), with scores from control samples grouping on the negative side of PC-1 axis, whilst scores related to OA clustered on positive side of the PC-1 axis. The loadings plot (Figure 6.7.B) was used to reveal the importance of the input variables on the PCA and positive loadings to all bands displayed in Figure 6.7.A, indicating higher amount of the molecular constituents associated with these vibrations, i.e., proteins, lipids and nucleic acids, in samples derived from plasma EVs in OA. The scores plot obtained by subjecting Raman signatures to PCA displayed poor discrimination between healthy control and OA samples (Figure 6.7.C). This was why we did not display the corresponding loadings plot.



**Figure 6.7. Principal component analysis scores and loadings plots.** Plots were obtained by subjecting infrared data to PCA (A and B); (C) PC scores plot of Raman data; Values in parentheses are the percentage total explained variance (TEV).

Raman and O-PTIR spectral data were used as input for PLS-DA in order to generate a model for classifying OA and control samples based on EV composition. In this study, a total of 130 spectra (10 spectra per animal; 50 spectra from healthy and 80 spectra from OA) were used as input data for PLS-DA. Each IR spectrum has 300 variables (O-PTIR intensities associated to each wavenumber between 1200-1800  $\text{cm}^{-1}$ ), whereas each Raman spectrum provides 480 variables. The classification models and confusion matrices obtained by PLS-DA using O-PTIR and Raman data are shown in Figure 6.8. Bootstrapping and permutation testing were performed 10,000 times to assess overall model performance and to decide whether the EV spectrum was classified as OA or control. PLS-DA model obtained from O-PTIR data achieved sensitivity, specificity, and positive predictive values of 97.5 %, 97.6 %, 96.7 %, while PLS-DA model generated by using Raman signatures as input data presented poor classification rates (sensitivity (66.37 %), specificity (66.37 %), and positive predictive values (64.62 %)). These findings agree with the results obtained by PCA, indicating superior ability of O-PTIR to discriminate healthy from OA samples.



**Figure 6.8. Classification model for partial least squares discriminant analysis of infrared and Raman spectra.** (A) Infrared and (B) Raman spectra showing classification rates for real (blue – from the 10,000 bootstrap analyses) and random (red – from the 10,000 permutation tests), with a sensitivity, specificity, and positive predictive value of 97.5 %, 97.6 %, 96.7 % for infrared, respectively. (C) and (D) are the average confusion matrices for infrared and Raman, respectively, with rows representing predicted classification and columns representing experimental.

#### 6.4. Discussion

This study investigated for the first time whether O-PTIR and Raman spectroscopies could be used to interrogate plasma-derived EVs in control and OA equine samples. We demonstrated that indeed the novel spectroscopy technique O-PTIR was able to determine differences in EV content attributed to disease pathology, while Raman spectroscopy provided poorer classification models. Thus O-PTIR could serve as a platform for as future biomarker studies in equine OA.

Clinical equine OA samples were used due to an interest in exploring the EV metabolome of equine OA. The fetlock joints were assessed for OA by histological scoring at post-mortem. The fetlock joint (metacarpophalangeal joint) is the most commonly afflicted joints in equine athletes (Bertoni *et al.*, 2020). Thoroughbred race horses are known to be a valuable model of natural occurring post traumatic osteoarthritis, with an increased prevalence of disease as a result of sustained repetitive impact, leading to subsequent joint injuries (Bertuglia *et al.*, 2016). As such our sample population was used as an appropriately characterised set of OA samples, with adequate volume to isolate EVs and use the proposed techniques to answer our research question. Additionally, we had extensive clinical records for our sample population. Finally, all horses were stabled, managed and raced at the same location enabling horses exposed to similar husbandry to be used.

Mankin score between control and diseased joints was significantly different ( $P < 0.0001$ ). However, synovitis score between groups was not ( $p = 0.12$ ), this may be reflective of the equine discipline the sample donors were used within, as horseracing involves a repetitive motion and large forces being applied to joints in the associated limbs, subsequently resulting in a degree of trauma to the joint capsule. In humans OA is often accompanied by inflammation caused by the immune response. However, we have described that there is no correlation between OA and synovitis score in horses with metacarpophalangeal OA (Gupta, Dimsaite and Peffers, 2020). Whilst we had extensive clinical and post-mortem records that did not indicate the horses had other underlying inflammatory conditions, without additional studies in other inflammatory conditions we cannot rule out that changes were due to inflammation as opposed to OA. Thus, OPTIR may be differentiating other factors not exclusive to OA.

EVs are a heterogenous group of nanoparticles, categorized based on size and biogenesis, however it is common practice to design experiments encompassing microvesicles and exosomes, due to the current inability of techniques to confidently isolate specific subgroups alone. This is reflective of the infancy of this research field. It is known that choice of isolation method can alter the heterogeneity of EV sample collected, with varying proportions of vesicles derived from both endosomal multivesicular bodies and plasma membrane budding as a result. The most common isolation methods

include size exclusion chromatography, precipitation and differential ultracentrifugation. As demonstrated by Brennan *et al* (Brennan *et al.*, 2020) in a study comparing human serum EVs, noting the number of EVs, protein and lipoprotein content varied between isolation method.

Plasma EV concentration ( $2.02 \times 10^9$  particles/ml) was quantified using NTA, an accepted method of EV evaluation known for its repeatability and reproducibility (Vestad *et al.*, 2017). The representative plasma sample shown reflects the biological sample heterogeneity, showing a range of EV sizes indicative of both exosome and microvesicles subgroups. The concentration determined was similar to those reported for plasma EVs in other species within the literature. For example, human plasma EVs were identified by Palviainen *et al* (Palviainen *et al.*, 2020) at  $2.46 \times 10^9 - 1.10 \times 10^{10}$  particles per ml. However, a study analysing plasma EVs across the duration of equine endurance racing found that baseline plasma EV concentration was  $5.6 \times 10^{12}$  particle per ml (de Oliveira *et al.*, 2021). The difference observed may be a result of horse breed and discipline used within such study. ExoView analysis identified EVs that were positive for the tetraspanin CD81 and CD9, however a low percentage of EVs were positive for the surface marker CD63. This may be a result of poor protein homology between equine and humans for this protein. However, a recent paper using intracellular trafficking demonstrated that CD63 expression in HeLa cells was specific to exosomes, and often a lack of CD63 expression may be due to small microvesicle production, referred to as ectosomes, and that this type of EV is far more prolific than CD63 positive exosomes (Kim *et al.*, 2019).

PCA and PLS-DA were used to analyse spectral data in order to evaluate the outputs obtained by an unsupervised (PCA) and a supervised (PLS-DA) method. PCA is the gold standard for unsupervised data analysis and highlights that EVs can be separated using O-PTIR but not from Raman data. PLS-DA is a popular method applied to metabolomics and spectroscopy data for supervised learning and hence PLS-DA was used to corroborate the PCA results. Infrared spectroscopy techniques have been used to probe EVs previously in order to identify structural components (Kim *et al.*, 2019) as well as proteins, lipid and nucleic acid components, as found in our study (Kim *et al.*, 2019). This is the first paper to our knowledge to probe OA EVs using Raman spectroscopy and O-PTIR spectroscopy which have the advantage that they use a very small sample volume. In other work, Zhai *et al* (Zhai *et al.*, 2019) found that in bone mineral carbonate content varied significantly with OA stage, with carbonate increasing with OA. They also identified using Fourier transform infrared (FT-IR) spectroscopy that acid phosphate, collagen maturity and crystallinity varied with OA. In addition, the use of infrared spectroscopy is compounded by the findings of Afara *et al* (Afara *et al.*, 2017) in a study utilising an experimental model of OA in rats. Here the spectral differences between control and OA samples could be correlated to Mankin score and glycosaminoglycan content. A previous study by our group used attenuated total reflection FT-IR (ATR-FTIR) spectroscopy on OA equine serum. This infrared

spectroscopy study found separation between groups with 100% sensitivity and specificity, and the six most significant peaks between groups was attributed to proteins and lipids. Similarly, this was observed within our current study, with increased abundance found within the OA group. The stated study postulated these observations may be associated to increased lipid and protein expression including increased expression of type 1 collagen, and decreased expression of type 2 collagen characteristic of OA (Paraskevaidi *et al.*, 2020).

Previously, changes in protein and lipid concentration in plasma and serum derived from OA patients has been described. One study utilised serum samples from horses to discriminate proteomic changes due to exercise or the development of early OA (Frisbie *et al.*, 2008). Researchers identified six biomarkers with the ability to discriminate OA from exercise groups. For example, the concentration of serum C1,2C (reflective of type 1 and 2 collagen degradation fragments) and collagen 1 was found to significantly increase in OA groups compared with exercise alone (Frisbie *et al.*, 2008). In addition, a multiplexed proteomic study on human OA serum identified a panel of 14 candidate biomarkers for OA, utilising cartilage, synovial fluid, chondrocytes and serum (Fernández-Puente *et al.*, 2017). These prospective biomarkers include von Willebrand factor (inflammation and haemostasis) and haptoglobin (an inflammation inducible plasma protein). Furthermore, a previous study in plasma identified different lipid profiles in OA using a destabilisation of the medial meniscus model in mice (Pousinis *et al.*, 2020). Altered lipids included classes of cholesterol esters, fatty acids, phosphatidylcholines, N-acylethanolamines, and sphingomyelins and some were attributed to cartilage degradation.

Raman spectroscopy has been employed to characterise EVs and their composition. It has been used to interrogate EVs undergoing autophagy (Chalapathi *et al.*, 2020), as well as distinguishing EVs derived from bovine placenta and mononuclear cells (Zhang, Silva, *et al.*, 2020), identifying differential features in Parkinson's disease pathology (Gualerzi, Picciolini, *et al.*, 2019) and sporadic Amyotrophic Lateral Sclerosis (Morasso *et al.*, 2020). Additionally, it has been applied to successfully discriminate between healthy and diseased joint tissues in order to identify subtle molecular and biochemical changes as a result of disease. Buchwald *et al* (Buchwald *et al.*, 2012) utilised Raman spectroscopy to identify compositional and structural changes in bone from the hip joints of OA patients demonstrating that subchondral bone from OA patients was less mineralised due to a decrease in hydroxyapatite. Furthermore, a study performed by de Souza *et al* using two *in vivo* experimental rat models of knee OA (treadmill exercise induced and collagenase induced) established molecular signatures unique to OA. Raman ratios relating to mineralization and tissue remodelling were significantly higher in OA groups. Specifically, the ratio between phosphate and amide III has been shown to reflect the degree of mineralisation and carbonate/ amide III is indicative of bone

remodelling. De Souza *et al* (De Souza *et al.*, 2014) also commented on the lack of literature available with regard to the use of Raman spectroscopy for OA research and the importance of this developing field. More recently, Hosu *et al* (Hosu *et al.*, 2019) reviewed the importance of Raman spectroscopy in identifying pathologically associated crystals such as monosodium urate and calcium pyrophosphate dihydrate in rheumatoid diseases.

Optical photothermal infrared spectroscopy requires minimal sample preparation enabling reduced analysis time when obtaining submicron spatial resolution. Subsequently O-PTIR is advantageous over other traditionally used methods such as Fourier transform infrared spectroscopy and quantum cascade laser microscopy (Kansiz *et al.*, 2021). This makes it a useful technique as it is also highly sensitive. Furthermore, the equipment used is smaller in size compared to other metabolomic techniques, such as nuclear magnetic resonance spectroscopy. Thus, having the possibility of placement 'stableside' or within an equine diagnostic laboratory. As such it has a greater capacity to be used in a clinical setting in the future. One disadvantage is that currently O-PTIR analysis of EVs requires sample concentration in order to achieve an appropriate signal.

We recognise a number of limitations in our study. We were restrained by the number of samples available to us, and our findings need validation in a larger cohort. Our sample was small due to the use of clinically sourced samples. Future studies will require replication of our analysis with a large cohort of samples. There are currently no definitive equine OA EV markers. Therefore, we cannot say definitively that the plasma-derived EVs used in this study are from the OA joint or due to OA. Thus, we cannot say definitively that OPTIR is not differentiating other factors, not exclusive to OA. We are currently undertaking a number of studies to identify equine EV markers specific for OA including mass spectrometry lipidomic, NMR lipidomic and small non-coding RNA sequencing studies of equine EVs. In our recent paper (Anderson *et al.*, 2022) we described a number of small non-coding RNAs changing in OA in both plasma and synovial fluid derived EVs. Unfortunately, we did not have any remaining plasma from the horses used in this study to complement our findings here and show the EVs interrogated were OA related. Thus, in the future additional studies will be needed to determine if the EVs isolated from plasma in this study are OA specific. In addition, large sample volumes were necessary to have an adequate number of EVs for analysis, providing an appropriate signal to noise ratio. Moreover, due to the large sample volumes required, repeated studies using other appropriate techniques such as NMR spectroscopy for validation were not possible. In our future studies minimum sample volume required will be optimized. Additionally, we used a single time point 'snap shot' of disease. Further work is needed to determine if O-PTIR is sensitive enough to determine differences in a range of different OA phenotypes and severities, and correlate differences to specific biological functions of EVs.

Overall this study demonstrates a ‘proof of concept’ with respect to the potential of Raman and OPTIR spectroscopy to be used as a diagnostic tool in clinical practice. Further work is required to identify if OA-related changes in plasma-derived EVs are related to the pathogenesis in the joint by utilising mechanistic study design, as well as exploring further validation with the use of additional metabolomics techniques- such as NMR metabolomics. We are currently quantifying the EV cargo using NMR metabolomics, mass spectrometry proteomics and sequencing platforms in order to provide complete characterisation of EVs in OA and determine their contribution to disease propagation.

## **6.5. Conclusion**

EVs derived from equine plasma in OA were probed using Raman and O-PTIR spectroscopy. O-PTIR spectroscopic analysis was found to be superior in classifying samples from OA patients compared to Raman spectroscopy. O-PTIR spectroscopy is an exciting potential platform for the analysis of plasma to diagnose OA in both human and horse, with this study pathing the way for future research to explore diagnostic capacity of the spectroscopic techniques further.

## **6.6. Ethics**

Plasma samples were collected in accordance with the Hong Kong Jockey Club owner consent regulations (VREC561). Samples were selected due to reflecting a natural model of post-traumatic osteoarthritis. All samples were from thoroughbred racehorses, and were collected between November 2005 and March 2009 from horses actively race training up to the time of death or had previously retired from active race training that were euthanized on welfare grounds.

## **6.7. Funding**

Emily Clarke is a self-funded PhD student. Mandy Peffers is funded through a Wellcome Trust Intermediate Clinical Fellowship (107471/Z/15/Z). Catarina Castanheira is funded through a Horse Trust PhD studentship (G5018). James Anderson’s postdoctoral position is funded through a Horserace Betting Levy Board Research Project Grant (T15). Jacob Hyett was supported by INSPIRE in conjunction with the Academy of Medical Sciences. Our work is also supported by the Medical Research Council (MRC) and Versus Arthritis as part of the MRC Versus Arthritis Centre for Integrated research into Musculoskeletal Ageing (CIMA).

## **6.8. Acknowledgments**

We would like to acknowledge to collaboration and support provided by the centre for metabolomics research.



## 7. Manuscript 3

### **Proteome and Phospholipidome Interrelationship of Synovial Fluid-derived Extracellular Vesicles in Equine Osteoarthritis: An Exploratory ‘Multi-Omics’ Study to Identify Composite Biomarkers**

**Emily J Clarke**<sup>1†</sup>, **Laura Varela**<sup>2,3†</sup>, Rosalind E Jenkins<sup>4</sup>, Estefanía Lozano-Andrés<sup>3,5</sup>, Anna Cywińska<sup>6</sup>, Maciej Przewozny<sup>7</sup>, P. René van Weeren<sup>2</sup>, Chris H.A. van de Lest<sup>2,3</sup>, Mandy Peffers<sup>1,\*</sup>, Marca H.M. Wauben<sup>3\*</sup>

<sup>1</sup> Department of Musculoskeletal Biology and Ageing Science, Institute of Life Course and Medical Sciences, University of Liverpool, Liverpool, United Kingdom

<sup>2</sup> Division Equine Sciences, Department of Clinical Sciences, Faculty of Veterinary Medicine, Utrecht University, Utrecht, the Netherlands

<sup>3</sup> Division Cell Biology, Metabolism & Cancer, Department of Biomolecular Health Sciences, Faculty of Veterinary Medicine, Utrecht University, Utrecht, the Netherlands

<sup>4</sup> Centre for Drug Safety Science Bioanalytical Facility, Liverpool Shared Research Facilities, Department of Pharmacology and Therapeutics, Institute of Systems, Molecular and Integrative Biology, University of Liverpool, Liverpool, United Kingdom

<sup>5</sup> Division of Infectious Diseases & Immunology, Department Biomolecular Health Sciences, Faculty of Veterinary Medicine, Utrecht University, Utrecht, the Netherlands

<sup>6</sup> Faculty of Biological and Veterinary Sciences, Nicolaus Copernicus University in Torun, 87-100 Torun, Poland

<sup>7</sup> EQUI VET SERWIS, Wygoda 6, 64-320, Buk, Poland

† \* authors contributed equally

#### **Keywords:**

**Osteoarthritis, synovial fluid, proteomics, lipidomics, equine, extracellular vesicles, biomarker**

#### **Declaration of author contributions**

**EJC:** Conceptualisation, Formal analysis, Funding acquisition, Investigation, Project administration, Validation, Visualisation, Writing - Original Draft, Writing - Review & Editing; **LV:** Conceptualisation, Formal analysis, Investigation, Project administration, Validation, Visualisation, Writing - Original Draft, Writing - Review & Editing; **RJ:** Data Curation, Formal analysis, Investigation, Validation, Writing - Review & Editing; **EL-A:** Investigation, Writing - Review & Editing; **AC:** Resources, Writing - Review & Editing; **MP:** Resources; **PRW:** Funding acquisition, Project administration, Supervision, Writing - Review & Editing; **CL:** Conceptualisation, Data Curation, Formal analysis, Validation, Supervision, Software, Writing - Review & Editing; **MW and MJP:** Conceptualisation, Project administration, Supervision,

## 7.1 Abstract

Osteoarthritis causes progressive joint deterioration, severe morbidity, and reduced mobility in both humans and horses. Currently, osteoarthritis is diagnosed at late stages through clinical examination and radiographic imaging, hence it is challenging to address and provide timely therapeutic interventions to slow disease progression or ameliorate symptoms. Extracellular vesicles are cell-derived vesicles that play a key role in cell-to-cell communication and are potential sources for composite biomarker panel discovery. We used a multi-omics strategy, combining proteomics and phospholipidomics, in an integral approach to identify composite biomarkers associated with purified extracellular vesicles from synovial fluid of healthy, mildly and severely osteoarthritic equine joints. Although the number of extracellular vesicles was unaffected by osteoarthritis, the proteome profiling of extracellular vesicles by mass spectrometry identified 37 differentially expressed proteins (non-adjusted  $p < 0.05$ ) following analysis of variance analysis and pairwise comparisons using a post hoc Tukey test across experimental groups, associated with significant canonical pathways, including Rho family GTPase signalling and complement activation associated with cartilage homeostasis and inflammation. Subsequently unveiling changes in disease and molecular functions during osteoarthritis development. Phospholipidome profiling by mass spectrometry showed a relative increase in sphingomyelin and a decrease in phosphatidylcholine, phosphatidylinositol, and phosphatidylserine in extracellular vesicles derived from osteoarthritic joints compared to healthy joints. Unsupervised data integration revealed positive correlations between the proteome and the phospholipidome. Comprehensive analysis showed that some phospholipids and their related proteins increased with the severity of osteoarthritis, while others decreased or remained stable. Altogether our data show interrelationships between synovial fluid extracellular vesicle-associated phospholipids and proteins responding to osteoarthritis pathology which could be explored as potential composite diagnostic biomarkers of disease.

## 7.2 Introduction

Osteoarthritis (OA) is the most prevalent joint disease and is one of the most important causes of pain and loss of quality of life in the older population (Allen, Thoma and Golightly, 2022). OA has often been classified as a chronic degenerative joint disease resulting from an imbalance between anabolic and catabolic processes in articular cartilage. However, OA has an important inflammatory component, the mediators of which trigger an aberrant remodelling of joint structures (Sokolove and Lepus, 2013). These may include synovial membrane dysfunction, abnormal bone proliferation, and subchondral bone sclerosis (Anderson, Phelan, Foddy, *et al.*, 2020a). Age, gender, obesity, genetics, activity level, joint loading, aberrant morphology and alignment, previous injuries, and muscle weakness are the most prevalent risk factors for OA (Roos and Arden, 2016). OA in horses is a major cause of lameness, with over 60% of lameness cases associated with a clinical diagnosis of OA (McIlwraith, Frisbie and Kawcak, 2012a). This results in impaired mobility, pain, poor performance, and early retirement, making equine OA a serious welfare issue that also leads to significant economic losses for the equine industry (C. Andersen, Jacobsen, *et al.*, 2022b).

Previously, it has been shown that human and equine OA pathogenesis follows a similar route from initial injury to disease progression and subsequent clinical signs, and as such, the horse is widely regarded as a clinically relevant model for musculoskeletal disease in humans (Ribitsch *et al.*, 2020). In addition, the horse's articular cartilage is comparable to that of humans with respect to both composition and thickness (Malda *et al.*, 2012). The horse as a model for disease offers numerous benefits, including the applicability of advanced diagnostic methodologies, such as magnetic resonance imaging (MRI) and arthroscopy, as well as serial sampling of biological material for analysis making it possible to monitor disease development, disease progression and response to intervention in great detail (Ribitsch *et al.*, 2020).

OA pathophysiology is not fully understood. The diagnosis is commonly based on clinical examination and radiographic imaging and, due to the insidious character of the disorder, is often made at late stages when cartilage damage is already substantial and far exceeds the tissue's capacity for intrinsic repair (Castanheira *et al.*, 2021). Therefore, it is paramount to identify biomarkers of disease that can be used to develop diagnostic tests that are both sensitive and specific for early OA, which could enable a timelier therapeutic intervention to decelerate disease progression.

In recent years, the concept of composite biomarkers has become popular; by definition, they are a non-linear combination of multiple measurements used to diagnose disease or predict outcomes (Kyriazakos *et al.*, 2021). Thus far, they have been used in neurological diseases such as Alzheimer's disease and bipolar disorder (Munkholm *et al.*, 2019), often using neuronal networks, artificial

intelligence or machine learning algorithms. Extracellular vesicles (EVs) can be considered a biological source for composite biomarker discovery.

EVs are nanoscale-sized vesicles with a phospholipid bilayer membrane secreted by cells and specialised in restoring homeostasis or facilitating intercellular communication (Buzas *et al.*, 2014). Furthermore, EVs transport bioactive molecules that can elicit a response in recipient cells, resulting in physiological and phenotypic changes (Russell *et al.*, 2019; Couch *et al.*, 2021). They are present in tissues and body fluids, such as blood, urine and synovial fluid (SF) (Boere, van de Lest, *et al.*, 2016; Erdbrügger *et al.*, 2021; Tóth *et al.*, 2021). It has been proposed that EVs may play a vital role in cartilage homeostasis and in the propagation of OA by promoting inflammation and regulating extracellular matrix (ECM) turnover (Malda *et al.*, 2016; Boere, Malda, Van De Lest, *et al.*, 2018; Anderson *et al.*, 2022; Varela *et al.*, 2023) EVs are found in abundance in SF due to its close proximity to EV-secreting cells found within the joint space and periarticular tissues, including but not limited to chondrocytes and synoviocytes (Esa, Connolly and Archer, 2019). For joint disorders such as OA, SF is thus a valuable source of biochemical information (Malda *et al.*, 2016; Clarke, Anderson and Peffers, 2021b; Varela *et al.*, 2023).

The translation of EV biomarkers to the clinic has been pioneered in the fields of cancer and neurodegenerative diseases (Zhao *et al.*, 2019; Kapogiannis, 2020). Nowadays, EVs are increasingly seen as a source for biomarker discovery for various disorders, including joint disease (Malda *et al.*, 2016; Boere, Malda, Van De Lest, *et al.*, 2018; Mustonen and Nieminen, 2021a). A comprehensive understanding of the molecular composition of EVs and their role in disease requires the interpretation of molecular intricacy by accounting for multiple biological levels, such as the proteome and phospholipidome (Phuyal *et al.*, 2015; Subramanian *et al.*, 2020a). Such a comprehensive experimental and data analysis approach provides a more thorough understanding of the complete spectrum of molecular changes contributing to cellular response, disease development and pathogenesis and is helpful for the identification of naturally occurring composite biomarkers. Recent studies in ovarian cancer (Cheng *et al.*, 2020) and Alzheimer's disease (Cohn *et al.*, 2021) have identified a relationship between the proteome and phospholipidome of EVs.

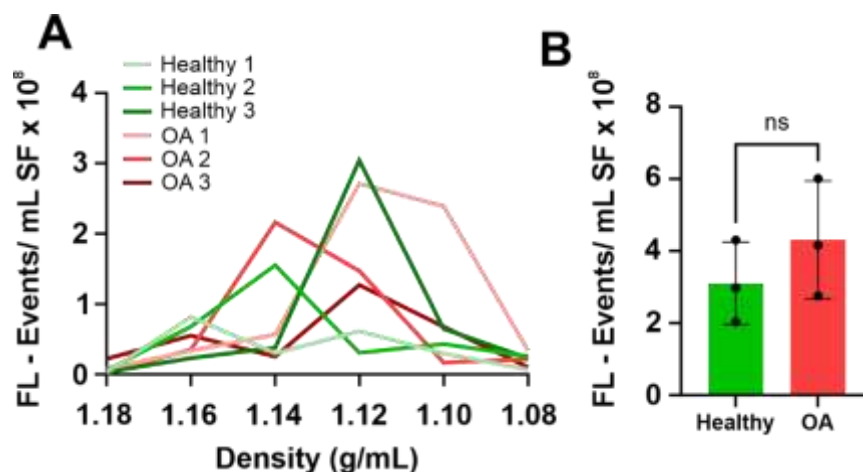
The present exploratory study exploited omics-based technologies to analyse the proteome and phospholipidome of SF-derived EVs (SF-EVs) to 1) enable comprehensive profiling of a healthy state versus clinically diagnosed mild and severe OA in horses and 2) identify candidate composite diagnostic biomarkers of OA.

## 7.3 Results

### 7.3.1 Extracellular Vesicle Characterisation

#### 7.3.1.1 Synovial Fluid-derived Extracellular Vesicle numbers do not differ between Osteoarthritic and Healthy Phenotypes

Recently we found that an inflammatory insult in the joint, such as lipopolysaccharide (LPS), can strongly affect the quantity of SF-EVs (Varela *et al.*, 2023). Therefore, we investigated, using the same technology, if the quantity of SF-EVs was altered as a result of OA using samples from equine patients with radiographically diagnosed OA and comparing these with samples from healthy joints. The quantity of EVs was assessed by single-EV fluorescence-based flow cytometric analysis of PKH-labelled EVs (Arkesteijn *et al.*, 2020; Varela *et al.*, 2023) on three representative samples of the group with healthy joints, two samples of the mild OA group and 1 of the severe OA group. The PKH+ events were measured in individual sucrose fractions ranging from 1.08 to 1.18 g/ml. The peak of fluorescent events was identified in the densities from 1.10 to 1.16 g/ml (Figure 7.1.A); those were considered the EV-enriched fractions and were used for calculating EV numbers (Figure 7.1.B). We did not observe statistically significant differences between the numbers of SF-EV from the healthy joints (where each sample consisted of SF-derived from three different horses) ( $3.1 \times 10^8$  per ml SF  $\pm 6.6 \times 10^7$ ; mean  $\pm$  SD) and OA samples (i.e. mild OA n=2 and severe OA n=1, each consisting of SF-derived from three different OA-diagnosed horses with the respective severity degree of OA) ( $4.0 \times 10^8$  per ml  $\pm 9.4 \times 10^7$ ; mean  $\pm$  SD).



**Figure 7.1. Quantitative flow cytometric analysis of extracellular vesicles isolated from equine joints with a healthy or osteoarthritic phenotype.** A) Single EV-based high-resolution FCM of representative healthy SF-EVs (n=3) and OA SF-EVs (n=2) from the mild OA group and from the severe OA group (n=1). Sucrose density gradient fractions containing EVs labelled with the lipophilic dye PKH67 were measured for 30 seconds. The majority of EVs floated at densities of 1.16-1.10 g/ml. FL – Events: Fluorescent Events. B) EV concentration in SF was calculated as the sum of single fluorescent events measurements (PKH67+ events) in EV-containing sucrose gradient densities (1.16 to 1.10 g/ml). Mean

± SD. ns: non-significance by Student's t-test. The uppermost point in the OA group reflects the severe OA phenotype.

### 7.3.2 Lipidomic Analysis

#### 7.3.2.1 Synovial Fluid-derived Extracellular Vesicle Phospholipid Profiles change during the Development of Osteoarthritis

Previously we had observed a drastic change in the phospholipidome following an inflammatory stimulus (Varela *et al.*, 2023). Here we analysed whether the phospholipid profile of the SF-EVs was modified as a result of OA. The phospholipidome profile of the SF-EV from healthy joints, mild OA, and severe OA was determined through a bioinformatics analysis that uncovered 280 lipid species after lipid annotation (and background adjustment), isotope and adduct correction and normalisation by the cumulative sum to unity. A PCA, an unsupervised dimensionality reduction method, revealed a combined explained variance of 69% with the first and second principal components (Figure 7.2.A).

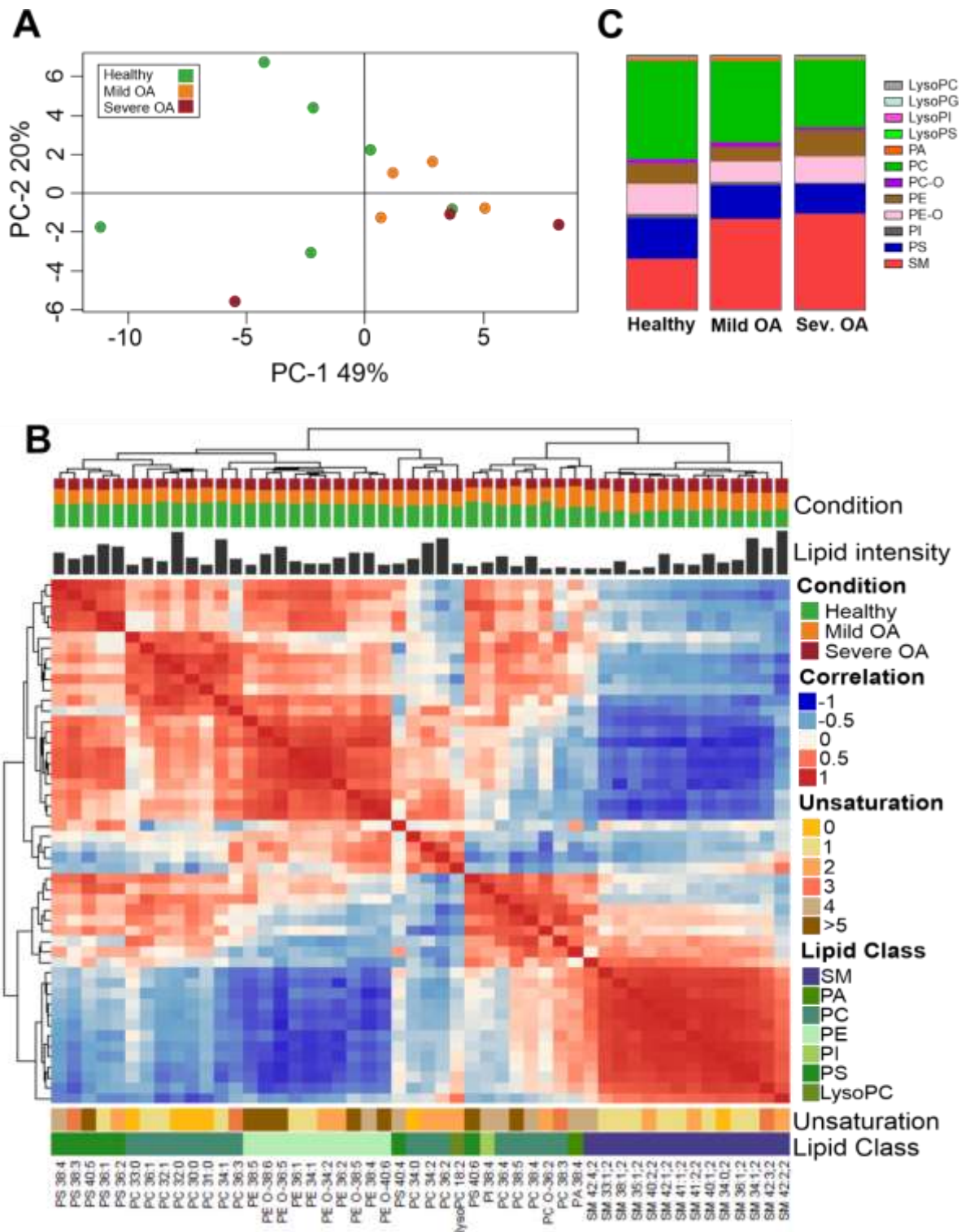
A Spearman correlation heatmap showed that the EV populations of the three different clinical groups differed in the distribution of their phospholipid composition (Figure 7.2.B). The heatmap was split into three sections (slices and clusters) based on Partitioning Around Medoids (PAM) clustering. For the first slice, the predominant lipid classes were phosphatidylserine (PS), ester-linked phosphatidylcholine (PC), ester-linked phosphatidylethanolamine (PE) and ether-linked phosphatidylethanolamine (PE-O), which account for half of the lipid distribution of EVs in the healthy joints but for less in both OA groups. The second slice included other members of the PS and PC classes, and the phosphatidic acid (PA), lysophosphatidylcholine (LysoPC), and phosphatidylinositol (PI) lipid classes. There were no clearly identified clusters in this slice. The third slice consisted solely of sphingomyelin (SM), and the distribution was one-third per group; thus, the OA-derived EVs had a higher presence than the EVs from healthy joints. These results showed a subtle variance among SF-EVs from the healthy and the mild and severe OA phenotypes.

#### 7.3.2.2. Differences in Lipid Class Composition of Synovial Fluid-derived Extracellular Vesicles are related to Osteoarthritis Progression

Having established a difference between the SF-EVs from healthy joints compared to mild OA and severe OA SF-EVs, we proceeded to analyse in more detail how the lipid classes were distributed in the respective groups (Figure 7.2.C, Supplementary Figure 10.3). The most abundant phospholipid classes in all three clinical groups were SM (20-40%), PC (25-40%), PS (12-16%), PE O- (8-12%) and PE (5- 10%) (Figure 7.2.C). However, a relative increase of SM was observed in the OA groups (healthy 19.9%, mild OA 35.5% and severe OA 37.5%), while the amounts of PC, PI and PS relatively decreased in OA groups which was most pronounced in the severe OA group (healthy: PC 38.3%, PI 1.73% and PS 16.0%; mild OA: PC 31.8%, PI 1.27% and PS 13.35%; severe OA group: PC 26.3%, PI 0.59% and PS

11.8% ). Additionally, compared to healthy SF-EVs, ether-linked phosphatidylcholine (PC O-) and PA classes demonstrated a relative rise in mild OA SF-EVs (healthy: PC O- 1.71% and PA 1.02% mild OA: PC O- 1.90% and PA 1.34%). However, the levels declined in severe OA-derived SF-EVs even more than the baseline levels in healthy joint derived EVs (severe OA: PC O- 1.19% and PA 0.55%). Inversely, both PE types (ester-linked and ether-linked) showed a reduction in the mild OA-derived EVs compared to the healthy joint derived EVs (healthy: PE 8.06% and PE O-11.8%; mild OA: PE 5.72% and PE O- 8.17%), while there was an increment in EVs isolated from the severe OA group (Severe OA: PE 10.2% and PE O- 10.2%) with the ester-linked PE class level even higher than in EVs derived from healthy joints.

Despite variations in the total lipid classes with respect to the whole phospholipidome, the individual lipid species contributing to the lipid classes were similarly distributed throughout the clinical groups following normalisation within each class (Supplementary Figure 10.3 ). Thus, the observed shifts in lipid classes cannot be directly attributed to changes in individual lipid species. Overall, these findings demonstrate that the phospholipidome is gradually transformed as OA develops.



**Figure 7.2. Lipidomic profile of equine synovial fluid-derived extracellular vesicles from healthy joints, mild and severe osteoarthritis.** Healthy samples (n=6), mild OA (n=4), severe OA (n=3). Each sample is comprised of a pool of three different biological replicates. Lipids were extracted from EVs isolated by differential centrifugation up to 100,000g, followed by purification with sucrose density gradients. (A) Principal component analysis of lipids isolated from the three different clinical groups. The principal components (PC)-1 and -2 explain 49% and 20% of the variance, respectively. (B) Lipid species correlation of SF-EVs. Combined heatmap (cluster dendrogram) of Lipid-Lipid Spearman correlations between the 50 most abundant lipid species in all EV sample groups. Lipid order was



based on Partitioning Around Medoids, also known as K-Medoids, a centroid-based clustering algorithm. On top of the figure is the cluster dendrogram. Below is the group distribution, the relative lipid intensity of each species, and the heatmap. Under the heatmap, the degree of saturation, the lipid class of each lipid, and the respective annotation of each lipid species are indicated. (C) Changes in EV lipid classes during OA development. Vertical slices plot of SF-EVs showing the relative molar abundances for individual lipid classes. Abbreviations: LysoPC, (lysophosphatidylcholine); LysoPG, (lysophosphatidylglycerol); LysoPI, (lysophosphatidylinositol); LysoPS, (lysophosphatidylserine); PC, (ester-linked phosphatidylcholine); PC O-, (ether-linked phosphatidylcholine); PE, (ester-linked phosphatidylethanolamine); PE O-, (ether-linked phosphatidylethanolamine); PI, (phosphatidylinositol); PS, (phosphatidylserine); SM, (sphingomyelin), PA (phosphatidic acid).

### 7.3.3 Proteomic Analysis

#### 7.3.3.1 Principal Component Analysis of Proteomes Demonstrates Variable Protein distribution according to Osteoarthritic Phenotype

Unsupervised multivariate analysis using PCA was conducted on the proteome of all samples exploring the variability between SF-EVs derived from healthy joints, mild OA and severe OA. A total of 5774 unique peptides were identified, translating to 290 proteins with no missing values. Missing values as such were imputed (using impute 2,1,1) using the following method: For the seven healthy samples, up to two missing values were imputed by inserting the mean of the healthy values for that particular protein. Similarly, for the four mild OA and three severe OA samples, up to one missing value was imputed by inserting the mean of the mild OA or severe OA values for that particular protein, resulting in a total of 598 proteins identified and quantified across all samples and used for statistical analysis. The first two components (Figure 7.3.A) reduce the total variation of all the individual data points by 36.4%.

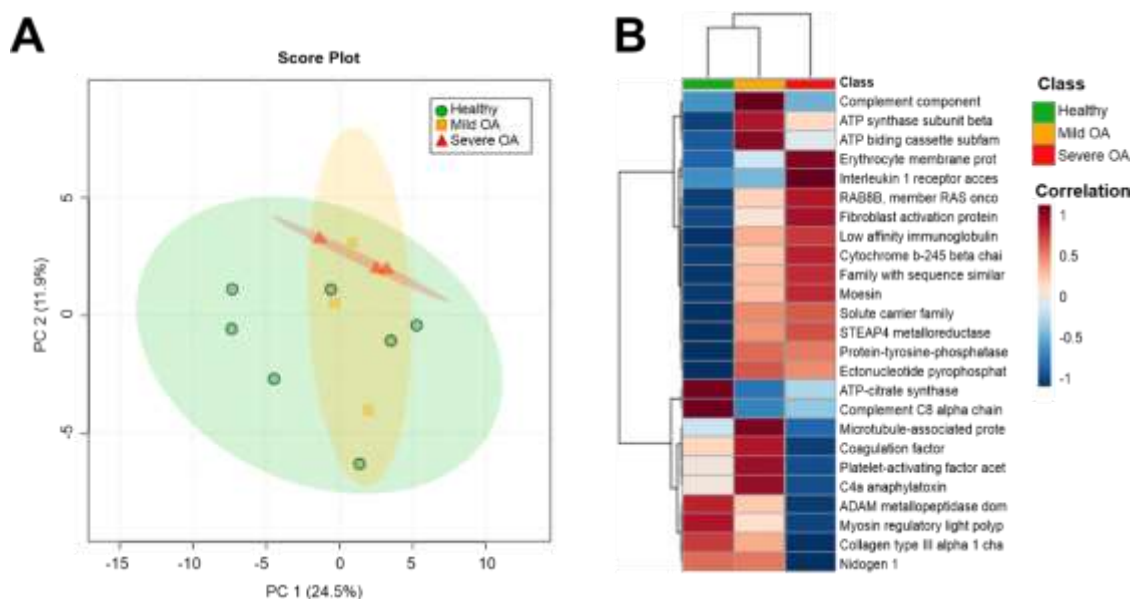
#### 7.3.3.2. Differentially Expressed Proteins identified across Osteoarthritic Phenotypes

Using ANOVA, 40 proteins were identified as being significantly differentially expressed ( $p < 0.05$ ) prior to false discovery rate (FDR) adjustment across all experimental groups. Unadjusted values were used due to this being an exploratory study, whereby multiple testing correction methods can fail to identify statistically significant values due to stringent thresholds (Pascovici *et al.*, 2016). Following post hoc Tukey analysis, a remaining 37 were significant ( $p < 0.05$ ). Table 7.1 demonstrates the top 25 differentially expressed proteins and their respective fold change expression, as well as the specific comparison found to be significant following post-hoc Tukey tests. It was revealed that microtubule-associated protein (ANOVA  $p = 0.006$ , test = severe OA compared to mild OA  $p = 0.006$ . and mild OA compared to healthy  $p = 0.03$ ) was present at higher levels in mild OA compared to the severe form of the disease. Further proteins with an increased expression in severe OA compared with the group with healthy joints were fibroblast activation protein alpha (ANOVA  $p = 0.03$ , Tukey test = severe OA compared to healthy  $p = 0.03$ ) and Interleukin 1 receptor accessory protein (ANOVA  $p = 0.02$ , Tukey test

= severe OA compared to healthy  $p = 0.02$ ). Conversely, platelet-activating factor acetylhydrolase IB subunit alpha (ANOVA  $p=0.004$ , Tukey test = severe OA compared to mild OA  $p= 0.003$ ) exhibited increased expression in mild OA but was decreased in severe OA, as shown in Table 7.1. Other significant ( $p<0.05$ ) proteins attributed to EVs that were identified in our dataset included RAB GTPases, such as RAB GDP dissociation inhibitor (ANOVA  $p=0.03$ , Tukey test = severe OA compared to healthy  $p= 0.02$ ) and RAB8 (ANOVA  $p=0.004$ , Tukey test = severe OA compared to mild OA  $p= 0.005$ , and mild OA compared to healthy  $p = 0.04$ ). Overall, a change in the proteome was observed in response to an altered OA phenotype, with significant proteins attributed to pathways known for propagating OA disease development within the joint.

### 7.3.3.3 A Stepwise Change in Protein Expression Correlates to Osteoarthritis Severity

Heatmap analysis was performed on SF-EV samples from healthy joints and mild and severe OA using the Ward clustering method and Pearson distance (Pang *et al.*, 2021), with selected proteins identified following ANOVA, visualising the top 25 most differential proteins. A stepwise expression change of 10 proteins was observed as OA severity increased, i.e., RAB8B ( $p=0.0039$ ), moesin ( $p=0.02$ ), fibroblast activation protein alpha ( $p=0.03$ ), cytochrome b-245 beta chain ( $p=0.016$ ), family with sequence similarity 171 ( $p=0.008$ ), solute carrier family 29 member 1 ( $p=0.02$ ), STEAP4 metalloredutase ( $p=0.02$ ), protein tyrosine phosphatase 1 ( $p=0.01$ ), and ectonucleotide pyrophosphatase ( $p=0.02$ ) (Figure 7.3.B and Table 1). It was found that four EV-associated proteins had an inverse correlation with an increased expression in mild OA but lower expression in EVs derived from severe OA patients (i.e., microtubule-associated protein ( $p=0.006$ ), coagulation factor V ( $p=0.01$ ), platelet-activating factor ( $p=0.004$ ) and c4a anaphylatoxin ( $p=0.01$ ) (Figure 7.3.B and Table 7.1).



**Figure 7.3. Proteomic profile of equine synovial fluid derived extracellular vesicles derived from healthy joints and from joints with mild and severe osteoarthritis.** A) Unsupervised multivariate analysis using principal component analysis. The first two principal components were plotted, accounting for ~36.4% of the variance. SF-EV samples were plotted based on acquired SWATH-MS data, after PQN normalisation and log transformation. Each plotted point represents a pooled SF-EV sample comprised of three biological replicates. B) Heatmap demonstrating mean average protein intensities between SF-EV healthy (green), mild OA (orange) and severe OA (red) phenotypes. Protein intensities were transformed and are displayed as colours ranging from red to blue. Both rows and columns are clustered using the Ward method, and distance was calculated using Pearson Distance.

**Table 7.1. Top 25 differentially expressed ( $p < 0.05$ ) proteins across synovial fluid derived extracellular vesicle samples derived from healthy joints and joints with mild osteoarthritis and severe osteoarthritis.** Following analysis of variance (ANOVA) and post hoc tukey test analysis, identifying significant experimental group comparisons and heatmap analysis.

Accession	Protein	ANOVA P value ( $p < 0.05$ )	FDR value	Experimental group comparisons							
				Severe Healthy	OA	Vs	Severe OA Vs mild OA	Mild Healthy	OA	Vs	
				Log fold change	2 Post hoc Tukey test p value		Log fold change	2 Post hoc Tukey test p value		Log fold change	2 Post hoc Tukey test p value
F6R528	Collagen type III alpha 1 chain	0.00239	0.599	-1.00	0.00183		-0.841	0.0175		-0.164	Ns
F7D3K4	Platelet-activating factor acetyl hydrolase IB subunit alpha	0.00389	0.599	-0.475	Ns		-0.800	0.00295		0.326	Ns
A0A5F5PPM3	RAB8B, member RAS oncogene family	0.00393	0.599	0.428	0.00486		0.140	Ns		0.288	0.0380
A0A3Q2H4M1	ATP-citrate synthase	0.00488	0.599	-0.244	Ns		0.106	Ns		-0.350	0.00538
A0A3Q2HW06	Microtubule-associated protein	0.00626	0.599	-0.186	Ns		-0.458	0.00621		0.272	0.0289
A0A5F5PGY6	Complement component C6	0.00761	0.599	0.014	Ns		-0.148	0.0373		0.163	0.00725
A0A5F5PQS3	Complement C8 alpha chain	0.00789	0.599	-0.255	Ns		0.066	Ns		-0.321	0.01040
A0A3Q2I4N2	Family with sequence similarity 171 member B	0.00813	0.599	0.162	0.0123		0.043	Ns		0.119	0.00813
A0A3Q2H905	Protein-tyrosine-phosphatase.1	0.0101	0.599	0.278	0.0369		-0.008	Ns		0.287	0.0186
F6U187	ATP synthase subunit beta	0.0112	0.599	0.129	Ns		-0.075	Ns		0.205	0.0103
F7DZ01	Coagulation factor V	0.0116	0.599	-0.174	Ns		-0.267	0.00912		0.093	Ns
A0A3Q2HG96	ADAM metallopeptidase domain 17	0.0140	0.599	-0.545	0.0109		-0.389	Ns		-0.155	Ns

<b>F6XS7</b>	C4a anaphylatoxin	0.0151	0.599	-0.106	Ns	-0.199	0.0119	0.092	Ns
<b>A0A3Q2HRQ8</b>	Solute carrier family 29 member 1	0.0151	0.599	0.185	0.0359	0.016	Ns	0.168	0.0364
<b>A0A3Q2ICY6</b>	Cytochrome b-245 beta chain	0.0159	0.599	0.334	0.0209	0.097	Ns	0.236	Ns
<b>F6XH19</b>	Nidogen 1	0.0161	0.599	-0.585	0.0167	-0.572	0.0332	-	Ns
<b>A0A3Q2GUV8</b>	ATP binding cassette subfamily A member 9	0.0192	0.599	0.208	Ns	-0.233	Ns	0.441	0.0152
<b>F7ALR7</b>	Ectonucleotide pyrophosphatase/phosphodiesterase 1	0.0202	0.599	0.266	Ns	-	Ns	0.294	0.0300
<b>A0A3Q2LMX0</b>	Erythrocyte membrane protein band 4.1 like 2	0.0207	0.599	0.272	0.0166	0.163	Ns	0.109	Ns
<b>F7AWQ9</b>	Interleukin 1 receptor accessory protein	0.0215	0.599	0.236	0.0193	0.208	Ns	0.027	Ns
<b>A0A3Q2KSS6</b>	Moesin	0.0219	0.599	0.159	0.0301	0.044	Ns	0.114	Ns
<b>A0A5F5PZW1</b>	Myosin regulatory light polypeptide 9	0.0223	0.599	-0.176	0.0182	-0.109	Ns	-	Ns
<b>F7A3D1</b>	STEAP4 metalloredutase	0.0236	0.599	0.498	0.0474	0.057	Ns	0.441	Ns
<b>A0A3Q2HB83</b>	Low affinity immunoglobulin gamma Fc region receptor III-B	0.0247	0.599	0.173	0.0392	0.037	Ns	0.136	Ns
<b>A0A3Q2HB68</b>	Fibroblast activation protein alpha	0.0250	0.599	0.404	0.0255	0.161	Ns	0.243	Ns

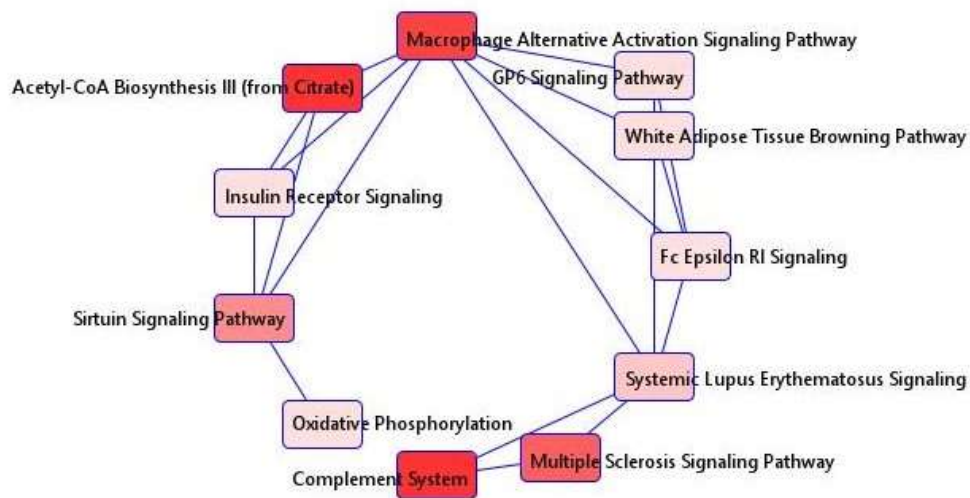
*Log2 fold change is provided in order to inform direction of expression for each comparison.*

#### **7.3.3.4 Functional Enrichment Analysis of the Synovial Fluid-derived Extracellular Vesicles Proteome Highlights Dysregulation in Pathways Associated with Cartilage Homeostasis and an Inflammatory Phenotype**

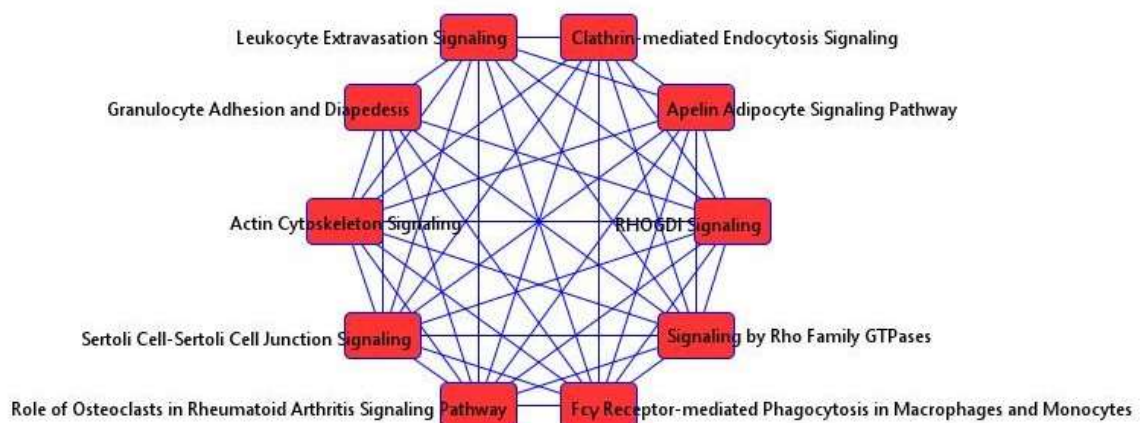
Functional enrichment analysis was performed in order to provide biological meaning to the identified and quantified proteome. In both mild OA and severe OA groups, the top canonical pathways were identified using the Ingenuity Knowledge Base Library and accounting for protein p-value following post hoc Tukey analysis and log2 fold change. It was found that signalling by Rho family GTPases ( $p=0.0000244$ ), clarithrin mediated endocytosis ( $p=0.000329$ ), liver x receptor/retinoid x receptor (LXR/RXR) activation ( $p=0.0353$ ), complement system activation ( $p=0.0107-0.000239$ ), and macrophage alternative action signalling ( $p=0.00604$ ) were all significant to OA pathology when considering EV cargo, as shown in Figure 7.4 A, B, and C. Additionally, significant diseases and functions in both severe and mild OA included inflammation of an organ ( $p=0.0231-0.0315$  (confidence interval)). Molecular functions found to be significant in severe OA compared to mild included injury

of joint ( $p= 0.00552$ ), and accumulation of macrophages (0.000414). Disease and molecular functions identified in a severe OA phenotype compared to healthy included: fibrosis ( $p = 0.0189$ ), systemic inflammation ( $p= 0.0211$ ), acute inflammation of tissue ( $p = 0.0289$ ) and osteoarthritis ( $p= 0.0316$ ). Finally, mild OA compared to healthy identified significant functions including: complement activation ( $p=0.000609$ ), development of articular cartilage ( $p=0.00374$ ), injury of joint ( $p=0.0118$ ), inflammation of joint ( $p=0.0169$ ), osteoarthritis ( $p=0.0280$ ) and chronic inflammation ( $p=0.0338$ ). A complete list of significant diseases and function can be found in Supplementary Table 10.5.

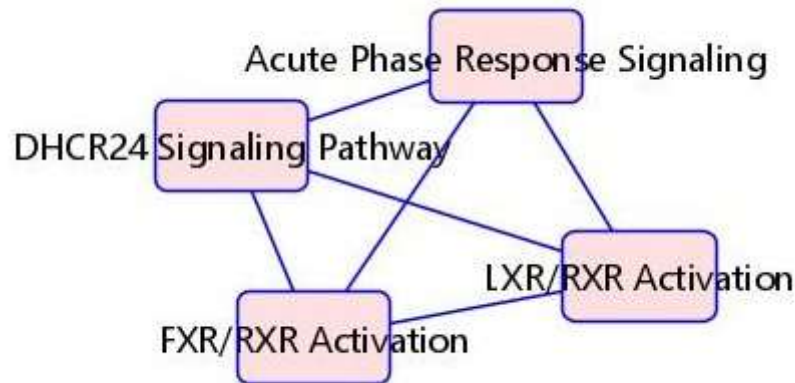
(A)



(B)



(C)



**Figure 7.4. Ingenuity Pathway Analysis networks providing an overview of significant related canonical pathways.** Analysis was conducted using the ingenuity knowledge base library and accounting for protein p-value and log<sub>2</sub> fold change following ANOVA and post hoc test analysis. (A) Mild OA compared to healthy (16 significant proteins), (B) Severe OA compared to healthy (20 significant proteins), (C) Severe OA compared with mild OA (9 proteins).

#### 7.3.4 Multi-Omic Integration

##### 7.3.4.1 Proteomics and Lipidomics Data Integration Demonstrates a High Correlation between Proteins and Phospholipids in Synovial Fluid-derived Extracellular Vesicles

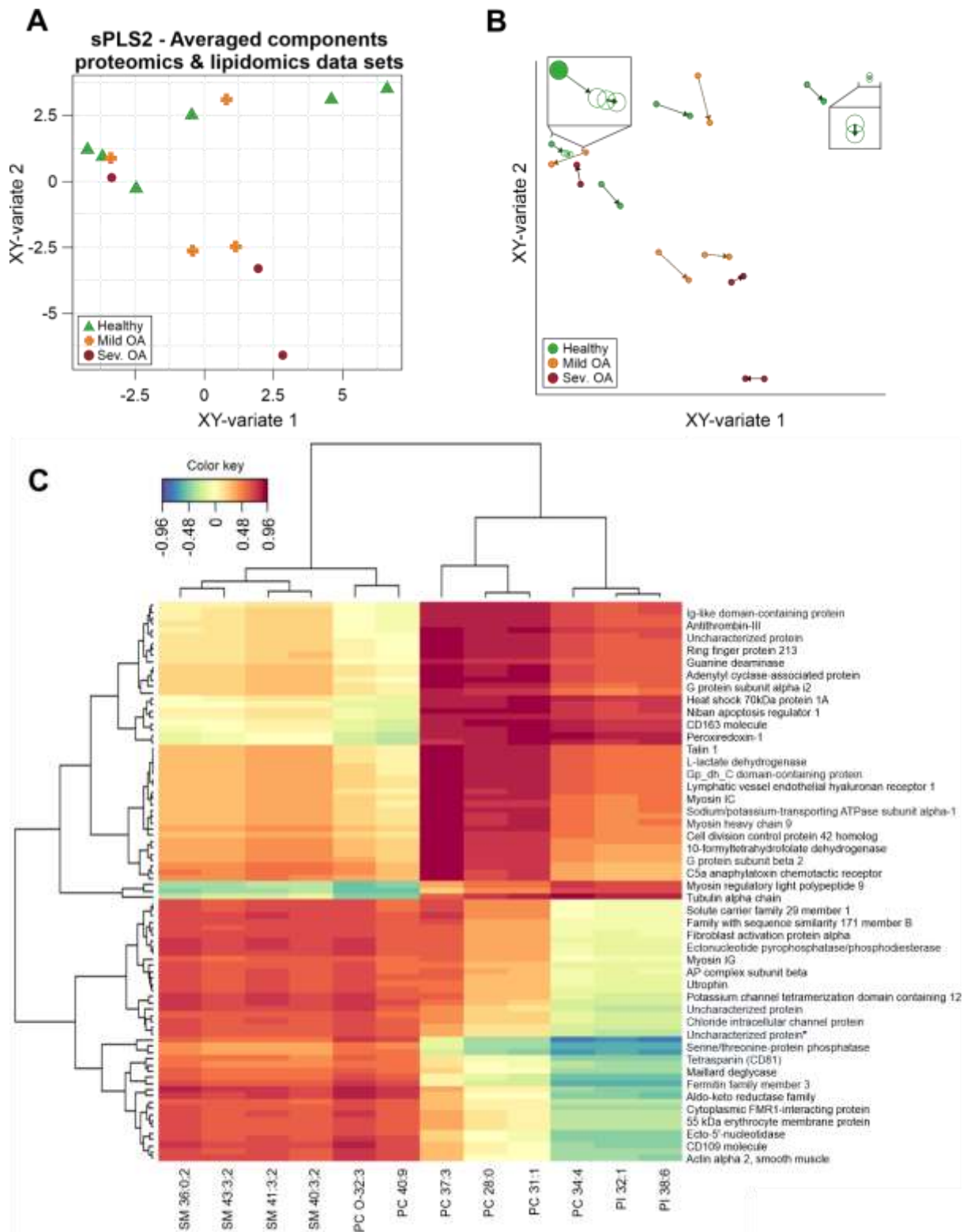
Integration of the proteome and phospholipidome datasets was performed to determine if biologically feasible correlates could be established; and thus, identify candidate composite protein-lipid biomarkers. An unsupervised approach was selected to integrate the dataset, consisting of a PCA assessment followed by sparse Partial Least Squares (sPLS2) regression which was tuned by cross-validation.

The initial exploratory analysis employing PCA was undertaken to recognise how the individual proteomic and lipidomic datasets behaved under the same normalisation conditions and to determine the optimal data integration model (Supplementary Figure 10.4). The omics datasets were normalised by the summed intensity of the sample, followed by centring and scaling of the data, thus subtracting the mean and dividing by the standard deviation. It was observed that clustering of the samples was comparable to the previous PCA (Figure 7.2.A, Figure 7.3.A).

Subsequently, to integrate the omics data sets, the unsupervised sPLS2 model was constructed separately for the proteomics and lipidomics data (Supplementary Figure 10.4.C and D). As an unsupervised analysis, the information about the groups (healthy joints, mild OA and severe OA) was not taken into consideration; however, the samples were labelled to understand how they clustered. In Supplementary Figure 10.4.C and 10.4.D, both sPLS2s project the respective data similarly, with the superior subspace primarily composed of SF-EV samples from healthy joints, the inferior one of mild OA and severe OA SF-EV samples and the top left subsection of overlapping samples from all groups.

Afterwards, both sPLS2s were averaged (Fig 7.5.A). The integrated averaged sPLS2 had a similar structure in components as the individual sPLS2. Figure 7.5.B assesses the degree of agreement between the proteomic and lipidomic datasets by plotting the position of each sample from both sPLS2s in the same space and connecting them with an arrow that indicates at its base the location in the proteomics data set and at the tip the location in the lipidomic data set. Most samples were located relatively close to each other indicating a correlation between the phospholipidome and proteome of SF-EVs.

This correlation was further explored with a Cluster Image Map (CIM) (Figure 7.5.C) to examine the connection between the features and components in a broad range, drawing attention to the relevant variables that collectively accounted for the covariance between the two datasets. According to the CIM, the phospholipid variables were divided into three slices that were either positively or negatively related to two main protein clusters. The left slice corresponded to 4 SMs (SM 36:0;2, SM 43:3;2, SM 41:3;2, SM 40:3;2), PC O-32:3, and PC 40:9, which had a positive association with the lower protein cluster. The middle slice, consisting of three PC species (PC 37:3, PC 28:0 and PC 31:1), had an inverse pattern of the cluster, with the upper group depicting the strongest association. Finally, the right slice, comprising the PC 34:4 and the two PI species (PI 32:1 and PI 38:6), had a similar association pattern as the middle one; however, the lower cluster exhibited a negative correlation, while the cluster above was positively correlated to the proteins.



**Figure 7.5. Unsupervised proteomic and lipidomic data integration.** Proteomic and lipidomic datasets from SF-EVs derived from healthy joints, mild OA and severe OA were normalised by the sum. (A) Sparse Partial Least Squares-2 regression (sPLS2) of SF-EV samples projected into the area covered by the averaged components of both datasets. Healthy SF-EVs (green triangle), mild OA SF-EVs (orange cross), and severe OA SF-EVs (Sev. OA; red circle). (B) Unsupervised multivariate sPLS2 arrow plot from the integration of proteomic and lipidomic data. The base of the arrow shows where a specific sample is in relation to the components of the proteomics dataset, and the tip of the arrow shows where the

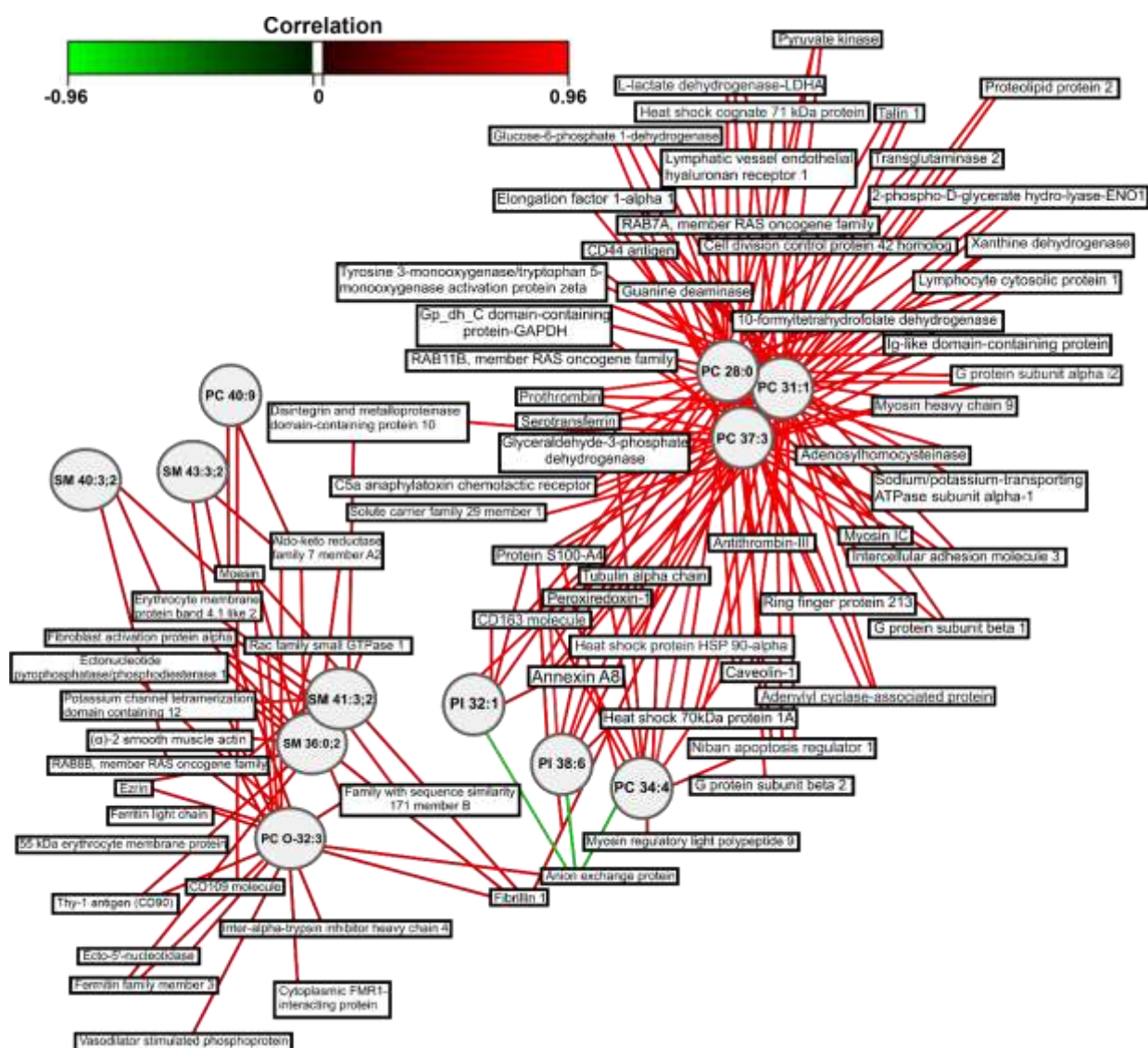


same sample is located concerning the components of the phospholipidomics dataset. Healthy SF-EVs (green circle), mild OA SF-EVs (orange circle), and severe OA SF-EVs (Sev. OA; red circle). The boxes zoom in on certain samples to better show the arrow direction. (C) Clustered Image Map from the sPLS2 data integration performed on the SF-EV omic datasets. The graphic shows the degree of similarity between the proteomic and lipidomic variables clustered over two dimensions and grouped using the Euclidean distance approach.

#### *7.3.4.2 Relevance Network for the Selection of Candidate Proteins and Phospholipids as Composite Osteoarthritis Biomarkers*

To better comprehend the correlation between the proteins and phospholipids, a relevance network plot was created (Figure 7.6). Three substructures could be identified from the network. The larger cluster contained the same lipids as the middle slice from the CIM (Figure 7.5.C; PC 28:0, PC 31:1 and PC 37:3), with all the correlations depicted being positive. The second substructure consisted of the right-side slice lipids from the CIM (Fig. 6.5.C; PC 34:4, PI 32:1, PI 38:6), with primarily positive correlations to the proteins except to the anion exchange protein. This cluster also overlapped with some of the same proteins as PC 28:0, PC 31:1 and PC 37:3. The third substructure was composed of the lipids from the left-side slice of the CIM (SM 36:0;2, SM 43:3;2, SM 41:3;2, SM 40:3;2, PC O-32:3, PC 40:9). This cluster displayed only positive correlation with the depicted proteins, including the anion exchange protein. Moreover, the proteins that correlated to phospholipids from the relevance network plot (Figure 7.6) were found to be associated with pathways such as actin cytoskeleton signalling ( $p=5.71 \times 10^{-7}$ ) and signalling by Rho family GTPases ( $p=5.89 \times 10^{-8}$ ), as shown in Table 7.2.

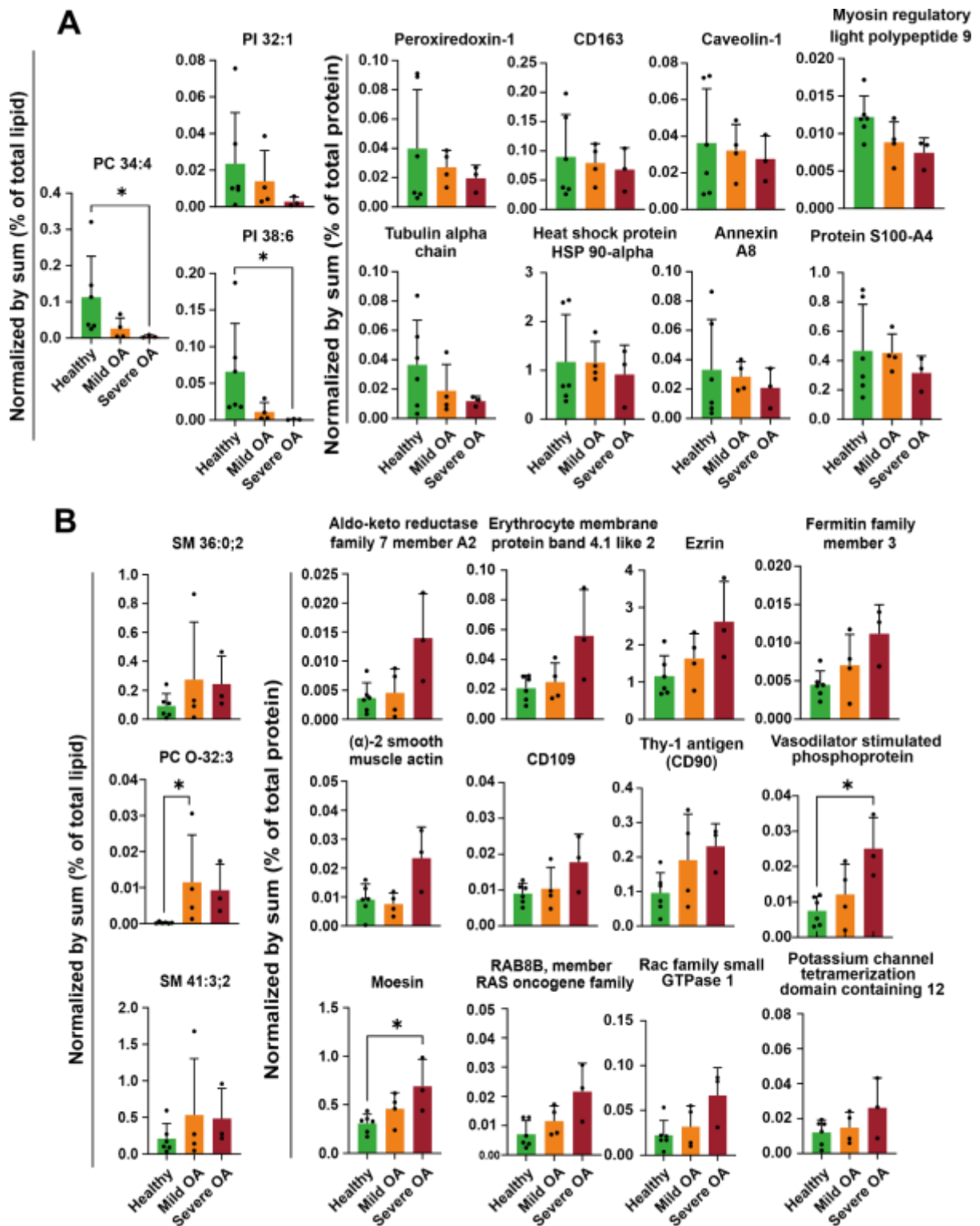
Since the sPLS2 analysis is an unsupervised approach (i.e., no information regarding the groups is entered in the model), neither the CIM nor the network explained how the SF-EV phospholipids and the correlated proteins relate to the healthy joints, mild OA and severe OA. To determine differences between the clinical groups, all lipids and proteins with a correlation above 0.754 based on the network (Figure 7.6) were assessed with a Kruskal-Wallis test (Figure 7.7). A significant decrease in PC 34:4 and PI 38:6, and decline in PI 32:1 and the related proteins showed a similar trend in SF-EVs derived from severe OA compared to healthy joints (Figure 7.7). Conversely, SM 36:0;2, SM 41:3;2 and PC O-32:3 and the correlated proteins showed a trend to increase with the severity of OA, with significant differences for PC O-32:3, moesin and vasodilator-stimulated phosphoprotein (Figure 7.7). A list of potential candidate proteins for composite biomarkers is provided in Supplementary Table 10.6.



**Figure 7.6.** Network representation derived from the sparsity in partial least squares regression models analysis of the proteomics and lipidomics integrated data. A relevance network plot with a correlation cutoff of 0.7 was created. Hence, only the variables with a correlation above 0.7 or below -0.7 are shown. The networks are bipartite, and each edge connects a protein (rectangle) to a phospholipid (circle) node based on a similarity matrix. The colour of the connecting lines represents positive (red) or negative (green) correlations.

**Table 7.2. Top 5 canonical pathways identified using Ingenuity Pathway Analysis.** Following input of proteins correlated to lipids.

Canonical Pathways	P-Value	Number of annotated molecules
Leukocyte extravasation signalling	1.64E-10	9/193
RHO GDI signalling	5.24E-10	9/220
Fcy Receptor-mediated phagocytosis in macrophages and monocytes	3.52E-8	6/94
Signalling by Rho Family GTPases	5.89E-8	8/267
Actin cytoskeleton signalling	5.71E-7	7/244



**Figure 7.7. Discovery of potential composite biomarkers for osteoarthritis.** Phospholipids and proteins were normalised by the sum of the total amount of material (i.e., lipid or protein). Healthy (green), mild OA (orange) and severe OA (red). \*  $p < 0.05$ , Kruskal-Wallis with Dunn's post hoc test A) Phospholipids and proteins that decreased with OA severity, B) phospholipids and proteins that increased with OA severity.

## 7.4 Discussion

In this exploratory study we designed a workflow for a multi-omics approach based on phospholipidomic and proteomic integration to identify composite SF-derived EV-biomarkers for OA, based on the analysis of EVs isolated from SF of horses with clinically defined OA (mild OA and severe OA), or from healthy equine joints. Hereto we investigated the phospholipidome and proteome of purified SF-EVs and designed a strategy for multi-omics data integration and differential expression analysis. To identify genuine composite EV-biomarkers, we used differential centrifugation followed by sucrose density gradient centrifugation to purify EVs from SF by removing most types of the contaminating lipoproteins and protein aggregates (Boere, van de Lest, *et al.*, 2016; Varela *et al.*, 2023). While the numbers of EVs in SF were unaffected by OA, consistent with other studies (Kolhe *et al.*, 2017; Mustonen *et al.*, 2022), the proteomic and phospholipidomic profiles of SF-EVs were correlated to the presence of OA .

We found that OA pathology directly impacted the phospholipidome at the lipid class level, showing gradual changes in several lipid classes associated with disease severity. The relative reduction in PC, PS and PI in mild OA and more drastically in severe OA, could be explained by the relative increase in SM. Since PC and SM are primarily located in the outer layer of the plasma membrane, the increase in SM disrupts the balance and reduces the amount of PC (Lorent *et al.*, 2020). Similarly, although PS and PI are predominantly found in the inner leaflet of the lipid bilayer, they can also be affected by an increase in SM. Furthermore, we found higher levels of PC compared to PC O-, while the PE and PE O- classes showed an opposite trend. These findings align with the lipidomics findings in the EV field and highlight the importance of ether lipids, especially PE O-, in EV biology, including membrane trafficking and cholesterol regulation (Honsho and Fujiki, 2017). SM, one of the main lipid classes detected in the SF-EVs, plays a crucial role in the plasma membrane composition, cellular proliferation, differentiation, growth, signal transduction, and apoptosis (Alaamery *et al.*, 2021). SMs are instrumental in the formation of lipid rafts enabling the selection of membrane proteins involved in signal transduction and intracellular transport (Pollet *et al.*, 2018). The notable increase of SMs with OA severity suggests that more lipid raft-like domains may be present in SF-EVs as the OA pathology progresses, facilitating and enhancing the cell-to-cell communication of SF-EVs.

Functional enrichment analysis of the differentially expressed SF-EV proteins identified a range of activated canonical pathways associated with disease phenotype. Specifically, Rho family GTPases, including RAC family small GTPase1 and ezrin were identified as activated in severe OA compared to healthy joints. Dysregulation of Rho GTPases has been implicated in rheumatic disorders in humans like rheumatoid arthritis, OA, and psoriatic arthritis, contributing to hypertrophic changes and

cartilage matrix destruction (Zhu, Dai, *et al.*, 2015; Rahmati *et al.*, 2020; Zeng *et al.*, 2022). Rac1, a pro-inflammatory factor, stimulates MMP13 production and upregulates markers of chondrocyte hypertrophy, such as COLX and ADAMTS-5 (Zeng *et al.*, 2022). Dysregulated activation of Rho GTPases, particularly CDC42, can lead to the degradation of articular chondrocytes through IL-6/STAT3 signalling (Hu *et al.*, 2018). The presence of these proteins in SF-EVs from diseased groups suggests their potential role in propagating disease within the joint by carrying cargo that induces phenotypic and metabolic changes.

Functional enrichment analysis also revealed disease and molecular functions related to complement system activation and macrophage alternative action signalling, with proteins such as complement C6 and ATP citrate lyase attributed to such pathways respectively. Complement system activation has previously been attributed to OA pathology, with its activation implicated in the formation of terminal complement complex (TCC) on chondrocytes, resulting in cell death, or the initiation of the production of matrix degrading enzymes, such as MMP13 (Wang *et al.*, 2011; Silawal *et al.*, 2018). These findings suggest the significant involvement of macrophages in OA pathogenesis. Previous studies have identified that an imbalance of macrophage subtypes (M1 and M2), can contribute to the chronic low-grade inflammation associated with OA and is implicated in OA pain mechanisms (Wu *et al.*, 2020). Additionally, macrophages play a crucial role in regulating inflammation and are known mediators of OA-related inflammation (Zhang, Cai and Bai, 2020). In addition, it was found that LXR/RXR signalling was dysregulated and was implicated in severe OA phenotypes compared with mild OA and had proteins such as inter alpha trypsin heavy chain 4 attributed to it. Previously, it has been shown that LXR/RXR signalling is dysregulated in OA tissue and associated with inflammation (Folkesson *et al.*, 2020), and has been identified in early and late stage OA (Wanner *et al.*, 2013). In addition, a reduction in LXR/RXR signalling has been found to contribute to catabolic processes in OA in human articular cartilage (Collins-Racie *et al.*, 2009). Further work should be done to elucidate if this signalling pathway is specifically a unique hallmark of later stage OA, or a specific endotype, hence its identification in some early OA cohorts.

Overall, the observed changes in both phospholipid classes and proteins between SF-EVs derived from healthy joints and OA patients and the gradual changes associated with the severity of OA, suggest that these SF-EV parameters may be used as natural composite biomarkers for OA diagnosis and progression. Our multi-omics integration approach, using unsupervised sPLS2 regression and PCA, indeed revealed a remarkably strong similarity in the space distribution induced by the SF-EV phospholipidome and proteome, indicating a strong interrelationship, which is mainly due to a strong correlation between specific phospholipids with a certain set of proteins. Functional enrichment

analysis of the proteins from this correlation network revealed several canonical pathways, such as signalling by Rho Family GTPases as previously identified and actin cytoskeleton signalling.

Integration of data revealed potential composite biomarkers consisting of downregulated and upregulated phospholipids and proteins as OA severity progressed. Downregulated proteins and the respective phospholipids were comprised of phospholipids PC 34:4, PI 32:1 and PI 38:6, and proteins such as heat shock protein 90 (HSP90AA1) and CD163. Interestingly, HSP90AA1 has been demonstrated to be down-regulated in blood and cartilage of human patients with OA, and levels correlated with the risk incidence of OA (Lorenzo-Gómez *et al.*, 2023), while CD163, a transmembrane protein of M2 macrophages (Hu *et al.*, 2017), was shown to decline as OA progressed in this study. It has been suggested that the inability of macrophages to transform from M1 to M2 might contribute to the onset and development of OA (Chen *et al.*, 2020).

Among the upregulated proteins, several structural proteins were detected, including  $\alpha$ -2 smooth muscle actin, erythrocyte membrane protein band 4.1-like 2 (EPB41L2), ezrin, and moesin. These proteins likely indicate changes in diseased joint tissues, which were reflected in the structural protein composition of SF-EVs.  $\alpha$ -smooth muscle actin is known to be expressed in fibroblast-like synoviocytes (FLSs) undergoing a change to a myofibroblast-like phenotype in the presence of transforming growth factor  $\beta$  (TGF $\beta$ ), linked to OA pathogenesis (Rice *et al.*, 2021), as well as to colocalise with fibronectin, which is associated with inflammation in OA. Ezrin, moesin, and EPB41L2 activation promote enhanced proliferation and formation of fibrillated OA cartilage by blocking cell-cell contact inhibition in chondrocytes (Housmans *et al.*, 2022). Ezrin has also been connected to the RhoGTPase signalling pathway in OA synovial fluid (Housmans *et al.*, 2022). Additionally, CD90 and CD109 transmembrane proteins, upregulated as OA progresses, regulate the pathological response in rheumatoid arthritis (RA) fibroblast-like synoviocytes, driving inflammation and fibrosis (Song *et al.*, 2019; Wiles *et al.*, 2023). The upregulated proteins were associated with phospholipids SM 36:0;2, SM 41:3;2, and PC O-32:3. The combinations of these proteins and phospholipids could potentially serve as candidate composite SF-EV biomarkers for OA onset and progression.

The inherent constraints of this exploratory study, such as relatively small clinical sample size and large volume of SF required, non-conformity of radiological and clinical parameters for OA severity assignment and lag in the development of analytical tools when comparing mass spectrometry proteomics and lipidomics pipelines, are important to overcome in future studies.

## 7.5 Conclusion

In summary, OA SF-EVs showed altered proteome and phospholipidome profiles associated with articular degeneration and inflammation, as identified by significant canonical pathways such as Rho family GTPase signalling and complement activation. The interplay between the proteomic and lipidomic changes highlights the functional interconnectedness of EV structure and contents in SF. These findings suggest a coordinated response reflected in EV composition, potentially propagating disease by inducing cellular changes. The approach followed in this exploratory study in equine OA highlights the potential for identifying important molecular mechanisms of OA and aims to serve as a framework for the discovery of SF-derived EV-based composite biomarkers having the potential to inform disease severity and enable targeted disease management in the future.

## 7.6 Funding

Author **L.V.** received funding from the EU's H2020 research and innovation program under Marie S. Curie COFUND RESCUE grant agreement No 801540. **E.C.** is a self-funded PhD student from the University of Liverpool and acquired funding from the EU Cost initiative (ExRNA path) cost action CA20110. **E.L.A.** received funding from the EU's H2020 research and innovation programme under the Marie Skłodowska-Curie grant agreement No 722148 (TRAIN-EV). **M.J.P.** and **E.C.** were also supported by the Medical Research Council (MRC) and Versus Arthritis as part of the MRC Versus Arthritis Center for Integrated Research into Musculoskeletal Aging (CIMA). M.J.P was supported by a Horserace Betting Levy Board grant (Prj794).

## 7.7 Acknowledgments

We thank Jeroen Jansen for running the MS for the lipidomics experiment. The authors acknowledge the use of the CDSS Bioanalytical Facility provided by Liverpool Shared Research Facilities, Faculty of Health and Life Sciences, University of Liverpool



## 8. Manuscript 4

### **Allogenic Platelet-rich Plasma and Platelet-rich Plasma Extracellular Vesicles Change the Proteome of Tenocytes in an *In Vitro* Equine Model of Tendon Inflammation, Resulting in the Identification of Potential Molecular Modes of Action of platelet-rich Plasma: A Pilot Study**

Emily J Clarke<sup>1</sup>, Anders Jensen<sup>1</sup>, Alexandra M Gillen<sup>2</sup>, David Bardell<sup>2</sup>, Mark Senior<sup>2</sup>, James R Anderson<sup>1</sup>, Agnieszka Turlo<sup>1</sup>, Mandy J Peffers<sup>1</sup>

<sup>1</sup> Department of Musculoskeletal and Ageing Science, Institute of Life Course and Medical Sciences, University of Liverpool, Liverpool, United Kingdom

<sup>2</sup> Department of Equine Clinical Science, Philip Leverhulme Equine Hospital, School of Veterinary Science, Leahurst Campus, University of Liverpool, Neston, Wirral, UK

#### **Key words:**

**Platelet-rich plasma, extracellular Vesicles, equine tendon injury, *in vitro*, proteomic**

#### **Declaration of author contributions**

**EJC:** Conceptualisation, Formal analysis, Investigation, Project administration, Validation, Visualisation, Writing - Original Draft, Writing – Review & Editing. **AJ:** data analysis, manuscript review and editing. **AMG:** clinical collaborator, PRP treatment analysis, manuscript review and editing, **DB:** Clinical collaborator, sample procurement, review and editing of manuscript. **MS:** clinical collaborator, sample procurement, review and editing of manuscript. **JRA:** conceptualisation, manuscript review and editing. **AT:** Conceptualisation, Project administration, Supervision, Writing – Review & Editing. **MJP:** Conceptualisation, Project administration, Supervision, Writing – Review & Editing

## 8.1 Abstract

Equine musculoskeletal injuries are highly prevalent across the athletic equine population. Following injury, the repaired structure is often inferior biomechanically, and prone to reinjury. Hemoderivative therapeutics such as platelet-rich plasma is a promising treatment option; however variable outcomes have been reported clinically due to lack of standardisation of composition. Platelet-rich plasma contains high concentrations of soluble growth factors as well as extracellular vesicles; nanoparticles involved in the facilitation of cell to cell communication through the delivery of biologically active cargo. This pilot study aimed to profile the proteome of platelet-rich plasma and platelet-rich plasma extracellular vesicles and determine their effect in an equine tendon inflammatory *in vitro* model. Plasma was isolated following double centrifugation, and platelet-rich plasma was produced using a commercial filtration kit. Extracellular vesicles were isolated from platelet-rich plasma and plasma using differential ultracentrifugation and characterised using the Exoview tetraspanin assay. Equine tenocytes were stimulated with interleukin 1 $\beta$  and tumour necrosis factor  $\alpha$  and subsequently treated with platelet-rich plasma or platelet-rich plasma extracellular vesicles. Proteomics was undertaken using data dependent acquisition liquid chromatography-tandem mass spectrometry on a QExactive HF Quadrupole-Orbitrap mass spectrometer. Resulting data was analysed using multivariate and univariate approaches. Platelet-rich plasma had a total of 575 quantifiable proteins, and platelet-rich plasma derived extracellular vesicles 209 proteins. Platelet-rich plasma and platelet-rich plasma extracellular vesicles were enriched in proteins associated with cellular waste disposal (microautophagy signalling pathway ( $p=4.37 \times 10^{-5}$ ) and inhibition of lipid metabolism (liver x receptor/ retinoid x receptor activation ( $p=1.02 \times 10^{-5}$ ), farnesoid x receptor/ retinoid x receptor activation ( $p=1.59 \times 10^{-5}$ )), compared to plasma or plasma derived extracellular vesicles respectively. Two-factor analysis of variance of proteins identified in equine tenocytes showed that experimental factors (inflammatory stimulation and/or treatments) had significant effect on the abundance of 18 proteins, differential proteins included collagen type 1 alpha 1 and sequestosome 1, with activity relating to collagen metabolism and nuclear factor kappa b signalling, respectively. This *in vitro* pilot study explored the effect of platelet-rich plasma and platelet-rich plasma derived extracellular vesicles in an equine tendon inflammatory model and identified differential proteins linked to potential molecular mechanisms, mediating the therapeutic effect observed clinically that requires further investigation and validation. We evidence that platelet-rich plasma extracellular vesicles do elicit an effect on stimulated tenocytes and thus may be involved in the mediation of platelet-rich plasma therapeutic effect. In the future platelet-rich plasma derived extracellular vesicles may serve as a viable 'off the shelf' therapeutic.

## 8.2 Introduction

Equine musculoskeletal injuries are highly prevalent within the performance horse population. This is often due to factors such as training frequency, intensity, surfaces and the equipment used (O'Brien, Marr and Thorpe, 2021). Injury to the musculoskeletal system accounted for 82% of all injuries to racehorses competing in the national hunt and flat races, of these 46% involved tendon or ligaments (Murray *et al.*, 2006; Thorpe, Clegg and Birch, 2010). The equine superficial digital flexor tendon (SDFT) is most prone to injury and is analogous to the human Achilles tendon. The SDFT is regarded as an energy storing tendon and is highly susceptible to injury due to experiencing large forces and repetitive loads during galloping and jumping (O'Brien, Marr and Thorpe, 2021). This accumulates micro damage due to exercise and ageing, predisposing it to rupture during normal activity (Patterson-Kane, Becker and Rich, 2012). Risk factors to impairment include breed, sex, age and weight along with variations in tendon vascular supply as well as flexibility and strength (Perkins, Reid and Morris, 2005; Lam *et al.*, 2007a, 2007b; Tamura, Kodaira and Yoshihara, 2018). A significant issue with injury to the SDFT is the incidence of reinjury and reduced biomechanical fortitude (Johnson *et al.*, 2021) which results in compromised welfare, pain and lameness in the equine athlete, and presents an economic burden to the equine industry.

Tendon is composed of a fibrous extracellular matrix (ECM) accompanied by a small number of resident tenocytes that maintain structure by producing matrix molecules including matrix metalloproteinases (MMPs) and tissue inhibitors of metalloproteinases (TIMPs) (Thorpe, Clegg and Birch, 2010). The matrix is predominantly comprised of type I collagen, with additional collagens, glycoproteins, proteoglycans and non-collagenous proteins. The structure is largely avascular which is postulated to promote poor healing (Thorpe, Clegg and Birch, 2010). Significant inflammation often accompanies injury, with many pro-inflammatory cytokines expressed by tenocytes and peritendinous tissues, such as tumour necrosis factor alpha (TNF- $\alpha$ ), interleukin 1 beta (IL-1 $\beta$ ) (Del Buono *et al.*, 2011; Chisari *et al.*, 2021). Tendon healing is often slow due to the poor innate regenerative properties. The repaired tissue is characterised by fibrosis and collagen type III, producing an inferior structure and subsequently contributing towards high re-injury rates (Beerts *et al.*, 2017). As a result, it is hypothesised that in order to maximise healing potential treatment should be administered between the inflammatory phases and proliferative phases of tendon injury healing (Beerts *et al.*, 2017).

Hemoderivative therapeutics, such as autologous platelet-rich plasma (PRP) have become a popular form of treatment for orthopaedic conditions such as tendon injury. This is due to its cost, ease to prepare, the minimal equipment required and its immunomodulatory effect (Brossi *et al.*, 2015). In addition it promotes haemostasis, anti-inflammatory cytokine release and release of important growth factors such as platelet-derived growth factor (PGF), transforming growth factor- $\beta$ 1 (TGF $\beta$ 1), transforming growth factor- $\beta$ 2 (TGF $\beta$ 2), vascular endothelial growth factor (VEGF), basic fibroblastic growth factor (FGF), and epidermal growth factor (EGF), following degranulation of alpha platelet granules (Bosch *et al.*, 2011; Brossi *et al.*, 2015; Wijekoon and de Silva, 2021). It is defined as having at least two times greater platelet count than baseline whole blood values (Fortier, 2010; Parrish *et al.*, 2016). In a randomised prospective trial using PRP a single intralesional treatment up to 8 weeks after the onset of clinical signs of tendon injury reduced lameness, and advanced the organisation of repair tissue (Geburek *et al.*, 2016). In addition, Bosch *et al.* demonstrated that PRP had the capacity to increase metabolic activity and improve the maturation of repaired tissue compared with no treatment, in experimentally induced tendon lesions (Bosch *et al.*, 2010). PRP's effect has also been investigated following surgically induced tendon injury. PRP induced significantly more neovascularisation than the placebo. However, PRP does present some disadvantage as clinical variables effect the autologous product composition, and level of activation (Bosch *et al.*, 2010). In addition, the lack of standardised PRP composition has contributed in variable clinical outcomes and a lack of reproducibility (Geburek *et al.*, 2016; Montano *et al.*, 2021).

Extracellular vesicles (EVs) have become an area of interest in understanding the mechanistic action of PRP, a factor that should be considered when producing an optimum formulation for PRP. EVs are nanoparticles secreted by most mammalian cells, enveloped in a phospholipid bilayer and are involved in intercellular communication, by transporting biologically active cargo between cells. EVs can be categorised by size, density and biochemical composition. Graca *et al.* (Graça *et al.*, 2022) explored the effect of platelet-derived EVs in a human bioengineered model of tendon injury and observed an increase in tenogenic markers, subsequently promoting a healthy ECM phenotype, remodelling and increasing the synthesis of anti-inflammatory mediators. Thus, EVs derived from platelets have the capacity to transfer platelet-derived content to cellular recipients and organs inaccessible to platelets (Tao, Guo and Zhang, 2017; Puhm, Boilard and MacHlus, 2021).

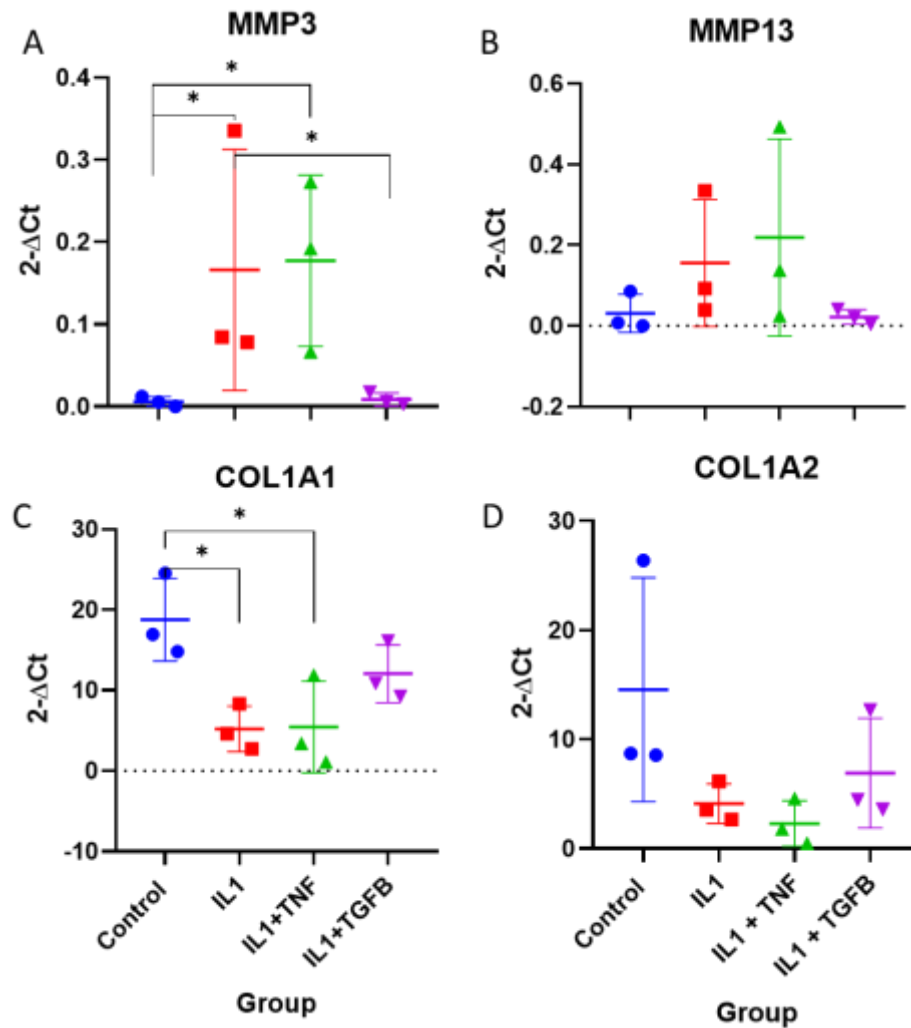
Furthermore, EVs have a low immunogenicity, are easily stored and obtained. Pre-clinical studies are aiming to quantify the effect of PRP-EVs therapeutically in order to determine if they are a viable superior alternative to cell-based regenerative therapeutics (Wu, Piao, *et al.*, 2021). Therefore, it is important to understand the composition of PRP and PRP-EVs, and the effect these EVs have in mediating the therapeutic effect observed in order to develop a therapeutic product that can deliver improved and reproducible clinical outcomes be that as a blood-based product, or EVs alone.

This pilot study aimed to profile PRP and PRP-EVs components and quantify the effect of PRP and PRP-EVs on an *in vitro* equine inflammatory tendon model. This was to establish (a) how PRP-EVs are involved in the mediation of PRP therapeutic activity, and (b) the potential molecular pathways PRP and PRP-EVs act on to deliver their therapeutic action.

## 8.3 Results

### 8.3.1. Optimisation of an In Vitro Inflammatory Model to Study Equine Tendon Injury

Gene expression analysis was conducted to determine the effect of cytokines on equine tenocytes. It was found that MMP3 expression significantly increased upon stimulation with IL-1 $\beta$  ( $p=0.0315$ ) and IL-1 $\beta$ /TNF- $\alpha$  ( $p=0.0415$ ), compared to control tenocytes. In addition, IL-1 $\beta$ /TGF- $\beta$  groups showed a decreased expression with MMP3, comparable to the control group (Figure 8.1.A). No significant difference was observed in MMP13 expression; however, a trend was evident increased expression upon stimulation by IL-1 $\beta$  or IL1/TNF- $\alpha$  (Figure 8.1.B). COL1A1 expression was significantly decreased compared to control upon inclusion of IL-1 $\beta$  ( $q=0.0239$ ) or IL-1 $\beta$ /TNF- $\alpha$  ( $q=0.0262$ ) (Figure 8.1.C). COL1A2 exhibited no significant change in expression following cytokine stimulation (Figure 8.1.D). Upon inclusion of TGF- $\beta$  gene expression levels alter upon cytokine stimulation to reflect that on the control group, demonstrating the capacity of TGF- $\beta$  to rescue the inflammatory phenotype. Across all genes measured the use of two cytokines rather than one resulted in an enhanced response. This preliminary study identified an effect upon stimulation with cytokines, principally IL-1 $\beta$  and TNF- $\alpha$ . A combination of both was putative to promoting a tendon inflammatory phenotype, and reflective of the natural disease. In clinical cases a number of cytokines interact in the tendon injury. In addition, a decrease of collagen 1 was quantified, characteristic of tendon injury. It has been previously identified that type 1 collagen expression decreased following injury, while collagen type 3 increased due to the formation of scar tissue (Voleti, Buckley and Soslowsky, 2012; Buckley *et al.*, 2013). Furthermore, the increased expression observed in MMPs was also synonymous with tendon injury, due to MMP's role in degrading the ECM that tenocytes are situated within. MMP's subsequently play a significant role in tendon remodelling and ECM homeostasis. A dysregulation of MMPs can result in tendon disturbance and damage, as a result of alteration to ECM architecture (Davis *et al.*, 2013; Del Buono *et al.*, 2013). An interesting finding from this small study was the ability for TGF- $\beta$  to rescue the tendon inflammatory phenotype, resulting in gene expression levels comparable to the control group. TGF- $\beta$  has many characterised roles following tendon injury such as: collagen synthesis, cell proliferation, cell differentiation, and cell adhesion, leading to tendon healing and tendon fibrosis (Kaji *et al.*, 2020; Li *et al.*, 2022). As a result of this study it was decided that a combination of IL-1 $\beta$  and TNF- $\alpha$  would be used for the main study in order to stimulate equine tenocytes in monolayer culture.



**Figure 8.1. Reverse transcription-quantitative polymerase chain reaction analysis of equine tenocytes (n=3) cytokine stimulation.** Control has no cytokine added; IL-1 had interleukin-1 $\beta$  added, IL-1+TNF- $\alpha$  had interleukin-1 $\beta$  and TNF- $\alpha$ ; and IL-1+TGF had interleukin-1 $\beta$  and TGF- $\beta$  added (n=3). Error bars are +/- standard deviation of the mean. (A) MMP3 gene expression following treatment with different cytokine combinations. Significant differences were found (Kruskal-Wallis:  $p=0.0118$ ) between control vs IL-1. ( $p=0.0315$ ), control vs IL-1 with TNF- $\alpha$  ( $p=0.0415$ ), IL-1 vs IL-1 with TGF- $\beta$  ( $p=0.0415$ ). (B) MMP13 gene expression following treatment with different cytokine combinations. No significant differences were found. (C) COL1A1 gene expression following treatment with different cytokine combinations. Significant differences were found (ANOVA=  $p=0.0170$ ), between control vs IL-1 ( $q=0.0239$ ) and control vs IL-1 with TNF- $\alpha$  ( $q=0.0262$ ). (D) COL1A2 gene expression following treatment with different cytokine combinations. No significant differences were found following Kruskal Wallis test. Across all box plots standard deviation of the mean error bars are shown and significance was denoted by \* = ( $p<0.05$ ), \*\* = ( $p<0.01$ ), \*\*\* = ( $p<0.001$ ).

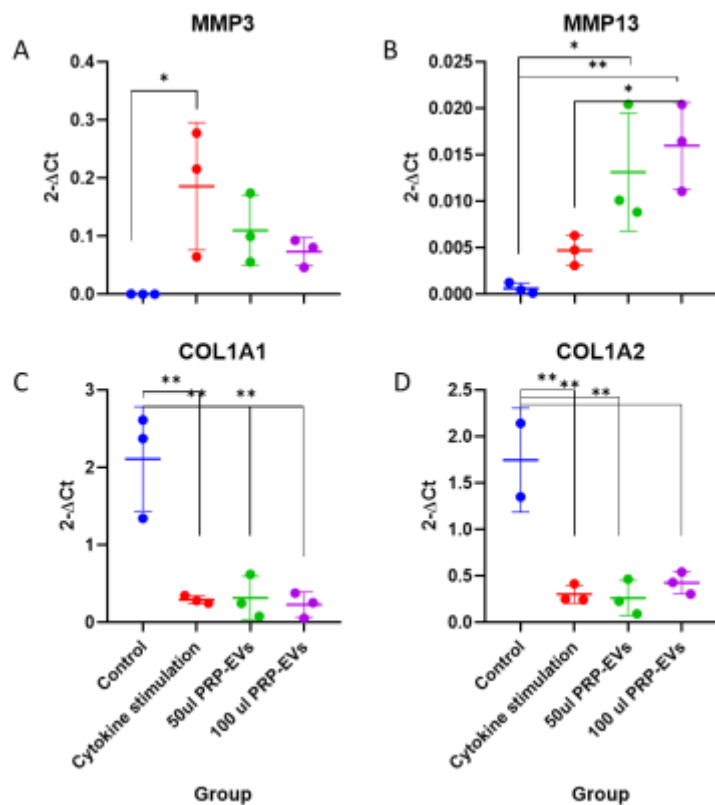
### 8.3.2. Determination of the most appropriate Platelet-rich Plasma Extracellular Vesicle Concentration to use in an *In Vitro* Equine Tendon Inflammatory Model

A significant increase ( $p=0.0298$ ) in MMP3 was observed compared to control in the IL1 $\beta$ +TNF- $\alpha$  treated group, reflective of a disease phenotype. No significant difference was determined between 50 $\mu$ l and 100 $\mu$ l PRP-EV treatment, however a trend can be observed that expression is decreasing within creased EV concentration, showing a shift toward returning to baseline expression levels (Figure 8.2.A). MMP13 expression changed with respect to IL1 $\beta$ +TNF- $\alpha$  stimulation, toward an increased expression, although this was not significant ( $p= 0.6199$ ). In addition, a significant increase in MMP13 expression was observed between IL1 $\beta$ +TNF- $\alpha$  and 100 $\mu$ l PRP-EVs ( $p=0.0375$ ), and between control and 50 $\mu$ l ( $p=0.021$ ) and 100 $\mu$ l of PRP-EV ( $p= 0.0013$ ) treatment (Figure 8.2.B). COL1A1 expression significant decreased in IL1 $\beta$ +TNF- $\alpha$  group compared to control ( $p=0.0016$ ). This was conserved across both 50  $\mu$ l ( $p=0.0017$ ) and 100 $\mu$ l PRP-EV ( $p= 0.0013$ ) groups (Figure 8.2.C). COL1A2 exhibited a similar pattern of expression across all comparisons as observed for COL1A1 (control and IL1 + TNF $\alpha$  ( $p= 0.0017$ ), control and 50  $\mu$ l PRP-EV treatment ( $p=0.014$ ), and control compared with 100  $\mu$ l PRP-EV treatment ( $p=0.0028$ )). Notably the increase in PRP-EV concentration results in a trend toward a marked increase COL1A2 expression (Figure 8.2.D). This preliminary study identified a cellular response following PRP-EV treatment in an *in vitro* equine tendon inflammatory model. Gene expression was as expected in both control equine tenocytes and those stimulated with IL-1 $\beta$ +TNF- $\alpha$  as previously identified. Upon PRP-EV treatment following cytokine stimulation PRP-EVs had the capacity to alter the expression of a selected panel of genes, namely MMP3, MMP13, COL1A1, and COL1A2. In some cases, this was therapeutically favourable, for example a trend toward a decrease in expression was observed with increased concentration of PRP-EV treatment with respect to MMP3, this was also observed with COL1A2. MMPs and collagens are significant molecules in relation to tendon injury and repair. Specifically, it is characteristic for collagen abundance to alter with injury (Hudson *et al.*, 2021), and an increase in MMP's is often observed, contributing towards extracellular matrix destruction (Del Buono *et al.*, 2013).



MMP3 expression increase has been speculated to be of great importance to prevent pathological alterations in tendons (Ireland *et al.*, 2001; Guo *et al.*, 2022). COL1A1 however did not show an observed improvement in expression following treatment. Converse to MMP3, MMP13 expression was seen to increase with increasing PRP-EV concentration. It has been reported previously that EVs can induce further production of MMPs and their subsequent release via EVs of recipient cells (Nawaz *et al.*, 2018). In addition it is interesting to note that MMP13 serves a different role compared to MMP3, as it the primary enzyme involved in the cleavage of type II collagen (Hu and Ecker, 2021).

This study was limited by a small sample size and panel of gene expression markers. However, it was decided based on this study that PRP-EVs derived from 100µl of PRP would be appropriate for the final study, due to eliciting the greatest and most therapeutically favourable cellular response with regard to MMP3 and COL1A2, when compared to PRP-EVs derived from 50 µl of PRP.



**Figure 8.2. Gene expression using analysis of equine tenocytes (n=3) following cytokine stimulation, and varying platelet-rich plasma derived extracellular vesicle concentration treatments.** Control was no cytokine added; IL+ TNFα had interleukin-1 and TNF-α; and both 50µl and 100 µl PRP-EV treatments were added to stimulated equine tenocytes. Data was analysed using a one-way ANOVA with multiple comparisons and a post hoc Tukey test, boxplots show standard deviation of the mean error bars. (A) MMP3 gene expression was found to significantly different between control and IL+TNF

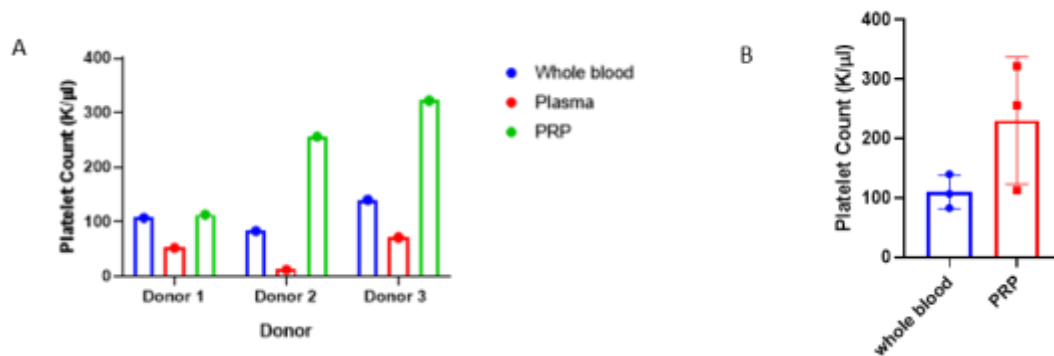
(p=0.0298). (B) MMP13 gene expression was found to significantly change with respect to control compared to 50  $\mu$ l PRP-EV treatment (p=0.021), control compared to 100  $\mu$ l PRP-EV treatment p=0.0071), and IL1+TNF $\alpha$  compared to 100  $\mu$ l PRP-EV treatment (p=0.0375). (C) COL1A1 gene expression was found to significantly vary between control and IL1+TNF (p=0.0016), control compared to 50  $\mu$ l PRP-EV treatment (p=0.0017) and control compared to 100  $\mu$ l PRP-EV treatment (p= 0.0013). (D) COL1A2 gene expression was found to change between control and IL1 + TNF $\alpha$  (p= 0.0017), control and 50  $\mu$ l PRP-EV treatment (p=0.014), and control compared with 100  $\mu$ l PRP-EV treatment (p=0.0028). Across all box plots significance was denoted by \* = (p<0.05), \*\* = (p<0.01), \*\*\* = (p<0.001).

### 8.3.3. Main Study

#### 8.3.3.1. Characterisation of Platelet-rich Plasma and Extracellular Vesicles

*Platelet-rich plasma was found to have a minimum of two times the number of platelets compared to matched whole blood sample*

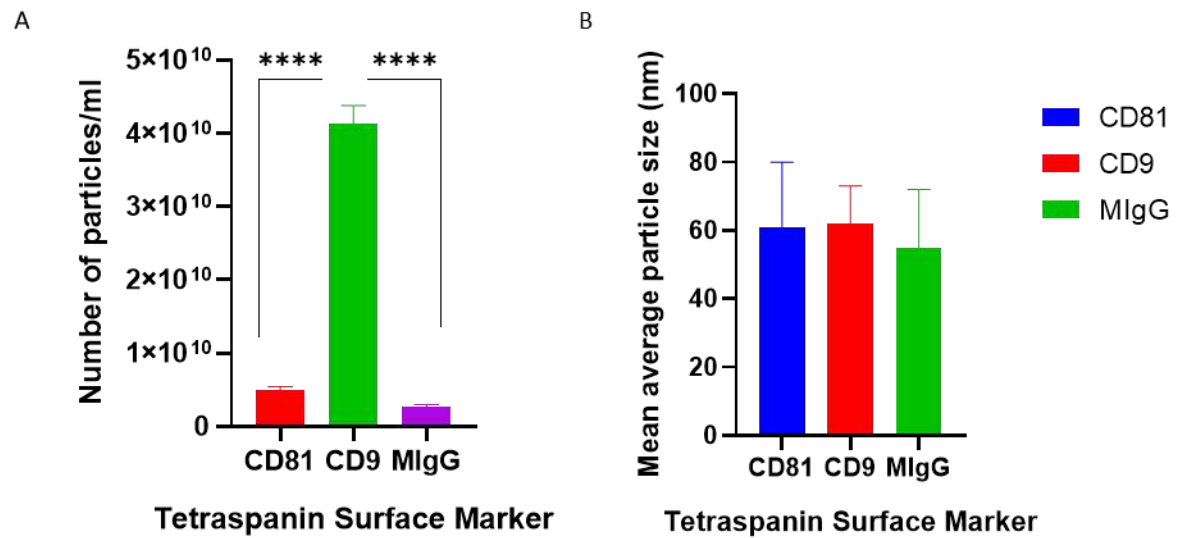
PRP was isolated from three equine donors, as shown in Figure 8.3.A. The platelet count for whole blood, plasma and PRP was measured. PRP was pooled for the *in vitro* experiments. PRP (691,000/ $\mu$ l +/- 61.9 (SEM)) had 2.09 times more platelets when compared to the baseline platelet count from whole blood (330,000/ $\mu$ l +/- 16.5 (SEM)), (Figure 8.3.B).



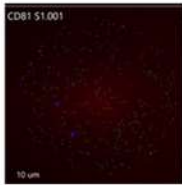
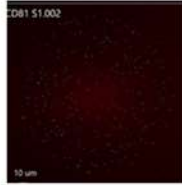
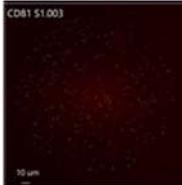
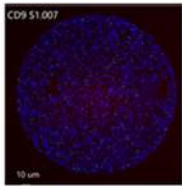
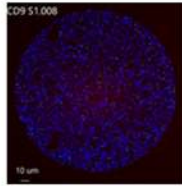
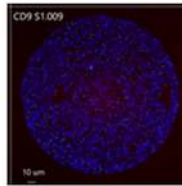

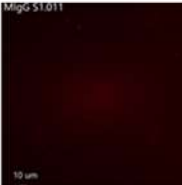

**Figure 8.3. Platelet-rich plasma characterisation.** (A) The platelet count (K/ $\mu$ l) per anonymised equine donor, from whole blood, plasma and platelet-rich plasma (PRP). (B) The mean (n=3) platelet count in plasma and PRP with standard deviation shown.

*Platelet-rich plasma derived extracellular vesicles were enriched in the expression of CD9*

PRP-EVs from a pooled sample of the previously analysed PRP was characterised using the Human Exoview Tetraspanin Assay. PRP-EVs expressed CD81 and CD9, but were most enriched for the CD9 surface marker (Figure 8.4.A and 8.4.B), with significant ( $p < 0.0001$ ) expression observed compared with CD81, and the negative control MIgG. CD63 was not reported here due to low particle counts for this tetraspanin; this has been attributed to poor protein homology between equine and human CD63 tetraspanin (Clarke, Johnson, *et al.*, 2022). It was identified that PRP-EVs had a concentration of  $5.23 \times 10^{10}$  particles/ml and plasma EVs had a concentration of  $6.91 \times 10^{10}$  particles/ml. As plasma EVs were not used in the *in vitro* equine tendon inflammatory model experiment, their characterisation data is not shown. PRP-EVs were visualized with fluorescent microscopy, highlighting tetraspanin expression and EV morphology (Figure 8.4.C).



C

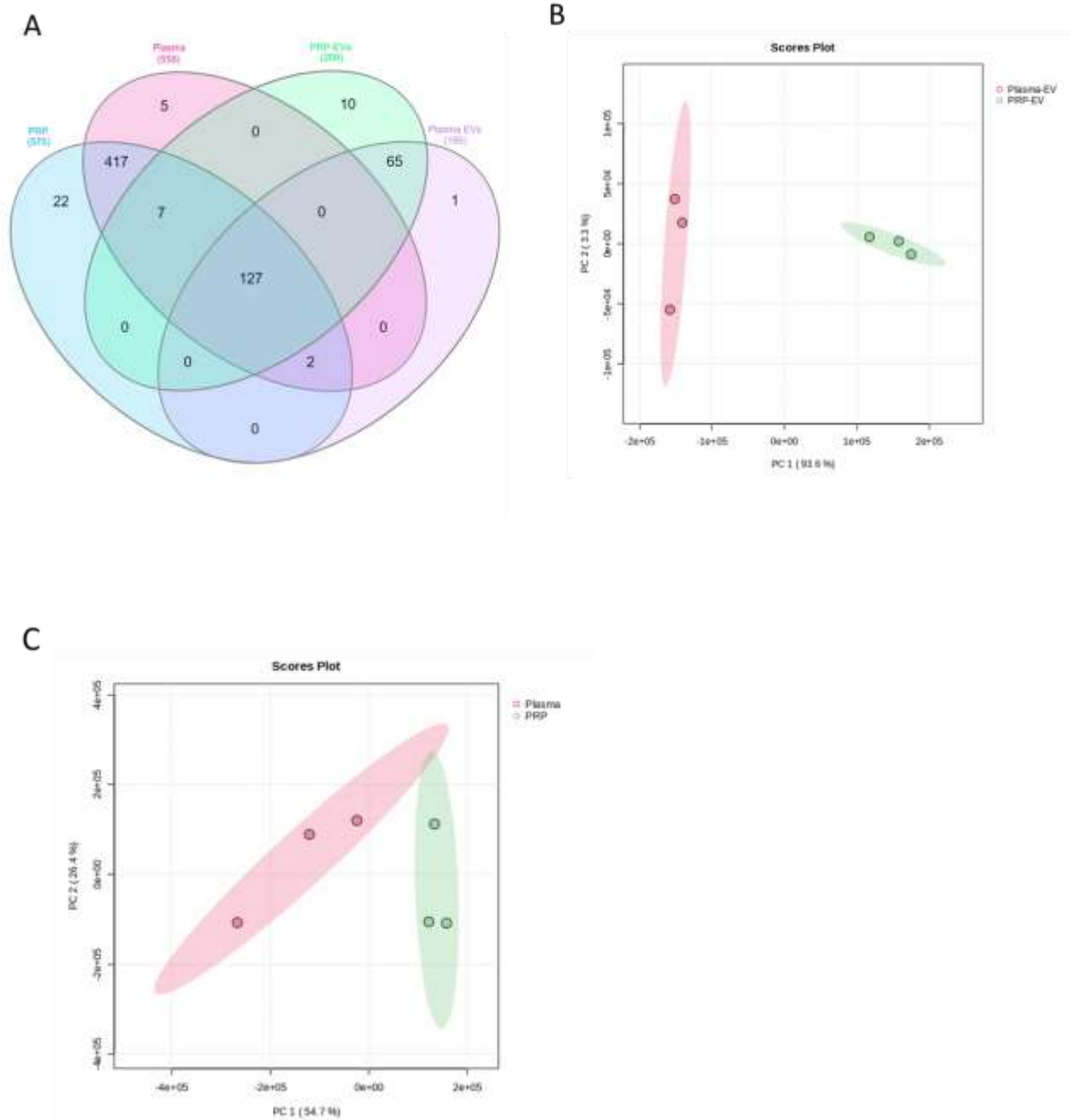
Surface Marker	Technical replicate 1	Technical replicate 2	Technical replicate 3
CD81			
CD9			
MIgG (negative control)			

**Figure 8.4. Exoview of platelet-rich plasma derived extracellular vesicles.** (A) Particle concentration (particles/ml) per EV surface marker for PRP-EVs, with MIgG acting as a negative control, (B) Mean average EV size per tetraspanin surface marker for PRP-EVs. Error bars are  $\pm$  standard deviation. (C) Visualization of PRP- EVs using Exoview Tetraspanin Assay. A fluorescent image of a representative spots (technical replicates) is shown with colour denoting surface tetraspanin positive identification blue-CD9, and green-CD81). (blue-CD9, and green-CD81). Significance denoted by \* ( $p < 0.05$ ), \*\* ( $p < 0.01$ ), \*\*\* ( $p < 0.001$ ), \*\*\*\* ( $p < 0.0001$ ), following Shapiro Wilks normality testing and one-way ANOVA with multiple comparisons, followed by a post hoc Tukey test undertaken in GraphPad Prism.

### *8.3.3.2. Platelet-rich Plasma and Platelet-rich Plasma Derived Extracellular Vesicle Proteomic Profiles*

*Distinct protein profiles were identified in platelet-rich plasma derived extracellular vesicles compared to matched plasma extracellular vesicles, and between platelet-rich plasma and plasma*

PRP, plasma, PRP-EVs and plasma-EVs (n=3) were analysed using mass spectrometry proteomics (Figure 8.5.A). PRP had a total of 575 quantified proteins, 22 of which were unique to PRP. Plasma had 558 proteins, five of which were unique to plasma. PRP- EVs had 209 proteins, with 10 proteins unique to PRP-EVs. Plasma EVs had 195 proteins quantified, with 1 unique protein found. T-test analysis identified 157 significant proteins ( $q < 0.05$ ) in PRP-EVs compared to plasma EVs (Supplementary Table 10.7), and 45 significant proteins ( $q < 0.05$ ) were identified in PRP compared with plasma (Supplementary Table 10.8). Unsupervised multivariate analysis of the proteome was then performed in the form of PCA on all quantified proteins following the removal of proteins with 50% or more missing values. It was found that principal component 1 (PC-1) had an explained variance of 93.6% when comparing PRP-EVs to plasma EVs (Figure 8.5.B), illustrating distinct differences in the proteome of varying EV sources. This analysis was repeated comparing plasma to PRP and it was found that PC-1 accounted for 54.7% of variation observed within the proteome dataset (Figure 8.5.C).



**Figure 8.5. Proteins identified and quantified between platelet-rich plasma and platelet-rich plasma derived extracellular vesicles with matched plasma samples.** (A) Venn diagram, (B) PCA of the proteome of plasma-EVs and PRP-EVs (n=3) following Pareto scaling, (C) PCA of the proteome of plasma and PRP (n=3), 95% confidence limit regions shown.

### 8.3.3.3. Functional Enrichment Analysis of Platelet-rich Plasma and Platelet-rich Plasma Derived Extracellular Vesicle Content

*Platelet-rich plasma was enriched with molecules associated with the regulation of cellular waste disposal, platelet-rich plasma extracellular vesicles showed a downregulation in lipid metabolism*

Functional enrichment analysis was performed using IPA software on differentially expressed proteins with and FDR p-value<0.05, and log fold change, as well as all identified proteins serving as background for analysis. The top five most significant canonical pathways for PRP versus plasma are in Table 8.1. The analysis was repeated to identify the top canonical pathways in PRP-EVs compared to plasma EVs as shown in table 8.2.

**Table 8.1. Top canonical pathways following Functional enrichment analysis using Ingenuity Pathway Analysis for platelet-rich plasma when compared to matched plasma.**

Enriched in	Disease and function	P value range	Pathway	Activation state	Z score	P value
PRP	Cellular function and Maintenance	4.23x10 <sup>-2</sup> – 1.86x10 <sup>-3</sup>	FAT10 signalling pathway	Not significant	N/A	6.15x10 <sup>-4</sup>
PRP	Cellular response to therapeutics	6.97x10 <sup>-3</sup> – 3.61 x10 <sup>-3</sup>	BAG2 signalling pathway	Not significant	N/A	1.8x10 <sup>-3</sup>
PRP	Tissue morphology	4.86x10 <sup>-2</sup> – 2.75x10 <sup>-3</sup>	Micro autophagy signalling pathway	Activated	3.873	4.37x10 <sup>-5</sup>
PRP	Organismal functions	4.49x10 <sup>-2</sup> – 1.05x10 <sup>-2</sup>	Inhibition of ARE mediated mRNA degradation pathway	Not significant	N/A	2.11x10 <sup>-3</sup>
PRP	Cellular assembly and organisation	4.23x10 <sup>-2</sup> – 1.86x10 <sup>-3</sup>	Protein ubiquitination pathway	Not significant	N/A	1.38x10 <sup>-4</sup>

Abbreviations: Human leukocyte antigen (HLA)-F adjacent transcript 10 (FAT10), Bcl-2-associated athanogene 2 (BAG2), AU-rich elements (ARE), messenger ribose nucleic acid (mRNA).

**Table 8.2. Top canonical pathways following Functional enrichment analysis using Ingenuity Pathway Analysis for platelet-rich plasma derived extracellular vesicles compared to matched plasma extracellular vesicles.**

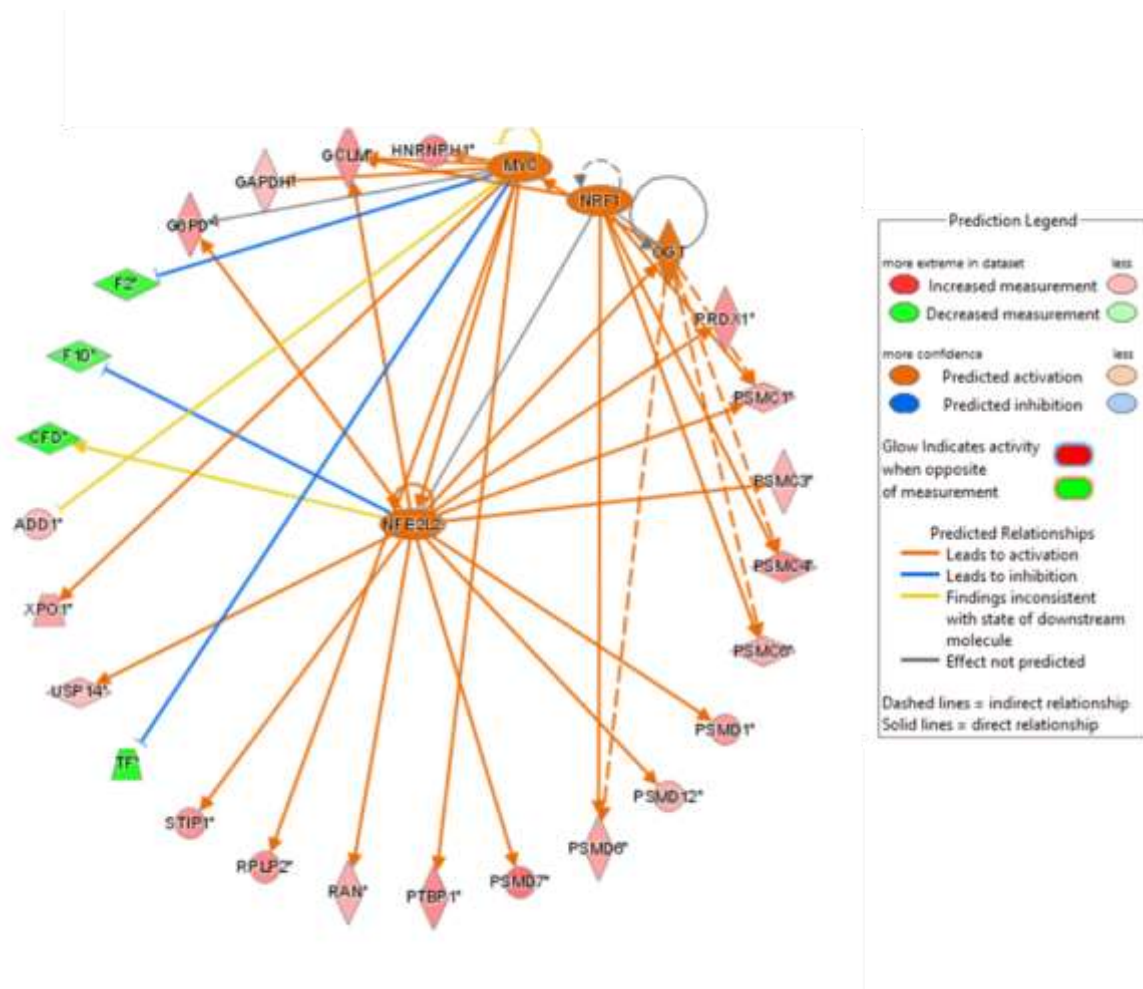
Enriched in	Disease and function	P value range	Pathway	Activation state	Z score	P value
PRP-EVs	Cell to cell signalling and interaction	4.65x10 <sup>-2</sup> – 1.70x10 <sup>-4</sup>	Acute phase response signalling	inhibited	-2.714	3.88x10 <sup>-5</sup>
PRP-EVs	Lipid metabolism	4.79x10 <sup>-2</sup> – 3.18x10 <sup>-4</sup>	LXR-RXR activation	inhibited	-3.771	1.02x10 <sup>-5</sup>
PRP-EVs	Molecular transport	3.85x10 <sup>-2</sup> – 3.18x10 <sup>-4</sup>	FXR/RXR activation	Not significant	N/A	1.59x10 <sup>-5</sup>
PRP-EVs	Cellular Movement	3.85x10 <sup>-2</sup> – 8.16x10 <sup>-5</sup>	DHCR24 signalling pathway	Inhibited	-4.123	9.29x10 <sup>-5</sup>
PRP-EVs	Tissue morphology	3.85x10 <sup>-2</sup> – 3.85x10 <sup>-3</sup>	Complement system	Activated	1.633	1.39x10 <sup>-2</sup>

Abbreviations: liver X receptor /retinoid X receptor (LXR/RXR), farnesoid X receptor/ retinoid X receptor (FXR-RXR), 24-dehydrocholesterol reductase (DHCR24).

*Predicted upstream regulators of platelet-rich plasma and platelet-rich plasma derived extracellular vesicles include NFE2L2 activation and inhibition of IL20 and STAT3 respectively*

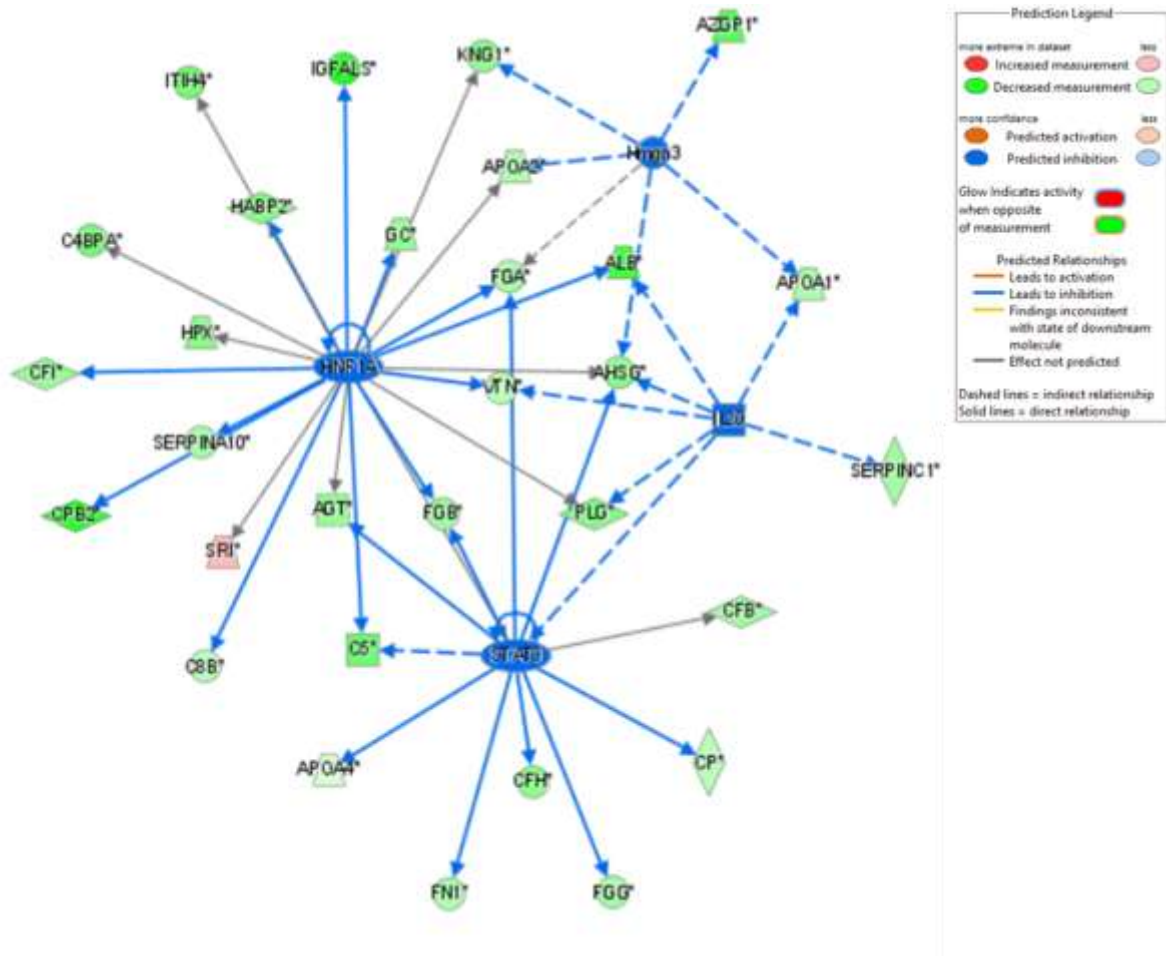
Following functional enrichment analysis upstream regulators were identified as enriched, and subsequently activated in PRP versus plasma. Activated upstream regulators included transcriptional regulators or enzymes. Of these, nuclear factor erythroid 2-related factor 2 (NFE2L2) (transcriptional

regulator,  $p=0.016$ ,  $z$  score = 2.959) was identified as a central upstream regulator within the network. Other activated upstream regulators included nuclear respiratory factor 1 (NRF1) (transcriptional regulator,  $p=0.00404$ ,  $z$  score = 2.236), O-GlcNAc transferase (OGT) (enzyme,  $p=0.0372$ ,  $z$  score= 2) and myelocytomatosis oncogene (MyC) (transcriptional regulator,  $p=0.446$ ,  $z$  score= 2.167), as shown in Figure 8.6. Conversely, the analysis was repeated for PRP-EVs versus plasma EVs, and it was found that specific upstream regulators were inhibited; signal transducers and activators of transcription 3 (STAT3) (transcriptional regulator,  $p= 0.024$ ,  $z$  score=-3.059), Interleukin 20 (IL20) (cytokine,  $p=0.00229$ ,  $z$  score= -2.449), hepatocyte nuclear factor-1 alpha (HNF1A) (transcriptional regulator,  $p=0.000147$ ,  $z$  score = -3.42), and high mobility group nucleosomal binding domain 3 (Hmgn3) (other,  $p= 0.00561$ ,  $z$  score = -2.236), as shown in Figure 8.7.



**Figure 8.6. A network showing activated upstream regulator nuclear factor erythroid 2-related factor 2, and associated proto-oncogene MyC, nuclear respiratory factor 1 and O-GlcNAc transferase, identified as enriched in platelet-rich plasma compared to plasma made in Ingenuity Pathway Analysis.** This is a graphical representation between molecules identified in our data. Green nodes; reflect decreased measurement and red nodes; highlight increased measurement within the dataset . Intensity of colour is related to higher fold change. Key to the main features in the networks is shown.



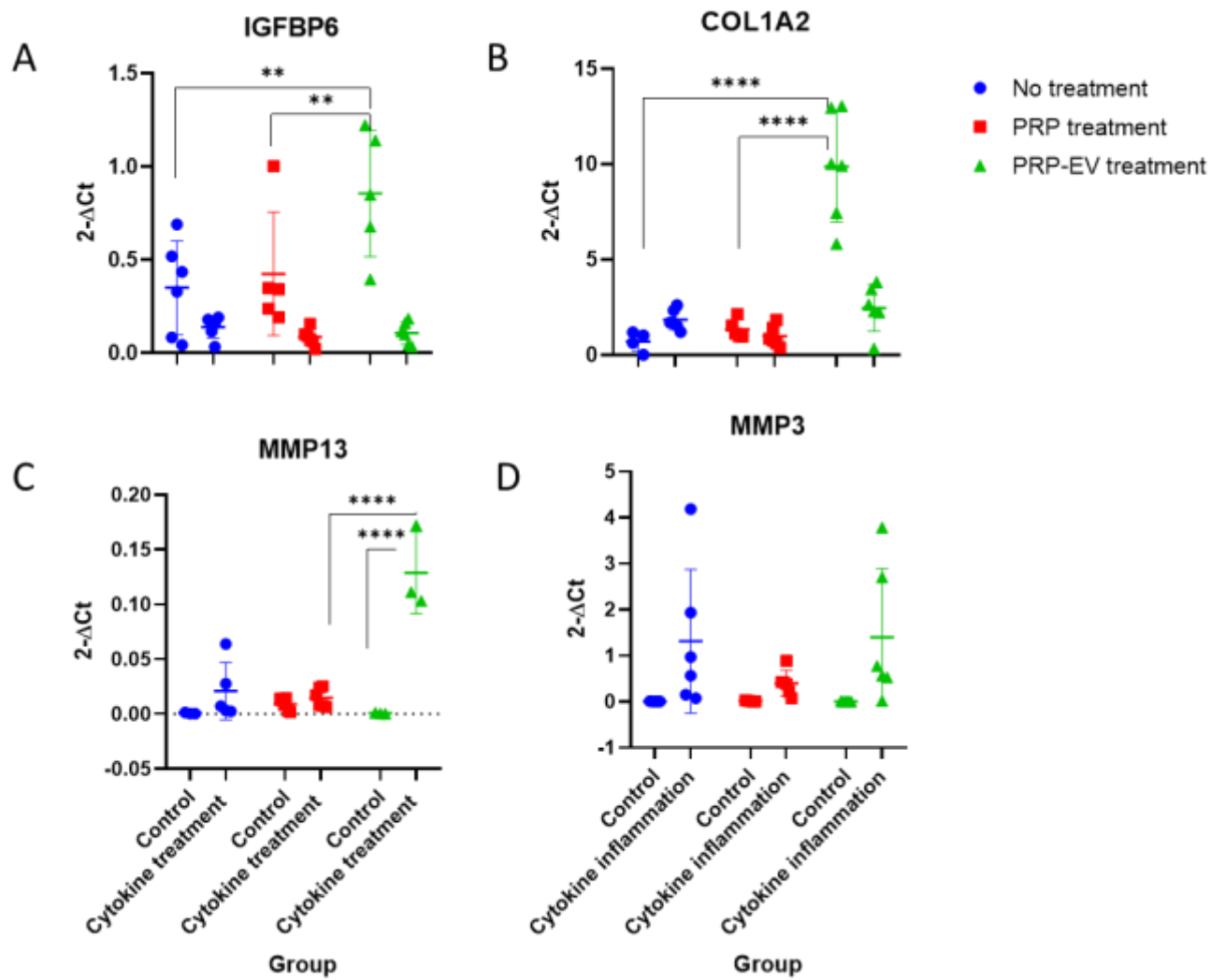


**Figure 8.7. A network showing activated upstream regulators, with the highest z score, identified as enriched in platelet-rich plasma derived extracellular vesicles compared to plasma derived extracellular vesicles.** This is a graphical representation between molecules identified in our data. Green nodes; reflect decreased measurement and red nodes; highlight increased measurement within the dataset. Intensity of colour is related to higher fold change. Key to the main features in the networks is shown.

#### 8.3.3.4. Gene Expression Analysis of In Vitro Tendon Inflammatory Model

*An increase in matrix metalloproteinases in tendon inflammatory model, and a decrease in tendon marker expression. Platelet-rich plasma treatment shows a trend towards decreasing matrix metalloproteinase expression*

Gene expression analysis was performed on a panel of protein coding genes, with statistical analysis using two-way ANOVA and post-hoc testing. IGFBP6 was found to have significant expression change with respect to both treatment and cytokine stimulation ( $p=0.0209$ ), and a loss of a healthy tendon phenotype. It was identified that PRP and PRP-EV treatment could not restore gene expression of IGFBP6 in equine tenocytes that received pro-inflammatory stimulation. Although, a significant increase in expression of IGFBP6 was observed when comparing no treatment and PRP treatment to that of EV treatment ( $p<0.01$ ) (Figure 8.8.A). COL1A2 was found to have significant expression changes with respect to both treatment ( $p<0.0001$ ) and cytokine stimulation ( $p=0.0001$ ). Increased expression in the control group following PRP-EV treatment, compared to no treatment and PRP treatment ( $q<0.0001$ ) (Figure 8.8.B) was observed. However, no significant increase in expression was observed in the cytokine stimulated groups following treatment. MMP13 expression was identified as significantly altered in relation to both treatment and cytokine stimulation following two-way ANOVA analysis ( $p<0.0001$ ). It was found to remain stable in all control associated groups. However, within the cytokine stimulation group differential expression was observed between no treatment and PRP-EV treatment ( $p<0.0001$ ), and PRP treatment compared to PRP-EV treatment ( $p<0.0001$ ). Whereby PRP treatment resulted in decreased expression compared to no treatment, and PRP-EV treatment resulted in significantly elevated levels of MMP13 (Figure 8.8.C). It was found that MMP3 expression remained low in all control groups, and increased following cytokine stimulation, though expression change was not significant. Following PRP treatment MMP3 expression decreases, however following PRP-EV treatment MMP3 expression increased when compared to all control groups, however this was not statistically significant following analysis (Figure 8.8.D).

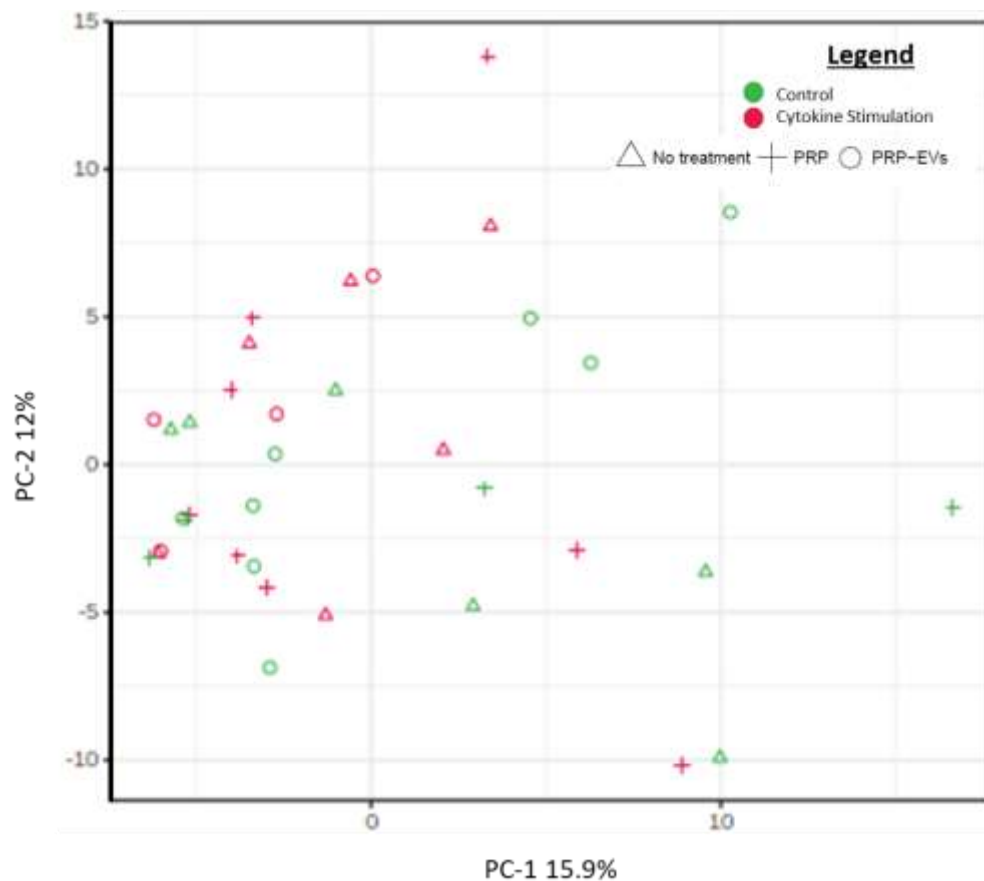


**Figure 8.8. Gene expression analysis of control and cytokine stimulated equine tenocytes following platelet-rich plasma and platelet-rich plasma derived extracellular vesicle treatments.** A) IGFBP6, B) COL1A2, C) MMP13, D) MMP3 using RT-qPCR and relative quantification methods ( $2^{-\Delta\text{Ct}}$ ). Significance is denoted by an adjusted p value \* ( $q < 0.05$ ), \*\* ( $q < 0.01$ ), \*\*\* ( $q < 0.001$ ), \*\*\*\* ( $q < 0.0001$ ), following two-way ANOVA analysis and multiple comparison testing. (A) COL1A2, (B) IGFBP6, (C) MMP3 and (D) MMP13.

### 8.3.3.5. Principal Component Analysis

#### *Platelet-rich plasma and platelet-rich plasma derived extracellular vesicles alter the cellular proteome of cytokine stimulated equine tenocytes*

A total of 1933 proteins were identified across all samples, with 1567 proteins quantified. Following the removal of contaminating blood-derived proteins and proteins with 25% or more missing values a total of 832 proteins were used for downstream analysis. Multiple factor PCA of the proteome of all experimental groups was performed considering cellular phenotype (control or following cytokine stimulation) and the effect of treatment (no treatment, PRP treatment and PRP-EV treatment). Using PCA there appeared to be a change following PRP or PRP-EV treatment (Figure 8.9.) with a shift towards that of control tenocytes when cells were treated with PRP or PRP-EVs following cytokine treatment.



**Figure 8.9. Unsupervised multivariate analysis using principal component analysis.** Red denotes cytokine treatment and green denotes control, a triangle symbolises no treatment, a cross represents

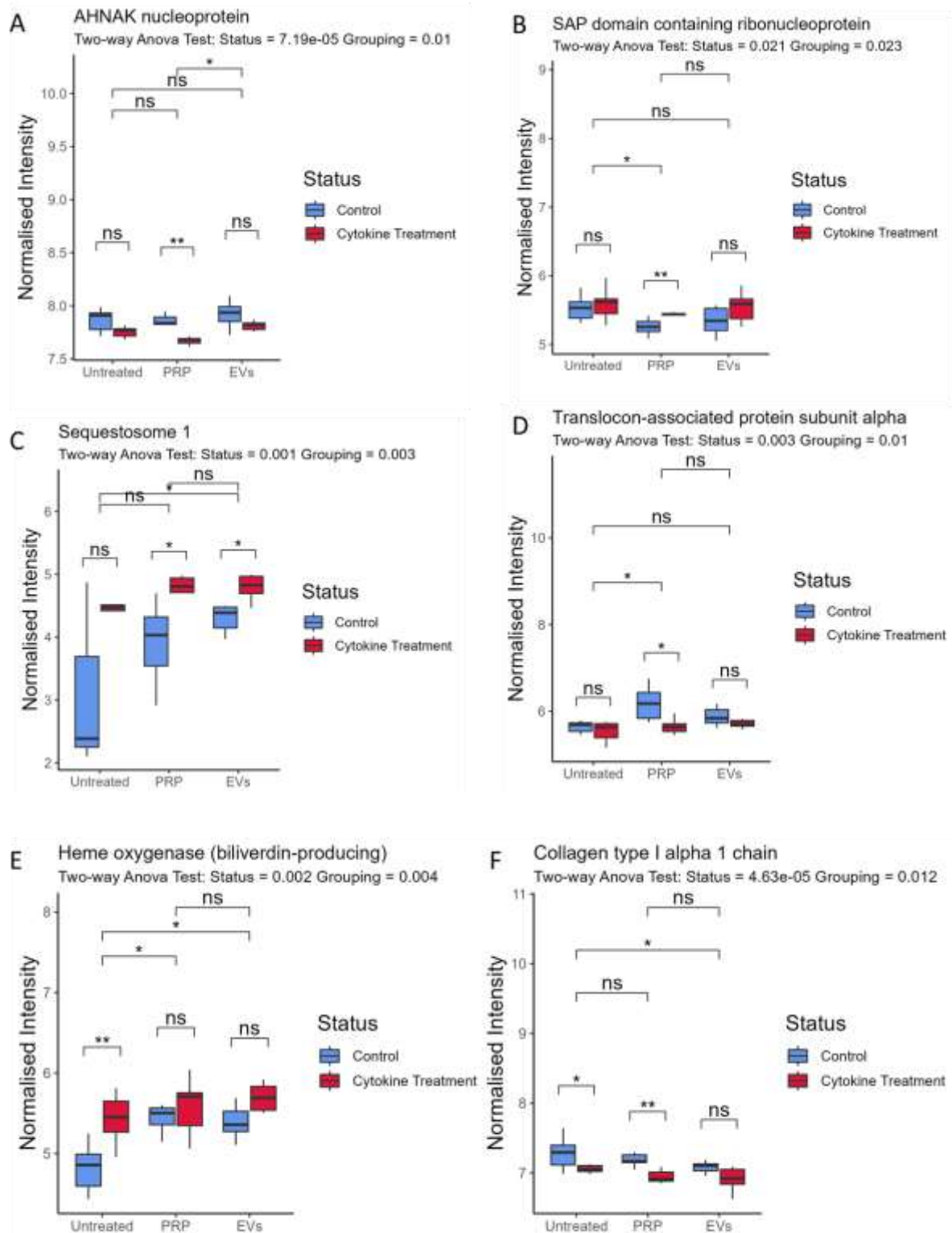
samples treated with PRP and a circle represents PRP-EV treatment. 95% confidence limit are also shown in PCA plots.

### 8.3.3.6. Cellular Proteome Analysis

#### *18 proteins changed following cytokine stimulation and treatment*

A two-way ANOVA was performed on all proteomics data from cellular lysates in order to account for both categorical variables within the study: cytokine stimulation (control or cytokine stimulation), and treatment (no treatment, PRP or PRP-EVs) and their effect on protein expression (Figure 8.10). Six significant proteins are shown and the remaining 12 can be found in Supplementary Figure 10.5. In total 18 proteins were identified as significant with respect to both categorical variables at an unadjusted  $p < 0.05$ . These proteins included the following with  $p$  values corresponding to the effect of cytokine stimulation and PRP or PRP-EV treatment, respectively: adenylate kinase 2 mitochondrial protein ( $p=0.035$  and  $p=0.038$ ) (Supplementary Figure 10.5.A), AHNAK nucleoprotein ( $p=7.19E-5$  and  $p=0.01$ ) (Figure 8.10.A), Beta-galactosidase ( $p=0.028$  and  $p=0.046$ ) (Supplementary Figure 10.5.B), centrosomal protein of 162kDa ( $p=0.013$  and  $p=0.019$ ) (Supplementary Figure 10.5.C), collagen type 1 alpha 1 chain ( $p=4.63E-5$  and  $p=0.012$ ) (Figure 8.9.F), D-3-phosphoglycerate dehydrogenase ( $p=0.047$  and  $p=0.034$ ) (Supplementary Figure 10.5.D), F-actin- capping protein subunit alpha ( $p=0.042$  and  $p=0.02$ ) (Supplementary Figure 10.5.E), heme oxygenase ( $p= 0.002$  and  $p=0.004$ ) (Figure 8.10.E), heterogeneous nuclear ribonucleoprotein U like 1 ( $p=0.011$  and  $p=0.035$ ) (Supplementary Figure 10.5.F), LRP chaperone MESD ( $p=0.038$  and  $p=0.043$ ) (Supplementary Figure 9.5.G), polyadenylate-binding protein ( $p=0.022$  and  $p=0.009$ ) (Supplementary Figure 10.5.H), protein disulphide isomerase ( $p=0.022$  and  $p= 0.012$ ) (Supplementary Figure 10.5.I), SAP domain containing ribonucleoprotein ( $p= 0.021$  and  $p=0.003$ ) (Figure 8.10.B), sequestosome 1 ( $p=0.001$  and  $p=0.036$ ) (Figure 8.10.C), small monomeric GTPase ( $p=0.017$  and  $p=0.036$ ) (Supplementary Figure 10.5.J), sulphide quinone oxidoreductase ( $p=0.022$  and  $p=0.022$ ) (Supplementary Figure 10.5.K), THADA armadillo repeat ( $p=0.02$  and  $p= 0.012$ ) (Supplementary Figure 10.5.L) and translocon associated protein subunit alpha ( $p=0.003$  and  $p=0.01$ ) (Figure 8.10.D) (All shown in supplementary Table 10.9 ).  $P$  values were subsequently used in pathway analysis as it has been reported that multiple testing correction methods can fail to identify statistically significant values due to stringent thresholds (Pascovici *et al.*, 2016).

Figure 8.10 depicts a selection of significant proteins identified following two-way ANOVA and post hoc Tukey test; Supplementary Figure 10.5 depicts the remaining 12 significant proteins. Figure 8.10.A demonstrates reduced expression of AHNAK nucleoprotein between control and cytokine treatment following PRP treatment ( $p < 0.01$ ). In addition, there was a significant difference in protein expression between PRP and PRP-EV treatment ( $p < 0.05$ ). Figure 8.10.B demonstrates a significant increase in SAP domain containing ribonucleoprotein between control and the cytokine following PRP treatment ( $p < 0.01$ ), and a difference in expression between no treatment and PRP treatment ( $p < 0.05$ ). Figure 8.10.C highlights a significant increase in sequestosome 1 between control and the cytokine following PRP and PRP-EV treatment ( $p < 0.05$ ). In addition, a difference in protein abundance between no treatment and PRP-EV treatment groups ( $p < 0.05$ ) was evident. Figure 8.10.D shows a significant decrease in translocon associated protein sub unit alpha expression between control and cytokine following PRP treatment ( $p < 0.05$ ) and a difference between no treatment and PRP treatment ( $p < 0.05$ ). Figure 8.10.E highlights a significant increase in heme oxygenase following cytokine treatment when compared to control ( $p < 0.01$ ), and a difference between no treatment and PRP and PRP-EV treatment groups ( $p < 0.05$ ). Finally, Figure 8.10.F shows a reduction in collagen 1 alpha 1 abundance between control and cytokine ( $p < 0.05$ ), and between control and cytokine treated with PRP ( $p < 0.01$ ) in both the control and PRP treated cytokine groups. It was also different between the control and that of PRP-EV treatment ( $p < 0.05$ ).



**Figure 8.10. Differential abundant proteins following cytokine stimulation of equine tenocytes and the effect of no treatment, platelet-rich plasma and platelet-rich plasma derived extracellular vesicle treatment.** As identified by a two-way ANOVA and post hoc tukey test A) AHNAK nucleoprotein, (B) SAP domain containing ribonucleoprotein, (C) sequestosome 1, (D) translocon associated protein subunit alpha, (E) heme oxygenase and (F) collagen type 1 alpha 1. Significance is denoted by \*( $p < 0.05$ ), \*\* ( $p < 0.01$ ), \*\*\* ( $p < 0.001$ ), \*\*\*\* ( $p < 0.0001$ ).

## 8.4 Discussion

This pilot study aimed to determine the effect of PRP and PRP-EVs on tendon inflammation using an *in vitro* model to ascertain how PRP-EVs may be involved in the mediation of PRP therapeutic outcomes and the potential molecular pathways eliciting their biological effect. To our knowledge this is the first study of its kind to explore the role of PRP-EVs in PRP therapeutic mediation *in vitro*. The rationale for determining the cargo of PRP-EVs was due to evidence demonstrating that platelets secrete a significant number of EVs (Tao, Guo and Zhang, 2017), thus it was hypothesised that EVs may be involved in the therapeutic action evident with PRP usage. PRP-EVs are a heterogenous population of EVs from multiple sources, such as leukocytes (T-cells and B cells) (Auber and Svenningsen, 2022), with an enrichment in platelet derived EVs. Many pre-clinical studies have evidenced the potential of PRP-EVs as a future therapeutic option, due to the smaller size of PRP-EVs being beneficial for their transfer across biological barriers which helps to retain stability in the extracellular environment (Wu, Piao, *et al.*, 2021). It was hypothesised that PRP and PRP-EVs treatment of cytokine stimulated tenocytes would result in a change in the phenotype of the cells as measured by the proteome. It was found that PRP and PRP-EVs were enriched in proteins associated with cellular waste disposal and lipid metabolism, respectively when compared to plasma and plasma-EVs. Whilst not significant there appeared to be reduction in the expression of matrix gene expression following PRP treatment. Proteomics revealed that PRP and PRP-EV treatment had a small effect on control equine tenocytes or those treated with cytokines (18 significant proteins across cytokine stimulation and treatment; no treatment, PRP, PRP-EVs). However, these proteins are associated with pathways such as collagen metabolism and NFkB signalling. As proteomic difference between PRP and PRP-EV treatment was not significant globally this is suggestive of PRP-EVs greater role in mediating PRP therapeutic action, and their potential as a therapeutic in their own right requiring further exploration.

PRP was characterised to determine the platelet count in PRP compared to whole blood. Mean PRP platelet count was greater than two times that of baseline whole blood, as per current literature that suggests PRP should have a platelet count at least 2 times greater than that of baseline plasma (Fortier, 2010; Parrish *et al.*, 2016). However, there is no definitive definition outlined by a medical or academic society, making comparisons between PRP research difficult to draw. A review comparing the PRP preparations from 33 commercially available systems found only 11 met the proposed  $1 \times 10^6$  platelets/ $\mu\text{l}$  suggested for medical and dental applications (Xu *et al.*, 2020). A number of classification systems in human associated research have been used to improve PRP characterisation and literature reporting, these include: Ehrenfest classification, platelets, activation, white blood cells (PAW) system,



dose, efficiency, preparation, activation (DEPA) system, and method, activation RBCs, spin, platelet concentration, image guided, leukocyte concentration, light activation (MARSPILL) system (Collins, Alexander and Barkatali, 2021). However, it is still controversial as to the appropriate leukocyte concentration for effective PRP use (Collins, Alexander and Barkatali, 2021). In addition, the preparation system can also affect PRP characteristics evidenced by a study that utilised a single-donor model in order to compare four commercially available systems and one laboratory based system, identifying significant biological variations (Magalon *et al.*, 2014).

PRP-EVs were isolated following dUC, and characterised using the Human Exoview Tetraspanin Chip Assay. Characterisation of EV samples is required to adhere to scientific reporting standards outlined by the international Society for Extracellular Vesicles (ISEV) (Théry *et al.*, 2018). This provides guidance on nomenclature, sample collection and pre-processing, EV separation and concentration, EV characterization, functional studies, and reporting requirements/exceptions. In this study it was found that PRP-EVs had a concentration of  $5.23 \times 10^{10}$  EVs/ml and were enriched for the expression of CD9 tetraspanin surface marker. Previous studies have postulated that tetraspanin enrichment may be indicative of extracellular function. It has been shown that enrichment of CD9 in platelets is associated with b3-integrins in both activated and non-activated forms (Spakova, Janockova and Rosocha, 2021). Plasma is rich in CD9+ EVs (Khanna, Salmond and Williams, 2023). Furthermore platelet-EVs are often enriched in CD63, due to these tetraspanin being an established surface marker of platelets, synonymous with the procoagulant activity of platelets (Heijnen *et al.*, 1999). A negligible number of PRP-EVs were found to be CD63+ in this study, however we have previously attributed this to poor protein homology between human and equines for this protein (Clarke, Lima, *et al.*, 2022). Additionally EV isolation technique has previously been reported to affect the subsequent heterogeneity of the EV population sampled (Vestad *et al.*, 2017; Anderson *et al.*, 2022; Clarke, Lima, *et al.*, 2022).

We interrogated the PRP and PRP-EV proteomes to determine significant pathways. It was found that enriched pathways in PRP included micro autophagy signalling pathway and the protein ubiquitination pathways. Microautophagy is recognised as a non-selective lysosomal degradative process, which engulfs cytoplasmic cargo at membrane boundaries via autophagic tubes (Kawamura *et al.*, 2012; Li, Li and Bao, 2012). It is involved in the maintenance of cellular size, membrane homeostasis and cellular survival under nitrogen restriction (Li, Li and Bao, 2012). In this study proteins such as proteasome 26s subunit ATPase 1, 2, 3, 4,5 and 6 were mapped to this activated pathway. Previous

studies have implicated autophagy more broadly in the development and repair of tendon following a traumatic injury, with autophagy of the endoplasmic reticulum found to regulate the secretion of type 1 procollagen, but reduce the mechanical strength of tendon when subject to tensile force (Montagna *et al.*, 2022). Furthermore, it has been shown that autophagy prevents the loss of stemness in tendon stem cells as a result of increased oxidative stress often seen at the site of tendon injury, by suppressing the accumulation of reactive oxygen species (ROS) (Chen *et al.*, 2016). As such it can be suggested that PRP may have the capacity to enhance the activity of such pathway, acting in a protective anti-oxidative capacity, protecting resident cells from damage. Protein ubiquitination is involved in the degradation of over 80% of proteins in cells, and is regarded as a reversible post-translational modification, which can occur due to the action of E1 ubiquitin-activating enzymes, E2 ubiquitin-conjugating enzymes, and E3 ubiquitin–ligase enzymes (Qu, Zou and Lin, 2021). Both ubiquitination and deubiquitination of proteins are involved in a variety of signal transduction pathways (Qu, Zou and Lin, 2021), and have been regarded as a new avenue for therapeutic research, with the emphasis placed on harnessing the targeted catalytic elimination of proteins (Ottis *et al.*, 2019). E3 ubiquitin-protein ligase plays a fundamental role in the maintenance of skeletal tissue through regulation of the mammalian hedgehog signalling pathway, with the loss of such protein linked to articular cartilage degradation, enlarged, abnormally shaped sesamoid bones and extensive heterotopic tissue metaplasia linked to calcification of tendons and ossification of synovium (Mellis *et al.*, 2021). In studies involving rotator cuff injury it has been found that the ubiquitin- proteasome pathway is a potent regulator of muscular atrophy and as such protein degradation can be attributed to such occurrence as a result of tendon injury (Sunil *et al.*, 2014). PRP is enriched for proteins that activate autophagic and ubiquitination processes, potentially promoting collagen metabolism, skeletal tissue homeostasis and the reduction of oxidative stress. This could have significant implications when considering the repair of tendon injury sites.

In addition to this, predicted upstream regulators of proteins enriched in PRP were also identified, namely NFE2L2 and NRF1 were both predicted to be activated. NFE2L2 is a transcription factor associated with the maintenance and adaptation of intracellular redox homeostasis (Fragoulis *et al.*, 2023), with the associated pathway involved in the cellular antioxidant defence system (Liu *et al.*, 2017). This property has been shown in a number of *in vitro* studies, such as that of Liu *et al* (Liu *et al.*, 2017), identifying that NFE2L2 could inhibit periodontal ligament stem cell apoptosis under excessive oxidative stress (Liu *et al.*, 2017). In addition, it has been evidenced to contribute toward

mechanotransduction in musculoskeletal tissues (Fragoulis *et al.*, 2023). Notably, Tognoloni *et al.* (Tognoloni *et al.*, 2023) showed that PRP could increase antioxidant defences of tenocytes through the activation of the NFE2L2 pathway. Hence this finding concurs with recent literature. In addition, NRF1 has been linked to the expression of nuclear and mitochondrial genes that promote mitochondrial biogenesis in order to meet the energetic demands of healing (Lippi, Longo and Maffulli, 2010; Thankam *et al.*, 2018). Its activation would be regarded therapeutically beneficial in the context of tendon injury and healing.

Following functional enrichment analysis of the proteome of PRP-EVs we identified acute phase response signalling (inhibited), LXR-RXR (inhibited) and FXR-RXR signalling (not stated) as canonical pathways associated with PRP-EV cargo. Acute phase response signalling has previously been associated with the enhancement of late stage healing in tendon injury, induced by IL-6, despite IL-6's role in inflammation and cellular response to tissue injury (Chisari *et al.*, 2021). It has however been directly attributed to inflammation due to its cytokine regulation, and involves multiple plasma proteins including C-reactive protein, serum amyloid A, transthyretin, fibronectin (Miroshnychenko *et al.*, 2020). This suggests that PRP-EVs could- potentially act in an anti-inflammatory manner by inhibiting acute phase response signalling. LXR-RXR signalling was predicted to be inhibited in this study, due to proteins clusterin, interleukin 1 receptor protein, transferrin, serpin family f member 1, and vitronectin. Liver X receptors (LXRs) are known as transcriptional regulators of lipid homeostasis, with anti-inflammatory properties (Ito *et al.*, 2015; Kong *et al.*, 2019), RXR is a nuclear hormone receptor of the retinoid family, that functions in conjunction with FXR and LXR. FXR-RXR signalling was attributed to the enrichment of proteins such as transferase and kinogen 1, and is involved in the activation of cholesterol homeostasis, triacylglyceride metabolism, and suppression of inflammatory processes (Kong *et al.*, 2019). In this study both LXR and FXR – RXR signalling were attributed to PRP-EV cargo. As such suggestive of PRP-EVs carrying cargo that can inhibit anti-inflammatory mechanisms. It has been demonstrated recently that PRP, and by association potentially PRP-EVs, can elicit an inflammatory response in human tendon fibroblasts *in vitro*, by stimulating TNF- $\alpha$  and NF $\kappa$ B pathways, resulting in the formation of ROS and the activation of oxidative stress pathways (Hudgens *et al.*, 2016). Thus it has been hypothesised that PRP may act by causing an acute inflammatory event that stimulates endogenous tissue regeneration responses (Hudgens *et al.*, 2016).

Upstream regulators were predicted for differentially abundant proteins in PRP-EVs compared with plasma EVs. These regulators included STAT3 and IL20, both of which were predicted to be inhibited. STAT3 has previously been found to exert effects on transcription genes by mediating cellular proliferation and the conversion of phenotype (Pan *et al.*, 2020). Its inhibition has been associated with a decrease in ECM production and fibroblast proliferation (Pan *et al.*, 2020). It was identified that the inhibited form of STAT3 following overexpression of heat shock protein 72 (HSP72) impaired collagen production and fibroblast proliferation (Pan *et al.*, 2020). Further to this, it has been shown that PRP can increase the proliferation of tendon cells by modulating STAT3 (Yu *et al.*, 2015). The potential inhibition of this pathway by PRP-EVs requires further *in vitro* investigation, as this is converse to cited literature and would not be therapeutically favourable. IL20 was also predicted to be inhibited. IL20 has been described as proinflammatory (Chen, Caspi and Chong, 2018), and has been shown to increase the production of pro-inflammatory molecules, such as MMP's and TNF- $\alpha$  in *in vitro* models of other musculoskeletal conditions, namely arthritis (Kragstrup *et al.*, 2017; Chen, Caspi and Chong, 2018). Subsequently, the inhibition identified would be preferable from a therapeutic in the context of tendinous injury, by inhibiting the development of an inflammatory phenotype.

Through gene expression analysis it was identified that the universal cross species tendon marker IGFBP6 (Turlo *et al.*, 2019) was significantly downregulated following cytokine treatment which is characteristic of an impaired tendon phenotype (Dahlgren, Mohammed and Nixon, 2006). In addition, gene expression analysis revealed increased expression of MMPs following cytokine stimulation, though this was not significant possibly due the heterogeneity of primary cells and low samples size. MMP increase is characteristic of tendon injury *in vivo* with MMPs often considered deleterious in the healing process of tendon (Del Buono *et al.*, 2013). It is postulated to be a factor predisposing a horse to tendon tears as MMPs are involved in the digestion of primary load bearing collagen fibres found in tendon (Davis *et al.*, 2013).

Predicted upstream regulators after comparing control to cytokine stimulated tenocytes included TNF activation and IL4 inhibition. TNF is a key proinflammatory cytokine associated with the acute inflammatory cascade following tendon injury, and is released in order to initiate cellular excavation and degradation, and subsequently responsible for the overt clinical signs of injury, including heat, inflammation and pain (Ellis, Schnabel and Berglund, 2022). A recent review by Morita *et al* found that

IL-1 $\beta$ , IL6, IL10 and TNF- $\alpha$  were most frequently investigated in human tendon tissues and animal models of tendon injury (Morita *et al.*, 2017). Specifically, TNF is associated with catabolic and anabolic effects, and is produced by damaged tenocytes and activates NF- $\kappa$ B signalling pathways resulting in the synthesis of molecules such as prostaglandin E2 and inducible nitric oxide synthase (Ellis, Schnabel and Berglund, 2022). Hence, the proteomic profile of cytokine stimulated tenocytes demonstrates the induction of an inflammatory phenotype, validating the *in vitro* experimental condition, and reflective of the naturally occurring phenotype. IL4 was also predicted to be inhibited, and is known to be a prototypic immunomodulatory t-helper cytokine, known for its profibrotic effects. It promotes proliferation of human primary tenocytes (Courneya *et al.*, 2010) and has been shown that mechanical stimulation improves of rotator cuff tendon bone healing via the activation of IL4/JAK/STAT signalling pathway, promoting macrophage polarisation to the M2 subtype (Y. Liu *et al.*, 2022). The subsequent predicted inhibition of this cytokine reflects impaired tendon homeostasis, a hallmark of injury and impaired function.

A global proteome shift was observed following multiple factor PCA in response to cytokine stimulation. Further analysis subsequently elucidated potential proteomic drivers of this variation. A total of 18 proteins were significant with respect to both cytokine stimulation and treatment (no treatment, PRP treatment and PRP-EV treatment). One of these proteins, sequestosome 1 is a protein that acts as a cargo receptor and is involved in the degradation of ubiquitinated proteins from both autophagic and proteasomal pathways (Philippe, 2020). In addition, sequestosome 1 is a regulator of NF $\kappa$ B signalling (Ratti and Berry, 2016). NF $\kappa$ B signalling is of primary importance to processes such as inflammation, cellular stress response and cellular survival (Rea *et al.*, 2013), and is a family of proteins that are known transcription factors, that are stimulated by pro-inflammatory cytokines, chemokines, stress-related factors and ECM degradation products. Upon stimulation NF $\kappa$ B molecules often trigger the expression of genes associated with tissue destruction (Rigoglou and Papavassiliou, 2013). Specifically, upon inflammatory stimulation the recruitment of I $\kappa$ B kinase complexes occurs, resulting in the phosphorylation of I $\kappa$ B and NF $\kappa$ B dimers translocate to the nucleus and stimulate transcription (Abraham *et al.*, 2019). Previous studies have implicated NF $\kappa$ B pathway signalling in tendinopathy. In murine tendon fibroblasts with cre-mediated overexpression of I $\kappa$ B, there was increased degeneration of mouse rotator cuff tendons which corresponded to increased levels of proinflammatory cytokines and innate immune cells within the joint (Abraham *et al.*, 2019). It has

been postulated that targeting of the NFkB pathway may serve as a prospective therapeutic approach in tendon disorders, and subsequent expression of sequestosome 1 would serve as a marker of this. Our study demonstrated that cytokine stimulation increases sequestosome 1 expression and that PRP does not significantly change its protein expression. However, PRP-EVs did, compared to no treatment, by further increasing the expression of sequestosome 1. Thus, the EV component of PRP may in fact elicit a localised inflammatory response, whereas other biological factors in PRP may prevent as great an effect from occurring.

Collagen type 1 alpha 1 was also observed as differentially abundant across experimental groups. Collagen type 1 alpha 1 is a component of type 1 collagen. Type 1 collagen is the most abundant protein in mammals and is the predominant collagen found in tendon (Salvatore *et al.*, 2020). Type 1 collagen expression has previously been found to decrease during the healing process following tendon injury, as type 3 collagen expression increases during early phases forming a randomly-orientated network around the site of injury (Voleti, Buckley and Soslowsky, 2012; Buckley *et al.*, 2013). Over time some of the granulated tissue is replaced with type 1 collagen. Subsequently type 3 collagen is associated with scar tissue following injury. In addition, an increase in the type 3/ type 1 collagen ratio has also been observed with age (Smith *et al.*, 1999) and pathology (Gonçalves-Neto *et al.*, 2002; Li *et al.*, 2023). Upon cytokine stimulation in this study tenocyte expression of collagen 1 alpha 1 decreased. PRP treatment did not significantly change collagen type 1 alpha 1 abundance compared to the non-treatment group, with collagen 1 alpha 1 having a significantly decreased expression in the cytokine stimulation group compared to control, irrespective of treatment. This is suggestive of PRP's inability to act on collagen metabolism. However, PRP-EV treatment of cytokine stimulated tenocytes was found to cause differential expression of collagen type 1 alpha 1 when compared with untreated groups, and no significant difference was observed between control and cytokine stimulation following PRP-EV treatment. Potentially PRP-EVs can alter collagen production to return to baseline, and components of PRP, namely platelets and plasma may contain biological agents that reduce this effect. Hence in order to determine this relationship further mechanistic studies are required to ascertain if PRP contains inhibitory biological agents as this will have implications on therapeutic efficacy.

Heme oxygenase demonstrated increased abundance following cytokine stimulation versus control. However, following PRP and PRP-EV treatment no significant difference was observed. Heme oxygenase is an enzyme involved in the degradation of endogenous iron protoporphyrin heme. It has

been attributed to reduction and oxidation homeostasis, and can decrease cellular oxidative damage (Consoli *et al.*, 2021). This is due to the heme-derived reaction products such as bilirubin, subsequently contributing to cytoprotection via antioxidant and immunomodulatory effects (Ryter, 2022). Its regulation in the case of tendon inflammation is important in reducing the effect of oxidative stress on injury.

AHNAK nucleoprotein abundance was not affected by cytokine stimulation compared to control. However, following PRP treatment its abundance was increased in the cytokine stimulated group. This was not conserved following PRP-EV treatment. AHNAK nucleoprotein is a scaffold protein characterised by its large size of 700kDa (Davis, Loos and Engelbrecht, 2014). The exact molecular function of AHNAK nucleoprotein is still being determined, but it is associated with cellular migration and is regarded as integral to muscle membrane repair (Zhu *et al.*, 2022). PRP treatment seems to change the expression of this protein significantly following cytokine stimulation but further work is required in the future to elucidate why this is.

There were inherent constraints associated within this study. Firstly, the low power of the study. As a result p values were used when analysing MS proteomic data from the *in vitro* experiment. This is however common practice in proteomic studies as multiple testing correction methods can fail to identify statistically significant values due to too stringent threshold in the case of underpowered studies (Pascovici *et al.*, 2016). Future studies should look to use a larger equine cohort. Moreover, the use of monolayer culture can alter the physiological outcomes observed in tendon injury-based studies, as they do not account for the three-dimensional environment tenocytes are situated within and their role in responding to external stimuli and biomechanical forces (Chien *et al.*, 2018; Atkinson *et al.*, 2020). Tenocytes in monolayer culture can be unstable phenotypically and dedifferentiate (Schulze-Tanzil *et al.*, 2004). Future studies may look to explore the use of bioengineering approaches such as musculoskeletal tissue on a chip technologies (Petta *et al.*, 2022). In addition, there were variables that could not be accounted for within this study that may affect reported outcomes, such as donor variation in EV uptake and response to PRP. Future studies could look to use bioluminescent (gaussian luciferase) or fluorescent (Cy5.5 or pHluorin) labelling approaches for imaging in order to visualise cellular uptake of EVs (Q. Liu *et al.*, 2022). In addition future studies could use stable isotope labelling by amino acids in cell culture approaches in order to label EV based proteins and quantify those proteins delivered to recipient cells (Kehrloesser *et al.*, 2023). Furthermore, this study was

unable to explore the effect of donor age, or how the duration of cytokine treatment and PRP or PRP-EV treatment exposure may affect the cellular phenotype on a transcriptional and proteomic level. Future studies may look to explore this, in particular to determine the optimum length of biological treatment exposure. Finally, allogenic PRP and subsequent PRP-EV treatment was used rather than the traditional autologous PRP product utilised in clinical practice, which may have elicited more of a cellular immune response compared to tendon cell culture where no white blood cells were present. However, it has been found that in cases where autologous PRP is not appropriate it can be used clinically, and reviews of a variety of studies have found it to be a safe alternative, though still highlighting issue surrounding efficacy (Akbarzadeh *et al.*, 2021).

## **8.5 Conclusion**

This *in vitro* pilot study exploring the effect of PRP and PRP-EVs in an equine tendon inflammatory model identified potential molecular mechanisms mediating the therapeutic effect observed *in vivo* upon clinical cases of tendon injury that require further investigation and validation, namely roles in collagen metabolism and NF- $\kappa$ B signalling in association with inflammation. Evidence was provided that PRP-EVs do elicit an effect on stimulated tenocytes and thus may be more significantly involved in the mediation of the therapeutic product, and at a minimum should be examined further when standardising PRP products. Ultimately considering the potential of an EV based product that can be available 'off the shelf' as a therapeutic in its own right, that could be used in both human and veterinary clinical settings.

## **8.6 Ethics**

Ethical approval was obtained from the University of Liverpool Veterinary Research Ethics Committee. Tenocyte samples from both our equine musculoskeletal biobank (VREC561) and clinical donors from the Philip Leverhulme equine hospital were used within this study (VREC561). Venous whole blood was collected from an abattoir (VREC561).

## **8.7 Funding**

E.C. is a self-funded PhD student from the University of Liverpool, but has previously secured funding from EUCost initiative (ExRNA path) cost action CA20110 and horserace betting levy board. M.P. and E.C. were also supported by the Medical Research Council (MRC) and Versus Arthritis as part of the



MRC Versus Arthritis Centre for Integrated Research into Musculoskeletal Aging (CIMA). A.T is supported by Horserace Betting Levy Board Equine Post-Doctoral Fellowship VET/2020-2 EPDF 8. This work was supported by the Horserace Levy Board and the Racing foundation small grant award scheme, project code SPj54.

## 9. General Discussion

Equine musculoskeletal diseases are a prevalent welfare and health concern within the equine athletic population (van Weeren and Back, 2016b; Mocchi *et al.*, 2020). There is a distinct lack of effective diagnostic tests to identify conditions such as osteoarthritis (OA) at early pathological stages to improve patient prognosis and management. In addition, treatment modalities available for OA and tendon injury are unable to reverse disease pathogenesis, and present with a range of limitations, effecting clinical outcomes (Brossi *et al.*, 2015; Devireddy *et al.*, 2017a; Barry, 2019; Wijekoon and de Silva, 2021). Thus, it is important to improve disease pathology understanding to facilitate the identification of biomarkers and determine the mechanisms and mediators of common regenerative therapeutics, namely mesenchymal stem cell therapy (MSC) and platelet-rich plasma (PRP) therapy.

Extracellular vesicles (EVs) are a promising avenue of research for both biomarker discovery and 'cell free' biological therapeutic alternatives (Tao, Guo and Zhang, 2017; Qiu *et al.*, 2019; Boulestreau *et al.*, 2020b; Mortati *et al.*, 2020; Wang *et al.*, 2020; Herrmann *et al.*, 2021b; Racchetti and Meldolesi, 2021a; Spakova, Janockova and Rosocha, 2021; Wu, Piao, *et al.*, 2021). A range of techniques and technologies have been employed to ascertain the biologically active cargo reflective of disease or therapeutic capacity. Techniques highlighted within this thesis include high throughput omics-based technologies, such as: Mass Spectrometry Proteomics and Lipidomics as well as Optical Photothermal Infrared Spectroscopy and Raman spectroscopy (Mallawaarachy *et al.*, 2017; Chen, Datta-Chaudhuri, *et al.*, 2019; Gatien *et al.*, 2019; Gualerzi, Picciolini, *et al.*, 2019; Almiñana *et al.*, 2021). This thesis has identified potential biomarkers of naturally occurring OA in equine plasma EVs using spectroscopic approaches, and synovial fluid EVs (SF-EVs) using both mass spectrometry proteomics and lipidomics, compared to clinically defined 'healthy' equine patients. In addition, temporal EV protein changes were identified following intraarticular treatment with integrin  $\alpha 10\beta 1$ -selected MSCs in a carpal osteochondral fragment model of equine osteoarthritis. This study resulted in the identification of potential molecular mechanisms of MSC therapy, elucidating the role of EVs in the mediation of the therapeutic. Finally, the proteomic composition of PRP and PRP-EVs was characterised, and the effect on an *in vitro* model of equine tendon inflammation determined. The main findings of these studies have been illustrated in Figure 9.1.

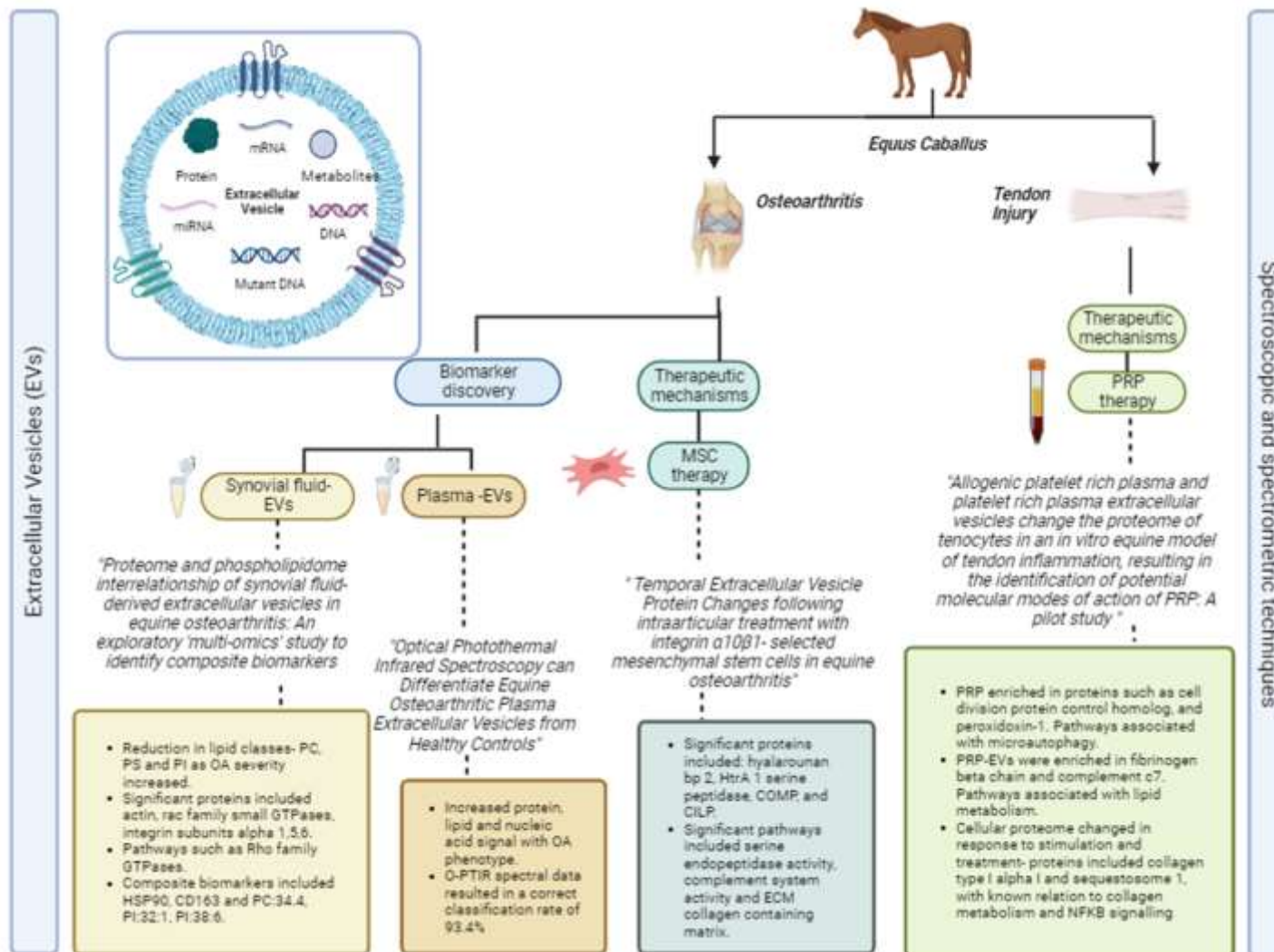


Figure 9.1. An overview of this PhD thesis. The primary research themes, and subsequent main findings across all results chapters.

### 9.1 Extracellular Vesicle Mediation of Mesenchymal Stem Cell Therapy in an Equine In Vivo Experimental Model of Osteoarthritis

The global temporal EV proteome following surgical induction of an equine OA phenotype and MSC therapeutic intervention was quantified for the first time. Adipose tissue derived  $\alpha$ 10-MSCs were injected intraarticularly into 6 horses 18 days post experimental OA induction. SF was collected via aseptic arthrocentesis. EVs were isolated using dUC, and characterised using nanoparticle tracking analysis and the Exoview Human Tetraspanin Assay and data independent acquisition (DIA) proteomics undertaken on the SF-EVs. The study quantified 442 proteins, and 48 proteins were differentially expressed ( $q < 0.05$ ) across all samples. Differentially abundant proteins were associated with serine endopeptidase activity, complement activation and collagen containing extracellular matrix (ECM). We provided tentative evidence of EVs mediating MSC therapy and a rationale for exploring the concept of a 'cell free' EV therapy.

Recent studies have demonstrated the restorative potential of EVs potential in equine joint diseases. A study by Kim *et al* (Kim *et al.*, 2020) used equine foetal bone marrow-derived cells (BMC)-derived nanoparticles (BMC-NPs) to determine if they could stimulate the survival of equine chondrocytes undergoing inflammatory cell death *in vitro*. Functionally, BMC-NPs promoted the growth of chondrocytes and reduced apoptosis induced by inflammatory cytokines (Kim *et al.*, 2020). Similarly, the effect of human MSC-EVs were examined *in vitro* in a bovine inflammatory model of OA. EV supplementation resulted in increased glycosaminoglycans (GAG) retention, and upregulation of the chondrogenic marker proteoglycan- 4 (PRG-4), however varying EV preparation resulted in inflammatory phenotype heterogeneity (Ossendorff *et al.*, 2023). Currently there are a number of MSC-EV based *in vitro* studies exploring their capacity to induce therapeutically favourable outcomes in models of OA (Vonk *et al.*, 2018; Capomaccio *et al.*, 2019; van Balkom *et al.*, 2019; Navarrete *et al.*, 2020; Arévalo-Turrubiarte *et al.*, 2021; Hotham *et al.*, 2021; Ai *et al.*, 2022). However, there is a distinct lack of suitable models to encapsulate the effect of a more dynamic *in vivo* environment, prior to clinical trials exploring the therapeutic use of EVs in orthopaedic conditions, and this requires redress.

We identified the pathway for serine endopeptidase activity was downregulated following MSC treatment, and this was hypothesised to be a potential molecular mechanism of MSC therapeutic intervention, as is observed that serine endopeptidase activity is increased in OA pathogenesis. This is further evidenced by a recent study using a bioinformatic approach in rheumatoid arthritis (RA) and OA, mapping a number of pathways including serine endopeptidase activity (Zhang *et al.*, 2021).

Serine endopeptidase activity is regarded as a component of inflammatory complement system activation. The complement system has been implicated in the pathogenesis of OA, and is associated with inflammation and proteolytic degradation (Schäfer and Grässel, 2022). *In vitro* studies utilised human osteochondral biopsies from OA patients to isolate chondrocytes and synoviocytes, cartilage and synovial tissues. These were cultured with or without interleukin 1 $\beta$  (IL-1 $\beta$ ) and it was identified that locally produced complement factors were activated indicative of innate immunity involvement in OA (Assirelli *et al.*, 2020). Proteomic and transcriptomic analysis of SF and synovial membranes from a human clinical cohort of OA patients were found to have significantly increased expression of complement components (Wang *et al.*, 2011). Furthermore *in vivo* investigation in mice deficient in complement component 5 (C5), C6 or the complement regulatory protein CD59a, found decreased expression of inflammatory and degradative molecules from C5 deficient mice (Wang *et al.*, 2011).

Thus, MSC therapeutic intervention and subsequent EVs appear to reduce the activation of this pathway in OA. Hence targeting the complement system and serine endopeptidases may serve as a potential OA therapeutic. In addition, EVs may serve as a treatment modality with significantly lower risk than that of anti-complement system drugs. For instance the use of anti-complement system drugs such as eculizumab in humans, may lead to an increased risk of infection, affecting cellular regeneration and metabolism, along with suppressing clearance of immune complexes (Schäfer and Grässel, 2022). Further work is required to determine how MSC-EVs specifically act on complement components, and techniques such as gel zymography and proteinase activity assays could be used in conjunction with *in vitro* experiments in order to explore the biological response of these pathways in a targeted manner.

## 9.2 Equine Plasma Extracellular Vesicle Biomarkers of Naturally Occurring Osteoarthritis

This thesis used novel spectroscopic approaches to probe the biological cargo of equine plasma-derived EVs from horses with OA as diagnosed at clinical examination, and for the first time demonstrated that infrared (IR) based spectroscopy techniques can be used to successfully interrogate and differentiate equine plasma-derived EVs in control and OA samples. Samples were sourced from the Hong Kong Jockey Club (HKJC). This population had the advantage that it was fairly homogenous; all Thoroughbred race horses were subjected to the same diets and training regimes. The aim of this specific study was to investigate the feasibility of spectroscopic techniques; Raman and

optical photothermal infrared spectroscopy (O-PTIR) spectroscopy to detect cargo changes in EVs as a result of OA pathology as potential disease biomarkers. EVs were isolated following differential ultracentrifugation (dUC) and characterised using nanoparticle tracking analysis (NTA), transmission electron microscopy (TEM) and the Human Exoview Tetraspanin Assay before analysis with the specific spectroscopic techniques.

Following computational classification modelling, cargo differences from O-PTIR infrared spectroscopy, distinguished between healthy and disease phenotypes, with a 93.4% classification rate. Inspection of the spectra identified enriched spectroscopic signal reflective of increased protein, lipid and nucleic acid abundance within the cargo of plasma EVs from OA horses. Previous studies utilising infrared spectroscopy techniques, such as near infrared (NIR) spectroscopy, have been able to resolve the composition of connective tissues, providing depth of analysis with respect to biomolecular, structural and functional properties allowing for the differentiation of ligament types (Afara *et al.*, 2021). These techniques have also been used to assess molecular markers of pain in human OA (Pollonini *et al.*, 2020). Further studies in humans have quantified the feasibility of NIR spectroscopy to diagnose OA in SF, characterised according to severity following the Kellgren and Lawrence classification criteria. Aquaphotomics was used and identified hydrogen bonds associated with different water species and this was correlated with OA occurrence and development (Zeng *et al.*, 2023). Therefore, IR based techniques can be used to detecting OA changes across a range of biofluids and tissues. During this current study Raman spectroscopy was not able to accurately differentiate healthy from disease, with a classification rate of 64.3%. However, previous human studies have probed hip cartilage with such spectroscopic technique with more favourable outcomes when using a different sample source. Decreased PG and GAG content with increasing OA severity was identified, and thus the capacity for Raman spectroscopy to serve as a complementary diagnostic tool for OA (Casal-Beiroa *et al.*, 2021).

In the horse IR based serum biomarker profiling has also been used to differentiate the early inflammatory phase of a traumatically induced longitudinal model of equine carpal OA. It was identified following classification models that OA compared to sham control had a classification rate of 52.7%, whereas comparing groups with respect to day had a 94% correct classification rate (Panizzi *et al.*, 2022). This finding is converse to the findings in our study as O-PTIR had the capacity to differentiate healthy from diseased plasma EVs with a classification rate of 93.4%, however the authors note the effect exercise may have on this model, and the effect of phenotype severity and study duration. In dogs, SF has also been probed exploring the composition in association with

naturally occurring OA following cranial cruciate ligament rupture. Similar to our findings IR based screening had a sensitivity, specificity and overall accuracy of 97.6%, 99.7% and 98.6%, respectively, following the implementation of predictive models (Malek *et al.*, 2020). This highlights its potential to be used in a diagnostic and clinical capacity.

Further studies are required to identify if IR based techniques can reproducibly identify compositional changes across biofluids, and biofluid-derived EVs to validate its use in a clinical setting. In addition, sample and technique optimisation must be conducted before clinical translation.

### *9.3 Equine Synovial Fluid-derived Extracellular Vesicle Proteomic and Phospholipidomic Biomarkers of Naturally Occurring Osteoarthritis*

This exploratory study examined the cargo of SF-EVs from horses with clinically diagnosed OA of varying severity (n=13; healthy = 7, moderate OA =4, and severe OA=3). We probed the EVs, integrating proteomic and phospholipidomic datasets following mass spectrometry analysis. Samples were isolated using dUC in conjunction with a sucrose density gradient, and characterised using Paul Karl Horan (PKH) staining and flow cytometry. We identified no change in EV concentration between disease states. Lipid abundance significantly varied between disease severity, and proteins that correlated with lipids were attributed to a range of molecular functions, including rho family GTPases activity, liver x receptor/ retinoid x receptor (LXR/RXR) dysregulation, along with complement system activation and clathrin mediated endocytosis.

The literature related to clathrin mediated endocytosis has shown it is related to the internalisation of EV cargo in order for a cellular response to be elicited. EV uptake cellular mechanisms have previously been explored in HeLa cells, identifying clathrin mediated endocytosis and micropinocytosis as playing a critical role in EV cargo transfer into cells (Costa Verdera *et al.*, 2017). This has been demonstrated across a range of pathologies and cell types such as cardiomyocytes (Eguchi *et al.*, 2019) and primary endothelial cells (Cronqvist *et al.*, 2020). Furthermore, Rho family GTPases were found to be activated. In an equine cartilage explant model rho family GTPases were upregulated with OA pathology, particularly in chondrocytes (Beier and Loeser, 2010), and involved in vesicle trafficking (Anderson, Phelan, Foddy, *et al.*, 2020b), as identified in our study. In addition, CDC42, a member Rho family GTPases critical to cartilage development, has been explored in a mouse OA model, due to it being highly expressed in cartilage and subchondral bone (Hu *et al.*, 2018). Its genetic disruption has

highlighted its importance in cartilage degeneration and subchondral bone deterioration in OA (Hu *et al.*, 2018). Studies interrogating the role of RAC1 (rac Family Small GTPase 1) ( a member of the Rho family GTPases, and mapped to such pathways in this study) in *in vitro* models of OA and *in vivo* models have also validated the pivotal significance of RAC1 in OA, identifying that upon RAC1 activation, increased expression of matrix metalloproteinase 13 (MMP13), a disintegrin and metalloproteinase with thrombospondin motifs – 5 (ADAMTS-5) and collagen type 10 (COLX) occurs in chondrocytes (Zhu, Lu, *et al.*, 2015).

The phospholipidome was also assessed in this study. There is a lack of animal-based EV studies probing the lipidome as OA biomarkers. However, other biofluids have been probed, including SF. A canine groove model of OA was used to study the SF lipidome in dogs, compared to human patients with early OA. In canines most lipid species were elevated in OA SF, with profiles reflecting early human OA (Kosinska *et al.*, 2016). However some variation between species was evident for phosphatidylcholine and sphingomyelin (Kosinska *et al.*, 2016). This study was also able to differentiate OA from healthy patients based on lipidomic variation, including phosphatidylcholine and sphingomyelin. It would be of interest to compare the equine lipidome to both human and canine, in order to extrapolate if the variation in lipid species expression is species specific in relation to OA. Human SF has also been profiled in a targeted manner from patients with varying OA grades, to provide deep phenotyping of OA. OA patients had higher levels of phosphatidylcholines, phosphatidylserines and phosphatidylinositols, and these could distinguish between two OA endotypes (Rocha *et al.*, 2021). Phosphatidylcholines and phosphatidylinositols were also differentially abundant in this study, however a decrease in their abundance was observed with OA.

Further studies have used lipidomics as a tool for OA biomarker discovery, identifying an altered lipid metabolism associated with OA and the release of arachidonic acid from phospholipids (Castro-Perez *et al.*, 2010). Further studies may look to utilise and explore other biological system levels (Gézi *et al.*, 2019; Subramanian *et al.*, 2020b; Guan *et al.*, 2021) such as the transcriptome or other aspects of the metabolome in order to encapsulate the dynamic *in vivo* system and interactions in order to provide further understanding surrounding the pathogenesis of OA.

#### *9.4 The Effect of Platelet-rich Plasma and Platelet-rich Plasma derived Extracellular Vesicles on Cytokine Stimulated Equine Tenocytes*



A study to profile Platelet-rich plasma (PRP) and Platelet-rich plasma derived extracellular vesicles (PRP-EV) proteomic composition, and explore their effect *in vitro* on a model of equine tendon inflammation was performed. PRP was produced and EVs isolated following dUC. PRP and PRP-EVs were characterised and then analysed using data dependent acquisition (DDA) mass spectrometry proteomics. PRP and PRP-EVs were enriched in proteins involved in cellular waste disposal and the inhibition of lipid metabolism respectively. Upon equine tenocyte treatment with PRP or PRP-EVs following cytokine stimulation it was found that differential proteins included collagen type 1 alpha 1 and sequestosome 1. Proteins known to have effects in relation to collagen metabolism and nuclear factor kappa B (NF- $\kappa$ B) signalling at the pathway, respectively.

Previous studies have explored the molecular mechanisms of PRP *in vitro* with a 'disease in a dish' model, using rabbit tendon stem progenitor cells. PRP releasate (PRP following platelet activation using calcium chloride) had the capacity to prevent tenogenic differentiation, and promote calcium deposition and proteoglycan (PG) accumulation suggestive of PRP's inability to reverse late stage tendinopathies (Zhang and Wang, 2014). This study did not identify proteins associated with proliferation, instead PRP and PRP-EVs were found to act on inflammatory components. In a further study, the effect of PRP *in vivo* in a rabbit model of tendon injury was determined. The effect of PRP on inflammatory, proliferative and remodelling phases of tendon injury was identified. The administration of PRP reduced the inflammatory phase and promoted tendon healing during the proliferative phase, evidenced by an increase in collagen 1 deposition, indicative of tendon maturation following treatment (Takamura *et al.*, 2017). Similar results were observed in an Achilles tendon rat tear model, whereby tendon remodelling was improved following PRP treatment in the short term (Parafioriti *et al.*, 2011). However, it was found as the study duration increased, no significant difference was found between PRP treated and non-treated groups, with respect to immunostaining or gene expression analysis (Parafioriti *et al.*, 2011).

During this study stimulated equine tenocytes were also treated with PRP-EVs, a heterogenous population of EVs that were most likely derived from platelets. As platelets are known to be the most significant source of EVs found in serum in humans, however it should be noted, that a limited number of EVs come from white blood cells (Brisson *et al.*, 2017; Tao, Guo and Zhang, 2017). The influence of platelet-derived EVs has been evaluated previously in a 3D human *in vitro* model of tendon injury, and it was found that EV treatment increased the expression of tenogenic markers, promoted a healthy ECM, and the synthesis of anti-inflammatory mediators (Graça *et al.*, 2022). This does not concur with

findings from our study, whereby PRP-EVs were enriched in proteins inhibiting lipid metabolism, subsequently reducing the activation of anti-inflammatory pathways, which requires further exploration and understanding. Moreover, platelet-derived EVs have been explored with respect to tenogenic differentiation. It was identified that platelet-derived EVs enhanced differentiation, reduced phenotypic drift, and improved the deposition of a tendon-like ECM (Graça *et al.*, 2023). Further work may look to elucidate the role of PRP-EVs in a larger cohort, while also applying the use of a more biologically appropriate *in vitro* model, that incorporate biomechanical stressors, and ECM components.

## 9.5 Further Work

### 9.5.1 Extracellular Vesicle Imaging and Tracking

Throughout this thesis a multi-omic approach has been used to characterise the cargo of EVs from various biological sources, and to quantify the cellular response to treatment. The thesis has primarily taken an exploratory approach to EV cargo biology, and further work should look to use more functional and mechanistic based techniques to understand EV interactions and validate hypotheses drawn from this thesis. One such approach that could be used in future studies would be EV imaging and tracking. This can be done in a variety of ways using radioactive, bioluminescent or fluorescent labelling systems in conjunction with flow cytometry or microscopy, in order to answer questions surrounding targeted cellular interaction, biodistribution, uptake and EV release (Verweij *et al.*, 2021). The most prominent form of EV labelling currently utilises luciferase enzymes tethered to cluster of differentiation 63 (CD63) (Gupta *et al.*, 2020). Studies have utilised imaging flow cytometry with small EVs labelled with CD63eGFP in order to develop reproducible protocols that can be used to assess EV heterogeneity (Görgens *et al.*, 2019), and the identification of *in vivo* biodistribution pattern variance based on EV subpopulations and route of injection (Gupta *et al.*, 2020).

Studies with respect to other pathologies exploring the labelling of MSC derived EVs have used aggregation – induced – emission luminogens, such as an aggregation-induced emission luminogen (AIEgen) DPA-SCP, to track EV movement in real time. These studies did not affect MSC-EV characteristics, had low toxicity, and had superior labelling efficiency when compared to commercial EV trackers such as PKH and 1,1'-dioctadecyl-3,3,3',3'-tetramethylindotricarbocyanine iodide (DiR) (Cao *et al.*, 2019). The methods identified that MSC-EVs had the capacity to reduce inflammatory cell infiltration and enhance antiapoptotic effects in a model of acute liver injury (Cao *et al.*, 2019). A further study evaluated the effect of five different optical or nuclear tracers often used to track EVs:

noncovalent fluorescent dye DiR, or covalent modification with indium-DTPA, or bioengineered with fluorescent (mCherry) or bioluminescent (Firefly and NanoLuc luciferase) proteins fused to the EV marker, CD63 (Lázaro-Ibáñez *et al.*, 2021). NanoLuc fused to CD63 altered EV biodistribution, which was suggestive of genetic modifications that may compromise physiology. Subsequently it was found that that radioactive tracing approaches offer more accurate tracking, and do not alter EV biodistribution in the way the former has been found to (Lázaro-Ibáñez *et al.*, 2021).

In the context of MSC-EVs and musculoskeletal disease, studies have utilised labelling techniques to track the effect of MSC-EVs in *in vitro* models of OA (such as IL-1 $\beta$  stimulation of chondrocytes). PKH26 labelled MSC-EVs promoted proliferation and reduced apoptosis in OA chondrocytes (Li *et al.*, 2020). Furthermore, strategies have been developed to improve the biodistribution of EVs in cartilage, due to the steric and electrostatic properties of the cartilage ECM presenting a challenge. Thus the surface charge of MSC-EVs was reversed with a novel cationic amphiphilic macromolecule namely  $\epsilon$ -polylysine-polyethylene-distearyl phosphatidylethanolamine (PPD) (Feng *et al.*, 2021). A fluorescent label was used in the form of DiO staining. It was found that EVs had improved cellular uptake and homeostasis modulation following PPD-EVs use (Feng *et al.*, 2021). This has also been shown with the evaluation of fluorescently labelled adipose derived MSC-EV kinetics in chondrocyte micromasses and cartilage explants from OA patients (Mortati *et al.*, 2020), utilising time-lapse quantitative microscopy techniques. The biodistribution varied between models, with micromasses displaying a more homogenous diffusion of EVs (Mortati *et al.*, 2020).

Future studies following the work from this thesis may look to use such labelling approaches to determine MSC-EV interaction *in vitro* in models of both tendon injury and OA. Exploring factors such as biodistribution, MSC-EV half-life and subsequent cellular response to varying doses would be informative. In addition, disease-associated EVs could be tracked to determine cellular localisation, or homing of EVs from similar cell sources, in order to understand disease pathology.

### 9.5.2 Development of Suitable *In Vitro* and *In Vivo* Models

During my work, both *in vivo* and *in vitro* models have been utilised in order to explore EVs in the context of disease pathogenesis and therapeutics. Within this body of work *in vitro* monolayer models were used in order to replicate tendon inflammation as associated with tendon injury. The suitability and appropriateness of *in vitro* models should be evaluated prior to experimental use in order to select

the most optimum model to answer a given research question. It has become paramount that novel models are developed in order to encapsulate both whole body physiology and functionality (Bersini *et al.*, 2016).

To address this, reductionist *ex vivo* models have become increasingly popular in order to study the behaviour of complex biological systems, providing the ability to control experimental conditions such as tissue specific response to stimuli and preserving the three-dimensional microenvironment (Szczesny, 2020). It has also been postulated that such reductionist approaches should be part of a stepwise strategy, utilising *in vitro*, *ex vivo* and *in silico* modelling in order to minimise *in vivo* studies and reflect the natural disease phenotype more closely (Ribitsch, Oreff and Jenner, 2021b).

An emerging bioengineering approach has also been established in more recent years, developing micro physiological systems, often referred to as 'organ, tissue or joint on a chip' technology (Ajalik *et al.*, 2022). These model systems have been designed to replace the need for *in vivo* animal studies, by emulating three dimensional tissue organisation and micro environment cues (Ajalik *et al.*, 2022). The primary challenges to the use of this technology include: incorporating biological barriers, simulating joint compartments and heterogenous tissue interfaces, simulating immune interactions and inflammatory factors, and simulating effects of *in vivo* loading. Thus far they have been utilised for a range of purposes, including : human intestine (Bein *et al.*, 2018), human liver (Moradi, Jalili-Firoozinezhad and Solati-Hashjin, 2020), female reproductive tract (Young and Huh, 2021), and to model diseases such as cancer (Liu *et al.*, 2022). The technology has been used to explore joint functionality and disease pathology, incorporating mechanical stimulation systems that mimic articular movement, multi-joint tissue cultures that enable crosstalk, and systems that aim to capture aspects of OA inflammation by incorporating immune cells (Banh *et al.*, 2022). Studies have used this technology to develop bovine cartilage shear damage models to explore the impact of surface injury on chondrocytes and ECM. This study identified that shear-induced damage resulted in reduced chondrocyte viability and affected ECM integrity (Trevino *et al.*, 2017). As a result of these studies, a natural progression for the work conducted in this thesis would be to adopt this technology, and optimise it for the study of joint diseases and tendon injury, in order to investigate *in vitro* the mechanisms of biologic-derived EVs in the context of disease, and their cellular interaction in order to ascertain their capacity to act as 'cell free' therapeutics.

In addition to the use of *in vitro* models throughout this thesis, large animal *in vivo* experimental models were also used. Large animal models present with a number of advantages over small animal

models. Firstly, they are physiologically, anatomically and phylogenetically more similar to humans than smaller species (Hotham and Henson, 2020). In addition, they are regarded as 'outbred' rather than 'inbred' as small rodent populations are, as a result matching the heterogeneity observed in humans (Hotham and Henson, 2020). Thus, working with larger animal models results in a greater sample yield for experiments. The use of animals in research is often critically evaluated as welfare and experimental best practice and the highest of ethical standards should always be maintained. There is increasing scrutiny of animal based studies by the general public, funding agencies and regulatory authorities (Allen *et al.*, 2017). A recent review of papers based on animal models use in scientific research in Turkey highlighted that over 40% over a 9 year period were never published, equating to orthopaedic researchers euthanising nearly 10,000 animals (Öztürk and Ersan, 2020; Leopold, 2021).

Scientists must evaluate the use of *in vivo* large animal models that require the termination of life in order to answer a research question, considering a thorough and methodical approach, and adherence to Animal Research: Reporting of *In Vivo* Experiments (ARRIVE) guidelines (Percie du Sert *et al.*, 2020). It has been suggested that if an animals life is to be taken for research purposes, there should be significant confidence that the questions being answered are of substantial importance, and have the capacity to meaningfully improve animal and human health (Leopold, 2021). As a result there is a shift towards the utilisation of 3Rs approaches (reduction, refinement and replacement) with respect to the use of animals in research (Allen *et al.*, 2017). This highlights the importance of the development of *in vitro* models such as 'joint/organ on a chip models'. Alternatively, the use of large animal *in vivo* models without animal sacrifice are also feasible. For example, a study previously used the *in vivo* equine synovitis model to determine the side effects of intraarticular corticosteroids. Acute inflammation was initiated through the injection of 1µg of lipopolysaccharide (Partridge *et al.*, 2022). The acute inflammation resolved itself within 24 hours, and equine participants were minimally affected long term. This may offer a more ethical alternative than the use of the carpal osteochondral fragment model in horses, for example.

### 9.5.3 One Medicine Approach to Research

Within this body of work equine musculoskeletal conditions have been the primary focus, however the equine system can serve as a model of human disease (McIlwraith, Frisbie and Kawcak, 2012a). Often experimental findings are corroborated by a diverse range of literature from numerous species,

such as canine, murine, bovine and human studies. This highlights the importance of a holistic one medicine approach to research, that is translational and has significant impact. Veterinary medicine has always recognised the interrelationship between humans and animals.

A one medicine approach to research ultimately maintains principles and recognises the connection between the health of human and animals, and providing impactful knowledge in both human and veterinary medical fields with respect to diagnosis, treatment and prevention strategies (Webb, Spaas and Guest, 2022). For example, regenerative medicine research has provided the necessary stage for translational research to use such approach in order to benefit humans and animals alike. It is recognised that clinical trials in companion animals with naturally occurring disease can often inform human clinical trials and improve their design and outcomes (Arzi *et al.*, 2021), serving as an intermediary between preclinical and clinical trials. They also provide a source of tissue for research, the genetic basis of analogous disease, a source for clinically applicable functional outcome measures, and can provide the opportunity for piloting new technologies and therapeutics (Meeson *et al.*, 2019). Thus, this approach could be used in the future to determine if biological differences between EV cargo in association with disease pathology are conserved across species in order to identify universal EV based biomarkers of disease.

#### 9.5.4 *Biologic Study Reporting Standards*

Regenerative therapeutics used in the treatment of orthopaedic conditions often referred to as ‘orthobiologics’ (Rodeo, 2019) have gained momentum in recent years. However, their use in clinical practice often yield varied outcomes. To ensure their successful use it is paramount that study reporting standards are universal to enable appropriate comparisons and conclusions to be drawn. Often challenges arise from inconsistent reporting of protocols, therapeutic characterisation, delivery and source heterogeneity. A recent review of level I and II clinical studies utilising PRP injection across medical specialities highlighted that of the 132 studies identified in humans, musculoskeletal conditions (OA and tendinopathy) accounted for 74% of all studies (Nazaroff *et al.*, 2021). Across all studies only 33% characterised the PRP composition used and only 17% reported the leukocyte component of PRP (Nazaroff *et al.*, 2021). The use of PRP in human medicine has subsequently been subject to legislation surrounding its clinical use and relevant manufacturing standards that must be upheld. This emphasises the need for the development of robust technologies in order to guarantee high therapeutic quality while maintaining good manufacturing practices (GMP) (Sebbagh *et al.*, 2023).

The use of MSCs clinically are also under scrutiny (Voga *et al.*, 2020). This makes between study comparisons and efficacy difficult to determine. A recent position statement by Guest *et al* (Guest *et al.*, 2022) outlining the minimal criteria for reporting veterinary and animal medicine research for mesenchymal stem/stem cells in orthopaedic applications suggested that MSC studies should report : plastic adherence, tri lineage differentiation, a minimum of two positive (CD90, CD73, CD105, CD29, CD44) and two negative surface markers ( CD79 $\alpha$ / CD19, CD14/CD11b, CD34, CD45) and MHC II expression.

The licensing strategies used in human MSCs can affect MSC phenotype and by proxy secreted factors including EVs. Licensing refers to the stimulation or activation of MSCs, and can effect of immunomodulation, ECM remodelling, vascular development, bioactive factor production, and endogenous stem/progenitor cell support (Koch and Schnabel, 2023). There is an unmet need to identify the optimal form of licensing in order to develop reliable and repeatable ‘off the shelf’ treatments that can be used in human and veterinary patients. Hence it is necessary that basic science studies report the form of licensing used. These requirements are important when considering the translation of research to human medical practice.

It is paramount that future studies involving the use of EVs derived from biologics provide the required information surrounding the biologic source, in order to adhere to reporting standards and avoid issues surrounding reproducibility and comparability of studies in the future.

#### 9.5.5 Mesenchymal Stem Cell Based Therapeutics- Challenges and Future Direction

The therapeutic potential of MSCs have provided both human and veterinary medicine the capacity to develop new treatment modalities that have considerable clinical potential. This is particularly important for musculoskeletal conditions due to the ability of MSCs to differentiate into tissue of mesoderm origin (De Schauwer *et al.*, 2013). However, the exact mechanism of action and definitive effectiveness remains unknown (Kang and Park, 2020). Thus far standards and regulatory frameworks do not exist for the use of MSCs clinically in veterinary medicine (Ivanovska *et al.*, 2022). This has resulted in veterinary stakeholders adhering to guidelines set out for human medical use (Devireddy *et al.*, 2017b). However, this presents with challenges as human guidelines do not account for species specific cell surface receptor variability, and antibody cross reactivity (Devireddy *et al.*, 2017b). A review of MSC therapeutic use in the canine species identified significant areas that were cause for

clinical variability, including :tissue source, donor age, cellular banking and cell media formulations (Ivanovska *et al.*, 2022). In addition, for commercialisation of an MSC based product cellular formulations must undergo release tests (Ivanovska *et al.*, 2022).

Future work must explore antibody cross reactivity between veterinary species, such as equine and canine as it is common practice that antibodies are often not validated for use with such sample source. This has resulted in significant challenges with respect to MSC veterinary research, but also EV characterisation. In addition, following studies identifying the most potent MSC source for specific pathology treatment, work could look to establish immortalised MSC cell lines in order to move towards the development of a standardised allogenic therapeutic. Recently, a limited number of allogenic equine MSC products have been approved for commercial use and include: AdStem™ (StemcellIX, allogenic stem cell therapy for OA in animals), Arti-Cell FORTE™ (Boehringer Ingelheim, chondrogenic induced equine allogenic peripheral blood derived mesenchymal stem cells, for the treatment of mild to moderate lameness linked to joint inflammation in horses) and RenuTend™ (Boehringer Ingelheim, tenogenic primed equine allogenic peripheral blood-derived mesenchymal stem cell, for the treatment of tendon and ligament injuries in horses).

#### 9.5.6 Adjuvant Therapeutics

Both MSC and PRP based therapeutics can be used in the treatment of OA and tendon injury in both horses and humans. A previous survey evaluated the use of MSCs, PRP, autologous conditioned serum (ACS), and autologous protein solution (APS) in horses. Of the 154 responses PRP accounted for 87.5% of responses with respect to the treatment of MSC conditions (Knott *et al.*, 2022), and PRP along with MSCs was most commonly utilised intralesionally for soft tissue injuries (Knott *et al.*, 2022). They have also been used as adjuvant therapies to primary treatment with evidence suggesting they can enhance the therapeutic effect observed upon treatment.

This was evidenced by numerous studies, for example 24 beagles were used as cranial cruciate ligament transection models of OA and subjected to the intra-articular injection of either phosphate-buffered saline (PBS), PRP, MSCs, and the MSC and PRP co-treatment (Yun, Ku and Kwon, 2016). It was identified that the combination of MSCs and PRP improved an OA phenotype by stimulating ECM synthesis, chondrocyte proliferation and inhibiting inflammatory activity, working in a synergistic manner (Yun, Ku and Kwon, 2016). This has also been reported in horses with tendonitis. MSCs derived from adipose tissue were expanded in the presence of autologous platelet lysate and subsequently



injected into the damaged tendon after being dispersed in activated PRP (Del Bue *et al.*, 2008). Of the 16 horses enrolled on the study 14 were able to return to normal activity and exhibited a functional recovery (Del Bue *et al.*, 2008).

Thus, it would be prudent to explore the effect of EVs from both PRP and MSCs in an adjuvant capacity *in vitro* to determine if previous findings are conserved. This could result in the possibility of an EV-based therapeutic with enhanced efficacy, compared to an EV therapeutic derived from one source.

## 9.6 Future Challenges

### 9.6.1 Extracellular Vesicle Standardisation

Interest in EVs has grown exponentially in recent years due to the accumulating evidence of their role in disease progression and therapeutic action (Erdbrügger and Lannigan, 2016). However, there are prominent challenges associated with EVs, particularly in veterinary practice. These include their standardisation, characterisation and analysis (Ramirez *et al.*, 2018). In order to address these rising concerns, the International Society for Extracellular Vesicles (ISEV) produced the minimal information for studies of extracellular vesicles (“MISEV”). This highlights that studies involving EVs should report all protocols used for EV separation to aid in reproducibility. In addition, characterisation must include identification of at least three positive EV protein markers (including at least one: transmembrane protein and cytosolic protein), and at least one negative protein marker, as well as EV quantification. It was recommended that single vesicles are also characterised using electron or atomic force microscopy, and/or single particle analysers (Théry *et al.*, 2018). Its first iteration was in 2014, and was updated in 2018 after consultation with over 400 EV researchers internationally (Witwer *et al.*, 2021).

In addition to MISEV guidelines, ISEV has supported the development of a number of frameworks and initiatives in order to encourage transparent reporting of EV research. An example of this includes EV-TRACK, a knowledgebase that centralises EV biology and methodology, in order to promote authors, reviewers, funders, and journal editors to adhere to experimental guidelines (Van Deun *et al.*, 2017a). EV-Track produces a metric that can be cited in peer reviewed publications, to reflect transparency of reporting experimental parameters (Van Deun *et al.*, 2017b). Further strategies developed in order to address the standardisation of EV research includes the minimal information about a flow cytometry

experiment in an EV specific reporting framework (MIFlowCyt-EV) (Welsh *et al.*, 2020). This framework provides guidance surrounding the reporting of EV detection parameters, measurement and experimental design. However it does not prescribe specific protocols in order to account for the rapid evolution of flow cytometry technology (Welsh *et al.*, 2020).

The issue of standardisation and characterisation requires consideration in the equine species, and the application of frameworks and guidelines to EV research in a veterinary context. Issues surrounding sample volume and technical challenges, such as the antibody cross reactivity previously discussed require addressing. This would enable veterinary research to make the same progress as its human counterparts. Further clarity surrounding nomenclature is necessary due to the ongoing discovery of EV subtypes, and investment from funding bodies is needed in order to further improve knowledge associated with EVs *in vivo* in transit, and the mechanisms used to deliver their cargo (van Niel *et al.*, 2022).

### 9.6.2 Clinical Translation of Extracellular Vesicles – Therapeutics and Diagnosis

EVs have been shown to hold significant promise with respect to diagnostics and therapeutics, courtesy of their endogenous characteristics. This has been evidenced by many studies, including that of Iyer *et al* (Iyer *et al.*, 2020), exploring the effect of PRP and MSC- EVs in a rat model of muscle injury. It found that EVs derived from PRP or MSCs could facilitate recovery by modulating inflammation, fibrosis, and myogenesis (Iyer *et al.*, 2020). However significant challenges need to be addressed in order to enable the clinical translation of EVs. These include scalability and standardization of generation, molecular characterization for design and regulation, therapeutic potency assessment, and targeted delivery (Gowen *et al.*, 2020; Bertoni *et al.*, 2021; Claridge *et al.*, 2021; Bertolino *et al.*, 2023).

Moreover, there are recognised challenges associated with EVs being used diagnostically in a clinical setting, such as the lack of simple and robust isolation methods, sample volume available, and sensitivity of analytical equipment used. Some commercially available preparation kits can be used in a clinical setting. For example, the Exoquick system has been used to successfully isolate EVs from gingival cervicular fluid in order to identify early biomarkers for the prediction of gestational diabetes mellitus in pre-symptomatic women (Monteiro *et al.*, 2018). Novel isolation systems are in the process of development to improve clinical translation. However, these developments alone do not address all the challenges present with respect to EV clinical translation.

It has been postulated that bioengineering approaches may offer sustainable solutions to the barriers harboured by EVs used in a therapeutic capacity. For example, by engineering EVs to contain specific pharmaceutical content (Claridge *et al.*, 2021; Bertolino *et al.*, 2023) by using RNAi, CRISPR/Cas9 and chemotherapeutics (Melling *et al.*, 2019). This can enhance their stability and modify surface epitopes to promote enhanced targeting of cells and tissues *in vivo* (Claridge *et al.*, 2021).

MSC-EV therapeutics offer several advantages over cell-based therapeutics, including a higher safety profile, lower immunogenicity, and the ability to cross biological barriers, and avoid complications that arise from stem cell-induced ectopic tumour formation, entrapment in lung microvasculature, and immune rejection (Gowen *et al.*, 2020; Bertoni *et al.*, 2021). Currently there are clinical studies evaluating and comparing the efficiency of autologous SF-derived MSCs and their corresponding EVs on knee injury in humans, receiving a single dose of MSCs ( $1 \times 10^6$  cells per kg) in the right knee and a single dose of their corresponding EVs in the left knee by intra-articular injection (Bertoni *et al.*, 2021). Nevertheless, there are specific challenges to be addressed in association with MSC-EVs and their clinical translation, surrounding the scalable production, batch to batch standardization and characterization of clinical grade EVs (Bertoni *et al.*, 2021). These could be addressed with the development of immortalised MSC lines, as previously discussed, or the use of induced pluripotent stem cells (Bertoni *et al.*, 2021).

In order to address the issue of clinical translation of EVs a number of task forces and committees have been established, such as the ISEV Task Force on Regulatory Affairs and Clinical Use of EV-based Therapeutics, as well as the Exosomes Committee from the International Society for Cell & Gene Therapy (ISCT) and the Extracellular Vesicle Translation to Clinical Perspectives (EVOLVE). The aim of these initiatives is to work collaboratively to demonstrate quality, safety and efficacy of EVs required for a medicinal product (Silva *et al.*, 2021). This provides information and recommendations regarding manufacturing, quality control, analytics, non-clinical development, and clinical trials, according to current European legislation.

### 9.6.3 Commercialisation of Extracellular Vesicle-based Therapeutics

The commercialisation of EV-based therapeutics is necessary to produce a universal 'cell free' product. A number of bioengineering approaches have been utilised to address this currently unmet need (Paolini *et al.*, 2022). Emphasis is placed on the use of membrane-based processes for isolation and the purification of EVs in combination with chromatographic techniques (Giancaterino and Boi, 2023).

Specific high yield EV manufacturing approaches involve the development of large-scale cell culture platforms, such as bioreactor culture systems. Further approaches include the induction of EV secretion through cellular stimuli (vesiculation buffer, sulfhydryl blocking agents, cytochalasin B, shear stress, high frequency ultrasound), and cell fragmentation with the creation of biomimetic vesicles (low frequency ultrasound, extrusion, and nitrogen cavitation) (Syromiatnikova, Prokopeva and Gomzikova, 2022).

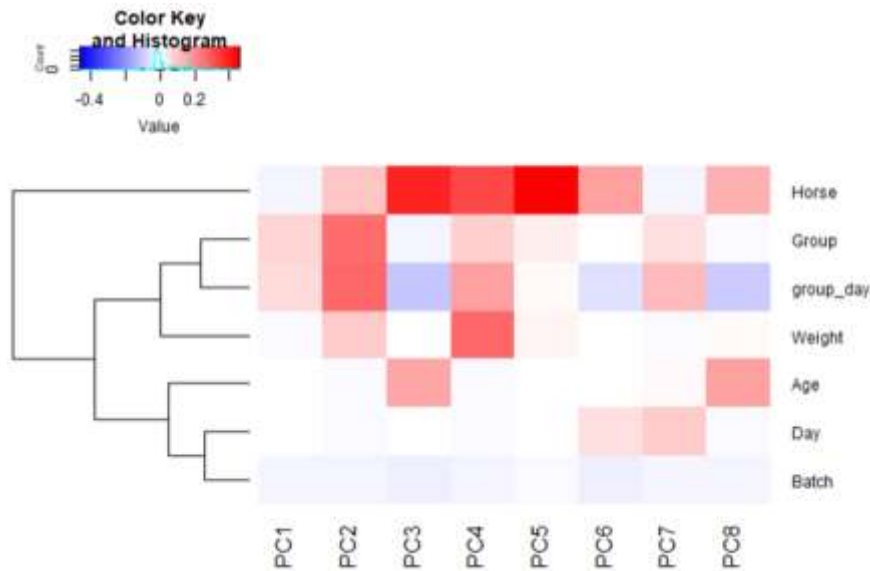
To address this developing area ISEV published the consensus and recommendations by ISEV members at a workshop entitled massivEVs, with representation from “The Extracellular Vesicle Foundry” (evFOUNDRY) and “Extracellular vesicles from a natural source for tailor-made nanomaterials” (VES4US) (Paolini *et al.*, 2022). This aimed to provide details with respect to manufacturing, upscaling challenges and directions for their resolution in EV research (Paolini *et al.*, 2022). An area of timely research includes the identification and validation of assays used for the quality control of EVs. This could ultimately promote interdisciplinary collaborations in order to take EV therapeutics to the commercial sector.

## **9.7 Conclusion**

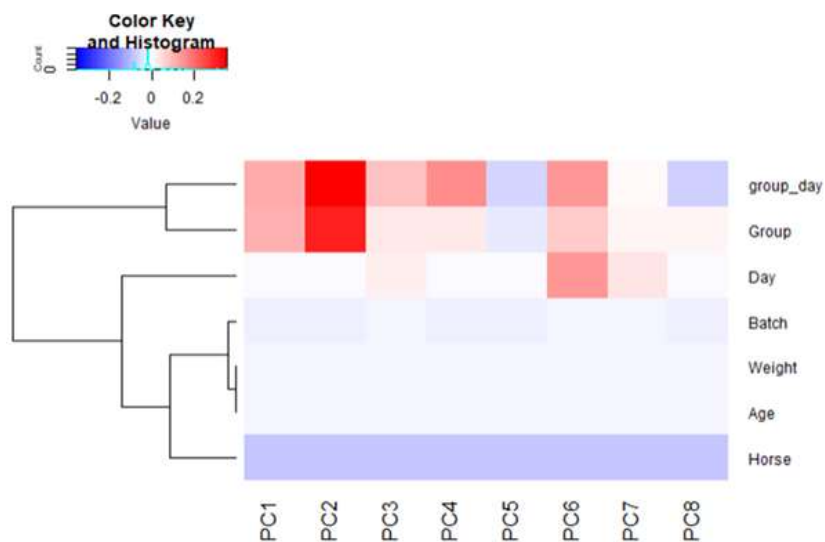
This thesis has identified potential biomarkers of naturally occurring OA intrinsic to EVs derived from both equine plasma and SF, from respective studies, by using a range of spectroscopic and spectrometric techniques. This has elucidated variation associated with joint disease with respect to the EV proteome, lipidome and transcriptome. The SF EV proteome changed on a global level as a result of MSC treatment, suggestive of the role of EVs in mediating the therapy. Mechanisms associated with serine endopeptidase and complement pathway regulation were identified. Finally, the effect of PRP and PRP-EVs on an *in vitro* model of equine tendon injury identified functional effects relating to inflammatory phenotypes in association with NF- $\kappa$ B signalling and collagen metabolism, which require further investigation. Future research directions should aim to use mechanistic approaches to explore EV cellular interaction and harnessing across species ‘one medicine’ approaches to enhance scientific impact and identify universal disease biomarkers. Priority should be given to prominent unmet needs, such as the requirement of suitable *in vitro* models, and the challenges associated with EV characterisation, clinical translation and commercialisation.

## 10. Supplementary Information

A



B



**Supplementary Figure 10.1. Clustering of experimental variables and confounding variables as drivers for explained variance for respective principal components before and after appropriate batch correction.** Proteomic data was normalised and log<sub>2</sub> transformed, with (A) showing the variables driving separation prior to batch correction, namely horse. (B) Following batch correction using ComBat it can be observed that group<sub>day</sub>, and group are the drivers of variation in the proteomic dataset.

**Supplementary Table 10.1. A table showing all 48 significant proteins.** Including accompanying accession number, FDR corrected P-Value, and direction of expression from MSC injection into the joint, to the end of the 70-day study. All proteins returning to baseline control after 70 days.

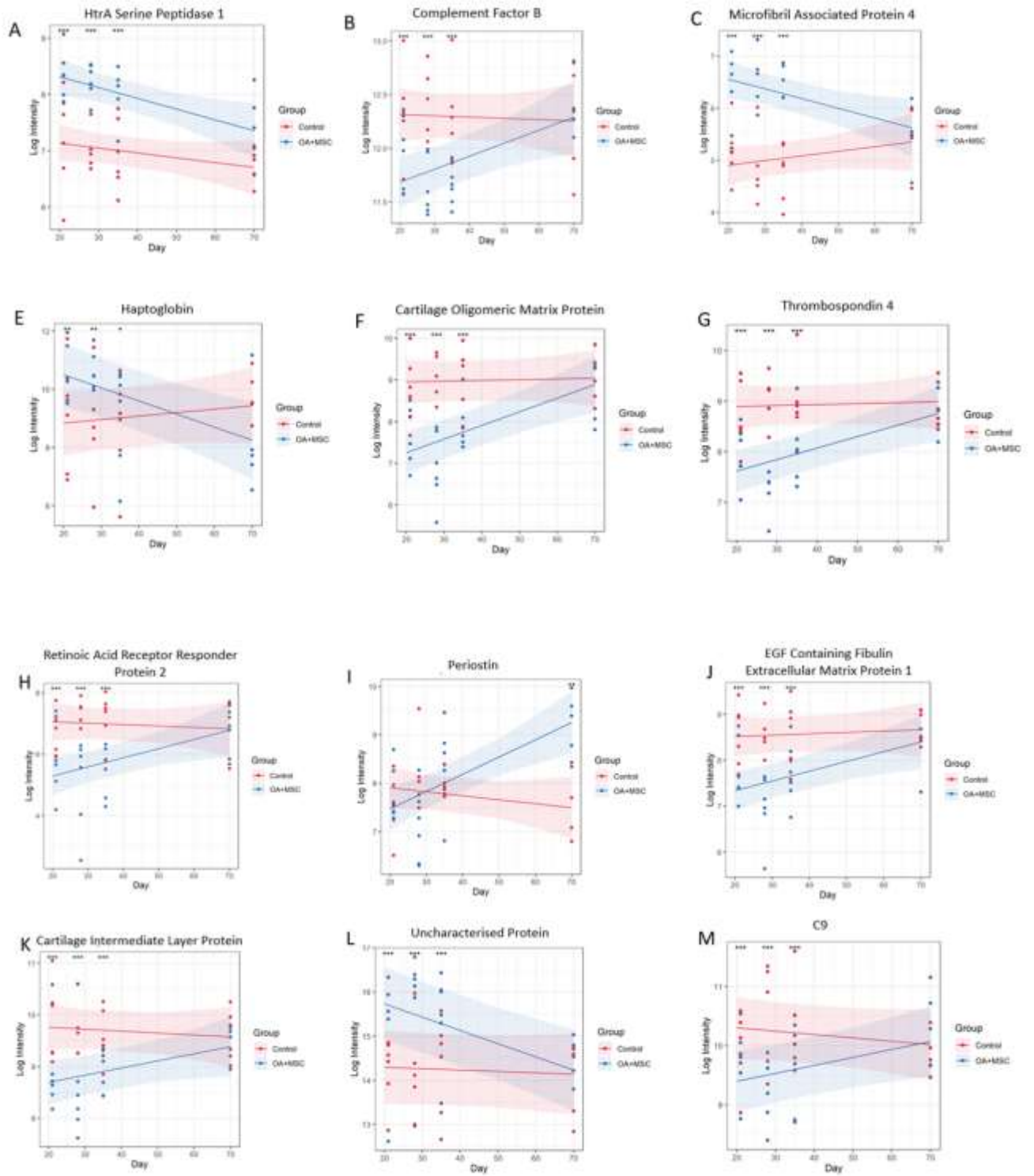
Protein	Accession number	P-Value (FDR adjusted)	Expression direction in OA+MSC group compared to control
Fibrinogen beta chain	F6PH38	0.000124457	Increase
Fibrinogen gamma chain	A0A5F5PPB8	0.00012875	Increase
Joining chain of multimeric IgA and IgM	A0A3Q2HW24	0.000256117	Increase
Dynein heavy chain domain 1	A0A3Q2HE28	0.000467924	Increase
Fibrinogen alpha chain	A0A3Q2HTG2	0.000527871	Increase
Gelsolin (Actin-depolymerizing factor, ADF) (Brevin)	Q28372	0.000558416	Decrease
Cartilage oligomeric matrix protein	A0A3Q2HRL2	0.001269811	Decrease
Microfibril associated protein 4	A0A3Q2HNNH0	0.001467511	Increase
Glutathione peroxidase	A0A5F5PST7	0.002535091	Decrease
Insulin like growth factor binding protein 6	F7DEB1	0.003249662	Decrease
Uncharacterized protein	A0A3Q2H908	0.003249662	Increase
Thrombospondin 4	F7E0P3	0.003398605	Decrease
Annexin	F7DE06	0.00767001	Increase
Chondroadherin	F6WD70	0.00767001	Decrease
Ectonucleotide pyrophosphatase/phosphodiesterase 2	A0A3Q2HYR4	0.009877629	Decrease
Sulfhydryl oxidase, EC 1.8.3.2	F6WR95	0.010834212	Decrease
CD5 molecule like	A0A3Q2HC10	0.011838064	Increase
Complement component C9	P48770	0.017797177	Decrease
Complement C8 alpha chain	A0A5F5PQS3	0.029587066	Decrease
Complement subcomponent C1r, EC 3.4.21.41	F6Z5L1	0.030381695	Increase
Histone H3	F6UU57	0.031141324	Increase
Fibulin-1	A0A3Q2GXX5	0.031158385	Decrease

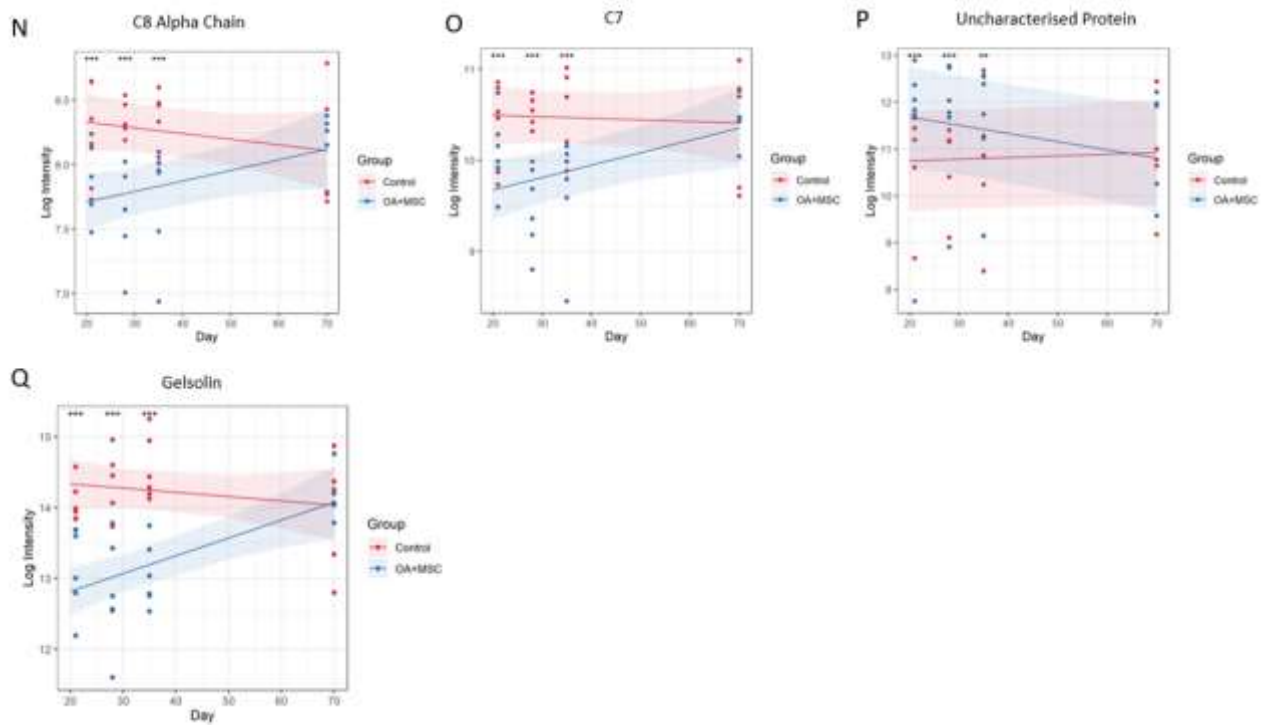
72 kDa type IV collagenase, EC 3.4.24.24 (72 kDa gelatinase) (Matrix metalloproteinase-2)	A0A3Q2H348	0.032777103	Decrease
Retinoic acid receptor responder protein 2 (Chemerin)	F7C5F1	0.032777103	Decrease
HtrA serine peptidase 1	A0A3Q2KX04	0.032777103	Increase
Rho-associated protein kinase 2, EC 2.7.11.1 (Rho-associated, coiled-coil-containing protein kinase 2) (Rho-associated, coiled-coil-containing protein kinase II) (p164 ROCK-2)	F6QSI7	0.032777103	Decrease
Serpin family F member 1	F7BKE1	0.032777103	Decrease
Periostin	F6Y0G5	0.032777103	Decrease
EGF containing fibulin extracellular matrix protein 1	F6PVG3	0.033746242	Decrease
Histone H4	A0A3Q2IAY9	0.034130559	Increase
Complement C7	A0A3Q2I4S4	0.034130559	Decrease
Haptoglobin	F6XWM5	0.034758356	Increase
MIA SH3 domain containing	F6VJF5	0.039924238	Decrease
Complement factor D, EC 3.4.21.46 (Adipsin) (C3 convertase activator) (Properdin factor D)	A0A3Q2LBP6	0.039924238	Decrease
Hyaluronan binding protein 2	F6VZ73	0.039924238	Decrease
Cartilage intermediate layer protein	F7C2J3	0.039924238	Decrease
WD repeat-containing protein 91	A0A3Q2L5K2	0.039924238	Decrease
Dynamin GTPase, EC 3.6.5.5	A0A3Q2H544	0.039924238	Decrease
Complement factor B, EC 3.4.21.47 (C3/C5 convertase)	A0A3Q2IDD2	0.039924238	Decrease
RAB10, member RAS oncogene family	A0A3Q2H5J5	0.043202308	No change

Secreted phosphoprotein 24 (Secreted phosphoprotein 2)	F7DIX7	0.043202308	Increase
Complement C2, EC 3.4.21.43 (C3/C5 convertase)	F6PPQ0	0.043202308	Decrease
Heat shock 70kDa protein 1A	F7DW69	0.043202308	Decrease
Titin	A0A5F5PSR4	0.043202308	Increase
Folate hydrolase 1B	A0A3Q2HLX0	0.043202308	Decrease
Complement C1s	F7BQD6	0.043202308	Increase
Uncharacterized protein	H9GZV1	0.043202308	Increase
EGF containing fibulin extracellular matrix protein 2	A0A5F5PL54	0.04772571	Decrease

*Abbreviations - RAB10 ( Ras-related protein Rab-10 ), RAS ( Rat sarcoma ), EGF (Epidermal growth factor ).*










**Supplementary Figure 10.2. Differentially abundant proteins mapped to one of the three most significant functional enrichment pathway.** Graphs demonstrating the results of significant ( $p \leq 0.05$ ) proteins identified after a linear mixed model was applied to the experimental cohort, comparing protein expression between experimental group (treatment OA+MSCs (treatment) and control over time (day 21, 28, 35 and 70), visualizing the expression change longitudinally. Pairwise comparisons were conducted post linear mixed model application to compare control and OA +MSCs protein expression per time point. Significance level, as determined by the generated FDR corrected P Value is shown using ( $p < 0.05$ , \*;  $p < 0.01$  \*\*,  $p < 0.001$ , \*\*\*,  $p < 0.0001$ , \*\*\*\*).

**Supplementary Table 10.2. Radiographic criteria used for the classification of the healthy, mild and severe osteoarthritis phenotypes.** Arrows indicate osteophyte formation and subchondral osteolysis, and R and L denote right or left limb.

Group	Description	Radiograph
Healthy	No lesions	

<p><b>Mild OA</b></p>	<p>Small osteophyte and subchondral osteolysis</p>	
<p><b>Severe OA</b></p>	<p>Bone deformation, narrowing of joint space, subchondral bone sclerosis, osteophytes.</p>	

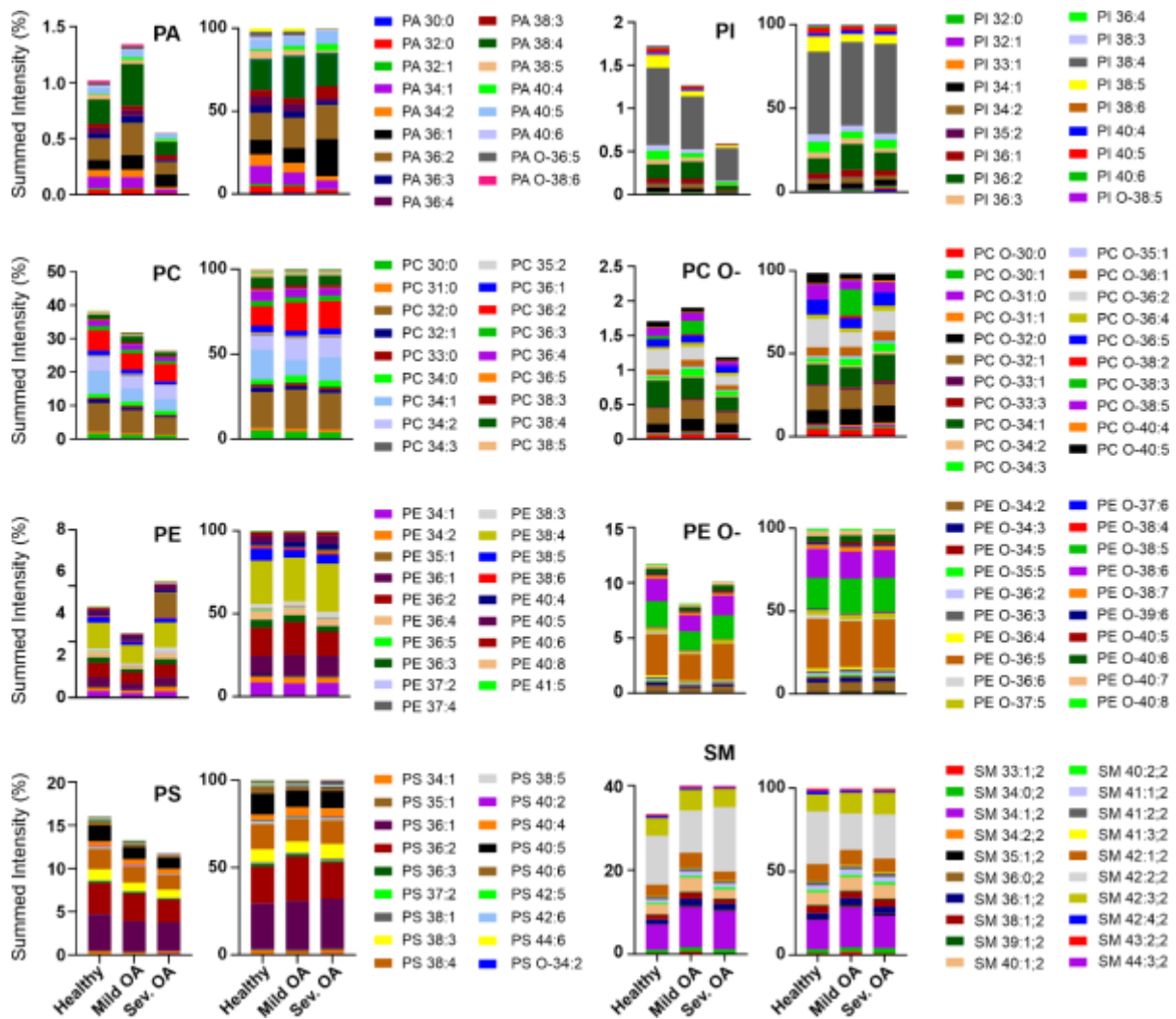
**Supplementary Table 10.3. Author Checklist: MIFlowCyt-Compliant Items.**

Requirement	Requested Information
<b>1.1. Purpose</b>	To investigate extracellular vesicle biomarker discovery in synovial fluid from healthy, mild and severe osteoarthritis (OA) equine samples by using a combined proteomics and lipidomics approach
<b>1.2. Keywords</b>	Osteoarthritis, synovial fluid, proteomics, lipidomics, equine, extracellular vesicles
<b>1.3. Experiment variables</b>	Healthy versus clinically relevant equine OA
<b>1.4. Organisation name and address</b>	Division Cell Biology, Metabolism & Cancer, Department of Biomolecular Health Sciences, Faculty of Veterinary Sciences Utrecht University Yalelaan 2, 3584 CM Utrecht, The Netherlands
<b>1.5. Primary contact name and email address</b>	Prof. Dr. M.H.M. Wauben M.H.M.Wauben@uu.nl
<b>1.6. Date or time period of experiment</b>	October 2022
<b>1.7. Conclusions</b>	The proteome and lipidome of SF-EVs are primarily positively correlated with activation of pathways related to chondrocyte dysregulation and inflammation. A series of phospholipids and proteins were proposed as alternatives for combined biomarker discovery, for example, PC O-32:3 and CD109.
<b>1.8. Quality control measures</b>	Procedural control for fluorescent stainings Serial dilutions Detergent treatment control
<b>2.1.1.1. (2.1.2.1., 2.1.3.1.) Sample description</b>	Synovial fluid from healthy equine joints, joints with diagnosed mild OA or severe OA
<b>2.1.1.2. Biological sample source description</b>	Synovial fluid
<b>2.1.1.3. Biological sample source organism description</b>	Horse (Equus caballus)
<b>2.1.2.2. Environmental sample location</b>	
<b>2.3. Sample treatment description</b>	For detergent treatment control samples were treated with 0.1% (v/v) triton X-100 (SERVA Electrophoresis GmbH, Heidelberg, Germany) final concentration for 30 seconds before reanalysis.
<b>2.4. Fluorescence reagent(s) description</b>	PKH67 (Sigma-Aldrich)
<b>3.1. Instrument manufacturer</b>	Becton Dickinson
<b>3.2. Instrument model</b>	BD Influx™ optimised instrument for detection of sub-micron sized particles as described previously.
<b>3.3. Instrument configuration and settings</b>	BD Influx optimised to measure small particles. All configuration details can be found in previous publications [32,33]. Briefly, samples were measured at a constant flow rate for 30 seconds using a fluorescence threshold on the 488 nm laser. The threshold level was set to detect 10-20 events per second when measuring a buffer control.
<b>4.1. List-mode data files</b>	All data files, including the quality control measure from 1.8, are available upon request.
<b>4.2. Compensation description</b>	No compensation was required due to instrument configuration.
<b>4.3. Data transformation details</b>	No data transformation was applied.

<b>4.4.1. Gate description</b>	No gates were applied
<b>4.4.2. Gate statistics</b>	The number of total events recorded in 30 seconds measurements are shown in the dot plots without any background correction.
<b>4.4.3. Gate boundaries</b>	N/A

**Supplementary Table 10.4.** MIFlowCyt-EV framework.

<b>1.1 Preanalytical variables conforming to MISEV guidelines</b>	Yes, all relevant data has been submitted to EV-TRACK for transparent reporting and centralising knowledge in extracellular vesicle research (EV-TRACK ID: EV230607).
<b>1.2 Experimental design according to MIFlowCyt guidelines</b>	Yes, MIFlowCyt checklist can be found as part of the supporting information of this manuscript in Suppl. Table 2.
<b>2.1 Sample staining details</b>	Yes, described in Materials and Methods.
<b>2.2 Sample washing details</b>	Yes, described in Materials and Methods.
<b>2.3 Sample dilution details</b>	Yes, described in Materials and Methods.
<b>3.1 Buffer-only controls</b>	Yes, relevant buffer controls were measured
<b>3.2 Buffer with reagent controls</b>	Yes. Data available upon request
<b>3.3 Unstained controls</b>	N/A
<b>3.4 Isotype controls</b>	N/A
<b>3.5 Single-stained controls</b>	N/A
<b>3.6 Procedural controls</b>	Yes. Available upon request
<b>3.7 Serial dilutions</b>	Yes, serial dilutions were performed in previous characterisation experiments to determine the ideal dilution used in this study. Data available upon request
<b>3.8 Detergent-treated controls</b>	Yes, sensitivity to triton X-100 was determined in previous characterisation experiments. Data available upon request
<b>4.1 Trigger channel(s) and threshold(s)</b>	The trigger channel used was on the fluorescent signal collected from the 488 nm laser (530/40 bandpass filter). The threshold level was set at 0.62, allowing an event rate of <20 events/second in a clean PBS sample. Additional details can be found in Materials and Methods.
<b>4.2 Flow rate / volumetric quantification</b>	Yes, low flow rate was kept constant and was measured for quantification purposes. The flow rate was estimated at 12.8 $\mu\text{L}/\text{min}$ .
<b>4.3 Fluorescence calibration</b>	N/A
<b>4.4 Scatter calibration</b>	N/A
<b>5.1 EV diameter/surface area/volume approximation</b>	N/A
<b>5.2 EV refractive index approximation</b>	N/A
<b>5.3 EV epitope number approximation</b>	N/A
<b>6.1 Completion of MIFlowCyt checklist</b>	Yes, see Suppl. Table 2
<b>6.2 Calibrated channel detection range</b>	As shown in previous publications, equivalent to 100 FITC MESF. See description in Arkesteijn GJA et al. [33].
<b>6.3 EV number/concentration</b>	Yes, see Figure 1.
<b>6.4 EV brightness</b>	N/A
<b>7.1 Sharing of data to a public repository</b>	Yes, all experimental details about the biological sample preparation can be found in EV-TRACK. All data files are available upon request.



**Supplementary Figure 10.3. Composition of individual lipid species in phosphatidic acid, phosphatidylinositol, ester-linked phosphatidylcholine, ether-linked phosphatidylcholine, ester-linked phosphatidylethanolamine, ether-linked phosphatidylethanolamine, phosphatidylserine, and sphingomyelin classes.** Lipid composition of the most abundant lipid classes of SF-EVs from healthy, mild OA, or severe OA horse patients. The left stacked bars graph in each class shows the lipid species' amount in the overall lipidome. The immediately right stacked bars graph displays the normalised amount of lipid species in each class. Samples were normalised for each class and SF-EV group by expressing the lipid intensity as a fraction of the sum of lipid intensities. Lipids were obtained from 100,000g purified SF-EVs with sucrose density gradients. Healthy samples (n=6), mild OA (n=4), severe OA (n=3).

**Supplementary Table 10.5. Significantly differentially expressed pathological functions.** As identified by ingenuity pathway analysis for each comparison.

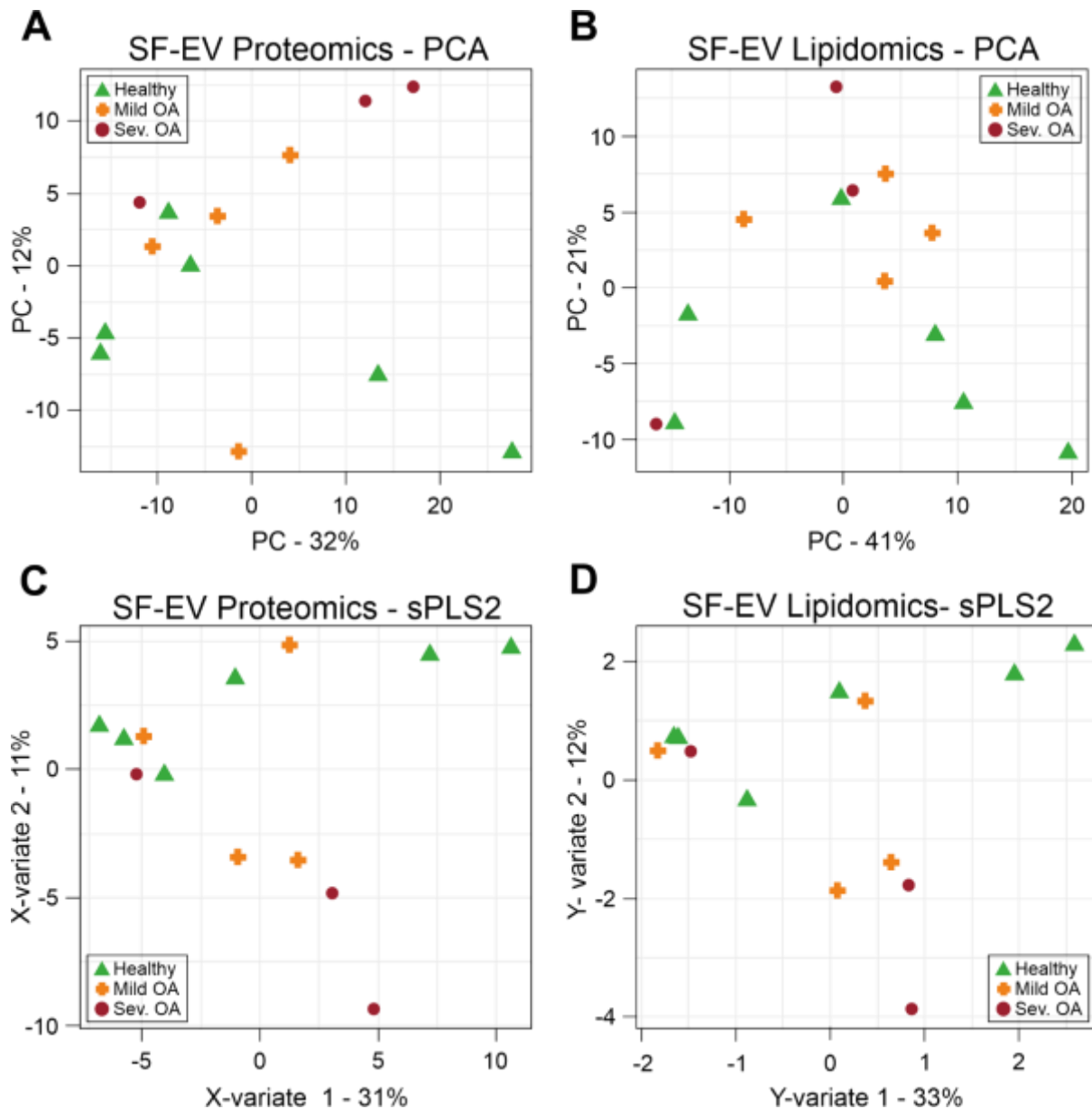
	<b>Disease or Function Annotation</b>	<b>p-value</b>
<b>Severe OA Vs mild OA</b>	Accumulation of macrophages	0.000414
	Stabilization of microtubules	0.000429
	Necrosis	0.000433
	Formation of microtubules	0.000563
	Translocation of microtubules	0.000582
	Outgrowth of microtubules	0.000582
	Quantity of filaments	0.00103
	Accumulation of microtubules	0.00146
	Conversion of neurons	0.00233
	Length of microtubules	0.00291
	Organization of microtubule organizing centers	0.0032
	Instability of microtubules	0.00349
	Regulation of actin cytoskeleton	0.00378
	Anchoring of microtubules	0.00436
	Activation of basophils	0.00552
	Injury of joint	0.00552
	Cell division of stem cells	0.00697
	Arrest in cell cycle progression of fibroblasts	0.00697
	Organization of basement membrane	0.00726
	Quantity of basophils	0.00755
	Induction of reactive oxygen species	0.00784
	Deposition of extracellular matrix	0.00784
	Quantity of microtubules	0.00842
	Abnormal morphology of basement membrane	0.00986
	Adhesion of macrophages	0.0107
	Activation of phagocytes	0.0119
	Complement activation	0.0171
	Phagocytosis of neutrophils	0.0185
	Organization of microtubules	0.0191



	Migration of cells	0.0198
	Polymerization of microtubules	0.0245
	Quantity of actin filaments	0.0259
	Adhesion of cell-associated matrix	0.0305
	Inflammation of organ	0.0315
	Apoptosis	0.0326
	Cell movement of phagocytes	0.0327
	Cell death of osteosarcoma cells	0.0389
<b>Severe OA vs healthy</b>	Organization of cytoskeleton	0.0000012
	Linkage of actin cytoskeleton	0.00000125
	Decapping of actin filaments	0.00000415
	Binding of actin cytoskeleton	0.00000871
	Clathrin mediated endocytosis	0.0000248
	Phagocytosis	0.0000418
	Proliferation of immune cells	0.000126
	Endocytosis	0.000256
	Adhesion of phagocytes	0.000285
	Morphology of cytoskeleton	0.00032
	Remodeling of actin cytoskeleton	0.000369
	Rac protein signal transduction	0.000387
	Maturation of phagosomes	0.000583
	Formation of vesicles	0.000712
	Trafficking of exocytic vesicle	0.00133
	Association of phospholipid vesicles	0.00133
	Endocytosis of plasma membrane	0.00133
	Blebbing	0.00134
	Quantity of phagocytes	0.00151
	Quantity of reactive oxygen species	0.00168
	Formation of reactive oxygen species	0.00168
	Cell movement of connective tissue cells	0.00171
	Necrosis	0.0018
	Oxidative stress	0.0019

Survival of synovial fibroblasts	0.002
Initiation of autophagy of cells	0.002
Proliferation of macrophages	0.00202
Migration of phagocytes	0.00299
Differentiation of phagocytes	0.00312
Transmigration of phagocytes	0.00362
Function of cytoskeleton	0.00399
Accumulation of proteoglycan	0.00465
Cell movement of neutrophils	0.00484
Apoptosis of chondrocyte cell lines	0.00598
Invasion of fibroblast-like synoviocytes	0.00598
Organization of extracellular matrix	0.00598
Migration of neutrophils	0.00625
Invasion of extracellular matrix	0.00664
Release of secretory vesicles	0.00664
Migration of osteoclasts	0.00664
Apoptosis	0.00669
Fusion of osteoclasts	0.00862
Fusion of osteoclast precursor cells	0.00928
Movement of vesicles	0.00994
Migration of fibroblast-like synoviocytes	0.0139
Accumulation of extracellular matrix	0.0165
Immune mediated inflammatory disease	0.0175
Quantity of chondrocytes	0.0185
Fibrosis	0.0189
Cellular infiltration by macrophages	0.0194
Morphology of bone	0.0195
Systemic inflammation	0.0211
Inflammation of organ	0.0231
Development of chondrocytes	0.027
Disruption of cytoskeleton	0.027
Acute inflammation of tissue	0.0289

	Differentiation of connective tissue cells	0.031
	Osteoarthritis	0.0316
<b>Mild OA vs healthy</b>	Complement activation	0.000609
	Coalignment of microfilaments	0.000624
	Necrosis	0.000961
	Chondrogenesis of bone marrow stem cells	0.00125
	Abnormal morphology of trabecular bone	0.00167
	Immune response of neutrophils	0.0017
	Development of articular cartilage	0.00374
	Morphogenesis of endochondral bone	0.00498
	Fusion of joint	0.00746
	Abnormal morphology of bone	0.00748
	Resorption of bone	0.00904
	Phagocytosis of phagocytes	0.00949
	Differentiation of osteoclasts	0.0116
	Injury of joint	0.0118
	Morphology of bone	0.0163
	Inflammation of joint	0.0169
	Mineralization of extracellular matrix	0.0198
	Activation of macrophages	0.0235
	Cell movement of phagocytes	0.0236
	Function of osteoblasts	0.0253
	Osteoarthritis	0.028
	Chronic inflammation	0.0338
	Function of osteoclasts	0.038
	Cell movement of macrophages	0.0381
	Phagocytosis of neutrophils	0.0392
	Cellular infiltration by phagocytes	0.0416



**Supplementary Figure 10.4. Normalisation of proteomics and lipidomics data for integrated analysis.** Healthy SF-EVs (green triangle, n=6), mild OA SF-EVs (orange cross, n=4), and severe OA SF-EVs (Sev. OA; red circle, n=3). Samples of both datasets were normalised by the sum. A-B) Principal component analysis (PCA) of the proteomics (A) and lipidomics (B) SF-EV datasets. C-D) Unsupervised multivariate Sparse Partial Least Squares regression (sPLS2) of the SF-EV samples in X-variate (for proteomics (C)) and Y-variate (for lipidomics (C)) components projected into the space spanned to the respective dataset.

**Supplementary Table 10.6. Candidate proteins for composite osteoarthritis biomarker discovery.**

	Protein	Membrane or cargo protein	Origin	Function	
<b>Group 1*– Downregulated proteins</b>					
<b>Enzymes (oxidative stress)</b>	Peroxiredoxin 1	Cargo	(Neumann, Cao and Manevich, 2009)	Dendritic cells (Théry <i>et al.</i> , 2001), spleen cells (Zöller <i>et al.</i> , 2018), osteoblasts (Xiao <i>et al.</i> , 2007), macrophages (Hassani and Olivier, 2013), thymus (Turiák <i>et al.</i> , 2011), pancreatic-β cells (Lee, Jeong and Lee, 2009), oligodendrocytes (Krämer-Albers <i>et al.</i> , 2007),	Modulation of redox signalling events for cellular protection (Collins <i>et al.</i> , 2016)
<b>Membrane proteins</b>	CD163 (Scavenger receptor cysteine-rich type 1 protein M130)	Transmembrane	(Etzerodt and Moestrup, 2013)	Macrophage (Etzerodt and Moestrup, 2013; Qu, Zhu and Zhang, 2022)	Receptor for clearance of oxidative and proinflammatory haemoglobin/haptoglobin complexes, stimulator of heme-oxygenase-1 and anti-inflammatory heme metabolites (Etzerodt and Moestrup, 2013)
<b>Membrane traffic</b>	Caveolin 1	Cargo	(Simón <i>et al.</i> , 2020)	Ubiquitously expressed in all cell types (Nwosu <i>et al.</i> , 2016)	Generation of caveolae (membrane curvatures) (Simón <i>et al.</i> , 2020)
<b>Structural and cytoskeleton-related molecules</b>	Myosin regulatory light polypeptide 9	Cargo	(Park <i>et al.</i> , 2011)	Smooth muscle, spleen, fibroblasts (all non-muscle tissues) (Park <i>et al.</i> , 2011), Astrocytes (Hallal <i>et al.</i> , 2019), hippocampus (Xu <i>et al.</i> , 2016), cancer (Matsushita <i>et al.</i> , 2021; Mujammami <i>et al.</i> , 2022)	Modulation of contractile activity of smooth muscle and non-muscle cells by phosphorylation (Kumar <i>et al.</i> , 1989)
	Tubulin alpha chain	Cargo	(Gasic, 2022)	Ubiquitously expressed in all cell types (Gasic, 2022)	Cellular morphology formation and maintenance, and intracellular transport, chromosomal segregation (Gasic, 2022)
<b>Chaperones</b>	Heat shock protein 90 alpha	Cargo	(Dempsey <i>et al.</i> , 2010)	Fibroblasts (Luga <i>et al.</i> , 2012), pancreatic-β cells (Lee, Jeong and Lee, 2009), oligodendrocytes (Krämer-Albers <i>et al.</i> , 2007), B cell (Clayton <i>et al.</i> , 2005), cancer (Bria <i>et al.</i> , 2015; Wei <i>et al.</i> , 2021; Zhong <i>et al.</i> , 2021; Mousavi <i>et al.</i> , 2023)	Protein folding, maturation, and involvement in signal transduction and transcriptional regulation (Calamia <i>et al.</i> , 2011)
<b>Endocytosis, exocytosis and trafficking</b>	Annexin A8	Cargo	(White <i>et al.</i> , 2002; Goebeler <i>et al.</i> , 2008)	Chondrocytes (White <i>et al.</i> , 2002), Leukocytes (Poeter <i>et al.</i> , 2014), osteoclasts (Crotti <i>et al.</i> , 2011), lung, liver, kidney, skin, placenta, and cornea (Grewal <i>et al.</i> , 2021)	Controls sorting and transport of late endosomes [100], chondrocyte differentiation marker under normal endochondral ossification (White <i>et al.</i> , 2002)

<b>Signal transduction</b>	Protein S100-A4	Cargo (Yammani, 2012), secreted (Chen <i>et al.</i> , 2015)	Chondrocytes (Yammani, 2012), macrophages (Chen <i>et al.</i> , 2015), fibroblasts, CD8+ T cells, monocytes, and eosinophils, cancer (Ambartsumian, Klingelhöfer and Grigorian, 2019)	Regulation of calcium homeostasis, cell growth and motility, cell differentiation, and cell survival (Yammani, 2012), promotion and induction of metastasis (Ambartsumian, Klingelhöfer and Grigorian, 2019)
<b>Group 2** – Upregulated proteins</b>				
<b>Metabolism</b>	Aldo-keto reductase family 7 member A2	Cargo	Cartilage (Vincourt <i>et al.</i> , 2006), cardiomyocytes (Quiñones-Lombraña, Intini and Blanco, 2019), brain, heart, kidney, liver, lung, prostate, skeletal muscle, small intestine, spleen (O'connor <i>et al.</i> , 1999)	Reduction of aldehydes and ketones to alcohols and metabolism of toxic aldehydes (Quiñones-Lombraña, Intini and Blanco, 2019)
<b>Structural and cytoskeleton-related molecules</b>	Erythrocyte membrane protein band 4.1. like 2	Cargo (Chishti <i>et al.</i> , 1998)	B cells (Buschow <i>et al.</i> , 2010), endothelial cells (de Jong <i>et al.</i> , 2012), Dendritic cells (Kowal <i>et al.</i> , 2016), Mesenchymal stem cells (Kim <i>et al.</i> , 2012), T cells (Németh <i>et al.</i> , 2017)	Role in the attachment of cytoplasmic proteins to the membrane, part of the FERM complex (composed of the 4.1 protein, ezrin, radixin, and moesin) (Chishti <i>et al.</i> , 1998)
	Ezrin	Cargo (Kawaguchi and Asano, 2022)	Chondrocytes (Housmans <i>et al.</i> , 2022), fibroblast (Quang <i>et al.</i> , 2000; Quan <i>et al.</i> , 2018), B cells (Buschow <i>et al.</i> , 2010), milk (van Herwijnen <i>et al.</i> , 2016), Dendritic cells (Kowal <i>et al.</i> , 2016), oligodendrocytes (Krämer-Albers <i>et al.</i> , 2007), cancer cells (Choi <i>et al.</i> , 2007; Paggetti <i>et al.</i> , 2015), macrophages (Kadiu <i>et al.</i> , 2012), monocytes (Bernimoulin <i>et al.</i> , 2009), T cells (Perez-Hernandez <i>et al.</i> , 2013), synovial fluid (György <i>et al.</i> , 2012)	Cross-linker between the actin cytoskeleton and the plasma membrane, part of the ERM complex (ezrin/radixin/moesin), also involved in signal transduction cell migration, and survival (Kawaguchi and Asano, 2022)
	Moesin	Cargo (Senju and Tsai, 2022)	B cell (Wubbolts <i>et al.</i> , 2003; Buschow <i>et al.</i> , 2010), milk (van Herwijnen <i>et al.</i> , 2016), Dendritic cells (Kowal <i>et al.</i> , 2016), endothelial cells (Peterson <i>et al.</i> , 2008), neutrophils (Dalli <i>et al.</i> , 2013), synovial fluid (György <i>et al.</i> , 2012)	Links cytoskeleton to the plasma membrane or integral membrane proteins (Senju and Tsai, 2022)
	Fermitin family member 3	Cargo (Stadtman and Zarbock, 2017)	B cells (Buschow <i>et al.</i> , 2010), cancer cells (Miguet <i>et al.</i> , 2006; Hurwitz <i>et al.</i> , 2016), Dendritic cells (Kowal <i>et al.</i> , 2016), endothelial cells (Peterson <i>et al.</i> , 2008), monocytes (Bernimoulin <i>et al.</i> , 2009), neutrophils (Dalli <i>et al.</i> , 2013), red blood cells (Bosman <i>et al.</i> , 2008), platelets (Garcia <i>et al.</i> , 2005)	Bind to the cytoplasmic regions of integrins and modulate their function (Fagerholm, Lek and Morrison, 2014; Stadtman and Zarbock, 2017)

	Actin alpha 2, smooth muscle (( $\alpha$ )-2 smooth muscle actin)	Cargo	Chondrocytes (Kinner and Spector, 2001), monocytes and macrophages (Ludin <i>et al.</i> , 2012), fibroblasts (Wang, Zohar and McCulloch, 2006; Z. Liu <i>et al.</i> , 2017; Rockey, Du and Shi, 2019)	Actin isoform contributes to cell-generated mechanical tension, cell structure, tissue remodelling and contraction (Wang, Zohar and McCulloch, 2006). Role in fibrosis (Mattey <i>et al.</i> , 1997; Song <i>et al.</i> , 2010; Rice <i>et al.</i> , 2021)	
	Vasodilator stimulated phosphoprotein	Cargo	Podocytes (Rachubik and Piwkowska, 2019), macrophages (Hu <i>et al.</i> , 2021) B cells (Miguet <i>et al.</i> , 2006; Buschow <i>et al.</i> , 2010), milk (van Herwijnen <i>et al.</i> , 2016), dendritic cells (Kowal <i>et al.</i> , 2016), endothelial cells (Peterson <i>et al.</i> , 2008), monocytes (Bernimoulin <i>et al.</i> , 2009), platelets (Garcia <i>et al.</i> , 2005; R. H. L. Li <i>et al.</i> , 2020), T cells (Perez-Hernandez <i>et al.</i> , 2013), cancer cells (Choi <i>et al.</i> , 2012; Tauro <i>et al.</i> , 2013; Hurwitz <i>et al.</i> , 2016)	Involved in adhesion, migration, cell-cell interaction, and regulation of pathways connected with actin cytoskeleton remodelling (Rachubik and Piwkowska, 2019). Associated with cell differentiation, mobility and tumour metastasis (Hu <i>et al.</i> , 2021)	
<b>Membrane proteins</b>	CD109	Transmembrane (Mii <i>et al.</i> , 2019)	Cancer cells (Choi <i>et al.</i> , 2012; Tauro <i>et al.</i> , 2013; Hurwitz <i>et al.</i> , 2016; Mallawaarachy <i>et al.</i> , 2017), T cells (Perez-Hernandez <i>et al.</i> , 2013), Dendritic cells (Kowal <i>et al.</i> , 2016), Mesenchymal stem cells (Kim <i>et al.</i> , 2012), endothelial cells (de Jong <i>et al.</i> , 2012), synovial tissue (Song <i>et al.</i> , 2019)	Modulation of pathological processes, such as osteoporosis, fibrosis and tumour metastasis (Song <i>et al.</i> , 2019), TGF- $\beta$ co-receptor and signalling inhibitor of TGF- $\beta$ in keratinocytes (Man <i>et al.</i> , 2012)	
	Thy-1 antigen/CD90	Transmembrane (Yang <i>et al.</i> , 2020)	T cells, NK cells, innate lymphoid cells (Schroeder <i>et al.</i> , 2023), fibroblasts (Wiles <i>et al.</i> , 2023), Mesenchymal stem cells (Kim <i>et al.</i> , 2012), cancer cells (Hurwitz <i>et al.</i> , 2016), endothelial cells, epithelial cells, neurons (Yang <i>et al.</i> , 2020)	Involved in cancer development and metastasis, cell proliferation, differentiation, cell migration, apoptosis, mechanotransduction and cell adhesion (Saalbach and Anderegg, 2019; Yang <i>et al.</i> , 2020)	
<b>Endocytosis, exocytosis and trafficking</b>	RAB8B, member oncogene family	RAS	Cargo and secreted	Sperm (Bae <i>et al.</i> , 2022), glioma cells (Vasileva <i>et al.</i> , 2022), and SARS-CoV-2 sera (Vastrad, Vastrad and Tengli, 2020)	Involved in membrane trafficking and the establishment of the Golgi apparatus (Bae <i>et al.</i> , 2022)
<b>Signal transduction</b>	Rac family small GTPase 1	Cargo and secreted	Hepatic cells (Liang <i>et al.</i> , 2022), range of eukaryotic cells (Arrazola Sastre <i>et al.</i> , 2020), equine synovial fluid and plasma (Koziy <i>et al.</i> , 2022)	Activated GTPases are involved in cellular proliferation, differentiation, motility, survival, and apoptosis (Arrazola Sastre <i>et al.</i> , 2020)	

<b>Transmembrane transport</b>	Potassium channel tetramerisation domain containing 12	Membrane	Cancer cells (Hasegawa <i>et al.</i> , 2013; Wang <i>et al.</i> , 2021) Serum (Okubo <i>et al.</i> , 2016)	Involved in neuronal excitability through GABBA receptor signalling. Also found to suppress Wnt/Notch signalling, stem cell factors, and chromatin remodelers (Ye <i>et al.</i> , 2020). Associated with tetramerisation and gating of ion channels, cytoskeleton regulation, and transcriptional repression (Liu, Xiang and Sun, 2013)
--------------------------------	--	----------	---	---

Abbreviations – CD163 ( Cluster of differentiation 163 ), Thy-1 ( Cluster of Differentiation 90 ), RAB8B (RAB8B, Member RAS Oncogene Family ), RAC ( Ras-related C3 botulinum toxin substrate 1), GTPase ( guanosine triphosphatease ).

\* Proteins from group 1 correlated to the following phospholipids: PC 34:4, PI 38:6, PI 32:1

\*\* Proteins from group 2 correlated to the following phospholipids: PC O-32:3, SM 36:0;2, SM 41:3



**Supplementary Table 10.7. A list of all differential ( $p < 0.005$ ) following false discovery rate correction proteins identified as enriched in platelet-rich plasma derived extracellular vesicles compared with plasma derived extracellular vesicles.** The table includes raw p value, FDR corrected p value and  $\log_2(\text{foldchange}/\text{FC})$  to inform direction of protein expression, as compared to plasma- EVs, n=3 samples used for analysis.

Protein	P value	FDR	$\log_2(\text{FC})$
Complement C7	2.03E-06	0.000244	-4.5452
Inhibitor of carbonic anhydrase	2.34E-06	0.000244	-4.1761
Serpin family A member 10	3.21E-06	0.000244	-2.4935
Coagulation factor XII	1.24E-05	0.00066	-5.262
Apolipoprotein E	1.45E-05	0.00066	-2.3441
Prothrombin	3.20E-05	0.001217	-2.6364
Serpin family F member 1	4.78E-05	0.001556	-2.2026
Kininogen 1	5.84E-05	0.001666	-3.2229
SH3 domain-binding glutamic acid-rich-like protein	8.76E-05	0.002197	6.144
Erythrocyte membrane protein band 4.2	9.64E-05	0.002197	5.5798
Antithrombin-III	0.00011	0.002276	-2.5928
Protein AMBP	0.00014	0.002325	-2.878
Vitamin D-binding protein	0.000153	0.002325	-3.0442
Afamin	0.000161	0.002325	-3.9464
Complement subcomponent C1r	0.000167	0.002325	-2.7964
Uncharacterized protein	0.000179	0.002325	-2.7227
Albumin	0.000182	0.002325	-5.2901
Selenium binding protein 1	0.000184	0.002325	2.5062
Fibrinogen beta chain	0.000232	0.002698	-2.7938
Complement factor I	0.000239	0.002698	-2.9471
Carboxypeptidase N subunit 2	0.000249	0.002698	-3.5797
Spectrin beta chain	0.000274	0.002837	4.3918
Quinoid dihydropteridine reductase	0.000288	0.002855	5.636
Anion exchange protein	0.00038	0.003607	4.9102
Ninjurin 1	0.000408	0.003707	5.2196
4.1m domain-containing protein	0.000423	0.003707	5.9118
Protein deglycase	0.000451	0.00381	3.5759
Complement C5	0.000468	0.003813	-3.8851
Neutral cholesterol ester hydrolase 1	0.000517	0.003986	2.7349
Alpha-2-macroglobulin	0.000546	0.003986	-1.6197
Fibrinogen gamma chain	0.00055	0.003986	-2.4735
Protein 4.1	0.000559	0.003986	4.0485
Spectrin alpha, erythrocytic 1	0.000578	0.003992	5.0741
Plasminogen	0.000597	0.004002	-3.6785
Complement factor B	0.000676	0.004403	-2.6604
Stomatin	0.000759	0.004806	4.4907
Tropomodulin 1	0.000923	0.005691	4.5901
CD58 molecule	0.000967	0.005799	7.7067
Actin alpha cardiac muscle 1	0.001014	0.00593	3.7589
Alpha-2-HS-glycoprotein	0.001068	0.006087	-3.2167

Aquaporin-1	0.001111	0.006181	6.3715
Kell metallo-endopeptidase	0.001204	0.006533	3.0223
Butyrophilin-like protein 10	0.001234	0.006545	3.1673
Butyrophilin-like protein 10	0.001358	0.006827	6.7399
Carbonic anhydrase	0.00136	0.006827	4.2354
Peroxiredoxin 2 OS	0.001404	0.006827	3.5368
Complement component 4 binding protein alpha	0.001407	0.006827	-3.842
Acylamino-acid-releasing enzyme	0.001542	0.007323	4.1524
Lactoylglutathione lyase	0.001659	0.00772	2.553
Interleukin 1 receptor accessory protein	0.001698	0.007741	-4.9837
Filamin A	0.001851	0.008275	-2.0026
Flotillin	0.0019	0.00833	5.7759
Ubiquitin-40S ribosomal protein S27a	0.002206	0.009386	6.2445
Clusterin	0.002223	0.009386	-2.2834
Alpha-2-glycoprotein 1, zinc-binding	0.002334	0.009559	-4.8202
Fibrinogen alpha chain	0.002348	0.009559	-2.4141
Alpha-synuclein	0.002452	0.009728	5.9383
Complement factor H	0.002475	0.009728	-3.1724
Carboxypeptidase B2	0.00261	0.010064	-5.8459
Tyrosine 3-monooxygenase/tryptophan 5-monooxygenase activation protein epsilon	0.002648	0.010064	4.7727
26S proteasome non-ATPase regulatory subunit 5	0.002725	0.010183	7.8939
Uncharacterized protein	0.002963	0.010812	-3.3483
Uncharacterized protein	0.002987	0.010812	-2.7906
Leucine rich alpha-2-glycoprotein 1	0.003057	0.01089	-3.1017
Hydroxyacylglutathione hydrolase	0.003233	0.01134	3.858
Actin, cytoplasmic 1	0.00346	0.011951	2.8775
IGv domain-containing protein	0.003531	0.011955	-2.2352
Butyrophilin-like protein 10	0.003566	0.011955	5.3708
Alpha-1B-glycoprotein	0.003707	0.012248	-2.8105
Ankyrin 1	0.003938	0.012657	4.9012
Flotillin	0.003984	0.012657	3.5465
Histone H2A	0.004003	0.012657	3.1223
2-hydroxyacyl-CoA lyase 2	0.004053	0.012657	4.6036
Anaphylatoxin-like domain-containing protein	0.00418	0.012724	-3.7128
Urea transporter	0.004186	0.012724	2.8193
Hemopexin	0.004328	0.012795	-3.2164
Glutathione S-transferase	0.004368	0.012795	2.1579
CDGSH iron sulfur domain 2	0.004377	0.012795	9.1939
Paraoxonase	0.004817	0.013733	-1.7181
Sodium/nucleoside cotransporter	0.004819	0.013733	6.1177
Angiotensinogen	0.004985	0.013919	-3.0493
Pregnancy zone protein	0.005006	0.013919	-1.1252
Hemoglobin subunit epsilon	0.005263	0.014458	2.6545
Vitronectin	0.005453	0.014802	-1.9535
Proteasome 20S subunit beta 1	0.005676	0.015226	4.4394
Complement C3	0.005936	0.015619	-2.0673

Ceruloplasmin	0.005977	0.015619	-1.9196
Hemoglobin subunit epsilon	0.006028	0.015619	6.3535
C-type lectin domain family 3 member B	0.006402	0.016401	-1.4742
Plasma retinol-binding protein	0.006525	0.016529	-3.0961
Fibrinogen alpha chain (Fragment)	0.006698	0.016783	-2.3054
Insulin like growth factor binding protein acid labile subunit	0.006826	0.016825	-6.8115
Glutathione peroxidase	0.006863	0.016825	-7.361
Complement component C8 beta chain	0.007252	0.017591	-1.9383
Growth differentiation factor 5	0.007489	0.017872	-1.784
Phosphatidylethanolamine binding protein 1	0.007525	0.017872	2.4854
Biliverdin reductase B	0.00784	0.018427	5.8074
Inter-alpha-trypsin inhibitor heavy chain 1	0.007927	0.018443	-1.7812
Complement C4-A	0.008389	0.019319	-2.6162
Inter-alpha-trypsin inhibitor heavy chain 2	0.008602	0.01933	-2.8638
Dematin actin binding protein	0.008634	0.01933	3.9006
Choline transporter-like protein	0.008656	0.01933	4.0416
Serpin family D member 1	0.008736	0.01933	-3.5409
Ankyrin 1	0.008817	0.01933	3.9167
Solute carrier family 14 member 1	0.009832	0.021044	3.8001
Biliverdin reductase B	0.009853	0.021044	2.0445
Rh associated glycoprotein	0.00997	0.021044	5.5265
Adenylate kinase isoenzyme 1	0.0101	0.021044	3.0054
Haptoglobin	0.010154	0.021044	-2.6583
Receptor expression-enhancing protein	0.010258	0.021044	4.8507
Fibronectin	0.010337	0.021044	-2.2283
Carbonic anhydrase	0.010469	0.021044	4.2464
Transitional endoplasmic reticulum ATPase	0.010515	0.021044	3.6277
Inter-alpha-trypsin inhibitor heavy chain 4	0.010522	0.021044	-4.0815
Sorcin	0.010635	0.021085	2.7669
NAD(P)(+)-arginine ADP-ribosyltransferase	0.011201	0.022017	7.2834
Galectin	0.01155	0.022508	6.5974
Fructose-bisphosphate aldolase	0.011689	0.022585	3.2734
Tyrosine 3-monooxygenase/tryptophan 5-monooxygenase activation protein beta	0.011799	0.022607	4.7806
Ig-like domain-containing protein	0.011939	0.022683	-2.1859
Grancalcin	0.012061	0.022727	8.6818
VAMP associated protein B and C	0.012256	0.022905	3.8556
SH3 domain-binding glutamic acid-rich-like protein	0.013854	0.025523	5.2242
Apolipoprotein A-II	0.013881	0.025523	-2.2631
Albumin	0.014593	0.026582	-1.8506
Apolipoprotein E	0.01469	0.026582	-1.1085
Complement factor properdin	0.015209	0.027304	-2.754
Alpha hemoglobin stabilizing protein	0.015872	0.028272	4.9154
Proteasome subunit alpha type	0.01712	0.030045	5.1547
BAG cochaperone 2	0.017131	0.030045	3.4146
Lactotransferrin	0.017395	0.030275	4.9391
UBA domain containing 1	0.018498	0.031951	3.1731

Dematin actin binding protein	0.019053	0.032663	4.3788
Uncharacterized protein	0.019446	0.033087	-1.5592
Ig-like domain-containing protein	0.019658	0.0332	-2.2826
Proteasome 26S subunit, ATPase 3	0.020306	0.034042	5.3532
Uncharacterized protein	0.020778	0.03458	4.6776
Globin B2	0.021237	0.035086	4.5677
Erythroblast membrane associated protein	0.02205	0.036168	5.3197
Long-chain-fatty-acid--CoA ligase	0.023686	0.038574	4.0618
Hydroxymethylbilane synthase	0.025315	0.040935	5.1038
Kininogen 1	0.026014	0.041663	-2.5838
Ig-like domain-containing protein	0.026131	0.041663	-2.2679
Apolipoprotein C-III	0.026594	0.042107	-1.9908
Proteasome subunit alpha type	0.026794	0.042132	4.3508
Solute carrier family 2, facilitated glucose transporter member 3	0.027282	0.042605	2.6098
Small VCP interacting protein	0.028687	0.044494	4.9987
Annexin	0.02963	0.045646	1.9908
Proteasome subunit alpha type	0.030047	0.045729	5.3203
Microfibril associated protein 4	0.030273	0.045729	2.3321
Hyaluronan binding protein 2	0.030285	0.045729	-2.9952
Tropomyosin 1	0.031701	0.047552	6.7709
Protein disulfide-isomerase	0.032116	0.047859	2.5513
Rab GDP dissociation inhibitor	0.032999	0.048831	1.7042
VAMP associated protein A	0.033197	0.048831	3.5415
Rh blood group CcEe antigens	0.033854	0.049479	4.1455
Proteasome 26S subunit, non-ATPase 11	0.034241	0.049726	3.3729

Abbreviations- A1M ( $\alpha$ 1-microglobulin)/bikunin precursor] (AMBP), cluster of differentiation 58 (CD58), Adenosine triphosphate (ATP), coenzyme A (CoA), nicotinamide adenine dinucleotide phosphate (NADP), adenosine diphosphate (ADP), vesicle associated membrane protein (VAMP), SRC Homology 3 Domain (SH3), Bcl-2-associated athanogene (BAG), ubiquitin-activating enzyme (UBA), valosin containing protein (VCP), ras-associated binding (RAB), guanosine diphosphate (GDP)

**Supplementary Table 10.8. A list of all differential ( $p < 0.005$ ) following false discovery rate correction proteins identified as enriched in platelet-rich plasma compared to plasma.** The table includes raw p value, FDR corrected p value and log<sub>2</sub>(foldchange/FC) to inform direction of protein expression, as compared to plasma, n=3 samples used for analysis.

Protein	P Value	FDR	log <sub>2</sub> (FC)
26S proteasome non-ATPase regulatory subunit 1	0.002031	0.03885	3.2083
Matrin 3	0.002293	0.039983	2.6117
GTP-binding nuclear protein Ran	0.003551	0.048414	2.6255
Uncharacterized protein	0.001524	0.038751	-2.406
Signal transducer and activator of transcription	0.003274	0.048414	2.3176
26S proteasome regulatory subunit 6B	0.001658	0.038751	3.7539
Phosphatidylcholine transfer protein	0.000282	0.028406	5.0689
Histone deacetylase 6	0.000568	0.030122	5.182
Proteasome 26S subunit, ATPase 6	0.001895	0.038751	2.8163

Biliverdin reductase B	0.003756	0.048414	5.5237
Polypyrimidine tract-binding protein 1	0.001884	0.038751	3.6077
DAZ associated protein 1	0.000973	0.033987	8.3881
40S ribosomal protein S25	0.000236	0.028406	7.5683
Glucose-6-phosphate 1-dehydrogenase	0.003171	0.048414	3.2262
Glyceraldehyde-3-phosphate dehydrogenase	0.000699	0.030797	4.3577
Parkinsonism associated deglycase	0.003584	0.048414	2.7332
Histone-arginine methyltransferase CARM1	0.001297	0.036634	7.9292
Phosphoribosyl pyrophosphate synthetase associated protein 1	0.002246	0.039983	2.6682
Complement C8 alpha chain	0.003387	0.048414	-1.0459
Ribonuclease A family member 4	0.000164	0.028406	-2.7486
Phosphatidylcholine transfer protein	0.00061	0.030122	3.4672
Proteasome 26S subunit, ATPase 3	0.000287	0.028406	2.432
Alpha hemoglobin stabilizing protein	0.000194	0.028406	9.9874
Cell division control protein 42 homolog	0.001595	0.038751	2.0937
Coagulation factor X	0.001963	0.038803	-2.2009
Ring finger protein 123	0.000427	0.029048	2.2796
60S acidic ribosomal protein P2	0.000441	0.029048	3.6042
Proteasome 26S subunit, ATPase 5	9.49E-05	0.028406	3.7367
Proteasome 26S subunit, ATPase 1	0.002684	0.043014	2.9469
Oxysterol-binding protein	0.001891	0.038751	5.0816
Ubiquitin specific peptidase 35	0.002575	0.042409	3.0118
Tumor susceptibility 101	0.003299	0.048414	2.6198
Protein phosphatase 2 scaffold subunit Alpha	0.002409	0.040814	3.0906
Charged multivesicular body protein 2A	0.001276	0.036634	2.5382
Protein-ribulosamine 3-kinase	0.001734	0.038751	6.6101
Heterogeneous nuclear ribonucleoprotein H1	0.000819	0.032366	3.9535
DnaJ heat shock protein family (Hsp40) member B2	0.002221	0.039983	4.044
Non-specific serine/threonine protein kinase	0.000727	0.030797	6.7791
26S proteasome non-ATPase regulatory subunit 9	0.000974	0.033987	2.4584
Acidic nuclear phosphoprotein 32 family member A	0.001137	0.036634	6.193
Biliverdin reductase B	0.003714	0.048414	3.3871
Peroxiredoxin-1	0.00371	0.048414	3.4861
Karyopherin subunit beta 1	0.000432	0.029048	3.1274
Coagulation factor V	0.001598	0.038751	-1.7302
GCS light chain	0.000502	0.029755	3.5237

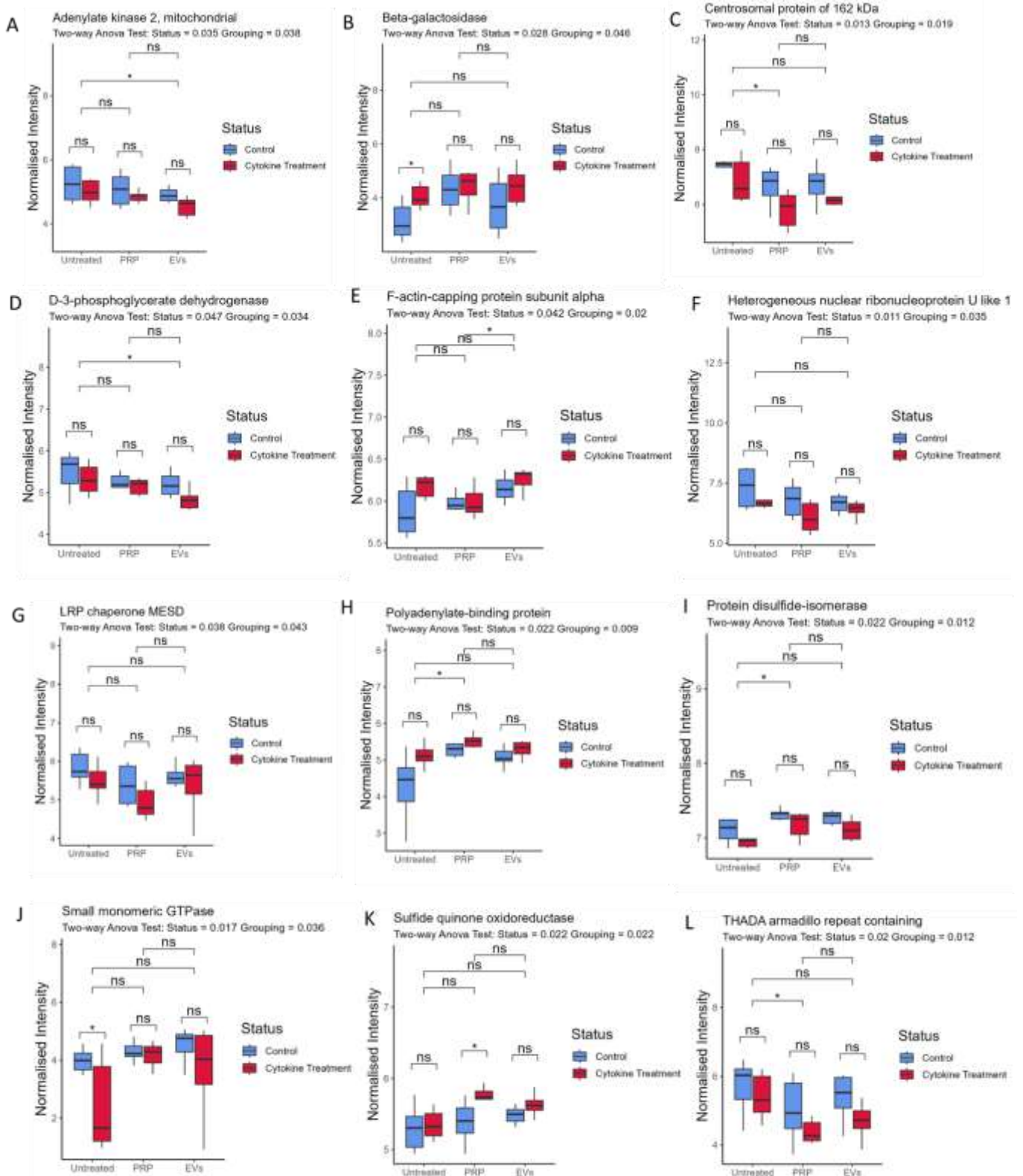
Abbreviations – Deleted in Zoospermia (DAZ), coactivator associated arginine methyltransferase (CARM1), deoxyribose nucleic acid (DNA), Adenosine triphosphate (ATP)

**Supplementary Table 10.9. A list of all 18 differential ( $p < 0.005$ ) proteins identified following two-way analysis of variance analysis and pairwise comparisons.** The included 18 proteins were identified as differential for both status (control or following cytokine stimulation) and grouping (treatment- no treatment, PRP or PRP-EVs). Raw P value and FDR corrected P value are shown.

Protein	Raw P Value		FDR	
	Status	Grouping	Status	Grouping

Adenylate kinase 2, mitochondrial	0.035	0.038	0.019988	0.154886
AHNAK nucleoprotein	7.19E-05	0.01	0.247373	0.254554
Beta-galactosidase	0.028	0.046	0.218243	0.271124
Centrosomal protein of 162 kDa	0.013	0.019	0.154886	0.189772
Collagen type I alpha 1 chain	4.63E-05	0.012	0.015446	0.154886
D-3-phosphoglycerate dehydrogenase	0.047	0.034	0.275074	0.243399
F-actin-capping protein subunit alpha	0.042	0.02	0.261403	0.192832
Heme oxygenase (biliverdin-producing)	0.002	0.004	0.116372	0.139
Heterogeneous nuclear ribonucleoprotein U like 1	0.011	0.035	0.154886	0.247373
LRP chaperone MESD	0.038	0.043	0.254554	0.264664
Polyadenylate-binding protein	0.022	0.009	0.195191	0.154886
Protein disulfide-isomerase	0.022	0.012	0.195191	0.154886
SAP domain containing ribonucleoprotein	0.021	0.023	0.195191	0.199813
Sequestosome 1	0.001	0.003	0.0834	0.116372
Small monomeric GTPase	0.017	0.036	0.181769	0.2502
Sulfide quinone oxidoreductase	0.022	0.022	0.195191	0.195191
THADA armadillo repeat containing	0.02	0.012	0.192832	0.154886
Translocon-associated protein subunit alpha	0.003	0.01	0.116372	0.154886

*Abbreviations – Neuroblast differentiation-associated protein (AHNAK), low density lipoprotein receptor-related protein (LRP), Serum amyloid P component (SAP), guanosine triphosphate (GTP), thyroid adenoma associated (THADA)*



**Supplementary Figure 10.5. Differential abundant proteins following cytokine stimulation of equine tenocytes and the effect of no treatment, platelet-rich plasma and platelet-rich plasma derived extracellular vesicle treatment.** As identified by a two-way ANOVA and post hoc Tukey test. A) Adenylate kinase 2, mitochondrial, (B) beta galactosidase, (C) centrosomal protein of 162 kDa, (D) D3-phosphoglycerate dehydrogenase, (E) f-actin capping protein subunit alpha (F) heterogenous nuclear ribonucleoprotein U like 1, (G) LRP chaperone MESD, (H) polyadenylate – binding protein, (I) protein

disulphide - isomerase, (J) small monomeric GTPase, (K) Sulphide quinone oxidoreductase and (L) THADA armadillo repeat containing .Significance is denoted by \*( $p < 0.05$ ), \*\* ( $p < 0.01$ ), \*\*\* ( $p < 0.001$ ), \*\*\*\* ( $p < 0.0001$ ).



# 11. Appendices

## A.11.1 Appendix 1: An Evaluation of Current Preventative Measures Used in Equine Practice to Maintain Distal Forelimb Functionality: A Mini Review

Emily J Clarke<sup>1</sup>, Alex Gillen<sup>2</sup>, Agnieszka Turlo<sup>1</sup>, Mandy J Peffers<sup>1</sup>

Institute of Life Course and Medical Sciences, Musculoskeletal and Ageing Science, William Henry Duncan Building, 6 West Derby Street, Liverpool, L7 8TX, UK.<sup>1</sup>

Philip Leverhulme Equine Hospital, Institute of Veterinary Science, University of Liverpool, Chester High Road, Neston, CH64 7TE.<sup>2</sup>

### **Author Contact Information:**

Corresponding author: Emily J Clarke ([eclarke@liverpool.ac.uk](mailto:eclarke@liverpool.ac.uk))

Mandy J Peffers ([peffs@liverpool.ac.uk](mailto:peffs@liverpool.ac.uk))

Agnieszka Turlo ([A.Turlo@liverpool.ac.uk](mailto:A.Turlo@liverpool.ac.uk))

Alex Gillen ([alexandra.gillen@liverpool.ac.uk](mailto:alexandra.gillen@liverpool.ac.uk))

**Keywords:** Equine, Joint, Distal limb, Compressive bandaging, Nutraceuticals, Therapeutic shoeing, Hoof trimming, Conformation

Published in *Frontiers in Veterinary Science* 2<sup>nd</sup> of November 2021. <https://doi.org/10.3389/fvets.2021.758970>

---

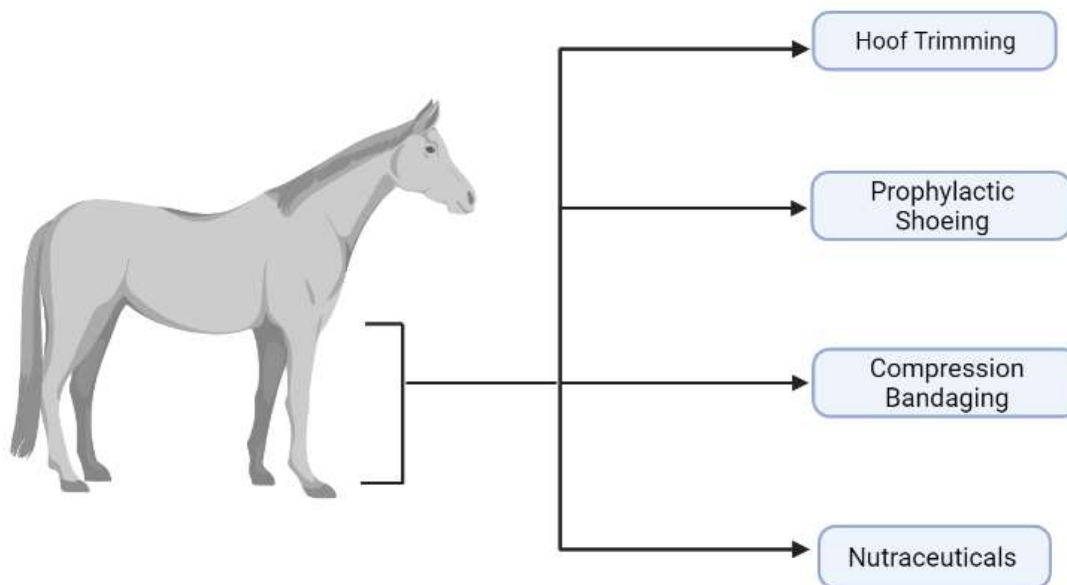
### **A.11.1.1. Abstract**

Horses are used in a variety of equestrian disciplines predisposing them to musculoskeletal injury or disease including osteoarthritis and tendinopathy. As a result, a number of preventative measures are used within equine medicine and husbandry, ranging from therapeutic shoeing to the use of nutraceuticals. Despite their popularity and routine use evidence base and clinical outcomes are variable, bringing into question the efficacy of these prophylactic measures. In recent years a small number of studies have been performed examining the effect of specific strategies in order to quantify the preventative and protective claims such modalities have on joint and forelimb health. Few have robustly demonstrated a capacity to protect the limb by reducing inflammation, or promoting regenerative pathways. The resounding theme that emerges in current research is the need for longitudinal studies to inform scientific conclusions surrounding single and multi-modal use.

Furthermore, there is a requirement to prioritise evidence-based medicine to inform optimal clinical practice.

#### **A.11.1.2 Introduction**

The equine musculoskeletal system has significant demands placed on it (Murray *et al.*, 2004), specifically articular structures and supporting tissues, leaving it vulnerable to injury and disease development that results in pain, lameness, and reduced mobility. Consequently, numerous preventative modalities are being used in an attempt to maintain optimum athletic performance and potentially reduce the onset of musculoskeletal disease. The forelimb incorporates the carpus, a compound joint, composed of three articulations; the antebrachio-carpal joint; the middle carpal joint, and the carpometacarpal joint, commonly referred to as the carpal joint in a research setting (Bertone, 2002). Soft tissue components include intercarpal ligaments, collateral ligaments, a fibrous joint capsule, and the palmar carpal ligament. The metacarpophalangeal joint is comprised of four bones; the third metacarpal bone, the proximal phalanx, and the paired proximal sesamoid bones (Bastiani *et al.*, 2014). As the carpal and metacarpophalangeal regions are imperative for equine locomotion, they can be highly susceptible to injury and disease, most notably tendinopathies and osteoarthritis. Tendon injury is a common impairment that can compromise the stability of the joint capsule, which can result in excessive wear due to uneven force distribution. When the tendon heals, it becomes biomechanically inferior to the original structure, increasing the likelihood of re-injury. Osteoarthritis (OA) is a common disease of the joint, and is considered to be responsible for up to 60% of all lameness cases (McIlwraith, Frisbie and Kawcak, 2012a). Osteoarthritis is a progressive degenerative pathology, characterised by an imbalance in metabolic activity, resulting in articular degradation, osteophyte formation, synovitis and subchondral bone sclerosis (Anderson, Phelan, Foddy, *et al.*, 2020a; Clarke, Anderson and Peffers, 2021a). Various preventative modalities are often used, including but not limited to foot trimming, therapeutic shoeing, compression bandaging, and nutraceuticals, in order to minimise damage to the associated structures (Figure A.2.6). This 'mini' review aims to evaluate the scientific evidence from the past ten years surrounding preventative measures used in equine practice to maintain distal forelimb functionality.



**Figure A.11.1. A visual summary of some the prevention modalities used in an attempt to maintain equine distal forelimb functionality.** Created with BioRender.com.

### A.11.1.3. Hoof Trimming

Equine hoof trimming aims to maintain a healthy, functional hoof and prevent lameness, supporting articular structures and subsequent soft tissues within the limb (Leśniak *et al.*, 2017). There are multiple hoof trimming strategies developed based on the dynamic-functional, natural-individual or static-geometric reference (Hagen *et al.*, 2018).

A study by Maeder *et al* (Maeder, Wuttke and Vogel, 2017) described, using a pressure measurement system, that initial contact and breakover showed marked inter-individual variability amongst the 70 warmblood horses included in the study. It was found that initial contact and centre of force were the most sensitive parameters affected by foot trimming, regardless of trimming practice, and that no significant long-term effects were concluded. The findings were thought to be determined by limb and body conformation, however, no significant long-term effects were concluded (Maeder, Wuttke and Vogel, 2017). In addition, Lesniak *et al* (Leśniak *et al.*, 2017) conducted a study that explored the linear and angular hoof variations pre- and post-farriery. Lesniak *et al* (Leśniak *et al.*, 2017) used 17 hoof and distal limb measurements from lateromedial and dorsopalmar digital photographs from 26 horses. They found that trimming practices resulting in a reduction of the dorsal wall and weight bearing resulted in increased vertical orientation of the hoof, improving dorsopalmar alignment (Leśniak *et al.*, 2017). This ultimately resulted in the suggestion of regular 4-6-week farriery appointments to provide optimal protection to palmar limb structures, such as the deep digital flexor tendon and

metacarpophalangeal joint (Leśniak *et al.*, 2017). However, this recommendation was formed despite the lack of significant results, and large inter-individual variation (Leśniak *et al.*, 2017).

Many factors may affect hoof growth and development, which may subsequently affect other areas of the distal limb, including the joints of the forelimb. These factors include: breed, diet, disease, height, pasture quality and lameness. Moeller *et al.* (Moeller *et al.*, 2019) examined the *in vitro* effect of hoof wall thinning, leading to increased deformability and resulting in damage to laminar tissue. This was undertaken using paired cadaver forelimbs of 12 horses. Each pair had the hoof wall from a single limb thinned by 25% (Moeller *et al.*, 2019). The contralateral hoof was used as a control within the study. Trimming the hoof was found to result in deformability of the entire hoof capsule, postulated to reduce damage to suspensory apparatus in the distal limb, such as tendons, ligaments and joints (Moeller *et al.*, 2019). In addition, there was significant disruption to suspensory apparatus of the distal phalanx in untrimmed hooves. This suggested a thinning of the hoof wall can decrease disruption to laminar tissue, supportive of hoof trimming as a prophylactic measure (Moeller *et al.*, 2019). However, it should be noted that this study was conducted *in vitro* and not *in vivo*. Therefore, the effect of the sole and frog have not been included. These structures may also be overloaded, and have a significant effect on the health and functionality of the distal limb and its joints (Moeller *et al.*, 2019). As such, the study does not reflect the physiology of live horses, therefore results may be affected by variables such as body and limb conformation, hoof shape, tension in tendons and ligaments, blood flow of structures, and speed of locomotion.

#### **A.11.1.4. Prophylactic Shoeing**

Prophylactic shoeing, or farriery, is often used in the management or prevention of orthopaedic conditions, steeped in the practical application of anatomical biomechanics. It is suggested that such practices can displace concussion, alter the locomotive interactions of the hoof with the ground, distribute forces more evenly through the distal limb, and stabilise movement within the distal interphalangeal joint (Wilson, McKenzie and Duesterdieck-Zellmer, 2018). Historically, this preventative modality has been used in practice, and recommended by farriers and clinicians through empirical evidence and tradition. However, very few controlled scientific studies have been conducted to rigorously ascertain the therapeutic efficacy of such strategy (Belknap and Geor, 2017). Multiple shoeing methods have been conceived, such as z-bar shoes (open area of shoe is intended to reduce weight bearing on the palmar area of the hoof, reducing trauma and promoting healing) (Chanda *et al.*, 2020), egg bar shoes (increase the weight-bearing surface and create a larger area of posterior support for the foot and leg) (Stutz *et al.*, 2018), toe wedges and heel wedges (used on the rear palmar aspect of a collapsed heel region of a hoof wall) (Hagen *et al.*, 2018). As such these interventions are

postulated to promote distal limb health, through supporting the joints of the lower limb and reducing unwanted biomechanical forces, applied by the farrier if adverse conformational traits are identified.

Scientific studies conducted in relation to prophylactic shoeing are limited in number. Hagen *et al* (2018) examined the forelimbs of 30 horses when barefoot, equipped with toe wedges and heel wedges at various angles, in order to examine the effect of hoof angulation on the dorsal metacarpophalangeal joint, deep digital flexor tendon, and superficial digital flexor tendon. It was found that the application of a toe wedge or heel wedge significantly affected the dorsal metacarpophalangeal joint. Despite this it was noted that individual toe conformation and the cross-sectional area of flexor tendons were likely to influence any effect seen on hoof angulation and the dorsal aspect of the metacarpophalangeal joint (Hagen *et al.*, 2018). Thus, any significant effects seen as a result of remedial shoeing must be considered with respect to individual toe conformation. However, it has not been quantified in relation to pathological state, and the effect this may have on the distal joints. In addition, there is no evidence demonstrating the effects of long-term angulation (Hagen *et al.*, 2018). Stutz *et al* (Stutz *et al.*, 2018) explored the effect of four shoeing methods (flat open shoe, rockered bar shoe, egg bar shoe, and unshod) on gait, measuring forelimb 'kinematic variables using an inertial measurement unit system'. It was found that 75% of horses showed a significant change in measured output in the presence of shoes (Stutz *et al.*, 2018). This was irrespective of shoe type, and independent of shoe geometry. It was also found that there were no differences between shoes when quantifying the non-podal kinematic variables investigated, notably in agreement with previously documented studies (Stutz *et al.*, 2018). Studies relating to therapeutic shoeing require further investigation, as it needs to be determined if therapeutic shoeing has a quantifiable benefit. Studies have previously found shod versus unshod can have a significant effect on the limb, however, significant effects have not been shown with different types of shoe.

#### **A.11.1.5. Compression Bandaging**

Compression bandages are used regularly within the veterinary profession, be it for the treatment of surgical or traumatic wounds, for protection of the distal limb, and reduction of fluid accumulation associated with inflammation, such as distal limb oedema. Compression bandaging relies on the concept of the venous muscle pump (Hettrick, 2009). Here hydrostatic pressure is created in the peripheral circulatory system as a result of the cardiovascular action of the heart. Various other structures of the circulatory system, such as the arteries and arterioles also contribute towards the pressure (Hettrick, 2009). These systems are subsequently affected by the contraction and relaxation of the musculature in the equine distal limb. Effectiveness of this technique is highly dependent on

the interface pressure applied, physical activity, and elastic properties of the bandaging material (Ruznan *et al.*, 2020).

Canada *et al* (Canada *et al.*, 2017) measured the effect of distal limb sub-bandage pressure over 96 hours in 8 horses. A distal limb compression bandage was used with the inclusion of cotton roll compressed with brown gauze and elastic layers. Alternatively, a polo wrap was also used in conjunction with a pillow pad. They found that the polo wraps effectiveness in reducing fluid accumulation was dependent on anatomical location but not time. It was also shown that pressure distribution was not uniform, and it was demonstrated that the polo wraps-maintained pressure for 24 hours, whereas the distal limb compression bandage maintained high pressures for 96 hours, without the need for reapplication. It was highlighted that, with regard to the application of compression bandages, there was variability in the technical skills the owners had. However, this study was conducted on healthy horses, thus the effects of compression bandaging in injured horses as well as its prophylactic value remain unknown. In another study by the same group, an observational study was undertaken on 8 healthy adult horses using six bandaging techniques. These were the distal limb compression bandage, double layer bandage, inner sanctum bandage, carpal compression bandage, tarsal compression bandage, and adhesive elastic carpal bandage. During the study, sub-bandage pressures were measured using a picopress compression system. It was found that distal limb compression and inner sanctum bandaging resulted in significantly higher pressures compared with the distal limb compression bandage. Additionally, pressure was found to decrease significantly after walking with the use of a carpal compression bandage (Canada *et al.*, 2018). Ultimately, the study concluded that clinician preference and clinical reasoning should guide bandaging protocols for the equine limb, emphasising that the adequate pressure ranges required to reduce oedema are still to be determined (Canada *et al.*, 2018). As a result, further work must look to quantify the most optimal pressure ranges to manage distal limb oedema, as well as the most appropriate duration of treatment, while determining the clinical efficacy.

#### **A.11.1.6. Nutraceuticals**

The nutraceutical industry is a growing area of preventive strategy in all companion animals, including the horse. Horse owners frequently supplement their horse's diets with various products in order to optimise equine health. A nutraceutical product can be defined as a substance which has a physiological benefit on the body, and that may provide prevention against chronic disease, such as is the case of management of equine osteoarthritis (Nasri *et al.*, 2014). They often provide what is perceived as additional vitamins, minerals and electrolytes. However, perceptions surrounding their use and scientific evidence of their benefit are varied, with many companies claiming to enhance

performance or alleviate health issues despite no significant evidence-based studies to support these claims. In addition, such modalities are not subject to robust regulations, and many are not subject to tests for safety or efficacy. Murray *et al* (Murray, Hanna and Hastie, 2018) conducted a survey of owners and professionals associated with the Irish equine industry. The survey had 134 responses (70% non-professionals and 30% professionals). Most notably 98% of professionals included a supplement in their horse's diet, whereas 86% of non-professionals gave a supplement (Murray, Hanna and Hastie, 2018). Joint supplements were the most commonly used supplement by all survey participants. Additionally, 53% of respondents sought advice from a feed merchant, followed by their veterinarian (46%) (Murray, Hanna and Hastie, 2018). Ninety-three percent of all respondents thought that nutraceuticals, such as feed supplements, had to meet legal standards, with 92% believing that supplements were always tested on horses before going to market.

It is often reported that the earliest recognisable feature of joint degeneration is loss of glycosaminoglycans from articular cartilage. As such, joint supplements are often used to replace these and are thought to be chondroprotective. These include chondroitin sulphate, glucosamine and hyaluronan. Chondroitin sulphate has reportedly resulted in the inhibition of degradative enzymes, and an increase in anti-inflammatory activity (Wright, 2010). Glucosamine is an amino-monosaccharide and a precursor of the disaccharide units of articular cartilage glycosaminoglycans, Chondrocytes synthesise glucosamine from glucose but when glucosamine is available it is preferentially incorporated into cartilage (Wright, 2010). Hyaluronan is a key component of synovial tissue and synovial fluid, functionally serving as a lubricant and shock absorber (Li *et al.*, 2019). These are often constituent components of supplements available for equines, and are often used due to their potential mechanisms of prevention.

Much *et al* (Much *et al.*, 2020) evaluated the use of oral joint supplementation on gait kinematics and biomarkers of cartilage metabolism. Twenty horses were used in the study, stratified by age, sex, bodyweight and lameness scores (Much *et al.*, 2020). Horses were randomly assigned one of two dietary treatments, a 100g placebo, or 100g of joint supplement containing glucosamine, chondroitin sulphate, hyaluronic acid, methylsulfonylmethane, turmeric, resveratrol, collagen, silica, and boron. It was found that horses treated with the supplement had an increased range of motion in the hock at walk and trot compared with control groups. This was suggestive of the hock being sensitive to biomechanical change due to supplementation (Much *et al.*, 2020). However, no change was observed between groups in serum and plasma biomarkers including a lack of alteration in the concentration of collagen metabolites and no change in systemic inflammation during the 28-day study period (Much *et al.*, 2020). Further to this, Gugliandolo *et al* (Gugliandolo *et al.*, 2020) investigated oral supplementation with ultra-micronized palmitoylethanolamide for joint disease and lameness

management in four jumping horses. Four jumping horses were evaluated for non-responsive lameness, which resulted in them being withdrawn from show jumping competitions (Gugliandolo *et al.*, 2020). Lameness was determined with the use of radiographic assessment, flexion tests and lameness evaluation in accordance with the American Association of Equine Practitioners (Gugliandolo *et al.*, 2020). After 4 months of treatment it was determined that all horses showed remissions of lameness, resulting in the reintroduction to work and show jumping competitions, without disease recurrence (Gugliandolo *et al.*, 2020). However, it should be noted that there was no appropriate control for this study and as such makes the study evidence weak.

Van de Water *et al* (Van De Water *et al.*, 2016) measured the preventative effects of two nutraceuticals on experimentally induced synovitis in horses. Twenty-four standardbred horses were allocated a supplement, either: multi ingredient (28 days), collagen hydrolysate (60 days), meloxicam (4 days) or a placebo (60 days). Synovitis was induced by intra-articular injection of 0.5ng of lipopolysaccharide into the right intercarpal joint (Van De Water *et al.*, 2016). Subsequently blood and synovial fluid samples were analysed. It was found that both nutraceutical groups resulted in significantly lower synovial fluid total protein, total nucleated cell count and prostaglandin E2 in comparison with placebo. However, no statistical differences were observed between treatment groups for interleukin 6, matrix metalloproteinases and glycosaminoglycans. The study concluded that the use of nutraceuticals could reduce inflammation in a model of joint synovitis. However, the nutraceuticals used did not alter cartilage turnover, resulting in biomarkers associated with the development of joint diseases remaining elevated, and subsequently non-responsive. Results of the studies described above lead to the question: should nutraceuticals be subject to stricter regulations, research and efficacy standards prior to being taken to market, in order to substantiate the claims made by their manufacturers.

#### **A.11.1.7. Conclusion**

There are multiple preventative modalities used in equine veterinary medicine that aim to maintain the functionality of the forelimb and joints. The lack of robust scientific studies is evident, with limited published literature within the last ten years and often contradictory findings, despite the increasing popularity of the discussed modalities. Amongst the papers that have been published distinct themes emerge, such as the effect of individual variability and the number of confounding variables that may affect the efficacy of such modalities, such as: breed, age, conformation, sex, and owner compliance. The importance of robust experimental design is emphasised, including a longitudinal approach to quantify the prevention of disease or injury. This review highlights the importance of evidence-based medicine, and its place in driving forward veterinary practice standards. It has become apparent that



in many cases joint injury and disease cannot be effectively prevented, substantiating the need for research into disease pathophysiology and potential therapeutics. That would result in better clinical outcomes than those that currently exist, promoting recovery and enabling a complete return to work, fundamentally prioritising animal health and welfare.

---

## References

- Abraham, A. *et al.* (2019) 'Targeting the NF- $\kappa$ B signaling pathway in chronic tendon disease', *Science Translational Medicine*, 11(481). doi: 10.1126/scitranslmed.aav4319.Targeting.
- Afara, I. O. *et al.* (2017) 'Monitoring osteoarthritis progression using near infrared (NIR) spectroscopy', *Scientific Reports*, 7(1), pp. 1–9. doi: 10.1038/s41598-017-11844-3.
- Afara, I. O. *et al.* (2021) 'Characterization of connective tissues using near-infrared spectroscopy and imaging', *Nature Protocols*, 16(2), pp. 1297–1329. doi: 10.1038/s41596-020-00468-z.
- Ai, M. *et al.* (2022) 'Human mesenchymal stem cells and derived extracellular vesicles reduce sensory neuron hyperexcitability and pain-related behaviors in a mouse model of osteoarthritis', pp. 1–37.
- Ajalik, R. E. *et al.* (2022) 'Human Organ-on-a-Chip Microphysiological Systems to Model Musculoskeletal Pathologies and Accelerate Therapeutic Discovery', *Frontiers in Bioengineering and Biotechnology*, 10(March), pp. 1–23. doi: 10.3389/fbioe.2022.846230.
- Akbarzadeh, S. *et al.* (2021) 'Allogeneic Platelet-Rich Plasma: Is It Safe and Effective for Wound Repair?', *European Surgical Research*, 62(1), pp. 1–9. doi: 10.1159/000514223.
- Alaamery, M. *et al.* (2021) 'Role of sphingolipid metabolism in neurodegeneration', *Journal of Neurochemistry*, 158(1), pp. 25–35. doi: 10.1111/jnc.15044.
- Allen, K. D., Thoma, L. M. and Golightly, Y. M. (2022) 'Epidemiology of osteoarthritis', *Osteoarthritis and Cartilage*, 30(2), pp. 184–195. doi: 10.1016/j.joca.2021.04.020.
- Allen, M. J. *et al.* (2017) 'Ethical use of animal models in musculoskeletal research', *Journal of Orthopaedic Research*, 35(4), pp. 740–751. doi: 10.1002/jor.23485.
- Almiñana, C. *et al.* (2021) 'Isolation and characterization of equine uterine extracellular vesicles: A comparative methodological study', *International Journal of Molecular Sciences*, 22(2), pp. 1–31. doi: 10.3390/ijms22020979.
- Ambartsumian, N., Klingelhöfer, J. and Grigorian, M. (2019) 'The Multifaceted S100A4 Protein in Cancer and Inflammation', in Heizmann, C. W. (ed.) *Calcium-Binding Proteins of the EF-Hand Superfamily: From Basics to Medical Applications*. New York, NY: Springer (Methods in Molecular Biology), pp. 339–365. Available at: [https://doi.org/10.1007/978-1-4939-9030-6\\_22](https://doi.org/10.1007/978-1-4939-9030-6_22).
- Andersen *et al.* (2022) 'Integrin  $\alpha$ 10 $\beta$ 1-selected equine mesenchymal stem cells reduce lameness

and joint degradation and increase immunomodulatory factors interleukin-10 and prostaglandin E2 in experimental post-traumatic osteoarthritis’.

Andersen, C., Jacobsen, S., *et al.* (2022a) ‘A detailed macroscopic scoring system for experimental post-traumatic Osteoarthritis in the equine middle carpal joint’, *BMC Research Notes*, 15(1), pp. 1–7. doi: 10.1186/s13104-022-06116-x.

Andersen, C., Jacobsen, S., *et al.* (2022b) ‘A detailed macroscopic scoring system for experimental post-traumatic Osteoarthritis in the equine middle carpal joint’, *BMC Research Notes*, 15(1), p. 226. doi: 10.1186/s13104-022-06116-x.

Andersen, C., Uvebrant, K., *et al.* (2022) ‘Human integrin  $\alpha 10\beta 1$ -selected mesenchymal stem cells home to cartilage defects in the rabbit knee and assume a chondrocyte-like phenotype’, *Stem Cell Research and Therapy*, 13(1), pp. 1–15. doi: 10.1186/s13287-022-02884-2.

Anderson, Phelan, Foddy, *et al.* (2020a) ‘Ex Vivo Equine Cartilage Explant Osteoarthritis Model: A Metabolomics and Proteomics Study’, *ACS Publications*, 19(9), pp. 3652–3667. doi: 10.1021/acs.jproteome.0c00143.

Anderson, Phelan, Foddy, *et al.* (2020b) ‘Ex Vivo Equine Cartilage Explant Osteoarthritis Model: A Metabolomics and Proteomics Study’, *ACS Publications*, 19(9), pp. 3652–3667. doi: 10.1021/acs.jproteome.0c00143.

Anderson, Phelan, Rubio-Martinez, *et al.* (2020) ‘Optimization of Synovial Fluid Collection and Processing for NMR Metabolomics and LC-MS/MS Proteomics’, *Journal of Proteome Research*, 19(7), pp. 2585–2597. doi: 10.1021/acs.jproteome.0c00035.

Anderson, J. *et al.* (2019) ‘The synovial fluid proteome differentiates between septic and nonseptic articular pathologies’, *Journal of Proteomics*. Available at: <https://www.sciencedirect.com/science/article/pii/S1874391919301332> (Accessed: 25 May 2021).

Anderson, J. *et al.* (2023) ‘Temporal Proteomic Landscape Of Plasma And Synovial Fluid Derived Extracellular Vesicles Using An Experimental Model Of Equine Osteoarthritis’, *International Journal of Molecular Sciences*, 31, p. S345. doi: 10.1016/j.joca.2023.01.386.

Anderson, J. R. *et al.* (2018) ‘Synovial Fluid Metabolites Differentiate between Septic and Nonseptic Joint Pathologies’, *Journal of Proteome Research*, 17(8), pp. 2735–2743. doi: 10.1021/acs.jproteome.8b00190.

Anderson, J. R. *et al.* (2022) ‘Small non-coding RNA landscape of extracellular vesicles from a post-traumatic model of equine osteoarthritis’, *Frontiers in Veterinary Science*, (1), p. 2022.03.10.483752.

doi: 10.1101/2022.03.10.483752.

Andia, I., Atilano, L. and Maffulli, N. (2021) 'Moving toward targeting the right phenotype with the right platelet-rich plasma (PRP) formulation for knee osteoarthritis', *Therapeutic Advances in Musculoskeletal Disease*, 13, pp. 1–9. doi: 10.1177/1759720X211004336.

Andreu, Z. and Yáñez-Mó, M. (2014) 'Tetraspanins in extracellular vesicle formation and function', *Frontiers in Immunology*, 5(SEP). doi: 10.3389/FIMMU.2014.00442/FULL.

Anjo, S. I., Santa, C. and Manadas, B. (2017) 'SWATH-MS as a tool for biomarker discovery: From basic research to clinical applications', *Proteomics*, 17(3–4). doi: 10.1002/pmic.201600278.

Arévalo-Turrubiarte, M. *et al.* (2021) 'Extracellular vesicles from equine mesenchymal stem cells decrease inflammation markers in chondrocytes in vitro', *Equine Veterinary Journal*, (April), pp. 1–11. doi: 10.1111/evj.13537.

Arévalo-Turrubiarte, M. *et al.* (2021) 'Extracellular vesicles from equine mesenchymal stem cells decrease inflammation markers in chondrocytes in vitro', *Equine Veterinary Journal*, (October), pp. 1–11. doi: 10.1111/evj.13537.

Arkesteijn, G. J. A. *et al.* (2020) 'Improved Flow Cytometric Light Scatter Detection of Submicron-Sized Particles by Reduction of Optical Background Signals', *Cytometry Part A*, 97(6), pp. 610–619. doi: 10.1002/cyto.a.24036.

Arrazola Sastre, A. *et al.* (2020) 'Small GTPases of the Ras and Rho Families Switch on/off Signaling Pathways in Neurodegenerative Diseases', *International Journal of Molecular Sciences*, 21(17), p. 6312. doi: 10.3390/ijms21176312.

Arzi, B. *et al.* (2021) 'Cell Therapy in Veterinary Medicine as a Proof-of-Concept for Human Therapies: Perspectives From the North American Veterinary Regenerative Medicine Association', *Frontiers in Veterinary Science*, 8(November), pp. 1–9. doi: 10.3389/fvets.2021.779109.

Aspden, R. M. and Saunders, F. R. (2019) 'Osteoarthritis as an organ disease: From the cradle to the grave', *European Cells and Materials*, 37, pp. 74–87. doi: 10.22203/eCM.v037a06.

Assirelli, E. *et al.* (2020) 'Complement Expression and Activation in Osteoarthritis Joint Compartments', *Frontiers in Immunology*, 11(October), pp. 1–10. doi: 10.3389/fimmu.2020.535010.

Atkinson, F. *et al.* (2020) 'Cyclical strain improves artificial equine tendon constructs in vitro', *Journal of Tissue Engineering and Regenerative Medicine*, 14(5), pp. 690–700. doi: 10.1002/term.3030.

Auber, M. and Svenningsen, P. (2022) 'An estimate of extracellular vesicle secretion rates of human

- blood cells', *Journal of Extracellular Biology*, 1(6). doi: 10.1002/jex2.46.
- Bae, J.-W. *et al.* (2022) 'Ras-related proteins (Rab) play significant roles in sperm motility and capacitation status', *Reproductive Biology*, 22(2), p. 100617. doi: 10.1016/j.repbio.2022.100617.
- Baker, M. J. *et al.* (2014) 'Using Fourier transform IR spectroscopy to analyze biological materials', *Nature Protocols*, 9(8), pp. 1771–1791. doi: 10.1038/nprot.2014.110.
- van Balkom, B. W. M. *et al.* (2019) 'Proteomic Signature of Mesenchymal Stromal Cell-Derived Small Extracellular Vesicles', *Proteomics*, 19(1–2), pp. 1–9. doi: 10.1002/pmic.201800163.
- Banas, A. M. *et al.* (2021) 'Comparing infrared spectroscopic methods for the characterization of Plasmodium falciparum-infected human erythrocytes', *Communications Chemistry*, 4(1), pp. 1–12. doi: 10.1038/s42004-021-00567-2.
- Banh, L. *et al.* (2022) 'Advances in organ-on-a-chip systems for modelling joint tissue and osteoarthritic diseases', *Osteoarthritis and Cartilage*, 30(8), pp. 1050–1061. doi: 10.1016/j.joca.2022.03.012.
- Barberini, D. J. *et al.* (2014) 'Equine mesenchymal stem cells from bone marrow, adipose tissue and umbilical cord: Immunophenotypic characterization and differentiation potential', *Stem Cell Research and Therapy*, 5(1), pp. 1–11. doi: 10.1186/scrt414.
- Barrachina, L. *et al.* (2018) 'Assessment of effectiveness and safety of repeat administration of proinflammatory primed allogeneic mesenchymal stem cells in an equine model of chemically induced osteoarthritis', pp. 1–17.
- Barry, F. (2019) 'MSC Therapy for Osteoarthritis: An Unfinished Story', *Journal of Orthopaedic Research*. John Wiley and Sons Inc., pp. 1229–1235. doi: 10.1002/jor.24343.
- Barth, A. (2007) 'Infrared spectroscopy of proteins', *Biochimica et Biophysica Acta - Bioenergetics*, 1767(9), pp. 1073–1101. doi: 10.1016/j.bbabi.2007.06.004.
- Bastiani, G. De *et al.* (2014) 'Association of ultrasound and anatomopathologic findings of equine metacarpophalangeal lesions', *Journal of Equine Veterinary Science*, 34(10), pp. 1218–1225. doi: <http://dx.doi.org/10.1016/j.jevs.2014.08.006>.
- Batson, E. L. *et al.* (2003) 'Are the material properties and matrix composition of equine flexor and extensor tendons determined by their functions?', *Equine Veterinary Journal*, 35(3), pp. 314–318. doi: 10.2746/042516403776148327.
- Battistelli, M. and Falcieri, E. (2020) 'Apoptotic bodies: Particular extracellular vesicles involved in

intercellular communication', *Biology*, 9(1). doi: 10.3390/biology9010021.

Beerts, C. *et al.* (2017) 'Tenogenically induced allogeneic peripheral blood mesenchymal stem cells in allogeneic platelet-rich plasma: 2-year follow-up after tendon or ligament treatment in horses', *Frontiers in Veterinary Science*, 4(SEP). doi: 10.3389/fvets.2017.00158.

Beier, F. and Loeser, R. F. (2010) 'Biology and pathology of rho GTPase, PI-3 kinase-Akt, and MAP kinase signaling pathways in chondrocytes', *Journal of Cellular Biochemistry*, 110(3), pp. 573–580. doi: 10.1002/jcb.22604.

Bein, A. *et al.* (2018) 'Microfluidic Organ-on-a-Chip Models of Human Intestine', *Cmgh*, 5(4), pp. 659–668. doi: 10.1016/j.jcmgh.2017.12.010.

Belknap and Geor (2017) 'Treatment of Laminitis: Digital Support and Stabilization of the Distal Phalanx Therapeutic Shoes: Application of Principles', pp. 341–353.

Benton, H. P., Want, E. J. and Ebbels, T. M. D. (2010) 'Correction of mass calibration gaps in liquid chromatography–mass spectrometry metabolomics data', *Bioinformatics*, 26(19), pp. 2488–2489. doi: 10.1093/bioinformatics/btq441.

Bernimoulin, M. *et al.* (2009) 'Differential stimulation of monocytic cells results in distinct populations of microparticles', *Journal of thrombosis and haemostasis: JTH*, 7(6), pp. 1019–1028. doi: 10.1111/j.1538-7836.2009.03434.x.

Bersini, S. *et al.* (2016) 'Engineered miniaturized models of musculoskeletal diseases', *Drug Discovery Today*, 21(9), pp. 1429–1436. doi: 10.1016/j.drudis.2016.04.015.

Bertolino, G. M. *et al.* (2023) 'Therapeutic potential in rheumatic diseases of extracellular vesicles derived from mesenchymal stromal cells', *Nature Reviews Rheumatology*. doi: 10.1038/s41584-023-01010-7.

Bertone, A. . (2002) 'The carpus. Adam's Lameness in Horses', in *Adam's Lameness in Horses*.

Available at:

[https://scholar.google.com/scholar?hl=en&as\\_sdt=0%2C5&q=Bertone%2C+A.L.%2C+2002.+The+carpus.+Adam%27s+Lameness+in+Horses+Fifth+Edition.+Philadelphia.+&btnG=](https://scholar.google.com/scholar?hl=en&as_sdt=0%2C5&q=Bertone%2C+A.L.%2C+2002.+The+carpus.+Adam%27s+Lameness+in+Horses+Fifth+Edition.+Philadelphia.+&btnG=).

Bertoni, L. *et al.* (2020) 'An experimentally induced osteoarthritis model in horses performed on both metacarpophalangeal and metatarsophalangeal joints: technical, clinical, imaging, biochemical, macroscopic and microscopic characterization', *PLoS ONE*, 15(6), pp. 1–22. doi: 10.1371/journal.pone.0235251.

- Bertoni, L. *et al.* (2021) 'Article evaluation of allogeneic bone-marrow-derived and umbilical cord blood-derived mesenchymal stem cells to prevent the development of osteoarthritis in an equine model', *International Journal of Molecular Sciences*, 22(5), pp. 1–18. doi: 10.3390/IJMS22052499.
- Bertuglia, A. *et al.* (2016) 'Osteoclasts are recruited to the subchondral bone in naturally occurring post-traumatic equine carpal osteoarthritis and may contribute to cartilage degradation', *Osteoarthritis and Cartilage*, 24(3), pp. 555–566. doi: 10.1016/j.joca.2015.10.008.
- Bhutada, S. *et al.* (2022) 'Forward and reverse degradomics defines the proteolytic landscape of human knee osteoarthritic cartilage and the role of the serine protease HtrA1', *Osteoarthritis and Cartilage*, 30, pp. 1091–1102. doi: 10.1016/j.joca.2022.02.622.
- Bligh, E. G. and Dyer, W. J. (1959) 'A rapid method of total lipid extraction and purification', *Canadian Journal of Biochemistry and Physiology*, 37(8), pp. 911–917. doi: 10.1139/o59-099.
- Bocsa, C. D. *et al.* (2019) 'Knee osteoarthritis grading by resonant Raman and surface-enhanced Raman scattering (SERS) analysis of synovial fluid', *Nanomedicine: Nanotechnology, Biology, and Medicine*, 20, p. 102012. doi: 10.1016/j.nano.2019.04.015.
- Boere, Lest, van de, *et al.* (2016) 'Synovial fluid pretreatment with hyaluronidase facilitates isolation of CD44+ extracellular vesicles', *Journal of Extracellular Vesicles*, 5(1), pp. 1–16. doi: 10.3402/jev.v5.31751.
- Boere, Lest, *et al.* (2016) 'Synovial fluid pretreatment with hyaluronidase facilitates isolation of CD44+ extracellular vesicles', *Journal of Extracellular Vesicles*, 5(1), p. 31751. doi: 10.3402/jev.v5.31751.
- Boere *et al.* (2020) 'Extracellular vesicles in synovial fluid from juvenile horses : No age-related changes in the quantitative profile', *Veterinary Journal*, pp. 91–93. doi: 10.1016/j.tvjl.2018.12.010.Extracellular.
- Boere, J., Malda, J., Van De Lest, C. H. A., *et al.* (2018) 'Extracellular vesicles in joint disease and therapy', *Frontiers in Immunology*. Frontiers Media S.A. doi: 10.3389/fimmu.2018.02575.
- Boere, J., Malda, J., van de Lest, C. H. A., *et al.* (2018) 'Extracellular Vesicles in Joint Disease and Therapy', *Frontiers in Immunology*, 9, p. 2575. doi: 10.3389/fimmu.2018.02575.
- Bogers, S. H. (2018) 'Cell-based therapies for joint disease in veterinary medicine: What we have learned and what we need to know', *Frontiers in Veterinary Science*. Frontiers Media S.A. doi: 10.3389/fvets.2018.00070.

Bosch *et al.* (2011) 'The effect of platelet-rich plasma on the neovascularization of surgically created equine superficial digital flexor tendon lesions', *Scandinavian Journal of Medicine and Science in Sports*, 21(4), pp. 554–561. doi: 10.1111/j.1600-0838.2009.01070.x.

Bosch, G. *et al.* (2010) 'Effects of platelet-rich plasma on the quality of repair of mechanically induced core lesions in equine superficial digital flexor tendons: A placebo-controlled experimental study', *Journal of Orthopaedic Research*, 28(2), pp. 211–217. doi: 10.1002/jor.20980.

Bosch, G. *et al.* (2011) 'Computerised analysis of standardised ultrasonographic images to monitor the repair of surgically created core lesions in equine superficial digital flexor tendons following treatment with intratendinous platelet rich plasma or placebo', *Veterinary Journal*, 187(1), pp. 92–98. doi: 10.1016/j.tvjl.2009.10.014.

Bosman, G. J. C. G. M. *et al.* (2008) 'The proteome of red cell membranes and vesicles during storage in blood bank conditions', *Transfusion*, 48(5), pp. 827–835. doi: 10.1111/j.1537-2995.2007.01630.x.

Boulestreau, J. *et al.* (2020a) 'Mesenchymal Stem Cell Derived Extracellular Vesicles in Aging', *Frontiers in Cell and Developmental Biology*. Frontiers Media S.A. doi: 10.3389/fcell.2020.00107.

Boulestreau, J. *et al.* (2020b) 'Mesenchymal Stem Cell Derived Extracellular Vesicles in Aging', *Frontiers in Cell and Developmental Biology*, 8(February), pp. 1–9. doi: 10.3389/fcell.2020.00107.

Bourdon, B. *et al.* (2021) 'Marine collagen hydrolysates downregulate the synthesis of pro-catabolic and pro-inflammatory markers of osteoarthritis and favor collagen production and metabolic activity in equine articular chondrocyte organoids', *International Journal of Molecular Sciences*, 22(2), pp. 1–32. doi: 10.3390/ijms22020580.

Brennan, K. *et al.* (2020) 'A comparison of methods for the isolation and separation of extracellular vesicles from protein and lipid particles in human serum', *Scientific Reports*, 10(1), pp. 1–13. doi: 10.1038/s41598-020-57497-7.

Bria, E. *et al.* (2015) 'Human epidermal growth factor receptor 2-positive breast cancer: heat shock protein 90 overexpression, Ki67 proliferative index, and topoisomerase II- $\alpha$  co-amplification as predictors of pathologic complete response to neoadjuvant chemotherapy with trastuz', *Clinical Breast Cancer*, 15(1), pp. 16–23. doi: 10.1016/j.clbc.2014.05.004.

Brisson, A. R. *et al.* (2017) 'Extracellular vesicles from activated platelets: a semiquantitative cryo-electron microscopy and immuno-gold labeling study', *Platelets*, 28(3), pp. 263–271. doi: 10.1080/09537104.2016.1268255.

Broeckx, Pille, *et al.* (2019) 'Evaluation of an osteochondral fragment-groove procedure for



induction of metacarpophalangeal joint osteoarthritis in horses', *American Journal of Veterinary Research*, 80(3), pp. 246–258. doi: 10.2460/ajvr.80.3.246.

Broeckx, Martens, *et al.* (2019) 'The use of equine chondrogenic-induced mesenchymal stem cells as a treatment for osteoarthritis : A randomised , double-blinded , placebo-controlled proof-of-concept study', *Equine Veterinary Journal*, 51, pp. 787–794. doi: 10.1111/evj.13089.

Brosseau, C. *et al.* (2018) 'CD9 tetraspanin: A new pathway for the regulation of inflammation?', *Frontiers in Immunology*, 9(OCT), pp. 1–12. doi: 10.3389/fimmu.2018.02316.

Brossi, P. M. *et al.* (2015) 'Platelet-rich plasma in orthopedic therapy: A comparative systematic review of clinical and experimental data in equine and human musculoskeletal lesions', *BMC Veterinary Research*, 11(1). doi: 10.1186/S12917-015-0403-Z.

Buchwald, T. *et al.* (2012) 'Identifying compositional and structural changes in spongy and subchondral bone from the hip joints of patients with osteoarthritis using Raman spectroscopy', *Journal of Biomedical Optics*, 17(1), p. 017007. doi: 10.1117/1.jbo.17.1.017007.

Buckley, M. R. *et al.* (2013) 'Distributions of types I, II and III collagen by region in the human supraspinatus tendon', *Connective Tissue Research*, 54(6), pp. 374–379. doi: 10.3109/03008207.2013.847096.

Del Bue, M. *et al.* (2008) 'Equine adipose-tissue derived mesenchymal stem cells and platelet concentrates: Their association in vitro and in vivo', *Veterinary Research Communications*, 32(SUPPL. 1). doi: 10.1007/S11259-008-9093-3.

Bundgaard, L. *et al.* (2018) 'Mapping of equine mesenchymal stromal cell surface proteomes for identification of specific markers using proteomics and gene expression analysis: An in vitro cross-sectional study 06 Biological Sciences 0601 Biochemistry and Cell Biology', *Stem Cell Research and Therapy*, 9(1). doi: 10.1186/s13287-018-1041-8.

Bundgaard, L. *et al.* (2020) 'Mass spectrometric analysis of the in vitro secretome from equine bone marrow-derived mesenchymal stromal cells to assess the effect of chondrogenic differentiation on response to interleukin-1 $\beta$  treatment', *Stem Cell Research and Therapy*, 11(1). doi: 10.1186/S13287-020-01706-7.

Del Buono, A. *et al.* (2011) 'Tendinopathy and inflammation: some truths.', *International journal of immunopathology and pharmacology*, 24(1 Suppl 2), pp. 45–50. doi: 10.1177/03946320110241s209.

Del Buono, A. *et al.* (2013) 'Metalloproteases and tendinopathy', *Muscles, Ligaments and Tendons Journal*, 3(1), pp. 51–57. doi: 10.11138/mltj/2013.3.1.051.

Buschow, S. I. *et al.* (2010) 'MHC class II-associated proteins in B-cell exosomes and potential functional implications for exosome biogenesis', *Immunology & Cell Biology*, 88(8), pp. 851–856. doi: 10.1038/icb.2010.64.

Buzas, E. I. *et al.* (2014) 'Emerging role of extracellular vesicles in inflammatory diseases', *Nature Reviews Rheumatology*, 10(6), pp. 356–364. doi: 10.1038/nrrheum.2014.19.

Cadby, J. A. *et al.* (2013) 'Further characterisation of an experimental model of tendinopathy in the horse', *Equine Veterinary Journal*, 45(5), pp. 642–648. doi: 10.1111/evj.12035.

Calamia, V. *et al.* (2011) 'Hsp90 $\beta$  inhibition modulates nitric oxide production and nitric oxide-induced apoptosis in human chondrocytes', *BMC Musculoskeletal Disorders*, 12, p. 237. doi: 10.1186/1471-2474-12-237.

Camargo Garbin, L., Lopez, C. and Carmona, J. U. (2021) 'A Critical Overview of the Use of Platelet-Rich Plasma in Equine Medicine Over the Last Decade', *Frontiers in Veterinary Science*, 8(March), pp. 1–10. doi: 10.3389/fvets.2021.641818.

Camper, L., Hellman, U. and Lundgren-åkerlund, E. (1998) 'Isolation, Cloning, and Sequence Analysis of the Integrin Subunit  $\alpha 10$ , a  $\alpha 1$ -associated Collagen Binding Integrin Expressed on Chondrocytes\*', *J Biol Chem*, 273(32), pp. 20383–20389.

Canada, N. C. *et al.* (2017) 'Measurement of distal limb sub-bandage pressure over 96 hours in horses', *Equine Veterinary Journal*, 49(3), pp. 329–333. doi: 10.1111/evj.12601.

Canada, N. C. *et al.* (2018) 'Effect of bandaging techniques on sub-bandage pressures in the equine distal limb, carpus, and tarsus', *Veterinary Surgery*, 47(5), pp. 640–647. doi: 10.1111/vsu.12914.

Cao, H. *et al.* (2019) 'In Vivo Real-Time Imaging of Extracellular Vesicles in Liver Regeneration via Aggregation-Induced Emission Luminogens', *ACS Nano*, 13(3), pp. 3522–3533. doi: 10.1021/acsnano.8b09776.

Capomaccio, S. *et al.* (2019) 'Equine adipose-derived mesenchymal stromal cells release extracellular vesicles enclosing different subsets of small RNAs', *Stem Cells International*, 2019. doi: 10.1155/2019/4957806.

Carneiro, D. de C. *et al.* (2023) 'Clinical Trials with Mesenchymal Stem Cell Therapies for Osteoarthritis: Challenges in the Regeneration of Articular Cartilage', *International Journal of Molecular Sciences*, 24(12). doi: 10.3390/ijms24129939.

Carrade, D. D. *et al.* (2012) 'Comparative Analysis of the Immunomodulatory Properties of Equine

- Adult-Derived Mesenchymal Stem Cells 1', *Cell Medicine*, 4(1), pp. 1–11. doi: 10.3727/215517912X647217.
- Casal-Beiroa, P. *et al.* (2021) 'Optical biomarkers for the diagnosis of osteoarthritis through raman spectroscopy: Radiological and biochemical validation using ex vivo human cartilage samples', *Diagnostics*, 11(3). doi: 10.3390/diagnostics11030546.
- Castanheira *et al.* (2021) 'Equine synovial fluid small non-coding RNA signatures in early osteoarthritis', *BMC Veterinary Research*, 17(1), p. 26. doi: 10.1186/s12917-020-02707-7.
- Castro-Perez, J. M. *et al.* (2010) 'Comprehensive LC-MSE lipidomic analysis using a shotgun approach and its application to biomarker detection and identification in osteoarthritis patients', *Journal of Proteome Research*, 9(5), pp. 2377–2389. doi: 10.1021/pr901094j.
- Cavallo, C. *et al.* (2021) 'Small Extracellular Vesicles from adipose derived stromal cells significantly attenuate in vitro the NF- $\kappa$ B dependent inflammatory/catabolic environment of osteoarthritis', *Scientific Reports*, 11(1). doi: 10.1038/S41598-020-80032-7.
- Chalapathi, D. *et al.* (2020) 'Surface-Enhanced Raman Spectroscopy as a Tool for Distinguishing Extracellular Vesicles under Autophagic Conditions: A Marker for Disease Diagnostics', *Journal of Physical Chemistry B*, 124(48), pp. 10952–10960. doi: 10.1021/acs.jpcc.0c06910.
- Chambers, M. C. *et al.* (2012) 'A cross-platform toolkit for mass spectrometry and proteomics', *Nature Biotechnology*, 30(10), pp. 918–920. doi: 10.1038/nbt.2377.
- Chanda, M. *et al.* (2020) 'The effect of the z-bar shoeing method on surface dimension of the hoof wall and time required for therapeutic shoeing in three horses with a sheared heel', *Journal of Applied Animal Research*, 48(1), pp. 406–412. doi: 10.1080/09712119.2020.1814785.
- Chargaff, E. and West, R. (1946) 'The biological significance of the thromboplastic protein of blood.', *The Journal of biological chemistry*, 166(1), pp. 189–197. doi: 10.1016/s0021-9258(17)34997-9.
- Chen, Tang, *et al.* (2019) 'High-Temperature Requirement A1 Protease as a Rate-Limiting Factor in the Development of Osteoarthritis', *American Journal of Pathology*, 189(7), pp. 1423–1434. doi: 10.1016/j.ajpath.2019.03.013.
- Chen, Datta-Chaudhuri, *et al.* (2019) 'Lipidomic characterization of extracellular vesicles in human serum', *Journal of Circulating Biomarkers*, 8, pp. 1–12. doi: 10.1177/1849454419879848.
- Chen, D. *et al.* (2022) 'Metabolomic analysis of extracellular vesicles from human synovial fluids', *Microchemical Journal*, 177, p. 107257. doi: 10.1016/j.microc.2022.107257.

- Chen, H. *et al.* (2016) 'Autophagy Prevents Oxidative Stress-Induced Loss of Self-Renewal Capacity and Stemness in Human Tendon Stem Cells by Reducing ROS Accumulation', *Cellular Physiology and Biochemistry*, 39(6), pp. 2227–2238. doi: 10.1159/000447916.
- Chen, J., Caspi, R. R. and Chong, W. P. (2018) 'IL-20 receptor cytokines in autoimmune diseases', *Journal of Leukocyte Biology*, 104(5), pp. 953–959. doi: 10.1002/JLB.MR1117-471R.
- Chen, L. *et al.* (2015) 'S100A4 promotes liver fibrosis via activation of hepatic stellate cells', *Journal of Hepatology*, 62(1), pp. 156–164. doi: 10.1016/j.jhep.2014.07.035.
- Chen, Y. *et al.* (2020) 'Macrophages in osteoarthritis: pathophysiology and therapeutics', *American Journal of Translational Research*, 12(1), pp. 261–268. Available at: <https://www.ncbi.nlm.nih.gov/pmc/articles/PMC7013211/>.
- Cheng, L. *et al.* (2020) 'Proteomic and lipidomic analysis of exosomes derived from ovarian cancer cells and ovarian surface epithelial cells', *Journal of Ovarian Research*, 13(1), pp. 1–13. doi: 10.1186/s13048-020-0609-y.
- Chien, C. *et al.* (2018) 'Optimizing a 3D model system for molecular manipulation of tenogenesis', *Connective Tissue Research*, 59(4), pp. 295–308. doi: 10.1080/03008207.2017.1383403.
- Chisari, E. *et al.* (2021) 'Tendon healing is adversely affected by low-grade inflammation', *Journal of Orthopaedic Surgery and Research*, 16(1), pp. 1–9. doi: 10.1186/s13018-021-02811-w.
- Chishti, A. H. *et al.* (1998) 'The FERM domain: a unique module involved in the linkage of cytoplasmic proteins to the membrane', *Trends in Biochemical Sciences*, 23(8), pp. 281–282. doi: 10.1016/S0968-0004(98)01237-7.
- Choi, D.-S. *et al.* (2007) 'Proteomic analysis of microvesicles derived from human colorectal cancer cells', *Journal of Proteome Research*, 6(12), pp. 4646–4655. doi: 10.1021/pr070192y.
- Choi, D.-S. *et al.* (2012) 'Quantitative proteomics of extracellular vesicles derived from human primary and metastatic colorectal cancer cells', *Journal of Extracellular Vesicles*, 1. doi: 10.3402/jev.v1i0.18704.
- Choi, H. *et al.* (2020) 'Heterogeneity of proteome dynamics between connective tissue phases of adult Tendon', *eLife*, 9, pp. 1–22. doi: 10.7554/eLife.55262.
- Chomczynski, P. and Sacchi, N. (1987) 'Single-step method of RNA isolation by acid guanidinium thiocyanate-phenol-chloroform extraction', *Analytical Biochemistry*, 162(1), pp. 156–159. doi: 10.1016/0003-2697(87)90021-2.

- Claridge, B. *et al.* (2021) *Development of Extracellular Vesicle Therapeutics: Challenges, Considerations, and Opportunities*, *Frontiers in Cell and Developmental Biology*. doi: 10.3389/fcell.2021.734720.
- Clarke, Lima, C., *et al.* (2022) 'Optical photothermal infrared spectroscopy can differentiate equine osteoarthritic plasma extracellular vesicles from healthy controls', *Analytical Methods*, p. 2022.03.11.483922. doi: 10.1101/2022.03.11.483922.
- Clarke, Johnson, *et al.* (2022) 'Temporal extracellular vesicle protein changes following intraarticular treatment with integrin  $\alpha 10\beta 1$ -selected mesenchymal stem cells in equine osteoarthritis', *Frontiers in Veterinary Science*, 9. doi: 10.3389/fvets.2022.1057667.
- Clarke, Anderson and Peffers (2021a) 'Nuclear magnetic resonance spectroscopy of biofluids for osteoarthritis', *British Medical Bulletin*, 137(1), pp. 28–41. doi: 10.1093/bmb/ldaa037.
- Clarke, Anderson and Peffers (2021b) 'Nuclear magnetic resonance spectroscopy of biofluids for osteoarthritis', *British Medical Bulletin*, 137(1), pp. 28–41. doi: 10.1093/bmb/ldaa037.
- Clayton, A. *et al.* (2005) 'Induction of heat shock proteins in B-cell exosomes', *Journal of Cell Science*, 118(Pt 16), pp. 3631–3638. doi: 10.1242/jcs.02494.
- Clements, P. E. *et al.* (2020) 'An investigation into the association between plantar distal phalanx angle and hindlimb lameness in a UK population of horses', *Equine Veterinary Education*, 32(S10), pp. 52–59. doi: 10.1111/eve.13186.
- Clutterbuck, A. L. *et al.* (2011) 'High throughput proteomic analysis of the secretome in an explant model of articular cartilage inflammation', *Journal of Proteomics*, 74(5), pp. 704–715. doi: 10.1016/J.JPROT.2011.02.017.
- Cocucci, E. and Meldolesi, J. (2015) 'Ectosomes and exosomes: shedding the confusion between extracellular vesicles', *Trends in Cell Biology*, 25(6), pp. 364–372. doi: 10.1016/j.tcb.2015.01.004.
- Cohn, W. *et al.* (2021) 'Multi-Omics Analysis of Microglial Extracellular Vesicles From Human Alzheimer's Disease Brain Tissue Reveals Disease-Associated Signatures', *Frontiers in Pharmacology*, 12(December), pp. 1–15. doi: 10.3389/fphar.2021.766082.
- Collins-Racie, L. A. *et al.* (2009) 'Global analysis of nuclear receptor expression and dysregulation in human osteoarthritic articular cartilage. Reduced LXR signaling contributes to catabolic metabolism typical of osteoarthritis', *Osteoarthritis and Cartilage*, 17(7), pp. 832–842. doi: 10.1016/j.joca.2008.12.011.

- Collins, J. A. *et al.* (2016) 'Oxidative Stress Promotes Peroxiredoxin Hyperoxidation and Attenuates Pro-survival Signaling in Aging Chondrocytes\*', *Journal of Biological Chemistry*, 291(13), pp. 6641–6654. doi: 10.1074/jbc.M115.693523.
- Collins, T., Alexander, D. and Barkatali, B. (2021) 'Platelet-rich plasma: a narrative review', *EFORT Open Reviews*, 64(4), pp. 225–235. doi: 10.1302/2058-5241.6.200017.
- Consoli, V. *et al.* (2021) 'Heme oxygenase-1 signaling and redox homeostasis in physiopathological conditions', *Biomolecules*, 11(4), pp. 1–23. doi: 10.3390/biom11040589.
- Cosenza, S. *et al.* (2017a) 'Mesenchymal stem cells derived exosomes and microparticles protect cartilage and bone from degradation in osteoarthritis', *Scientific Reports*, 7(1), p. 16214. doi: 10.1038/s41598-017-15376-8.
- Cosenza, S. *et al.* (2017b) 'Mesenchymal stem cells derived exosomes and microparticles protect cartilage and bone from degradation in osteoarthritis', *Scientific Reports*, 7(1). doi: 10.1038/s41598-017-15376-8.
- Costa, F. R. *et al.* (2023) 'Intra-Articular Hyaluronic Acid in Osteoarthritis and Tendinopathies: Molecular and Clinical Approaches', *Biomedicines*, 11(4), pp. 1–14. doi: 10.3390/biomedicines11041061.
- Costa Verdera, H. *et al.* (2017) 'Cellular uptake of extracellular vesicles is mediated by clathrin-independent endocytosis and macropinocytosis', *Journal of Controlled Release*, 266, pp. 100–108. doi: 10.1016/j.jconrel.2017.09.019.
- Couch, Y. *et al.* (2021) 'A brief history of nearly EV-erything – The rise and rise of extracellular vesicles', *Journal of Extracellular Vesicles*, 10(14). doi: 10.1002/jev2.12144.
- Courneya, J. P. *et al.* (2010) 'Interleukins 4 and 13 modulate gene expression and promote proliferation of primary human tenocytes', *Fibrogenesis and Tissue Repair*, 3(1), pp. 1–8. doi: 10.1186/1755-1536-3-9.
- Cronqvist, T. *et al.* (2020) 'Placental syncytiotrophoblast extracellular vesicles enter primary endothelial cells through clathrin-mediated endocytosis', *Placenta*, 100, pp. 133–141. doi: 10.1016/j.placenta.2020.07.006.
- Crook, T. C. *et al.* (2008) 'Comparative anatomy and muscle architecture of selected hind limb muscles in the Quarter Horse and Arab', *Journal of Anatomy*, 212(2), pp. 144–152. doi: 10.1111/j.1469-7580.2007.00848.x.

- Crotti, T. N. *et al.* (2011) 'Bone matrix regulates osteoclast differentiation and annexin A8 gene expression', *Journal of Cellular Physiology*, 226(12), pp. 3413–3421. doi: 10.1002/jcp.22699.
- Cvjetkovic, A. *et al.* (2016) 'Detailed Analysis of Protein Topology of Extracellular Vesicles—Evidence of Unconventional Membrane Protein Orientation', *Scientific Reports*, 6(1), p. 36338. doi: 10.1038/srep36338.
- Dahlgren, L. A., Mohammed, H. O. and Nixon, A. J. (2006) 'Expression of insulin-like growth factor binding proteins in healing tendon lesions', *Journal of Orthopaedic Research*, 24(2), pp. 183–192. doi: 10.1002/jor.20000.
- Dalli, J. *et al.* (2013) 'Heterogeneity in neutrophil microparticles reveals distinct proteome and functional properties', *Molecular & cellular proteomics: MCP*, 12(8), pp. 2205–2219. doi: 10.1074/mcp.M113.028589.
- Davis, M. E. *et al.* (2013) 'MMP inhibition as a potential method to augment the healing of skeletal muscle and tendon extracellular matrix', *Journal of Applied Physiology*, 115(6), pp. 884–891. doi: 10.1152/jappphysiol.00137.2013.
- Davis, T. A., Loos, B. and Engelbrecht, A. M. (2014) 'AHNAK: The giant jack of all trades', *Cellular Signalling*, 26(12), pp. 2683–2693. doi: 10.1016/j.cellsig.2014.08.017.
- Delco, M. L. *et al.* (2020) 'Integrin  $\alpha 10\beta 1$ -Selected Mesenchymal Stem Cells Mitigate the Progression of Osteoarthritis in an Equine Talar Impact Model', *American Journal of Sports Medicine*, 48(3), pp. 612–623. doi: 10.1177/0363546519899087.
- Demichev, V. *et al.* (2020) 'DIA-NN: neural networks and interference correction enable deep proteome coverage in high throughput', *Nature Methods*, 17(1), pp. 41–44. doi: 10.1038/s41592-019-0638-x.
- Dempsey, N. C. *et al.* (2010) 'Differential heat shock protein localization in chronic lymphocytic leukemia', *Journal of Leukocyte Biology*, 87(3), pp. 467–476. doi: 10.1189/jlb.0709502.
- Deng, Z. *et al.* (2021) 'Interleukin 1 beta-induced chloride currents are important in osteoarthritis onset: An in vitro study', *Acta Biochimica et Biophysica Sinica*, 53(4), pp. 400–409. doi: 10.1093/abbs/gmab010.
- Van Deun, J. *et al.* (2017a) 'EV-TRACK: transparent reporting and centralizing knowledge in extracellular vesicle research', *Nature Methods*, 14(3), pp. 228–232. doi: 10.1038/nmeth.4185.
- Van Deun, J. *et al.* (2017b) 'EV-TRACK: Transparent reporting and centralizing knowledge in

extracellular vesicle research', *Nature Methods*, 14(3), pp. 228–232. doi: 10.1038/nmeth.4185.

Devireddy *et al.* (2017a) 'Questions and Challenges in the Development of Mesenchymal Stromal/Stem Cell-Based Therapies in Veterinary Medicine', *liebertpub.com*, 23(5), pp. 462–470. doi: 10.1089/ten.teb.2016.0451.

Devireddy *et al.* (2017b) 'Questions and Challenges in the Development of Mesenchymal Stromal/Stem Cell-Based Therapies in Veterinary Medicine', *Tissue Engineering - Part B: Reviews*, 23(5), pp. 462–470. doi: 10.1089/ten.teb.2016.0451.

Dominici, M. *et al.* (2006) 'Minimal criteria for defining multipotent mesenchymal stromal cells. The International Society for Cellular Therapy position statement', *Cytotherapy*, 8(4), pp. 315–317. doi: 10.1080/14653240600855905.

Dyson, S. (2017) 'Equine performance and equitation science: Clinical issues', *Applied Animal Behaviour Science*, 190, pp. 5–17. doi: 10.1016/j.applanim.2017.03.001.

Eguchi, S. *et al.* (2019) 'Cardiomyocytes capture stem cell-derived, anti-apoptotic microRNA-214 via clathrin-mediated endocytosis in acute myocardial infarction', *Journal of Biological Chemistry*, 294(31), pp. 11665–11674. doi: 10.1074/jbc.RA119.007537.

Elahi, S. A. *et al.* (2023) 'Contribution of collagen degradation and proteoglycan depletion to cartilage degeneration in primary and secondary osteoarthritis: an in silico study', *Osteoarthritis and Cartilage*, 31(6), pp. 741–752. doi: 10.1016/j.joca.2023.01.004.

Ellis, I. M., Schnabel, L. V. and Berglund, A. K. (2022) 'Defining the profile: Characterizing cytokines in tendon injury to improve clinical therapy', *Journal of Immunology and Regenerative Medicine*, 16(February), p. 100059. doi: 10.1016/j.regen.2022.100059.

Erdbrügger, U. *et al.* (2021) 'Urinary extracellular vesicles: A position paper by the Urine Task Force of the International Society for Extracellular Vesicles', *Journal of Extracellular Vesicles*, 10(7), p. e12093. doi: 10.1002/jev2.12093.

Erdbrügger, U. and Lannigan, J. (2016) 'Analytical challenges of extracellular vesicle detection: A comparison of different techniques', *Cytometry Part A*, 89(2), pp. 123–134. doi: 10.1002/cyto.a.22795.

Esa, A. *et al.* (2019) 'Extracellular vesicles in the synovial joint: Is there a role in the pathophysiology of osteoarthritis?', *Malaysian Orthopaedic Journal*, 13(1), pp. 1–7. doi: 10.5704/MOJ.1903.012.

Esa, A., Connolly, K. and Archer, C. (2019) 'Extracellular Vesicles in the Synovial Joint: Is there a Role



in the Pathophysiology of Osteoarthritis?', *Malaysian Orthopaedic Journal*, 13(1), pp. 1–7. doi: 10.5704/MOJ.1903.012.

Etzerodt, A. and Moestrup, S. K. (2013) 'CD163 and Inflammation: Biological, Diagnostic, and Therapeutic Aspects', *Antioxidants & Redox Signaling*, 18(17), pp. 2352–2363. doi: 10.1089/ars.2012.4834.

Everts, P. *et al.* (2020) 'Platelet-rich plasma: New performance understandings and therapeutic considerations in 2020', *International Journal of Molecular Sciences*, 21(20), pp. 1–36. doi: 10.3390/ijms21207794.

Fagerholm, S. C., Lek, H. S. and Morrison, V. L. (2014) 'Kindlin-3 in the immune system', *American Journal of Clinical and Experimental Immunology*, 3(1), pp. 37–42. Available at: <https://www.ncbi.nlm.nih.gov/pmc/articles/PMC3960760/>.

Feng, C. *et al.* (2018) 'Efficacy and Persistence of Allogeneic Adipose-Derived Mesenchymal Stem Cells Combined with Hyaluronic Acid in Osteoarthritis After Intra-articular Injection', 24, pp. 219–233. doi: 10.1089/ten.tea.2017.0039.

Feng, K. *et al.* (2021) 'Reversing the surface charge of MSC-derived small extracellular vesicles by  $\epsilon$ PL-PEG-DSPE for enhanced osteoarthritis treatment', *Journal of Extracellular Vesicles*, 10(13). doi: 10.1002/jev2.12160.

Fernández-Puente, P. *et al.* (2017) 'Multiplexed mass spectrometry monitoring of biomarker candidates for osteoarthritis', *Journal of Proteomics*, 152, pp. 216–225. doi: 10.1016/j.jprot.2016.11.012.

Ferreira, P. M. *et al.* (2020) 'Mode of induction of platelet-derived extracellular vesicles is a critical determinant of their phenotype and function', *Scientific Reports*, 10(1), p. 18061. doi: 10.1038/s41598-020-73005-3.

Folkesson, E. *et al.* (2020) 'Proteomic comparison of osteoarthritic and reference human menisci using data-independent acquisition mass spectrometry', *Osteoarthritis and Cartilage*, 28(8), pp. 1092–1101. doi: 10.1016/j.joca.2020.05.001.

Fortier, L. (2010) *Clinical Use of Stem Cells, Marrow Components, and Other Growth Factors*. Second Edi, *Diagnosis and Management of Lameness in the Horse: Second Edition*. Second Edi. Elsevier Inc. doi: 10.1016/B978-1-4160-6069-7.00073-0.

Fragoulis, A. *et al.* (2023) 'The Contribution of the Nrf2/ARE System to Mechanotransduction in Musculoskeletal and Periodontal Tissues', *International Journal of Molecular Sciences*, 24(9). doi:

10.3390/ijms24097722.

Frisbie *et al.* (2002) 'Treatment of experimental equine osteoarthritis by in vivo delivery of the equine interleukin-1 receptor antagonist gene', *Gene Therapy*, pp. 12–20. doi: 10.1038/sj/gt/3301608.

Frisbie, D. D. *et al.* (1997) 'Effects of triamcinolone acetonide on an in vivo equine osteochondral fragment exercise model', *EQUINE VETERINARY JOURNAL*, 29, pp. 349–359.

Frisbie, D. D. *et al.* (2008) 'Changes in synovial fluid and serum biomarkers with exercise and early osteoarthritis in horses', *Osteoarthritis and Cartilage*, 16(10), pp. 1196–1204. doi: 10.1016/j.joca.2008.03.008.

Frisbie, D. D. *et al.* (2009) 'Evaluation of Adipose-Derived Stromal Vascular Fraction or Bone Marrow-Derived Mesenchymal Stem Cells for Treatment of Osteoarthritis', *JOURNAL OF ORTHOPAEDIC RESEARCH DECEMBER*, (December), pp. 1675–1680. doi: 10.1002/jor.20933.

Furstenberg, R. *et al.* (2012) 'Chemical imaging using infrared photothermal microspectroscopy', *Next-Generation Spectroscopic Technologies V*, 8374(May 2012), p. 837411. doi: 10.1117/12.919574.

Gaesser, A. M. *et al.* (2021) 'Evaluation of Autologous Protein Solution Injection for Treatment of Superficial Digital Flexor Tendonitis in an Equine Model', *Frontiers in Veterinary Science*, 8(July), pp. 1–13. doi: 10.3389/fvets.2021.697551.

Garcia, B. A. *et al.* (2005) 'The platelet microparticle proteome', *Journal of Proteome Research*, 4(5), pp. 1516–1521. doi: 10.1021/pr0500760.

Gardiner, C. *et al.* (2013) 'Extracellular vesicle sizing and enumeration by nanoparticle tracking analysis', *Journal of Extracellular Vesicles*, 2(1), pp. 1–11. doi: 10.3402/jev.v2i0.19671.

Gardner, P. *et al.* (2021) 'Analysis of fixed and live single cells using optical photothermal infrared with concomitant Raman spectroscopy', *Analytical Chemistry*, 93(8), pp. 3938–3950. doi: 10.1021/acs.analchem.0c04846.

Gasic, I. (2022) 'Regulation of Tubulin Gene Expression: From Isotype Identity to Functional Specialization', *Frontiers in Cell and Developmental Biology*, 10. Available at: <https://www.frontiersin.org/articles/10.3389/fcell.2022.898076>.

Gatien, J. *et al.* (2019) 'Metabolomic Profile of Oviductal Extracellular Vesicles across the Estrous Cycle in Cattle', *International Journal of Molecular Sciences*, 20(24), p. 6339. doi: 10.3390/ijms20246339.

Ge, R. *et al.* (2022) 'Quantitative proteomics reveals potential anti-inflammatory protein targets of radial extracorporeal shock wave therapy in TNF- $\alpha$ -induced model of acute inflammation in primary human tenocytes', *Heliyon*, 8(12), p. e12008. doi: 10.1016/j.heliyon.2022.e12008.

Geburek, F. *et al.* (2016) 'Effect of intralesional platelet-rich plasma (PRP) treatment on clinical and ultrasonographic parameters in equine naturally occurring superficial digital flexor tendinopathies - a randomized prospective controlled clinical trial', *BMC Veterinary Research*, 12(1). doi: 10.1186/s12917-016-0826-1.

Gézi, A. *et al.* (2019) 'Systems biology approaches to investigating the roles of extracellular vesicles in human diseases', *Experimental & Molecular Medicine*, 51(3), pp. 1–11. doi: 10.1038/s12276-019-0226-2.

Giancaterino, S. and Boi, C. (2023) 'Alternative biological sources for extracellular vesicles production and purification strategies for process scale-up', *Biotechnology Advances*, 63(December 2022), p. 108092. doi: 10.1016/j.biotechadv.2022.108092.

Gillet, L. C. *et al.* (2012) 'Targeted data extraction of the MS/MS spectra generated by data-independent acquisition: A new concept for consistent and accurate proteome analysis', *Molecular and Cellular Proteomics*, 11(6), pp. 1–17. doi: 10.1074/mcp.O111.016717.

Goebeler, V. *et al.* (2008) 'Annexin A8 Regulates Late Endosome Organization and Function', *Molecular Biology of the Cell*, 19(12), pp. 5267–5278. doi: 10.1091/mbc.E08-04-0383.

Gonçalves-Neto, J. *et al.* (2002) 'Changes in collagen matrix composition in human posterior tibial tendon dysfunction', *Joint Bone Spine*, 69(2), pp. 189–194. doi: 10.1016/S1297-319X(02)00369-X.

Goodacre, R. *et al.* (2021) 'Imaging isotopically labeled bacteria at the single-cell level using high-resolution optical infrared photothermal spectroscopy', *Analytical Chemistry*, 93(6), pp. 3082–3088. doi: 10.1021/acs.analchem.0c03967.

Görgens, A. *et al.* (2019) 'Optimisation of imaging flow cytometry for the analysis of single extracellular vesicles by using fluorescence-tagged vesicles as biological reference material', *Journal of Extracellular Vesicles*, 8(1). doi: 10.1080/20013078.2019.1587567.

Gowen, A. *et al.* (2020) 'Mesenchymal Stem Cell-Derived Extracellular Vesicles: Challenges in Clinical Applications', *Frontiers in Cell and Developmental Biology*, 8(March), pp. 1–8. doi: 10.3389/fcell.2020.00149.

Graça, A. L. *et al.* (2022) 'Therapeutic Effects of Platelet-Derived Extracellular Vesicles in a Bioengineered Tendon Disease Model', *International Journal of Molecular Sciences*, 23(6). doi:

10.3390/ijms23062948.

Graça, A. L. *et al.* (2023) 'Platelet-Derived Extracellular Vesicles Promote Tenogenic Differentiation of Stem Cells on Bioengineered Living Fibers', *International Journal of Molecular Sciences*, 24(4). doi: 10.3390/ijms24043516.

Grewal, T. *et al.* (2021) 'Annexin Animal Models—From Fundamental Principles to Translational Research', *International Journal of Molecular Sciences*, 22(7), p. 3439. doi: 10.3390/ijms22073439.

Gu, Z., Eils, R. and Schlesner, M. (2016) 'Complex heatmaps reveal patterns and correlations in multidimensional genomic data', *Bioinformatics*, 32(18), pp. 2847–2849. doi: 10.1093/bioinformatics/btw313.

Gualerzi, A. *et al.* (2017) 'Raman spectroscopy uncovers biochemical tissue-related features of extracellular vesicles from mesenchymal stromal cells', *Scientific Reports*, 7(1), pp. 1–11. doi: 10.1038/s41598-017-10448-1.

Gualerzi, A., Picciolini, S., *et al.* (2019) 'Raman profiling of circulating extracellular vesicles for the stratification of Parkinson's patients', *Nanomedicine: Nanotechnology, Biology, and Medicine*, 22, p. 102097. doi: 10.1016/j.nano.2019.102097.

Gualerzi, A., Kooijmans, S. A. A., *et al.* (2019) 'Raman spectroscopy as a quick tool to assess purity of extracellular vesicle preparations and predict their functionality', *Journal of Extracellular Vesicles*, 8(1). doi: 10.1080/20013078.2019.1568780.

Guan, F. *et al.* (2021) 'Simultaneous metabolomics and proteomics analysis of plasma-derived extracellular vesicles', *Analytical Methods*, 13(16), pp. 1930–1938. doi: 10.1039/d1ay00060h.

Guest, D. J. *et al.* (2022) 'Position Statement: Minimal Criteria for Reporting Veterinary and Animal Medicine Research for Mesenchymal Stromal/Stem Cells in Orthopedic Applications', *Frontiers in Veterinary Science*, 9(March), pp. 1–5. doi: 10.3389/fvets.2022.817041.

Gugliandolo, E. *et al.* (2020) 'Oral Supplementation with Ultramicronized Palmitoylethanolamide for Joint Disease and Lameness Management in Four Jumping Horses: A Case Report', *Animals*, 10(9), p. 1469. doi: 10.3390/ani10091469.

Guo, R. *et al.* (2022) 'Association between matrix metalloproteinase-3 gene polymorphisms and tendon-ligament injuries: evidence from a meta-analysis', *BMC Sports Science, Medicine and Rehabilitation*, 14(1), pp. 1–12. doi: 10.1186/s13102-022-00421-5.

Gupta, D. *et al.* (2020) 'Quantification of extracellular vesicles in vitro and in vivo using sensitive

bioluminescence imaging', *Journal of Extracellular Vesicles*, 9(1). doi: 10.1080/20013078.2020.1800222.

Gupta, S., Dimsaite, I. and Peffers, M. . (2020) 'Does equine osteoarthritis have an inflammatory component?', *Insider Imprint*.

Gurung, S. *et al.* (2021) 'The exosome journey: from biogenesis to uptake and intracellular signalling', *Cell Communication and Signaling : CCS*, 19, p. 47. doi: 10.1186/s12964-021-00730-1.

György, B. *et al.* (2012) 'Improved flow cytometric assessment reveals distinct microvesicle (cell-derived microparticle) signatures in joint diseases', *PLoS One*, 7(11), p. e49726. doi: 10.1371/journal.pone.0049726.

Hagen, J. *et al.* (2018) 'Immediate effects of an artificial change in hoof angulation on the dorsal metacarpophalangeal joint angle and cross-sectional areas of both flexor tendons', *Veterinary Record*, 182(24), pp. 692–692. doi: 10.1136/vr.104700.

Halekoh, U. and Højsgaard, S. (2014) 'A kenward-Roger approximation and parametric bootstrap methods for tests in linear mixed models-the R package pbkrtest', *Journal of Statistical Software*, 59(9), pp. 1–32. doi: 10.18637/jss.v059.i09.

Hallal, S. *et al.* (2019) 'Extracellular Vesicles Released by Glioblastoma Cells Stimulate Normal Astrocytes to Acquire a Tumor-Supportive Phenotype Via p53 and MYC Signaling Pathways', *Molecular Neurobiology*, 56(6), pp. 4566–4581. doi: 10.1007/s12035-018-1385-1.

Haltmayer, E. *et al.* (2019) 'Co-culture of osteochondral explants and synovial membrane as in vitro model for osteoarthritis', *PLoS ONE*, 14(4), pp. 1–19. doi: 10.1371/journal.pone.0214709.

Hasegawa, T. *et al.* (2013) 'Use of potassium channel tetramerization domain-containing 12 as a biomarker for diagnosis and prognosis of gastrointestinal stromal tumor', *Human Pathology*, 44(7), pp. 1271–1277. doi: 10.1016/j.humpath.2012.10.013.

Hassani, K. and Olivier, M. (2013) 'Immunomodulatory Impact of Leishmania-Induced Macrophage Exosomes: A Comparative Proteomic and Functional Analysis', *PLoS Neglected Tropical Diseases*, 7(5), p. e2185. doi: 10.1371/journal.pntd.0002185.

Heijnen, H. F. G. *et al.* (1999) 'Activated platelets release two types of membrane vesicles: Microvesicles by surface shedding and exosomes derived from exocytosis of multivesicular bodies and  $\alpha$ -granules', *Blood*, 94(11), pp. 3791–3799. doi: 10.1182/blood.v94.11.3791.

Herrmann, M. *et al.* (2021a) 'Extracellular Vesicles in Musculoskeletal Pathologies and Regeneration',

*Frontiers in Bioengineering and Biotechnology*, 8. doi: 10.3389/FBIOE.2020.624096.

Herrmann, M. *et al.* (2021b) 'Extracellular Vesicles in Musculoskeletal Pathologies and Regeneration', *Frontiers in Bioengineering and Biotechnology*, 8(January). doi: 10.3389/fbioe.2020.624096.

van Herwijnen, M. J. C. *et al.* (2016) 'Comprehensive Proteomic Analysis of Human Milk-derived Extracellular Vesicles Unveils a Novel Functional Proteome Distinct from Other Milk Components', *Molecular & cellular proteomics: MCP*, 15(11), pp. 3412–3423. doi: 10.1074/mcp.M116.060426.

Hettrick, H. (2009) 'The Science of Compression Therapy for Chronic Venous Insufficiency Edema', *The Journal of the American College of Certified Wound Specialists*, 1(1), pp. 20–24. doi: 10.1016/j.jcws.2008.10.002.

Honsho, M. and Fujiki, Y. (2017) 'Plasmalogen homeostasis - regulation of plasmalogen biosynthesis and its physiological consequence in mammals', *FEBS letters*, 591(18), pp. 2720–2729. doi: 10.1002/1873-3468.12743.

Horie, M. *et al.* (2009) 'Intra-articular Injected Synovial Stem Cells Differentiate into Meniscal Cells Directly and Promote Meniscal Regeneration Without Mobilization to Distant Organs in Rat Massive Meniscal Defect', *Stem Cells*, 27(4), pp. 878–887. doi: 10.1634/stemcells.2008-0616.

Hosu, C. D. *et al.* (2019) 'Raman spectroscopy applications in rheumatology', *Lasers in Medical Science*, 34(4), pp. 827–834. doi: 10.1007/s10103-019-02719-2.

Hotham, W. E. *et al.* (2021) 'The anti-inflammatory effects of equine bone marrow stem cell-derived extracellular vesicles on autologous chondrocytes', (July). doi: 10.1002/vro2.22.

Hotham, W. E. and Henson, F. M. D. (2020) 'The use of large animals to facilitate the process of MSC going from laboratory to patient—"bench to bedside"', *Cell Biology and Toxicology*, 36(2), pp. 103–114. doi: 10.1007/S10565-020-09521-9.

Housmans, B. A. C. *et al.* (2022) 'Synovial fluid from end-stage osteoarthritis induces proliferation and fibrosis of articular chondrocytes via MAPK and RhoGTPase signaling', *Osteoarthritis and Cartilage*, 30(6), pp. 862–874. doi: 10.1016/j.joca.2021.12.015.

Hu, H. *et al.* (2021) 'Role of vasodilator-stimulated phosphoprotein in RANKL-differentiated murine macrophage RAW264.7 cells: Modulation of NF- $\kappa$ B, c-Fos and NFATc1 transcription factors', *Experimental and Therapeutic Medicine*, 21(5), pp. 1–9. doi: 10.3892/etm.2021.9856.

Hu, J. M. *et al.* (2017) 'CD163 as a marker of M2 macrophage, contribute to predict aggressiveness

and prognosis of Kazakh esophageal squamous cell carcinoma', *Oncotarget*, 8(13), pp. 21526–21538. doi: 10.18632/oncotarget.15630.

Hu, Q. and Ecker, M. (2021) 'Overview of MMP-13 as a promising target for the treatment of osteoarthritis', *International Journal of Molecular Sciences*, 22(4), pp. 1–22. doi: 10.3390/ijms22041742.

Hu, X. *et al.* (2018) 'Cdc42 Is Essential for Both Articular Cartilage Degeneration and Subchondral Bone Deterioration in Experimental Osteoarthritis', *Journal of Bone and Mineral Research*, 33(5), pp. 945–958. doi: 10.1002/jbmr.3380.

Huang, Q. *et al.* (2015) 'SWATH enables precise label-free quantification on proteome scale', *Proteomics*, 15(7), pp. 1215–1223. doi: 10.1002/pmic.201400270.

Hudgens, J. L. *et al.* (2016) 'Platelet-Rich Plasma Activates Proinflammatory Signaling Pathways and Induces Oxidative Stress in Tendon Fibroblasts', *American Journal of Sports Medicine*, 44(8), pp. 1931–1940. doi: 10.1177/0363546516637176.

Hudson, D. M. *et al.* (2021) 'Age-related type I collagen modifications reveal tissue-defining differences between ligament and tendon', *Matrix Biology Plus*, 12, p. 100070. doi: 10.1016/j.mplus.2021.100070.

Hurwitz, S. N. *et al.* (2016) 'Proteomic profiling of NCI-60 extracellular vesicles uncovers common protein cargo and cancer type-specific biomarkers', *Oncotarget*, 7(52), pp. 86999–87015. doi: 10.18632/oncotarget.13569.

Ireland, D. *et al.* (2001) 'Multiple changes in gene expression in chronic human Achilles tendinopathy', *Matrix Biology*, 20(3), pp. 159–169. doi: 10.1016/S0945-053X(01)00128-7.

Ito, A. *et al.* (2015) 'LXRs link metabolism to inflammation through Abca1-dependent regulation of membrane composition and TLR signaling', *eLife*, 4(JULY 2015), pp. 1–23. doi: 10.7554/eLife.08009.

Ivanovska, A. *et al.* (2022) 'Manufacturing Mesenchymal Stromal Cells for the Treatment of Osteoarthritis in Canine Patients: Challenges and Recommendations', *Frontiers in Veterinary Science*, 9(June), pp. 1–22. doi: 10.3389/fvets.2022.897150.

Iyer, S. R. *et al.* (2020) 'Exosomes Isolated From Platelet-Rich Plasma and Mesenchymal Stem Cells Promote Recovery of Function After Muscle Injury', *American Journal of Sports Medicine*, 48(9), pp. 2277–2286. doi: 10.1177/0363546520926462.

Jackson, C. E. *et al.* (2017) 'Effects of Inhibiting VPS4 Support a General Role for ESCRTs in

- Extracellular Vesicle Biogenesis', *Biophysical Journal*, 113(6), pp. 1342–1352. doi: 10.1016/j.bpj.2017.05.032.
- Jammes, M. *et al.* (2023) 'Equine osteoarthritis: Strategies to enhance mesenchymal stromal cell-based acellular therapies', *Frontiers in Veterinary Science*, 10(2). doi: 10.3389/fvets.2023.1115774.
- Jeucken, A. *et al.* (2019) 'A Comprehensive Functional Characterization of Escherichia coli Lipid Genes', *Cell Reports*, 27(5), pp. 1597-1606.e2. doi: 10.1016/j.celrep.2019.04.018.
- Johal, K. S., Lees, V. C. and Reid, A. J. (2016) 'Europe PMC Funders Group Adipose-derived stem cells : selecting for translational success', 10(1), pp. 79–96. doi: 10.2217/rme.14.72.Adipose-derived.
- Johnson, S. A. *et al.* (2021) 'Longitudinal tendon healing assessed with multi-modality advanced imaging and tissue analysis', *Equine Veterinary Journal*, (January), pp. 1–16. doi: 10.1111/evj.13478.
- de Jong, O. G. *et al.* (2012) 'Cellular stress conditions are reflected in the protein and RNA content of endothelial cell-derived exosomes', *Journal of Extracellular Vesicles*, 1. doi: 10.3402/jev.v1i0.18396.
- Jr, G. de O. *et al.* (2021) 'Effects of endurance racing on horse plasma extracellular particle miRNA', *Wiley Online Library*, 53(3), pp. 618–627. doi: 10.1111/evj.13300.
- Kadiu, I. *et al.* (2012) 'Biochemical and Biologic Characterization of Exosomes and Microvesicles as Facilitators of HIV-1 Infection in Macrophages', *Journal of immunology (Baltimore, Md. : 1950)*, 189(2), pp. 744–754. doi: 10.4049/jimmunol.1102244.
- Kaji, D. A. *et al.* (2020) 'Tgfb signaling is required for tenocyte recruitment and functional neonatal tendon regeneration', *eLife*, 9, pp. 1–19. doi: 10.7554/eLife.51779.
- Kamm, J. L., Nixon, A. J. and Witte, T. H. (2010) 'Cytokine and catabolic enzyme expression in synovium, synovial fluid and articular cartilage of naturally osteoarthriticequine carpi', *Equine Veterinary Journal*, 42(8), pp. 693–699. doi: 10.1111/j.2042-3306.2010.00140.x.
- Kang, M. H. and Park, H. M. (2020) 'Challenges of stem cell therapies in companion animal practice', *Journal of Veterinary Science*, 21(3), pp. 1–22. doi: 10.4142/JVS.2020.21.E42.
- Kansiz, M. *et al.* (2021) 'Optical Photothermal Infrared Microspectroscopy Discriminates for the First Time Different Types of Lung Cells on Histopathology Glass Slides', *Analytical Chemistry*, 93(32), pp. 11081–11088. doi: 10.1021/acs.analchem.1c00309.
- Kapogiannis, D. (2020) 'Exosome Biomarkers Revolutionize Preclinical Diagnosis of Neurodegenerative Diseases and Assessment of Treatment Responses in Clinical Trials', in Vlamos, P. (ed.). Springer International Publishing (Advances in Experimental Medicine and Biology), p. 149. doi:



10.1007/978-3-030-32633-3\_19.

Kawaguchi, K. and Asano, S. (2022) 'Pathophysiological Roles of Actin-Binding Scaffold Protein, Ezrin', *International Journal of Molecular Sciences*, 23(6), p. 3246. doi: 10.3390/ijms23063246.

Kawamura, N. *et al.* (2012) 'Delivery of endosomes to lysosomes via microautophagy in the visceral endoderm of mouse embryos', *Nature Communications*, 3(May). doi: 10.1038/ncomms2069.

Kearney, C. M. *et al.* (2022) 'Treatment Effects of Intra-Articular Allogenic Mesenchymal Stem Cell Secretome in an Equine Model of Joint Inflammation', *Frontiers in Veterinary Science*, 9(June), pp. 1–13. doi: 10.3389/fvets.2022.907616.

Keerthikumar, S. *et al.* (2016) 'ExoCarta: A Web-Based Compendium of Exosomal Cargo', *Journal of Molecular Biology*, 428(4), pp. 688–692. doi: 10.1016/j.jmb.2015.09.019.

Kehrloesser, S. *et al.* (2023) 'Cell-of-origin–specific proteomics of extracellular vesicles', *PNAS Nexus*, 2(4), pp. 1–12. doi: 10.1093/pnasnexus/pgad107.

Khanna, K., Salmond, N. and Williams, K. C. (2023) 'Nanoscale Advances Separation and isolation of CD9-positive extracellular vesicles from plasma using flow'. doi: 10.1039/d3na00081h.

Kim, H.-S. *et al.* (2012) 'Proteomic Analysis of Microvesicles Derived from Human Mesenchymal Stem Cells', *Journal of Proteome Research*, 11(2), pp. 839–849. doi: 10.1021/pr200682z.

Kim, K. H. *et al.* (2020) 'Nanoparticles from equine fetal bone marrow-derived cells enhance the survival of injured chondrocytes', *Animals*, 10(10), pp. 1–17. doi: 10.3390/ani10101723.

Kim, S. *et al.* (2022) 'Metabolic discrimination of synovial fluid between rheumatoid arthritis and osteoarthritis using gas chromatography/time-of-flight mass spectrometry', *Metabolomics*, 18(7), pp. 1–10. doi: 10.1007/s11306-022-01893-9.

Kim, S. Y. *et al.* (2019) 'High-fidelity probing of the structure and heterogeneity of extracellular vesicles by resonance-enhanced atomic force microscopy infrared spectroscopy', *Nature Protocols*, 14(2), pp. 576–593. doi: 10.1038/s41596-018-0109-3.

Kinner, B. and Spector, M. (2001) 'Smooth muscle actin expression by human articular chondrocytes and their contraction of a collagen-glycosaminoglycan matrix in vitro', *Journal of Orthopaedic Research: Official Publication of the Orthopaedic Research Society*, 19(2), pp. 233–241. doi: 10.1016/S0736-0266(00)00081-4.

Klymiuk, M. C. *et al.* (2019) 'Exosomes isolation and identification from equine mesenchymal stem cells', *BMC Veterinary Research*, 15(1). doi: 10.1186/s12917-019-0190-9.

10.1186/S12917-019-1789-9.

Knott, L. E. *et al.* (2022) 'Current use of biologic therapies for musculoskeletal disease: A survey of board-certified equine specialists', *Veterinary Surgery*, 51(4), pp. 557–567. doi: 10.1111/vsu.13805.

Koch, D. W. *et al.* (2022) 'Interleukin-1 $\beta$  in tendon injury enhances reparative gene and protein expression in mesenchymal stem cells', *Frontiers in Veterinary Science*, 9. doi: 10.3389/fvets.2022.963759.

Koch, D. W. and Schnabel, L. V (2023) 'Currents in One Health Mesenchymal stem cell licensing : enhancing MSC function as a translational approach for the treatment of tendon injury The Pathophysiology of Tendon Injury', *American Journal of Veterinary Research*, pp. 1–8.

Kolhe, R. *et al.* (2017) 'Gender-specific differential expression of exosomal miRNA in synovial fluid of patients with osteoarthritis', *Scientific Reports*, 7(1), p. 2029. doi: 10.1038/s41598-017-01905-y.

Kolhe, R. *et al.* (2020) 'Sex-Specific Differences in Extracellular Vesicle Protein Cargo in Synovial Fluid of Patients with Osteoarthritis', *Life*, 10(12), p. 337. doi: 10.3390/life10120337.

Kong, Z. *et al.* (2019) 'Multi-omics analysis reveals up-regulation of APR signaling, LXR/RXR and FXR/RXR activation pathways in holstein dairy cows exposed to high-altitude hypoxia', *Animals*, 9(7), pp. 1–15. doi: 10.3390/ani9070406.

Konoshenko, M. Y. *et al.* (2018) 'Isolation of Extracellular Vesicles: General Methodologies and Latest Trends', *BioMed Research International*. Hindawi Limited. doi: 10.1155/2018/8545347.

Kosinska, M. K. *et al.* (2016) 'Comparative lipidomic analysis of synovial fluid in human and canine osteoarthritis', *Osteoarthritis and Cartilage*, 24(8), pp. 1470–1478. doi: 10.1016/j.joca.2016.03.017.

Kowal, J. *et al.* (2016) 'Proteomic comparison defines novel markers to characterize heterogeneous populations of extracellular vesicle subtypes', *Proceedings of the National Academy of Sciences of the United States of America*, 113(8), pp. E968-977. doi: 10.1073/pnas.1521230113.

Koziy, R. V *et al.* (2022) 'Discovery proteomics for the detection of putative markers for eradication of infection in an experimental model of equine septic arthritis using LC-MS/MS', *Journal of Proteomics*, 261, p. 104571. doi: 10.1016/j.jprot.2022.104571.

Kragstrup, T. W. *et al.* (2017) 'Increased interleukin (IL)-20 and IL-24 target osteoblasts and synovial monocytes in spondyloarthritis', *Clinical and Experimental Immunology*, 189(3), pp. 342–351. doi: 10.1111/cei.12973.

Krämer-Albers, E.-M. *et al.* (2007) 'Oligodendrocytes secrete exosomes containing major myelin and

stress-protective proteins: Trophic support for axons?', *PROTEOMICS – Clinical Applications*, 1(11), pp. 1446–1461. doi: 10.1002/prca.200700522.

Kumar, C. C. *et al.* (1989) 'Characterization and differential expression of human vascular smooth muscle myosin light chain 2 isoform in nonmuscle cells', *Biochemistry*, 28(9), pp. 4027–4035. doi: 10.1021/bi00435a059.

Kuyinu, E. L. *et al.* (2016) 'Animal models of osteoarthritis: Classification, update, and measurement of outcomes', *Journal of Orthopaedic Surgery and Research*. BioMed Central Ltd. doi: 10.1186/s13018-016-0346-5.

Kyriazakos, S. *et al.* (2021) 'Discovering Composite Lifestyle Biomarkers With Artificial Intelligence From Clinical Studies to Enable Smart eHealth and Digital Therapeutic Services', *Frontiers in Digital Health*, 3, p. 648190. doi: 10.3389/fdgth.2021.648190.

Lam *et al.* (2007a) 'Descriptive analysis of retirement of Thoroughbred racehorses due to tendon injuries at the Hong Kong Jockey Club (1992-2004)', *Equine Veterinary Journal*, 39(2), pp. 143–148. doi: 10.2746/042516407X159132.

Lam *et al.* (2007b) 'Evaluation of detailed training data to identify risk factors for retirement because of tendon injuries in Thoroughbred racehorses', *American Journal of Veterinary Research*, 68(11), pp. 1188–1197. doi: 10.2460/ajvr.68.11.1188.

Latifkar, A. *et al.* (2019) 'New insights into extracellular vesicle biogenesis and function', *Journal of Cell Science*, 132(13), pp. 1–9. doi: 10.1242/JCS.222406.

Lázaro-Ibáñez, E. *et al.* (2021) 'Selection of fluorescent, bioluminescent, and radioactive tracers to accurately reflect extracellular vesicle biodistribution in vivo', *ACS Nano*, 15(2), pp. 3212–3227. doi: 10.1021/acsnano.0c09873.

Lee, H. S., Jeong, J. and Lee, K.-J. (2009) 'Characterization of vesicles secreted from insulinoma NIT-1 cells', *Journal of Proteome Research*, 8(6), pp. 2851–2862. doi: 10.1021/pr900009y.

Leek, J. T. *et al.* (2012) 'The SVA package for removing batch effects and other unwanted variation in high-throughput experiments', *Bioinformatics*, 28(6), pp. 882–883. doi: 10.1093/bioinformatics/bts034.

Leonard, N. A. *et al.* (2021) 'Stromal cells promote matrix deposition, remodelling and an immunosuppressive tumour microenvironment in a 3d model of colon cancer', *Cancers*, 13(23). doi: 10.3390/cancers13235998.

- Leopold, S. S. (2021) 'Editorial: In Musculoskeletal Research, Too Many Animals are Being Harmed for Too Small a Return', *Clinical Orthopaedics and Related Research*, 479(3), pp. 427–428. doi: 10.1097/CORR.0000000000001661.
- Leśniak, K. *et al.* (2017) 'Does a 4–6 week shoeing interval promote optimal foot balance in the working equine?', *Animals*, 7(4). doi: 10.3390/ani7040029.
- Li *et al.* (2020) 'hBMSC-Derived Extracellular Vesicles Attenuate IL-1 $\beta$ -Induced Catabolic Effects on OA-Chondrocytes by Regulating Pro-inflammatory Signaling Pathways', *Frontiers in Bioengineering and Biotechnology*, 8. doi: 10.3389/fbioe.2020.603598.
- Li, H. *et al.* (2019) 'Nanotherapy: Nanotherapy in Joints: Increasing Endogenous Hyaluronan Production by Delivering Hyaluronan Synthase 2 (Adv. Mater. 46/2019)', *Advanced Materials*, 31(46), p. 1970331. doi: 10.1002/adma.201970331.
- Li, R. H. L. *et al.* (2020) 'Assessment of P2Y<sub>12</sub> Inhibition by Clopidogrel in Feline Platelets Using Flow Cytometry Quantification of Vasodilator-Stimulated Phosphoprotein Phosphorylation', *Frontiers in Veterinary Science*, 7. Available at: <https://www.frontiersin.org/articles/10.3389/fvets.2020.00267>.
- Li, S. *et al.* (2023) 'Combined Verapamil-Polydopamine Nanoformulation Inhibits Adhesion Formation in Achilles Tendon Injury Using Rat Model', *International Journal of Nanomedicine*, 18, pp. 115–126. doi: 10.2147/IJN.S377600.
- Li, W. W., Li, J. and Bao, J. K. (2012) 'Microautophagy: Lesser-known self-eating', *Cellular and Molecular Life Sciences*, 69(7), pp. 1125–1136. doi: 10.1007/s00018-011-0865-5.
- Li, Y. *et al.* (2022) 'Transforming growth factor- $\beta$  signalling pathway in tendon healing', *Growth Factors*, 40(3–4), pp. 98–107. doi: 10.1080/08977194.2022.2082294.
- Liang, X.-H. *et al.* (2022) 'Identification of potential biomarkers for diagnosis of hepatocellular carcinoma', *Experimental and Therapeutic Medicine*, 23(1), pp. 1–10. doi: 10.3892/etm.2021.10973.
- Lima, C., Muhamadali, H. and Goodacre, R. (2021) 'The Role of Raman Spectroscopy within Quantitative Metabolomics', *Annual Review of Analytical Chemistry*, 14, pp. 323–345. doi: 10.1146/annurev-anchem-091420-092323.
- Lin, Jianjing *et al.* (2021) 'The Role of Extracellular Vesicles in the Pathogenesis, Diagnosis, and Treatment of Osteoarthritis', *Molecules*, 26(16), p. 4987. doi: 10.3390/molecules26164987.
- Lippi, G., Longo, U. G. and Maffulli, N. (2010) 'Genetics and sports', *British Medical Bulletin*, 93(1), pp. 27–47. doi: 10.1093/bmb/ldp007.

- Liu *et al.* (2017) 'Nrf2 inhibits periodontal ligament stem cell apoptosis under excessive oxidative stress', *International Journal of Molecular Sciences*, 18(5). doi: 10.3390/ijms18051076.
- Liu, Shortt, *et al.* (2020) 'Extracellular Vesicles Released From Articular Chondrocytes Play a Major Role in Cell–Cell Communication', *Journal of Orthopaedic Research*, 38(4), pp. 731–739. doi: 10.1002/jor.24525.
- Liu, Cheng, *et al.* (2020) 'Therapeutic effects and perspective of stem cell extracellular vesicles in aging and cancer'. doi: 10.1002/jcp.30212.
- Liu *et al.* (2022) 'Recent Advances of Organ-on-a-Chip in Cancer Modeling Research', *Biosensors*, 12(11), pp. 1–31. doi: 10.3390/bios12111045.
- Liu, Q. *et al.* (2022) 'Tracking tools of extracellular vesicles for biomedical research', *Frontiers in Bioengineering and Biotechnology*, 10(November), pp. 1–13. doi: 10.3389/fbioe.2022.943712.
- Liu, X. *et al.* (2019) 'Exosomes derived from platelet-rich plasma present a novel potential in alleviating knee osteoarthritis by promoting proliferation and inhibiting apoptosis of chondrocyte via Wnt/ $\beta$ -catenin signaling pathway', *Journal of Orthopaedic Surgery and Research*, 14(1). doi: 10.1186/S13018-019-1529-7.
- Liu, Y. *et al.* (2022) 'Mechanical stimulation improves rotator cuff tendon-bone healing via activating IL-4/JAK/STAT signaling pathway mediated macrophage M2 polarization', *Journal of Orthopaedic Translation*, 37(October), pp. 78–88. doi: 10.1016/j.jot.2022.08.008.
- Liu, Z. *et al.* (2017) 'Vascular disease-causing mutation, smooth muscle  $\alpha$ -actin R258C, dominantly suppresses functions of  $\alpha$ -actin in human patient fibroblasts', *Proceedings of the National Academy of Sciences*, 114(28), pp. E5569–E5578. doi: 10.1073/pnas.1703506114.
- Liu, Z., Xiang, Y. and Sun, G. (2013) 'The KCTD family of proteins: structure, function, disease relevance', *Cell & Bioscience*, 3(1), p. 45. doi: 10.1186/2045-3701-3-45.
- Löfgren, M. *et al.* (2018) 'Time-dependent changes in gene expression induced in vitro by interleukin-1 $\beta$  in equine articular cartilage', *Research in Veterinary Science*, 118(April), pp. 466–476. doi: 10.1016/j.rvsc.2018.04.013.
- Lorent, J. H. *et al.* (2020) 'Plasma membranes are asymmetric in lipid unsaturation, packing and protein shape', *Nature Chemical Biology*, 16(6), pp. 644–652. doi: 10.1038/s41589-020-0529-6.
- Lorenzo-Gómez, I. *et al.* (2023) 'Defective chaperone-mediated autophagy is a hallmark of joint disease in patients with knee osteoarthritis', *Osteoarthritis and Cartilage*, 31(7), pp. 919–933. doi:

10.1016/j.joca.2023.02.076.

Ludin, A. *et al.* (2012) 'Monocytes-macrophages that express  $\alpha$ -smooth muscle actin preserve primitive hematopoietic cells in the bone marrow', *Nature Immunology*, 13(11), pp. 1072–1082. doi: 10.1038/ni.2408.

Luga, V. *et al.* (2012) 'Exosomes Mediate Stromal Mobilization of Autocrine Wnt-PCP Signaling in Breast Cancer Cell Migration', *Cell*, 151(7), pp. 1542–1556. doi: 10.1016/j.cell.2012.11.024.

Macrì, S. *et al.* (2013) 'The Directive 2010/63/EU on animal experimentation may skew the conclusions of pharmacological and behavioural studies', *Scientific Reports*, 3, pp. 1–9. doi: 10.1038/srep02380.

Maeder, D., Wuttke, W. and Vogel, M. (2017) 'Immediate, short and long-term effects of hoof trimming on hoof-ground contact in the horse at the walk', *The Australian Equine Veterinarian*.

Magalon, J. *et al.* (2014) 'Characterization and comparison of 5 platelet-rich plasma preparations in a single-donor model', *Arthroscopy - Journal of Arthroscopic and Related Surgery*, 30(5), pp. 629–638. doi: 10.1016/j.arthro.2014.02.020.

Malda, J. *et al.* (2012) 'Comparative study of depth-dependent characteristics of equine and human osteochondral tissue from the medial and lateral femoral condyles', *Osteoarthritis and Cartilage*, 20(10), pp. 1147–1151. doi: 10.1016/j.joca.2012.06.005.

Malda, J. *et al.* (2016) 'Extracellular vesicles — new tool for joint repair and regeneration', *Nature Reviews. Rheumatology*, 12(4), pp. 243–249. doi: 10.1038/nrrheum.2015.170.

Malek, S. *et al.* (2020) 'Infrared spectroscopy of synovial fluid as a potential screening approach for the diagnosis of naturally occurring canine osteoarthritis associated with cranial cruciate ligament rupture', *Osteoarthritis and Cartilage Open*, 2(4), pp. 1–7. doi: 10.1016/j.ocarto.2020.100120.

Mallawaaratchy, D. M. *et al.* (2017) 'Comprehensive proteome profiling of glioblastoma-derived extracellular vesicles identifies markers for more aggressive disease', *Journal of Neuro-Oncology*, 131(2), pp. 233–244. doi: 10.1007/s11060-016-2298-3.

Maly, K. *et al.* (2021) 'Comp and tsp-4: Functional roles in articular cartilage and relevance in osteoarthritis', *International Journal of Molecular Sciences*, 22(5), pp. 1–23. doi: 10.3390/ijms22052242.

Man, X.-Y. *et al.* (2012) 'CD109, a TGF- $\beta$  co-receptor, attenuates extracellular matrix production in scleroderma skin fibroblasts', *Arthritis Research & Therapy*, 14(3), p. R144. doi: 10.1186/ar3877.

Marr, N. *et al.* (2023) 'The tendon interfascicular basement membrane provides a vascular niche for CD146+ cell subpopulations', *Frontiers in Cell and Developmental Biology*, 10(January), pp. 1–14. doi: 10.3389/fcell.2022.1094124.

Martins, M. C. *et al.* (2018) 'Effects of stanozolol on normal and IL-1 $\beta$ -stimulated equine chondrocytes in vitro', *BMC Veterinary Research*, 14(1), pp. 1–7. doi: 10.1186/s12917-018-1426-z.

Mathieu, M. *et al.* (2020) 'Specificities of exosome versus small ectosome secretion revealed by live intracellular tracking and synchronized extracellular vesicle release of CD9 and CD63', *Nature Cell Biology*, p. 2020.10.27.323766. doi: 10.1038/s41467-021-24384-2.

Mathieu, M. *et al.* (2021) 'Specificities of exosome versus small ectosome secretion revealed by live intracellular tracking of CD63 and CD9', *Nature Communications*, 12(1), p. 4389. doi: 10.1038/s41467-021-24384-2.

Matsushita, K. *et al.* (2021) 'Clinicopathological significance of MYL9 expression in pancreatic ductal adenocarcinoma', *Cancer Reports*, 5(10), p. e1582. doi: 10.1002/cnr2.1582.

Matsuyama, T., Murakami, T. and Fujita, M. (1986) 'Extracellular vesicle formation and biosurfactant production by *Serratia marcescens*', *Journal of General Microbiology*, 132(4), pp. 865–875. doi: 10.1099/00221287-132-4-865.

Mattey, D. L. *et al.* (1997) 'Transforming growth factor beta 1 and interleukin 4 induced alpha smooth muscle actin expression and myofibroblast-like differentiation in human synovial fibroblasts in vitro: modulation by basic fibroblast growth factor', *Annals of the Rheumatic Diseases*, 56(7), pp. 426–431. doi: 10.1136/ard.56.7.426.

McCoy, A. M. *et al.* (2020) 'Differential gene expression analysis reveals pathways important in early post-traumatic osteoarthritis in an equine model', *BMC Genomics*, 21(1), pp. 1–12. doi: 10.1186/s12864-020-07228-z.

McIlwraith, C. W. *et al.* (2010) 'The OARSI histopathology initiative - recommendations for histological assessments of osteoarthritis in the horse', *Osteoarthritis and Cartilage*, 18(SUPPL. 3), pp. S93–S105. doi: 10.1016/j.joca.2010.05.031.

McIlwraith, C. W. (2010) 'Use of synovial fluid and serum biomarkers in equine bone and joint disease: a review', *Equine Veterinary Journal*, 37(5), pp. 473–482. doi: 10.2746/042516405774480102.

McIlwraith, C. W., Anderson, T. M. and Sanschi, E. M. (2003) 'Conformation and musculoskeletal problems in the racehorse', *Clinical Techniques in Equine Practice*, 2(4), pp. 339–347. doi:

10.1053/j.ctep.2004.04.006.

McIlwraith, C. W., Frisbie, D. D. and Kawcak, C. E. (2012a) 'The horse as a model of naturally occurring osteoarthritis', *Bone & Joint Research*, 1(11), pp. 297–309. doi: 10.1302/2046-3758.111.2000132.

McIlwraith, C. W., Frisbie, D. D. and Kawcak, C. E. (2012b) 'The horse as a model of naturally occurring osteoarthritis', *Bone & Joint Research*, 1(11), pp. 297–309. doi: 10.1302/2046-3758.111.2000132.

McLeod, C. M. *et al.* (2017) 'ON THE ORIGIN AND IMPACT OF MESENCHYMAL STEM CELL HETEROGENEITY : NEW INSIGHTS AND EMERGING TOOLS FOR SINGLE CELL ANALYSIS', pp. 217–231. doi: 10.22203/eCM.v034a14.

Meeremans, M. *et al.* (2021) 'The Lack of a Representative Tendinopathy Model Hampers Fundamental Mesenchymal Stem Cell Research', *Frontiers in Cell and Developmental Biology*, 9(May), pp. 1–28. doi: 10.3389/fcell.2021.651164.

Meeson, R. L. *et al.* (2019) 'Spontaneous dog osteoarthritis — a One Medicine vision', *Nature Reviews Rheumatology*, 15(5), pp. 273–287. doi: 10.1038/s41584-019-0202-1.

Melling, G. E. *et al.* (2019) 'The Challenges and Possibilities of Extracellular Vesicles as Therapeutic Vehicles', *European Journal of Pharmaceutics and Biopharmaceutics*, 144(July), pp. 50–56. doi: 10.1016/j.ejpb.2019.08.009.

Mellis, D. *et al.* (2021) 'Ubiquitin-protein ligase Ubr5 cooperates with hedgehog signalling to promote skeletal tissue homeostasis', *PLoS Genetics*, 17(4). doi: 10.1371/journal.pgen.1009275.

Miguet, L. *et al.* (2006) 'Proteomic analysis of malignant lymphocyte membrane microparticles using double ionization coverage optimization', *Proteomics*, 6(1), pp. 153–171. doi: 10.1002/pmic.200500133.

Mihály, J. *et al.* (2017) 'Characterization of extracellular vesicles by IR spectroscopy: Fast and simple classification based on amide and C[sbnd]H stretching vibrations', *Biochimica et Biophysica Acta - Biomembranes*, 1859(3), pp. 459–466. doi: 10.1016/j.bbamem.2016.12.005.

Mii, S. *et al.* (2019) 'CD109: a multifunctional GPI-anchored protein with key roles in tumor progression and physiological homeostasis', *Pathology International*, 69(5), pp. 249–259. doi: 10.1111/pin.12798.

Milne, S. *et al.* (2006) 'Lipidomics: An analysis of cellular lipids by ESI-MS', *Methods*, 39(2), pp. 92–



103. doi: 10.1016/j.ymeth.2006.05.014.

Miroshnychenko, O. *et al.* (2020) 'Proteomic analysis of platelet-rich and platelet-poor plasma', *Regenerative Therapy*, 15, pp. 226–235. doi: 10.1016/j.reth.2020.09.004.

Mocchi, M. *et al.* (2020) 'Veterinary Regenerative Medicine for Musculoskeletal Disorders: Can Mesenchymal Stem/Stromal Cells and Their Secretome Be the New Frontier?', *Cells*, 9(6), p. 1453. doi: 10.3390/cells9061453.

Moeller, S. *et al.* (2019) 'The influence of trimming of the hoof wall on the damage of laminar tissue after loading: An in vitro study', *The Veterinary Journal*, 250, pp. 63–70. doi: 10.1016/j.tvjl.2019.07.002.

Mohammadi, A. *et al.* (2022) 'Site- and Zone-Dependent Changes in Proteoglycan Content and Biomechanical Properties of Bluntly and Sharply Grooved Equine Articular Cartilage', *Annals of Biomedical Engineering*, 50(12), pp. 1787–1797. doi: 10.1007/s10439-022-02991-4.

te Moller, N. C. R. *et al.* (2021) 'Structural, compositional, and functional effects of blunt and sharp cartilage damage on the joint: A 9-month equine groove model study', *Journal of Orthopaedic Research*, 39(11), pp. 2363–2375. doi: 10.1002/jor.24971.

Montagna, C. *et al.* (2022) 'Autophagy guards tendon homeostasis', *Cell Death and Disease*, 13(4). doi: 10.1038/s41419-022-04824-7.

Montano, C. *et al.* (2021) 'The Use of Platelet-Rich Plasma for Treatment of Tenodesmic Lesions in Horses: A Systematic Review and Meta-Analysis of Clinical and Experimental Data', *mdpi.com*. doi: 10.3390/ani11030793.

Monteiro, L. J. *et al.* (2018) 'Oral extracellular vesicles in early pregnancy can identify patients at risk of developing gestational diabetes mellitus', *PLoS ONE*, 14(6), pp. 1–13. doi: 10.1371/journal.pone.0218616.

Moradi, E., Jalili-Firoozinezhad, S. and Solati-Hashjin, M. (2020) 'Microfluidic organ-on-a-chip models of human liver tissue', *Acta Biomaterialia*, 116, pp. 67–83. doi: 10.1016/j.actbio.2020.08.041.

Morasso, C. F. *et al.* (2020) 'Raman spectroscopy reveals biochemical differences in plasma derived extracellular vesicles from sporadic Amyotrophic Lateral Sclerosis patients', *Nanomedicine: Nanotechnology, Biology, and Medicine*, 29, p. 102249. doi: 10.1016/j.nano.2020.102249.

Morita, W. *et al.* (2017) 'Cytokines in tendon disease: A systematic review', *Bone and Joint Research*, 6(12), pp. 656–664. doi: 10.1302/2046-3758.612.BJR-2017-0112.R1.

- Mortati, L. *et al.* (2020) 'In vitro study of extracellular vesicles migration in cartilage-derived osteoarthritis samples using real-time quantitative multimodal nonlinear optics imaging', *Pharmaceutics*, 12(8), pp. 1–18. doi: 10.3390/pharmaceutics12080734.
- Mousavi, S. M. *et al.* (2023) 'Exosomes released from U87 glioma cells treated with curcumin and/or temozolomide produce apoptosis in naive U87 cells', *Pathology - Research and Practice*, 245, p. 154427. doi: 10.1016/j.prp.2023.154427.
- Much, M. L. *et al.* (2020) 'Evaluation of an oral joint supplement on gait kinematics and biomarkers of cartilage metabolism and inflammation in mature riding horses', *Translational Animal Science*, 4(3). doi: 10.1093/tas/txaa150.
- Mujammami, M. *et al.* (2022) 'Proteomic Analysis of Endometrial Cancer Tissues from Patients with Type 2 Diabetes Mellitus', *Life (Basel, Switzerland)*, 12(4), p. 491. doi: 10.3390/life12040491.
- Munkholm, K. *et al.* (2019) 'A multisystem composite biomarker as a preliminary diagnostic test in bipolar disorder', *Acta Psychiatrica Scandinavica*, 139(3), pp. 227–236. doi: 10.1111/acps.12983.
- Murray, J. K. *et al.* (2004) 'Factors influencing risk of injury to horses falling during eventing', *Veterinary Record*, 154(7), pp. 207–208. doi: 10.1136/vr.154.7.207.
- Murray, J. M. D., Hanna, E. and Hastie, P. (2018) 'Equine dietary supplements: An insight into their use and perceptions in the Irish equine industry', *Irish Veterinary Journal*, 71(1). doi: 10.1186/s13620-018-0115-3.
- Murray, R. C. *et al.* (2006) 'Association of type of sport and performance level with anatomical site of orthopaedic injury diagnosis', *Equine Veterinary Journal*, 38(SUPPL.36), pp. 411–416. doi: 10.1111/j.2042-3306.2006.tb05578.x.
- Mustonen *et al.* (2021a) 'Characterization of hyaluronan-coated extracellular vesicles in synovial fluid of patients with osteoarthritis and rheumatoid arthritis', *BMC Musculoskeletal Disorders*, 22(1). doi: 10.1186/S12891-021-04115-W.
- Mustonen *et al.* (2021b) 'Characterization of hyaluronan-coated extracellular vesicles in synovial fluid of patients with osteoarthritis and rheumatoid arthritis', *BMC Musculoskeletal Disorders*, 22(1), p. 247. doi: 10.1186/s12891-021-04115-w.
- Mustonen *et al.* (2023) 'Equine osteoarthritis modifies fatty acid signatures in synovial fluid and its extracellular vesicles', *Arthritis Research & Therapy*, 25(1), p. 39. doi: 10.1186/s13075-023-02998-9.
- Mustonen, A. M. *et al.* (2022) 'Counts of hyaluronic acid-containing extracellular vesicles decrease in

naturally occurring equine osteoarthritis', *Scientific Reports*, 12(1), pp. 1–12. doi: 10.1038/s41598-022-21398-8.

Mustonen and Nieminen (2021a) 'Extracellular vesicles and their potential significance in the pathogenesis and treatment of osteoarthritis', *Pharmaceuticals*, 14(4). doi: 10.3390/PH14040315.

Mustonen and Nieminen (2021b) 'Extracellular Vesicles and Their Potential Significance in the Pathogenesis and Treatment of Osteoarthritis', *Pharmaceuticals*, 14(4), p. 315. doi: 10.3390/ph14040315.

Al Naem, M. *et al.* (2020) 'Therapeutic mesenchymal stromal stem cells: Isolation, characterization and role in equine regenerative medicine and metabolic disorders', *Stem Cell Reviews and Reports*. Springer, pp. 301–322. doi: 10.1007/s12015-019-09932-0.

Najar, M. *et al.* (2018) 'Mesenchymal stromal cells of the bone marrow and natural killer cells: cell interactions and cross modulation', *Journal of Cell Communication and Signaling*, 12(4), pp. 673–688. doi: 10.1007/s12079-018-0448-4.

Nasri, H. *et al.* (2014) 'New concepts in nutraceuticals as alternative for pharmaceuticals', *International journal of preventive medicine*. Available at: <https://www.ncbi.nlm.nih.gov/pmc/articles/pmc4336979/> (Accessed: 16 March 2021).

Navarrete, F. *et al.* (2020) 'Distinctive Cellular Transcriptomic Signature and MicroRNA Cargo of Extracellular Vesicles of Horse Adipose and Endometrial Mesenchymal Stem Cells from the Same Donors', *Cellular Reprogramming*, 22(6), pp. 311–327. doi: 10.1089/cell.2020.0026.

Nawaz, M. *et al.* (2018) 'Review extracellular vesicles and matrix remodeling enzymes: The emerging roles in extracellular matrix remodeling, progression of diseases and tissue repair', *Cells*, 7(10), pp. 1–26. doi: 10.3390/cells7100167.

Nazaroff, J. *et al.* (2021) 'Reporting in clinical studies on platelet-rich plasma therapy among all medical specialties: A systematic review of Level I and II studies', *PLoS ONE*, 16(4 April), pp. 1–11. doi: 10.1371/journal.pone.0250007.

Neagu, A.-N. *et al.* (2022) 'Applications of Tandem Mass Spectrometry (MS/MS) in Protein Analysis for Biomedical Research', *Molecules*.

Nelson, B. B. *et al.* (2019) 'Evaluation of equine articular cartilage degeneration after mechanical impact injury using cationic contrast-enhanced computed tomography', *Osteoarthritis and Cartilage*, 27(8), pp. 1219–1228. doi: 10.1016/j.joca.2019.04.015.

- Németh, A. *et al.* (2017) 'Antibiotic-induced release of small extracellular vesicles (exosomes) with surface-associated DNA', *Scientific Reports*, 7, p. 8202. doi: 10.1038/s41598-017-08392-1.
- Neumann, C. A., Cao, J. and Manevich, Y. (2009) 'Peroxisome and its role in cell signaling', *Cell cycle (Georgetown, Tex.)*, 8(24), pp. 4072–4078. doi: 10.4161/cc.8.24.10242.
- Ni, Z. *et al.* (2019) 'The exosome-like vesicles from osteoarthritic chondrocyte enhanced mature IL-1 $\beta$  production of macrophages and aggravated synovitis in osteoarthritis', *Cell Death and Disease*, 10(7). doi: 10.1038/s41419-019-1739-2.
- Ni, Z. *et al.* (2020) 'Exosomes: roles and therapeutic potential in osteoarthritis', *Bone Research*, 8(1). doi: 10.1038/s41413-020-0100-9.
- Nichols, A. E. C., Best, K. T. and Loisel, A. E. (2019) 'The cellular basis of fibrotic tendon healing: challenges and opportunities', *Translational Research*, 209, pp. 156–168. doi: 10.1016/j.trsl.2019.02.002.
- van Niel, G. *et al.* (2022) 'Challenges and directions in studying cell–cell communication by extracellular vesicles', *Nature Reviews Molecular Cell Biology*, 23(5), pp. 369–382. doi: 10.1038/s41580-022-00460-3.
- Nielsen, F. M. *et al.* (2016) 'Discrete adipose-derived stem cell subpopulations may display differential functionality after in vitro expansion despite convergence to a common phenotype distribution', *Stem Cell Research & Therapy*, pp. 1–13. doi: 10.1186/s13287-016-0435-8.
- Nwosu, Z. C. *et al.* (2016) 'Caveolin-1 in the regulation of cell metabolism: a cancer perspective', *Molecular Cancer*, 15(1), p. 71. doi: 10.1186/s12943-016-0558-7.
- O'Brien, C., Marr, N. and Thorpe, | Chavaunne (2021) '| INTRODUC TI ON-THE TR AINING ENVIRONMENT-WHY IS THE S DF T MOS T AT RIS K? Microdamage in the equine superficial digital flexor tendon', *Equine Vet J*, 53, pp. 417–430. doi: 10.1111/evj.13331.
- O'Brien, C., Marr, N. and Thorpe, C. (2021) 'Microdamage in the equine superficial digital flexor tendon', *Equine Veterinary Journal*, 53(3), pp. 417–430. doi: 10.1111/evj.13331.
- O'connor, T. *et al.* (1999) 'Major differences exist in the function and tissue-specific expression of human aflatoxin B1 aldehyde reductase and the principal human aldo-keto reductase AKR1 family members', *The Biochemical Journal*, 343 Pt 2(Pt 2), pp. 487–504. Available at: <http://www.ncbi.nlm.nih.gov/pubmed/10510318>.
- Okubo, K. *et al.* (2016) 'Identification of Novel and Noninvasive Biomarkers of Acute Cellular

Rejection After Liver Transplantation by Protein Microarray', *Transplantation Direct*, 2(12), p. e118. doi: 10.1097/TXD.0000000000000630.

Oláh, T. *et al.* (2021) 'Comparative anatomy and morphology of the knee in translational models for articular cartilage disorders. Part I: Large animals', *Annals of Anatomy*, 235, p. 151680. doi: 10.1016/j.aanat.2021.151680.

Olive, J. *et al.* (2017) 'Metacarpophalangeal joint injury patterns on magnetic resonance imaging: A comparison in racing Standardbreds and Thoroughbreds', *Veterinary Radiology and Ultrasound*, 58(5), pp. 588–597. doi: 10.1111/vru.12512.

de Oliveira, G. P. *et al.* (2021) 'Effects of endurance racing on horse plasma extracellular particle miRNA', *Equine Veterinary Journal*, 53(3), pp. 618–627. doi: 10.1111/evj.13300.

Ossendorff, R. *et al.* (2023) 'Immunomodulatory potential of mesenchymal stromal cell-derived extracellular vesicles in chondrocyte inflammation', *Frontiers in Immunology*, 14(July), pp. 1–12. doi: 10.3389/fimmu.2023.1198198.

Otahal, A. *et al.* (2021) 'Effects of Extracellular Vesicles from Blood-Derived Products on Osteoarthritic Chondrocytes within an Inflammation Model', *mdpi.com*. doi: 10.3390/ijms22137224.

Ottis, P. *et al.* (2019) 'Cellular Resistance Mechanisms to Targeted Protein Degradation Converge Toward Impairment of the Engaged Ubiquitin Transfer Pathway', *ACS Chemical Biology*, 14(10), pp. 2215–2223. doi: 10.1021/acscchembio.9b00525.

Öztürk, A. and Ersan, Ö. (2020) 'Are the Lives of Animals Well-spent in Laboratory Science Research? A Study of Orthopaedic Animal Studies in Turkey', *Clinical Orthopaedics and Related Research*, 478(9), pp. 1965–1970. doi: 10.1097/CORR.0000000000001335.

Paggetti, J. *et al.* (2015) 'Exosomes released by chronic lymphocytic leukemia cells induce the transition of stromal cells into cancer-associated fibroblasts', *Blood*, 126(9), pp. 1106–1117. doi: 10.1182/blood-2014-12-618025.

Palviainen, M. *et al.* (2020) 'Extracellular vesicles from human plasma and serum are carriers of extravesicular cargo—Implications for biomarker discovery', *PLoS ONE*, 15(8 August), pp. 1–19. doi: 10.1371/journal.pone.0236439.

Pan, Z. *et al.* (2020) 'Upregulation of HSP72 attenuates tendon adhesion by regulating fibroblast proliferation and collagen production via blockade of the STAT3 signaling pathway', *Cellular Signalling*, 71(December 2019), p. 109606. doi: 10.1016/j.cellsig.2020.109606.

- Pang, Z. *et al.* (2020) 'MetaboAnalystR 3.0: Toward an Optimized Workflow for Global Metabolomics', *Metabolites*. doi: 10.3390/metabo10050186.
- Pang, Z. *et al.* (2021) 'MetaboAnalyst 5.0: narrowing the gap between raw spectra and functional insights', *Nucleic Acids Research*, 49(W1), pp. W388–W396. doi: 10.1093/nar/gkab382.
- Panizzi, L. *et al.* (2022) 'Infrared spectroscopy of serum fails to identify early biomarker changes in an equine model of traumatic osteoarthritis', *Osteoarthritis and Cartilage Open*, 4(4), p. 100297. doi: 10.1016/j.ocarto.2022.100297.
- Paolini, L. *et al.* (2020) 'Fourier-transform Infrared (FT-IR) spectroscopy fingerprints subpopulations of extracellular vesicles of different sizes and cellular origin', *Journal of Extracellular Vesicles*, 9(1). doi: 10.1080/20013078.2020.1741174.
- Paolini, L. *et al.* (2022) 'Large-scale production of extracellular vesicles: Report on the "massivEVs" ISEV workshop', *Journal of Extracellular Biology*, 1(10). doi: 10.1002/jex2.63.
- Parafioriti, A. *et al.* (2011) 'Single injection of platelet-rich plasma in a rat Achilles tendon tear model', *Muscles, Ligaments and Tendons Journal*, 1(2), pp. 41–47.
- Paraskevaidi, M. *et al.* (2020) 'Attenuated total reflection Fourier-transform infrared (ATR-FTIR) spectroscopy to diagnose osteoarthritis in equine serum', *Equine Veterinary Journal*, 52(1), pp. 46–51. doi: 10.1111/evj.13115.
- Paraskevaidi, M. *et al.* (2021) 'Clinical applications of infrared and Raman spectroscopy in the fields of cancer and infectious diseases', *Applied Spectroscopy Reviews*, 56(8–10), pp. 804–868. doi: 10.1080/05704928.2021.1946076.
- Park, I. *et al.* (2011) 'Myosin regulatory light chains are required to maintain the stability of myosin II and cellular integrity', *Biochemical Journal*, 434(1), pp. 171–180. doi: 10.1042/BJ20101473.
- Parrish, W. R. *et al.* (2016) 'Normal platelet function in platelet concentrates requires non-platelet cells: A comparative in vitro evaluation of leucocyte-rich (type 1a) and leucocyte-poor (type 3b) platelet concentrates', *BMJ Open Sport and Exercise Medicine*, 2(1), pp. 1–8. doi: 10.1136/bmjsem-2015-000071.
- Partridge, E. *et al.* (2022) 'Residual effects of intra-articular betamethasone and triamcinolone acetonide in an equine acute synovitis model', *Equine Veterinary Journal*, (March 2022), pp. 905–915. doi: 10.1111/evj.13899.
- Pascovici, D. *et al.* (2016) 'Multiple testing corrections in quantitative proteomics: A useful but blunt

- tool', *Proteomics*, 16(18), pp. 2448–2453. doi: 10.1002/pmic.201600044.
- Pathan, M. *et al.* (2019) 'Vesiclepedia 2019: a compendium of RNA, proteins, lipids and metabolites in extracellular vesicles', *Nucleic Acids Research*, 47(D1), pp. D516–D519. doi: 10.1093/nar/gky1029.
- Patterson-Kane, J. C., Becker, D. L. and Rich, T. (2012) 'The Pathogenesis of Tendon Microdamage in Athletes: The Horse as a Natural Model for Basic Cellular Research', *Journal of Comparative Pathology*, 147(2–3), pp. 227–247. doi: 10.1016/j.jcpa.2012.05.010.
- Peal, B. T. *et al.* (2020) 'Synovial fluid lubricin and hyaluronan are altered in equine osteochondral fragmentation, cartilage impact injury, and full-thickness cartilage defect models', *Journal of Orthopaedic Research*, 38(8), pp. 1826–1835. doi: 10.1002/jor.24597.
- Peffers, M. J. *et al.* (2015) 'Comprehensive protein profiling of synovial fluid in osteoarthritis following protein equalization', *Osteoarthritis and Cartilage*, 23(7), pp. 1204–1213. doi: 10.1016/j.joca.2015.03.019.
- Peffers, M. J., Liu, X. and Clegg, P. D. (2013) 'Transcriptomic signatures in cartilage ageing', *Arthritis Research and Therapy*, 15(4). doi: 10.1186/ar4278.
- Pellequer, Y. *et al.* (2021) 'Development of a new methodology to determine size differences of nanoparticles with nanoparticle tracking analysis', *Applied Nanoscience (Switzerland)*, 11(7), pp. 2129–2141. doi: 10.1007/s13204-021-01932-2.
- Percie du Sert, N. *et al.* (2020) 'The ARRIVE guidelines 2.0: Updated guidelines for reporting animal research\*', *Journal of Cerebral Blood Flow and Metabolism*, 40(9), pp. 1769–1777. doi: 10.1177/0271678X20943823.
- Perez-Hernandez, D. *et al.* (2013) 'The intracellular interactome of tetraspanin-enriched microdomains reveals their function as sorting machineries toward exosomes', *The Journal of Biological Chemistry*, 288(17), pp. 11649–11661. doi: 10.1074/jbc.M112.445304.
- Perez-Riverol and Csordas (2019) 'The PRIDE database and related tools and resources in 2019: improving support for quantification data', *Nucleic Acid Res.* Available at: <https://academic.oup.com/nar/article-abstract/47/D1/D442/5160986> (Accessed: 25 May 2021).
- Perkins, N. R., Reid, S. W. J. and Morris, R. S. (2005) 'Risk factors for injury to the superficial digital flexor tendon and suspensory apparatus in Thoroughbred racehorses in New Zealand', *New Zealand Veterinary Journal*, 53(3), pp. 184–192. doi: 10.1080/00480169.2005.36503.
- Peterson, D. B. *et al.* (2008) 'Comparative proteomic analysis of PAI-1 and TNF-alpha-derived

- endothelial microparticles', *Proteomics*, 8(12), pp. 2430–2446. doi: 10.1002/pmic.200701029.
- Petta, D. *et al.* (2022) 'Musculoskeletal tissues-on-a-chip: Role of natural polymers in reproducing tissue-specific microenvironments', *Biofabrication*, 14(4). doi: 10.1088/1758-5090/ac8767.
- Philippe, C. (2020) *Linking amyotrophic lateral sclerosis and frontotemporal dementia, Diagnosis and Management in Dementia: The Neuroscience of Dementia, Volume 1*. Elsevier Inc. doi: 10.1016/B978-0-12-815854-8.00004-5.
- Phuyal, S. *et al.* (2015) 'The Ether Lipid Precursor Hexadecylglycerol Stimulates the Release and Changes the Composition of Exosomes Derived from PC-3 Cells', *Journal of Biological Chemistry*, 290(7), pp. 4225–4237. doi: 10.1074/jbc.M114.593962.
- Pitt, J. J. (2009) 'Principles and Applications of Liquid Chromatography- Mass Spectrometry in Clinical Biochemistry', *Clinical Biochemistry Reviews*, 30(February), pp. 19–34.
- Poeter, M. *et al.* (2014) 'Annexin A8 controls leukocyte recruitment to activated endothelial cells via cell surface delivery of CD63', *Nature Communications*, 5(1), p. 3738. doi: 10.1038/ncomms4738.
- Pollet, H. *et al.* (2018) 'Plasma Membrane Lipid Domains as Platforms for Vesicle Biogenesis and Shedding?', *Biomolecules*, 8(3), p. 94. doi: 10.3390/biom8030094.
- Pollonini, L. *et al.* (2020) 'Functional Near-Infrared Spectroscopy to Assess Central Pain Responses in a Nonpharmacologic Treatment Trial of Osteoarthritis', *Journal of Neuroimaging*, 30(6), pp. 808–814. doi: 10.1111/jon.12782.
- Pousinis, P. *et al.* (2020) 'Lipidomic identification of plasma lipids associated with pain behaviour and pathology in a mouse model of osteoarthritis', *Metabolomics*, 16(3), pp. 1–13. doi: 10.1007/s11306-020-01652-8.
- Price, J., Gardiner, C. and Harrison, P. (2021) 'Platelet-enhanced plasma: Characterization of a novel candidate resuscitation fluid's extracellular vesicle content, clotting parameters, and thrombin generation capacity', *Transfusion*, 61(7), pp. 2179–2194. doi: 10.1111/trf.16423.
- Pugliese, B. R. *et al.* (2020) 'Effect of Fatigue on Equine Metacarpophalangeal Joint Kinematics—A Single Horse Pilot Study', *Journal of Equine Veterinary Science*, 86, p. 102849. doi: 10.1016/j.jevs.2019.102849.
- Puhm, F., Boilard, E. and MacHlus, K. R. (2021) 'Platelet extracellular vesicles; beyond the blood', *Arteriosclerosis, Thrombosis, and Vascular Biology*, 41(1), pp. 87–96. doi: 10.1161/ATVBAHA.120.314644.



- Qiu, G. *et al.* (2019) 'Functional proteins of mesenchymal stem cell-derived extracellular vesicles', *Stem Cell Research and Therapy*, 10(1), pp. 1–11. doi: 10.1186/s13287-019-1484-6.
- Qu, J., Zou, T. and Lin, Z. (2021) 'The roles of the ubiquitin–proteasome system in the endoplasmic reticulum stress pathway', *International Journal of Molecular Sciences*, 22(4), pp. 1–21. doi: 10.3390/ijms22041526.
- Qu, M., Zhu, H. and Zhang, X. (2022) 'Extracellular vesicle-mediated regulation of macrophage polarization in bacterial infections', *Frontiers in Microbiology*, 13. Available at: <https://www.frontiersin.org/articles/10.3389/fmicb.2022.1039040>.
- Quan, C. *et al.* (2018) 'Ezrin regulates skin fibroblast size/mechanical properties and YAP-dependent proliferation', *Journal of Cell Communication and Signaling*, 12(3), pp. 549–560. doi: 10.1007/s12079-017-0406-6.
- Quang, C. T. *et al.* (2000) 'Ezrin function is required for ROCK-mediated fibroblast transformation by the Net and Dbl oncogenes', *The EMBO Journal*, 19(17), pp. 4565–4576. doi: 10.1093/emboj/19.17.4565.
- Quiñones-Lombraña, A., Intini, A. and Blanco, J. G. (2019) 'Insights into the transcriptional regulation of the anthracycline reductase AKR7A2 in human cardiomyocytes', *Toxicology letters*, 307, pp. 11–16. doi: 10.1016/j.toxlet.2019.02.015.
- Racchetti, G. and Meldolesi, J. (2021a) 'biomedicines Extracellular Vesicles of Mesenchymal Stem Cells: Therapeutic Properties Discovered with Extraordinary Success', *mdpi.com*. doi: 10.3390/biomedicines9060667.
- Racchetti, G. and Meldolesi, J. (2021b) 'Extracellular vesicles of mesenchymal stem cells: Therapeutic properties discovered with extraordinary successok', *Biomedicines*, 9(6), pp. 1–15. doi: 10.3390/biomedicines9060667.
- Rachubik, P. and Piwkowska, A. (2019) 'The role of vasodilator-stimulated phosphoprotein in podocyte functioning', *Cell Biology International*, 43(10), pp. 1092–1101. doi: 10.1002/cbin.11149.
- Rahmati, S. *et al.* (2020) 'Rho-GTPase pathways may differentiate treatment response to TNF-alpha and IL-17A inhibitors in psoriatic arthritis', *Scientific Reports*, 10(1), p. 21703. doi: 10.1038/s41598-020-78866-2.
- Ramirez, M. I. *et al.* (2018) 'Technical challenges of working with extracellular vesicles', *Nanoscale*, 10, p. 881. doi: 10.1039/c7nr08360b.

- Ratneswaran, Rockel and Kapoor (2020) 'Understanding osteoarthritis pathogenesis: a multiomics system-based approach', *Current Opinion in Rheumatology*.
- Ratti, E. and Berry, J. D. (2016) *Amyotrophic Lateral Sclerosis 1 and Many Diseases, Genomics, Circuits, and Pathways in Clinical Neuropsychiatry*. Elsevier Inc. doi: 10.1016/B978-0-12-800105-9.00042-1.
- Rea, S. L. *et al.* (2013) 'New insights into the role of sequestosome 1/p62 mutant proteins in the pathogenesis of paget's disease of bone', *Endocrine Reviews*, 34(4), pp. 501–524. doi: 10.1210/er.2012-1034.
- Reesink, H. L. *et al.* (2018) 'Galectins-1 and-3 increase in equine post-traumatic osteoarthritis', *Frontiers in Veterinary Science*, 5(NOV), pp. 1–11. doi: 10.3389/fvets.2018.00288.
- Ribitsch, I. *et al.* (2020) 'Large Animal Models in Regenerative Medicine and Tissue Engineering: To Do or Not to Do', *Frontiers in Bioengineering and Biotechnology*, 8, p. 972. doi: 10.3389/fbioe.2020.00972.
- Ribitsch, I., Oreff, G. L. and Jenner, F. (2021a) 'animals Regenerative Medicine for Equine Musculoskeletal Diseases', *mdpi.com*. doi: 10.3390/ani11010234.
- Ribitsch, I., Oreff, G. L. and Jenner, F. (2021b) 'Regenerative medicine for equine musculoskeletal diseases', *Animals*, 11(1), pp. 1–30. doi: 10.3390/ani11010234.
- Rice, S. J. *et al.* (2021) 'Genetic and Epigenetic Fine-Tuning of TGFB1 Expression Within the Human Osteoarthritic Joint', *Arthritis & Rheumatology*, 73(10), pp. 1866–1877. doi: 10.1002/art.41736.
- Rigoglou, S. and Papavassiliou, A. G. (2013) 'The NF- $\kappa$ B signalling pathway in osteoarthritis', *International Journal of Biochemistry and Cell Biology*, 45(11), pp. 2580–2584. doi: 10.1016/j.biocel.2013.08.018.
- Rikkert, L. G. *et al.* (2018) 'Journal of Extracellular Vesicles Quality of extracellular vesicle images by transmission electron microscopy is operator and protocol dependent Quality of extracellular vesicle images by transmission electron microscopy is operator and protocol dependent', *Taylor & Francis*, 8(1). doi: 10.1080/20013078.2018.1555419.
- Rivers-Auty, J. *et al.* (2018) 'Redefining the ancestral origins of the interleukin-1 superfamily', *Nature Communications*, 9(1), pp. 1–12. doi: 10.1038/s41467-018-03362-1.
- Rocha, B. *et al.* (2021) 'Targeted phospholipidomic analysis of synovial fluid as a tool for osteoarthritis deep phenotyping', *Osteoarthritis and Cartilage Open*, 3(4), p. 100219. doi:

10.1016/j.ocarto.2021.100219.

Rockey, D. C., Du, Q. and Shi, Z. (2019) 'Smooth Muscle  $\alpha$ -Actin Deficiency Leads to Decreased Liver Fibrosis via Impaired Cytoskeletal Signaling in Hepatic Stellate Cells', *The American Journal of Pathology*, 189(11), pp. 2209–2220. doi: 10.1016/j.ajpath.2019.07.019.

Rodeo, S. (2019) 'The Need for Minimum Reporting Standards for Studies of "Biologics" in Sports Medicine', *American Journal of Sports Medicine*, 47(11), pp. 2531–2532. doi: 10.1177/0363546519872219.

Roelofs, A. J. *et al.* (2017) 'Joint morphogenetic cells in the adult mammalian synovium', *Nature Communications*, 8(May), pp. 1–14. doi: 10.1038/ncomms15040.

Rohart, F. *et al.* (2017) 'mixOmics: An R package for 'omics feature selection and multiple data integration', *PLOS Computational Biology*. Edited by D. Schneidman, 13(11), p. e1005752. doi: 10.1371/journal.pcbi.1005752.

Roos, E. M. and Arden, N. K. (2016) 'Strategies for the prevention of knee osteoarthritis', *Nature Reviews. Rheumatology*, 12(2), pp. 92–101. doi: 10.1038/nrrheum.2015.135.

Routh, J. *et al.* (2020) 'An investigation of the association between hindlimb conformation and suspensory desmopathy in sports horses', *Equine Veterinary Education*, 32(S10), pp. 183–192. doi: 10.1111/eve.13089.

Rowbotham, T. J. (1980) 'Preliminary report on the pathogenicity of *Legionella pneumophila* for freshwater and soil amoebae', *Journal of Clinical Pathology*, 33(12), pp. 1179–1183. doi: 10.1136/jcp.33.12.1179.

Rozanova, S. *et al.* (2021) 'Quantitative Mass Spectrometry-Based Proteomics: An Overview', in *Quantitative Methods in Proteomics*, pp. 85–116. doi: 10.1007/978-1-0716-1024-4\_8.

RStudio (2015) 'Integrated Development for R.', p. R Studio.

RStudio (2020) 'RStudio: Integrated Development Environment for R'. Boston, MA: RStudio, PBC. Available at: <http://www.rstudio.com/>.

Russell, A. E. *et al.* (2019) 'Biological membranes in EV biogenesis, stability, uptake, and cargo transfer: an ISEV position paper arising from the ISEV membranes and EVs workshop', *Journal of Extracellular Vesicles*, 8(1), p. 1684862. doi: 10.1080/20013078.2019.1684862.

Russo, M. *et al.* (2020) 'Raman Spectroscopic Stratification of Multiple Myeloma Patients Based on Exosome Profiling', *ACS Omega*, 5(47), pp. 30436–30443. doi: 10.1021/acsomega.0c03813.

- Ruznan, W. *et al.* (2020) 'Understanding stress-strain behavioral change in fabrics for compression bandaging', *journals.sagepub.com*. doi: 10.1177/1534734620912093.
- Ryter, S. W. (2022) 'Heme Oxygenase-1: An Anti-Inflammatory Effector in Cardiovascular, Lung, and Related Metabolic Disorders', *Antioxidants*, 11(3), pp. 1–26. doi: 10.3390/antiox11030555.
- Saalbach, A. and Andereg, U. (2019) 'Thy-1: more than a marker for mesenchymal stromal cells', *The FASEB Journal*, 33(6), pp. 6689–6696. doi: 10.1096/fj.201802224R.
- Salvatore, L. *et al.* (2020) 'An insight on type I collagen from horse tendon for the manufacture of implantable devices', *International Journal of Biological Macromolecules*, 154, pp. 291–306. doi: 10.1016/j.ijbiomac.2020.03.082.
- Samvelyan, H. J. *et al.* (2020) 'Models of Osteoarthritis: Relevance and New Insights', *Calcified Tissue International*. Springer, p. 3. doi: 10.1007/s00223-020-00670-x.
- dos Santos, R. G. *et al.* (2021) 'The regenerative mechanisms of platelet-rich plasma: A review', *Cytokine*, 144(April). doi: 10.1016/j.cyto.2021.155560.
- Schäfer, N. and Grässel, S. (2022) 'Involvement of complement peptides C3a and C5a in osteoarthritis pathology', *Peptides*, 154(May). doi: 10.1016/j.peptides.2022.170815.
- De Schauwer, C. *et al.* (2013) 'Mesenchymal stem cell therapy in horses: Useful beyond orthopedic injuries?', *Veterinary Quarterly*, 33(4), pp. 234–241. doi: 10.1080/01652176.2013.800250.
- Schlueter, A. E. and Orth, M. W. (2004) 'Equine osteoarthritis: a brief review of the disease and its causes', *Equine and Comparative Exercise Physiology*, 1(4), pp. 221–231. doi: 10.1079/ECP200428.
- Schramme, M. *et al.* (2010) 'A surgical tendonitis model in horses: Technique, clinical, ultrasonographic and histological characterisation', *Veterinary and Comparative Orthopaedics and Traumatology*, 23(4), pp. 231–239. doi: 10.3415/VCOT-09-10-0106.
- Schroeder, J.-H. *et al.* (2023) 'CD90 is not constitutively expressed in functional innate lymphoid cells', *Frontiers in Immunology*, 14, p. 1113735. doi: 10.3389/fimmu.2023.1113735.
- Schulze-Tanzil, G. *et al.* (2004) 'Cultivation of human tenocytes in high-density culture', *Histochemistry and Cell Biology*, 122(3), pp. 219–228. doi: 10.1007/s00418-004-0694-9.
- Schuurman, S. O., Kersten, W. and Weijs, W. A. (2003) 'The equine hind limb is actively stabilized during standing', *Journal of Anatomy*, 202(4), pp. 355–362. doi: 10.1046/j.1469-7580.2003.00166.x.
- Seabaugh, K. A. *et al.* (2022) 'Examining the Effects of the Oral Supplement *Biota orientalis* in the

Osteochondral Fragment-Exercise Model of Osteoarthritis in the Horse', *Frontiers in Veterinary Science*, 9(June), pp. 1–10. doi: 10.3389/fvets.2022.858391.

Sebbagh, P. *et al.* (2023) 'Current Status of PRP Manufacturing Requirements & European Regulatory Frameworks: Practical Tools for the Appropriate Implementation of PRP Therapies in Musculoskeletal Regenerative Medicine', *Bioengineering*, 10(3). doi: 10.3390/bioengineering10030292.

Senju, Y. and Tsai, F.-C. (2022) 'A biophysical perspective of the regulatory mechanisms of ezrin/radixin/moesin proteins', *Biophysical Reviews*, 14(1), pp. 199–208. doi: 10.1007/s12551-021-00928-0.

Shakya, B. R. *et al.* (2020) 'Detection of experimental cartilage damage with acoustic emissions technique: An in vitro equine study', *Equine Veterinary Journal*, 52(1), pp. 152–157. doi: 10.1111/evj.13132.

Shariatzadeh, M., Song, J. and Wilson, S. L. (2019) 'The efficacy of different sources of mesenchymal stem cells for the treatment of knee osteoarthritis', *Cell and Tissue Research*, pp. 399–410. doi: 10.1007/s00441-019-03069-9.

Silawal, S. *et al.* (2018) 'Osteoarthritis and the complement cascade', *Clinical Medicine Insights: Arthritis and Musculoskeletal Disorders*, 11. doi: 10.1177/1179544117751430.

Silva, A. K. A. *et al.* (2021) 'Development of extracellular vesicle-based medicinal products: A position paper of the group "Extracellular Vesicle translation to clinical perspectives – EVOLVE France"', *Advanced Drug Delivery Reviews*, 179, p. 114001. doi: 10.1016/j.addr.2021.114001.

Simón, L. *et al.* (2020) 'Caveolin-1 function at the plasma membrane and in intracellular compartments in cancer', *Cancer Metastasis Reviews*, 39(2), pp. 435–453. doi: 10.1007/s10555-020-09890-x.

Singh, Y. P. *et al.* (2021) 'Overcoming the Dependence on Animal Models for Osteoarthritis Therapeutics – The Promises and Prospects of In Vitro Models', *Advanced Healthcare Materials*, 10(20). doi: 10.1002/adhm.202100961.

Smith, A. D. *et al.* (2014) 'Magnetic Resonance Imaging Scoring of an Experimental Model of Osteoarthritis in the Equine Carpus', *Osteoarthritis Research Society International Proceedings*, 57(5), pp. 502–514. doi: 10.1111/vru.12369.

Smith, R. K. *et al.* (1999) 'Should equine athletes commence training during skeletal development?: changes in tendon matrix associated with development, ageing, function and exercise.', *Equine*

- veterinary journal. Supplement*, 30, pp. 201–209. doi: 10.1111/j.2042-3306.1999.tb05218.x.
- Smith, R. K. W. and McIlwraith, C. W. (2021) ‘“One Health” in tendinopathy research: Current concepts’, *Journal of Orthopaedic Research*, 39(8), pp. 1596–1602. doi: 10.1002/jor.25035.
- Sokolove, J. and Lepus, C. M. (2013) ‘Role of inflammation in the pathogenesis of osteoarthritis: latest findings and interpretations’, *Therapeutic Advances in Musculoskeletal Disease*, 5(2), pp. 77–94. doi: 10.1177/1759720X12467868.
- Song, G. *et al.* (2019) ‘CD109 regulates the inflammatory response and is required for the pathogenesis of rheumatoid arthritis’, *Annals of the Rheumatic Diseases*, 78(12), pp. 1632–1641. doi: 10.1136/annrheumdis-2019-215473.
- Song, H. Y. *et al.* (2010) ‘Synovial fluid of patients with rheumatoid arthritis induces  $\alpha$ -smooth muscle actin in human adipose tissue-derived mesenchymal stem cells through a TGF- $\beta$ 1-dependent mechanism’, *Experimental & Molecular Medicine*, 42(8), pp. 565–573. doi: 10.3858/emm.2010.42.8.057.
- de Sousa, E. B. *et al.* (2019) ‘Osteoarthritic synovial fluid modulates cell phenotype and metabolic behavior in vitro’, *Stem Cells International*, 2019. doi: 10.1155/2019/8169172.
- De Souza, R. A. *et al.* (2014) ‘Raman spectroscopy detection of molecular changes associated with two experimental models of osteoarthritis in rats’, *Lasers in Medical Science*, 29(2), pp. 797–804. doi: 10.1007/s10103-013-1423-1.
- Spakova, T., Janockova, J. and Rosocha, J. (2021) ‘Characterization and therapeutic use of extracellular vesicles derived from platelets’, *International Journal of Molecular Sciences*, 22(18). doi: 10.3390/ijms22189701.
- Stadtman, A. and Zarbock, A. (2017) ‘The role of kindlin in neutrophil recruitment to inflammatory sites’, *Current Opinion in Hematology*, 24(1), pp. 38–45. doi: 10.1097/MOH.0000000000000294.
- Stutz, J. C. *et al.* (2018) ‘Effect of three types of horseshoes and unshod feet on selected nonpodal forelimb kinematic variables measured by an extremity mounted inertial measurement unit sensor system in sound horses at the trot under conditions of treadmill and soft geotextile surface exercise’, *Veterinary Record Open*, 5(1), p. 237. doi: 10.1136/vetreco-2017-000237.
- Subramanian, I. *et al.* (2020a) ‘Multi-omics Data Integration, Interpretation, and Its Application’, *Bioinformatics and Biology Insights*, 14, p. 117793221989905. doi: 10.1177/1177932219899051.
- Subramanian, I. *et al.* (2020b) ‘Multi-omics Data Integration, Interpretation, and Its Application’,

*Bioinformatics and Biology Insights*, 14, pp. 7–9. doi: 10.1177/1177932219899051.

Sulaiman, S. S. *et al.* (2020) 'Comparison of synovial fluid proteome profiles between chemically induced rabbit model and surgically induced rabbit model in mimicking early osteoarthritis', *Osteoarthritis and Cartilage*, 28(2020), p. S349. doi: 10.1016/j.joca.2020.02.546.

Sunil, K. *et al.* (2014) 'Differential ubiquitin-proteasome and autophagy signaling following rotator cuff tears and suprascapular nerve injury', *Journal of Orthopaedic Research*. doi: 10.1002/jor.22482.Differential.

Syromiatnikova, V., Prokopeva, A. and Gomzikova, M. (2022) 'Methods of the Large-Scale Production of Extracellular Vesicles', *International Journal of Molecular Sciences*, 23(18). doi: 10.3390/ijms231810522.

Szczesny, S. E. (2020) 'Ex vivo models of musculoskeletal tissues', *Connective Tissue Research*, 61(3–4), pp. 245–247. doi: 10.1080/03008207.2020.1742418.

Takamura, M. *et al.* (2017) 'The effect of platelet-rich plasma on Achilles tendon healing in a rabbit model', *Acta Orthopaedica et Traumatologica Turcica*, 51(1), pp. 65–72. doi: 10.1016/j.aott.2016.12.001.

Tamura, Kodaira and Yoshihara (2018) 'A retrospective cohort study investigating risk factors for the failure of Thoroughbred racehorses to return to racing after superficial digital flexor tendon injury', *Veterinary Journal*. Available at: <https://www.sciencedirect.com/science/article/pii/S1090023318300662> (Accessed: 16 March 2021).

Tan, S. S. H. *et al.* (2021) 'Mesenchymal Stem Cell Exosomes for Cartilage Regeneration: A Systematic Review of Preclinical in Vivo Studies', *Tissue Engineering - Part B: Reviews*, 27(1), pp. 1–13. doi: 10.1089/TEN.TEB.2019.0326.

Tao, Guo and Zhang (2017) 'Platelet-derived extracellular vesicles: An emerging therapeutic approach', *International Journal of Biological Sciences*, 13(7), pp. 828–834. doi: 10.7150/ijbs.19776.

Tauro, B. J. *et al.* (2013) 'Oncogenic H-ras reprograms Madin-Darby canine kidney (MDCK) cell-derived exosomal proteins following epithelial-mesenchymal transition', *Molecular & cellular proteomics: MCP*, 12(8), pp. 2148–2159. doi: 10.1074/mcp.M112.027086.

Taylor, S. *et al.* (2007) 'Mesenchymal stem cell therapy in equine musculoskeletal disease: scientific fact or clinical fiction?', *Wiley Online Library*, 39(2), pp. 172–180. doi: 10.2746/042516407X180868.

Teeple, E. *et al.* (2013) 'Animal models of osteoarthritis: Challenges of model selection and analysis',

*AAPS Journal*, pp. 438–446. doi: 10.1208/s12248-013-9454-x.

Temple-Wong, M. *et al.* (2020) 'Effects of an articular cartilage lubrication with a viscosupplement in vitro and in vivo following osteochondral fractures in horses', *American veterinary medical association*, 82(8), pp. 611–618.

Teng, F. and Fussenegger, M. (2021) 'Shedding Light on Extracellular Vesicle Biogenesis and Bioengineering', *Advanced Science*, 8(1), pp. 1–17. doi: 10.1002/adv.202003505.

Thampi, P. *et al.* (2021) 'Surface Topography as a Tool to Detect Early Changes in a Post-Traumatic Equine Model of Osteoarthritis', *Journal of Orthopaedic Research*, (February), pp. 1–9. doi: 10.1002/jor.25175.

Thankam, F. G. *et al.* (2018) 'Amplification of Mitochondrial Activity in the Healing Response Following Rotator Cuff Tendon Injury', *Scientific Reports*, 8(1), pp. 1–14. doi: 10.1038/s41598-018-35391-7.

Theodossiou, S. K. and Schiele, N. R. (2019) 'Models of tendon development and injury', *BMC Biomedical Engineering*, 1(1), pp. 1–24. doi: 10.1186/s42490-019-0029-5.

Théry, C. *et al.* (2001) 'Proteomic Analysis of Dendritic Cell-Derived Exosomes: A Secreted Subcellular Compartment Distinct from Apoptotic Vesicles<sup>1</sup>', *The Journal of Immunology*, 166(12), pp. 7309–7318. doi: 10.4049/jimmunol.166.12.7309.

Théry, C. *et al.* (2018) 'Minimal information for studies of extracellular vesicles 2018 (MISEV2018): a position statement of the International Society for Extracellular Vesicles and update of the MISEV2014 guidelines', *Journal of Extracellular Vesicles*, 7(1). doi: 10.1080/20013078.2018.1535750.

Thorpe, C. T., Clegg, P. D. and Birch, H. L. (2010) 'A review of tendon injury: Why is the equine superficial digital flexor tendon most at risk?', *Equine Veterinary Journal*, pp. 174–180. doi: 10.2746/042516409X480395.

Thysen, S. *et al.* (2015) 'Targets, models and challenges in osteoarthritis research', *dmm.biologists.org*. doi: 10.1242/dmm.016881.

Tofiño-Vian, M. *et al.* (2018) 'Microvesicles from Human Adipose Tissue-Derived Mesenchymal Stem Cells as a New Protective Strategy in Osteoarthritic Chondrocytes', *Cellular Physiology and Biochemistry*, 47(1), pp. 11–25. doi: 10.1159/000489739.

Tognoloni, A. *et al.* (2023) 'Platelets Rich Plasma Increases Antioxidant Defenses of Tenocytes via Nrf2 Signal Pathway', *International Journal of Molecular Sciences*, 24(17). doi:



10.3390/ijms241713299.

Tossetta, G. *et al.* (2022) 'The multifaced role of HtrA1 in the development of joint and skeletal disorders', *Bone*, 157(February), p. 116350. doi: 10.1016/j.bone.2022.116350.

Tóth, E. Á. *et al.* (2021) 'Formation of a protein corona on the surface of extracellular vesicles in blood plasma', *Journal of Extracellular Vesicles*, 10(11), p. e12140. doi: 10.1002/jev2.12140.

Trevino, R. L. *et al.* (2017) 'Development of a Cartilage Shear-Damage Model to Investigate the Impact of Surface Injury on Chondrocytes and Extracellular Matrix Wear', *Cartilage*, 8(4), pp. 444–455. doi: 10.1177/1947603516681133.

Turiák, L. *et al.* (2011) 'Proteomic characterization of thymocyte-derived microvesicles and apoptotic bodies in BALB/c mice', *Journal of Proteomics*, 74(10), pp. 2025–2033. doi: 10.1016/j.jprot.2011.05.023.

Turlo, A. J. *et al.* (2018) 'Donor age affects proteome composition of tenocyte-derived engineered tendon', *BMC Biotechnology*, 18(1). doi: 10.1186/s12896-018-0414-5.

Turlo, A. J. *et al.* (2019) 'Insulin-like growth factor binding protein (Igfbp6) is a cross-species tendon marker', *European Cells and Materials*, 38, pp. 123–136. doi: 10.22203/eCM.v038a10.

Uvebrant *et al.* (2019) 'Integrin  $\alpha 10\beta 1$ -selected Equine MSCs have Improved Chondrogenic Differentiation, Immunomodulatory and Cartilage Adhesion Capacity', *Annals of Stem Cell Research Research*.

Varas, L. *et al.* (2007) 'Growth Factor-2-Treated Mesenchymal Stem Cells with', 978, pp. 965–978. doi: 10.1089/scd.2007.0049.

Varela, L. *et al.* (2023) 'Acute joint inflammation induces a sharp increase in the number of synovial fluid EVs and modifies their phospholipid profile', *Biochimica et Biophysica Acta (BBA) - Molecular and Cell Biology of Lipids*, 1868(10), p. 159367. doi: 10.1016/j.bbalip.2023.159367.

Varela, L., Clarke, E. and van de Lest van Weeren A4 - Marca, Wauben A4 - Mandy, Peffers, C. H. A. A.-R. (2023) 'Proteome and phospholipidome interrelationship of synovial fluid-derived extracellular vesicles in equine osteoarthritis: An exploratory “multi-omics” study towards combined biomarkers'. Utrecht University. doi: 10.24416/UU01-Q25GD7.

Vasileva, N. S. *et al.* (2022) 'Transcriptome Changes in Glioma Cells Cultivated under Conditions of Neurosphere Formation', *Cells*, 11(19), p. 3106. doi: 10.3390/cells11193106.

Vastrad, B., Vastrad, C. and Tengli, A. (2020) 'Bioinformatics analyses of significant genes, related

pathways, and candidate diagnostic biomarkers and molecular targets in SARS-CoV-2/COVID-19', *Gene Reports*, 21, p. 100956. doi: 10.1016/j.genrep.2020.100956.

Vences-Catalán, F. *et al.* (2021) 'Targeting the tetraspanin CD81 reduces cancer invasion and metastasis', 118. doi: 10.1073/pnas.2018961118/-/DCSupplemental.

Verweij, F. J. *et al.* (2021) 'The power of imaging to understand extracellular vesicle biology in vivo', *Nature Methods*, 18(9), pp. 1013–1026. doi: 10.1038/s41592-021-01206-3.

Vestad, B. *et al.* (2017) 'Size and concentration analyses of extracellular vesicles by nanoparticle tracking analysis: a variation study', *Journal of Extracellular Vesicles*, 6(1). doi: 10.1080/20013078.2017.1344087.

Villanueva, R. A. M. and Chen, Z. J. (2019) 'ggplot2: Elegant Graphics for Data Analysis (2nd ed.)', *Measurement: Interdisciplinary Research and Perspectives*, 17(3), pp. 160–167. doi: 10.1080/15366367.2019.1565254.

Vincourt, J.-B. *et al.* (2006) 'Establishment of a Reliable Method for Direct Proteome Characterization of Human Articular Cartilage\*', *Molecular & Cellular Proteomics*, 5(10), pp. 1984–1995. doi: 10.1074/mcp.T600007-MCP200.

van der Vlist, E. J. *et al.* (2012) 'Fluorescent labeling of nano-sized vesicles released by cells and subsequent quantitative and qualitative analysis by high-resolution flow cytometry', *Nature Protocols*, 7(7), pp. 1311–1326. doi: 10.1038/nprot.2012.065.

Voga, M. *et al.* (2020) 'Stem Cells in Veterinary Medicine—Current State and Treatment Options', *Frontiers in Veterinary Science*, 7(May), pp. 1–20. doi: 10.3389/fvets.2020.00278.

Voleti, P. B., Buckley, M. R. and Soslowsky, L. J. (2012) 'Tendon healing: Repair and regeneration', *Annual Review of Biomedical Engineering*, 14, pp. 47–71. doi: 10.1146/ANNUREV-BIOENG-071811-150122.

Vonk, L. A. *et al.* (2018) 'Mesenchymal stromal/stem cell-derived extracellular vesicles promote human cartilage regeneration in vitro', *Theranostics*, 8(4), pp. 906–920. doi: 10.7150/thno.20746.

Wagner, F. C. *et al.* (2021) 'Biplanar high-speed fluoroscopy of pony superficial digital flexor tendon (Sdft)—an in vivo pilot study', *Veterinary Sciences*, 8(6). doi: 10.3390/vetsci8060092.

Wang, J., Zohar, R. and McCulloch, C. A. (2006) 'Multiple roles of alpha-smooth muscle actin in mechanotransduction', *Experimental Cell Research*, 312(3), pp. 205–214. doi: 10.1016/j.yexcr.2005.11.004.

Wang, Jian *et al.* (2020) 'Roles of Exosomes from Mesenchymal Stem Cells in Treating Osteoarthritis', *liebertpub.com*, 22(3), pp. 107–117. doi: 10.1089/cell.2019.0098.

Wang, Q. *et al.* (2011) 'Identification of a central role for complement in osteoarthritis', *Nature Medicine*, 17(12), pp. 1674–1679. doi: 10.1038/nm.2543.

Wang, Y. *et al.* (2017) 'Exosomes from embryonic mesenchymal stem cells alleviate osteoarthritis through balancing synthesis and degradation of cartilage extracellular matrix', *Stem Cell Research and Therapy*, 8(1), pp. 1–13. doi: 10.1186/s13287-017-0632-0.

Wang, Z. *et al.* (2021) 'KCTD12 is a prognostic marker of breast cancer and correlates with tumor immune cell infiltration', *Translational Cancer Research*, 10(1), pp. 261–272. doi: 10.21037/tcr-20-2099.

Wanner, J. P. *et al.* (2013) 'Proteomic profiling and functional characterization of early and late shoulder osteoarthritis', *Arthritis Research and Therapy*, 15(6), p. 1. doi: 10.1186/ar4369.

Van De Water, E. *et al.* (2016) 'The preventive effects of two nutraceuticals on experimentally induced acute synovitis', *Wiley Online Library*, 49(4), pp. 532–538. doi: 10.1111/evj.12629.

Watkins, A. *et al.* (2021) 'Investigation of synovial fluid lubricants and inflammatory cytokines in the horse: a comparison of recombinant equine interleukin 1 beta-induced synovitis and joint lavage models', *BMC Veterinary Research*, 17(1). doi: 10.1186/S12917-021-02873-2.

Webb, T. L., Spaas, J. H. and Guest, D. J. (2022) 'Editorial: One Health and Veterinary Regenerative Medicine: Translational Applications', *Frontiers in Veterinary Science*, 9(July), pp. 9–11. doi: 10.3389/fvets.2022.959564.

van Weeren, P. R. and Back, W. (2016a) 'Musculoskeletal Disease in Aged Horses and Its Management', *Veterinary Clinics of North America - Equine Practice*, pp. 229–247. doi: 10.1016/j.cveq.2016.04.003.

van Weeren, P. R. and Back, W. (2016b) 'Musculoskeletal Disease in Aged Horses and Its Management', *Veterinary Clinics of North America - Equine Practice*. W.B. Saunders, pp. 229–247. doi: 10.1016/j.cveq.2016.04.003.

Wei, W. *et al.* (2021) 'Plasma Levels of Heat Shock Protein 90 Alpha Associated With Colorectal Cancer Development', *Frontiers in Molecular Biosciences*, 8, p. 684836. doi: 10.3389/fmolb.2021.684836.

Welsh, J. A. *et al.* (2020) 'MIFlowCyt-EV: a framework for standardized reporting of extracellular

- vesicle flow cytometry experiments', *Journal of Extracellular Vesicles*, 9(1), p. 1713526. doi: 10.1080/20013078.2020.1713526.
- White, A. H. *et al.* (2002) 'Annexin VIII Is Differentially Expressed by Chondrocytes in the Mammalian Growth Plate During Endochondral Ossification and in Osteoarthritic Cartilage', *Journal of Bone and Mineral Research*, 17(10), pp. 1851–1858. doi: 10.1359/jbmr.2002.17.10.1851.
- Wijekoon, H. M. S. and de Silva, D. D. N. (2021) 'Current Evidence on Using Platelet Rich Plasma as a Therapeutic Modality for Veterinary Orthopedic Conditions', *World's Veterinary Journal*, 11(1), pp. 73–78. doi: 10.54203/scil.2021.wvj10.
- Wiles, A. K. *et al.* (2023) 'Activated CD90/Thy-1 fibroblasts co-express the  $\Delta$ 133p53 $\beta$  isoform and are associated with highly inflamed rheumatoid arthritis', *Arthritis Research & Therapy*, 25(1), p. 62. doi: 10.1186/s13075-023-03040-8.
- Wilkinson, D. J. *et al.* (2019) 'Serine proteinases in the turnover of the cartilage extracellular matrix in the joint: implications for therapeutics', *British Journal of Pharmacology*, 176(1), pp. 38–51. doi: 10.1111/bph.14173.
- Wilson, J. M., McKenzie, E. and Duesterdieck-Zellmer, K. (2018) 'International survey regarding the use of rehabilitation modalities in horses', *Frontiers in Veterinary Science*, 5(JUN). doi: 10.3389/fvets.2018.00120.
- Withrow, J. *et al.* (2016) 'Extracellular vesicles in the pathogenesis of rheumatoid arthritis and osteoarthritis', *Arthritis Research and Therapy*, 18(1), pp. 1–12. doi: 10.1186/s13075-016-1178-8.
- Witwer, K. W. *et al.* (2021) 'Updating MISEV: Evolving the minimal requirements for studies of extracellular vesicles', *Journal of Extracellular Vesicles*, 10(14). doi: 10.1002/jev2.12182.
- Wolf, P. (1967) 'The nature and significance of platelet products in human plasma.', *British journal of haematology*, 13(3), pp. 269–288. doi: 10.1111/j.1365-2141.1967.tb08741.x.
- Woodell-May, J. E. and Sommerfeld, S. D. (2020) 'Role of Inflammation and the Immune System in the Progression of Osteoarthritis', *Journal of Orthopaedic Research*, 38(2), pp. 253–257. doi: 10.1002/jor.24457.
- Wright, I. M. (2010) 'Oral supplements in the treatment and prevention of joint diseases: a review of their potential application to the horse', *Equine Veterinary Education*, 13(3), pp. 135–139. doi: 10.1111/j.2042-3292.2001.tb00078.x.
- Wu, Hu, *et al.* (2021) 'clusterProfiler 4.0: A universal enrichment tool for interpreting omics data',

- The Innovation*, 2(3), p. 100141. doi: 10.1016/j.xinn.2021.100141.
- Wu, Zhang, *et al.* (2021) 'Extracellular vesicles: A bright star of nanomedicine', *Biomaterials*, 269. doi: 10.1016/J.BIOMATERIALS.2020.120467.
- Wu, Piao, *et al.* (2021) 'Platelet-rich plasma-derived extracellular vesicles: A superior alternative in regenerative medicine?', *Cell Proliferation*, 54(12), pp. 1–13. doi: 10.1111/cpr.13123.
- Wu, C. L. *et al.* (2020) 'The role of macrophages in osteoarthritis and cartilage repair', *Osteoarthritis and Cartilage*, 28(5), pp. 544–554. doi: 10.1016/j.joca.2019.12.007.
- Wubbolts, R. *et al.* (2003) 'Proteomic and biochemical analyses of human B cell-derived exosomes. Potential implications for their function and multivesicular body formation', *The Journal of Biological Chemistry*, 278(13), pp. 10963–10972. doi: 10.1074/jbc.M207550200.
- Wunderli, S. L., Blache, U. and Snedeker, J. G. (2020) 'Tendon explant models for physiologically relevant in vitro study of tissue biology—a perspective', *Connective Tissue Research*, 61(3–4), pp. 262–277. doi: 10.1080/03008207.2019.1700962.
- Xiao, Z. *et al.* (2007) 'Analysis of the extracellular matrix vesicle proteome in mineralizing osteoblasts', *Journal of Cellular Physiology*, 210(2), pp. 325–335. doi: 10.1002/jcp.20826.
- Xu, B. *et al.* (2016) 'Quantitative protein profiling of hippocampus during human aging', *Neurobiology of Aging*, 39, pp. 46–56. doi: 10.1016/j.neurobiolaging.2015.11.029.
- Xu, J. *et al.* (2020) 'Platelet-rich plasma and regenerative dentistry', *Australian Dental Journal*, 65(2), pp. 131–142. doi: 10.1111/adj.12754.
- Yammani, R. R. (2012) 'S100 proteins in cartilage: Role in arthritis', *Biochimica et Biophysica Acta*, 1822(4), pp. 600–606. doi: 10.1016/j.bbadis.2012.01.006.
- Yang, J. *et al.* (2020) 'The multiple roles of Thy-1 in cell differentiation and regeneration', *Differentiation*, 113, pp. 38–48. doi: 10.1016/j.diff.2020.03.003.
- Ye, R. *et al.* (2020) 'KCTD12 promotes G1/S transition of breast cancer cell through activating the AKT/FOXO1 signaling', *Journal of Clinical Laboratory Analysis*, 34(8), p. e23315. doi: 10.1002/jcla.23315.
- Yeung, C. Y. C., Zhang, C., *et al.* (2020) 'Comparison of tenocyte populations from the core and periphery of equine tendons', *Journal of Proteome Research*, 19(10), pp. 4137–4144. doi: 10.1021/acs.jproteome.0c00591.

Yeung, C. Y. C., Schoof, E. M., *et al.* (2020) 'Proteomics identifies differences in fibrotic potential of extracellular vesicles from human tendon and muscle fibroblasts', *Cell Communication and Signaling*, 18(1), pp. 1–15. doi: 10.1186/s12964-020-00669-9.

Young, R. E. and Huh, D. D. (2021) 'Organ-on-a-chip technology for the study of the female reproductive system', *Advanced Drug Delivery Reviews*, 173, pp. 461–478. doi: 10.1016/j.addr.2021.03.010.

Yu, T. Y. *et al.* (2015) 'Platelet-rich plasma increases proliferation of tendon cells by modulating Stat3 and p27 to up-regulate expression of cyclins and cyclin-dependent kinases', *Cell Proliferation*, 48(4), pp. 413–420. doi: 10.1111/cpr.12189.

Yue, B. *et al.* (2020) 'Exosome biogenesis, secretion and function of exosomal miRNAs in skeletal muscle myogenesis', *Wiley Online Library*, 53(7). doi: 10.1111/cpr.12857.

Yun, S., Ku, S. K. and Kwon, Y. S. (2016) 'Adipose-derived mesenchymal stem cells and platelet-rich plasma synergistically ameliorate the surgical-induced osteoarthritis in Beagle dogs', *Journal of Orthopaedic Surgery and Research*, 11(1), pp. 1–12. doi: 10.1186/s13018-016-0342-9.

Zeng, R. *et al.* (2022) 'Rho GTPase signaling in rheumatic diseases', *iScience*, 25(1), p. 103620. doi: 10.1016/j.isci.2021.103620.

Zeng, R. *et al.* (2023) 'Early osteoarthritis diagnosis based on near-infrared spectroscopy combined with aquaphotomics', *Spectrochimica Acta - Part A: Molecular and Biomolecular Spectroscopy*, 302(February), p. 123120. doi: 10.1016/j.saa.2023.123120.

Zhai, M. *et al.* (2019) 'Fourier transform infrared spectroscopy research on subchondral bone in osteoarthritis', *Spectrochimica Acta - Part A: Molecular and Biomolecular Spectroscopy*, 218, pp. 243–247. doi: 10.1016/j.saa.2019.04.020.

Zhang, Ge, *et al.* (2020) 'Data-Independent Acquisition Mass Spectrometry-Based Proteomics and Software Tools: A Glimpse in 2020', *Proteomics*, 20(17–18), pp. 1–12. doi: 10.1002/pmic.201900276.

Zhang, Silva, *et al.* (2020) 'Raman Spectroscopy characterization extracellular vesicles from bovine placenta and peripheral blood mononuclear cells', *PLoS ONE*, 15(7), pp. 1–16. doi: 10.1371/journal.pone.0235214.

Zhang, Cai and Bai (2020) 'Macrophages regulate the progression of osteoarthritis', *Osteoarthritis and Cartilage*, 28(5), pp. 555–561. doi: 10.1016/j.joca.2020.01.007.

Zhang, J. and Wang, J. H. C. (2014) 'PRP treatment effects on degenerative tendinopathy - An in

- vitromodel study', *Muscles, Ligaments and Tendons Journal*, 4(1), pp. 10–17. doi: 10.32098/mltj.01.2014.03.
- Zhang, R. *et al.* (2021) 'Identification of differential key biomarkers in the synovial tissue between rheumatoid arthritis and osteoarthritis using bioinformatics analysis', *Clinical Rheumatology*, 40(12), pp. 5103–5110. doi: 10.1007/s10067-021-05825-1.
- Zhang, S. *et al.* (2018) 'MSC exosomes mediate cartilage repair by enhancing proliferation, attenuating apoptosis and modulating immune reactivity', *Biomaterials*, 156, pp. 16–27. doi: 10.1016/j.biomaterials.2017.11.028.
- Zhao, Z. *et al.* (2019) 'Extracellular vesicles as cancer liquid biopsies: from discovery, validation, to clinical application', *Lab on a Chip*, 19(7), pp. 1114–1140. doi: 10.1039/C8LC01123K.
- Zhong, B. *et al.* (2021) 'Plasma Heat Shock Protein 90 Alpha: A Valuable Predictor of Early Chemotherapy Effectiveness in Advanced Non-Small-Cell Lung Cancer', *Medical Science Monitor: International Medical Journal of Experimental and Clinical Research*, 27, p. e924778. doi: 10.12659/MSM.924778.
- Zhou, Y. and Wang, J. H. C. (2016) 'PRP Treatment Efficacy for Tendinopathy: A Review of Basic Science Studies', *BioMed Research International*. doi: 10.1155/2016/9103792.
- Zhu, D. *et al.* (2022) 'Inhibition of AHNAK nucleoprotein 2 alleviates pulmonary fibrosis by downregulating the TGF- $\beta$ 1/Smad3 signaling pathway', *Journal of Gene Medicine*, 24(9), pp. 1–10. doi: 10.1002/jgm.3442.
- Zhu, S., Dai, J., *et al.* (2015) 'Down-Regulation of Rac GTPase-Activating Protein OCRL1 Causes Aberrant Activation of Rac1 in Osteoarthritis Development', *Arthritis & Rheumatology*, 67(8), pp. 2154–2163. doi: 10.1002/art.39174.
- Zhu, S., Lu, P., *et al.* (2015) 'Inhibition of Rac1 activity by controlled release of NSC23766 from chitosan microspheres effectively ameliorates Osteoarthritis development in vivo', *Annals of the Rheumatic Diseases*, 74(1), pp. 285–293. doi: 10.1136/annrheumdis-2013-203901.
- Zhu, Z. *et al.* (2020) 'Regeneration-Related Functional Cargoes in Mesenchymal Stem Cell-Derived Small Extracellular Vesicles', *liebertpub.com*, 29(1), pp. 15–24. doi: 10.1089/scd.2019.0131.
- Zöller, M. *et al.* (2018) 'Immunoregulatory Effects of Myeloid-Derived Suppressor Cell Exosomes in Mouse Model of Autoimmune Alopecia Areata', *Frontiers in Immunology*, 9, p. 1279. doi: 10.3389/fimmu.2018.01279.

Züllig, T., Trötz Müller, M. and Köfeler, H. C. (2020) 'Lipidomics from sample preparation to data analysis: a primer', *Analytical and Bioanalytical Chemistry*, 412(10), pp. 2191–2209. doi: 10.1007/s00216-019-02241-y.



## Publications

**Clarke, E.J.**, Anderson, J.R. and Peffers, M.J., 2021. Nuclear magnetic resonance spectroscopy of biofluids for osteoarthritis. *British medical bulletin*, 137(1), pp.28-41.

**Clarke, E.J.**, Gillen, A., Turlo, A. and Peffers, M.J., 2021. An Evaluation of Current Preventative Measures Used in Equine Practice to Maintain Distal Forelimb Functionality: A Mini Review. *Frontiers in Veterinary Science*, p.1323.

**Clarke, E.J.**, Lima, C., Anderson, J.R., Castanheira, C., Beckett, A., James, V., Hyett, J., Goodacre, R. and Peffers, M.J., 2022. Optical photothermal infrared spectroscopy can differentiate equine osteoarthritic plasma extracellular vesicles from healthy controls. *Analytical Methods*, 14(37), pp.3661-3670.

Anderson, J.R., Jacobsen, S., Walters, M., Bundgaard, L., Diendorfer, A., Hackl, M., **Clarke, E.J.**, James, V. and Peffers, M.J., 2022. Small non-coding RNA landscape of extracellular vesicles from a post-traumatic model of equine osteoarthritis. *Frontiers in Veterinary Science*, p.1170.

**Clarke, E.J.**, Lima, C., Anderson, J.R., Castanheira, C., Hyett, J., Goodacre, R. and Peffers, M.J., 2022. Novel Spectroscopy Techniques Used To Interrogate Equine Osteoarthritic Extracellular Vesicles. *Osteoarthritis and Cartilage*, 30, pp.S95-S96.

**Clarke EJ**, Johnson E, Caamaño Gutierrez E, Andersen C, Berg LC, Jenkins RE, Lindegaard C, Uvebrant K, Lundgren-Åkerlund E, Turlo A, James V, Jacobsen S, Peffers MJ. 2022. Temporal extracellular vesicle protein changes following intraarticular treatment with integrin  $\alpha 10\beta 1$ -selected mesenchymal stem cells in equine osteoarthritis. *Front Vet Sci*.

Collins J, Kim C, Coleman A, Little A, Perez M, **Clarke EJ**, Diekman B, Peffers M J, Chubinskaya S, Tomlinson R, Freeman T, Loeser R ( submitted 2023). Cartilage-specific Sirt6 loss represses IGF-1 signaling and enhances osteoarthritis severity in mice. Submitted to *Annals in Rheumatic Disease* (May 2023).

Anderson, J.R., Johnson, E., Jenkins, R.E., Jacobsen, S., Green, D., Walters, M., Bundgaard, L., Hausmans, B., van den Akker, G., Welting, T., Chabronova, A., Kharaz, Y., **Clarke, E.J.**, James, V., Peffers, M.J. (submitted 2023). Multi-omic temporal landscape of plasma and synovial fluid-derived extracellular vesicles using an experimental model of equine osteoarthritis. Submitted to *International Journal of Molecular Medicine*,

**Clarke, E.J.**, Varela, L, Jenkins, R.E, Lozano-Andres, E, Cywinska, A, Przewozny,M., van Weeren, R., Van de Lest,C., Peffers, M.J., (submitted 2023) Wauben, M. Proteome and phospholipidome interrelationship of synovial fluid-derived extracellular vesicles in equine osteoarthritis: An exploratory multi-omics study to identify composite biomarkers. Submitted to BBA Molecular Basis of Disease.



Cite this: DOI: 10.1039/d2ay00779g

## Optical photothermal infrared spectroscopy can differentiate equine osteoarthritic plasma extracellular vesicles from healthy controls

Emily J. Clarke,<sup>†\*</sup> Cassio Lima,<sup>†‡</sup> James R. Anderson,<sup>†§</sup> Catarina Castanheira,<sup>¶</sup> Alison Beckett,<sup>||</sup> Victoria James,<sup>||</sup> Jacob Hyett,<sup>¶</sup> Royston Goodacre,<sup>||</sup> and Mandy J. Peffers<sup>¶</sup>

Equine osteoarthritis is a chronic degenerative disease of the articular joint, characterised by cartilage degradation resulting in pain and reduced mobility and thus is a prominent equine welfare concern. Diagnosis is usually at a late stage through clinical examination and radiographic imaging, whilst treatment is symptomatic not curative. Extracellular vesicles are nanoparticles that are involved in intercellular communication. The objective of this study was to investigate the feasibility of Raman and Optical Photothermal Infrared Spectroscopies to detect osteoarthritis using plasma-derived extracellular vesicles, specifically differentiating extracellular vesicles in diseased and healthy controls within the parameters of the techniques used. Plasma samples were derived from thoroughbred racehorses. A total of 14 samples were selected (control;  $n = 6$  and diseased;  $n = 8$ ). Extracellular vesicles were isolated using differential ultracentrifugation and characterised using nanoparticle tracking analysis, transmission electron microscopy, and human tetraspanin chips. Samples were then analysed using combined Raman and Optical Photothermal Infrared Spectroscopies. Infrared spectra were collected between 950–1800  $\text{cm}^{-1}$ . Raman spectra had bands between the wavelengths of 900–1800  $\text{cm}^{-1}$  analysed. Spectral data for both Raman and Optical Photothermal Infrared Spectroscopy were used to generate clustering via principal components analysis and classification models were generated using partial least squared discriminant analysis in order to characterize the techniques' ability to distinguish diseased samples. Optical Photothermal Infrared Spectroscopy could differentiate osteoarthritic extracellular vesicles from healthy with good classification (93.4% correct classification rate) whereas Raman displayed poor classification (correct classification rate = -64.3%). Inspection of the infrared spectra indicated that plasma-derived extracellular vesicles from osteoarthritic horses contained increased signal for proteins, lipids and nucleic acids. For the first time we demonstrated the ability to use optical photothermal infrared spectroscopy combined with Raman spectroscopy to interrogate extracellular vesicles and osteoarthritis-related samples. Optical Photothermal Infrared Spectroscopy was superior to Raman in this study, and could distinguish osteoarthritis samples, suggestive of its potential use diagnostically to identify osteoarthritis in equine patients. This study demonstrates the potential of Raman and Optical Photothermal Infrared Spectroscopy to be used as a future diagnostic tool in clinical practice, with the capacity to detect changes in extracellular vesicles from clinically derived samples.

Received 12th May 2022  
Accepted 25th August 2022

DOI: 10.1039/d2ay00779g

rsc.li/methods

## Introduction

Osteoarthritis (OA) is a common degenerative disease of the synovial joint, characterised by catabolic processes observed in articular cartilage, and a notable imbalance in bone remodeling. It results in pain, inflammation and reduced mobility.<sup>1</sup> OA is the most prevalent cause of equine lameness, with over 60% of horses developing OA within their lifetime; a significant welfare concern.<sup>2</sup> It is a complex heterogeneous condition of multiple causative factors, including mechanical, genetic, metabolic and inflammatory pathway involvement.<sup>3</sup> OA pathophysiology is conserved across species, resulting in synovitis,

\*Department of Musculoskeletal Biology and Ageing Science, Institute of Life Course and Medical Sciences, University of Liverpool, William Henry Duncan Building, 6 W Derby St, Liverpool L7 8TX, UK. E-mail: eclarke@liverpool.ac.uk

†Centre for Metabolomics Research, Biochemistry and Systems Biology, Institute of Systems, Molecular and Integrative Biology, University of Liverpool, Biosciences Building, Crown Street, Liverpool, L69 7BE, UK

‡Biomedical Electron Microscopy Unit, University of Liverpool, UK

§School of Veterinary Medicine and Science, University of Nottingham, Sutton Bonington, Loughborough LE12 5RD, UK

¶ Co-first authors.



Invited Review

## Nuclear magnetic resonance spectroscopy of biofluids for osteoarthritis

Emily J Clarke\*, James R Anderson, and Mandy J Peffers

Institute of Life Course and Medical Sciences, Musculoskeletal and Ageing Science, William Henry Duncan Building, 6 West Derby Street, Liverpool L7 8TX, UK

\*Correspondence address. Institute of Life Course and Medical Sciences, Musculoskeletal and Ageing Science, William Henry Duncan Building, 6 West Derby Street, Liverpool, L7 8TX, UK. E-mail: eclarke@liverpool.ac.uk

Received 6 July 2020; Revised 1 October 2020; Accepted 24 October 2020

### Abstract

**Background:** Osteoarthritis is a common degenerative musculoskeletal disease of synovial joints. It is characterized by a metabolic imbalance resulting in articular cartilage degradation, reduced elastoviscosity of synovial fluid and an altered chondrocyte phenotype. This is often associated with reduced mobility, pain and poor quality of life. Subsequently, with an ageing world population, osteoarthritis is of increasing concern to public health. Nuclear magnetic resonance (NMR) spectroscopy can be applied to characterize the metabolomes of biofluids, determining changes associated with osteoarthritis pathology, identifying potential biomarkers of disease and alterations to metabolic pathways.

**Sources of data:** A comprehensive search of PubMed and Web of Science databases using combinations of the following keywords: 'NMR Spectroscopy', 'Blood', 'Plasma', 'Serum', 'Urine', 'Synovial Fluid' and 'Osteoarthritis' for articles published from 2000 to 2020.

**Areas of agreement:** The number of urine metabolomics studies using NMR spectroscopy to investigate osteoarthritis is low, whereas the use of synovial fluid is significantly higher. Several differential metabolites have previously been identified and mapped to metabolic pathways involved in osteoarthritis pathophysiology.

**Areas of controversy:** Conclusions are sometimes conservative or over-inflated, which may reflect the variation in reporting standards. NMR

© The Author(s) 2020. Published by Oxford University Press.

This is an Open Access article distributed under the terms of the Creative Commons Attribution License (<http://creativecommons.org/licenses/by/4.0/>), which permits unrestricted reuse, distribution, and reproduction in any medium, provided the original work is properly cited.





# An Evaluation of Current Preventative Measures Used in Equine Practice to Maintain Distal Forelimb Functionality: A Mini Review

Emily J. Clarke<sup>1\*</sup>, Alex Gillen<sup>2</sup>, Agnieszka Turlo<sup>1</sup> and Mandy J. Peffers<sup>1</sup>

<sup>1</sup> Institute of Life Course and Medical Sciences, Musculoskeletal and Ageing Science, Liverpool, United Kingdom, <sup>2</sup> Philip Laverhulme Equine Hospital, Institute of Veterinary Science, University of Liverpool, Liverpool, United Kingdom

Horses are used in a variety of equestrian disciplines predisposing them to musculoskeletal injury or disease including osteoarthritis and tendinopathy. As a result, a number of preventative measures are used within equine medicine and husbandry, ranging from therapeutic shoeing to the use of nutraceuticals. Despite their popularity and routine use evidence base and clinical outcomes are variable, bringing into question the efficacy of these prophylactic measures. In recent years a small number of studies have been performed examining the effect of specific strategies in order to quantify the preventative and protective claims such modalities have on joint and forelimb health. Few have robustly demonstrated a capacity to protect the limb by reducing inflammation, or promoting regenerative pathways. This review focusses on performance horses specifically, and the resounding theme that emerges in current research is the need for longitudinal studies to inform scientific conclusions surrounding single and multi-modal use. Furthermore, there is a requirement to prioritise evidence-based medicine to inform optimal clinical practice.

**Keywords:** equine, joint, distal limb, preventative, osteoarthritis, tendon, function

## OPEN ACCESS

### Edited by:

Micaela Sgorbini,  
University of Pisa, Italy

### Reviewed by:

Ilana Nocera,  
University of Pisa, Italy  
Riccardo Rimovati,  
University of Bologna, Italy

### \*Correspondence:

Emily J. Clarke  
eclarke@liverpool.ac.uk

### Specialty section:

This article was submitted to  
Comparative and Clinical Medicine,  
a section of the journal  
Frontiers in Veterinary Science

Received: 15 August 2021

Accepted: 12 October 2021

Published: 02 November 2021

### Citation:

Clarke EJ, Gillen A, Turlo A and  
Peffers MJ (2021) An Evaluation of  
Current Preventative Measures Used  
in Equine Practice to Maintain Distal  
Forelimb Functionality: A Mini Review.  
Front. Vet. Sci. 8:758970.  
doi: 10.3389/fvets.2021.758970

## INTRODUCTION

The equine musculoskeletal system has significant demands placed on it (1), specifically articular structures and supporting tissues, leaving it vulnerable to injury and disease development that results in pain, lameness, and reduced mobility. Consequently, numerous preventative modalities are being used in an attempt to maintain optimum athletic performance and potentially reduce the onset of musculoskeletal disease. The forelimb incorporates the carpus, a compound joint, composed of three articulations; the antebrachio-carpal joint; the middle carpal joint, and the carpometacarpal joint, commonly referred to as the carpal joint in a research setting (2). Soft tissue components include intercarpal ligaments, collateral ligaments, a fibrous joint capsule, and the palmar carpal ligament. The metacarpophalangeal joint is comprised of four bones; the third metacarpal bone, the proximal phalanx, and the paired proximal sesamoid bones (3). As the carpal and metacarpophalangeal regions are imperative for equine locomotion, they can be highly susceptible to injury and disease, most notably tendinopathies and osteoarthritis. Tendon injury is a common impairment that can compromise the stability of the joint capsule, which can result in excessive wear due to uneven force distribution. When the tendon heals, it becomes



## OPEN ACCESS

EDITED BY  
Debbie Guest,  
Royal Veterinary College (RVC),  
United Kingdom

REVIEWED BY  
Eric Barrey,  
INRA UMR1313 Genetique Animale et  
Biologie Integrative, France  
Krishna Prahlad Maremanda,  
Texas A&M University, United States  
Mohammed Zayed,  
National Center for Geriatrics and  
Gerontology (NCGG), Japan

## \*CORRESPONDENCE

Mandy J. Peffers  
peffs@liv.ac.uk

## SPECIALTY SECTION

This article was submitted to  
Veterinary Regenerative Medicine,  
a section of the journal  
Frontiers in Veterinary Science

RECEIVED 21 March 2022

ACCEPTED 18 July 2022

PUBLISHED 08 August 2022

## CITATION

Anderson JR, Jacobsen S, Walters M,  
Bundgaard L, Diendorfer A, Hackl M,  
Clarke EJ, James V and Peffers MJ  
(2022) Small non-coding RNA  
landscape of extracellular vesicles  
from a post-traumatic model of  
equine osteoarthritis.  
*Front. Vet. Sci.* 9:901269.  
doi: 10.3389/fvets.2022.901269

## COPYRIGHT

© 2022 Anderson, Jacobsen, Walters,  
Bundgaard, Diendorfer, Hackl, Clarke,  
James and Peffers. This is an  
open-access article distributed under  
the terms of the Creative Commons  
Attribution License (CC BY). The use,  
distribution or reproduction in other  
forums is permitted, provided the  
original author(s) and the copyright  
owner(s) are credited and that the  
original publication in this journal is  
cited, in accordance with accepted  
academic practice. No use, distribution  
or reproduction is permitted which  
does not comply with these terms.

# Small non-coding RNA landscape of extracellular vesicles from a post-traumatic model of equine osteoarthritis

James R. Anderson<sup>1</sup>, Stine Jacobsen<sup>2</sup>, Marie Walters<sup>2</sup>,  
Louise Bundgaard<sup>2</sup>, Andreas Diendorfer<sup>3</sup>, Matthias Hackl<sup>3</sup>,  
Emily J. Clarke<sup>1</sup>, Victoria James<sup>4</sup> and Mandy J. Peffers<sup>1\*</sup>

<sup>1</sup>Department of Musculoskeletal and Ageing Science, Institute of Life Course and Medical Sciences, University of Liverpool, Liverpool, United Kingdom, <sup>2</sup>Department of Veterinary Clinical Sciences, University of Copenhagen, Taastrup, Denmark, <sup>3</sup>TAmRNA, TAmRNA GmbH, Vienna, Austria, <sup>4</sup>School of Veterinary Medicine and Science, University of Nottingham, Loughborough, United Kingdom

Extracellular vesicles comprise an as yet inadequately investigated intercellular communication pathway in the field of early osteoarthritis. We hypothesised that the small non-coding RNA expression pattern in synovial fluid and plasma would change during progression of experimental osteoarthritis. In this study, we conducted small RNA sequencing to provide a comprehensive overview of the temporal expression profiles of small non-coding transcripts carried by extracellular vesicles derived from plasma and synovial fluid for the first time in a posttraumatic model of equine osteoarthritis. Additionally, we characterised synovial fluid and plasma-derived extracellular vesicles with respect to quantity, size, and surface markers. The different temporal expressions of seven microRNAs in plasma and synovial fluid-derived extracellular vesicles, eca-miR-451, eca-miR-25, eca-miR-215, eca-miR-92a, eca-miR-let-7c, eca-miR-486-5p, and eca-miR-23a, and four snoRNAs, U3, snord15, snord46, and snord58, represent potential biomarkers for early osteoarthritis. Bioinformatics analysis of the differentially expressed microRNAs in synovial fluid highlighted that in early osteoarthritis these related to the inhibition of cell cycle, cell cycle progression, DNA damage and cell proliferation as well as increased cell viability and differentiation of stem cells. Plasma and synovial fluid-derived extracellular vesicle small non-coding signatures have been established for the first time in a temporal model of osteoarthritis. These could serve as novel biomarkers for evaluation of osteoarthritis progression or act as potential therapeutic targets.

## KEYWORDS

osteoarthritis, extracellular vesicles, small non-coding RNA, synovial fluid, plasma

## Introduction

Osteoarthritis (OA) is a degenerative joint disease characterised by deterioration of articular cartilage and accompanied by changes in the bone and soft tissues of the joint (1), which adversely impact the health of equine athletes. It is a major welfare issue resulting in substantial morbidity and mortality (2). Lameness resulting from OA is a



## OPEN ACCESS

EDITED BY  
Scott J. Roberts,  
Royal Veterinary College (RVC),  
United Kingdom

REVIEWED BY  
Jayesh Duthia,  
Royal Veterinary College (RVC),  
United Kingdom  
Luca Melotti,  
University of Pavia, Italy

\*CORRESPONDENCE  
Emily J. Clarke  
eclarke@liverpool.ac.uk

SPECIALTY SECTION  
This article was submitted to  
Veterinary Regenerative Medicine,  
a section of the journal  
Frontiers in Veterinary Science

RECEIVED 29 September 2022  
ACCEPTED 10 November 2022  
PUBLISHED 24 November 2022

## CITATION

Clarke EJ, Johnson E, Caamaño  
Gutierrez E, Andersen C, Berg LC,  
Jenkins RE, Lindgaard C, Uvebrant K,  
Lundgren-Åkerlund E, Turlo A,  
James V, Jacobsen S and Peffers MJ  
(2022) Temporal extracellular vesicle  
protein changes following  
intraarticular treatment with integrin  
 $\alpha 10\beta 1$ -selected mesenchymal stem  
cells in equine osteoarthritis.  
Front Vet Sci 9:1057667.  
doi: 10.3389/fvets.2022.1057667

## COPYRIGHT

© 2022 Clarke, Johnson, Caamaño  
Gutierrez, Andersen, Berg, Jenkins,  
Lindgaard, Uvebrant,  
Lundgren-Åkerlund, Turlo, James,  
Jacobsen and Peffers. This is an  
open-access article distributed under  
the terms of the Creative Commons  
Attribution License (CC BY). The use,  
distribution or reproduction in other  
forums is permitted, provided the  
original author(s) and the copyright  
owner(s) are credited and that the  
original publication in this journal is  
cited, in accordance with accepted  
academic practice. No use, distribution  
or reproduction is permitted which  
does not comply with these terms.

# Temporal extracellular vesicle protein changes following intraarticular treatment with integrin $\alpha 10\beta 1$ -selected mesenchymal stem cells in equine osteoarthritis

Emily J. Clarke<sup>1\*</sup>, Emily Johnson<sup>2</sup>, Eva Caamaño Gutierrez<sup>2</sup>,  
Camilla Andersen<sup>3</sup>, Lise C. Berg<sup>3</sup>, Rosalind E. Jenkins<sup>4</sup>,  
Casper Lindgaard<sup>2</sup>, Kristina Uvebrant<sup>5</sup>,  
Evy Lundgren-Åkerlund<sup>6</sup>, Agnieszka Turlo<sup>1</sup>, Victoria James<sup>7</sup>,  
Stine Jacobsen<sup>1</sup> and Mandy J. Peffers<sup>1</sup>

<sup>1</sup>Institute of Life Course and Medical Sciences, University of Liverpool, Liverpool, United Kingdom, <sup>2</sup>Computational Biology Faculty, Liverpool Shared Research Facilities, Faculty of Health and Life Sciences, University of Liverpool, Liverpool, United Kingdom, <sup>3</sup>Department of Veterinary Clinical Sciences, University of Copenhagen, Copenhagen, Denmark, <sup>4</sup>Department of Pharmacology and Therapeutics, Institute of Systems, Molecular and Integrative Biology, Centre for Drug Safety Science, Biomedical Faculty, Liverpool Shared Research Facilities, University of Liverpool, Liverpool, United Kingdom, <sup>5</sup>Birsteå AB, Linné, Sweden, <sup>6</sup>School of Veterinary Medicine and Science, University of Nottingham, Nottingham, United Kingdom

**Introduction:** Equine osteoarthritis (OA) is a heterogeneous, degenerative disease of the musculoskeletal system with multifactorial causation, characterized by a joint metabolic imbalance. Extracellular vesicles are nanoparticles involved in intracellular communication. Mesenchymal stem cell (MSC) therapy is a form of regenerative medicine that utilizes their properties to repair damaged tissues. Despite its wide use in veterinary practice, the exact mechanism of action of MSCs is not fully understood. The aim of this study was to determine the synovial fluid extracellular vesicle protein cargo following integrin  $\alpha 10\beta 1$ -selected mesenchymal stem cell (integrin  $\alpha 10$ -MSC) treatment in an experimental model of equine osteoarthritis with longitudinal sampling.

**Methods:** Adipose tissue derived, integrin  $\alpha 10$ -MSCs were injected intraarticularly in six horses 18 days after experimental induction of OA. Synovial fluid samples were collected at day 0, 18, 21, 28, 35, and 70. Synovial fluid was processed and extracellular vesicles were isolated and characterized. Extracellular vesicle cargo was then analyzed using data independent acquisition mass spectrometry proteomics.

**Results:** A total of 442 proteins were identified across all samples, with 48 proteins differentially expressed (FDR  $\leq 0.05$ ) between sham-operated control joint without MSC treatment and OA joint treated with MSCs. The most significant pathways following functional enrichment analysis of the differentially abundant protein dataset were serine endopeptidase activity ( $p = 0.023$ ), complement activation (classical pathway) ( $p = 0.025$ ), and collagen containing extracellular matrix ( $p = 0.034$ ). Due to the lack of an OA group without MSC treatment, findings cannot be directly correlated to only MSCs.





## TRANSLATIONAL SCIENCE

Cartilage-specific *Sirt6* deficiency represses IGF-1 and enhances osteoarthritis severity in mice

John A Collins<sup>1,2</sup>, C James Kim<sup>1</sup>, Ashley Coleman<sup>1</sup>, Abreah Little<sup>1</sup>,  
 Matheus M Perez<sup>1</sup>, Emily J Clarke<sup>3</sup>, Brian Diekman<sup>2</sup>, Mandy J Peffers<sup>3</sup>,  
 Susanna Chubinskaya<sup>4</sup>, Ryan E Tomlinson<sup>1</sup>, Theresa A Freeman<sup>1</sup>, Richard F Loeser<sup>2</sup>

Handling editor: Jozef S Smolen

Additional supplemental material is published online only. To view, please visit the journal online (<http://dx.doi.org/10.1136/ard-2023-224385>).

<sup>1</sup>Department of Orthopaedic Surgery, Thomas Jefferson University, Philadelphia, Pennsylvania, USA

<sup>2</sup>Department of Medicine, Division of Rheumatology, Allergy and Immunology and the Thurston Arthritis Research Center, The University of North Carolina at Chapel Hill, Chapel Hill, North Carolina, USA

<sup>3</sup>Institute of Life Course and Medical Sciences, University of Liverpool, Liverpool, UK

<sup>4</sup>Department of Pediatrics, Rush University Medical Center, Chicago, Illinois, USA

Correspondence to: Dr John A Collins, Department of Orthopaedic Surgery, Thomas Jefferson University, Philadelphia, Pennsylvania 19107, USA; [john.collins2@jefferson.edu](mailto:john.collins2@jefferson.edu)

Received 4 May 2023  
 Accepted 22 July 2023



© Author(s) for their employer(s) 2023. Re-use permitted under CC BY. Published by BMJ.

To cite: Collins JA, Kim CJ, Coleman A, et al. *Ann Rheum Dis* Epub ahead of print: [please include Day Month Year], doi:10.1136/ard-2023-224385

## ABSTRACT

**Objectives** Prior studies noted that chondrocyte SIRT6 activity is repressed in older chondrocytes rendering cells susceptible to catabolic signalling events implicated in osteoarthritis (OA). This study aimed to define the effect of *Sirt6* deficiency on the development of post-traumatic and age-associated OA in mice.

**Methods** Male cartilage-specific *Sirt6*-deficient mice and *Sirt6* intact controls underwent destabilisation of the medial meniscus (DMM) or sham surgery at 16 weeks of age and OA severity was analysed at 6 and 10 weeks postsurgery. Age-associated OA was assessed in mice aged 12 and 18 months of age. OA severity was analysed by micro-CT, histomorphometry and scoring of articular cartilage structure, toluidine blue staining and osteophyte formation. SIRT6-regulated pathways were analysed in human chondrocytes by RNA-sequencing, qRT-PCR and immunoblotting.

**Results** *Sirt6*-deficient mice displayed enhanced DMM-induced OA severity and accelerated age-associated OA when compared with controls, characterised by increased cartilage damage, osteophyte formation and subchondral bone sclerosis. In chondrocytes, RNA-sequencing revealed that SIRT6 depletion significantly repressed cartilage extracellular matrix (eg, COL2A1) and anabolic growth factor (eg, insulin-like growth factor-1 (IGF-1)) gene expression. Gain-of-function and loss-of-function studies in chondrocytes demonstrated that SIRT6 depletion attenuated, whereas adenoviral overexpression or MDI-800-induced SIRT6 activation promoted IGF-1 signalling by increasing Akt<sup>ser473</sup> phosphorylation.

**Conclusions** SIRT6 deficiency increases post-traumatic and age-associated OA severity in vivo. SIRT6 profoundly regulated the pro-anabolic and pro-survival IGF-1/Akt signalling pathway and suggests that preserving the SIRT6/IGF-1/Akt axis may be necessary to protect cartilage from injury-associated or age-associated OA. Targeted therapies aimed at increasing SIRT6 function could represent a novel strategy to slow or stop OA.

## INTRODUCTION

The highly conserved NAD<sup>+</sup>-dependent family of sirtuin deacetylases and mono-ADP ribosyltransferases (sirtuins 1–7) are key epigenetic regulators that control age-associated cell signalling pathways and promote longevity in various model organisms.<sup>1,2</sup> Efforts to elucidate the precise roles of the nuclear localised sirtuin 6 (SIRT6) in ageing and disease have come to the fore since the finding that global loss of *Sirt6* in mice leads to a progeroid phenotype,

## WHAT IS ALREADY KNOWN ON THIS TOPIC

⇒ Sirt6 activity significantly declines in ageing chondrocytes, which promotes catabolic signalling events implicated in osteoarthritis (OA) development and progression.  
 ⇒ Sirt6 regulates multiple pathways necessary for chondrocyte homeostasis but the effect of Sirt6 deficiency on OA development in vivo and the specific Sirt6-associated mechanisms responsible remain largely unexplored.

## WHAT THIS STUDY ADDS

⇒ Cartilage-specific *Sirt6* deficiency enhances post-traumatic OA and accelerates age-associated OA in mice.  
 ⇒ Depletion of chondrocyte Sirt6 significantly represses insulin-like growth factor-1 (IGF-1) signalling and downregulates multiple cartilage extracellular matrix components including COL2A1.  
 ⇒ Genetic and pharmacological activation of Sirt6 promotes pro-survival and pro-anabolic IGF-1/Akt activation in human chondrocytes.

## HOW THIS STUDY MIGHT AFFECT RESEARCH, PRACTICE OR POLICY

⇒ The SIRT6/IGF-1 signalling axis is an important mediator of cartilage integrity and the chondrocyte phenotype.  
 ⇒ Targeted therapies that promote chondrocyte SIRT6 activity during ageing and in response to injury represents a novel strategy to reduce OA severity.

metabolic dysfunction and death within 4 weeks of birth.<sup>3</sup> Conversely, transgenic overexpression of *Sirt6* governs metabolic signalling events during ageing to extend lifespan in both male and female mice.<sup>3,4</sup> Several lines of evidence demonstrate that SIRT6 regulates an array of age-associated biological processes including DNA repair, cellular metabolism, oxidative stress, inflammation, autophagy and senescence.<sup>1,2</sup> As such, maintenance of SIRT6 activity during ageing, or in response to stress, is considered important for the prevention of ageing diseases such as cardiovascular disease, various metabolic and neurodegenerative disorders including diabetes and Alzheimer's, certain cancers and arthritis.<sup>1,2,7,8</sup>



# Extracellular vesicles in osteoarthritis: from biomarkers to therapeutic potential

Equine osteoarthritis is a leading welfare concern. Currently, it can only be diagnosed in its late stages – radiographically and upon clinical examination. There are no curative therapeutic options, with treatment aiming to provide symptom relief and reduce the rate of progression. Thus far, no biochemical diagnostic panels have been produced to diagnose osteoarthritis in its infancy, nor have there been transformative therapeutics to improve disease management. As such, the exploration has continued, with attention now focused on the emerging role of extracellular vesicles in the pathogenesis of osteoarthritis, their potential to carry biomarkers of disease and their therapeutic capacity in the context of popular regenerative therapeutics, such as mesenchymal stromal cell therapy. This article provides a brief overview of the role of extracellular vesicles in equine osteoarthritis for veterinary clinicians, and the future directions this growing field may explore. <https://doi.org/10.1080/09687692.2023.214344>

Emily J Clarke, PhD candidate<sup>1</sup>; Mandy J Peffers, Professor<sup>1</sup>; <sup>1</sup>Department of Musculoskeletal Biology and Ageing Science, Institute of Life Course and Medical Sciences, University of Liverpool, Liverpool, United Kingdom; Corresponding author: Emily J Clarke, [eclarke@liverpool.ac.uk](mailto:eclarke@liverpool.ac.uk)

**Key words:** equine osteoarthritis | extracellular vesicles | biomarkers | biological therapies | cell-free therapies

**Submitted:** 12 July 2023; accepted for publication following double-blind peer review: 16 August 2023

Horses are used in a variety of disciplines – including dressage, show jumping, eventing and racing – and the equine athlete is predisposed to the development of musculoskeletal injuries. Injury can be career limiting and present as a significant equine welfare concern. Poor performance can be the result of pain and the onset of lameness; however, riders and trainers may be unwilling to recognise behavioural changes as a manifestation of impaired welfare.

Equine osteoarthritis is a major cause of lameness, with over 60% of horses reported to develop osteoarthritis within their lifetime (McIlwraith et al, 2012a). However, its prevalence is thought to be much higher, with 80–90% of horses older than 15 years developing this chronic condition (Schluter and Orth, 2004). It was first reported in 1938 and received clinical interest in 1966 at the American Association of Equine Practitioners. In 1975, it was established that cartilaginous lesions should act as objective criteria for the diagnosis of osteoarthritis (McIlwraith et al, 2012b).

## Clinical signs and symptoms of equine osteoarthritis

Today, it is understood that osteoarthritis is a disease of the entire joint, including cartilage, subchondral bone, ligaments, synovial

membrane and periarticular tissues. It is recognised as incorporating multiple disorders characterised by a common end stage: the progressive deterioration of articular cartilage accompanied by changes in bone and soft tissue. As a disease of multifactorial origin, underlying factors include traumatic injury and idiopathic causes such as ageing. Osteoarthritis pathophysiology results in synovitis, cartilage degradation, osteophyte formation, subchondral bone sclerosis, fibrosis and reduced elastoviscosity of synovial fluid found within the joint capsule, as shown in Figure 1 (Clarke et al, 2021). Clinical diagnosis is founded upon radiographic and physical examination as well as reported history (Castanheira et al, 2021).

Osteoarthritis is regarded as a chronic degenerative disease taking many years to develop. Development can often be the result of trauma or injury as well as idiopathic causes such as ageing (Castanheira et al, 2021). In the horse, the risk of trauma induced osteoarthritis is often increased because of the athletic discipline the horse undertakes, with orthopaedic problems being the primary cause of loss of use and death in athletic horses. This results in more than 70% of days-lost to training in both show jumpers and racehorses (Rabitich et al, 2021). Factors that may predispose a horse to osteoarthritis include age, mechani-



Article

# Multi-Omic Temporal Landscape of Plasma and Synovial Fluid-Derived Extracellular Vesicles Using an Experimental Model of Equine Osteoarthritis

James R. Anderson <sup>1,\*</sup>, Emily Johnson <sup>2,†</sup>, Rosalind Jenkins <sup>3,†</sup>, Stine Jacobsen <sup>4</sup>, Daniel Green <sup>1</sup>, Marie Walters <sup>4</sup>, Louise Bundgaard <sup>4</sup>, Bas A. C. Hausmans <sup>5</sup>, Guus van den Akker <sup>5</sup>, Tim J. M. Welting <sup>5</sup>, Alzbeta Chabronova <sup>1</sup>, Yalda A. Kharaz <sup>1</sup>, Emily J. Clarke <sup>1</sup>, Victoria James <sup>6</sup> and Mandy J. Peffers <sup>1,\*</sup>

- <sup>1</sup> Department of Musculoskeletal and Ageing Science, Institute of Life Course and Medical Sciences, University of Liverpool, Liverpool L7 8TX, UK; yaldak@liv.ac.uk (Y.A.K.)
- <sup>2</sup> Computational Biology Facility, Liverpool Shared Research Facilities, Faculty of Health and Life Sciences, University of Liverpool, Liverpool L7 8TX, UK
- <sup>3</sup> CDSS Biosanalytical Facility, Liverpool Shared Research Facilities, Department Pharmacology and Therapeutics, University of Liverpool, Liverpool L7 8TX, UK
- <sup>4</sup> Department of Veterinary Clinical Sciences, University of Copenhagen, Taastrup, DK-1870 Copenhagen, Denmark
- <sup>5</sup> Laboratory for Experimental Orthopedics, Department of Orthopedic Surgery, Maastricht University, 6229 Maastricht, The Netherlands; b.hausmans@maastrichtuniversity.nl (B.A.C.H.)
- <sup>6</sup> School of Veterinary Medicine and Science, University of Nottingham, Sutton Bonington, Loughborough, Nottingham LE12 5RD, UK
- \* Correspondence: peffs@liv.ac.uk
- † These authors contributed equally to this work.



**Citation:** Anderson, J.R.; Johnson, E.; Jenkins, R.; Jacobsen, S.; Green, D.; Walters, M.; Bundgaard, L.; Hausmans, B.A.C.; van den Akker, G.; Welting, T.J.M.; et al. Multi-Omic Temporal Landscape of Plasma and Synovial Fluid-Derived Extracellular Vesicles Using an Experimental Model of Equine Osteoarthritis. *Int. J. Mol. Sci.* **2023**, *24*, 14888. <https://doi.org/10.3390/ijms241914888>

**Academic Editor:**  
Regina Golob-Gornitz

**Received:** 3 August 2023  
**Revised:** 26 September 2023  
**Accepted:** 28 September 2023  
**Published:** 4 October 2023



Copyright: © 2023 by the authors. Licensee MDPI, Basel, Switzerland. This article is an open access article distributed under the terms and conditions of the Creative Commons Attribution (CC BY) license (<https://creativecommons.org/licenses/by/4.0/>).

**Abstract:** Extracellular vesicles (EVs) contribute to osteoarthritis pathogenesis through their release into joint tissues and synovial fluid. Synovial fluid-derived EVs have the potential to be direct biomarkers in the causal pathway of disease but also enable understanding of their role in disease progression. Utilizing a temporal model of osteoarthritis, we defined the changes in matched synovial fluid and plasma-derived EV small non-coding RNA and protein cargo using sequencing and mass spectrometry. Data exploration included time series clustering, factor analysis and gene enrichment interrogation. Chondrocyte signalling was analysed using luciferase-based transcription factor activity assays. EV protein cargo appears to be more important during osteoarthritis progression than small non-coding RNAs. Cluster analysis revealed plasma-EVs represented a time-dependent response to osteoarthritis induction associated with supramolecular complexes. Clusters for synovial fluid-derived EVs were associated with initial osteoarthritis response and represented immune/inflammatory pathways. Factor analysis for plasma-derived EVs correlated with day post-induction and were primarily composed of proteins modulating lipid metabolism. Synovial fluid-derived EVs factors represented intermediate filament and supramolecular complexes reflecting tissue repair. There was a significant interaction between time and osteoarthritis for CRE, NFkB, SRE, SRF with a trend for osteoarthritis synovial fluid-derived EVs at later time points to have a more pronounced effect.

**Keywords:** extracellular vesicles; osteoarthritis; multi-omics


## 1. Introduction

Osteoarthritis (OA) is the most common equine joint disease characterised by cartilage degradation and changes to other joint tissues [1], severely affecting welfare and performance leading to early retirement [2]. It results in substantial morbidity and mortality [3]. Despite the huge socioeconomic importance of OA, our understanding of the pathophysiological mechanisms involved is limited [4]. Characterised by synovitis [5],

# Conference presentations & posters

## ISEV 2021- The characterisation of equine synovial fluid and plasma EVs (poster)


### The Characterisation of Equine Synovial Fluid and Plasma Extracellular Vesicles



**NanoView**  
BIOSCIENCES

**Chen E.J.<sup>1</sup>, Anderson J.P., Hayward L.P., Tully D., Hogg P., Jones P.** *University of Liverpool*

<sup>1</sup>Research Centre for Equine Health, University of Liverpool, Leahurst, Neston, Wirral, Merseyside, L69 3GE, UK  
<sup>2</sup>Department of Veterinary Clinical Science, University of Liverpool, Leahurst, Neston, Wirral, Merseyside, L69 3GE, UK  
<sup>3</sup>Department of Veterinary Pathology, University of Liverpool, Leahurst, Neston, Wirral, Merseyside, L69 3GE, UK



**UNIVERSITY OF**  
**LIVERPOOL**


**Introduction**

Extracellular vesicles (EVs) are secreted by a diverse range of cells, contributing to intercellular communication, assisting in tumour cell development, acting as potential disease biomarkers and therapeutic targets. The ability to characterise EV surface markers, allowing for the identification of EVs, is essential for the identification of EVs. However, until now the identification of antibodies for equine EV surface proteins has been problematic, as there are a low number of antibodies available for equine-specific proteins. In our knowledge this is the first study of its kind to characterise equine EVs, specifically the membrane sub-population. This is fundamental in defining the role of EVs in pathophysiology and immunomodulation, representing the capacity to be used to monitor clinical practice.

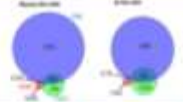
**Aims**

- To determine if the NanoView Human antibodies show cross-reactivity with equine proteins.
- To characterise equine EVs in accordance with MISEV 2018 guidelines, using the NanoView system.

**Materials & Methods**




**Colocalization Analysis**



Colocalization analysis from the NanoView system allows for the identification of EVs from the surface of EVs using the NanoView system. This allows for the identification of EVs from the surface of EVs using the NanoView system.

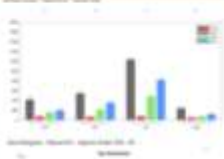
**Background – The NanoView System**




- Isolated EVs from the NanoView system are then used to assess the ability of the NanoView system to identify EVs from the surface of EVs.
- EVs are then processed and separated by antibody immunoprecipitation, enabling single-antibody characterisation.
- Characterisation and distribution of surface marker identification and colocalisation are discussed.


**Results**

**Equine Synovial Fluid**



**Equine Plasma**





NanoView system analysis of EVs identified the plasma protein concentration to be 0.000000 particles per EV and the EV concentration to be 0.000000 particles per EV.

The NanoView system identified human antibodies cross-reactivity for EVs in equine synovial fluid and plasma. The EVs in equine synovial fluid and plasma are 1.000000 larger than EVs.


**Discussion**

- The NanoView system is able to characterise EVs using the NanoView system.
- The NanoView system is able to characterise EVs using the NanoView system.
- Additional analysis from a wider population of samples is needed.
- We intend to further explore this group of markers using complementary immunoprecipitation analysis of the EV surface proteins.

**Conclusion**

- The NanoView system is able to characterise EVs using the NanoView system.
- The NanoView system is able to characterise EVs using the NanoView system.
- The NanoView system is able to characterise EVs using the NanoView system.

**Acknowledgements**



**wellcome trust** **CIMA** **ISEV**



**ASEV 2021- Characterisation of Equine EVs from In Vitro, Ex Vivo and In Vivo Models of Equine OA (oral presentation)**

**Characterisation of Equine Extracellular Vesicles from *In Vitro*, *Ex Vivo* and *In Vivo* Models of Equine Osteoarthritis**



2020-2021  
PUBLIC INVOLVEMENT PANEL  
UNIVERSITY OF LIVERPOOL

ASEV Young Scientists Meeting 2021

Emily Clarke BSC(Hons) MRAS AFHEA, PhD student  
University of Liverpool, Institute of Life course & Medical sciences



CIMA



wellcome



NanoView  
NANOSCIENCE




UNIVERSITY OF LIVERPOOL



**UKEV 2021 poster**

**Novel Spectroscopy Techniques Used to Interrogate Equine Osteoarthritic (OA) Extracellular Vesicles (EVs)**




PEPERS LAB

Emily J Clarke<sup>1</sup>, Cassin Lima<sup>1</sup>, James R Anderson<sup>1</sup>, Caterina Caporaso<sup>1</sup>, Jacob Myers<sup>1</sup>, Roy Goodacre<sup>1</sup> and Manly J Palfrey<sup>2</sup>

<sup>1</sup>University of Liverpool, Institute of Life Course and Medical Sciences, William Morris Research Building, 6th Floor, 6, Liverpool, Liverpool, L69 3GB, UK


<sup>2</sup>University of Liverpool, Institute of Health, Molecular and Integrative Biology Research Building, Crown Road, Liverpool, Liverpool, L69 3GB, UK



UNIVERSITY OF LIVERPOOL

(1) Background

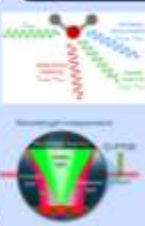
- Osteoarthritis common degenerative disease of the synovial joints in humans and horses.
- Causes pain, reduced mobility and inflammation.
- Important to understand mechanisms by which osteoarthritis develops, in order to identify potential diagnostic biomarkers and therapeutic targets.



(2) Raman and O-PTIR

**Raman spectroscopy** can probe molecular structure with optical penetration and enhanced sensitivity (O-PTIR) using microbeams.

- Highly sensitive
- Non-destructive technique
- Composition, phase, crystallinity and molecular interactions
- Low sample volumes required



(4) Results

**Conclusions**

"With the development of osteoarthritis the extracellular vesicle membrane composition changes, contributing towards the propagation of disease throughout the joint."

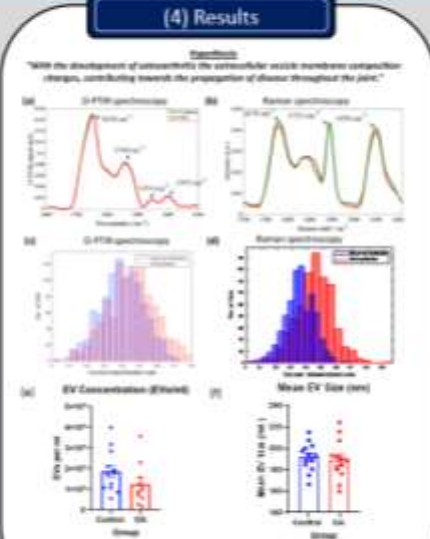






Figure 1 - (a) O-PTIR spectra, (b) Raman spectra (O-PTIR overlaid) (c) EV concentration measured for the EVs using O-PTIR and Raman data, (d) EV number - O-PTIR concentration measured and (e) and (f) EV number highlighting mean size difference between OA and control EVs.

(3) Materials & Methods




(5) Conclusions

- No difference in biochemical composition between diseased and control extracellular vesicle membranes.
- Limitations include the power of the study, and severity of osteoarthritic phenotype in sample donors.
- Further work will look to explore if this finding is consistent across biofluids relevant to osteoarthritic disease, and if extracellular vesicle metabolism and proteomic cargo alters as a result of disease.
- Further methods may look to use nuclear magnetic resonance spectroscopy to explore metabolic and lipidic components of the EV membrane.

**Acknowledgements:**    **wellcome trust**

# OARSI 2022- Optical Photothermal Infrared Spectroscopy To Distinguish Equine Osteoarthritic Extracellular Vesicles (poster)


## Optical Photothermal Infrared Spectroscopy To Distinguish Equine Osteoarthritic Extracellular Vesicles



**PEPPERS LAB**

**Emily J Clarke<sup>1</sup>, Cassio Lima<sup>2</sup>, James R Anderson<sup>1</sup>, Catarina Castanheira<sup>1</sup>, Jacob Hyett<sup>1</sup>, Royston Goodacre<sup>2</sup> and Mandy J Peffers<sup>1</sup>**

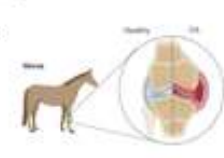
<sup>1</sup>University of Liverpool, Institute of Life Course and Biological Sciences, William Henry Charles Building, 6 W Derby St, Liverpool L7 8TC  
<sup>2</sup>University of Liverpool, Institute of Systems, Molecular and Integrative Biology, Biosciences Building, Crown Street, Liverpool, L69 7GE



**UNIVERSITY OF LIVERPOOL**

### Osteoarthritis

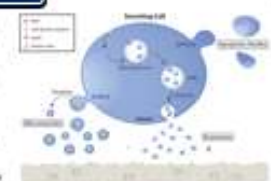
- Osteoarthritis is a common degenerative disease of the synovial joint in humans and horses.
- Causes pain, reduced mobility and inflammation.
- Important to understand mechanisms by which osteoarthritis develops, in order to identify potential diagnostic biomarkers and therapeutic targets.



**Figure 1:** Overview of equine osteoarthritis and the molecular changes associated with pathological changes to the joint.

### Extracellular Vesicles

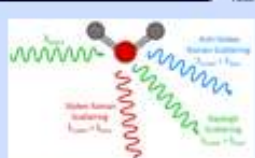
- Nanoparticles enveloped by a phospholipid bilayer membrane.
- Secreted by most mammalian cells.
- Involved in intercellular communication.
- Classified as apoptotic bodies (100nm-5000nm), microvesicles (100nm-1000nm) and exosomes (30-250nm).




**Figure 2:** Overview of extracellular vesicle biogenesis.

### Raman and O-PTIR

Highly sensitive, non-destructive technique, non-contact, phase, crystallinity and molecular interactions; low sample volumes required.



**Figure 3:** Principle of Raman Scattering.



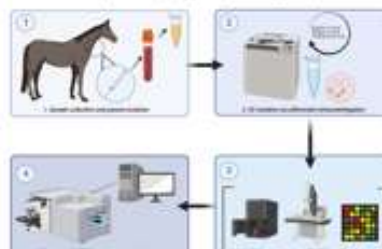
**Figure 4:** Principle of optical photothermal infrared spectroscopy.

**Raman Spectroscopy:** Photons from a monochromatic source interact with the sample and a small fraction of them are inelastically scattered. The energy difference between incident and scattered photons corresponds to a Raman shift and it is associated with the chemical structure of molecules in the sample.

**Infrared spectroscopy:** is based on the absorption of infrared radiation by molecular vibrations from bonds that possess an electric dipole moment that can change by atomic displacement.

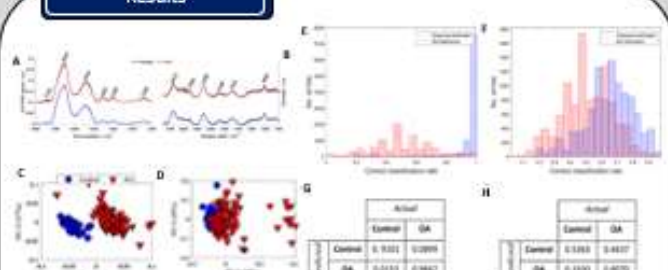
### Materials & Methods

With the development of osteoarthritis plasma extracellular vesicle cargo changes, monitoring towards the progression of disease throughout the joint?



**Figure 5:** Overview of the workflow for the study. Extracellular vesicles were collected from the synovial fluid (SB) of 10 samples from healthy control and OA horses.

### Results



**Figure 6:** Representative regions of average spectra. (A) for horse and (B) Raman spectra collected from healthy control (blue) and joint OA (red) joint samples. Peaks are offset for clarity. PCA scores and loading plots. Plot scores obtained by subjecting to least squares PCA (LSP) PCA scores plot of Raman Aids (C). Values on axes are the percentage total explained variance (PEV). Qualitative scores for PEV of infrared and Raman spectra. (D) Infrared and (E) Raman spectra of using classification rates for real data - from the 10,000 Raman spectra and spectrum sets - from the 10,000 permeation rates, with a correct classification rate of 74.1% for infrared and 64.5%, (F) and (G) are the average confusion matrices for infrared and Raman, respectively, with rows representing post-test classification and columns representing expected results.

	Control	OA
Control	0.7012	0.2988
OA	0.2513	0.7487

	Control	OA
Control	0.5183	0.4817
OA	0.4333	0.5667


### Conclusions

- Optical Photothermal Infrared spectroscopy could differentiate control and osteoarthritic vesicles from healthy control with great classification (74.1% correct classification rate and 64.5% correct classification rate) (correct classification rate = 67.3%).
- Regardless of the infrared spectra indicated that photoacoustic spectroscopy can be used to measure extracellular vesicle concentration in synovial fluid for protein, lipid and nucleic acids.
- Insensitivity - number of samples available for analysis is not sufficient in a larger cohort, large sample collection is necessary to see an adequate number of EVs for analysis.
- A further work is needed to determine if O-PTIR is sensitive enough to determine differences in a range of different OA phenotypes and severities, and possible differences in the specific biological functions of EVs.
- We are currently modifying the EV cargo using DNA microarrays, mass spectrometry proteomics and various platforms in order to provide complete characterization of EVs in OA and determine their role further in disease progression.
- Overall this study demonstrates the potential of Raman and O-PTIR spectroscopy to be used as a diagnostic tool in osteoarthritis.


### Preprint

**bioRxiv**  
THE PREPRINT SERVER FOR BIOLOGY

Optical photothermal infrared spectroscopy can differentiate equine osteoarthritic plasma extracellular vesicles from healthy controls  
Clarke et al., 2022



### Acknowledgements:




[@E\\_Clarke\\_Sci](#) [@LabPeppers](#) [@LivuniILCaMS](#)




Cutting edge OA 2022- Characterisation of equine EVs and metabolomic / proteomic cargo in an in vivo model of OA treated with MSCs ( oral presentation and poster)

## Exploring the Proteome of Equine Extracellular Vesicles from an *In Vivo* model of Osteoarthritis Treated Intraarticularly with Mesenchymal Stromal Cells



**Emily J Clarke<sup>1</sup>, Alex P Shephard<sup>2</sup>, Camilla Andersen<sup>3</sup>, Louise Sundgaard<sup>3</sup>, Rosalind Jenkins<sup>4</sup>, Stine Jacobsen<sup>4</sup> and Mandy J Peffers<sup>1</sup>**

<sup>1</sup>University of Liverpool, Institute of Life Course and Medical Sciences, William Henry Dawson Building, 6 W Derby St, Liverpool L7 8TS |  
<sup>2</sup>Novartis Biosciences Ltd, 95, Mollat Avenue, Science Park, Sandilands Road, Mollat, Mollat, Wiltshire, Wiltshire, Wiltshire, Wiltshire, Wiltshire  
<sup>3</sup>University of Copenhagen, Department of Veterinary Clinical Science, Artibejsgade 35, 2300 København K |  
<sup>4</sup>University of Liverpool, Department of Pharmacology and Therapeutics, Institute of Systems, Molecular and Integrative Biology, MRC Centre for Drug Safety Science



### Osteoarthritis

- Osteoarthritis is a common degenerative disease of the synovial joint in humans and horses.
- Causes pain, reduced mobility and inflammation.
- Important to understand mechanisms by which osteoarthritis develops, in order to identify potential diagnostic biomarkers and therapeutic targets.




Figure 1: Overview of equine osteoarthritis and the molecular changes associated with pathological changes (taken with permission)

### Extracellular Vesicles

- Nanoparticles enveloped by a phospholipid bilayer membrane.
- Secreted by most mammalian cells.
- Involved in intercellular communication.
- Classified as apoptotic bodies (1000nm-5000nm), microvesicles (100nm-1000nm) and exosomes (30-150nm).

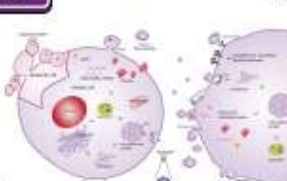
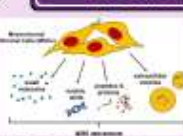


Figure 2: Overview of extracellular vesicle types

### MSC Therapy



- Injected intracellularly
- Harvested from stromal marrow from dermal or bone or adipose tissue from tail base or head
- Can be autologous or allogeneic
- Therapeutic benefits have been observed
- MSCs are multipotent progenitor cells that self-renew and differentiate
- MSCs have immunosuppressive properties and an ability to migrate to site of injury
- Provides repair and regeneration
- Mechanism of action unknown, EVs and secretome thought to contribute

Figure 3: Overview of MSCs





Figure 4: MSCs in Osteoarthritis

### SWATH Proteomics



- Proteins are analysed by liquid chromatography coupled to ion- mobility mass spectrometry according to the modified data-independent acquisition (DIA) mode
- DIA-MS approach, all ions are isolated by the first mass analyser can be transferred to the second mass analyser by the second mass analyser

Figure 5: SWATH proteomics pipeline

- Comparison to DDA (Data Dependent Acquisition) (one made from scratch)
- High throughput, accuracy, repeatability, sensitive up to 1000 proteins per run
- Quantitatively identify nearly all detectable proteins, including low abundance proteins

### Materials & Methods

\*The experimental flow chart depicts the workflow towards the therapeutic mechanism of MSC therapy in an equine model of OA\*




Figure 6: Materials & Methods

### Samples & Model

- Deep Descriptive (regret model) comparisons (one across a sham control - from region on the distal end of the distal femur)
- The study was approved by the Danish Animal Experimentation Inspectorate (N2020-16-003) and also by the Ethical Committee of the University of Copenhagen (project no. 32020-04)
- 60 horses, 60 times of age (one horse)
- Injecting MSCs (one side, one eye) 3 times

Group	Number	Sex	Age	Eye
Control	30	15	15	15
MSC	30	15	15	15
MSC + MSC	30	15	15	15
MSC + MSC + MSC	30	15	15	15

### Results

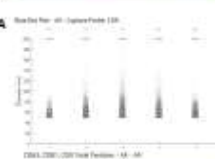


Figure 7: EVs purified from synovial fluid were analysed using western blotting...

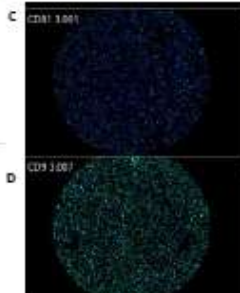


Figure 8: EVs were analysed for CD9, CD63, and CD81...

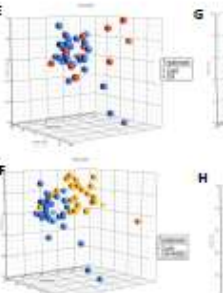


Figure 9: 3D scatter plots of protein abundance...

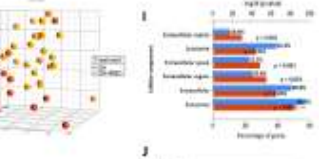


Figure 10: Bar chart of protein abundance...

### Conclusions

- Significant differences between EVs due to disease pathology, and upon therapeutic intervention. These results highlight potential mechanisms of action of MSC therapy, including cellular differentiation, proliferation and organisation of joint-related tissues.
- This is the first time to our knowledge that the EV proteome derived from synovial fluid has been analysed following biological treatment for OA, while also exploring time related change with longitudinal sampling.
- Highlights the effect of MSC derived EVs in an in vivo model of chronic disease, providing evidence that extracellular vesicles contribute towards the therapeutic mechanisms observed with MSC therapy, and hence may serve as a potential alternative to cellular therapeutics.
- Further to this we provide evidence of a time related effect associated with the delivery of MSC therapy and its molecular mechanisms.
- Matched NMR metabolomic analysis to be conducted and multi-omic integration.

@E\_Clarke\_Sci 
 @LabPeppers 
 @LivuniILCaMS

### Acknowledgements:



# UKEV 2022 Characterization of extracellular vesicle cargo in equine osteoarthritis through a SWATH-MS proteomics approach (poster)

## Characterization of extracellular vesicle cargo in equine osteoarthritis through a SWATH-MS proteomics approach

Emily J Clarke<sup>1</sup>, James R Anderson<sup>1</sup>, Rosalind Jenkins<sup>2</sup> and Mandy J Peffers<sup>1</sup>

<sup>1</sup>University of Liverpool, Institute of Life Course and Medical Sciences, L7 8TX and <sup>2</sup>University of Liverpool, Centre for Drug Safety Science Bioanalytical Facility



### INTRODUCTION

- Osteoarthritis is a common degenerative disease of the synovial joint in humans and horses.
- Causes pain, reduced mobility and inflammation.
- Important to understand mechanisms by which osteoarthritis develops, in order to identify potential diagnostic biomarkers and therapeutic targets.

### OBJECTIVE

- To produce two SWATH-MS proteomic libraries from equine synovial fluid and plasma derived extracellular vesicles (EVs), which can be used in the proteomic analysis of EVs in equine osteoarthritis research.

### Background

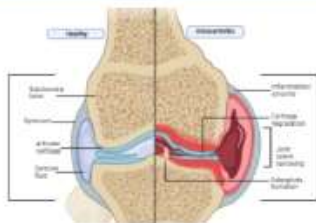


Figure 1 - Overview of osteoarthritis - the molecular changes.

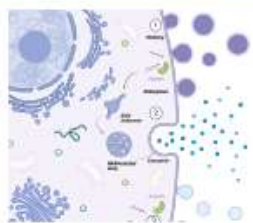


Figure 2 - Overview of extracellular vesicle biogenesis.

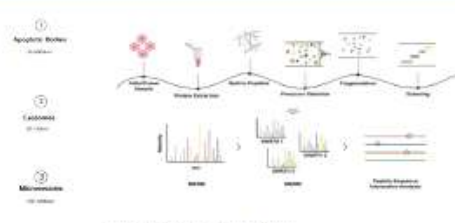
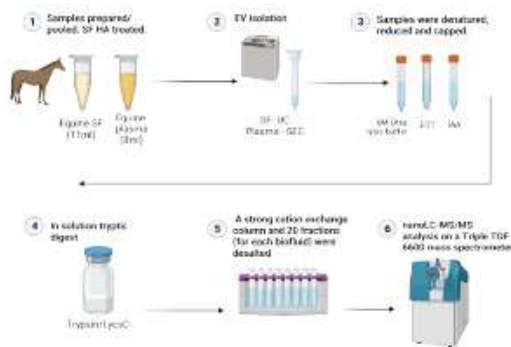


Figure 3 - SWATH proteomics pipeline.

### Methods



### Results

- The plasma library identified 392 proteins
- The SF library 2448 protein with FDR 5%
- 12.8% of proteins overlapped between biofluids.
- Based on cellular compartments we show a significant enrichment of the exosome and extracellular component in both biofluids.
- We identified the top canonical pathways as EIF2 signaling ( $p=3.2E-71$ ) and acute phase response signaling ( $p=2.2E-41$ ); top upstream regulators as MYC ( $p=9.8E-76$ ) and TGF $\beta$  ( $p=1.5E-38$ ) for SF and plasma respectively.

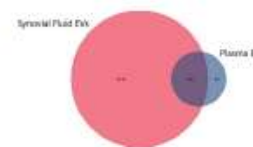


Figure 4 - A venn diagram showing the unique and shared proteins between equine synovial fluid EVs and plasma EVs.



Figure 5 - Funrich pathway analysis results for both plasma and synovial fluid EVs

Figure 6 - Top networks identified using Ingenuity pathway analysis.

### Discussion

- To our knowledge this is the most comprehensive proteome of EVs derived from SF, highlighting the potential for SWATH-MS in EV cargo proteomics.
- These results laydown the foundation for future proteomics studies in our lab.
- We have characterised the protein cargo of SF-EVs after MSC treatment in experimentally induced equine OA. The QR code below takes you to our recently published paper in Frontiers in Veterinary Science utilising the SF-EV library.




### Acknowledgements





**TERMIS 2023 Proteomic characterisation of equine platelet-rich plasma and their extracellular vesicles (poster)**


## Proteomic Characterisation of Equine Platelet Rich Plasma and Their Extracellular Vesicles



**PEFFERS LAB**

**Emily J Clarke<sup>1</sup>, Veronica Foisor<sup>2</sup>, Josephine Hamilton<sup>3</sup>, Alex Gillen<sup>4</sup>, Mark Senior<sup>5</sup>, Agnieszka Turlo<sup>3</sup> and Mandy J Peffers<sup>1</sup>**

University of Liverpool, Institute of Life Course and Medical Sciences, William Henry Duncan Building, 6 W Derby St, Liverpool L7 8TX.<sup>1</sup>  
 NanoViz Biotechnology Unit 05, Mollern Hills Science Park, Gerstethor Road, Malvern WR14 3ZZ.<sup>2</sup>  
 Philip Leverhulme Equine Hospital, Institute of Veterinary Science, University of Liverpool, Liverpool, United Kingdom<sup>3</sup>



**UNIVERSITY OF LIVERPOOL**

### Equine Tendon Injury & PRP

- Tendon injury can affect up to 40% of horses.
- Superficial digital flexor tendon is especially prone to injuries.
- Tendon functional competence and structural integrity rely on homeostasis of tendon cell metabolism and extracellular matrix macromolecules.
- Analogous pathology with both human Achilles tendinopathy (superficial digital flexor tendon).
- There are no treatments that currently improve the structural and functional outcomes.
- Platelet rich plasma (PRP) is injected intratendinously.
- Harvested from blood.
- Local delivery of concentrated growth factors.
- Clinical outcomes can be varied.




Figure 1: Equine lower limb anatomy (left) and human limb anatomy (right), highlighting the analogous structures between both species.




Figure 2: (left) PRP tubes (middle) PRP and (right) PRP being injected into a horse's lower limb.

### Extracellular Vesicles

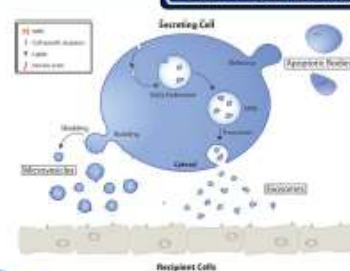


Figure 3: Overview of extracellular vesicle biogenesis.

- Nanoparticles enveloped by a phospholipid bilayer membrane.
- Secreted by most mammalian cells.
- Involved in intercellular communication.
- Classified as apoptotic bodies (1000nm-5000nm), microvesicles (100nm-1000nm) and exosomes (30-150nm).

### Conclusions

1. PRP-EV proteomic cargo was explored in order to find their potential role in the therapeutic mechanisms of PRP.
2. Significantly different proteomes were observed between PRP and plasma, as well as their respective EVs.
3. PRP cargo was significantly attributed to TGFβ1 signalling, PRP-EV cargo was significantly attributed to fatty acid metabolism and its downregulation.
4. EVs should be explored further when considering optimal PRP composition to improve PRP efficacy in clinical practice.

### Methods

**Hypothesis**  
 "We hypothesised that PRP has an altered proteome compared to matched plasma, enriched in proteins that contribute towards therapeutic action. Respective EVs are also variable, with PRP EVs containing unique proteins suggestive of a specific role in mediating PRP therapy."

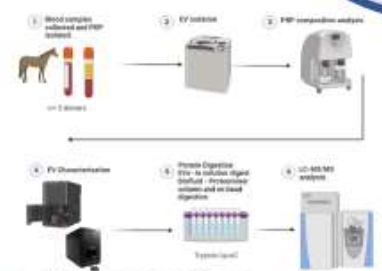


Figure 4: An overview of the experimental methods for this study.

### Results

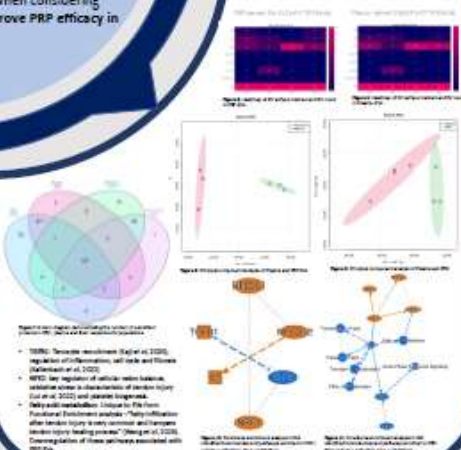


Figure 5: Proteomic analysis of PRP and EVs. The top row shows fluorescence microscopy images of EVs. The middle row shows Venn diagrams and dot plots comparing PRP and EV proteomes. The bottom row shows network diagrams of protein interactions.


Key findings:  
 - TGFβ1: TGFβ1 signalling pathway (Kojima et al. 2020), regulation of proliferation, cell cycle and fibrosis (Kawabuchi et al. 2022).  
 - FFA: Key regulator of cellular metabolism, oxidative stress and inflammation of tendon injury (Liu et al. 2022) and muscle hypertrophy.  
 - Other key molecules: Linkage to the TGFβ1 signalling pathway and its downregulation. Functional enrichment analysis: "TGFβ1 signalling after tendon injury in rat normal and chronic tendon injury loading model" (Shen et al. 2020).  
 - Downregulation of these pathways associated with PRP/EVs.

[eclarke@liverpool.ac.uk](mailto:eclarke@liverpool.ac.uk)

Emily Clarke

@E\_Clarke\_Sci @LabPeffers @LivuniILCaMS

**Acknowledgements:**





**EuPA-BSPR 2023 Proteome and phospholipidome interrelationship of synovial fluid-derived extracellular vesicles in equine osteoarthritis: An exploratory multi-omics study to identify composite biomarkers**

Proteome and phospholipidome interrelationship of synovial fluid-derived extracellular vesicles in equine osteoarthritis: An exploratory 'multi-omics' study towards combined biomarkers



Emily Clarke, Laura Varela, Rosalind E Jenkins, Estefania Lozano-Andrés, Anna Cywińska, Maciej Przewozny, P. René van Weeren, Chris H.A. van de Lest, Mandy Peffers, Marca H.M. Wauben



BSPR/EuPA Newcastle 2023

